AN ABSTRACT OF THE THESIS OF

William W. Deaton, III for the degree of Master of Science

in Chemical Engineering presented on October 15, 1979

Title: SOLIDS MOVEMENT IN A TUBE-FILLED FLUIDIZED BED

Abstract approved: Redacted for Privacy

Thomas J. Fitzgerald

Mixing of ferrite tracer with silica sand was studied in a 0.91 m x 0.91 m cold fluidized bed. Inductance probes located inside dummy heat transfer tubes [in a 4 x 4 x 4 array] were used to monitor a ferrite tracer with physical properties similar to coal as it moved and dispersed from its injection port above the bed. Increases in superficial gas velocity were found to enhance mixing. Tracer appeared to circulate down the sides and up the interior of the bed.

Solids Movement in a Tube-Filled Fluidized Bed

by

William W. Deaton, III

A THESIS

submitted to

Oregon State University

in partial fulfillment of
the requirements for the
degree of

Master of Science

Completed October 1979

Commencement June 1980

APPROVED:

Redacted for Privacy

Professor of Chemical Engineering
in charge of major

Redacted for Privacy

Head of Department of Chemical Engineering

Redacted for Privacy

Dean of Graduate School

Date thesis is presented October 15, 1979

Typed by Margi Wolski for William W. Deaton, III

ACKNOWLEDGEMENTS

I would like to express my gratitude to Professor Thomas J. Fitzgerald for his originality, unwavering enthusiasm and scientific zeal. Also, I wish many thanks to Steve Crane, Rich Fobes and Riley Chan - all of whom have contributed so much to the success of this project. To Professor Charles E. Wicks: Thanks for your genuine concern and assistance. I was the friend "in need" and you were the friend "in deed." And finally, I want to thank Kathy M. Deaton, my wife, whose compassion, understanding and assistance was invaluable during our two year stay at Oregon State University. This work was supported by grant number RP-315-1 from the Electric Power Research Institute.

NOMENCLATURE

Symbol	Description	Dimensions
A_t	cross sectional area	L^2
B	reciprocal time constant	t^{-1}
$\bar{C}^*$	average concentration sensed by all channels over the last ten seconds of a run	ML^{-3}
$\tilde{C}_i$	average concentration measured on channel i over a one second time interval	ML^{-3}
C_i^*	maximum concentration of channel i over the last 20 seconds of a run	ML^{-3}
$C_{i,j}$	concentration measured by channel i at time increment j	ML^{-3}
C_{p_s}	specific heat of solids	$EM^{-1}T^{-1}$
C_t	tracer concentration	ML^{-3}
$\tilde{C}_i/\bar{C}_i^*$	normalized tracer concentration	---
$\bar{C}_j$	mean concentration of all channels calculated for time interval j	ML^{-3}
C_θ	$(\bar{C}_j/\bar{C}^*)$, normalized mean concentration	---
D	overall dispersion coefficient	L^2t^{-1}
D_{sa}, D_{sr}	axial and radial dispersion coefficients	L^2t^{-1}
$\bar{d}_p$	mean surface particle diameter	L
d_{p_i}	average diameter of size interval i	L
g	acceleration of gravity, 9.8 m/s (32.2 FPS)	Lt^{-2}

Nomenclature, continued

Symbol	Description	Dimensions
J_v	vertical flux of solids	$ML^{-2}t^{-1}$
K_{ea}	effective axial thermal conductivity	$EL^{-1}T^{-1}$
MSMM	mean square measure of mixing (Chapter V)	ML^{-3}
OMT	overall mixing time (Chapter IV): time required for all channels to register their average final or "equilibrium" values. More precisely, it is the time for the slowest or worst channel to fall within the noise band about the equilibrium concentration.	t
OMT	overall mixing time (Chapter V): the time required for the MSMM curve to fall within the noise band about the equilibrium concentration.	t
OMT	overall mixing time (Chapter VI): time for the tracer to enter the "noise band" about the equilibrium concentration of the mass balance curve or the normalized tracer average concentration curve.	t
P	pressure	FL^{-2}
t	time	t
Δt	time interval	t
U, U_o	superficial gas velocity	Lt^{-1}
U_{mf}	superficial gas velocity at minimum fluidizing conditions	Lt^{-1}
v_d	driving voltage of the inductance circuit	V

Nomenclature, continued

Symbol	Description	Dimensions
v_l	inductive voltage component	V
V_l	amplitude of the inductive voltage component	V
v_{out}	output voltage of the circuit	V
v_r	resistive voltage component	V
V_r	amplitude of the resistive voltage component	V
ΔV	voltage difference	V
ΔV	average voltage difference	V
W	weight of solids	M
x	distance	L
x_i	fraction of material in size interval i	---
X_s	concentration of tracer in solids mix	MM^{-1}
$\overline{(\Delta Z)^2}$	mean square distance	L^2

Greek Symbols

$\bar{\rho}, \rho_s, \rho_g$	mean bed density, solid density, gas density	ML^{-3}
ν	kinematic viscosity	L^2t^{-1}
ω	frequency	t^{-1}

TABLE OF CONTENTS

TABLE OF CONTENTS

LIST OF FIGURES

LIST OF TABLES

SOLIDS MOVEMENT IN A TUBE-FILLED FLUIDIZED BED

I. INTRODUCTION

Fluidization is a curious term created by engineers and scientists to describe a man-produced and natural-occurring phenomena. Davidson and Harrison [10] define gas fluidization as the "technique of giving to solid particles the properties of a [fluid] by forcing gas ... up through a bed of solid particles at a flow-rate sufficient to support them." According to Kunii and Levenspiel [21], gas fluidization is "the operation by which fine solids are transformed into a fluid-like state through contact with a gas ..." By any definition, fluidization is now used for many important industrial applications and has, therefore, become the subject of intensive research and development.

In an attempt to develop cheap, reliable and environmentally safe fuels, both government and industry have instigated additional research in the area of fluidized coal combustion. Bituminous-coal-fired burners no longer meet the revised requirements and regulations of society. For example, since these burners cannot control sulfur dioxide (SO_2) emissions, this task must be done separately with expensive scrubbing systems. Fluidized bed combustors, on the other hand, operate isothermally at relatively low combustion temperatures (750-800°C) and, thereby, inhibit NO_x emissions while providing optimum

conditions for the retention of sulfur by limestone or dolomite in the bed. In general, fluidized coal combustors, as opposed to standard burners of the past decades, are extremely versatile.

Gas-fluidized beds are recognized for their good solids-mixing properties. In fact, for many gas-solid reactions fluidized beds mix rapidly enough to be considered well-mixed reactors. Unfortunately, this is not the case for large-scale fluidized bed coal combustors. Coal particles burn to completion in a few minutes, and evolve large quantities of combustible and polluting gases (e.g., sulfur dioxide) only seconds after their introduction to the bed. Thus, it is generally accepted that a very large number of feed points must be used to inject the coal in order to consider the media well-mixed.

Most previous solids-mixing studies involve fine particle systems with a mean surface diameter, $\overline{d}_p$, less than 0.5 mm (0.02 in) and relatively low superficial gas velocities, less than 1.8 m/sec (6 ft/sec). Fluidized beds of intermediate particles (0.5 mm (0.02 in) to 1.5 mm (0.06 in) in diameter) and large particles (greater than 1.5 mm (0.06 in)) have only recently become a topic of investigation, primarily as a result of the increasing importance of several new processes such as fluidized bed combustion of coal.

Fluidized bed coal combustors typically use dolomite or limestone particles of diameter greater than 0.5 mm (0.02 in) to prevent the formation of sulfur dioxide produced by burning sulfur-containing

coal. To be more specific, limestone particles in the bed are calcined to form calcium oxide which then combines with oxygen and sulfur dioxide produced by coal combustion to form calcium sulfate, a solid waste. One to two percent of the bed material is coal. The heat produced in the bed is transferred to an immersed horizontal tube bank. These heat exchange tubes are used for steam generation in electric power plants and for liquid and gas heating in the process industries.

In the design of a large-scale fluidized bed combustor it is important to know just how fast solids move and disperse throughout the bed. This problem is the motivation of our study. It is significant to note that experiments dealing with modeling parameters of solids movement need not be conducted in a hot bed where tracer monitoring is extremely difficult. Solids movement is strongly dependent on bubble size and frequency, and, therefore, it can be modeled quite well at room temperature. The bed media (its physical properties and amount) and geometry (.91 m x .91 m (3' x 3') with an array of dummy heat transfer tubes immersed in the bed media) and the range of superficial gas velocities presented in this study are all roughly representative of fluidized bed combustors.

II. PREVIOUS WORK

2.1 Background

Studies of solids movement in gas-fluidized beds have shown that bubbles are principally responsible for mixing and circulation of solids. In small particle beds ($\bar{d}_p$ < 0.5 mm (0.02 in)) rising bubbles carry along wakes of solids and associated gases, as demonstrated by Davidson and Harrison [10], Woolard and Potter [44], and Abrahami and Resnick [1]. "The shedding and replenishment of solids in the wakes of bubbles appears to be the major mechanism of solids transport in these beds" [21]. On the other hand, in large particle beds ($\bar{d}_p$ > 1.5 mm (0.059 in)) the solids transport mechanism is almost entirely bubble-induced drift or displacement according to Cranfield [9]. In the intermediate regime (0.5 mm (0.02 in) < $\bar{d}_p$ < 1.5 mm (0.059 in)) both mixing mechanisms participate. Our study is in the intermediate regime with $\bar{d}_p$ = 0.8 mm (0.03 in).

There exist four major differences between our study and those done previously.

(1) Our bed has an immersed tube array.

(2) Many of our experiments are done at relatively high superficial gas velocities.

(3) We use intermediate-sized bed media ($\bar{d}_p \simeq$ 0.8 mm (0.03 in)); and large tracer ($\bar{d}_p \simeq$ 5.08 mm (0.2 in)) for runs 50-73,

$\overline{d}_p \simeq$ 1.6 mm (0.06 in)) for runs 74-114).

(4) The tracer sensing probes are inductor coils inside the tubes of the array; accordingly, the probes are in situ and non-disruptive.

2.2 Early Experimental Studies and Modeling

2.2.1 Diffusion Model

Bart [2] carried out tracer studies in a 31.8 mm (1.25 in) I. D. tube and modeled the mixing with the diffusion equation (and appropriate boundary conditions),

$$\frac{\partial C_t}{\partial t} = D_{sa} \frac{\partial^2 C_t}{\partial x^2}$$

where C_t is the concentration of tracer (kg/m^3), D_{sa} is the axial dispersion coefficient of solids (m^2/sec), t is time (seconds) and x is axial distance (m).

Stemerding and Reman [39] followed an indirect method, introduced by Gilliland and Mason [15], where they determined the axial diffusion coefficient of solids from knowledge of the axial temperature distribution in a long, narrow fluidized bed. When heat is supplied to the top of the bed electrically and removed from the bottom with a cool water reservoir, the apparent axial thermal conductivity, K_{ea}, can be used to calculate an apparent axial diffusion coefficient (D_{sa}) for

solids mixing:

$$D_{sa} = \frac{K_{ea}}{C_{ps}\bar{\rho}}$$

where C_{ps} is the specific heat of the solids (J/Kg °K), $\bar{\rho}$ is the average bed density (Kg/m^3) and K_{ea} is the effective thermal conductivity (W/m °K).

Lewis, Gilliland and Girouard [24] extended Gilliland's approach to study radial or lateral transport by insertion of a vertical electric heating element along the axes of 50.8 mm (2 in), 74.7 mm (2.94 in) and 146.1 mm (5.75 in) diameter beds and cooling the outer walls of these cylindrical beds. Kunii, Yoshida and Levenspiel [22] interpreted this data in terms of the diffusion model and found that lateral and axial diffusion coefficients increase as particle size becomes smaller.

May [29] experimented in fluid bed units up to 1.52 m (5 ft) in diameter using cracking catalyst and incipient bubbling velocities. Radioactively tagged particles were injected at the top of the bed and monitored at various locations below. In the .381 m (15 in) diameter unit, the data fit the diffusion model fairly well. On the other hand, data from the larger units were much more erratic. Although, according to May, there was evidence in the larger units of a gross circulation pattern with smaller scale mixing superimposed on it. May also observed that mixing of .050 Kg (0.11 lbs) of catalyst with

14,800 Kg (15 tons) of catalyst was complete in less than a minute in the 1.52 m (15 ft) unit.

Hayakawa et al. [16] monitored the spread of solids in fluidized-packed beds (where fine glass spheres were fluidized in the voids of Raschig rings made of metal screens) by the change in electrical resistance during the mixing of conductive and non-conductive materials. From their results, one can conceivably postulate a diffusion mechanism.

Brotz [5] and, eventually, others (Gabor [13] and Mori and Nakamura [32]) studied lateral diffusion in a shallow rectangular fluidized bed by measuring the rate of approach to equilibrium (i.e., a uniform solid concentration) after rapid removal of a plate separating two regions of different tracer concentrations.

Several researchers [21, 10] claim that the diffusion model fails to explain the wide variation in reported data. The reason for this failure is the presence of large bubbles, which precludes the use of any model whose basis lies in a diffusion type of mechanism (that is, a mechanism requiring a large number of small, random mixing steps).

2.2.2 Two-Stirred Tank Model

Katz and Zenz [18] describe the mixing of solids in terms of a flux of solids across a horizontal plane using the following differential equation:

$$W_1 \frac{dX_{s_1}}{dt} = -W_2 \frac{dX_{s_2}}{dt} = J_v A_t (X_{s_1} - X_{s_2})$$

where W_1 and W_2 are the weights of solids (Kg) in regions 1 and 2, X_{s_1} and X_{s_2} are the concentrations of tracer (Kg tracer/Kg total solids) in the upper (1) and lower (2) regions, J_v is the vertical flux of solids across the horizontal boundary (Kg/m^2 sec) and A_t is the cross sectional area of the bed (m^2).

Physically, J_v is a flux at the center of the bed and it tells nothing about how much material crosses the horizontal interface at distinct locations. Since the model is a poor fit to reality, J_v values can only be considered as a rough approximation of the flux of solids up or down a bed.

2.2.3 Movement of a Single Particle

Toomey and Johnstone [42] used a high speed filming technique in a bed of 376 micron (0.0148 in) diameter glass spheres and reported no change of sign in the vertical particle velocity component along the wall of their 120 mm (4.72 in) diameter fluidized bed, i.e. the velocity component was always downward. After observing these experiments, Leva [23] claimed that the mean particle velocity is lower than the superficial fluid velocity and that both of these velocities are somehow positively related. In other words, as the superficial gas velocity

increases, the mean particle velocity also increases.

Kondukov et al. [19] studied the movement of individualized radioactively tagged particles in a fluidized bed. Besides observing that particles wander everywhere in the bed, he noticed a rapid upward movement compared to a slow pulsating migration downward. Thus, solids spend a considerable portion of their time drifting downward, but they are occasionally blown up to the top of the bed.

Leva [23], in a study similar to that of Kondukov, noticed active zones above the bottom portion of the bed, where tagged particles moved down the wall and, then, suddenly away. Todes and Bondareva [3, 4, 41] drew an analogy between this motion and turbulent pulsations of fluids after viewing their motion pictures of fluidized steel spheres. Massmilla and Westwater [26] conducted a similar study and also observed particle pulsations.

2.3 Proposed Mechanisms and Modeling Efforts

2.3.1 Background

As mentioned previously, most recent studies have focused on bubble wake and drift mechanisms of solids mixing in vigorously fluidized beds without tubes. Sutherland [40] and Rowe and Sutherland [36] examined mixing of a layer of nickel shot in long, narrow fluidized beds of copper shot. They observed very slow mixing at gas velocities

close to U_{mf} (the minimum fluidization gas velocity) and significant improvements in mixing at velocities only 1.3 times U_{mf}. Thus, one would be led to conclude that mixing of solids in gas fluidized beds must be a function of the size and number of rising bubbles in the bed.

A major difference between fluidized beds of large and small particles is their respective relationships of superficial gas velocity to rising bubble velocity. In beds of small particles ($\bar{d}_p$ < 0.5 mm (0.02 in)), the rising velocity of bubbles exceeds the superficial gas velocity and, therefore, the bubbles are referred to as fast bubbles. On the other hand, beds of large particles ($\bar{d}_p$ > 0.5 mm (0.02 in)) are characterized by slow bubbles since the air velocity through the emulsion phase is greater than the bubble rise velocity. A closer inspection of the small and large particle regimes is now in order.

2.3.2 The Small Particle Regime - Bubble Wake Transport

Rowe and Partridge [35] have shown in small particle beds ($\bar{d}_p$ < 0.5 mm (0.02 in)) that solids are entrained in the wake (a small turbulent region of solids located immediately underneath a bubble) of upward rising gas bubbles. The solids are supported under the bubble by upward rising gas. These investigators approximate that the wake of the bubble is 30% of the bubble volume. Thus, movement of solids results from wake transport, i.e. bubble wake shedding and replenishment, in beds of small particles.

Nguyen et al. [33] studied the interrelation between bubbles, solids movement and gas backmixing in their 1.22 meter (4 foot) square bed without internals. Their data demonstrates that the countercurrent backmixing model (or bubbling bed model), which incorporates the bubble wake mechanism, is an acceptable description of small particle fluidized beds. They conclude that in large fluidized beds, gas velocity and, thus, the number and size of bubbles have a very pronounced and direct effect on solids mixing.

While the countercurrent backmixing model proves to be very powerful in small particle beds operating at low velocities, it cannot be used in its present form to account for turbulent and fast bubbling regimes, where definite single bubbles are practically nonexistent. Mireur and Bischoff emphasize this conclusion in a recent study where they state that

> most commercial fluidized beds are operated under conditions where the gas flow rate is many times (5-10-20) the minimum. Here, the bed is a churning mass with bubbles of many sizes colliding, etc., and it is difficult to see how a direct bubble model could be used. In other words, there would always be a certain number of empirical parameters regarding bubble size distributions [etc. required] ... [31, p. 840]

2.3.3 The Large Particle Regime - Bubble Drift Transport

Cranfield [9] investigated solids mixing in fluidized beds (20 x 610 mm (0.79 x 42.02 in) and 610 x 610 mm (42.02 x 42.02 in)) of

large particles (1.52 mm (0.0598 in) < $\overline{d}_p$ < 1.76 mm (0.0693 in), 1025 Kg/m^3 (13.17 lb/ft^3) < $\overline{\rho}_s$ < 1150 Kg/m^3 (14.77 lb/ft^3)). After comparing the mixing caused by a single bubble with that resulting from a sphere drawn up manually through a quiescent bed, he concluded that material was vertically transported by bubble-induced drift only. He, also, asserted that the net vertical transport of solids was a function of bubble flow, time and bed level.

In his investigation, Cranfield noticed the existence of specific particle zones.

> At the distributor, particles are mixed by the jetting gas, and in the freely bubbling zone they are mixed by randomly superimposed, bubble-induced drift. In the [3] bed there are descending wall layers for solid return arising from the lateral displacement of surface material by erupting bubbles. [9, p. 59]

According to Cranfield, "the net lateral particle displacement induced by a rising bubble was negligible, but considerable lateral displacement of the bed surface material and deposition of underlying material on the surface occurred upon the eruption of [a] bubble" [9, p. 60]. He suggests forced circulation (e.g., "Gulf-stream" generated circulation) to increase lateral mixing and, therefore, improve dispersion of fuel from a feed point in large particle fluidized combustors.

H. Masson [27] experimented in a two-dimensional bed and observed solids circulation patterns. In accord with other investigators he, also, detected mixing of solids in the bubble wakes and local

motions, on the scale of a bubble diameter, as described by a "drift effect."

Only a few other studies have been conducted using large particles. Brotz [5] investigated axial diffusion, using colored particles for tracer, in a bed consisting of particles 2-10 mm (0.08 - 0.33 in) in diameter. Highley and Merrick [17] used a 1.52 m (5 ft) diameter bed of coal particles ranging from 0.55 to 1.77 mm (0.022 to 0.067 in). They determined diffusion coefficients by removing radioactive tracer at various vertical and radial positions in the bed. Burovoi and Svetozarova [6] used a continuous flow bed to determine axial diffusion coefficients of 0.5 - 4.0 mm (0.02 - 0.16 in) particles. Geldart and Cranfield [14] modeled vertical transport of magnetic tracer particles (1-2 mm (0.030-0.079 in)) with the two-stirred tank model.

2.3.4 Residence Time Distributions (RTDs) and Compartmental Modeling

The measurement and analysis of residence time distribution is an important tool in the study of continuous flow systems. Fluidized beds with a constant inflow and outflow of solids can be analyzed with compartmental RTD models. These models represent the bed as interconnected compartments, which may exhibit well-mixed behavior, plug flow, short circuiting, dead space, channeling, etc., Combinations

of these compartments are arranged so as to best approximate an experimentally obtained solids RTD. Comparmental modeling can be used to predict conversions of solids exiting a gas-solid fluidized bed reactor. However, this approach cannot describe mixing and conversions in specific regions of a bed. In flowing beds of large particles ($\bar{d}_p \geqslant 1.6$ mm (0.063 in)), Cranfield [9] found that particle residence times approximated those of well-mixed beds.

K. Schugerl [38] measured conversion profiles and residence time distributions to determine the degree of backmixing along the walls and in the center of fluidized bed reactors. He observed three distinct mixing regions in the bed. Directly above the gas distributors only slight mixing occurs because of the low bubble frequency and small mean bubble diameter. Adjacent to the walls, mixing is significantly better; while in the center region, the best mixing is observed. Schugerl explains the distinct wall and center regions by a low intensity of radial mixing.

2.3.5 Overall Effective Measures of Mixing

Trawinski [43], Matheson et al. [28], and Furukawa and Omae [12] attempted to describe particle mixing in terms of an overall effective viscosity of fluidized beds. Kramers [20], in a more perceptive and detailed study, demonstrated that the effective viscosity varies at different locations within a fluidized bed by measuring vertical

viscosity profiles. Liu and Orr [25] extended Kramers' work and obtained local values of the effective viscosity at various points along the vertical axis of an air-fluidized bed. Schugerl [38], in accord with Kramers, Liu and Orr, insisted that fluidized beds are highly complex systems and, therefore, cannot be described by a single characteristic parameter, e.g. an overall mixing coefficient or an overall viscosity, etc.. "Depending on the sampling technique and the location of the sample, one can obtain values [of a single characteristic parameter] which are one order of magnitude different" [38, p. 267].

2.4 Closure

At present, no general correlation exists for calculating solids mixing in tube-filled fluidized beds of intermediate and large particles. Some researchers are trying to make an analogy with molecular and turbulent diffusion and, in this way, describe mixing by an effective diffusivity, viscosity, mixing coefficient, etc. of the fluidized bed. Zabrodsky [45] asserts that practical calculations using such effective measures are still far in the future. More information is required on the effects of particle properties (size, density and sphericity), the diameter of the bed, internals (like heat transfer tubes), superficial gas velocity, amount of bed media, etc. to develop a correlation for effective measures of mixing which is consistent with particle movement studies in industrial-scale units. These variables are among

those considered in the present study. We plan to contribute to the reservoir of data required to obtain such correlations; although Schugerl may be correct in his claim that the data is too complex to allow for such a reduction.

III. APPARATUS AND MATERIALS

3.1 Background

Numerous techniques have been employed to study solids movement in fluidized beds. Methods that involve injecting colored or otherwise tagged particles and then slumping (i.e., defluidizing) the bed for a layer by layer examination are very poor. Besides being time consuming and difficult, the defluidizing time of one or two seconds reduces the accuracy of tracer migration measurements, significantly. In addition, Donlevy [11] has shown that the slumping process is accompanied by segregation of different sizes of particles.

Another method proposed by Highley and Merrick [17] makes use of a sample thief to collect samples at various positions in the bed. This technique is limited by the number of samples that can be collected during the time tracer is dispersing in the bed. It also tends to disrupt solids movement and circulation in the bed.

In situ detection of radioactive tracer has been employed by some researchers [17, 19, 29]. Besides being hazardous, this tracer technique gives relatively "noisy" data because the intensity of radiation detected by a probe varies with the density of the bed media between the probe and the radioactive source. Thus, the occurrence of a bubble near a probe would increase the amount of radiation sensed by the detector and make the tracer appear to have moved closer to it,

Calculations show that even at steady state, the tracer signal would fluctuate by at least an order of magnitude.

Our experiments use a ferromagnetic substance with soft-magnetic properties, ie. the particles can be collected with a magnet, but do not become permanently magnetized. The presence of particles in any region of the bed is detected by means of inductor coils within dummy heat transfer tubes immersed in the bed, which is nondisruptive. Ferrite particles in the vicinity of an induction coil increase the inductance of the coil by an amount proportional to the volume fraction occupied by these particles. Also, ferrite material can be incorporated in a polyester casting resin, thus providing tracer material of any size and a range of possible densities.

The sensitivity of our coils is high enough and their stability is good enough to allow the use of low concentrations of tracer (e.g. one volume percent). Also, the response time of our technique is less than one one-hundredth of a second, which makes it possible to catch many transients that go undetected by sampling techniques. Thus, we have developed a very flexible technique for tracer studies while avoiding the inherent difficulties and inaccuracies of previous techniques.

3.2 The Test Facility

The 0.91 m by 0.91 m (3 ft by 3 ft) cross section fluidized bed is used for solids movement studies (see Figures 3.1 and 3.2). Air is

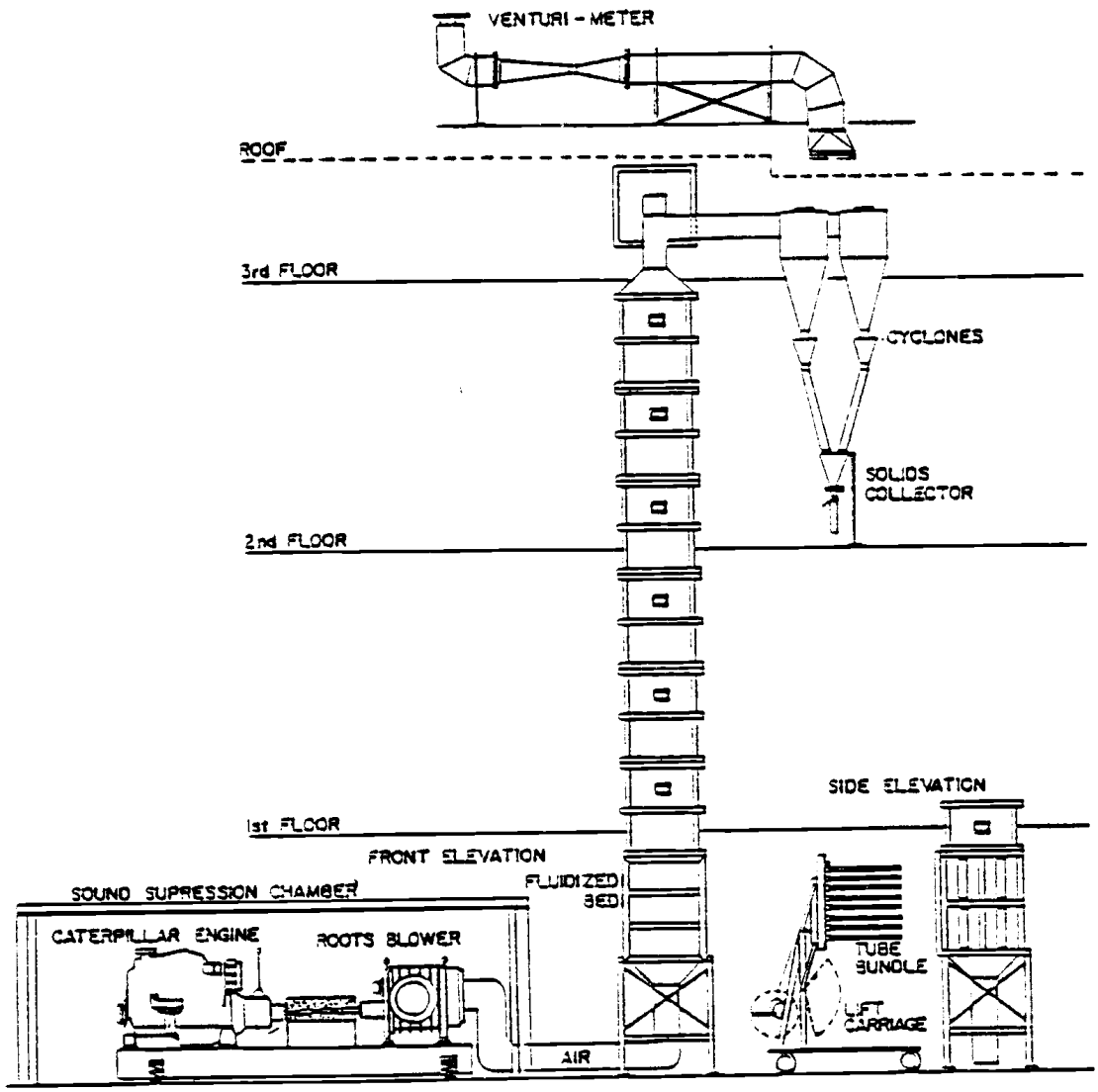

Figure 3.1. The general layout of the experimental apparatus.

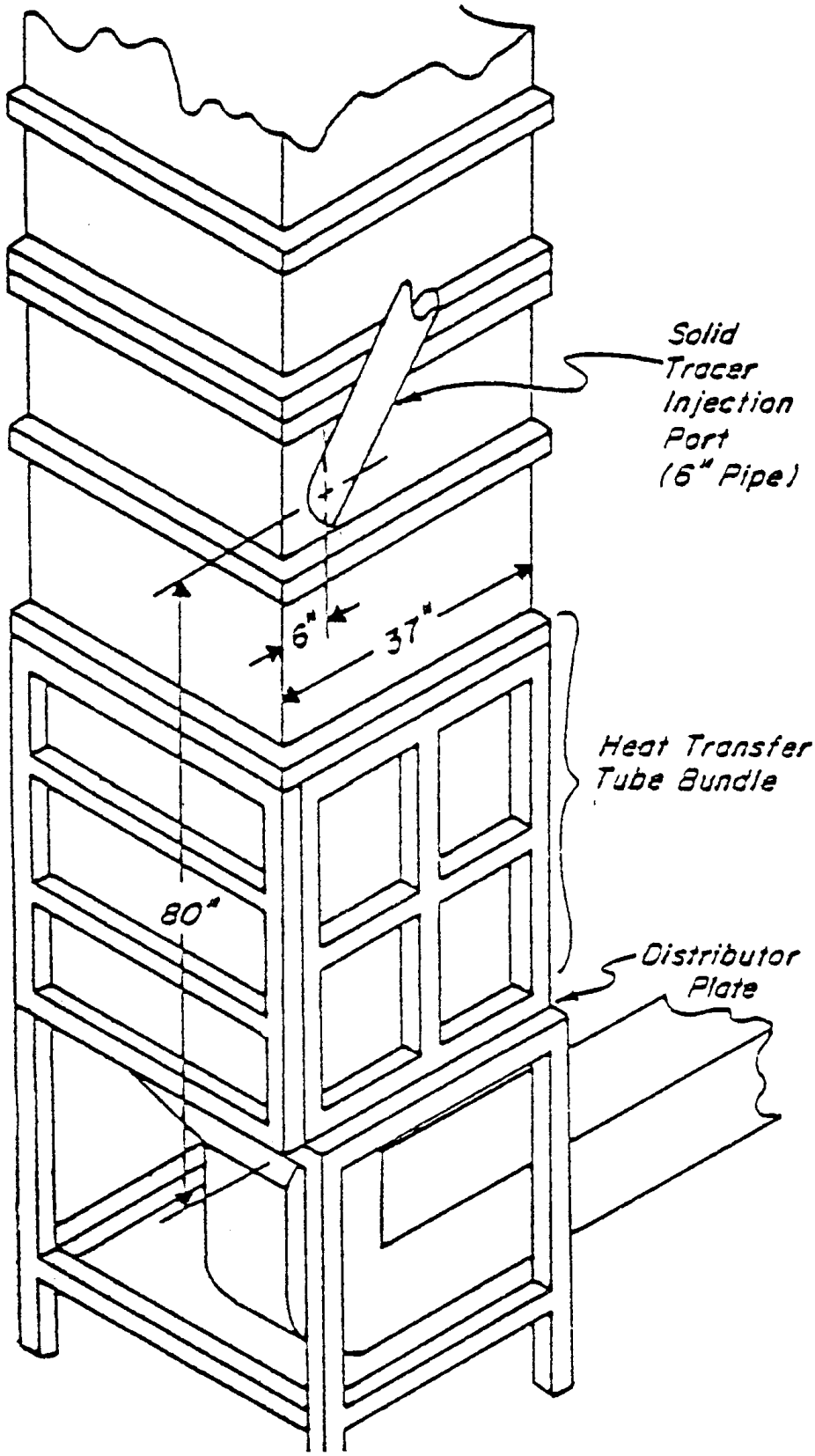

Figure 3.2. Sketch of the .91 m x .91 m (3 ft. x 3 ft.) fluidized bed.

supplied to this bed by a Root Positive Displacement Blower (maximum pressure drop: 51.7 KPa (7.5 psi), maximum flow rate: 3.78 m^3/s (134 ft^3/s)), which is driven by a 242 KW (325 HP) diesel engine. The blower and engine are located in a sound-proof chamber. Although the bed operates isothermally, air temperatures range between 25°C (77°F) and 55°C (130°F) depending on whether the bed has been warmed-up. On exiting the sound proof chamber, the air passes through a butterfly valve and enters the bed through a wind box (Figure 3.3), which ensures an even distribution of gas to the distributor plate. It, then, passes through the perforated "sandwich" design distributor plate (Figure 3.4), which consists of two 10 gage mild steel plates with a wire screen (No. 20 Tyler Mesh) between them. The plates have 5.55 mm (7/32 in) diameter holes placed on 19.05 mm (3/4 in) centers in square pitch. The open area of a plate is 6.68 percent, which allows for superficial gas velocities up to 3.81 m/s (12.5 ft/s) with 1361 Kg (3000 lbs) of bed media. The pressure drop across the distributor plate is high enough to achieve uniform flow through the openings and, thereby, avoid channeling. The ratio of the pressure drop across the distributor to that across the bed is approximately 40 percent. For the fine particle (EI-70) experiments every other row of holes on the distributor plate was sealed with tape.

After passage through the free-board, the exit gas stream is distributed into four cyclone separators (Figure 3.5) operating in

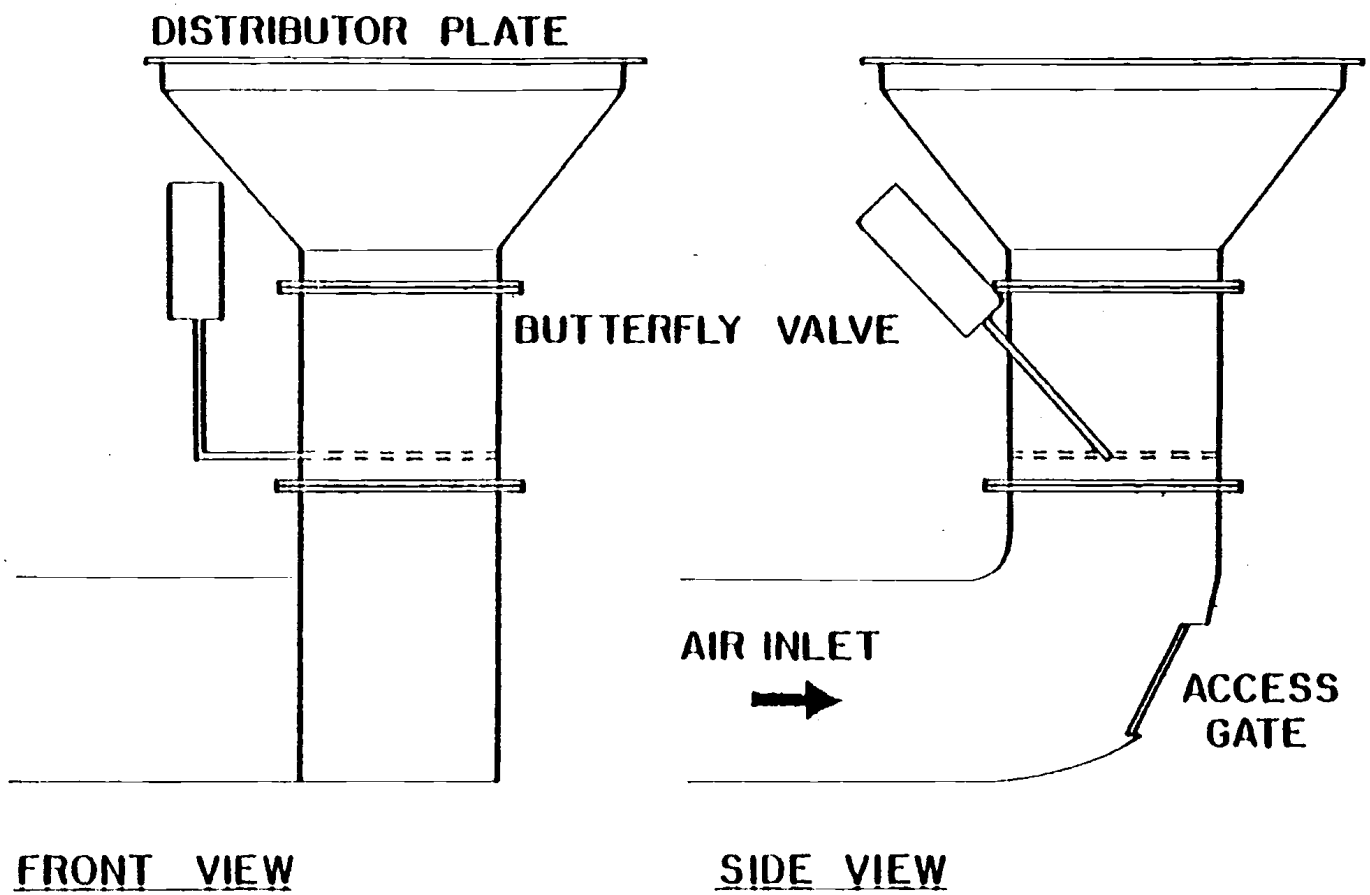

Figure 3.3. The wind box.

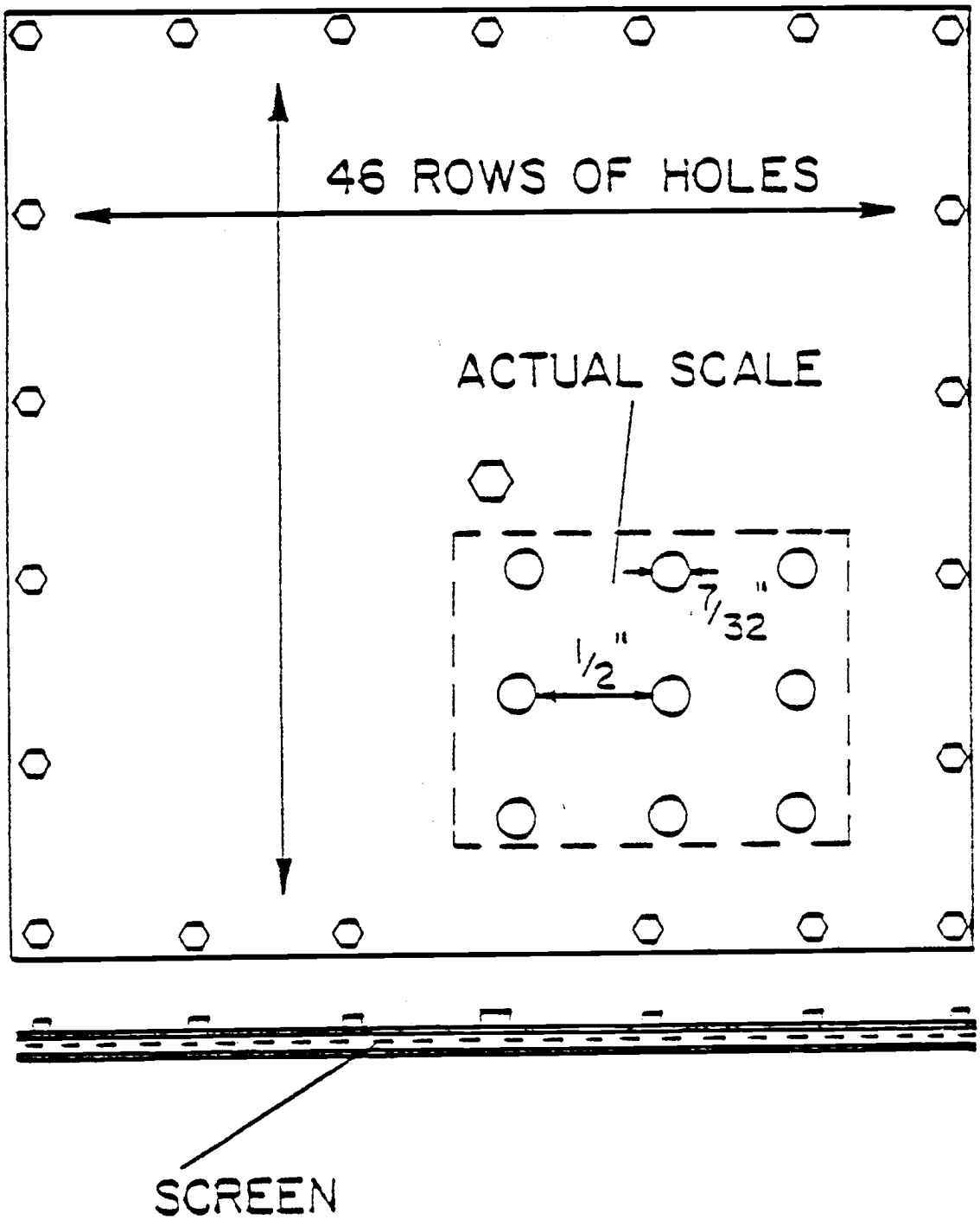

Figure 3.4. The perforated, "sandwich" design distributor plate.

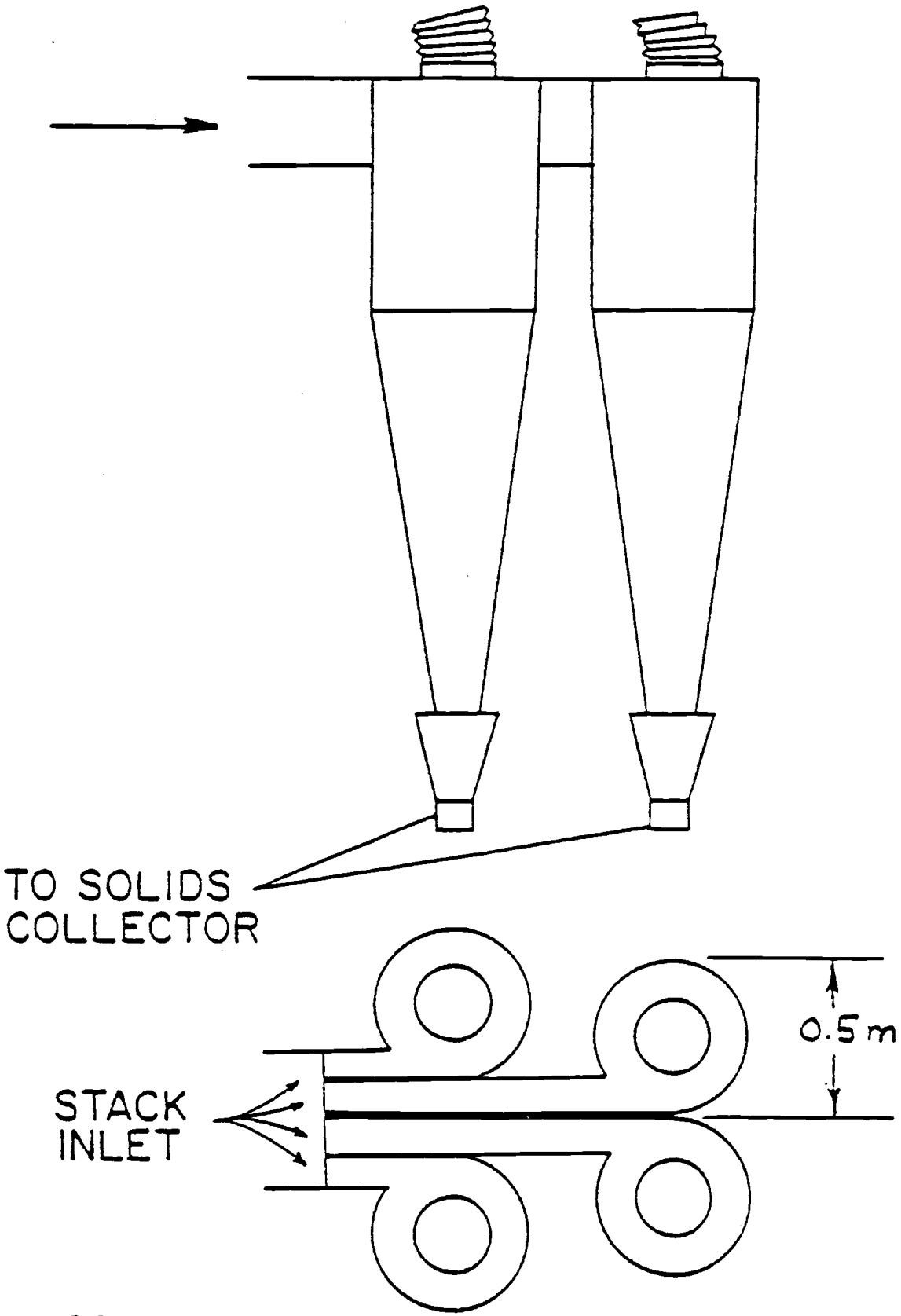

Figure 3.5. Cyclone separators operating in parallel (front and top view).

parallel. All entrained fines are removed from the gas in these separators and the particle-free gas then flows through a calibrated venturi meter (refer to Figure 3.1) which allows for calculation of the superficial gas velocity through the system (with minimal pressure drop due to the measurement).

3.3 The Tube Array

The heat transfer tube array is a steel frame holding 50.8 mm (2 in) O.D., horizontal, fiberglass tubes (Figure 3.6). The array has an equilateral triangular pitch with 101.6 mm (4 in) horizontal, center to center tube spacing. The fiberglass tubes are supported by vertical rods and plastic spacers (which provide vertical separation of the tubes). Installation of the tube bundle is done with the lift carriage (refer to Figure 3.1) and hooks in the back of the bed. The array can be installed at two different levels; with its bottom either at 254 mm (10 in) or 508 mm (20 in) above the distributor plate.

3.4 Bed Media

According to E. C. McKenzie [30], a bed of coal ash and limestone has a density of about 2700 Kg/m^3 (167.4 lb/ft^3). In an attempt to model the real situation, we used silica sand (EI-16, Wedron Silica Div.) as bed media. This sand has a surface mean particle diameter of 0.8 mm (0.03 in), a density of 2700 Kg/m^3 (167.4 lb/ft^3) and a

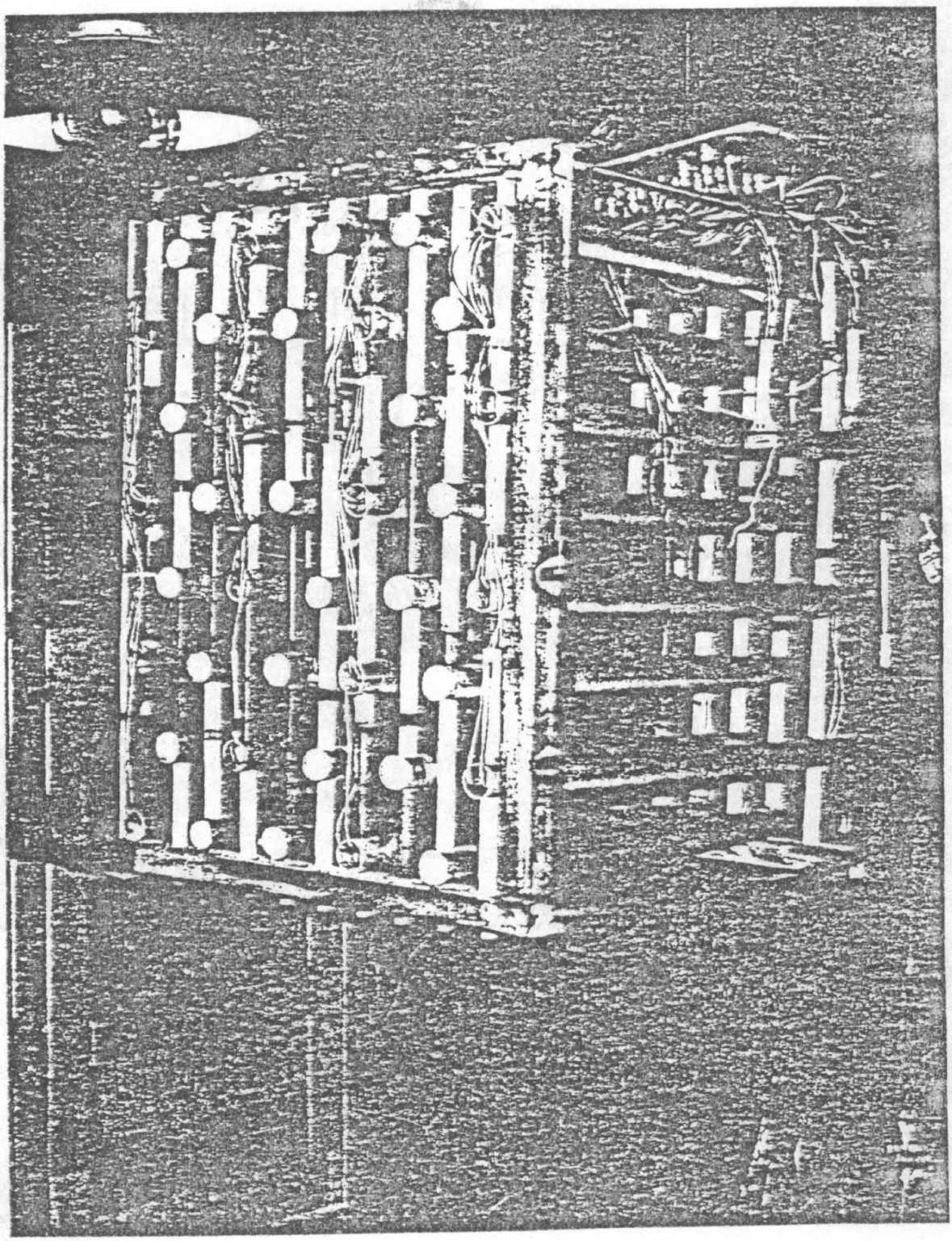

Figure 3.6. Photograph of the dummy heat transfer tubes. The tubes with wires coming from them each contain four inductor coils.

minimum fluidization velocity, U_{mf}, of .459 m/sec (1.51 ft/sec) [8]. Three fine particle runs were conducted with EI-70 sand, which has a surface mean particle diameter, d_p, of 0.17 mm (0.0068 in) and a density about the same as EI-16 sand.

3.5 Ferrite Tracer Particles

It was necessary to make special ferrite tracer particles because most ferromagnetic substances have a specific gravity above 4 -- far too dense to simulate the behavior of coal ($\rho_{coal} \simeq 1.5$). A specific gravity of about 2.4 was obtained by mixing ferrite particles with an acrylic casting resin. Small 5 mm (0.2 in) cubes were cut out of thin layers of this resin when it was only partially hardened. These tracer cubes were used for runs 50-73. After run 73, the ferrite was crushed until it had a surface mean diameter, $\bar{d}_p$, of 1.6 mm (0.06 in), as calculated by:

$$\bar{d}_p = \sum_i \frac{1}{(x/d_p)_i}$$

where x_i is the fraction of material in size interval i and d_{p_i} is the average diameter of that size interval. A Ro-Tap Tyler sieve shaker was used for screen analysis of these tracer particles and the EI-16 and EI-70 sand (see Appendix A for sieve analyses).

3.6 Tracer Injection and Removal

Tracer is introduced in a slug above the fluidized bed. The injection port is about 2.03 m (80 in) above the distributor plate (refer to Figure 3.2). After a tracer run is made, the ferrite material is separated from the sand. This is accomplished by refluidizing the bed and draining the sand-ferrite mixture, at a fixed rate, onto a conveyor belt, which passes over a magnetic drum (see Figure 3.7). The non-ferrite material falls off the edge of the drum into a barrel; the ferrite material clings to the belt until the belt separates from the drum, where the ferrite material drops into a bucket. A vibrating tray controls the rate of solids feed onto the conveyor belt (see Figure 3.8).

3.7 The Probes[1]

Sixty-four inductance probes were used to measure the concentration of ferrite tracer as it spread throughout the bed (Figure 3.9). The arrangement of the tubes and the location of the inductor coils within the array is shown in Figure 3.10. Each inductor coil monitors the concentration of ferrite in a volume with a radius of about 100 mm (4 in) from the center of the coil (see Figure 3.11). The

[1] The inductance probe method was conceived and developed by Dr. Thomas J. Fitzgerald.

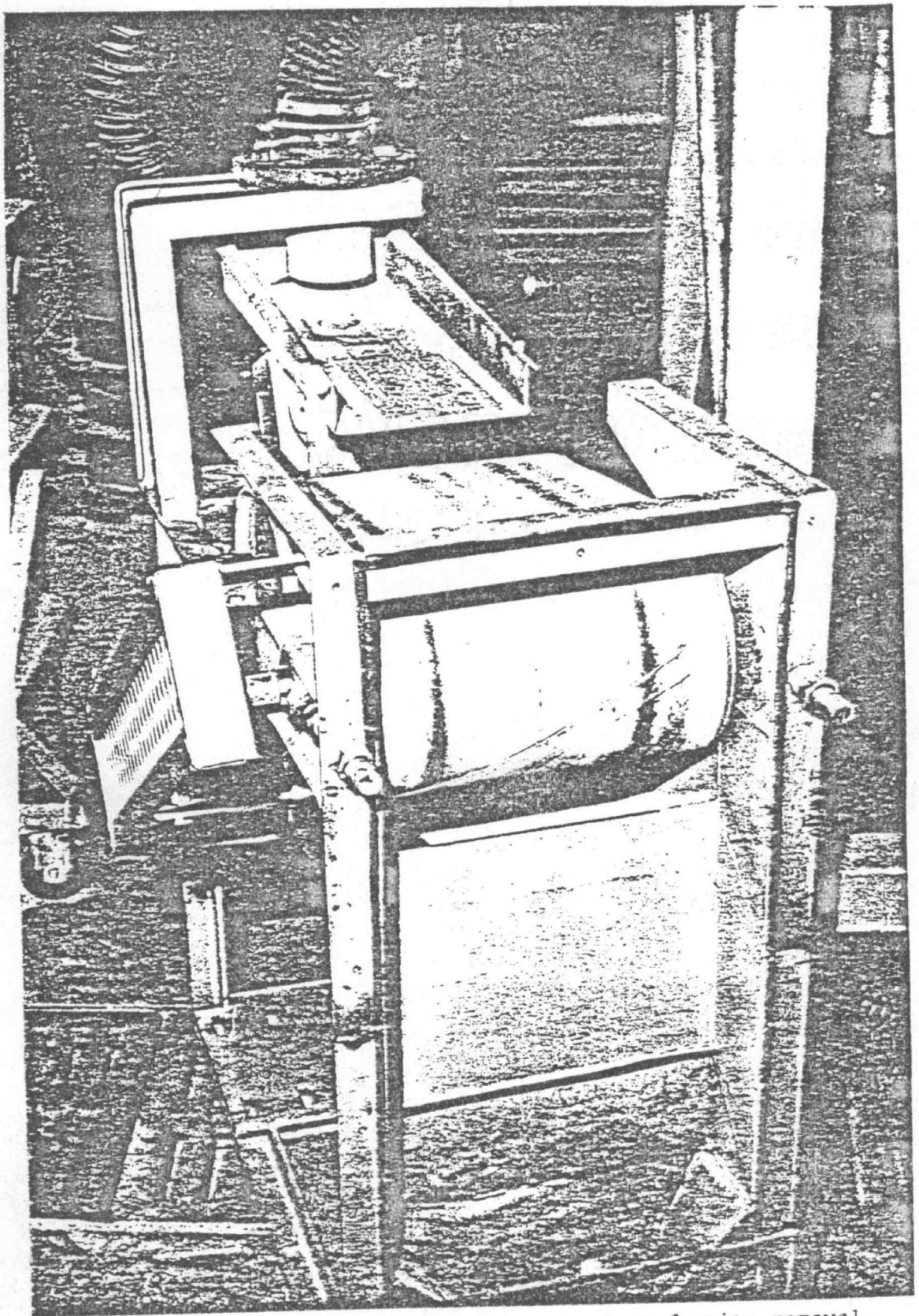

Figure 3.7. Photograph of the magnetic drum ferrite removal system.

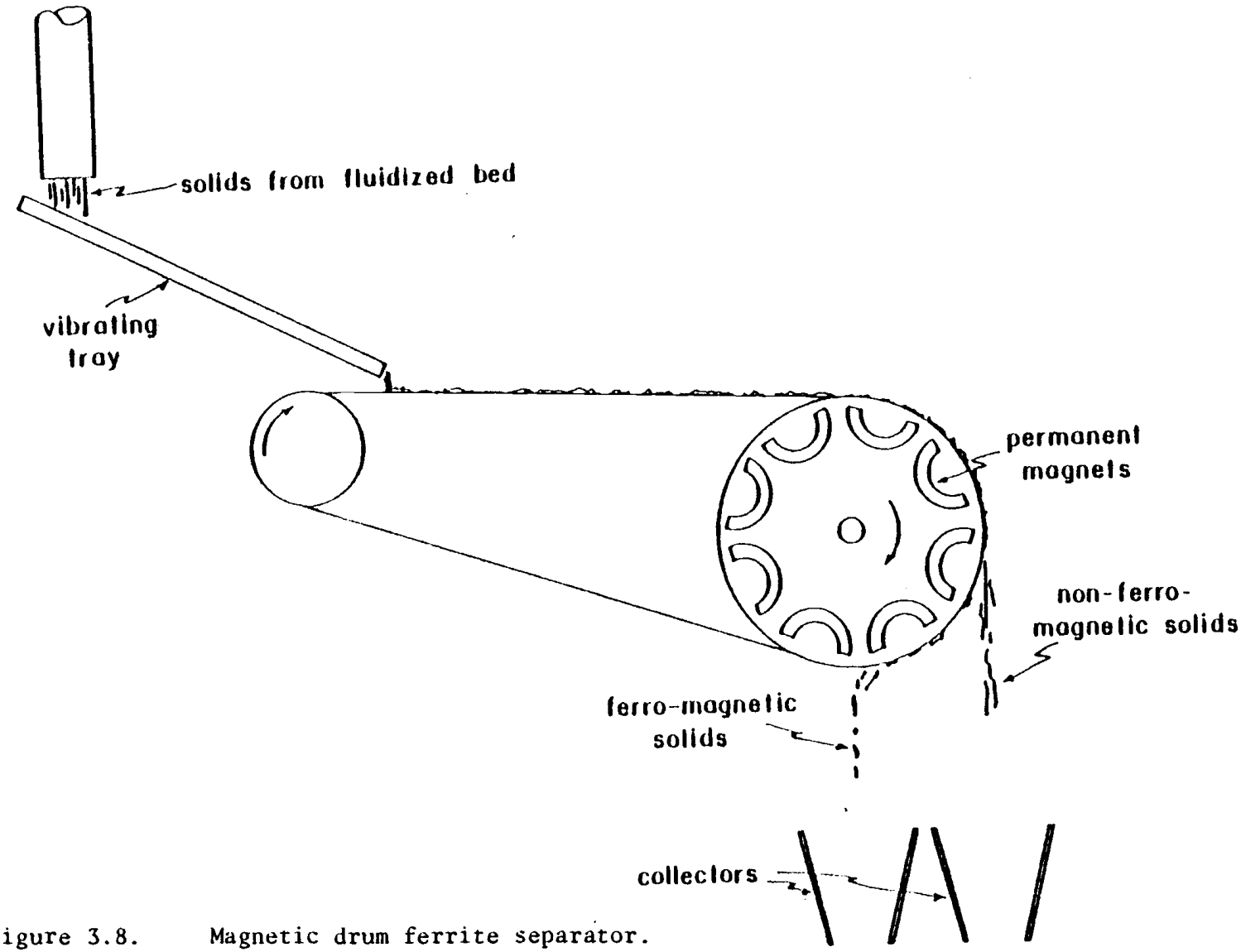

Figure 3.8. Magnetic drum ferrite separator.

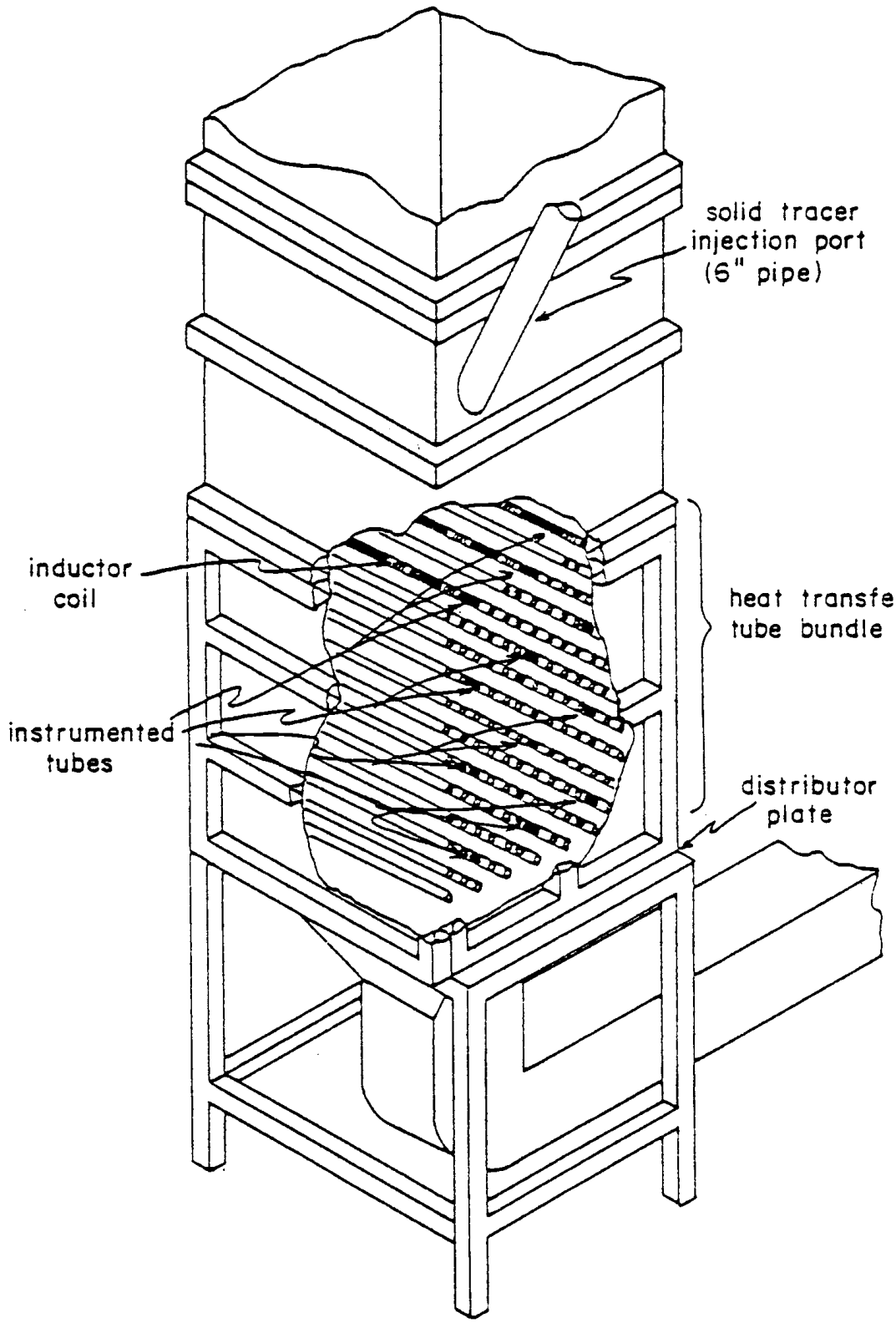

Figure 3.9. Location of heat transfer tube bundle and inductor coils in the bed.

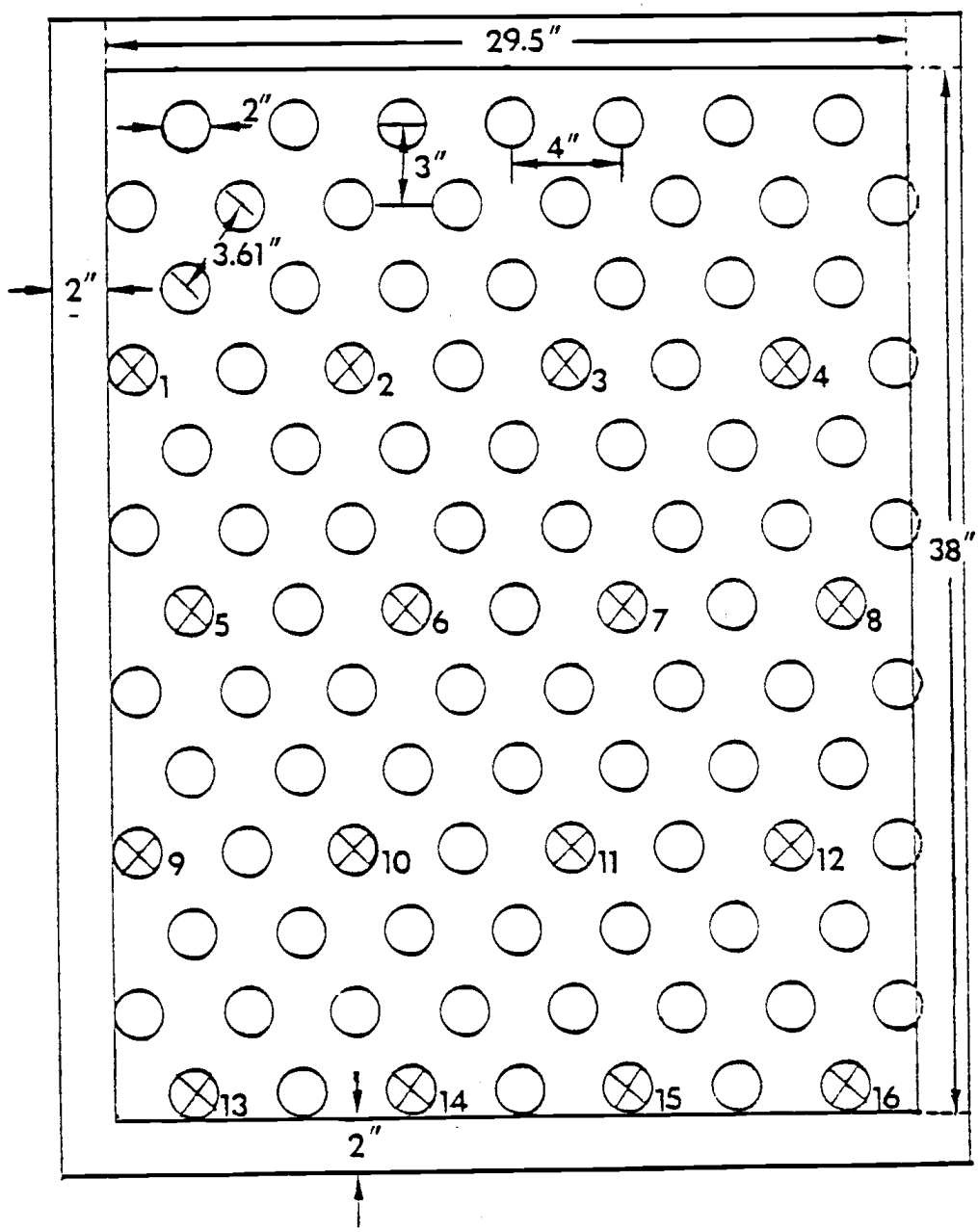

Figure 3.10. Arrangement of tubes in the .91 m x .91 m (3 ft. x 3 ft.) bed, end view. There are four inductor coils in each tube marked by an X. These coils are spaced at 203 mm (8 in) intervals along the length of the tube.

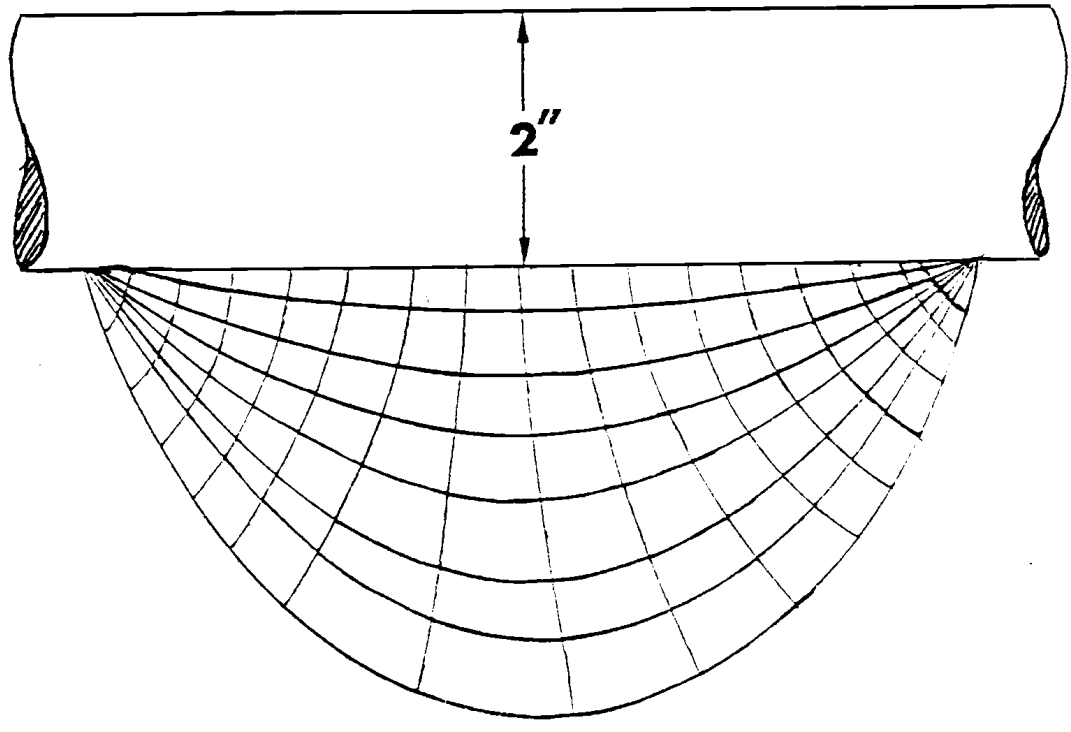

Figure 3.11. Magnetic lines of force surrounding a probe were determined by two methods: (1.) A coil (20 turns of No. 28 wire) was connected to earphones and rotated in the field until a 4 K-Hz sine wave signal generated in the probe was inaudible in the earphones; i.e. the coil was perpendicular to a line of force. This was done at discrete points along distinguishable lines force. The figure is a diagrammatic account of what was heard. (Note that the sensitivity of the probe at a particular location in its field is, ideally, inversely portional to the area of the curvilinear square at that location.). (2.) The probe was connected to the inductance circuit and voltage values were recorded for a ferrite cube (5.08 mm) moved about in the field of the probe. The results of this analysis were incorporated into the figure also.

inductor coils consist of approximately 1200 turns of fine wire (#34 gage) wound on a plastic tube, which is approximately 41 mm (1.6 in) in diameter (see Figures 3.12 and 3.13). A ferrite core was placed inside the coil to increase the sensitivity of the probe and improve the uniformity of the magnetic lines of force within the probe's pick-up volume. Each probe has an inductance of 0.1 Henry and is used in a balanced active bridge circuit for monitoring ferrite concentration in the fluidized bed. When ferrite is near a probe, its inductance is increased and the bridge goes out of inductive balance. The resulting output signal (which is measured in Volts) is linear with respect to ferrite concentration (see Figure 3.14).

Before conducting experiments, the inductance probes were calibrated to give a uniform response to a ferrite rod with a diameter of 6.35 mm (.25 in) and a length of 152.4 mm (6.0 in). The computer was programmed to print out voltage values for all 64 probes while the ferrite rod was held adjacent to each individual probe. Once these voltages were known (along with "zero" reference voltages), a range of sensitivity was determined for each probe. These sensitivity ranges were then scaled to a common range. Thus, all channels were comparable on the same basis. Scaling values for each of the 64 channels are tabulated in Appendix B.

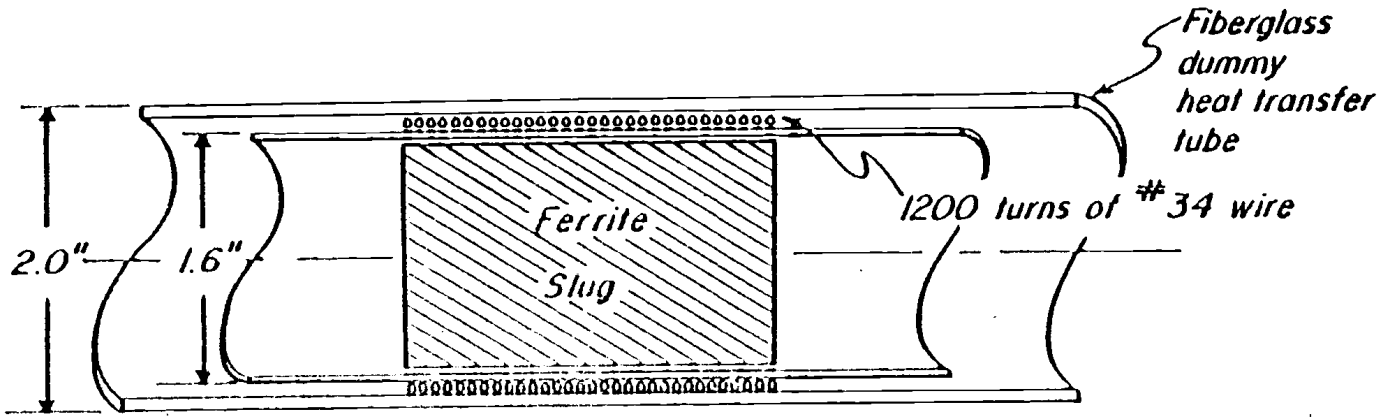

Figure 3.12. Inductor coil for sensing ferrite tracer in the fluidized bed.

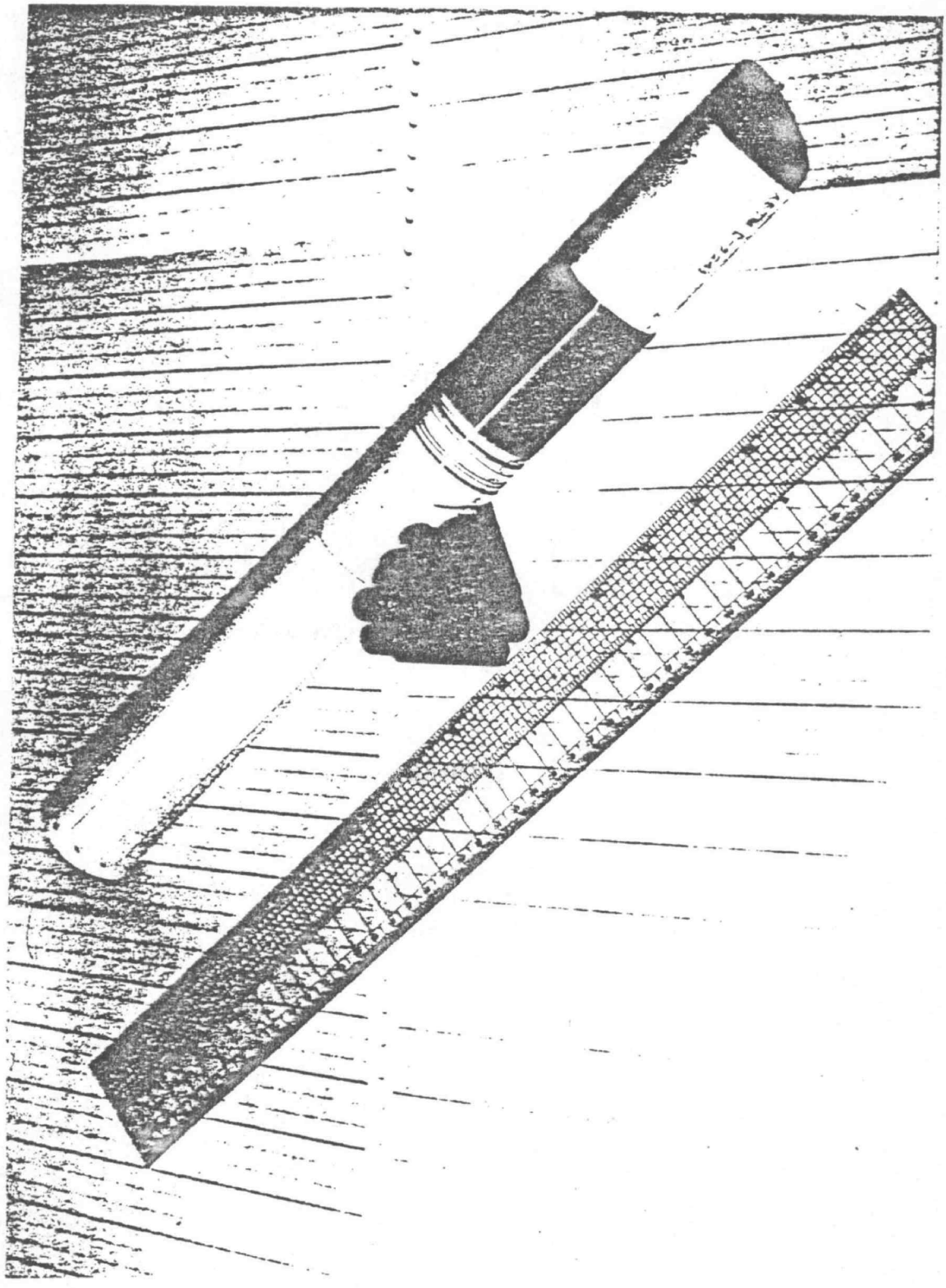

Figure 3.13. Prototype inductor coil.

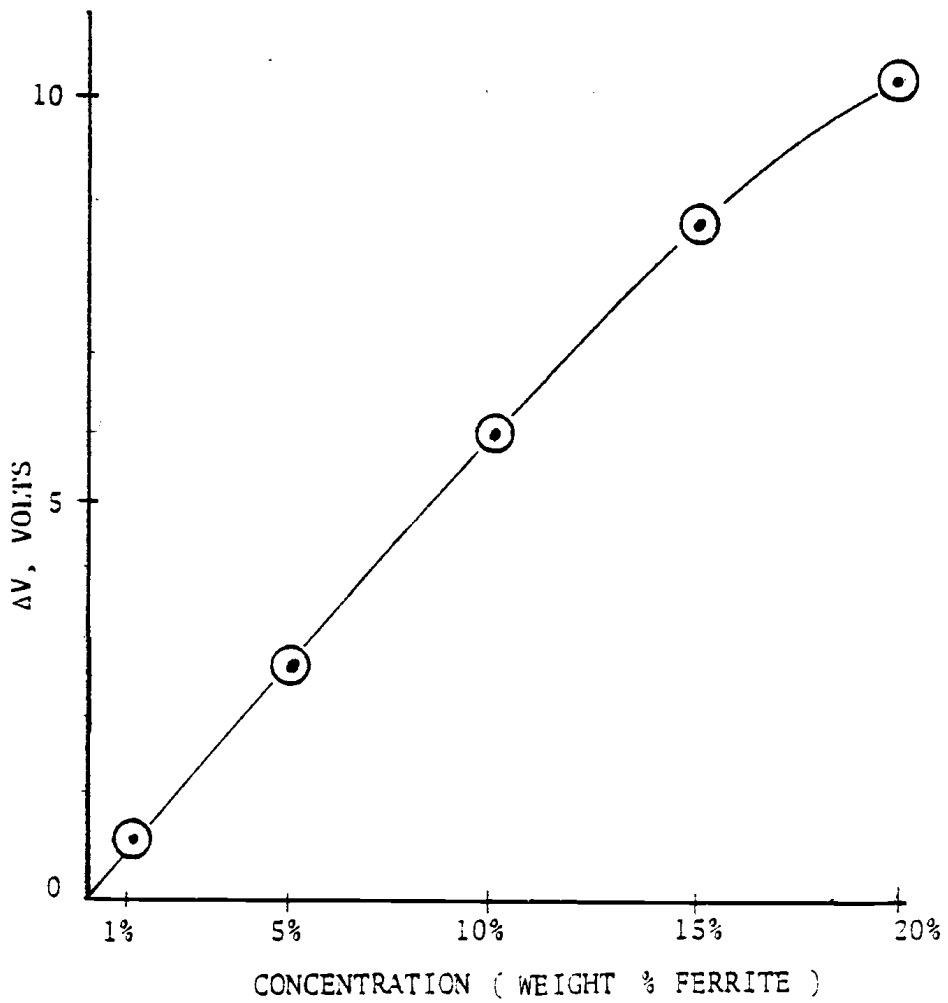

Figure 3.14. Calibration plot of a typical probe. Note that the voltage change varies proportionally with concentration (up to about 15 weight percent ferrite).

3.8 The Inductance Bridge Circuit

The sensitive inductance bridge circuit used for detecting ferrite tracer is shown and described fully in Appendix C. Briefly, one leg of the bridge is the 0.1 Henry torroid located on the printed circuit card; the other inductance leg is the 0.1 Henry inductor coil located within a dummy heat transfer tube. When one volume percent of ferrite tracer passes within the pick-up region of an inductor probe, the inductance of the probe is increased by approximately one percent (or one Volt) and this imbalance is detected by the bridge.

3.9 Data Acquisition

The inductance probe signals were sampled 40 times per second by an analog-to-digital converter. Data was collected on all 64 channels for approximately 10 seconds before injecting the tracer in order to determine accurately the background or zero level for each of the inductor coils. Then, a slug of tracer was introduced through an injection port above the bed or, more exactly, 2.03 m (80 in) above the distributor plate. Data was logged for another 50 seconds in runs 50-73, making a total of 60 seconds. The length of the data record taken for runs 74-114 was increased to a total of 100 seconds.

A Nova 840 system was used for all data collection and some processing. The CDC 3300 computer was used for more complicated

analysis and lengthier calculations. A block diagram of possible computer links is provided in Figure 3.15.

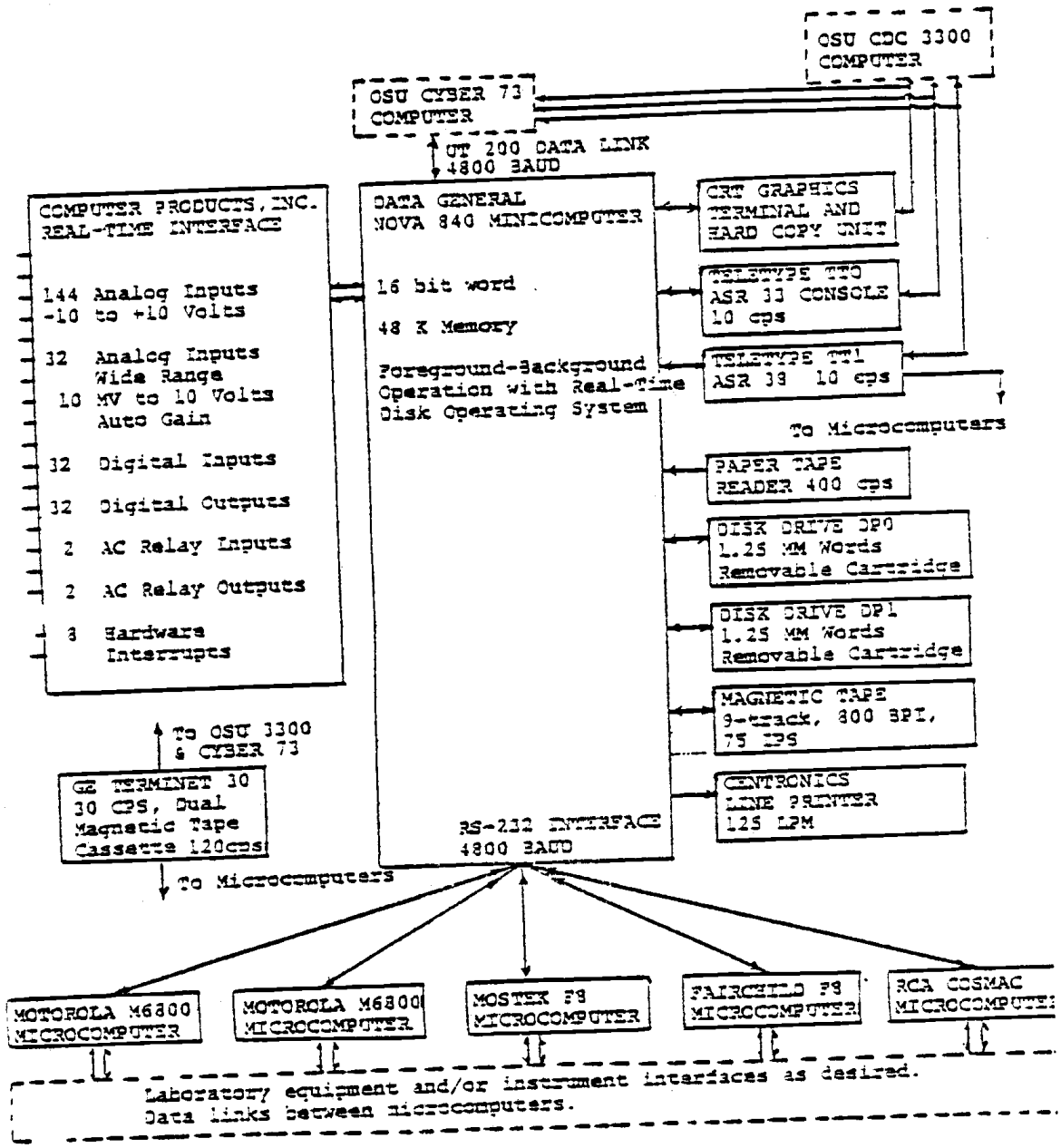

Figure 3.15. Block diagram of the Chemical Engineering Department minicomputer facility.

IV. RESULTS AND DISCUSSION

4.1 Background

In these experiments, sixty-four inductance probes were used to measure the concentration of ferrite material as it spread throughout the .91 m x .91 m (3 ft x 3 ft) bed. The tube array with these sixty-four probes was shown in Figures 3.6 and 3.10. Concentration versus time graphs have been plotted (see Figure 4.3) for each of the sixty-four data channels (connecting the probes, inductance circuits and the computer). As mentioned in Figure 3.6, each of the sixteen dummy heat transfer tubes contains four probes. The channels corresponding to these four probes have been labeled A, B, C, and D on the concentration versus time plots shown in Figure 4.1, which is the key to the actual plots. Thus, the four probes in tube "one" are represented as 1A, 1B, 1C and 1D on the plots.

Collected data has been smoothed to attenuate the effect of bubbles passing the probes, that is "bubble noise." The procedure used to smooth the raw data collected from each probe is described here. Step 1: Choose the maximum of the first twenty raw data points and use this value as the first "smoothed" data point. Step 2: Next, skip the first ten raw data points and choose the maximum of the following twenty consecutive raw data points to be the second "smoothed" data point. Step 3: Now, skip the first twenty raw data

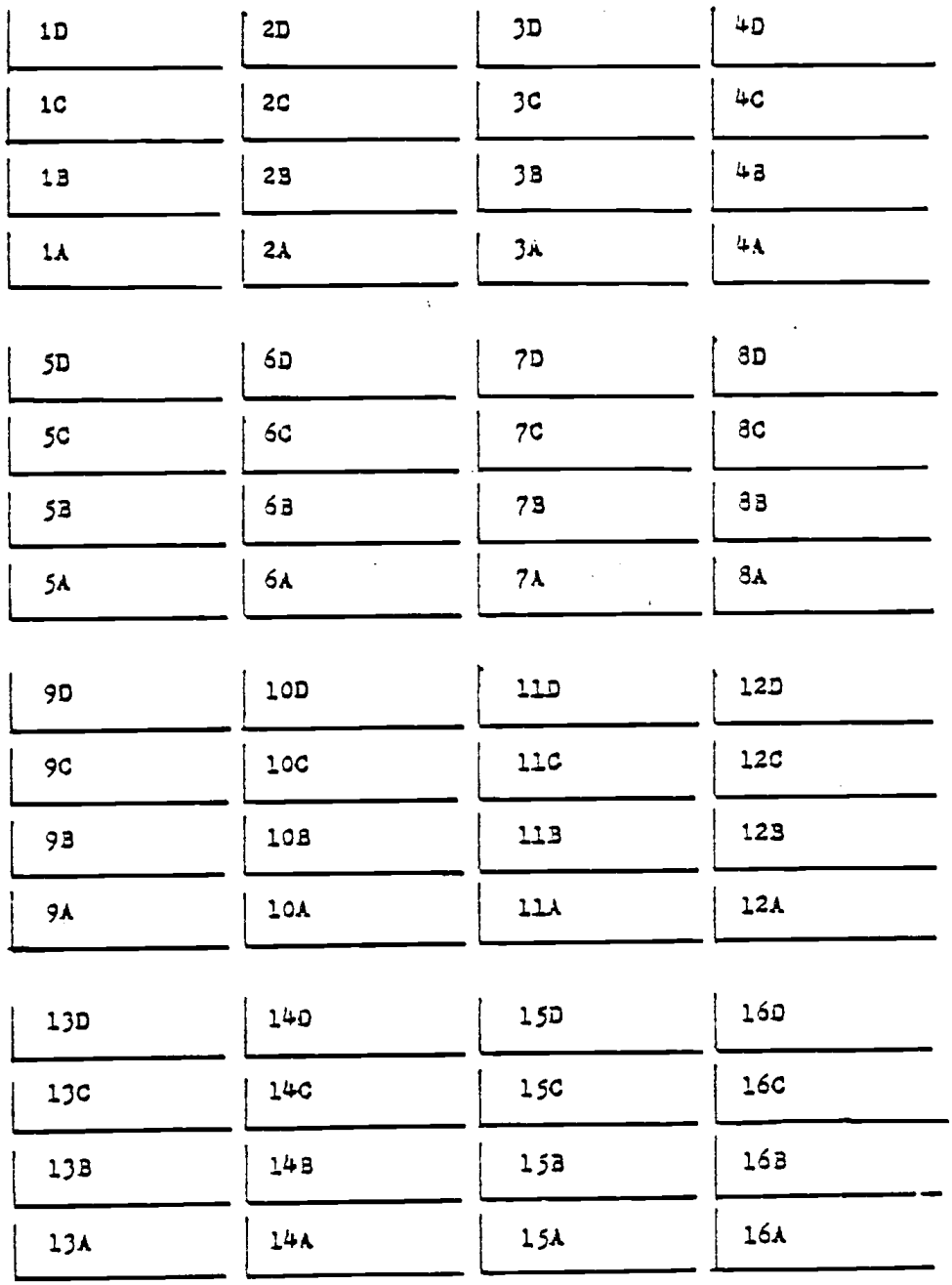

Figure 4.1. Tube array: Concentration versus time plots (key) - injection port above 1A and 2A.

points and choose the maximum lying in the twenty raw data points that follow to represent the third "smoothed" data point and so forth until all the raw data have been smoothed. Thus, "smoothed" data were obtained for each channel by taking the maximum in a set of twenty consecutive raw data points and overlapping these sets of twenty by ten. Since twenty consecutive raw data points correspond to a half second of data collection on an individual channel, this smoothing procedure ignores the effects of bubble-caused signal dropouts of less than a half-second duration.

A significant amount of statistical noise was eliminated when a larger number of tracer particles were used. Runs 50 to 73 were made with large ferrite tracer particles ($\bar{d}_p \simeq 5.08$ mm (0.2 in)), whereas runs 74-114 were made with finer tracer particles ($\bar{d}_p \simeq 1.6$ mm (0.06 in)). Since the same weight of tracer was used in both sets of runs, the total number of tracer particles was drastically different. The ratio of particles between the two sets was approximately sixteen to one. Only a small number of tracer particles were detected by a probe at any given time. Therefore, the random replacement of these particles within the detection range of the probe caused concentration fluctuations even after the tracer was well-mixed; this was especially true in runs 50-73. We expected these fluctuations to be described by Poisson statistics, i.e. the standard deviation of the number of detected particles should be the square root of the mean (or average) number of

detected particles. It follows that with sixteen times as many particles, the standard deviation in the number of detected particles should increase by a factor of four. However, since there were sixteen times as many particles, the relative fluctuation, which is equal to the standard deviation divided by the mean, should decrease by a factor of four. Thus, there was four times as much noise due to particle replacement in Runs 50 to 73 as there was in runs 74 to 112. In fact, most of the noise in runs 50 to 73 was caused by random particle replacement. This conclusion was based on the following simple experiment. We repeated run 70 (see run 73) using only one-quarter the amount of tracer and renormalized the measured response by multiplying by four. The relative noise was found to increase by approximately a factor of two -- which was consistent with the hypothesis.

Fifty-eight experimental runs were made in the .91 m x .91 m (3 ft x 3 ft) test facility using 102 mm (4 in) tube spacing and EI-16 sand ($\bar{d}_p \simeq$ 0.8 mm (0.03 in)). The superficial gas velocities ranged from 1.52 m/s (5 FPS) to 3.35 m/s (11 FPS), while the distance between the distributor plate and the bottom of the tube array was set at either .254 m (10 in) or .508 m (20 in). The bed inventories used were 907 Kg (2000 lbs), 1134 Kg (2500 lbs) and 1361 Kg (3000 lbs). As mentioned previously, runs 50-73 were conducted with 5.08 mm (0.20 in) ferrite tracer cubes, whereas runs 74-114 were made with 1.6 mm (0.06 in) diameter tracer.

Three fine sand (EI-70 , $\bar{d}_p \simeq 0.17$ mm (.0068 in)), runs were made at superficial gas velocities of 0.30 m/s (1 FPS) and 1.22 m/s (4 FPS). The heights of the tube array above the distributor plate and the tube spacing were the same as those used for the EI-16 sand experiments. However, only 907 Kg (2000 lbs) of bed media was used in each of these fine particle runs. These runs were more difficult to perform than others because of excessive elutriation. As much as 640 Kg (1400 lbs) of sand was entrained into the cyclones at higher gas velocities (> 1.52 m/s (5 FPS)).

Output from one particular channel has been enlarged and described in Figure 4.2. Sixty-four such plots of channel outputs are shown for each run (see Figure 4.3). Observations and descriptions precede the page of plots for a particular run. The quantities following an observation run number are: the height of the tube array above the distributor plate (m), the weight of sand used in the bed (Kg) and the superficial gas velocity (m/s). The run numbers referred to in parentheses are runs made at the same three conditions. Table 4.1 shows the experimental conditions of each particular run.

Several terms, which are used frequently in the text of the observations, will be described here along with a few comments for future reference.

(1) Rise time: Channels that don't have peaks are characterized by rise times (or lag times). Essentially, the rise

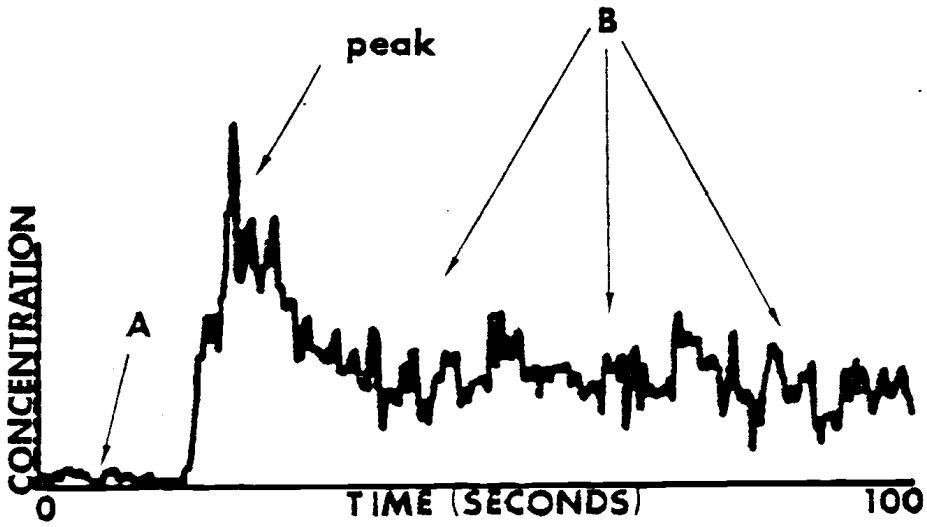

Figure 4.2. Typical output from a channel.

Output from the channel shown above has been divided into three major parts:

I. the A region, which consists of background or reference data on concentration values taken before injection of tracer,

II. the peak, which corresponds to a large clump of tracer passing the probe at that particular instant,

III. the B region, which is the relatively well-mixed regime (i.e., tracer concentration varies about a constant average concentration).

Note: The concentration scale is measured in data units. Usually the ordinate (concentration) ranges from zero to 200 data units. There are 0.05 volts per data unit. Thus, the ordinate ranges from 0 to 1 volt. It is important to remember that a volt is approximately the same as one volume percent tracer in the vicinity of the probe.

Table 4.1

SUMMARY OF EXPERIMENTS

Sand Size: EI-16 ($\bar{d}_p \simeq$ 0.8 mm (0.03 in))
Tracer Size: $\bar{d}_p \simeq$ 5.08 mm (0.20 in)
Tube Spacing: 0.12 m (4 in)

Run Number	Weight of sand kg (lb)	Height of Array Above Distributor m (in)	Superficial Gas Velocity m/s (ft/s)
50	907 (2000)	.254 (10)	2.13 (7)
51	907 (2000)	.254 (10)	2.74 (9)
52	907 (2000)	.254 (10)	3.35 (11)
53	1134 (2500)	.254 (10)	1.52 (5)
54	1134 (2500)	.254 (10)	1.98 (6.5)
55	1134 (2500)	.254 (10)	2.74 (9)
56	1134 (2500)	.254 (10)	3.35 (11)
57	1361 (3000)	.254 (10)	1.52 (5)
58	1361 (3000)	.254 (10)	2.13 (7)
59	1361 (3000)	.254 (10)	2.74 (9)
60	1361 (3000)	.254 (10)	3.35 (11)
61	1361 (3000)	.508 (20)	3.35 (11)
62	1361 (3000)	.508 (20)	2.74 (9)
63	1361 (3000)	.508 (20)	2.13 (7)
64	1361 (3000)	.508 (20)	1.52 (5)
65	1134 (2500)	.508 (20)	1.52 (5)
66	1134 (2500)	.508 (20)	2.13 (7)
67	1134 (2500)	.508 (20)	2.74 (9)
68	1134 (2500)	.508 (20)	3.35 (11)
69	907 (2000)	.508 (20)	1.52 (5)
70	907 (2000)	.508 (20)	2.13 (7)
71	907 (2000)	.508 (20)	2.74 (9)
72	907 (2000)	.508 (20)	3.35 (11)
73	907 (2000)	.508 (20)	2.13 (7)

Table 4.1 (continued)

SUMMARY OF EXPERIMENTS

Sand Size: EI-16 ($d_p \simeq 0.8$ mm (0.03 in))
Tracer Size: $d_p \simeq 1.6$ mm (0.06 in)
Tube Spacing: 0.102 m (4in)

Run Number [2]	Weight of sand kg (lb)	Height of Array Above Distributor m (in)	Superficial Gas Velocity m/s (ft/s)
74	907 (2000)	.508 (20)	0.91 (3)
75	907 (2000)	.508 (20)	2.13 (7)
76	907 (2000)	.508 (20)	1.52 (5)
77	907 (2000)	.508 (20)	3.35 (11)
78	907 (2000)	.508 (20)	2.74 (9)
79	1134 (2500)	.508 (20)	1.52 (5)
80	1134 (2500)	.508 (20)	2.13 (7)
81	1134 (2500)	.508 (20)	2.74 (9)
82	1134 (2500)	.508 (20)	3.35 (11)
83	1361 (3000)	.508 (20)	1.52 (5)
84	1361 (3000)	.508 (20)	2.13 (7)
85	1361 (3000)	.508 (20)	2.74 (9)
86	1361 (3000)	.508 (20)	3.35 (11)
87	907 (2000)	.508 (20)	0.30 (1)
88	1361 (3000)	.254 (10)	1.52 (5)
89	1361 (3000)	.254 (10)	2.13 (7)
90	1361 (3000)	.254 (10)	2.74 (9)
91	1361 (3000)	.254 (10)	3.05 (10)
92	1134 (2500)	.254 (10)	1.52 (5)
93	1134 (2500)	.254 (10)	2.13 (7)
95	1134 (2500)	.254 (10)	3.35 (11)
96	907 (2000)	.254 (10)	1.52 (5)
97	907 (2000)	.254 (10)	2.13 (7)
98	907 (2000)	.254 (10)	2.74 (9)
99	907 (2000)	.254 (10)	3.35 (11)
102	1134 (2500)	.254 (10)	1.52 (5)
103	1134 (2500)	.254 (10)	2.13 (7)
104	1134 (2500)	.254 (10)	2.74 (9)
105	1134 (2500)	.254 (10)	3.20 (10.5)
106	907 (2000)	.254 (10)	1.52 (5)
107	907 (2000)	.254 (10)	2.13 (7)
108	907 (2000)	.254 (10)	2.74 (9)
109	907 (2000)	.254 (10)	3.35 (11)
110	1134 (2500)	.508 (20)	1.52 (5)
111	1134 (2500)	.508 (20)	3.35 (11)
112	1361 (3000)	.508 (20)	1.52 (5)
113	907 (2000)	.254 (10)	0.30 (1)
114	907 (2000)	.254 (10)	1.22 (4)

[2] Runs 87, 113 and 114 were conducted with EI-70 sand ($d_p \simeq 0.17$ mm (.0068 in))

time is the time it takes one of these "peak-less" channels to attain its final concentration value, i.e. its quasi-equilibrium state.

(2) Overall mixing time (OMT) is the time required for all channels to register their average final or "equilibrium" values. More precisely, it is the time for the slowest or worst channel to fall within the noise band about the equilibrium concentration. Thus, this is a worst case measure of mixing.

(3) The right and left sides of the bed are the same as the right and left columns of plots, respectively. Sometimes reference is made to the front and back of the bed. The front is the left column of plots (i.e., tubes 1, 5, 9 and 13) and the back is the right column of plots (i.e., tubes 4, 8, 12 and 16).

(4) The tracer injection port is located above and between channels 1A and 2A.

(5) The interior of the bed is defined to be channels B and C on probes 2, 3, 6, 7, 10, 11, 14 and 15.

(6) Two different ordinate scales were used for plotting the runs. The single scale (which was used for runs 50-73, 81, 84, and 85) has a maximum ordinate of 200 data units or 1.0 Volt. The double scale (which was used for runs

74-80, 82, 83 and 86-114) has a maximum ordinate value of 100 data units, i.e. 0.5 Volts.

(7) Malfunctioning channels were usually omitted from the data and subsequent data analysis.

(8) The time scale (abcissa) of each of the 64 plots ranges from 0 to 100 seconds for runs 74-114 and 0 to 60 seconds for runs 50-73.

4.2 Observations

Run 50: .254 m (10"), 907 kg (2000#), 2.13 m/s (7FPS),
(see runs 97 and 107)

1. It appears that the pulse of tracer moves mostly along the wall opposite the injection port.
2. The tracer clumps tend to persist longer in run 50 than in the finer tracer runs conducted under the same conditions (runs 97 and 107).
3. Run 50 shows more noise (Poisson) than runs 97 and 107.
4. Rise times are comparable in all three runs with a maximum at channel 16A of 10 to 12 seconds.
5. Bubbles seem to avoid the left side of the bed in all three runs. A dense solid phase in this region must be typical of these conditions.

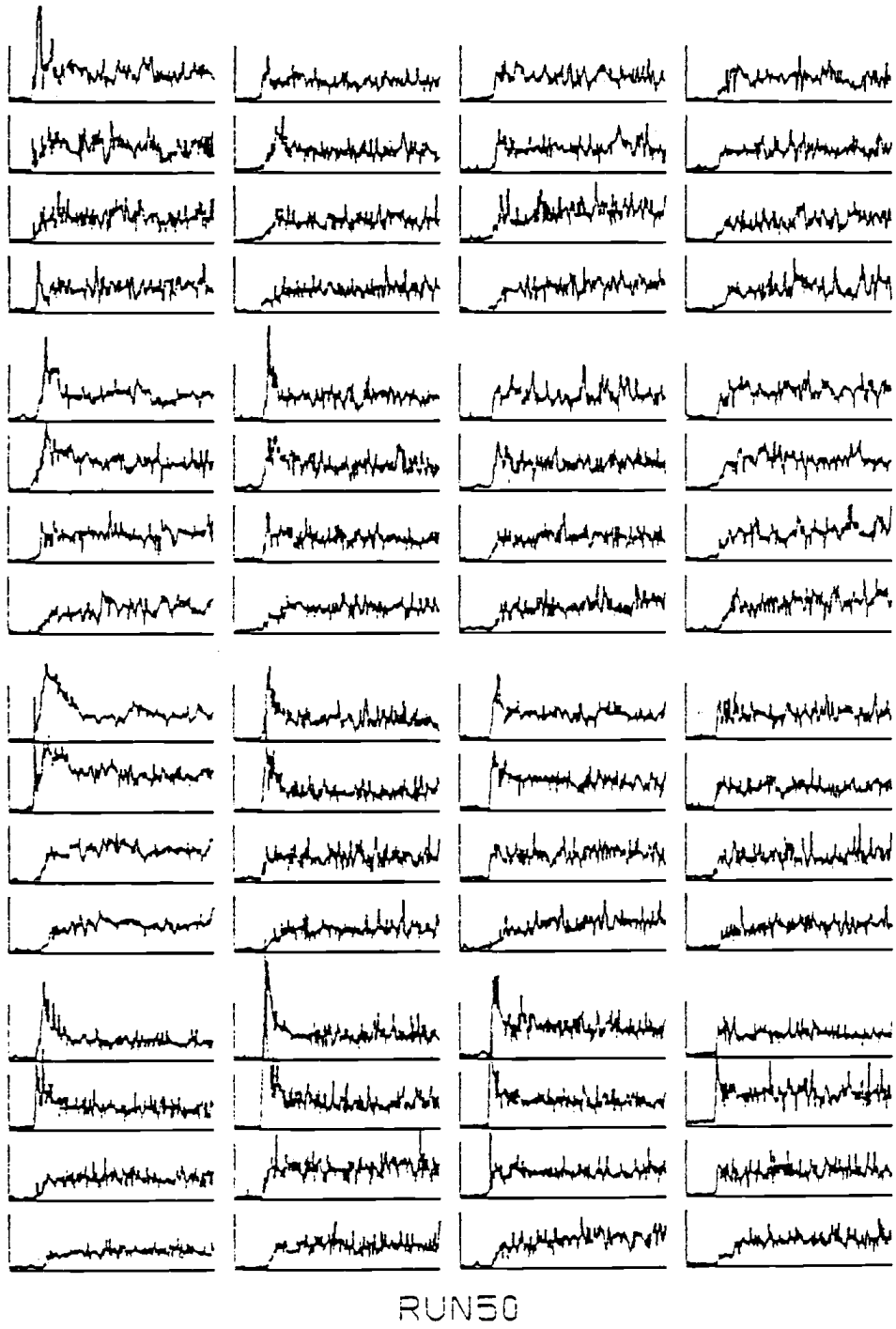

Figure 4.3. Tube array : Concentration versus time plots for runs 50-114.

Run 51: .254 m (10"), 907 kg (2000#), 2.74 m/s (9FPS), (see Runs 98 and 108)

1. Mixing is much faster in this run than in run 50. The only peaks occur in channels 1D, 2D and 5D.
2. The same general pattern of mixing exists, though. Tracer moves down the side of the bed faster than it disperses toward the interior of the bed.
3. Runs 98 and 108, which are at the same conditions, show a clump of tracer moving down the right side of the bed. In all three runs, bubbles are concentrated at the bottom of the bed and in the interior. Also, these runs indicate a dense region about tube 9.

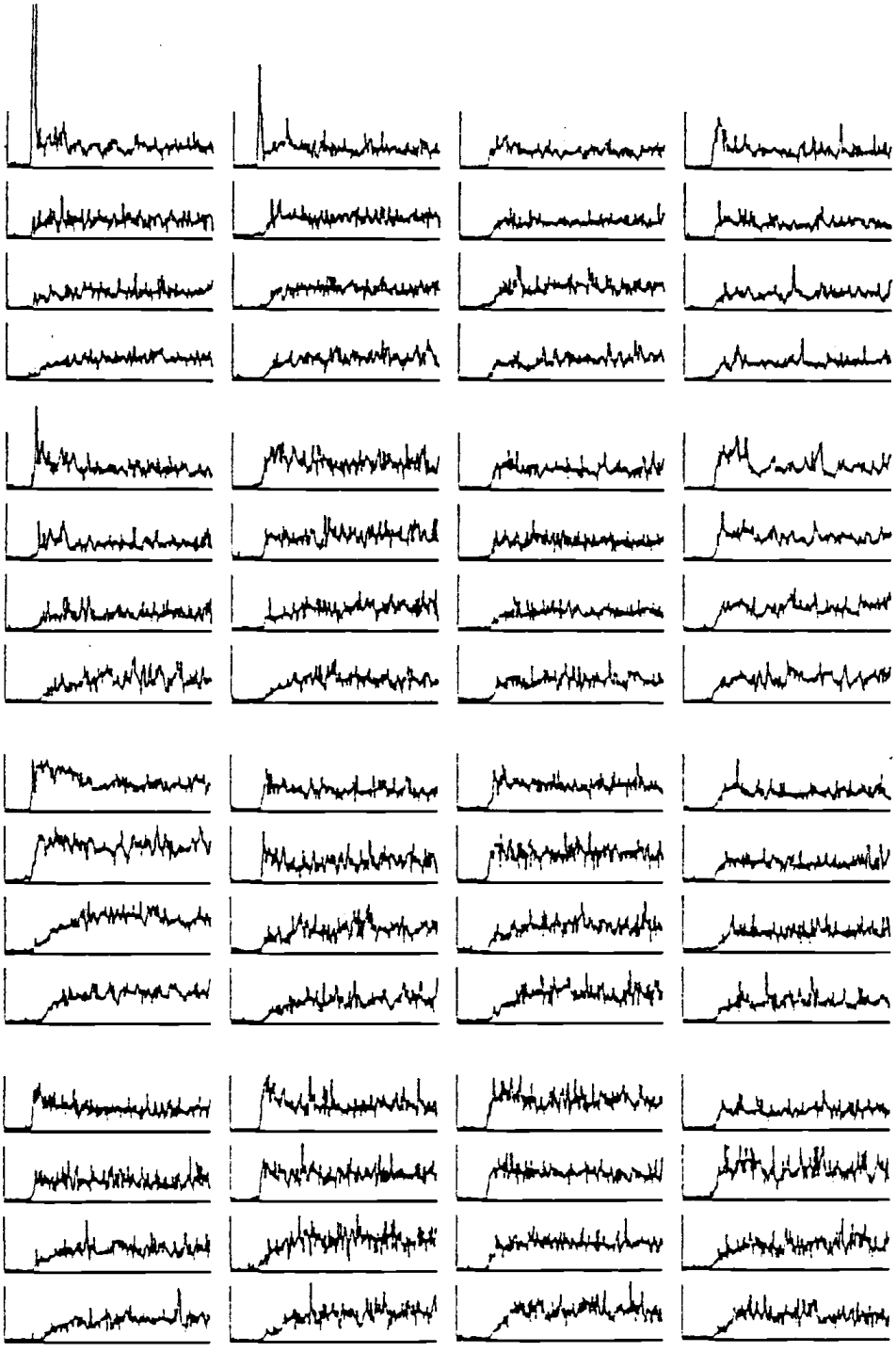

Figure 4.3. (Continued)

Run 52: .254 m (10"), 907 kg (2000#), 3.35 m/s (11FPS), (see Runs 99 and 109)

1. Tracer was able to spread about the top of the bed.
2. Peaks are much smaller at this high velocity.
3. Tracer seems to be fairly well mixed by the time it sifts down to the second row of tubes.
4. High average concentrations exist in the center of the bed after about 25 seconds. Apparently the tracer has gone down the walls of the bed and then back up the center (but at a slower rate--therefore causing accumulation as seen in channels A, B, C and D of tubes 10, 11, 14 and 15).
5. Runs 99 and 109 (which were conducted under the same conditions) have about the same rise times in the bottom of the bed as Run 52. The 3 runs show slightly different behavior in the top two rows of probes. Run 99 has definite spikes at the injection point (2A and 1A), whereas runs 52 and 109 have only small peaks which are on the other side of the bed (the "D" side). This lack of replication is inherent in the mixing process.
6. Bubble data appears to be the same in all three runs.

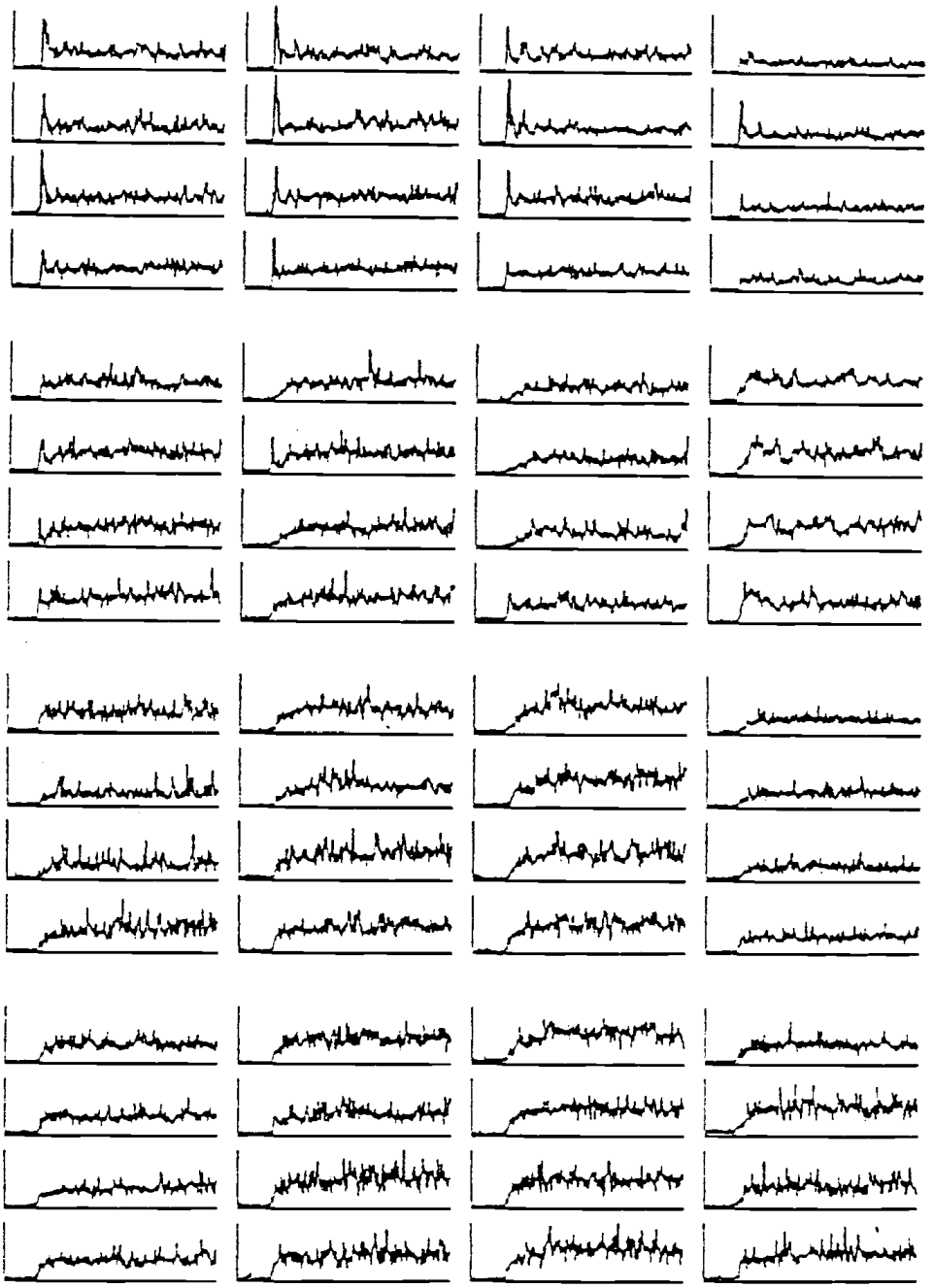

Figure 4.3. (Continued)

Run 53: .254 m (10"), 1134 kg (2500#), 1.52 m/s (5FPS),
(see Runs 92 and 102)

1. The tracer appears to move quite rapidly down the sides. A pulse appears on channel 9B, C and 13B, C at the same time it appears at the top of the bed (1C). This clump of tracer slipped down the wall and avoided detection until it reached Channel 9C. A similar clump exists in the subsequent reruns under these same conditions (runs 92 and 102).
2. Bubble movement occurs mostly in the interior and along the right side of the bed in all three runs (92, 102, 53). A dense phase of solids is seen by channels A, B, C and D in Tubes 1, 5 and 9.

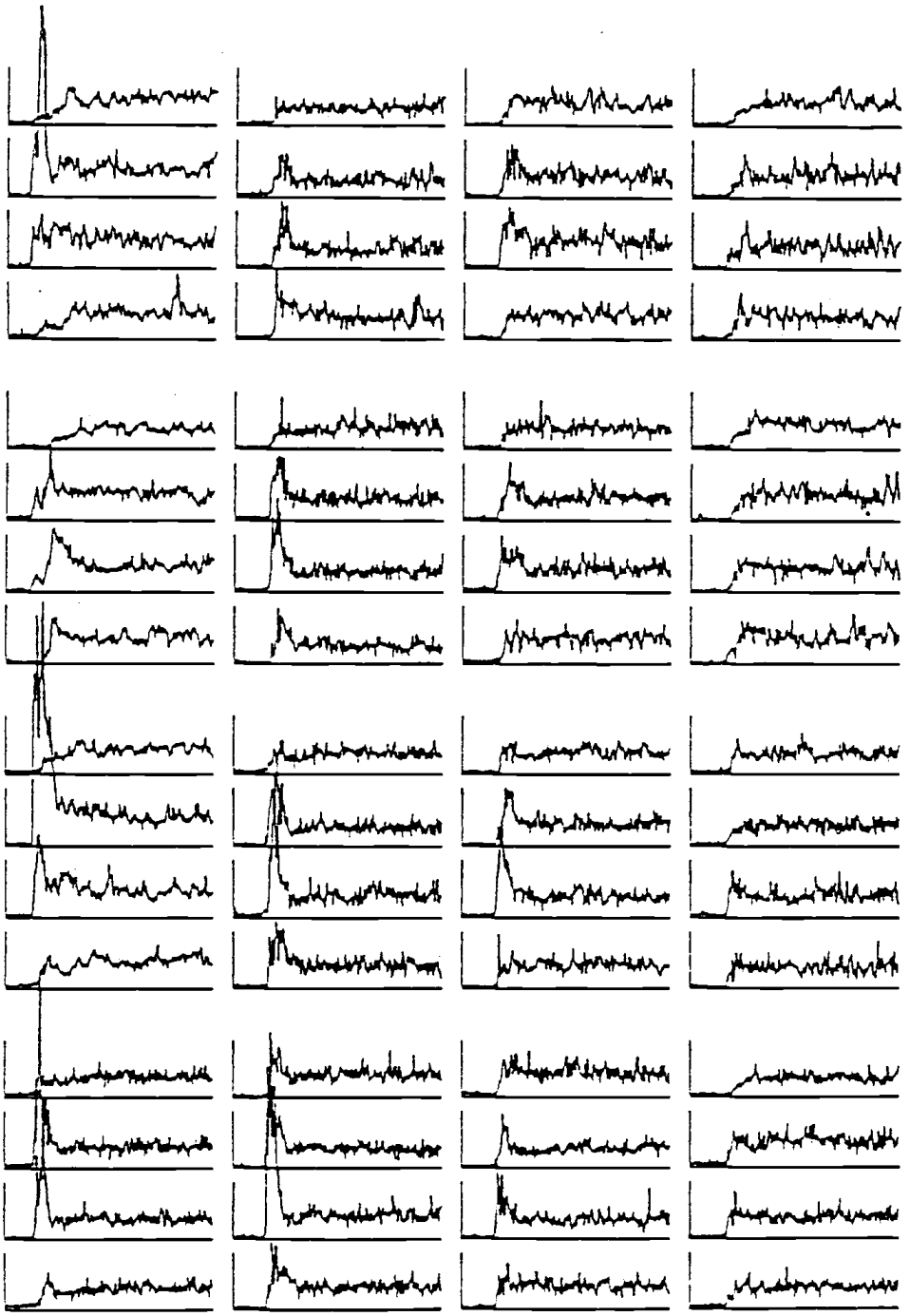

Figure 4.3. (Continued)

Run 54: .254 m (10"), 1134 kg (2500#), 2.13 m/s (7FPS), (see Runs 93 and 103).

1. This runs shows more persistent clumps of tracer than its counterparts (runs 93 and 103). Again, this is probably a coincidence, which indicates a lack of reproducibility in the mixing process.
2. The rise times are about the same in all three runs. Mixing times are also about equal.
3. Channel 9, in all three runs, indicates that a dense solid region exists. Run 54 does not show this effect nearly as much as runs 93 and 103. Bubble movement is virtually the same for all three runs in other regions of the bed.

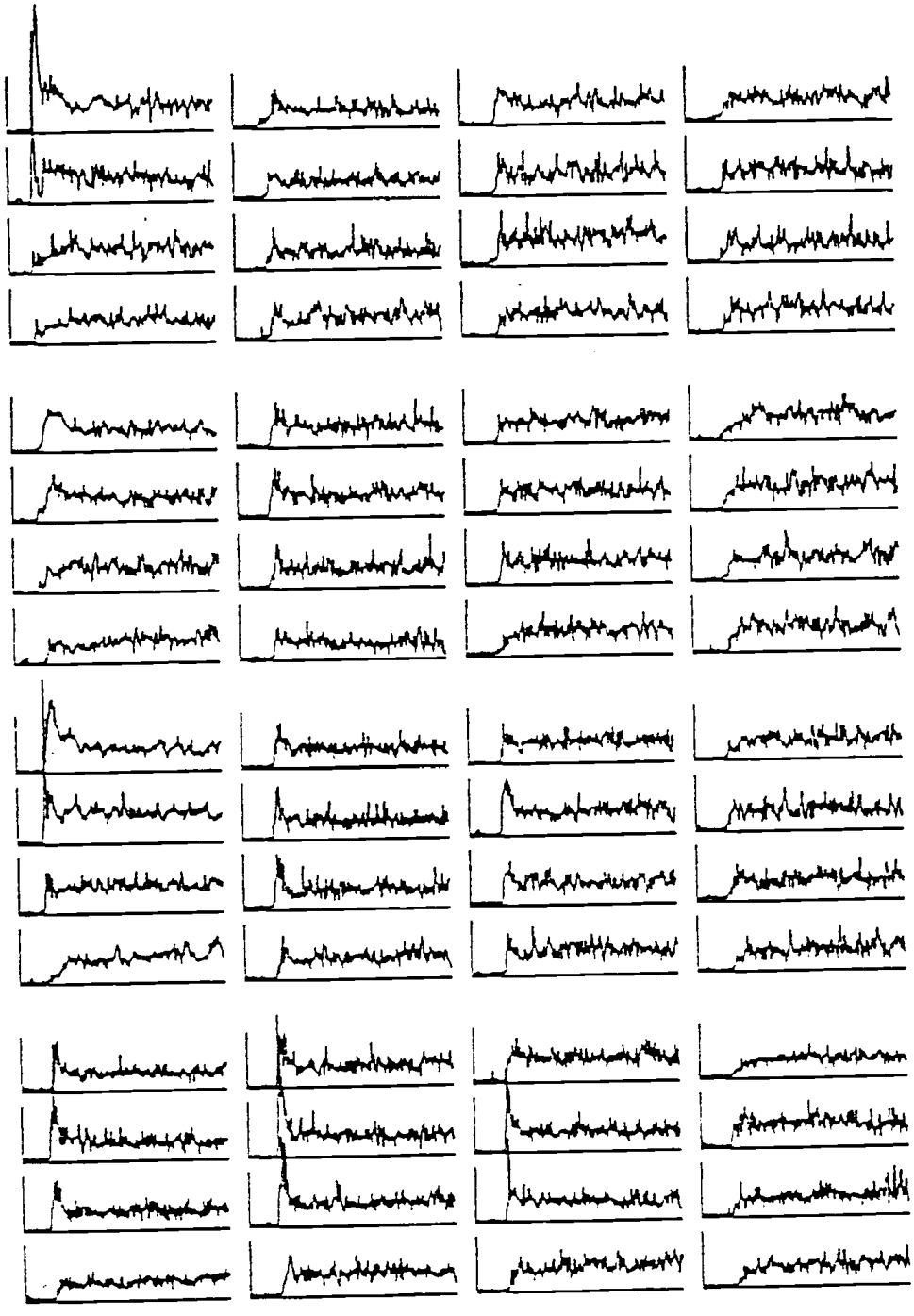

Figure 4.3. (Continued)

Run 56: .254 m (10"), 1134 (2500#), 3.35 m/s (11FPS), (see Runs 95 and 105)

1. Bubble movement is about the same in all three runs (95, 105, 56), except around channels 9A, B, C and D. Run 95 shows a dense phase of solids in this region, whereas runs 56 and 106 are more uniform throughout the bed.
2. Clumps are virtually absent in these runs, except for some small spikes about the point of injection.
3. Rise times are fairly uniform throughout all three runs. Thus, the overall mixing times of these runs are equal.

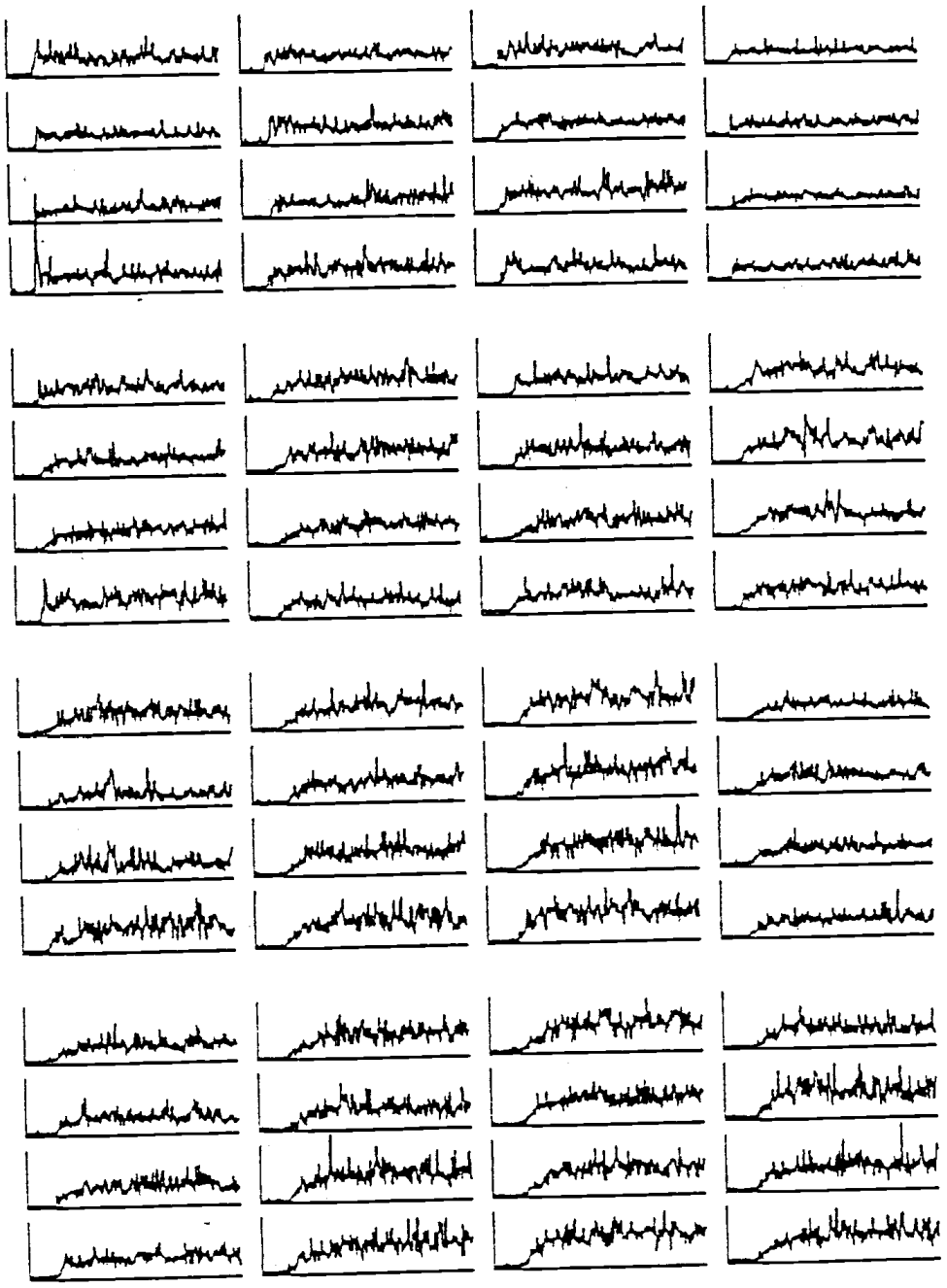

Figure 4.3. (Continued)

Run 57: .254 m (10"), 1361 kg (3000#), 1.52 m/s (5FPS), (see Run 88)

1. The dense phase shown in channels 1, 5 and 9 of run 88 is not apparent in this run. Much of this effect is due to the Poisson noise superimposed on the data of run 57.
2. Again, some tracer has avoided detection by probes 5 and 9 and then appears in channels 13B and 14B.
3. The right side of the bed has an absence of peaks or clumps as is the case with run 88.
4. Mixing at the bottom is sluggish compared with the top as a comparison of rise times demonstrates.

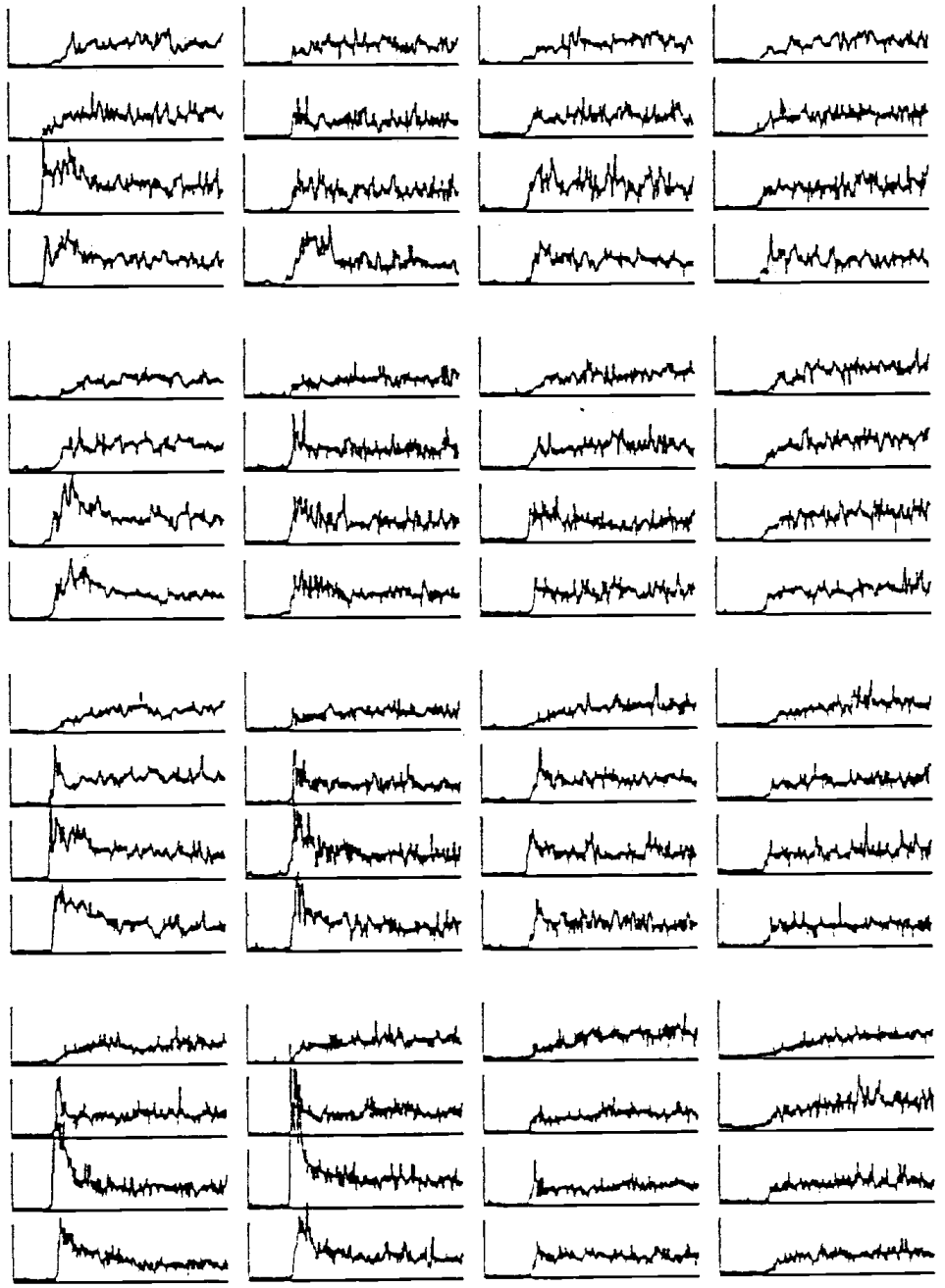

Figure 4.3. (Continued)

Run 58: .254 m (10"), 1361 kg (3000#), 2.13 m/s (7FPS), (see Run 89)

1. As in run 89, tracer is fairly well mixed by the time it reaches the array.
2. The rise times of both runs are comparable.
3. Bubbles are well dispersed at the bottoms of both beds. Along tube 9, run 58 doesn't register a dense phase as run 89 does. Again, this effect is probably due to Poisson noise.
4. Mixing appears to be slower on the sides of the bed than in the middle of the bed.

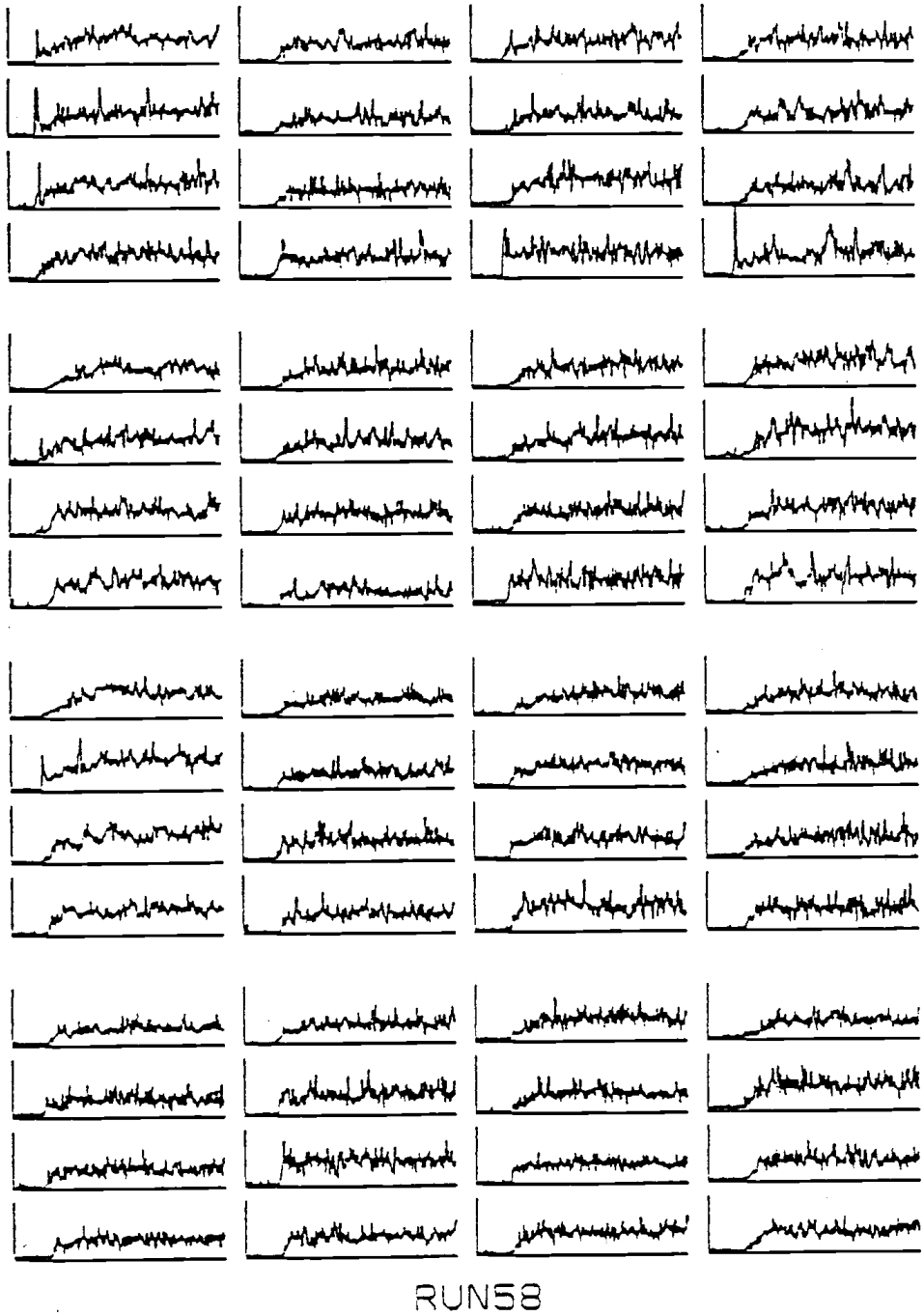

Figure 4.3. (Continued)

Run 59: .254 m (10"), 1361 kg (3000#), 2.74 m/s (9FPS),
(see Run 90)

1. Not as many clumps appear in this run as in run 90.
2. Rise times vary a bit from channel to channel in these runs. Overall mixing time is about the same, though.
3. In run 90, channels 8 and 9 show dense solid phases. These are not seen in run 59. This is probably due to Poisson "noise."

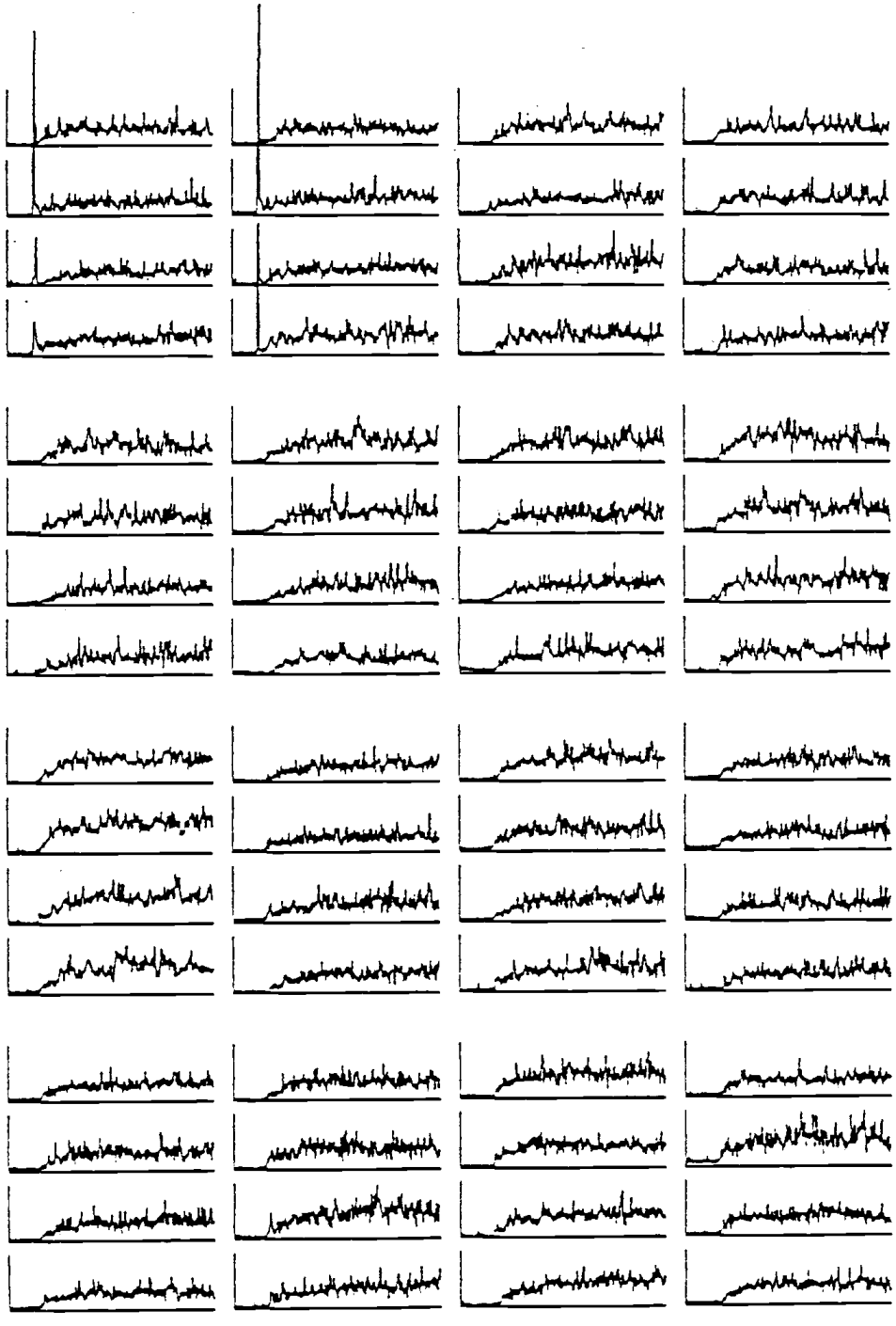

Figure 4.3. (Continued)

Run 60: .254 m (10"), 1361 kg (3000#), 3.35 m/s (11FPS),
(see Run 91)

1. Peaks appear near the point of injection, whereas in run 90 they are seen in channels 4A and B. This could be the result of larger tracer particles.
2. Again, the dense regions around tubes 8 and 9 in run 91 don't show up in run 60.
3. Rise times for each channel vary between these runs. Overall mixing time is about the same in both beds, though.

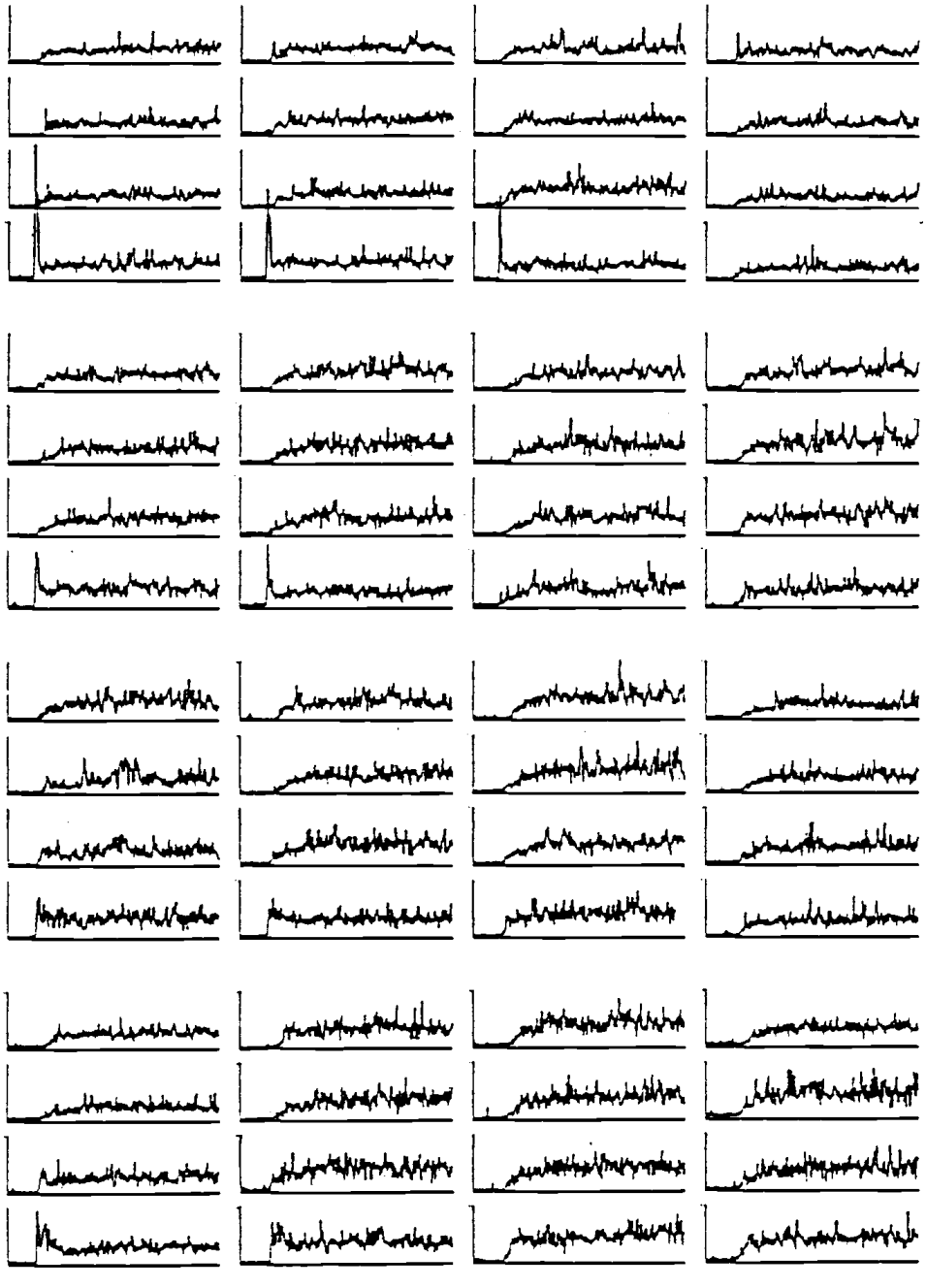

Figure 4.3. (Continued)

Run 61: .508 m (20"), 1361 kg (3000#), 3.35 m/s (11FPS),
(see Run 86)

1. Rise times are about the same in both runs. Their overall mixing is also approximately equal.
2. Although clumps appear in different channels for each run, their sizes are roughly equal. Therefore the clump disappearance time is about the same for both runs. Again, for the heavier tracer particles the clumps appear right below the port of injection, whereas the clumps of smaller tracer particles first appear at the back (or right side) of the bed.
3. The effect of Poisson noise is evident in these two runs.
4. Bubbles seem to move in the same areas in both runs, i.e. more freely in the interior than along the sides. The "D" side of the bed inhibits movement the most.

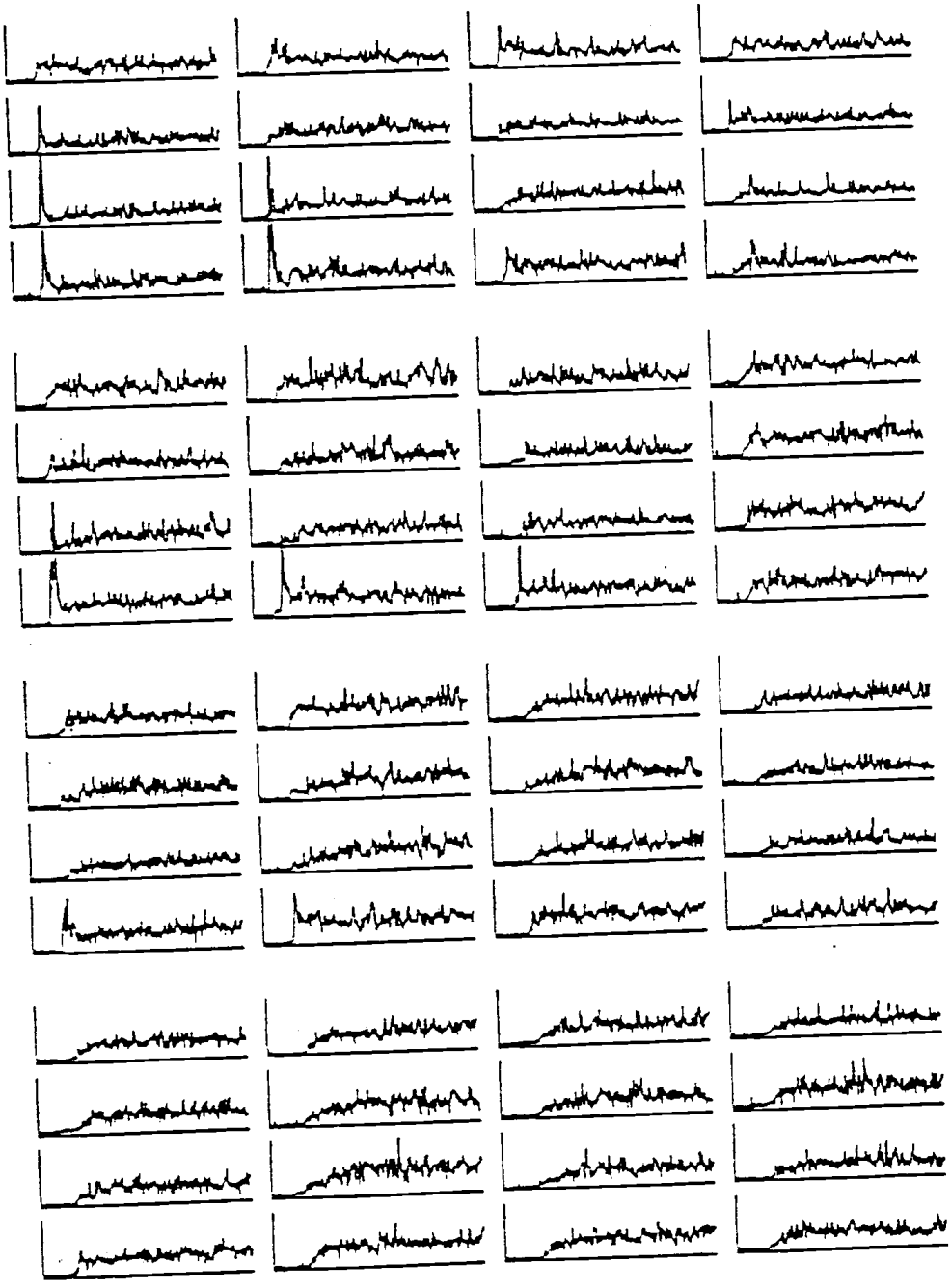

Figure 4.3. (Continued)

Run 62: .508 m (20"), 1361 kg (3000#), 2.74 m/s (9FPS), (see Run 85)

1. Rise times are similar in each run.
2. Many peaks are the same (2A, 5A). Mixing times are approximately equal in both runs.
3. Circulation of solids is similar to that in run 85.
4. Bubble data is obscured by Poisson noise in this run.
5. Bubbles move freely about the bed.

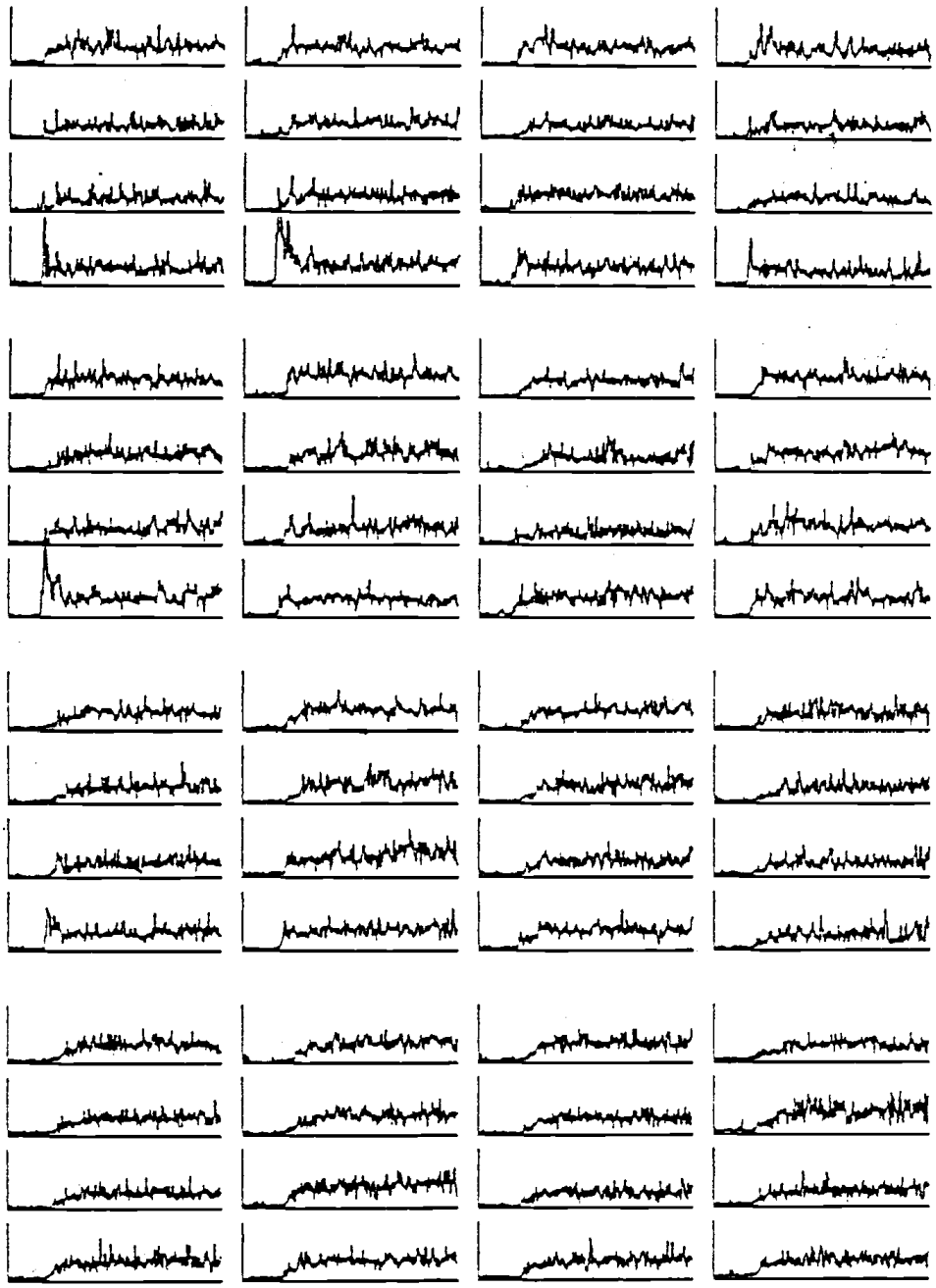

Figure 4.3. (Continued)

Run 63: .508 m (20"), 1361 kg (3000#), 2.13 m/s (7FPS),
(see Run 84)

1. Peaks are virtually absent. In run 84, some large peaks appear at the point of tracer injection (1A, 2A).
2. Rise times are about equal in both runs. Thus, the overall mixing time is the same.
3. Compare channel 6A to its neighbors in both runs. It seems to be out of calibration in Run 84.
4. Circulation of tracer and bubbles seems about the same in both runs.

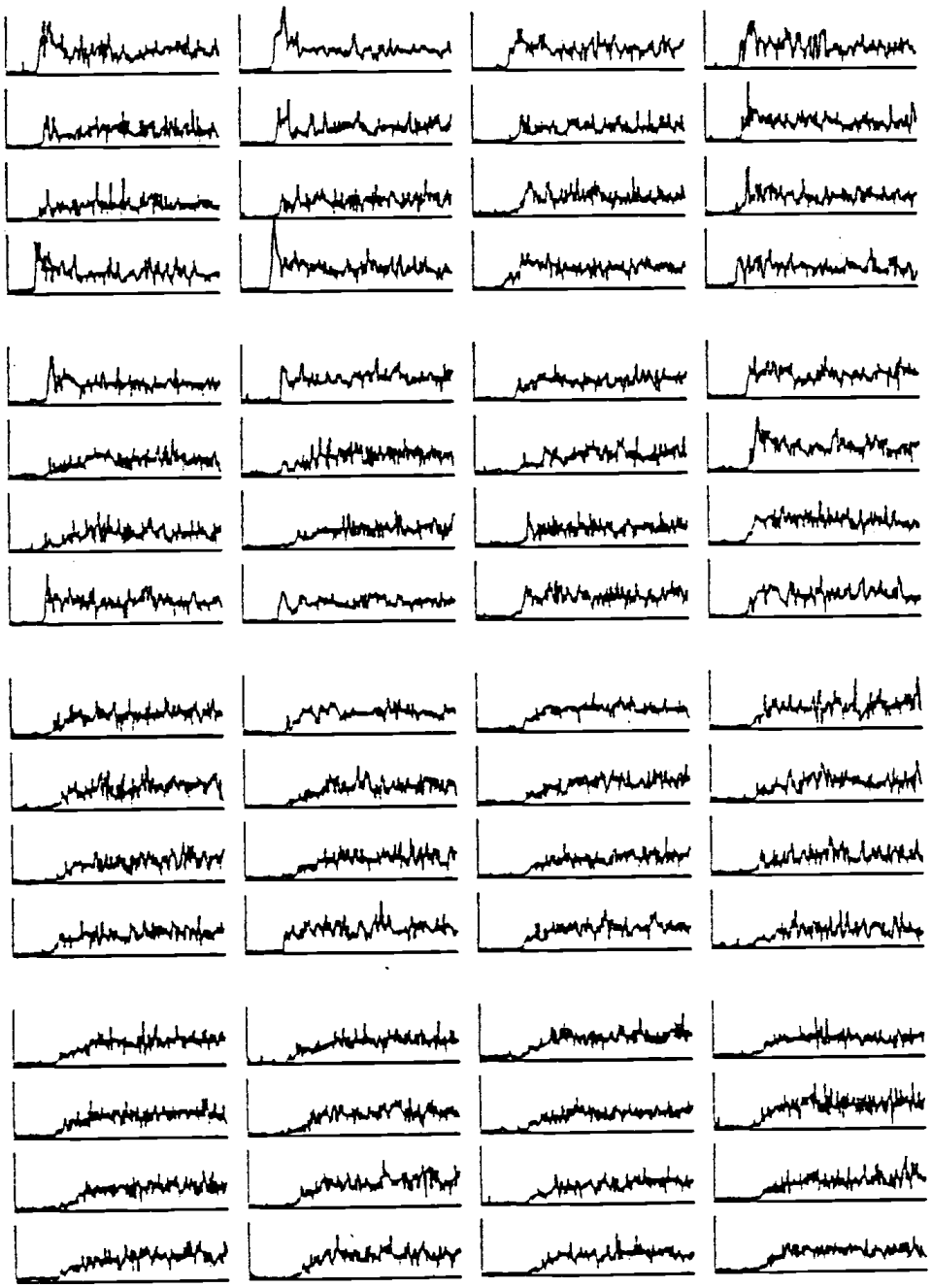

Figure 4.3. (Continued)

Run 64: .508 m (20"), 1361 kg (3000#), 1.52 m/s (5FPS),
(see Run 83)

1. Channel 10D is malfunctioning.
2. In both runs, corner flow is accentuated. The tracer falls down the corner adjacent to the injection port and down the walls. It then catches on upward current at the bottom of the bed and moves upward in the interior of the bed.
3. Bubbles are concentrated more in the interior and right side of the bed in run 84. On the left side of the bed, bubbles are either smaller (not large enought to cause as much noise) or scarcer. These effects are obscured by Poisson noise in run 64.
4. Rise times and mixing in both runs are comparable.

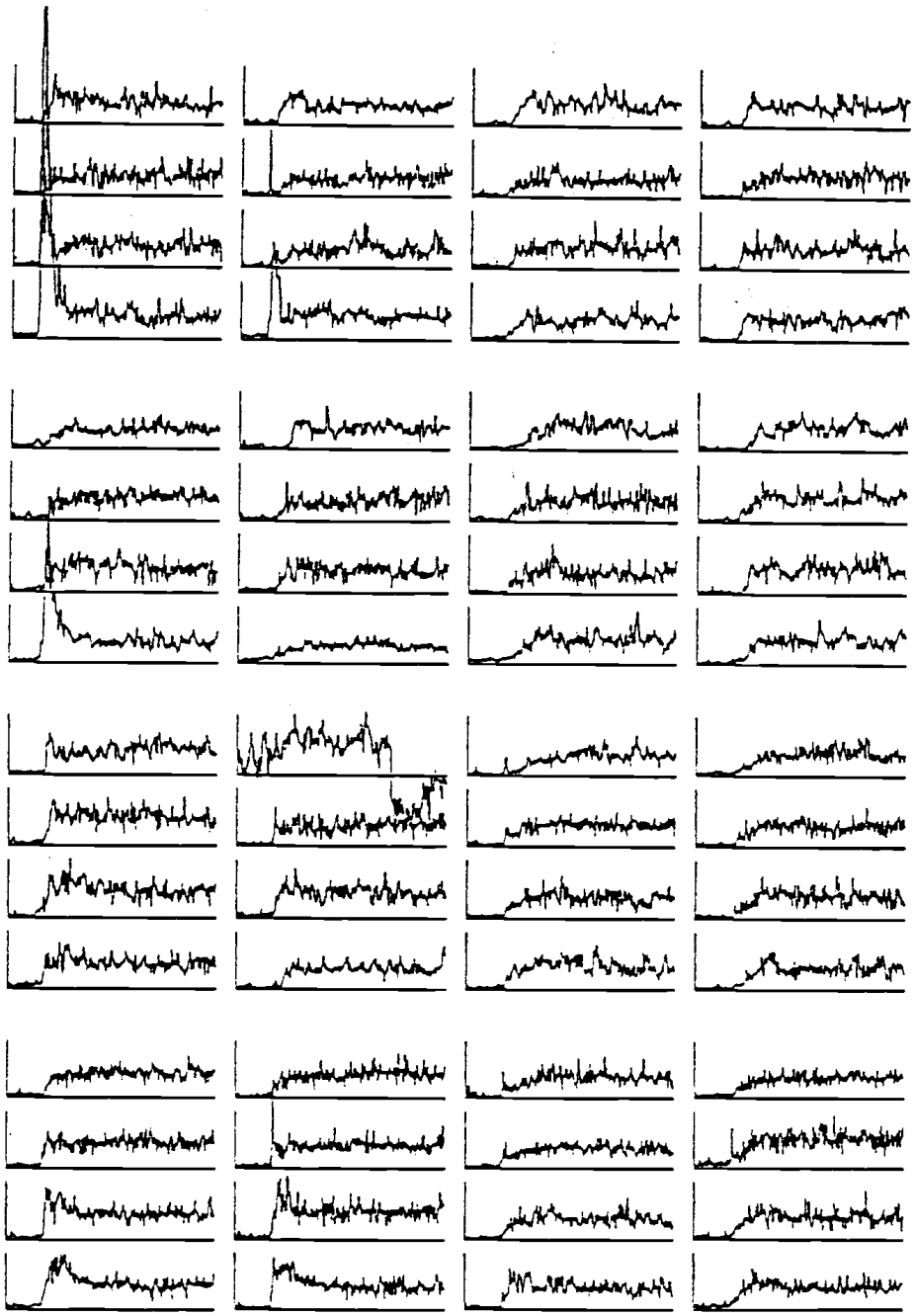

Figure 4.3. (Continued)

Run 65: .508 m (20"), 1134 kg (2500#), 1.52 m/s (5FPS), (see Run 79)

1. Clumps of tracer seem to persist longer in Run 79 than in Run 65. Only a couple of small peaks appear in the bottom three rows of probes (see 5A, D). This seems to indicate that small particles move differently than the large particles.
2. The rise times or lags in run 65 are greater than those in run 79, which indicates poor mixing in the bottom of the bed.
3. Solids tend to move down the corners and sides of the bed, whereas bubbles prefer the center of the bed.
4. The overall mixing time is approximately the same in both runs.

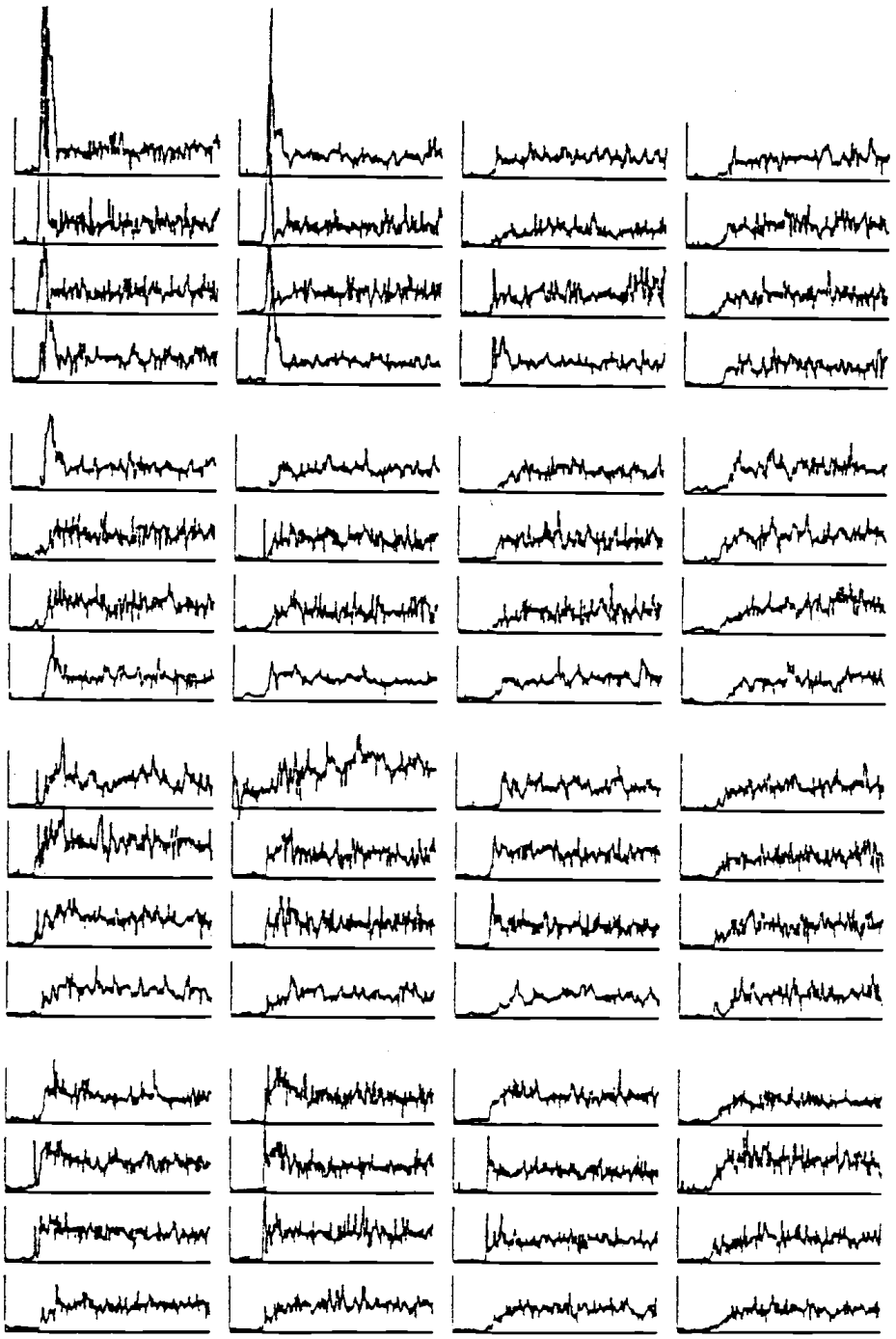

Figure 4.3. (Continued)

Run 66: .508 m (20"), 1134 kg (2500#), 2.13 m/s (7FPS), (see Run 80)

1. Peak disappearance or clump dispersion time is about the same in both runs.
2. Rise times appear a bit longer in Run 66 than those in Run 80 (see channels 16A, B, C, D).
3. Fluctuations from bubbles are more pronounced in the bottom and center or interior regions of these beds.
4. Tracer moves down the corner adjacent to the injection port.
5. Overall mixing times in both runs are comparable.

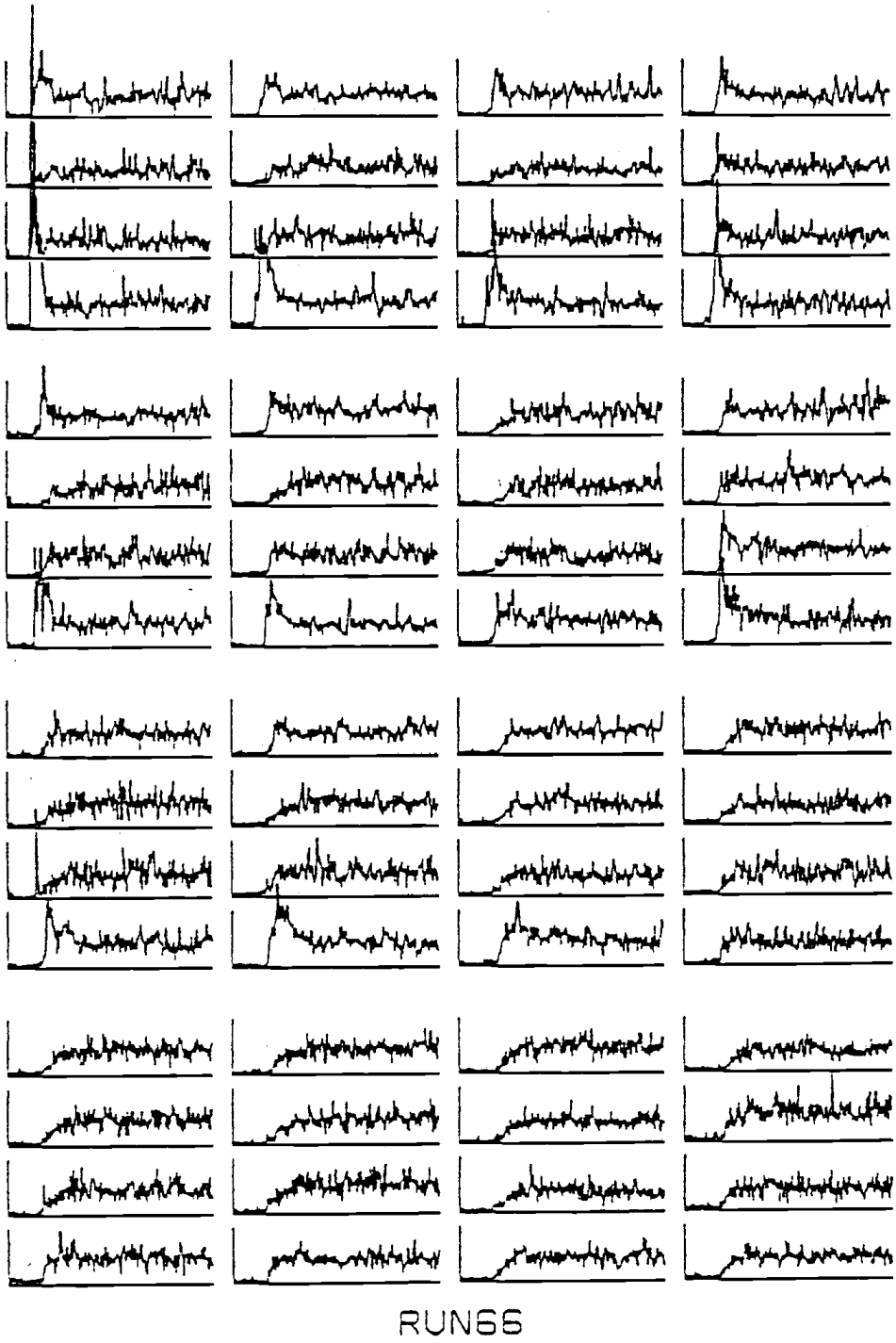

Figure 4.3. (Continued)

Run 67: .508 m (20"), 1134 kg (2500#), 2.74 m/s (9FPS),
(see Run 81)

1. Clumps disappear rapidly in both runs. No clumps make it past the second row of probes, except 10A, Run 67.
2. In the top row of probes tracer appears to move laterally against the tubes more readily than along the tubes. It definitely prefers to move along the walls as opposed to the interior.
3. Bubbles seem to move uniformly throughout the bed. They are smaller and more uniform in the bottom of the bed.

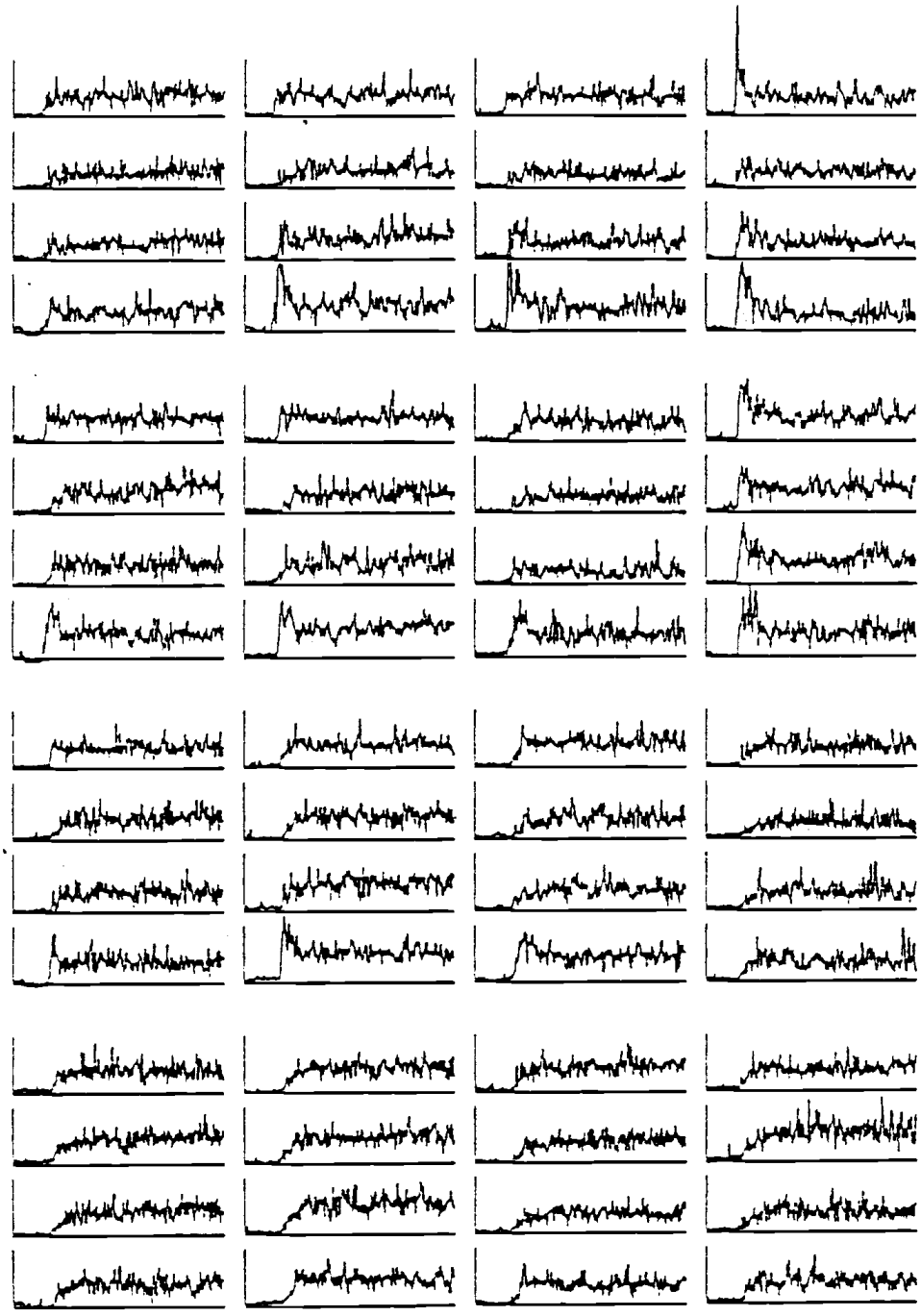

Figure 4.3. (Continued)

Run 68: .508 m (20"), 1134 kg (2500#), 3.35 m/s (11FPS), (see Run 82).

1. Peak disappearance time is more prolonged in this run than in the smaller-tracer run, number 82.
2. Also lag times appear a little bit worse in this run than in its counterpart. See channels 16A, B and C, especially. This is probably due to the difference in movement between large and small particles.
3. Bubbles are evenly dispersed throughout the bed.

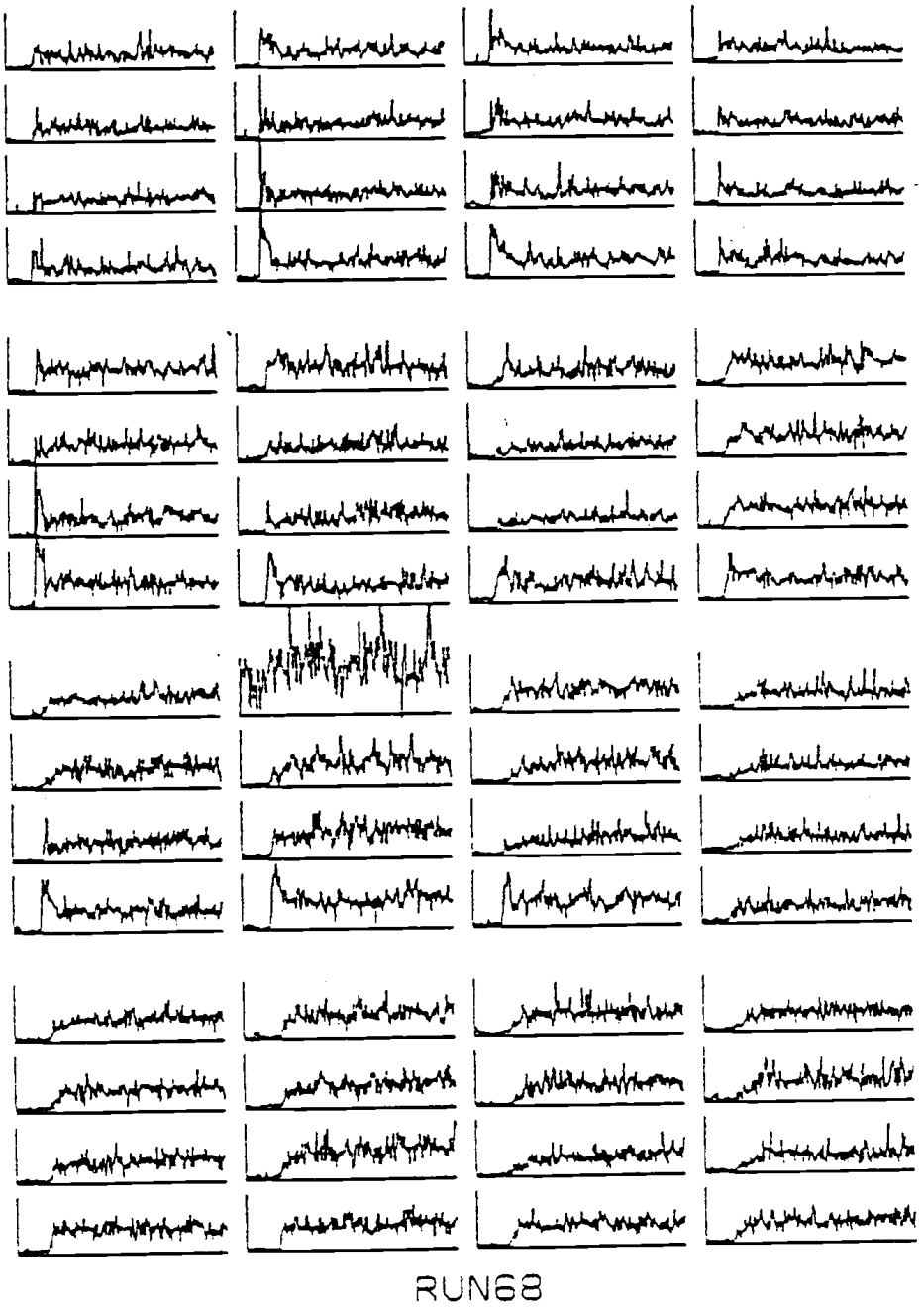

Figure 4.3. (Continued)

Run 69: .508 m (20"), 907 kg (2000#), 1.52 m/s (5FPS),
(see Run 76)

1. Sluggish mixing exists in both of these runs.
2. It appears that the top row of probes in run 69 is mostly out of the bed and in the freeboard.
3. Bubbles move freely in the interior regions of the bed. The difference in concentrations in the top row of tubes of runs 69 and 76 is due to the fact that small particles are more readily entrained in the freeboard than large ones.
4. Lag times are roughly the same in both runs.

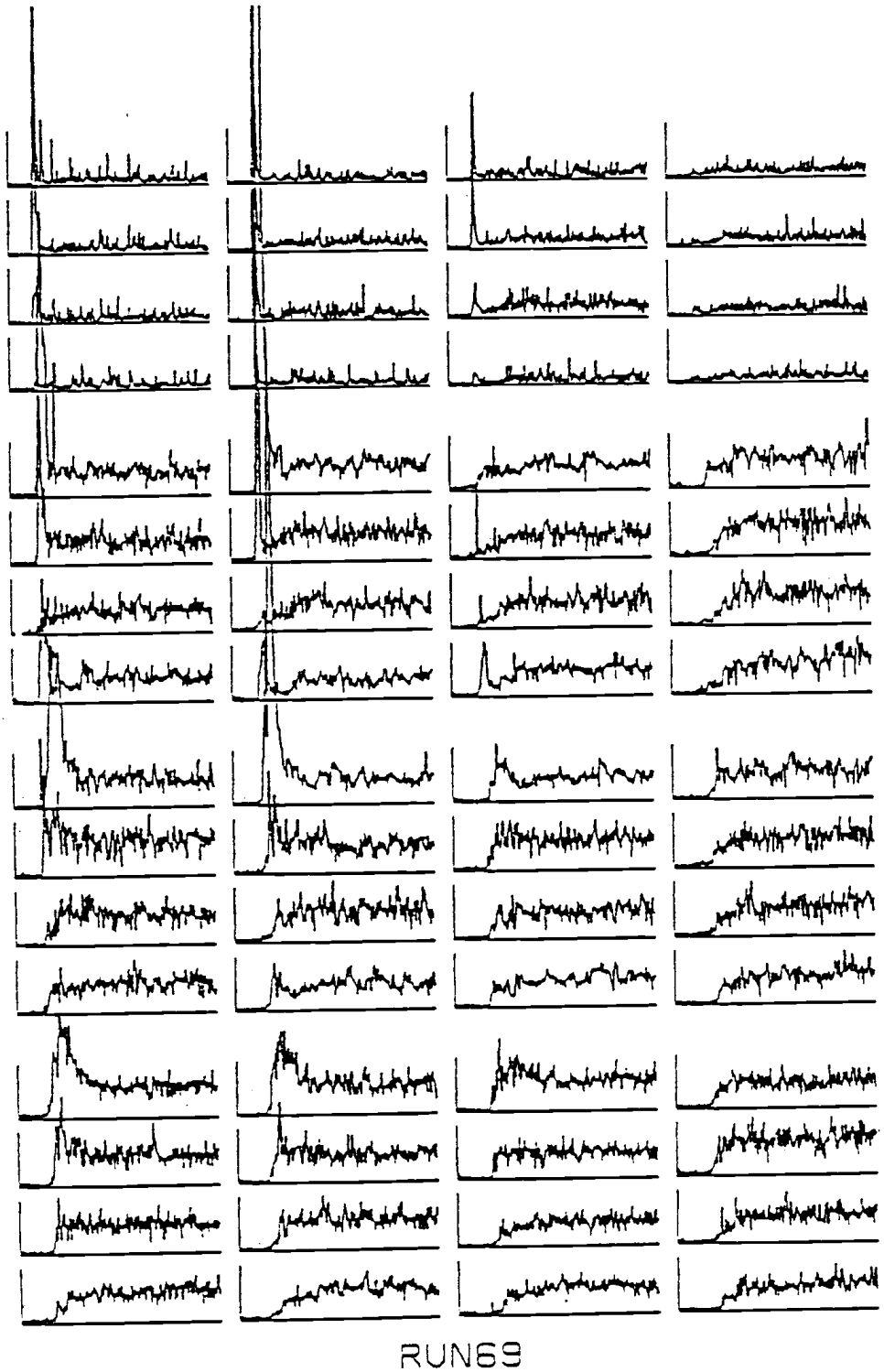

Figure 4.3. (Continued)

Run 70: .508 m (20"), 907 kg (2000#), 2.13 m/s (7FPS),
(see Run 75)

1. Clumps manage to make it to the bottom of these beds before dispersing. Mixing has improved significantly in these runs over that observed at 5 FPS.
2. Bubbles movement is relatively uninhibited in the interior of the bottom 2 rows of probes. There may well be a dense phase near the walls as is evident in run 75.
3. Lag times are generally longer in run 70 than those in run 75. This may be due to the fact that in run 75 the lighter tracer spreads across the top of the bed more rapidly.

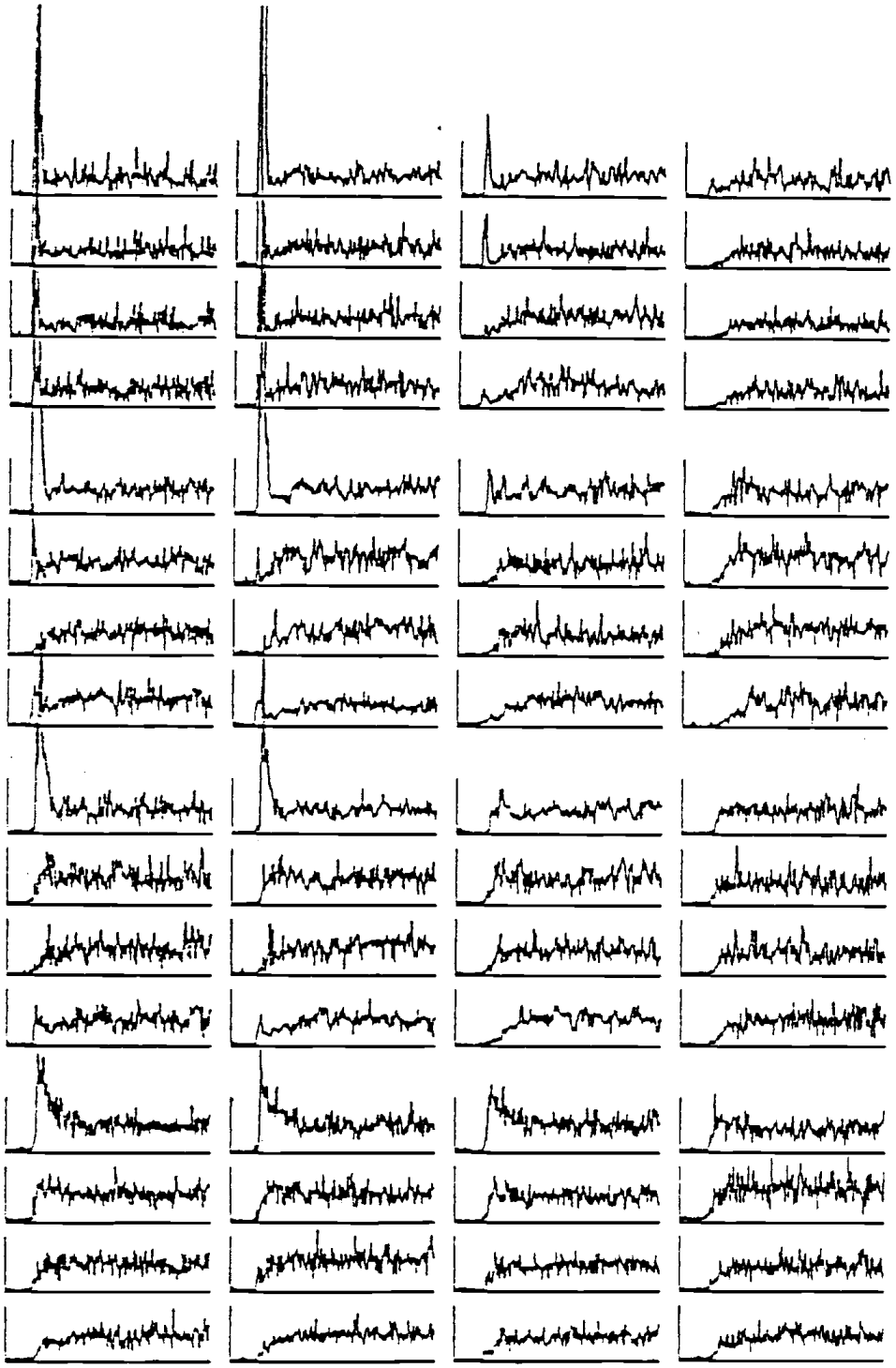

Figure 4.3. (Continued)

Run 71: .508 m (20"), 907 kg (2000#), 2.74 m/s (9FPS), (same as Run 78)

1. In this run tracer clumps are detected below the second row of probes, whereas in run 78 they have been essentially eliminated. Tracer movement is better across the top in run 78.
2. Lag times in these two runs are about the same. In general, overall mixing time is also equivalent.
3. Bubbles are evenly dispersed in the interior of the bed at each particular level.

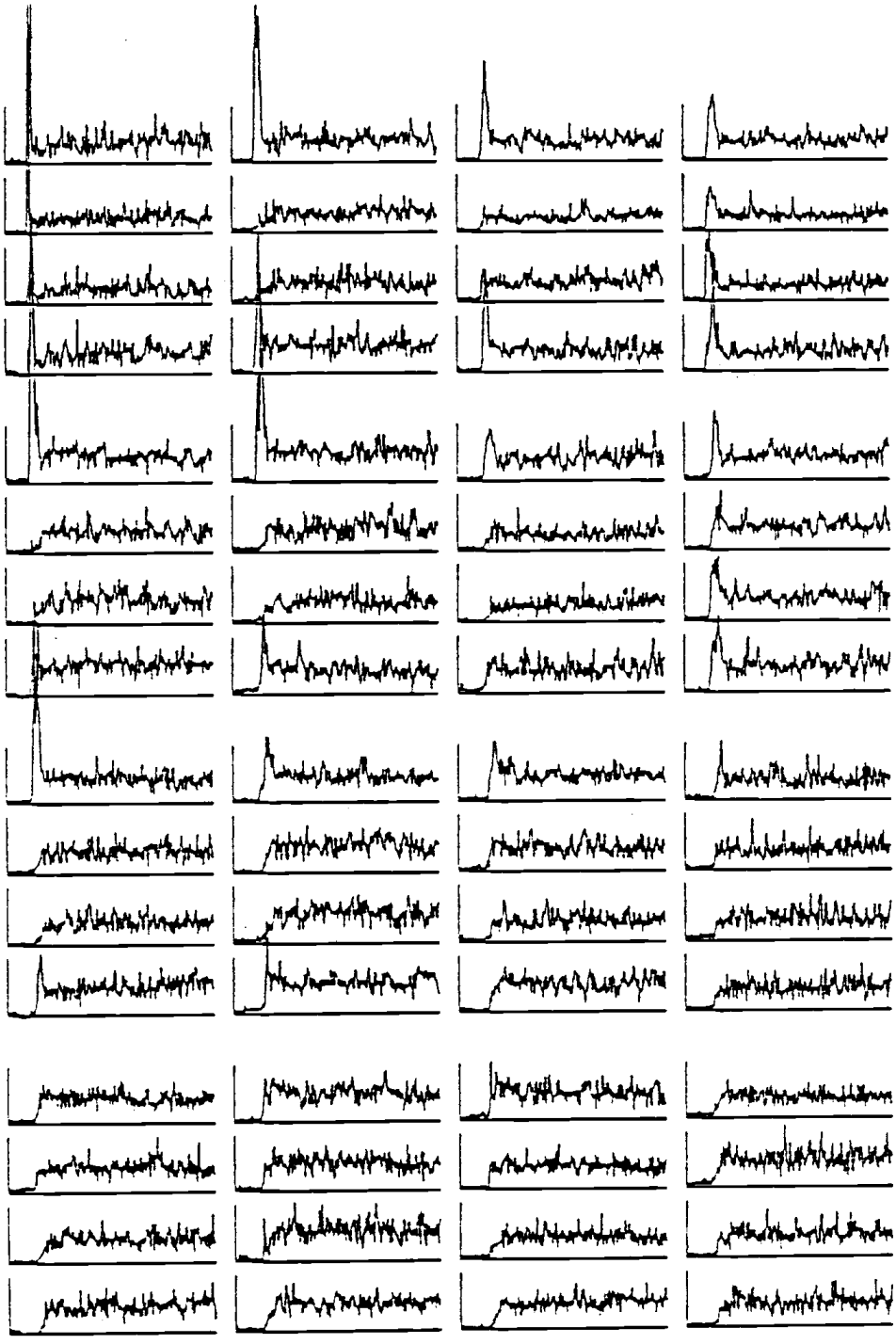

Figure 4.3. (Continued)

Run 72: .508 m (20"), 907 kg (2000#), 3.35 m/s (11FPS),
(see Run 77)

1. Mixing is quite rapid in both of these runs. Lag times compare favorably in both.
2. Clumps disperse at about the same rates in these runs.
3. Bubbles populate the bottom two rows of probes uniformly with the exception of 10A and D. However, in the upper portion of these beds, bubbles seem to move preferentially in the interior.

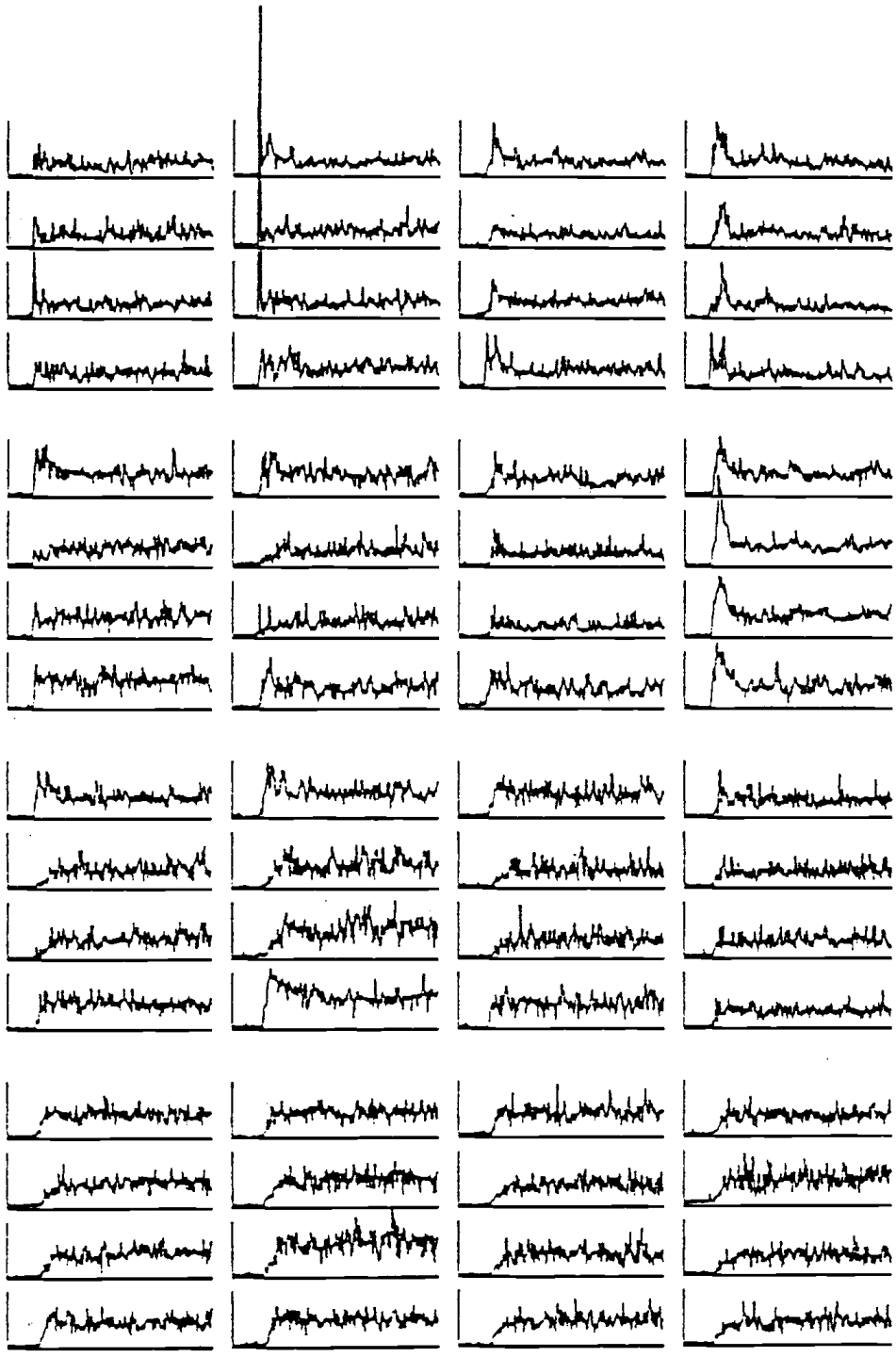

Figure 4.3. (Continued)

Run 73: .508 m (20"), 907 kg (2000#), 2.13 m/s (7FPS),
(see Run 70)

The conditions of this run were the same as run 70, except only one-quarter as much tracer was used. The relative noise was found to increase by a factor of two, which was consistent with our Poisson model.

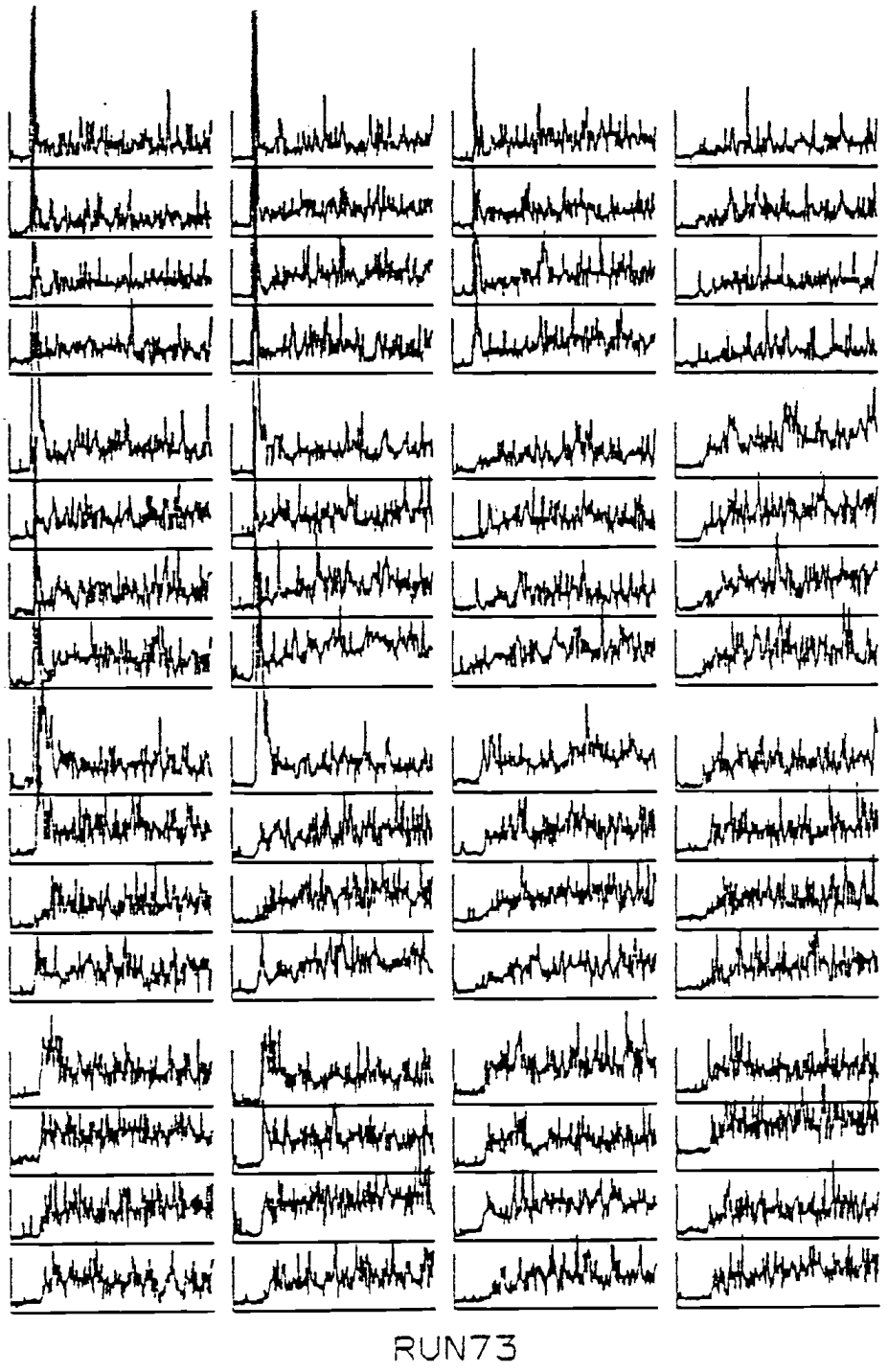

Figure 4.3. (Continued)

Run 74: .508 m (20"), 907 kg (2000#), . 91 m/s (3FPS)

1. At this low velocity, the peaks are very large and mixing is quite slow.
2. Since only 2000# of sand is used and the array is in the 20" position, the upper row of tubes (1, 2, 3, 4) don't see very much tracer (just a few small spikes at the beginning of the run). These tubes are out of the bed and in the freeboard.
3. Tracer seems to clump together for about ten seconds along the wall as seen in channels (9D, 10D, 11D).
4. The rate at which the tracer falls down the side of the bed (the side opposite the tracer injection port) seems to decrease as a comparison between channels (9D, 10D, 11D) and (13D, 14D, 15D) demonstrates.
5. All clumps of tracer seem to disappear after about 25 seconds. The channels showing the slowest mixing are 9D, 10D, 11D.

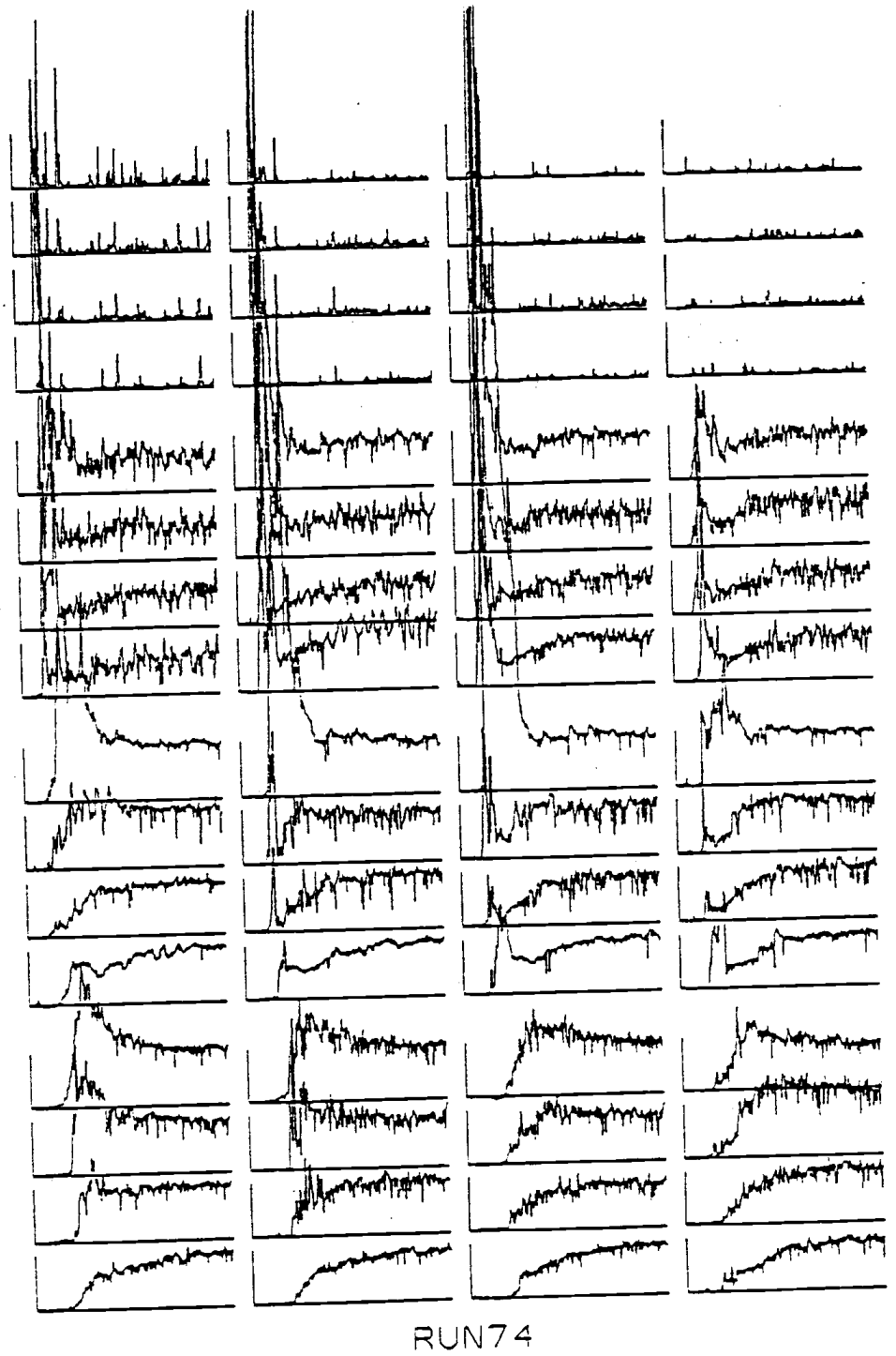

Figure 4.3. (Continued)

Run 75: .508 m (20"), 907 kg (2000#), 2.13 m/s (7FPS),
(see Run 70)

1. The higher velocity accounts for the more rapid mixing in Run 75 when compared to Run 74.
2. The clumpiness of the tracer has been greatly reduced as can be seen by the areas under the pulses or spikes. All tracer pulses or peaks disappear within 12 seconds of its injection into the bed (channel 10A controls this rate).
3. The tracer seems well mixed by the time it reaches the bottom row of probes, i.e., peaks are absent.
4. Lateral mixing seems a bit faster than axial mixing.
5. Lateral mixing along the tubes seems better than against the tubes. Compare channels 9D, 10D, 11D ("against") with 9B, C, D ("along").

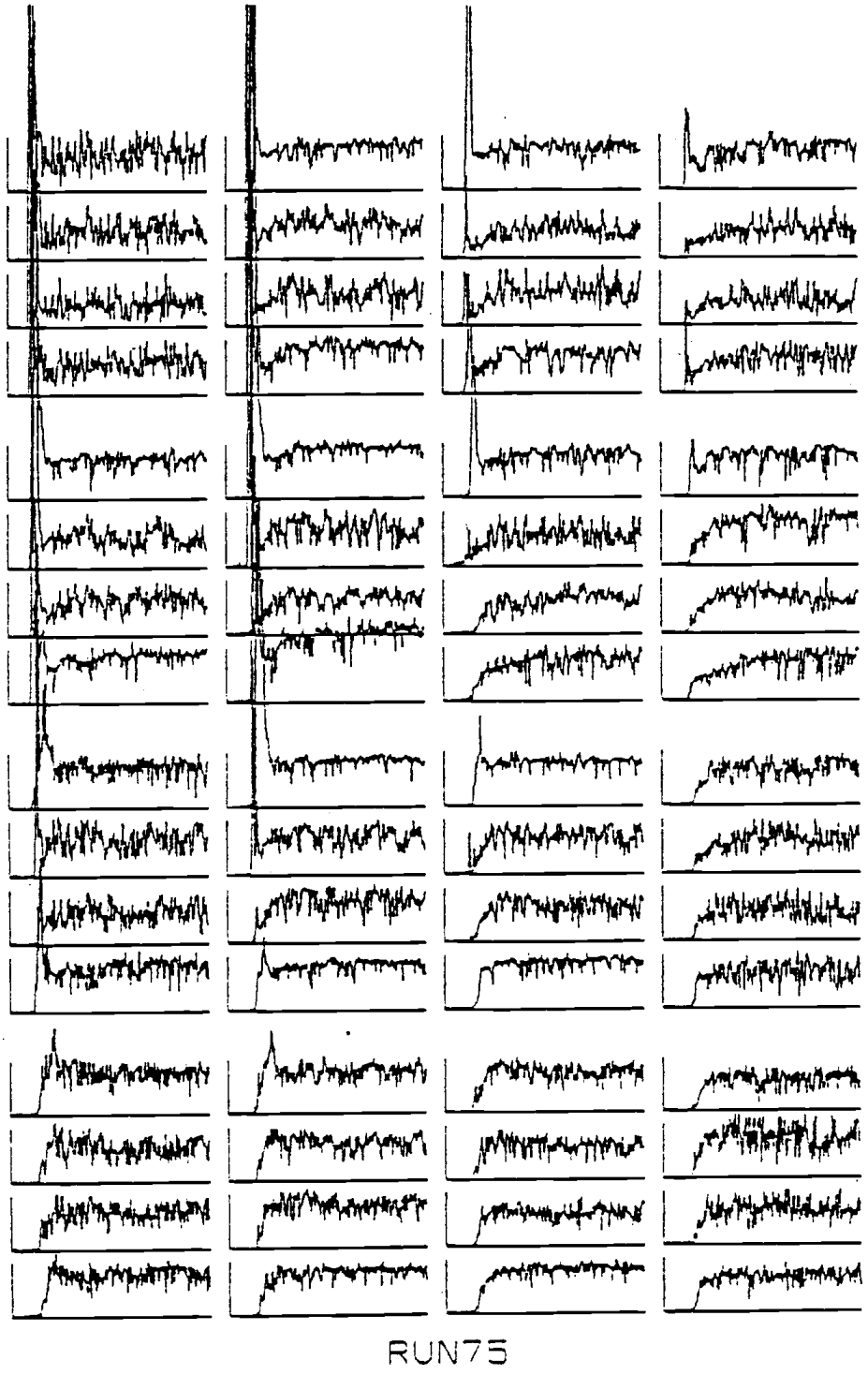

Figure 4.3. (Continued)

Run 76: .508 m (20"), 907 kg (2000#), 1.52 m/s (5FPS), (see Run 69)

1. The areas underneath the peaks resemble those at 7 FPS more closely than those at 3 FPS. Therefore, the rate of mixing is not necessarily related to the velocity in a linear or proportional manner. It is probably related to the velocity taken to an exponent greater than one.
2. Initially the tracer sifts down the side of the bed at a greater rate than it moves across the bed.
3. After complete mixing, it appears that some tracer has accumulated. (see Channels A and D on tubes 6, 7, 10, 11)
4. Channel 6A is either way out of calibration or has a lot of tracer around it--every run has this problem. It could be a pinch point, as it is similar to its neighbors.
5. Clumps seem to disappear in about 5 seconds around the sides of the bed. Those in the vicinities of 5D, 6D and 9D persist the longest. Interior channels seem to have a rise time of about 20 seconds (see channel 7B).

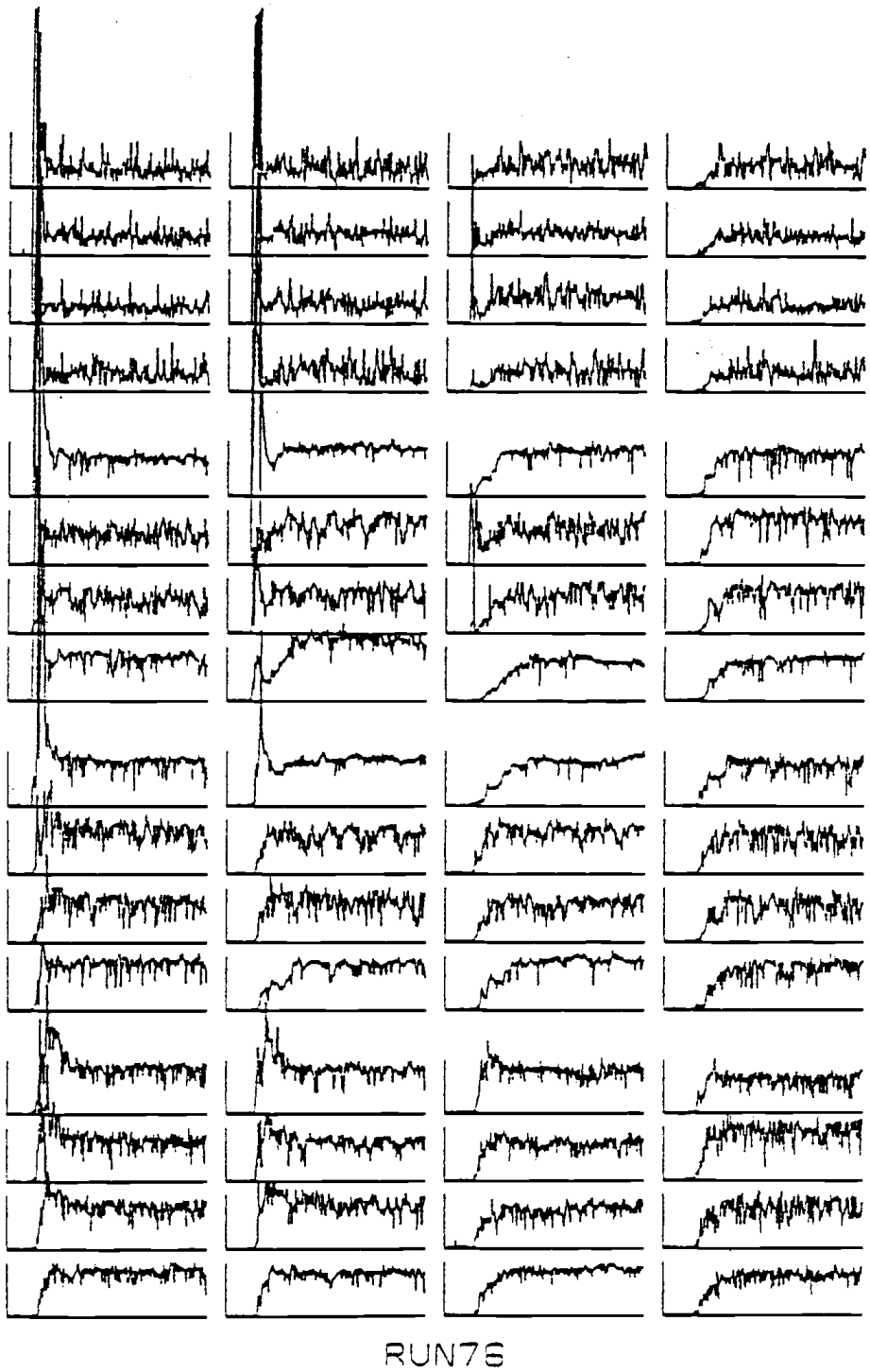

Figure 4.3. (Continued)

Run 77: .508 m (20"), 907 kg (2000#), 3.35 m/s (11FPS), (see Run 72)

1. At this high velocity the tracer appears to hit the top of the bed and drift to the side opposite the injection port.
2. Channels 6D, 7D, 8A, B, C, D seem to indicate that very few bubbles or voids exist along the sides of the bed. In the interior of the bed (Channels B and C of tubes 2, 3, 6, 7, 10, 11, 14, 15) much more bubble noise or oscillations on the plot are seen.
3. The tracer has moved over the tubes in cross flow to the back of the bed. It then appears to move down the sides of the bed and up the center.
4. All tracer is well mixed by the time it reaches the third row of probes (i.e., 9, 10, 11, 12).
5. It takes approximately 15 seconds for the tracer to reach the interior probes (see channels 6B, 7B) as compared to 12 seconds for the wall probes (see channels 5B, 8B).

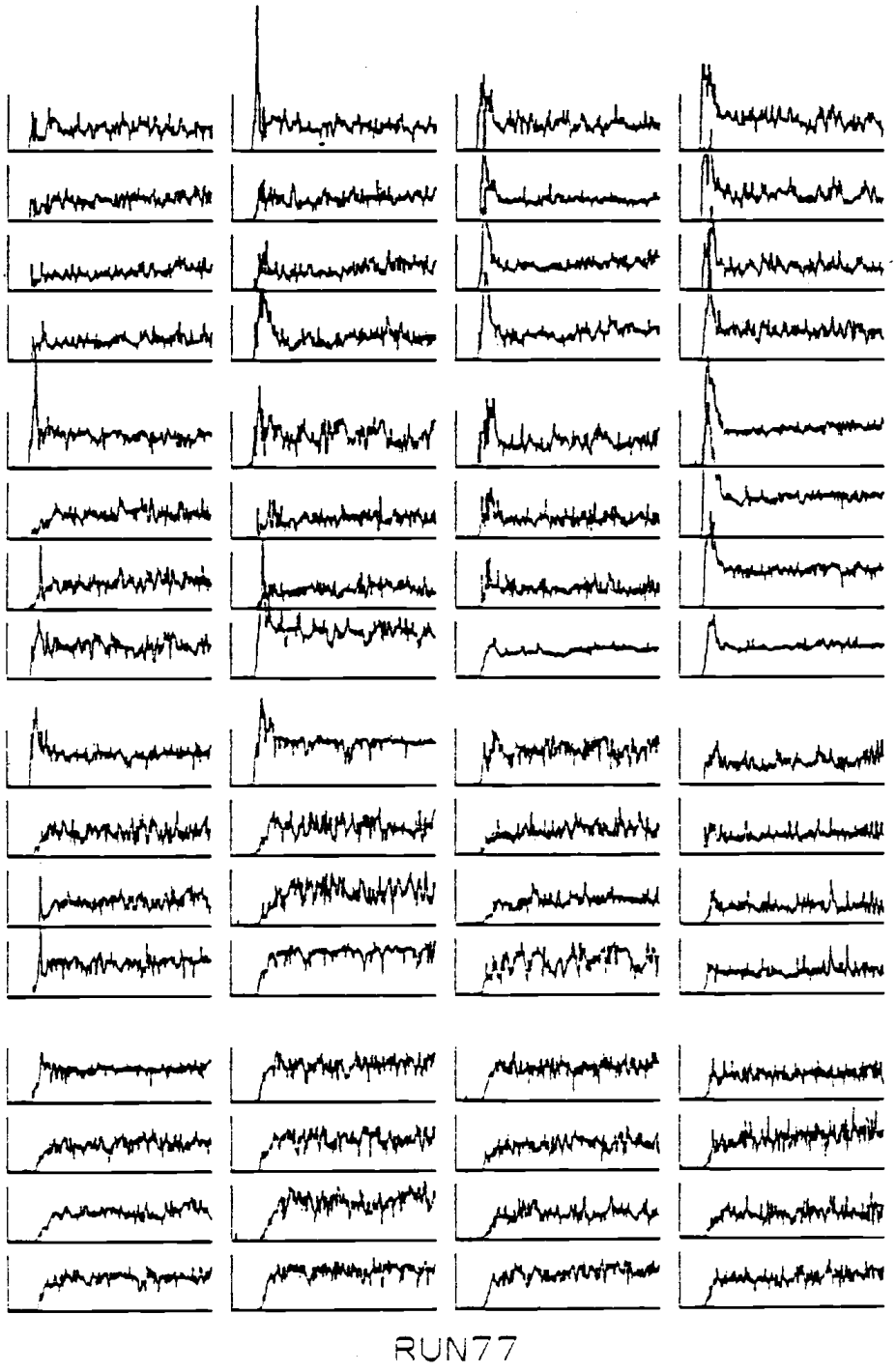

Figure 4.3. (Continued)

Run 78: .508 m (20"), 907 kg (2000#), 2.74 m/s (9FPS), (see Run 71)

1. Again the tracer is driven in crossflow against the tubes to the back wall of the bed where tube 4 is. From here it moves down the wall at a greater rate and it moves toward the interior of the bed. It appears that the tracer reaches interior channels such as 6B, C and 7B, C as much as 5 seconds later than it passes wall channels like 5A, B, C, D and 8A, B, C, D.
2. All tracer is mixed by the time it reaches the third row of tubes (i.e., 9, 10, 11, 12).
3. The time for the last clump of tracer to mix after its introduction is about 10 seconds (see channels 8A, 11A).

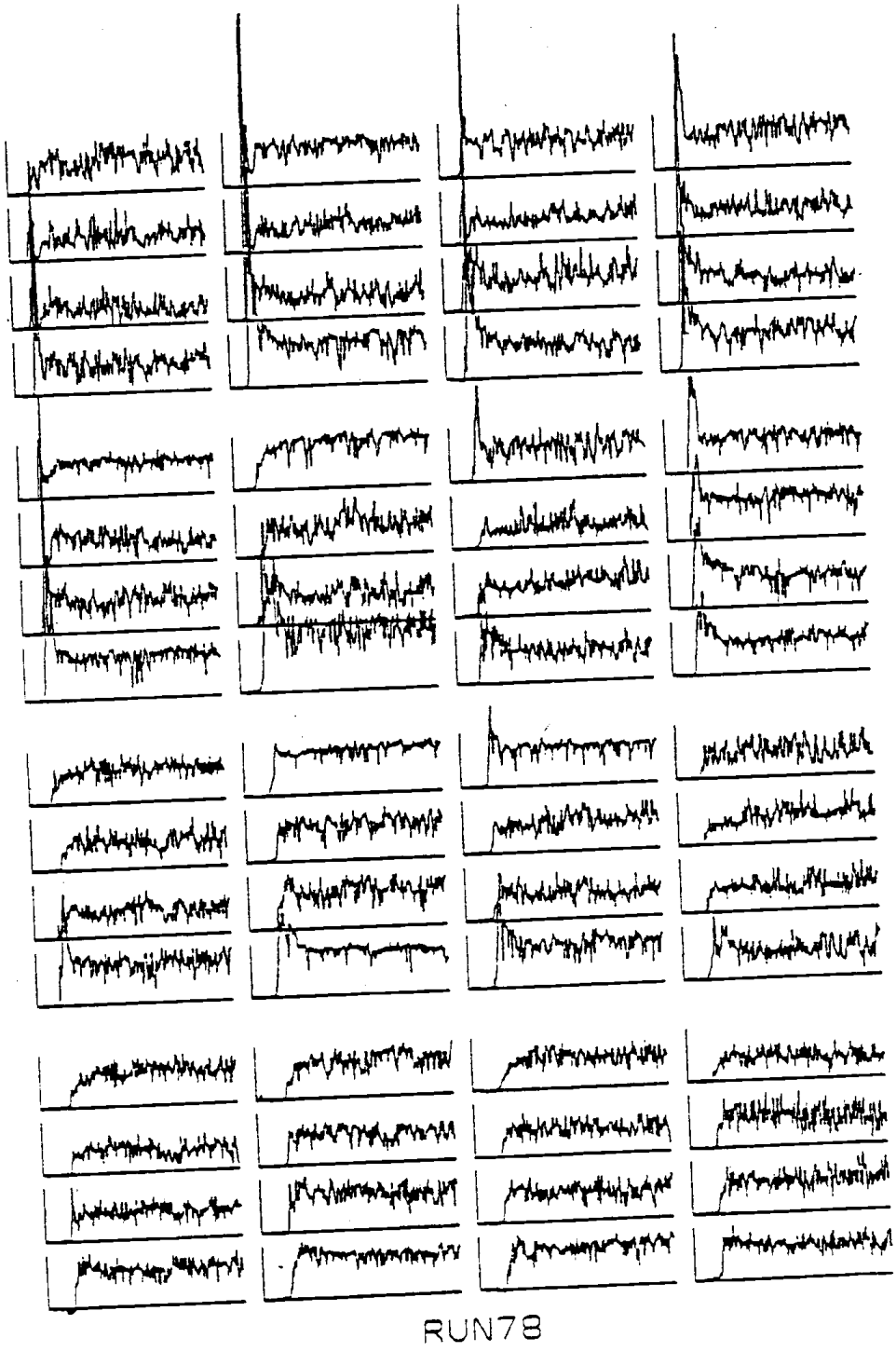

Figure 4.3. (Continued)

Run 79: .508 m (20"), 1134 kg (2500#), 1.52 m/s (5FPS),
(see Runs 65 and 110)

1. Tracer mixing seems fairly sluggish in that it takes 20 seconds approximately for the last clump to disappear. This last clump is around channel 9A.
2. With a higher inventory of sand in the bed, the tracer has time to cross the bed even at this low velocity. This would explain the peaks in channels 4A, B, C and D.
3. The higher inventory of sand gives better spreading or mixing of tracer than is found in Run 76.
4. It appears that tracer slides down the back and front walls of the bed (parallel to the tubes) faster than it moves down side walls (normal to the tubes).
5. The tracer movement appears to be down the walls and up the interior of the bed.
6. There appears to be a higher average voidage in the middle of the bed (especially at the top) than along the walls. A comparison of channels 6D and C or 7D and C or 11D and C will readily show this fact. D channels, of course, are wall channels, whereas C channels are interior channels.

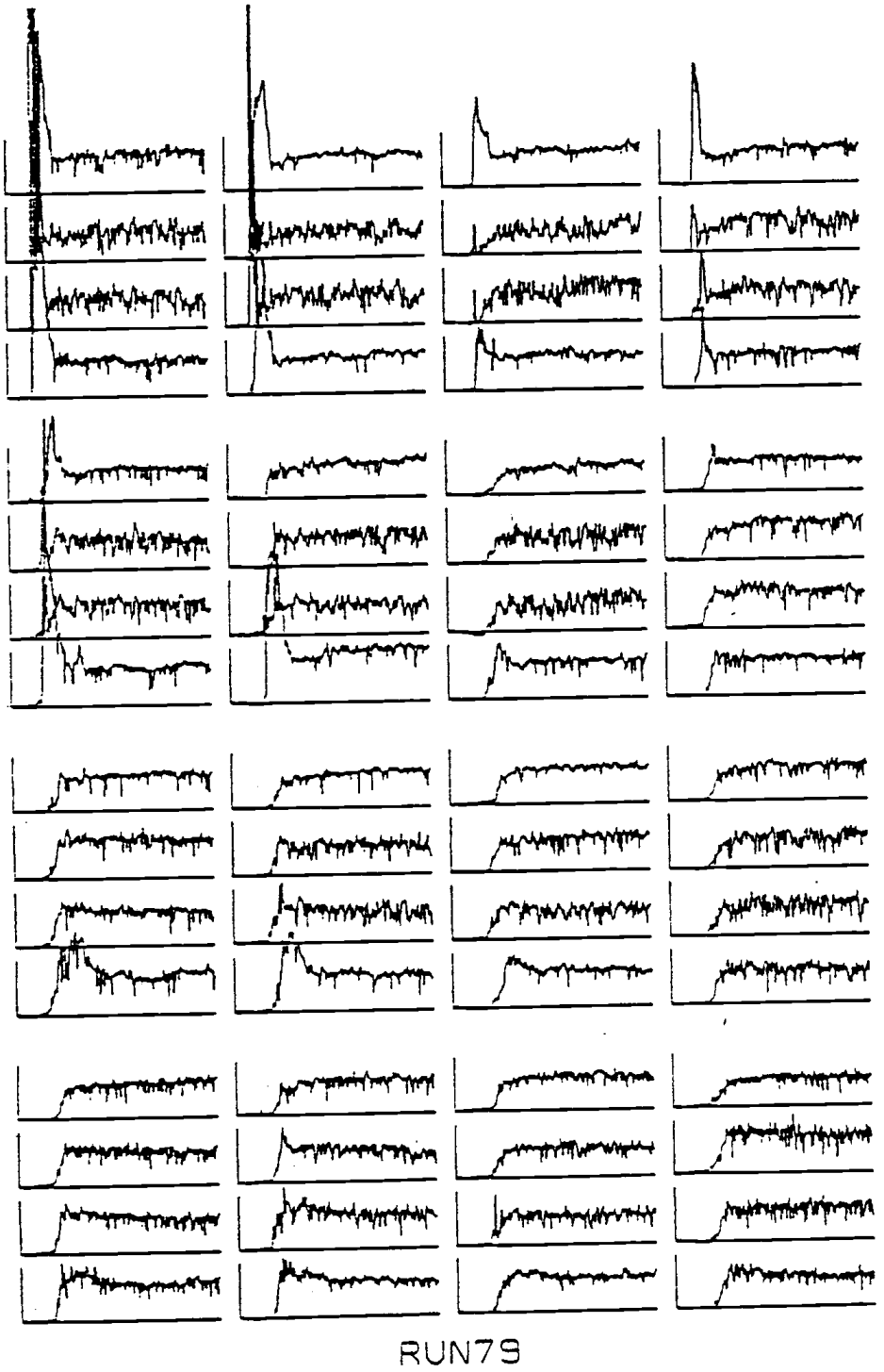

Figure 4.3. (Continued)

Run 80: .508 m (20"), 1134 kg (2500#), 2.13 m/s (7FPS), (see Run 65)

1. The time required for disappearance of clumps is approximately 17 seconds as can be seen on channel 10A.
2. Tracer moves across the tubes and drops down the wall in clumps. It disappears by the time the last row is reached.
3. Transport across the tubes appears faster than along the tubes.
4. It appears that movement down the sides of the bed is faster than into the interior for the first two rows of probes, but for the last two rows, tracer movement seems to be about the same. This observation helps substantiate the claim that tracer goes down the sides and up the middle or interior of the bed.

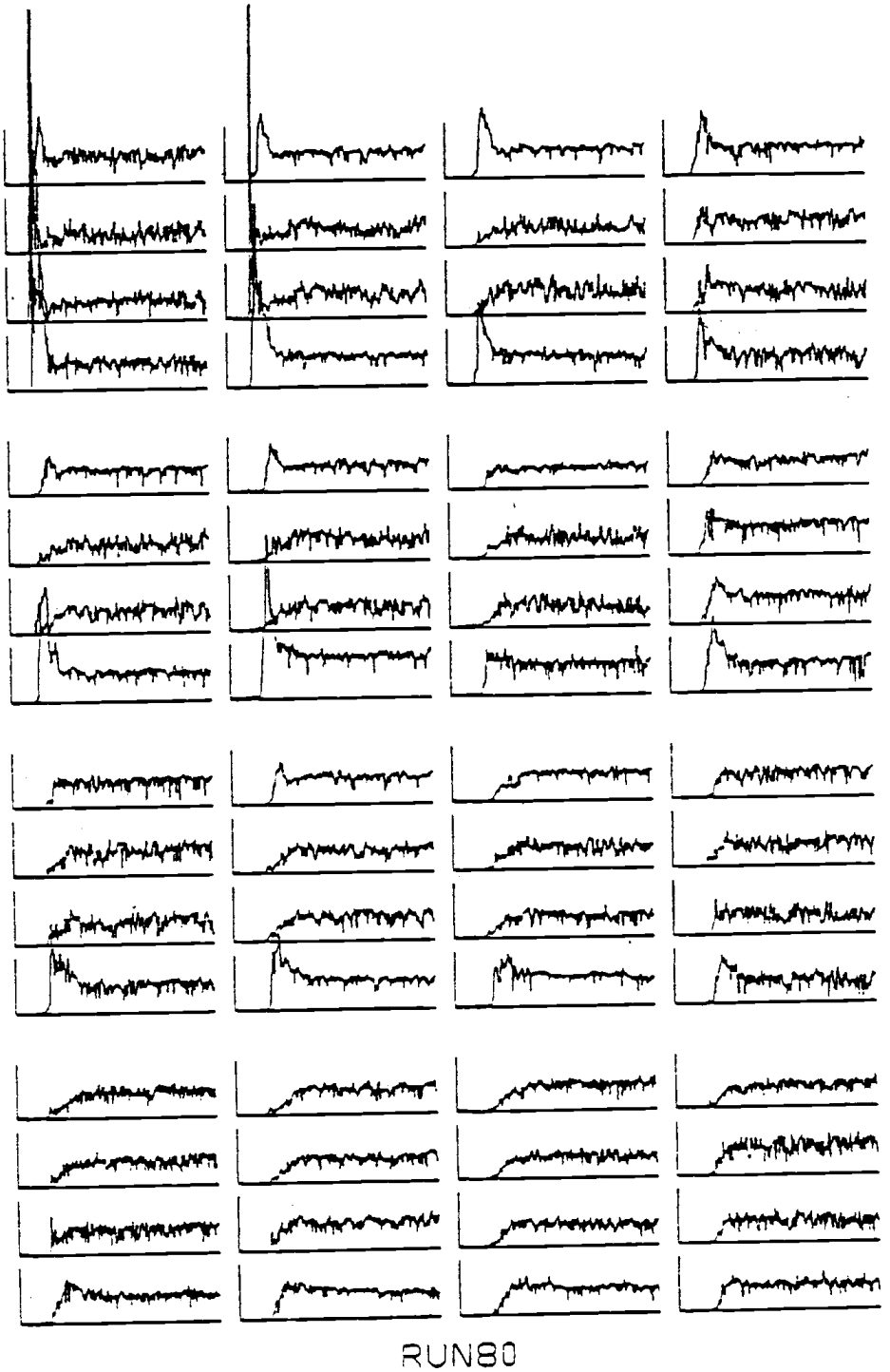

Figure 4.3. (Continued)

Run 81: .508 m (20"), 1134 kg (2500#), 2.74 m/s (9FPS), (see Run 67)

1. Much faster mixing occurs in this run compared to that at 7 FPS. The maximum amount of time for clumps to disperse is about 16 seconds (see channel 3D).
2. No peaks (or clumps) appear by the time the tracer reaches the third and fourth rows of probes.
3. Slow rise times, i.e. "approaches" to final concentrations, in channels A, B, C, D of tubes 13, 14, 15 and 16 indicate poor mixing in the bottom of the bed.
4. On the top row along the back wall (where the D channels are) crossflow lateral movement predominates.
5. Again it appears that tracer circulates down the walls and up the interior of the bed.
6. It appears that the tracer moves mostly down the right side of the diagram, that is, along tubes 4, 8, 12 and 16.

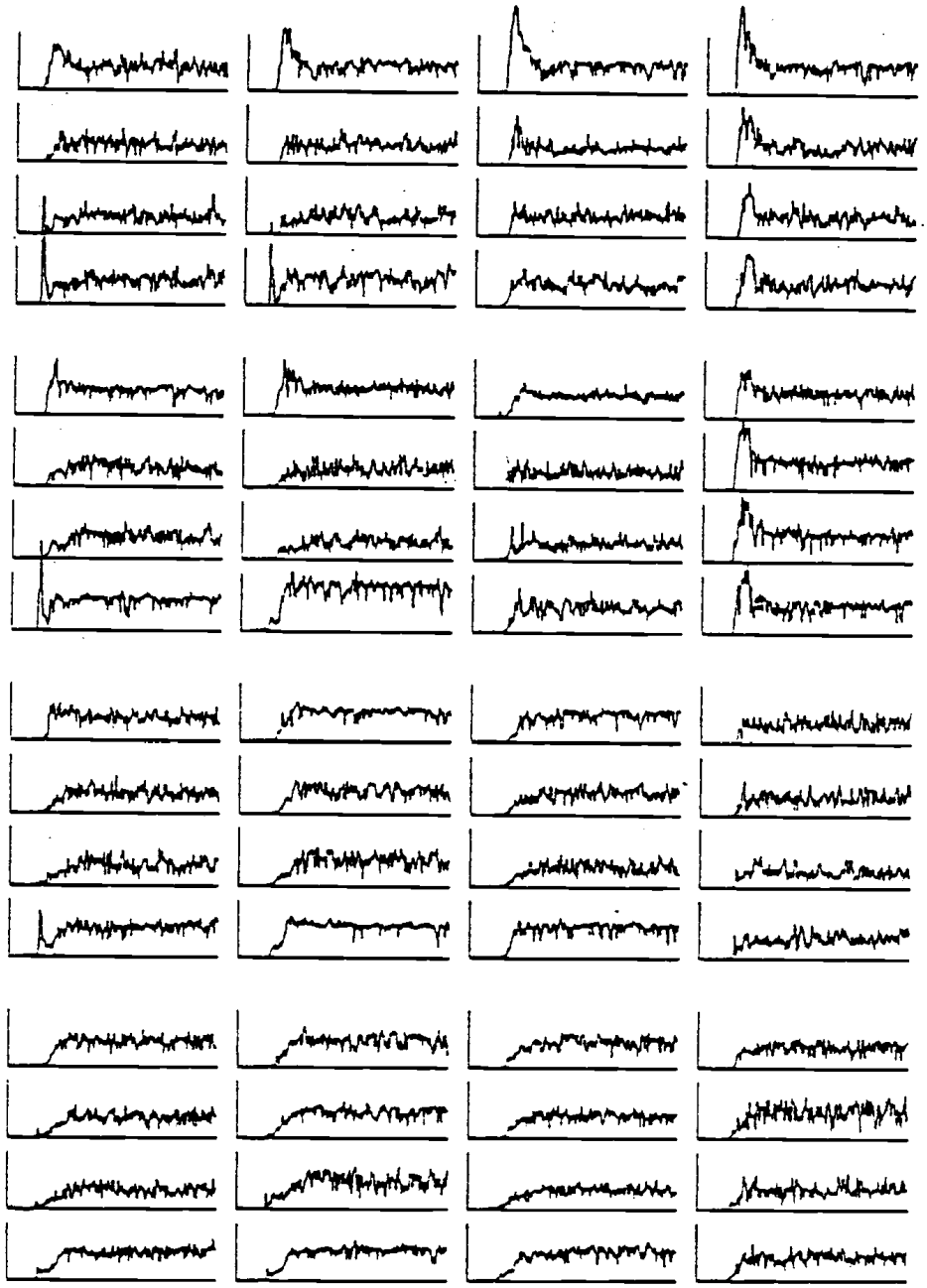

Figure 4.3. (Continued)

Run 82: .508 m (20"), 1134 kg (2500#), 3.35 m/s (11FPS), (see Runs 68 and 111)

1. The circulation of the tracer in this run is similar to that of Run 81, only faster.
2. The time of disappearance of the last clump of tracer is approximately 16 seconds (see channel 8A).
3. Comparison of the channels on tubes 8 and 7 indicate that the tracer is moving down the side and up the middle or interior of the bed.
4. The tracer appears to be well mixed across the top of the bed at the beginning of the run. The only persistent clump, as previously mentioned, is 8A.

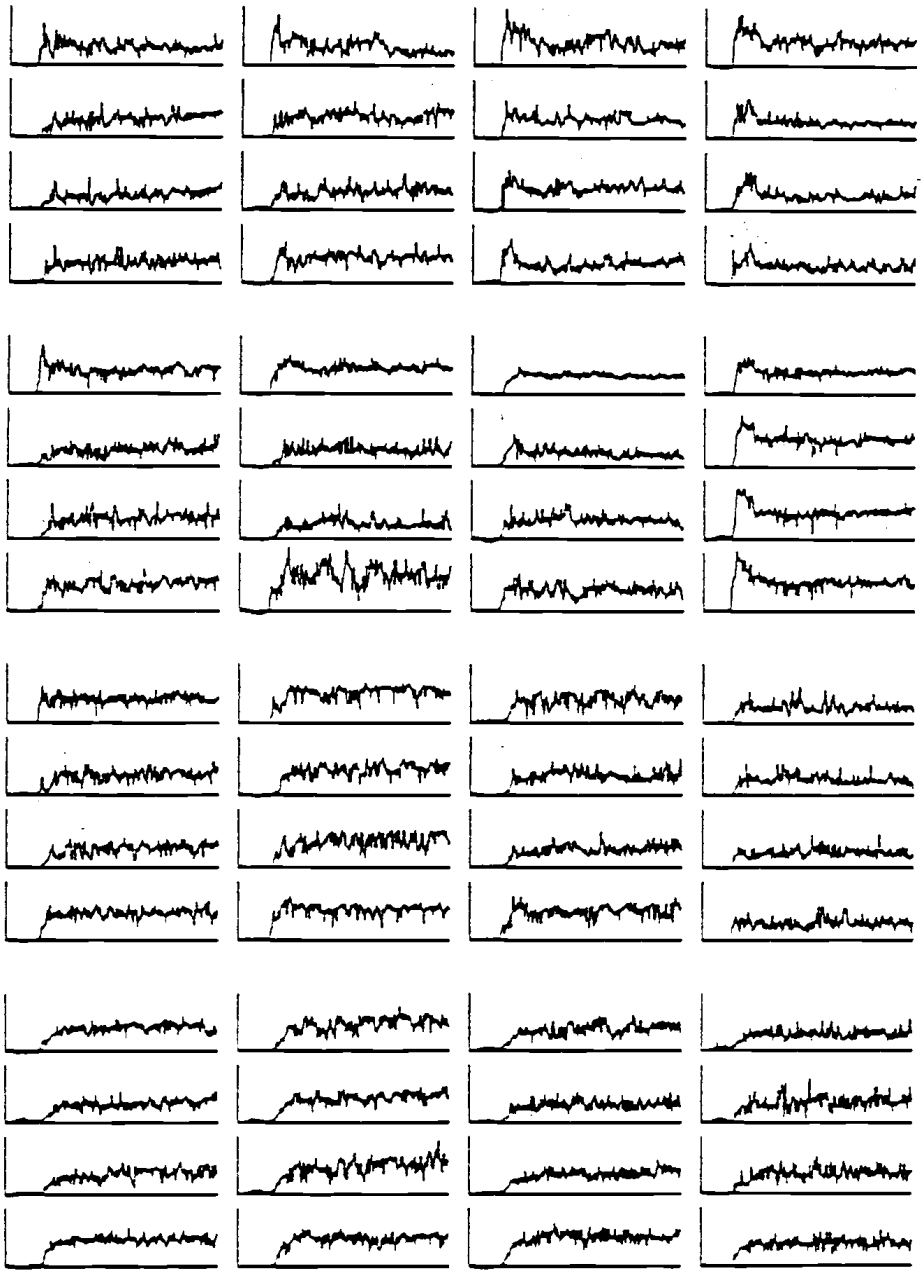

Figure 4.3. (Continued)

Run 83: .508 m (20"), 1361 kg (3000#), 1.52 m/s (5FPS), (see Runs 64 and 112)

1. The time for dispersion of the last clump of tracer is approximately 20 seconds as can be seen in channels 5A and 9A.
2. The tracer seems to move along the tubes while above the probes. Then, it mostly comes down the "A" side of the bed. Observe the peaks in channels 1A, 2A, 5A, 6A, 9A.
3. Except for the lag time the interior concentrations remain fairly constant from the time of initial sensing of tracer throughout the run. By looking at these lag times, we see that about 30 seconds are required for complete mixing of the tracer from the time of its injection.
4. Again, observe the enhanced dilution effect at the top of the bed as a result of a large inventory of sand. For a comparison, see runs 76 and 79.
5. Lateral mixing at the top of the bed appears relatively slow (channel 2A versus 3C).
6. The wall region appears to be mixing slowly with long rise times. The smooth tracer curves indicate that few bubbles exist near these probes as compared to the jagged tracer curves in the interior of the bed (see channels 7C and D).
7. Corner flow seems accentuated in this run. Channels 1A, 5A, 9A verify this.

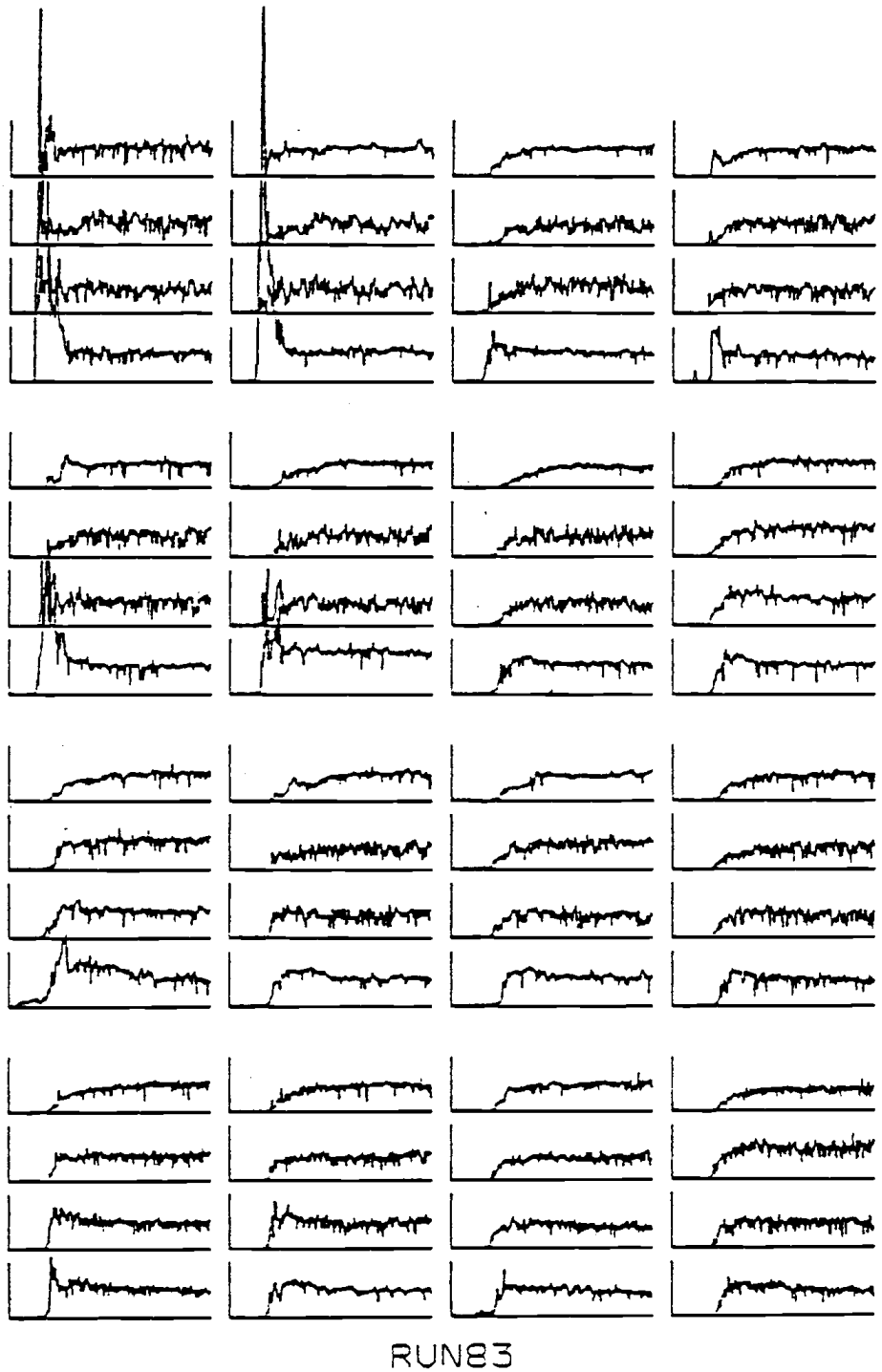

Figure 4.3. (Continued)

Run 84: .508 m (20"), 1361 kg (3000#), 2.13 m/s (7FPS), (see Run 63)

1. The clump disappearance time is about 5 seconds. This means that the rate of mixing at 7 FPS is about twice the rate of mixing at 5 FPS.
2. Dilution in this bed occurs even above the array as the lack of clumps or peaks indicates.
3. It takes about 15 to 20 seconds for the concentration along the back wall to reach equilibrium (see probes 9B, D, 11D, 14D, 15D).
4. The tracer appears to move around the sides (see Channels 1A, B, C, D, 2A, D, 3A, D, and 4A, B, C, D), then down all the walls and up the middle or center of the bed.
5. All tracer appears to be well mixed by the time it reaches the second row of probes from the top.
6. At the top of the bed the tracer moves more rapidly along tube 1 than against probes (1D, 2D, 3D, and 4D). It then increases in rate of movement along tube 4, which is adjacent to the wall.
7. Mixing appears slower at the bottom of the bed as evidenced by long rise times. Thus, the overall mixing time is affected by these lower channels.

Run 84: continued

8. Channels 1A and 5A show the tendency of the tracer to move rapidly down the corner.

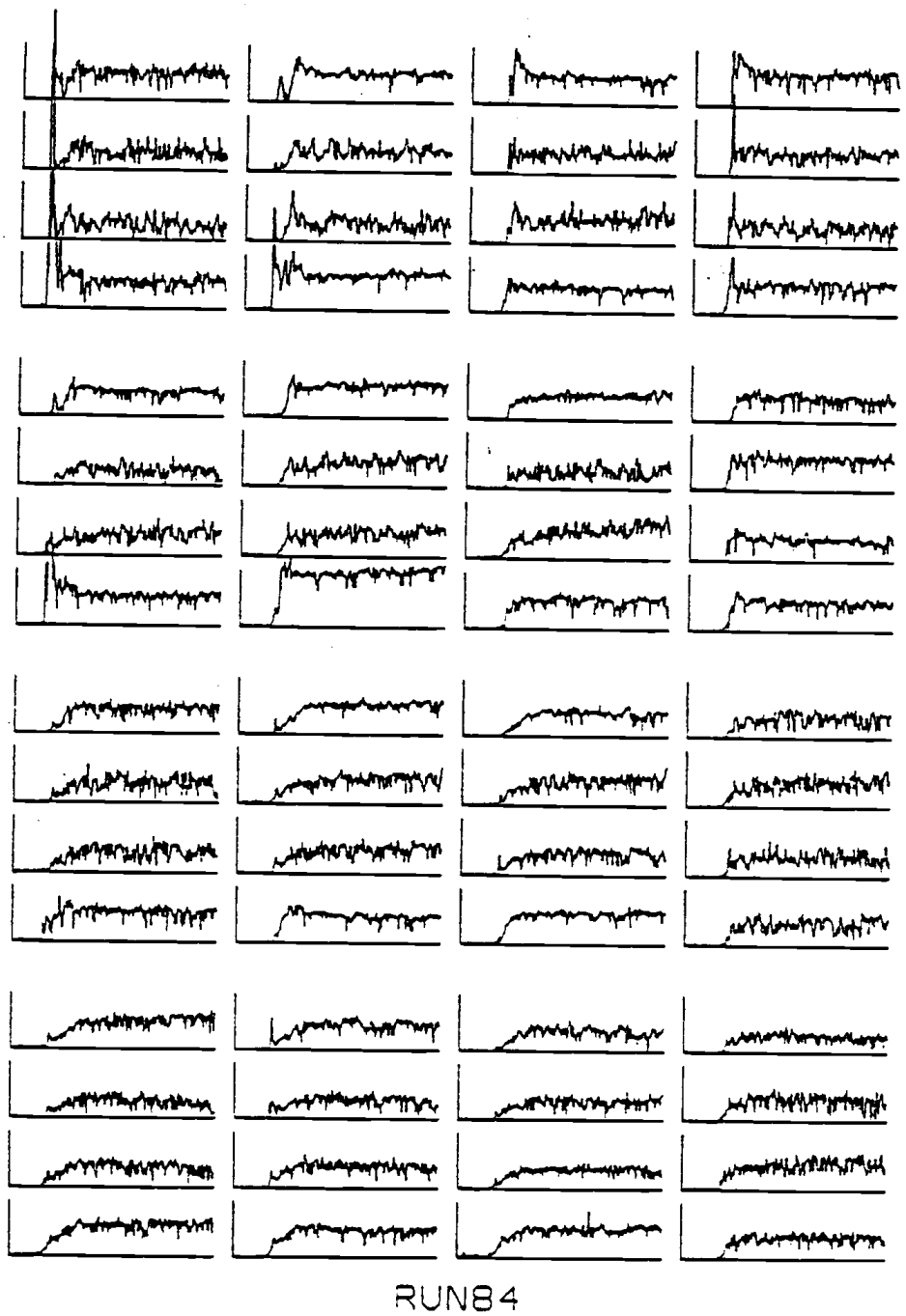

Figure 4.3. (Continued)

Run 85: .508 m (20"), 1361 kg (3000#), 2.74 m/s (9FPS), (see Run 62)

1. The time for disappearance of clumps is about 7 seconds. See channel 6A. Also notice that mixing in the bottom takes about 10 to 15 seconds as shown by the rise times on these lower channels.
2. Again, the tracer circulates along the walls in the bed. The solids prefer the wall regions and corner regions of the bed, whereas the bubbles concentrate in the interior of the bed.
3. The tracer is well mixed by the time it reaches the third row of probes. Mixing seems faster with the larger inventory of sand (3000#) as compared to smaller inventories in Runs 78 and 81.
4. Tracer is well mixed within a few seconds across the top of the bed. The variations in concentrations at the top disappear in about seven seconds (see Channels 5A, 6A, 8A).

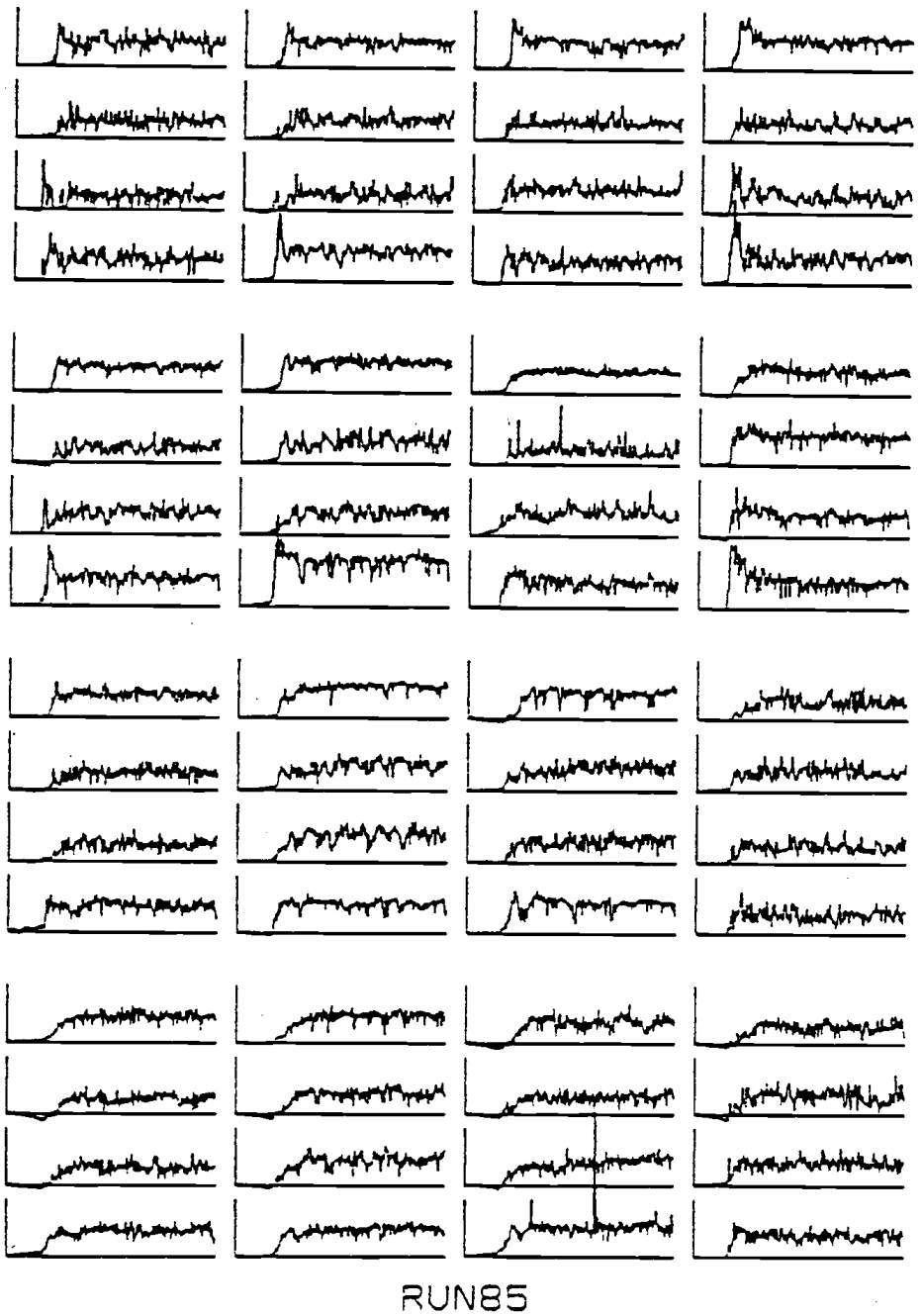

Figure 4.3. (Continued)

Run 86: .508 m (20"), 1361 kg (3000#), 3.35 m/s (11FPS), (see Run 61)

1. Mixing is very rapid here (see channel 7C, an obvious glitch).
2. The only peaks occur in channels 4A, C, D, and 8B, C, D along the wall, so the tracer moves in clumps down this wall.
3. The channels in tubes 9, 10, 11 and 12 indicate that considerable voidage exists in the bottom of the bed.
4. The clumps near 8A and B persist longer than those at 9 FPS. However, mixing in the bottom of the bed is faster, with a rise time of approximately 7 seconds.

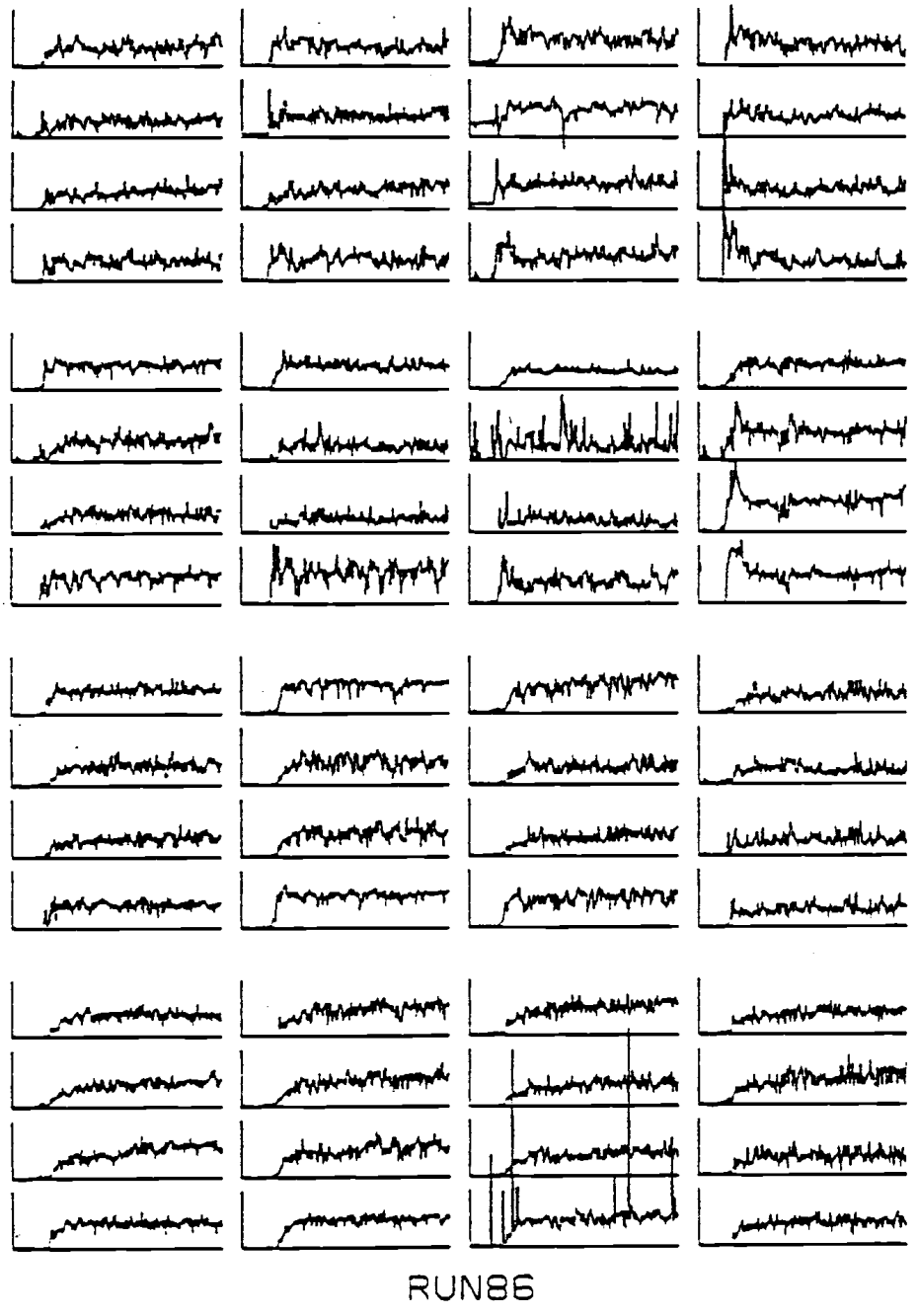

Figure 4.3. (Continued)

Run 87: .508 m (20"), 907 kg (2000#), .30 m/s (1FPS), EI70 sand (d_p 0.17 mm (.0068 in))

1. This is one of three runs down with fine sand nd the results differ dramatically from those of EI-16 sand. The tracer moves in clumps for quite awhile due to the low velocity required to keep EI-70 sand from elutriating.
2. In the top row of the tubes, channels 1B, C and 2B, C seem to reach a uniform concentration level about one-half the value of the lower rows of probes. Also, observe that the rest of the top probes register zero concentration levels. Evidently, low bed expansion at this reduced superficial gas velocity is responsible for the top row of tubes being out of the bed and in the freeboard. The unusual concentrations observed on channels 1B, C and 2B and C must be the result of lee stack.
3. There exist especially sharp peaks (or large clumps of tracer) in the following channels: 5A, B, C, D, 6A, B, C, 7C, 11C, 9C.
4. Apparently, the tracer prefers to move down the "1, 5, 9, 13" tube side of the bed, i.e. the front of the bed.

Run 87: continued

5. Smaller bubbles in the bed seem to cause the reduced bed expansion observed. This is the reason that the top row of tubes is in the freeboard. Also, note that at all points in the the bed few bubbles persist for more than a half second. Data was smoothed with a peak following filter over half-second intervals. Therefore, the relative infrequency of dropouts indicates that either bubbles were small (could not envelope a probe) or few.

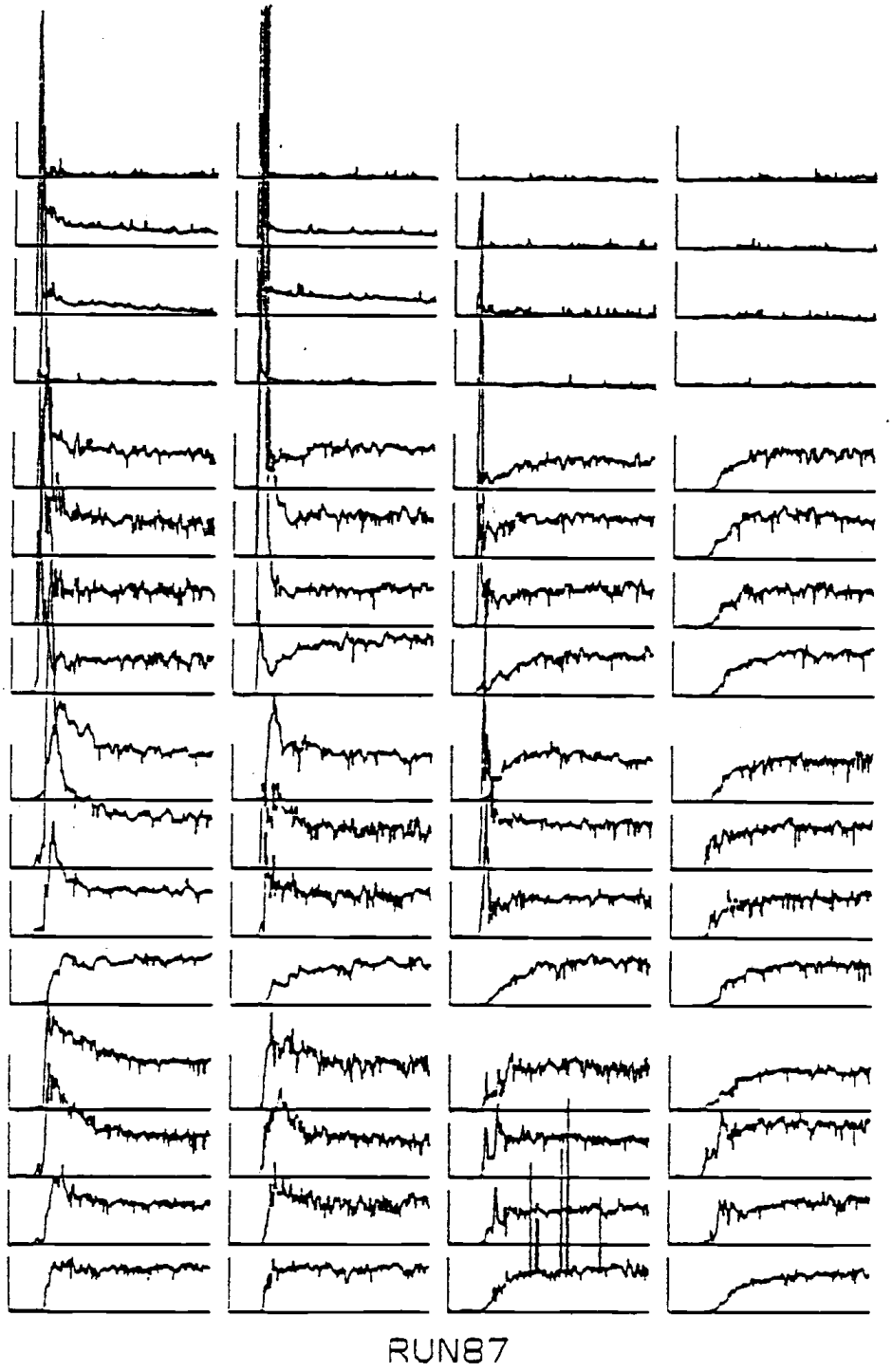

Figure 4.3. (Continued)

Run 88: .254 m (10"), 1361 kg (3000#), 1.52 m/s (5FPS), (see Run 57)

1. Since the array has been lowered to 10 inches, the top two rows of tubes (probes) look very similar to the lower rows of the array at the 20-inch position above the distributor, i.e., both exhibit an absence of clumps or peaks.
2. Strangely enough, the bottom two rows show clumping or accumulation (poor mixing) of tracer. This clumping occurs mostly along the wall and a slight bit in the interior probes. Check channels: 9A, B, 13A, B, 10A, D, 14A, B. The peculiar spike in 9B and 13B is probably tracer that slid down the wall outside the range of detection of the probes.
3. The time for clumps to disperse is approximately 15 seconds as seen in channel 9A. The time for the bed to reach uniformity is somewhere between 20 and 30 seconds (see channel 16A).
4. The whole right side of the diagram appears well mixed. Therefore, good lateral mixing exists across the tubes and up the center of the bed.
5. Mixing at the bottom of the bed is sluggish compared to the top. Comparison of time constants or rise times and corresponding driving forces will verify this fact. In addition, the peaks on the left side of the diagram versus the slow rise

Run 88: continued

times, especially at the bottom, show bad mixing. Compare channels 16A and 4A.

6. Lateral mixing is much slower at the bottom of the bed. Again, compare rise times at the top and bottom.
7. The absence of bubbles in tubes 1, 5, 9 indicate a dense phase of the downflowing material.

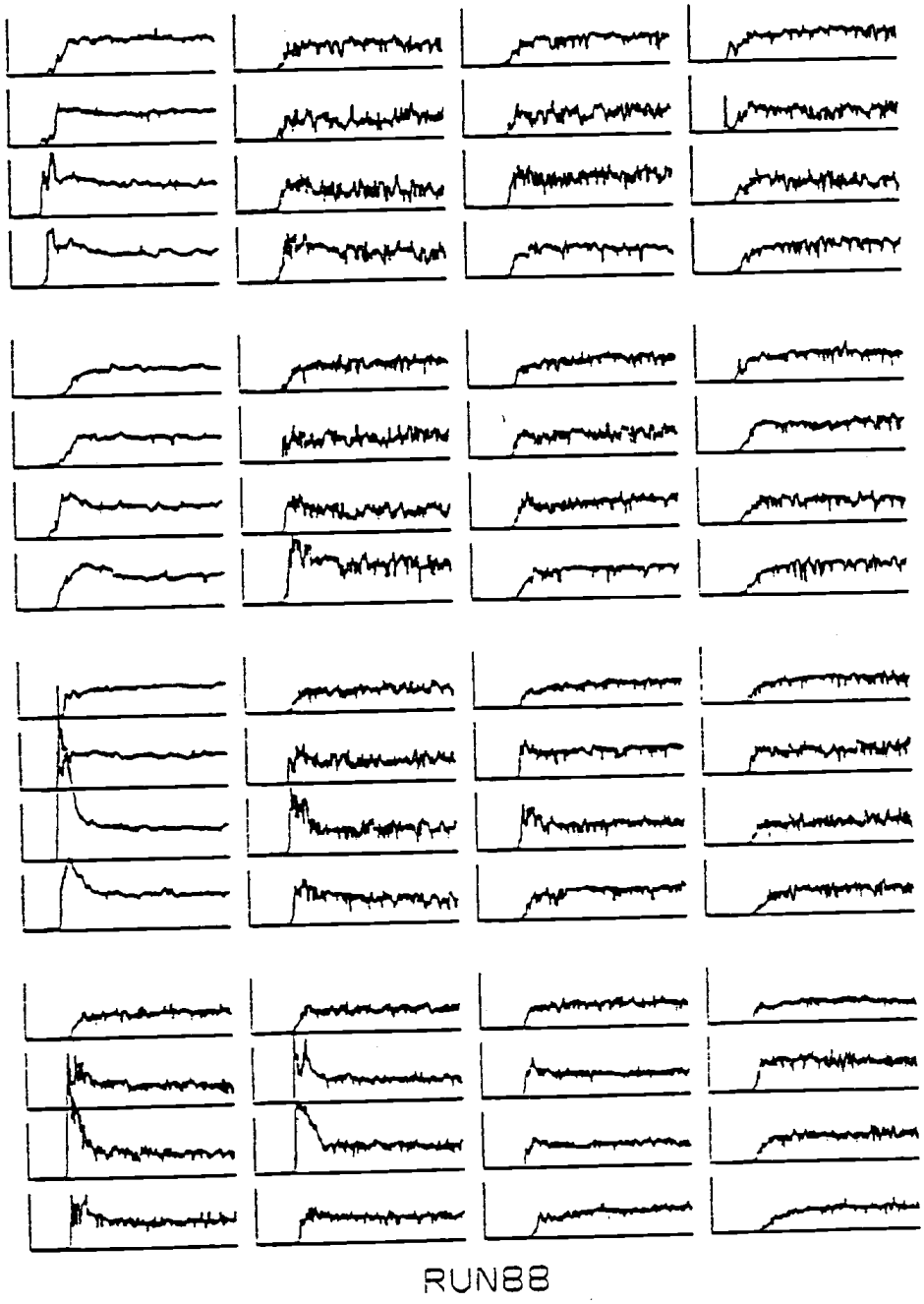

Figure 4.3. (Continued)

Run 89: .254 m (10"), 1361 kg (3000#), 2.13 m/s (7FPS), (see Run 58)

1. The tracer appears to be well mixed by the time it reaches the tube array.
2. The maximum rise time is about 20 seconds as shown by channels 16A, 15A, B, 10A, D. Therefore the overall mixing time is also about 20 seconds at the walls.
3. This mixing is vastly better than that found in Runs 75, 80, and 84 (which were all at the same gas velocity). The greater bed inventory and lower height of the array are responsible for this. The peaks disappear faster, but the rise time on the bottom is about the same.
4. Bubbles seem fairly well dispersed at the bottom of the bed. The channels on tube 9 indicate a dense phase in this region. Otherwise the rest of the bed has more or less uniform voidage.
5. Mixing is sluggish at the bottom of the bed. Also, mixing is slower on the sides than in the middle of the bed as can be shown by comparison of rise times (see channels 11B, C and 12B, C).

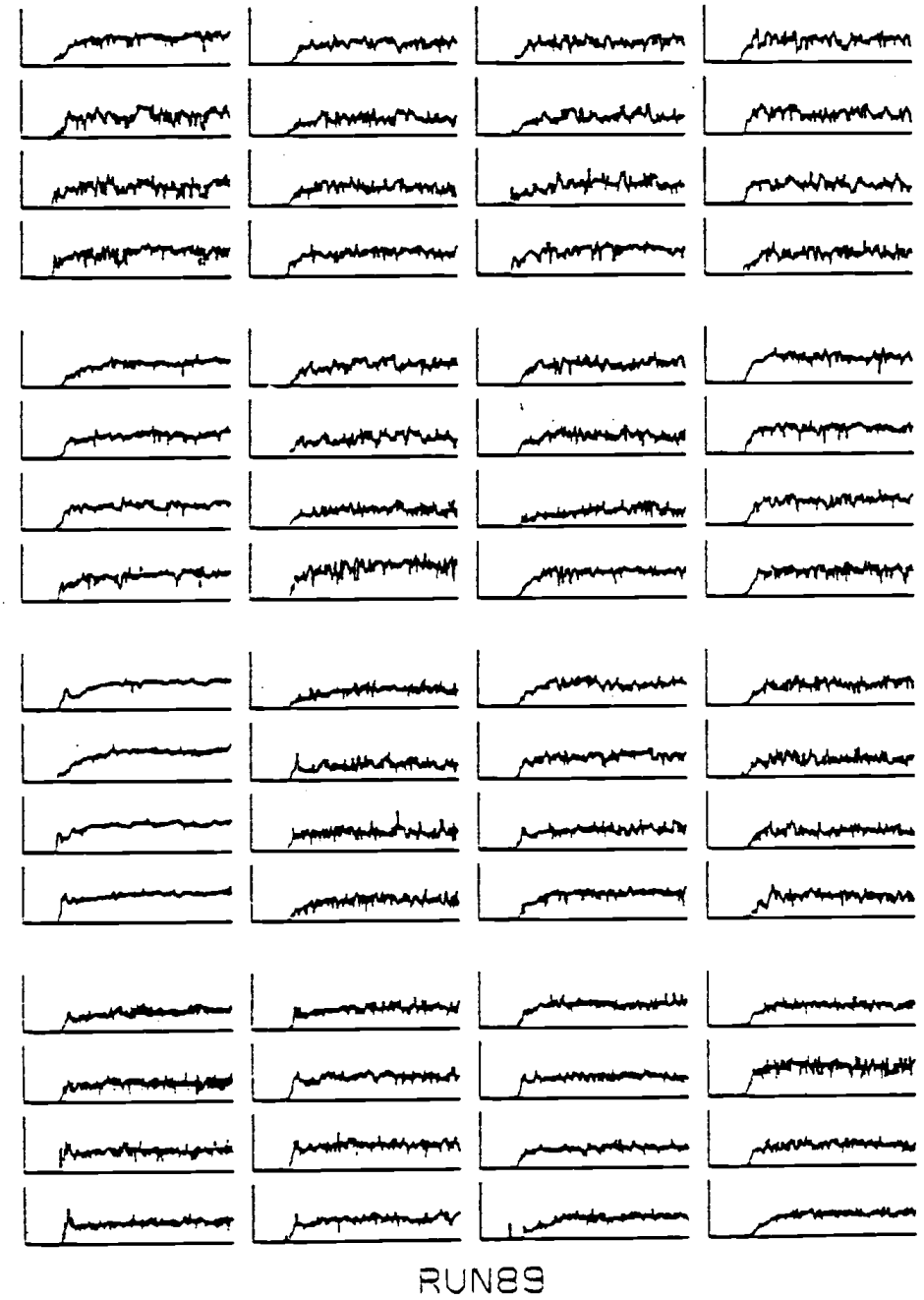

Figure 4.3. (Continued)

Run 90: .254 m (10"), 1361 kg (3000#), 2.74 m/s (9FPS), (see Run 59)

1. Clump disappearance time is about 13 seconds as seen from channels 8A and B.
2. The rise times of the interior and lower channels are relatively short compared to the clump disappearance time given above. The only ones with significant lag are 11B and D, 10B, C, D, 9A, B, C, D.
3. Tracer is fairly well mixed, although some has moved across the tubes and down the right side quickly enough to cause a couple of peaks.
4. Again, greater inventory has resulted in better mixing as compared to other runs at the same gas velocity (Runs 78, 81, 85).
5. It appears that bubbles move mostly in the center of the bed (see channels B and C on tubes 2, 3, 6, 7, 10, 11, 14 and 15) and along the left side (tbues 1, 5, 13). For some reason the regions around tubes 8 and 9 are more dense than others.

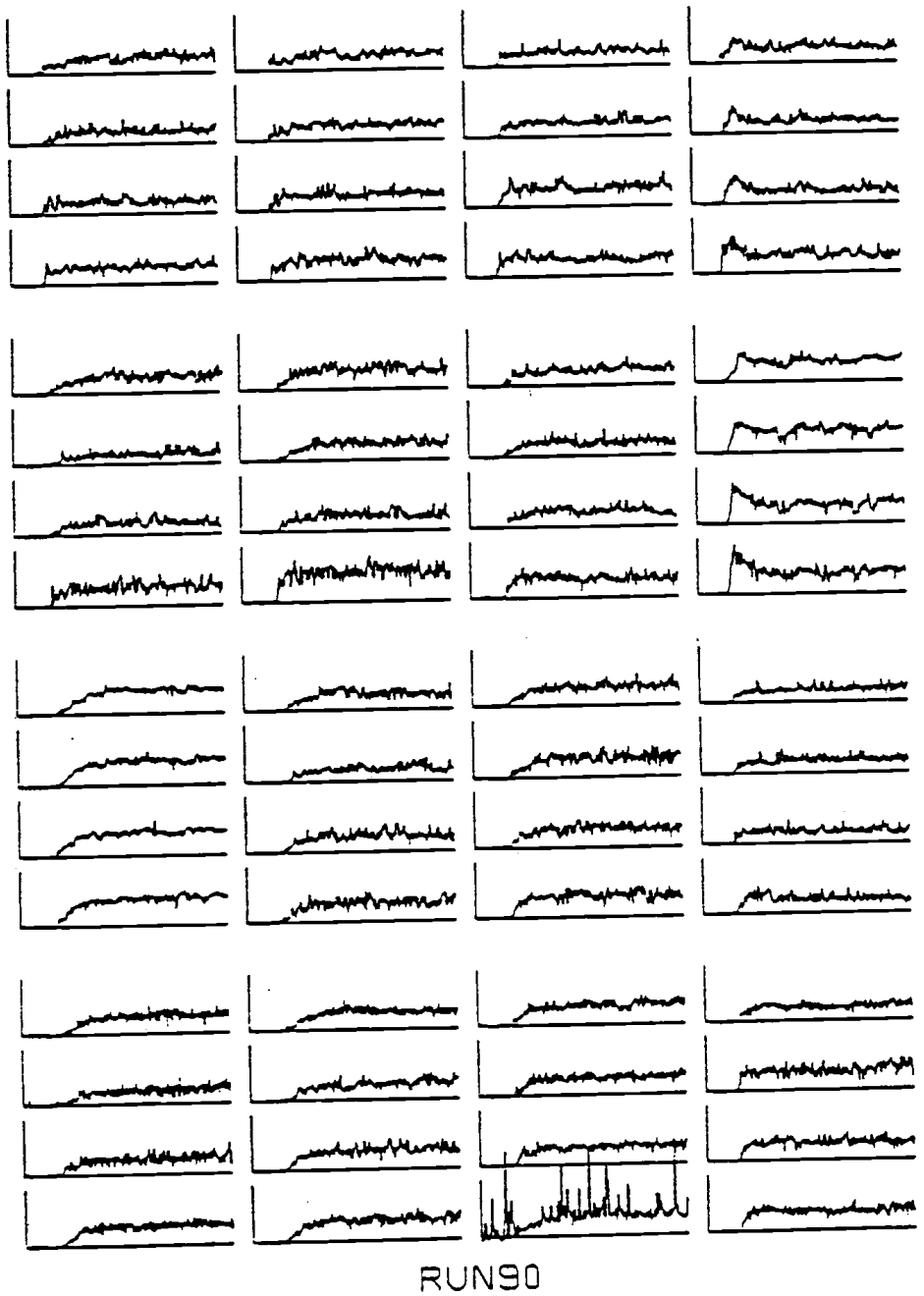

Figure 4.3. (Continued)

Run 91: .254 m (10"), 1361 kg (3000#), 3.35 m/s (11FPS), (see Run 60)

1. The peaks are sharper than those in run 90 and therefore the clump disappearance time is slightly less. Compare channels 4A and B.
2. The rise time is a bit faster at 11 FPS. See channels 16A, B and C in run 90 and compare with run 91.
3. Run 86 (3000#, 20", 11 FPS) shows much worse mixing, which retlects the fact that the array is 10" deeper in the bed. Compare tubes at the same height.
4. It appears that bubbles move mostly in the center of the bed and along the left side. For some reason the regions around tubes 8 and 9 are more dense with solids than others.
5. Channel 12 shows a low concentration but little fluctuation which possibly indicates that the solids are flowing constantly over the tube, but the tube is not immersed in the solids.

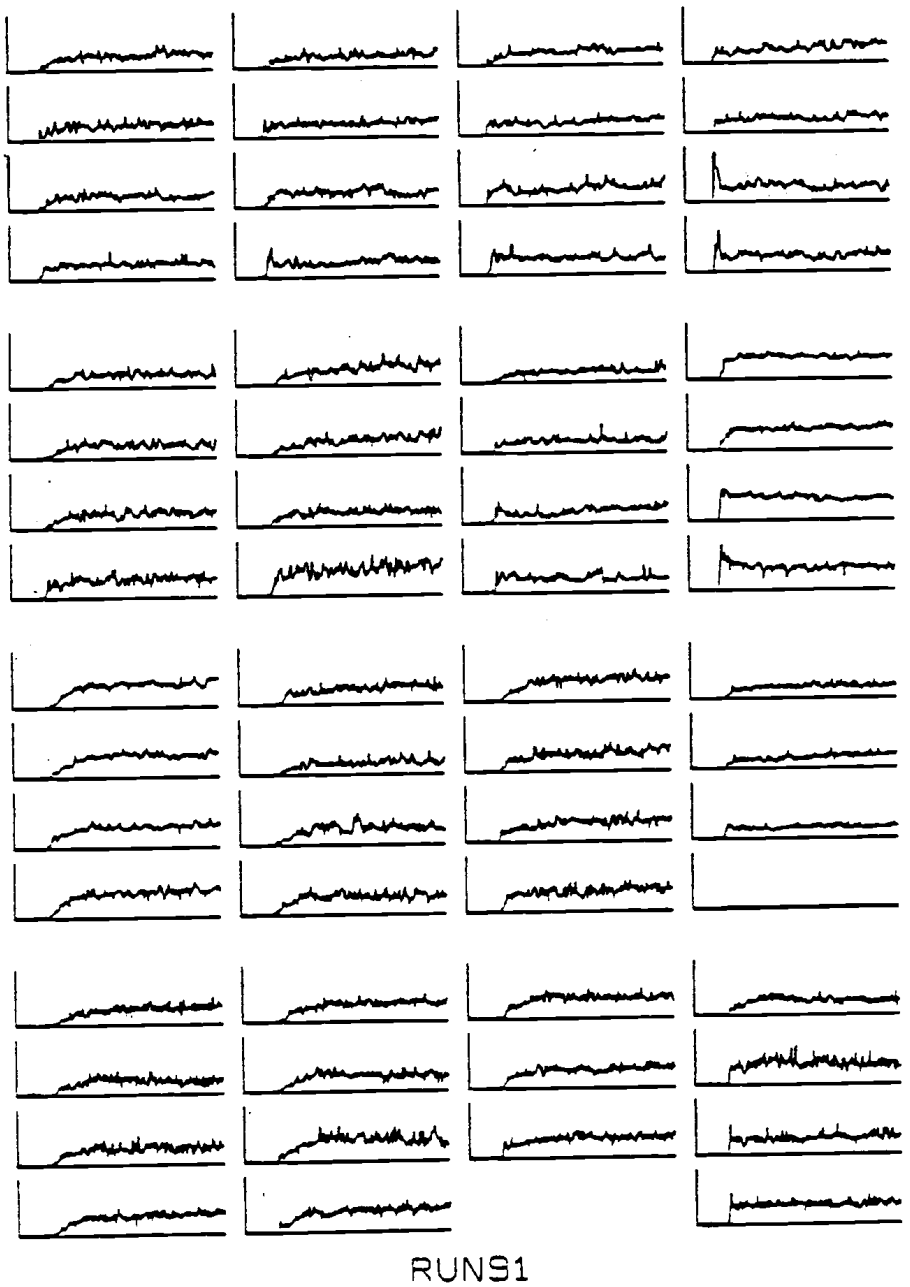

Figure 4.3. (Continued)

Run 102: .254 m (10"), 1134 kg (2500#), 1.52 m/s (5FPS), (see Run 92)

1. Clump disappearance time is approximately 20 seconds (channel 9B).
2. Overall mixing time (rise times are quite fast), is approximately 15 to 20 seconds (see channel 16D).
3. Mixing seems fairly rapid, except for a clump of tracer that slipped down along the wall and avoided detection (at tube 5) until it reached channel 9C.
4. Bubbles prefer to move upward through the center and to a lesser extent along the walls. Tubes 1, 5 and 9 indicate a lack of bubbles or a dense phase.
5. Tracer appears to come down the left side and then it sweeps back up the center. Follow Channels 1B, C, 2A, 9B, C, 13B, C, 14B, C, 15B, C, 10B, C, 11B, C on upward.
6. 3000# (Run 88) gives better results. Peaks disappear quicker.

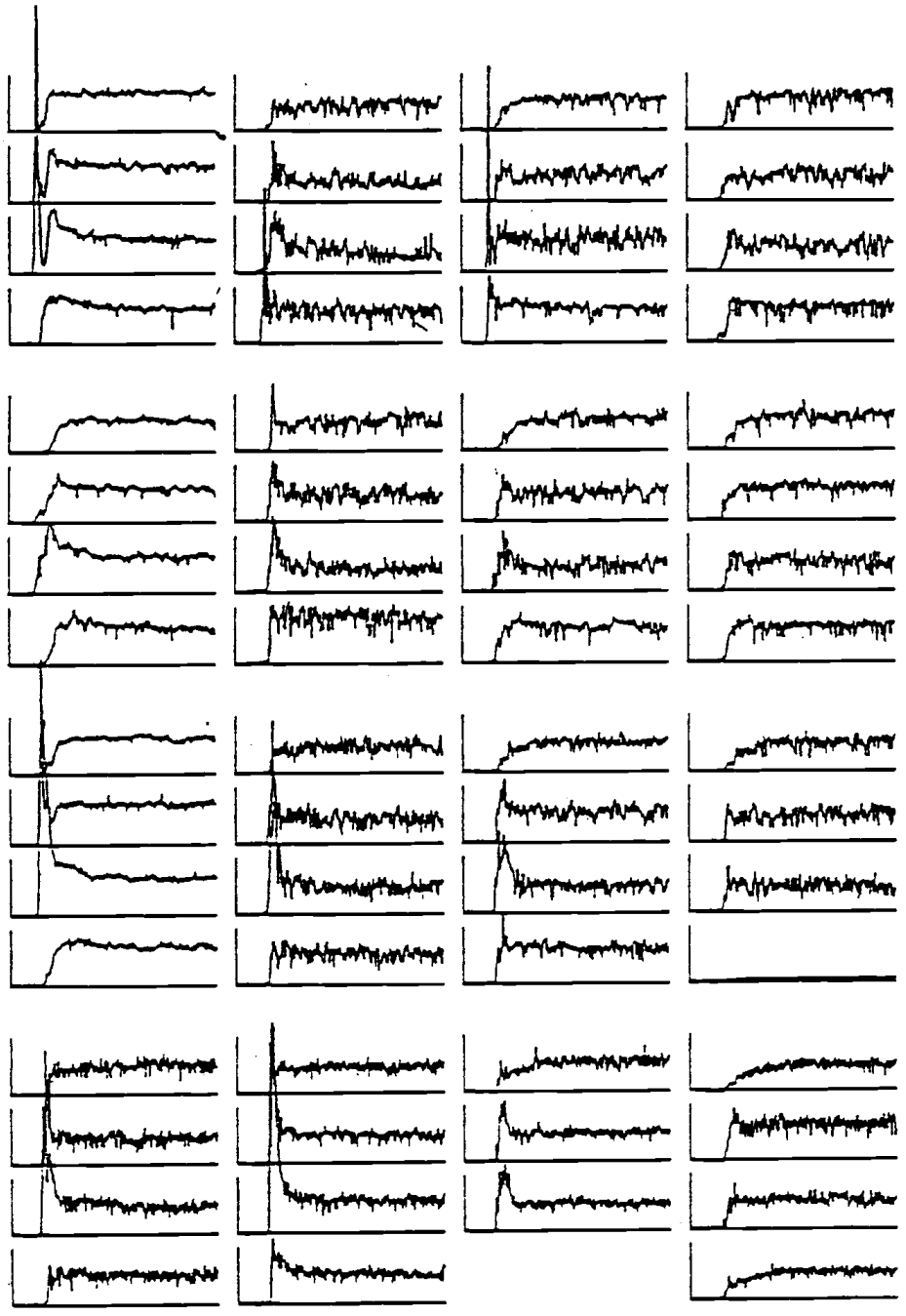

Figure 4.3. (Continued)

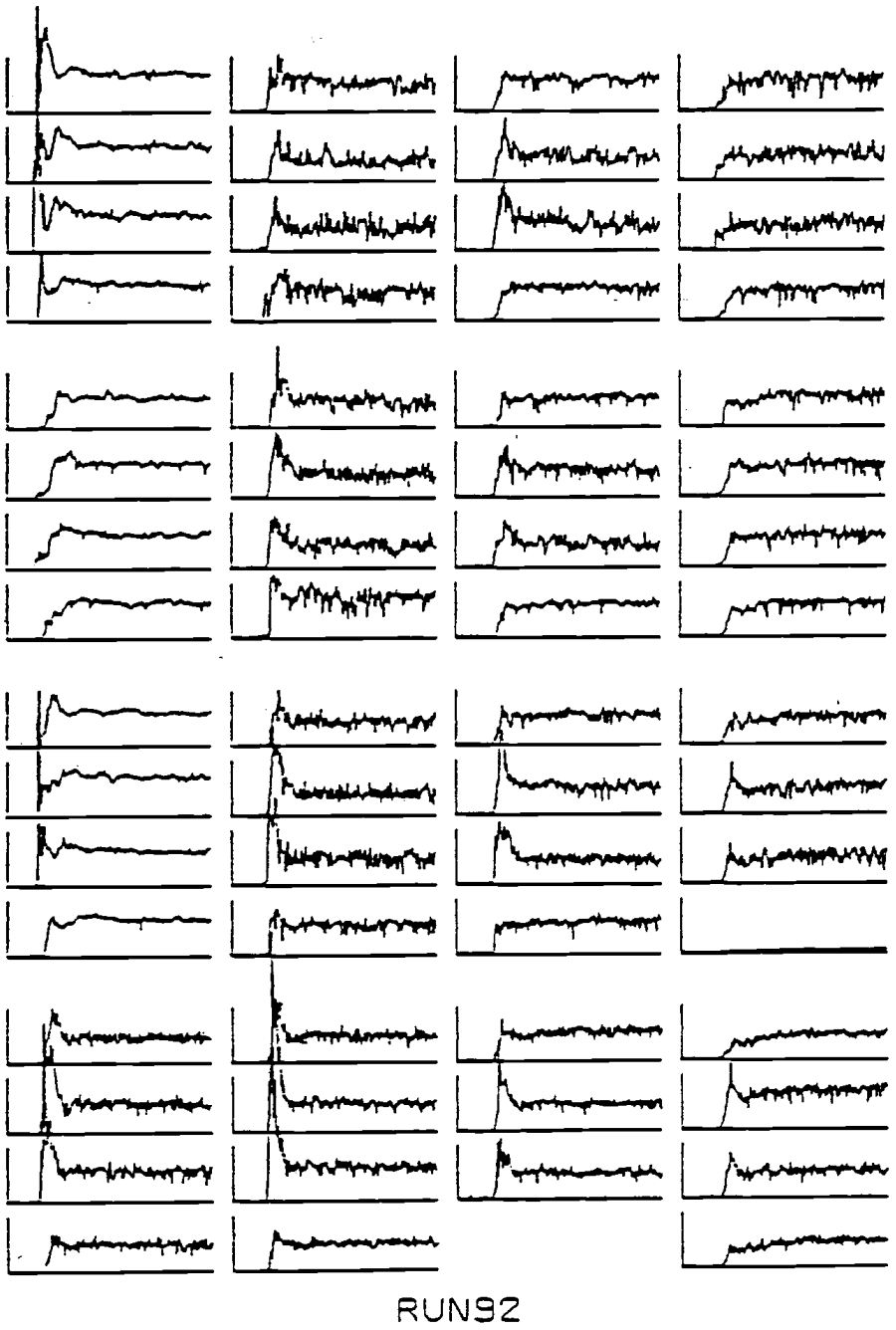

Figure 4.3. (Continued)

Run 103: .254 m (10"), 1134 kg (2500#), 2.13 m/s (7FPS), (see Run 93)

1. A great deal of improvement has been attained over run 102. Virtually all peaks have been eliminated with the exception of one registering in channel 9B (which has a disappearance time of about 5-7 seconds).
2. It appears that the rise times may be longer than those in run 102. For example, compare any of the channels in the right hand column (where this etfect seems most pronounced). Overall mixing occurs about 10 seconds after introduction of tracer to the bed (see channels 8B, 16C).
3. As can be seen from the rise times in the curves, the tracer circulates down the sides adjacent to the injection port and up the center. Pay special attention to the rise times as the tracer moves up the center (i.e., 14B, C, 15B, C, 10B, C, 11B, C, 6B, C, 7B, C, 3B, C). Tracer is hardly detected at the intermediate levels. The tracer also migrates down the other sides and corners of the bed, but after a slight time lag.
4. Notable gains in mixing are achieved as a result of increased bed inventory. Compare this run with run 107.

Run 103: continued

5. Bubbles seem to move mainly in the center regions. Bubble movement is retarded quite a bit along the wall adjacent to tube 9, which indicates a dense solid phase.

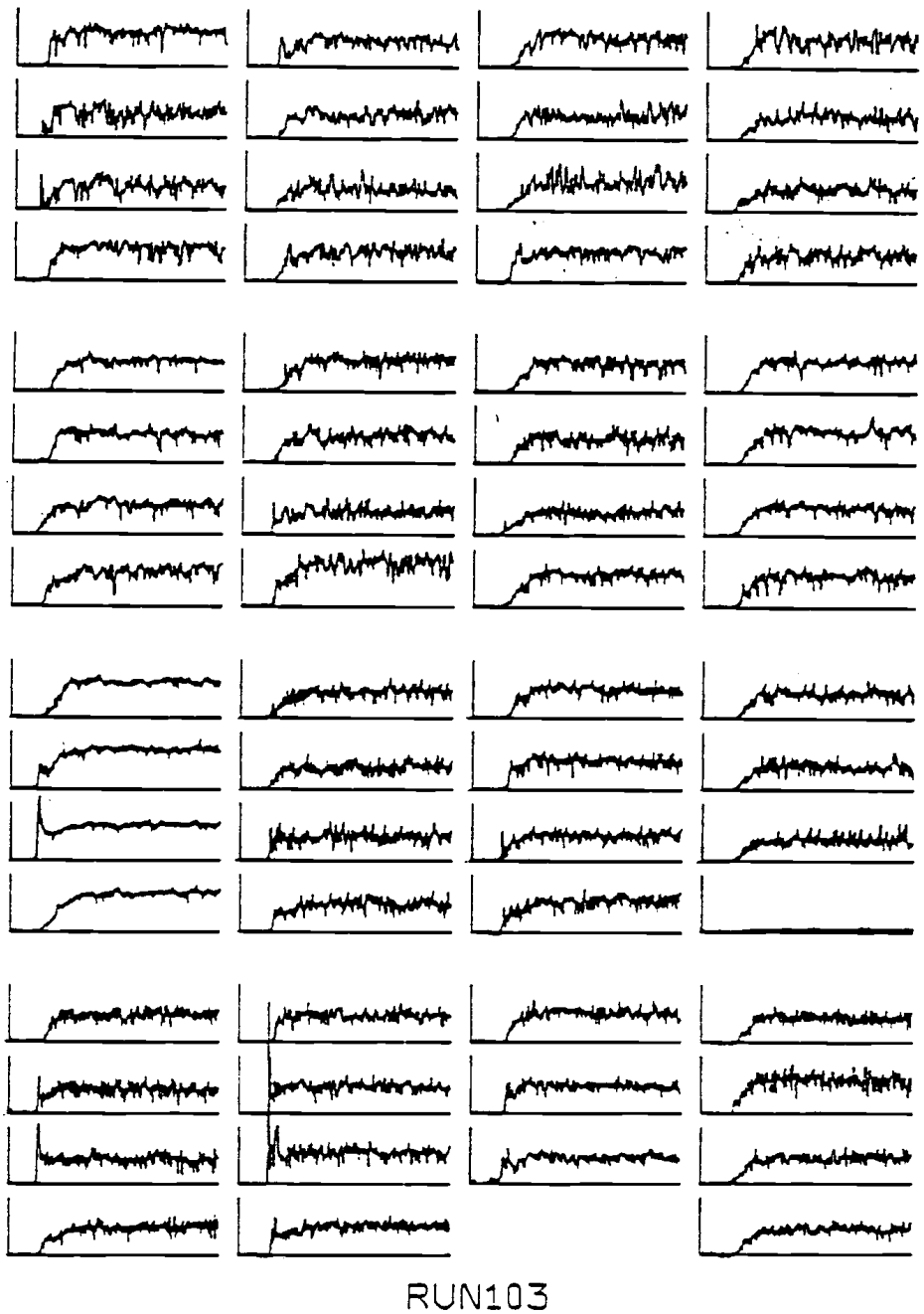

Figure 4.3. (Continued)

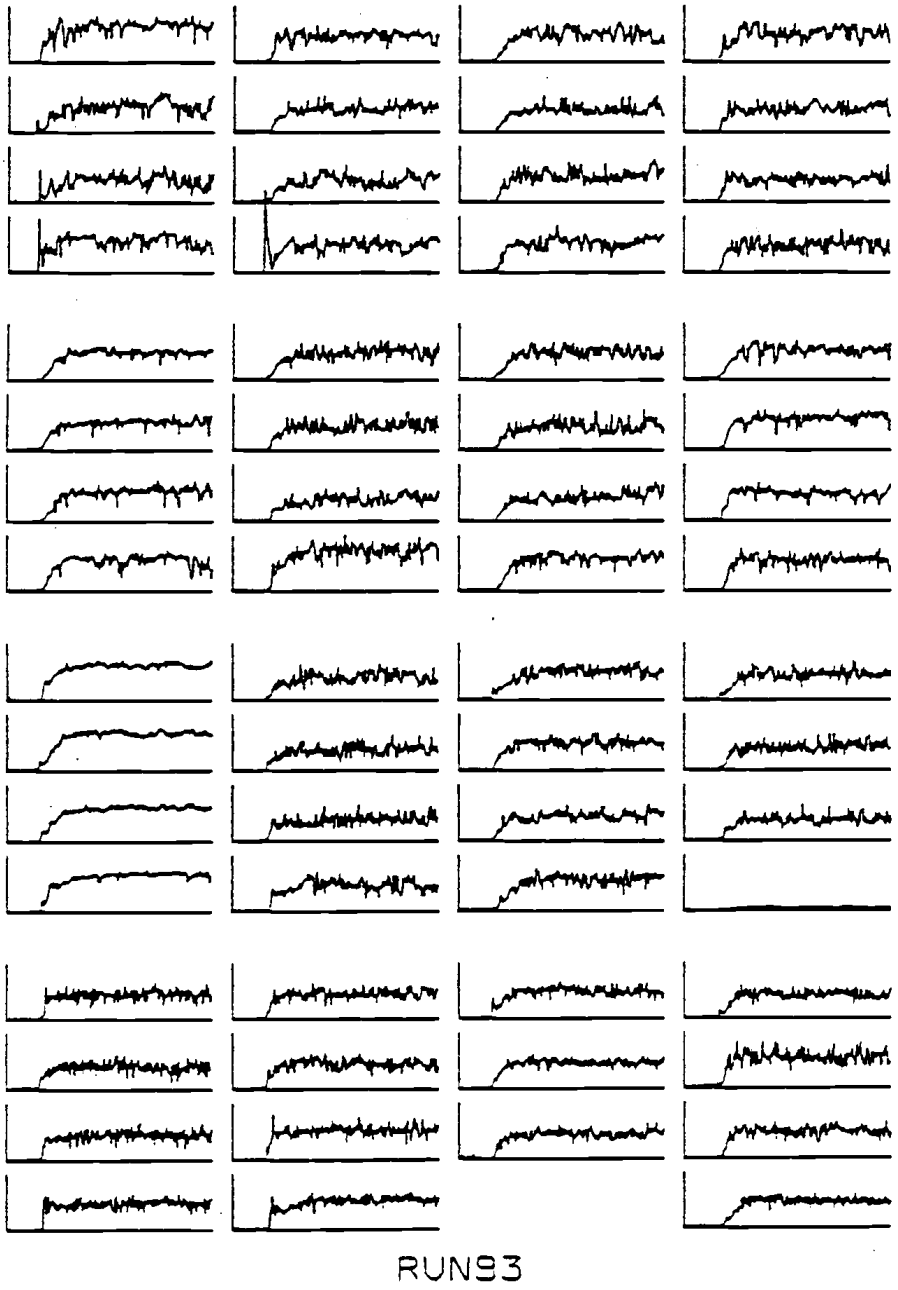

Figure 4.3. (Continued)

Run 104: .254 m (10"), 1134 kg (2500#), 2.74 m/s (9FPS)

1. At this velocity, tracer seems to clump along the right side of the bed. About 10 seconds of mixing is sufficient to eliminate all clumps. The persistent clumps are seen on channels 8A, B, C and D. Mixing is not as good as at 7 FPS.
2. The rise times on the left side of the bed (or diagram) are significantly longer than those on the right side and even some of those in the interior. Compare the interior channels 10B and C with wall channels 9B and C. The maximum rise time is about 15 to 20 seconds as channel 13C indicates. Therefore, the overall mixing time is controlled by the rise time.
3. A clump of tracer moves down the right side of the bed.
4. Overall mixing is still good under these conditions. But a reduced bed inventory would not be that much worse. Compare this with run 108 (10", 2000#, 9 FPS). Mixing along the bottom in run 108 is faster.
5. Bubbles are concentrated in the bottom and interior of the bed. Along the left wall, adjacent to tube 9, bubble movement is significantly hindered.

Run 104: continued

6. A restriction to solids flow must exist in the bottom of the bed. Tubes 4 and 8 show high concentrations, whereas tube 12 (below 8) shows a low concentration of tracer. Thus, tube 8 acts like a bottleneck to solids movement at these conditions. This may account for the long rise times observed throughout the bottom half of the bed. Due to this bottleneck, mixing in run 104 is worse than that in 103.

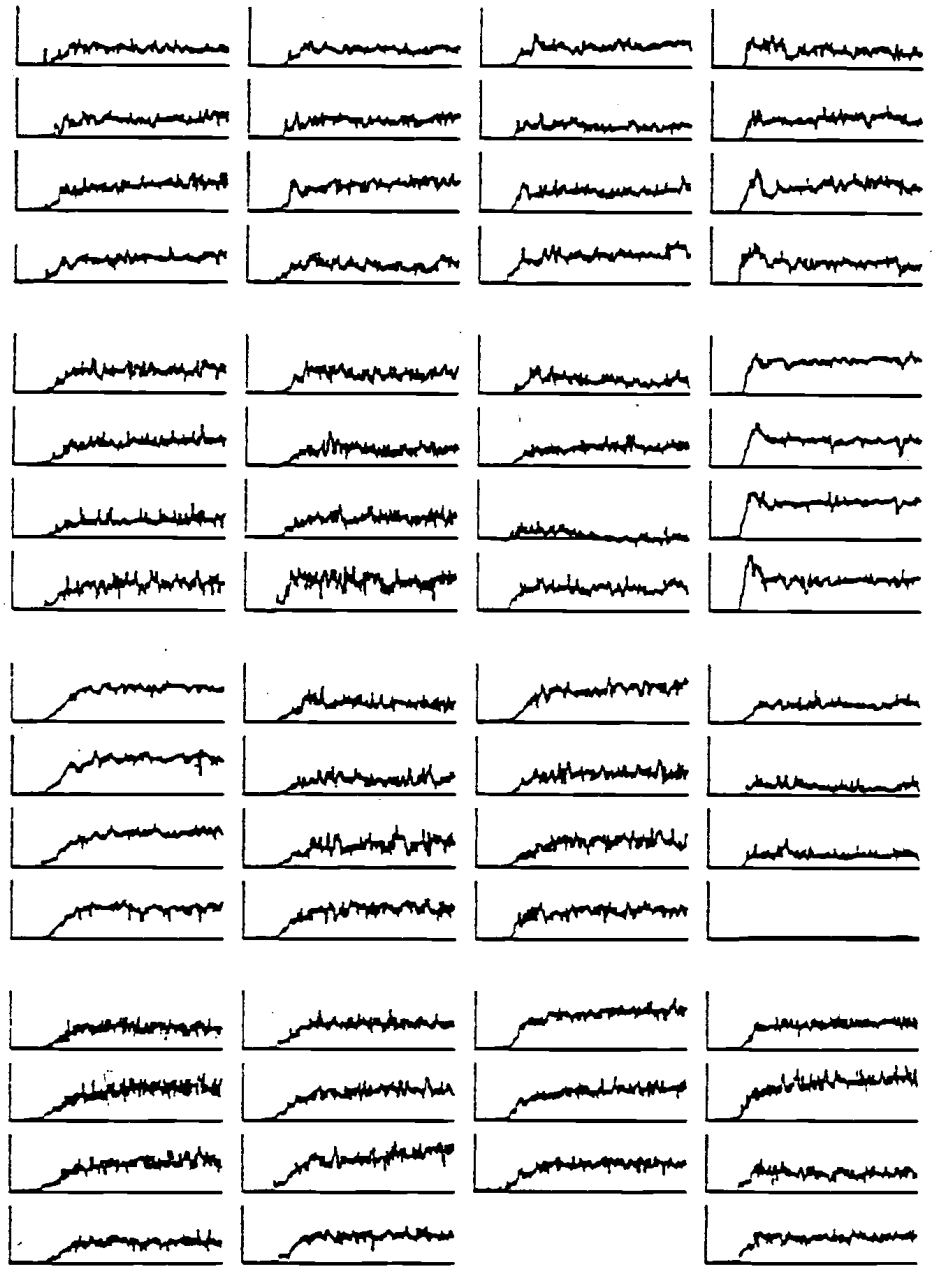

Figure 4.3. (Continued)

Run 105: .254 m (10"), 1134 kg (2500#), 3.35 m/s (11FPS), (see Run 95)

1. There appear to be no clumps of tracer in the bed.
2. Rise times seem almost uniform (within a few seconds of each other) around the walls of the bed. For example, in the second row compare channels 5A, B, C, D, 6A, D, 7A, D, 8A, B, C, D. Also rise times in the center of the bed appear almost uniform (see channels 14B, C, 15B, C, 10B, C, 11B, C). Overall mixing time is about 10 seconds.
3. Since the rise times are so close, it is hard to distinguish a path of tracer circulation.
4. This bed inventory gives somewhat better mixing than the 2000# bed of run 109.
5. Bubbles move freely about the bottom, interior and left side of the bed when compared to the right side of the bed.

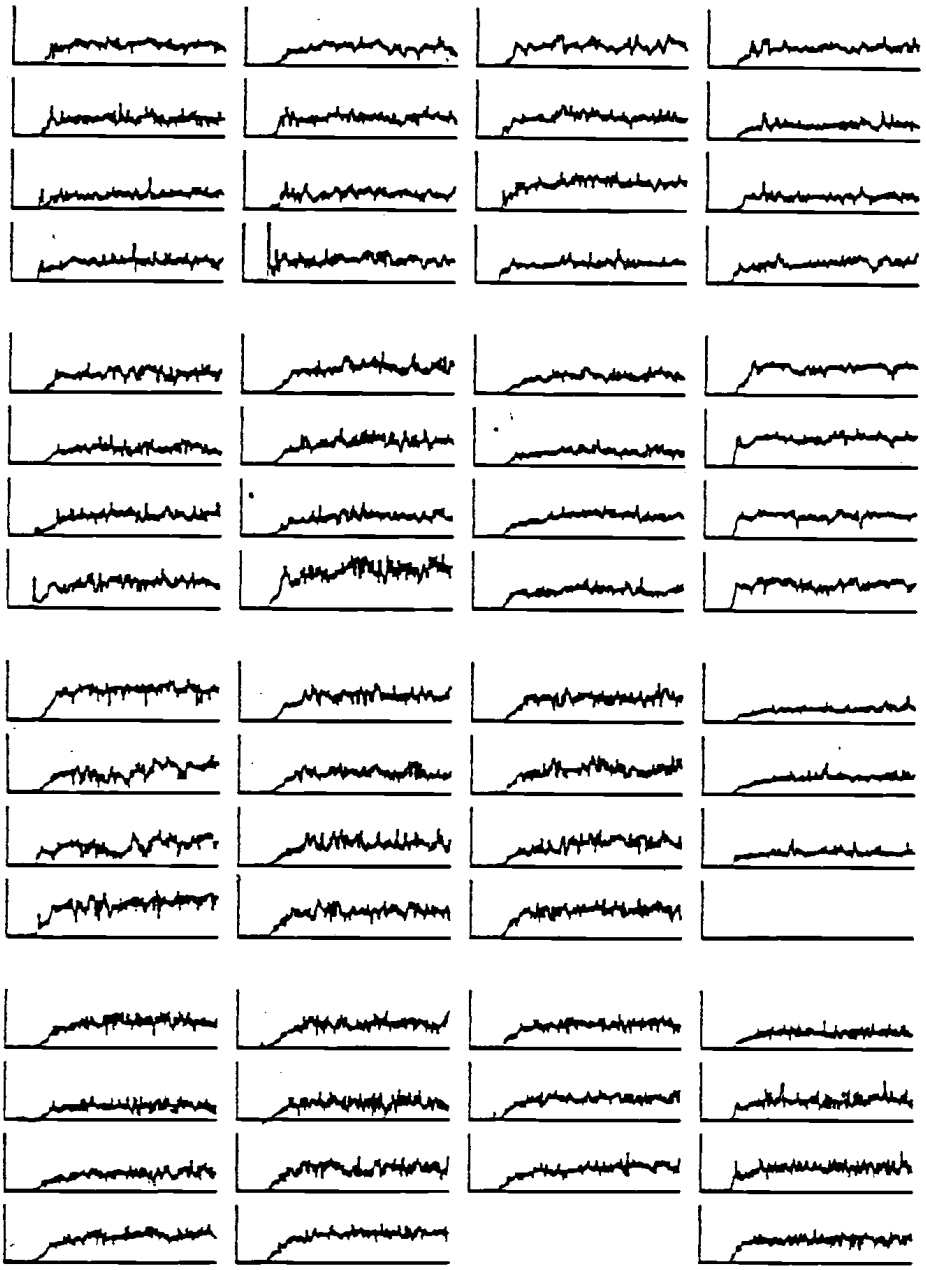

Figure 4.3. (Continued)

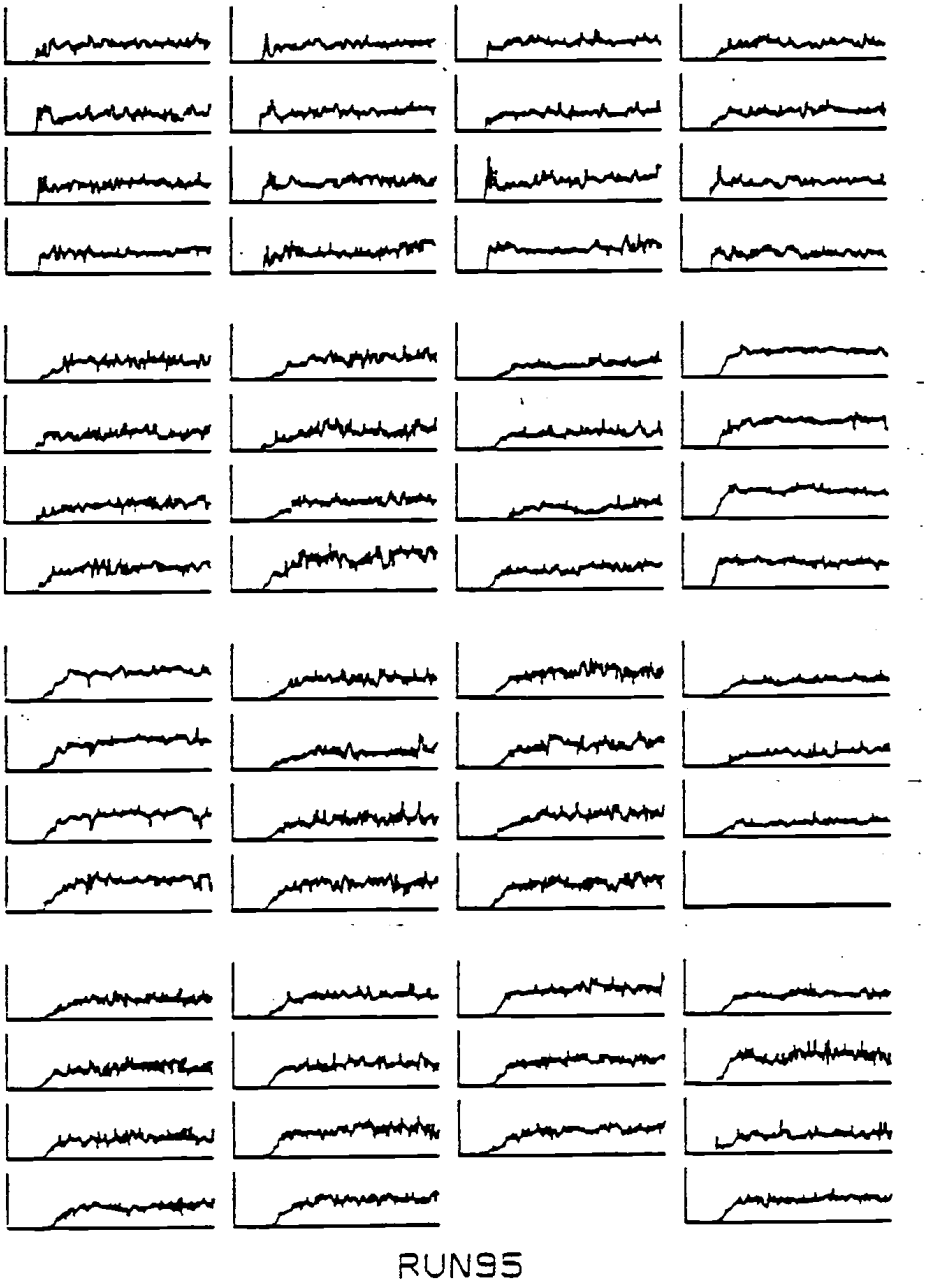

Figure 4.3. (Continued)

Run 106: .254 m (10"), 907 kg (2000#), 1.52 m/s (5FPS), (see Run 96)

1. Mixing is quite sluggish. Clumps move throughout the bed before dispersing. The maximum time necessary for clump dispersion is about eight seconds as channels 11C and 7C indicate. Interestingly enough, both of these channels are interior channels. So clumps are holding together even in the upswing through the center of the bed. These interior peaks are not as pronounced in run 76 (20", 2000#, 5 FPS), which may indicate good mixing under the array.
2. Rise times are relatively quick compared to those of Run 76 for the left side of the bed. The opposite case holds for the right side. About 7 or 8 seconds are required for the slowest channel (13A) to reach its final equilibrium concentration.
3. Circulation of tracer seems more random under these conditions. It appears to move down the sides of injection and up through the center.
4. Bubbles are sparse along the left side (tubes 1, 5 and 9), which indicates a dense region of solids. Concentration of bubbles along the bottom of the bed is fairly uniform.

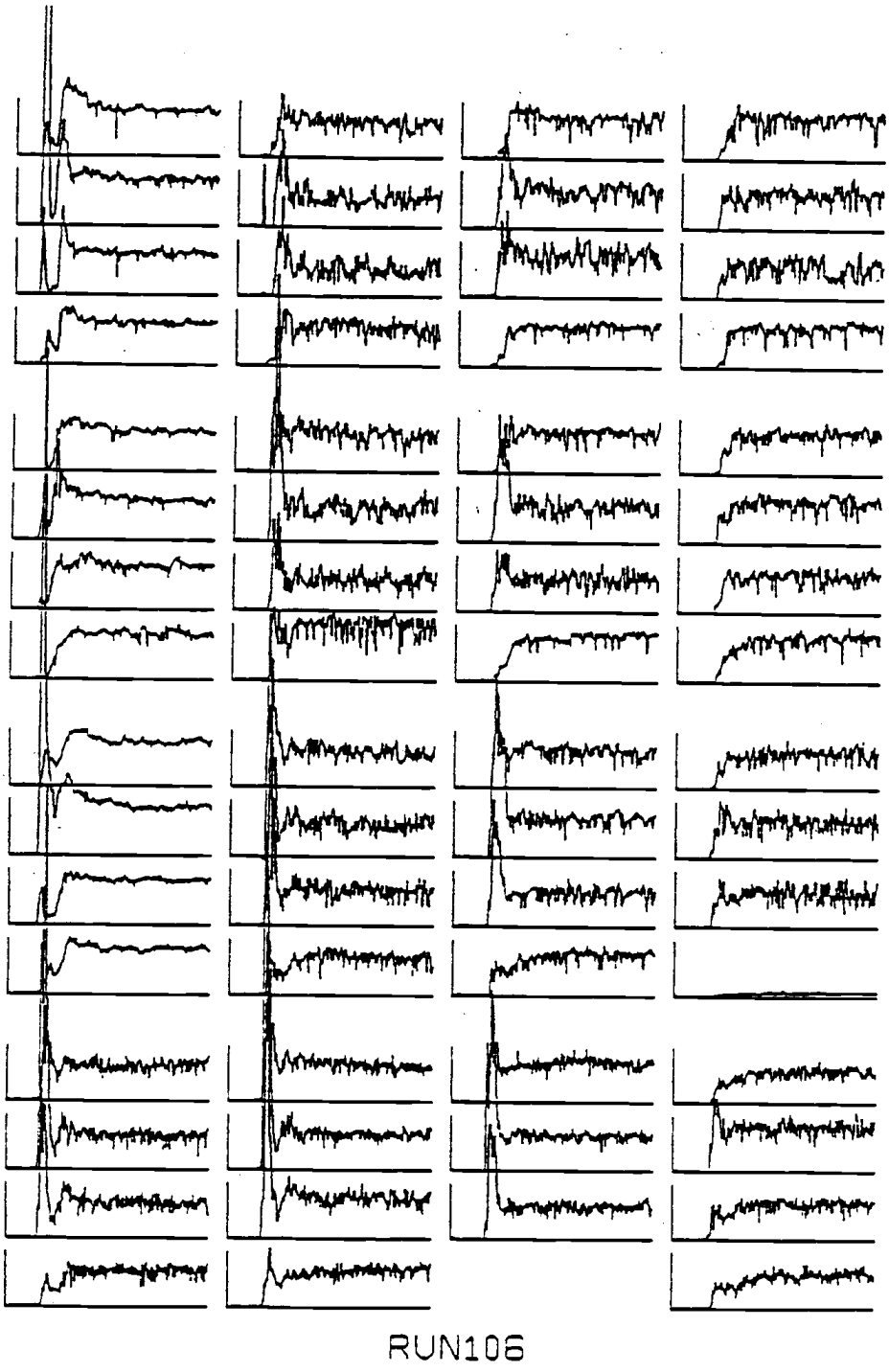

Figure 4.3. (Continued)

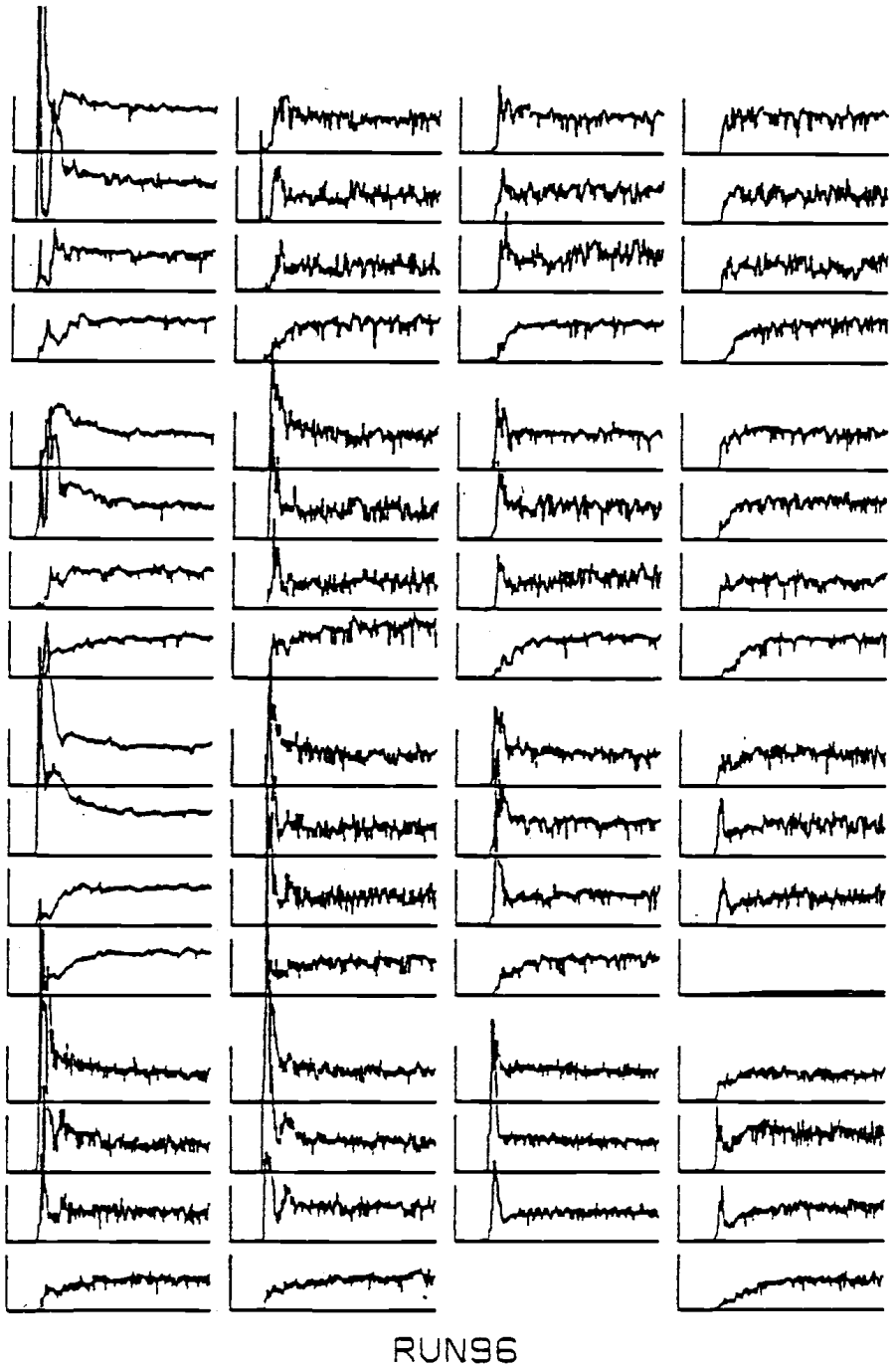

Figure 4.3. (Continued)

Run 107: .254 m (10"), 907 kg (2000#), 2.13 m/s (7FPS), (see Run 97)

1. A couple of clumps of tracer manage to avoid detection until they reach the lower part of the array. They appear to move up the center of the array. (see channels 13B, 14A, B, C, 15B, C, 10B, C).
2. Mixing is considerably better here than in Run 106 (at 5 FPS). The time required for clumps to disappear is about 5 to 10 seconds (14B). The maximum rise time (channel 16A) is approximately 10 to 12 seconds. Clumps are smaller though.
3. As usual, bubble concentration in the bottom of the array is fairly uniform. As the bubbles move up the bed, they migrate toward the center. The left side shows a lack of bubbles or a dense phase of solids.
4. The long rise time of channel 4 indicates that vertical mixing is better than lateral mixing.

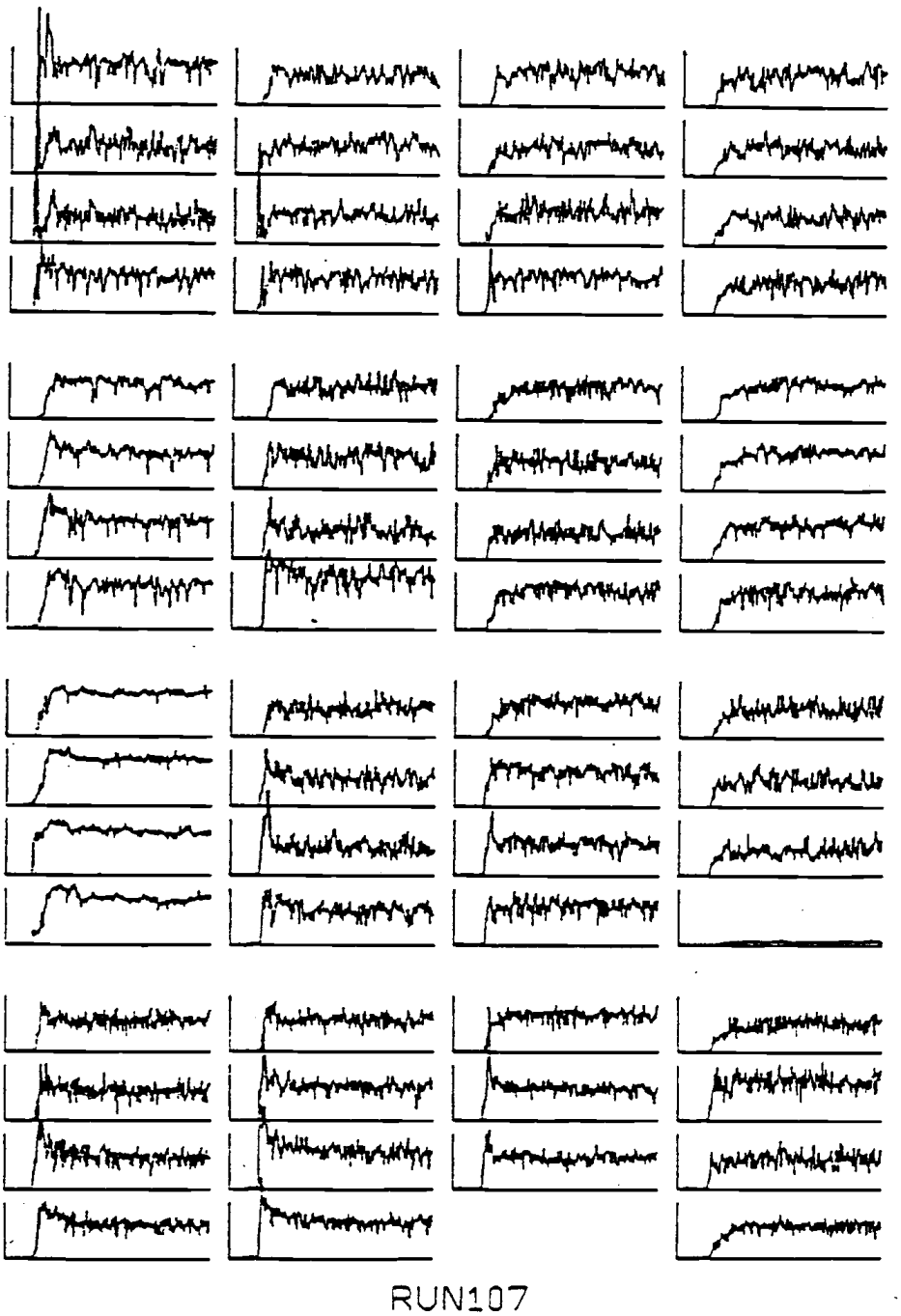

Figure 4.3. (Continued)

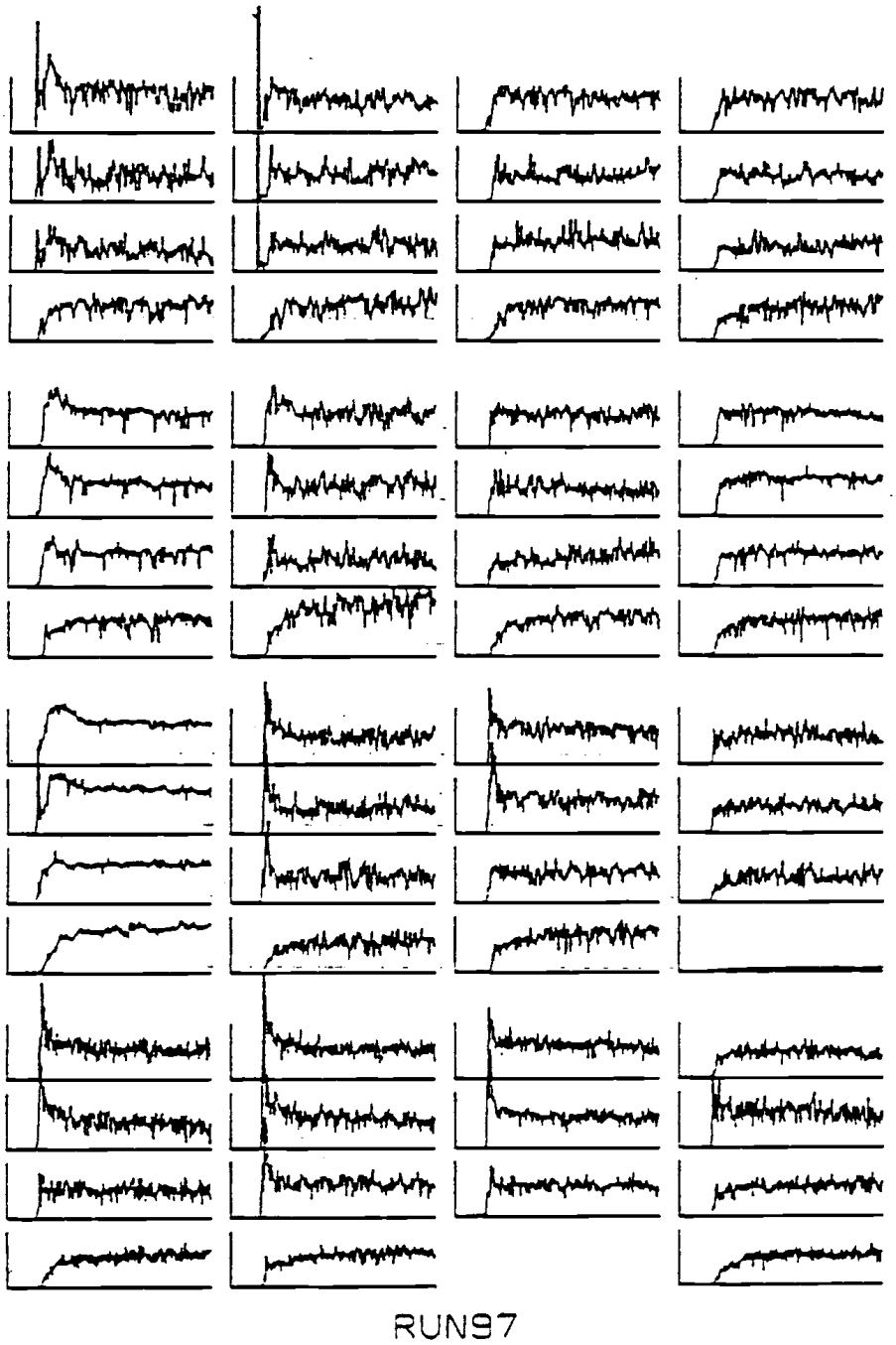

Figure 4.3. (Continued)

Run 108: .254 m (10"), 907 kg (2000#), 2.74 m/s (9FPS), (see run 98)

1. In comparison with run 107, the clumps are smaller but persist longer. Therefore, mixing is not greatly enhanced at this higher gas velocity. Clumps have moved to the right side of the bed.
2. Rise times are slower at the bottom of the bed compared to run 107. Throughout the rest of the bed they are roughly equal.
3. Circulation in the bed is complementary with that in run 107, i.e., tracer falls down the right side and up the center of the bed.
4. More bubbles exist along the left side of the bed because of a higher superficial gas velocity. The concentration of bubbles in the center of the bed is greater than that about the sides and corners of the bed.

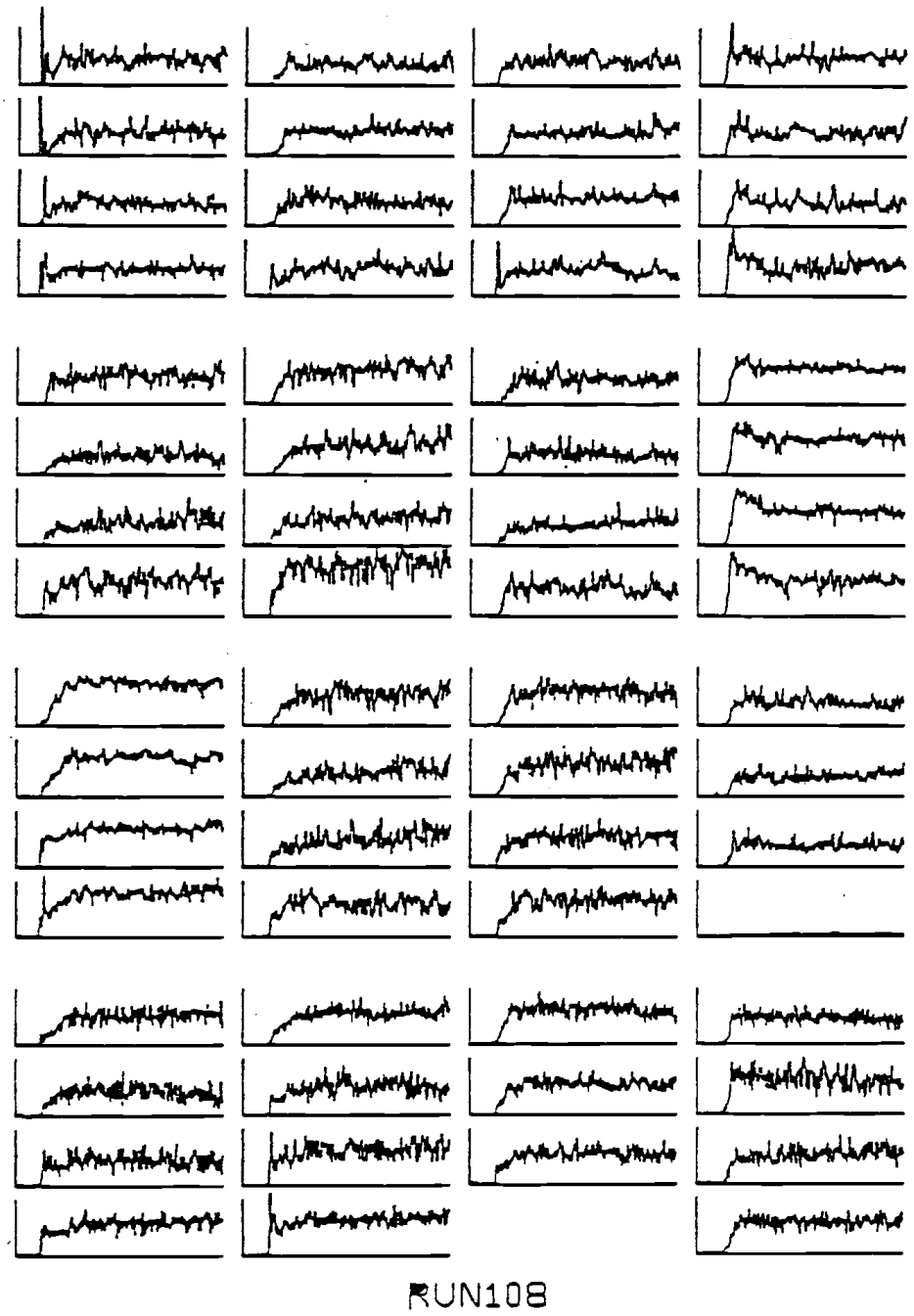

Figure 4.3. (Continued)

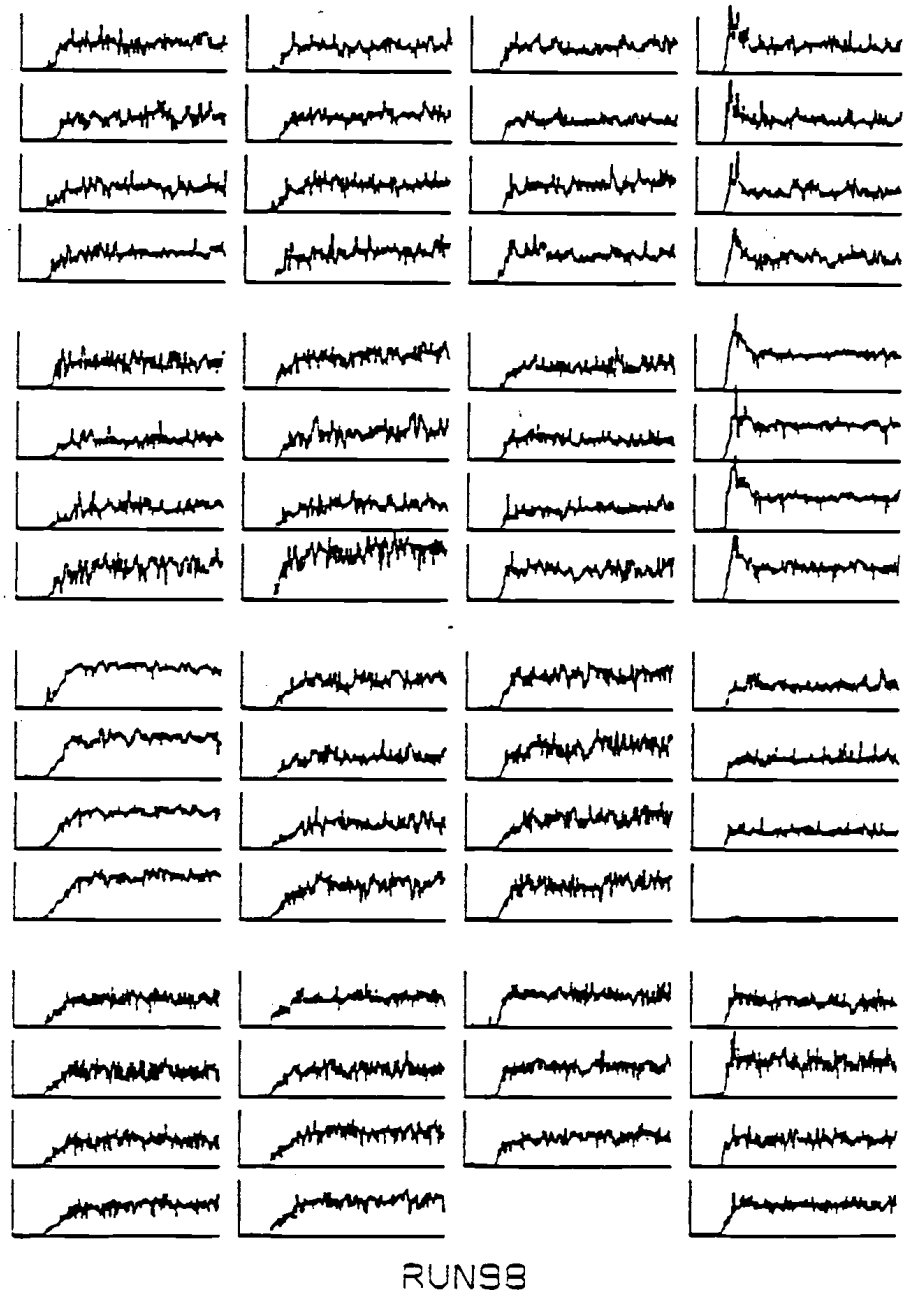

Figure 4.3. (Continued)

Run 109: .254 m (10"), 907 kg (2000#), 3.35 m/s (11FPS),
(see run 99)

1. Mixing is quite fast. The only peaks or clumps are detected by channels 1D, 2D and 3D. These are small and require just 3-6 seconds to disperse. Within 10 seconds mixing is complete (bottom probes).
2. Clumps of tracer appear to shoot across the bed in the first instants after injection of tracer. No clumps are able to sift below the top row.
3. Vertical mixing along the walls (1D to 5D and 2D to 6D) seems better than lateral mixing along the tubes (1A to 1D and 2A to 2D).
4. Bubbles seem well dispersed throughout the bed.
5. Again, observe the "pinch effect" or bottleneck about tube 8 which causes lower concentration of tracer around tube 12.

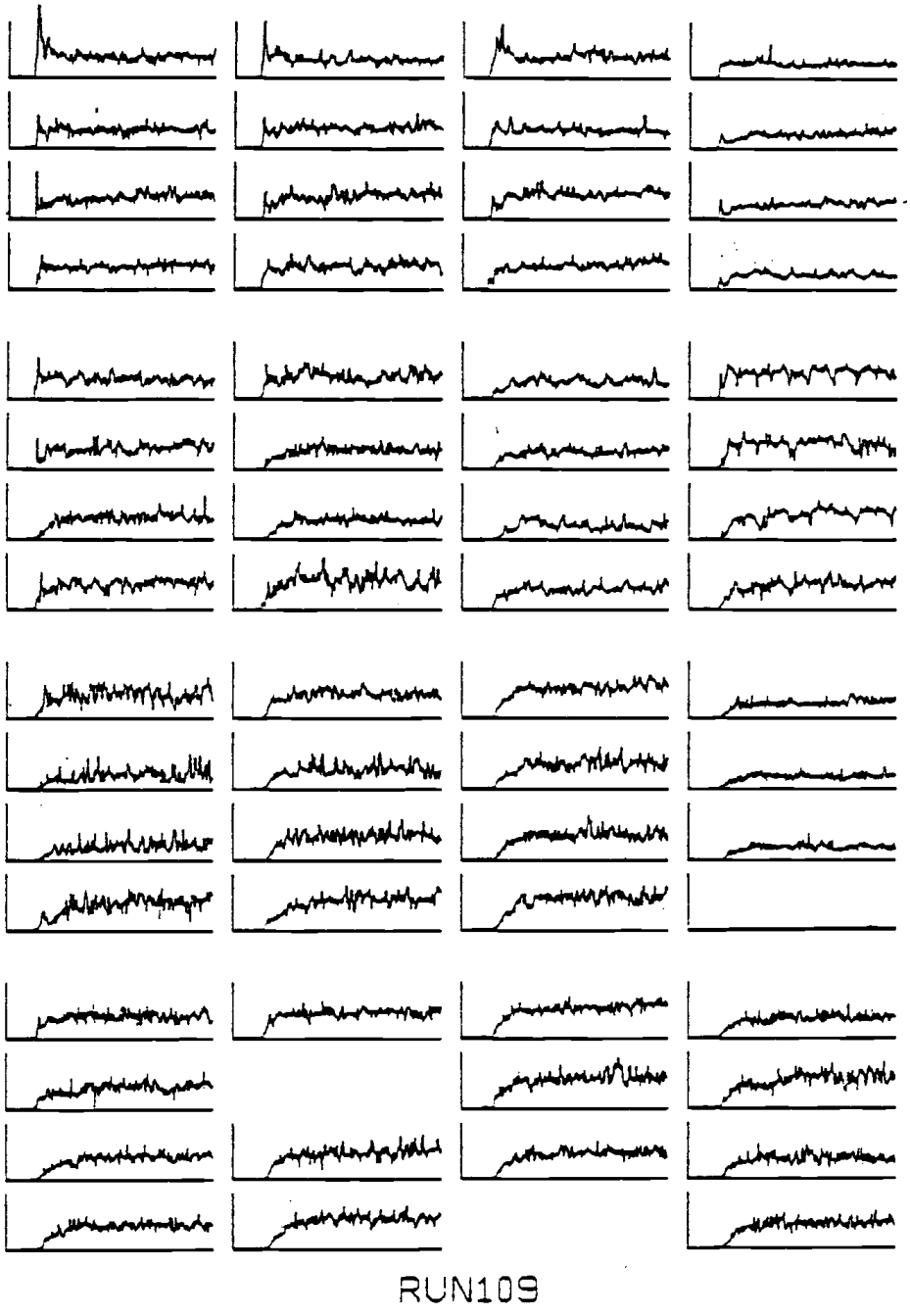

Figure 4.3. (Continued)

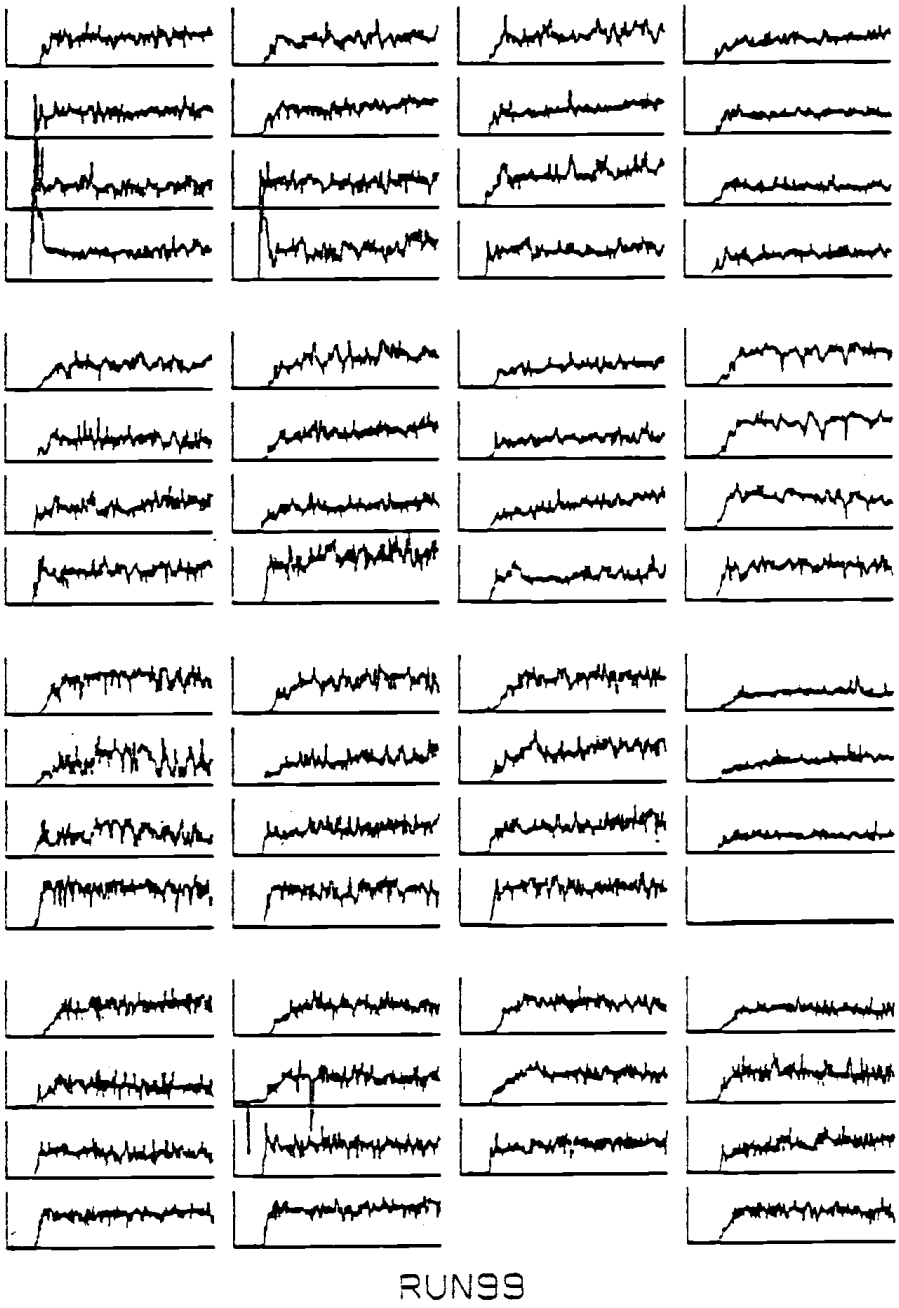

Figure 4.3. (Continued)

Run 110: .508 m (20"), 1134 kg (2500#), 1.52 m/s (5FPS), (see Run 79)

1. Mixing in this run is slightly better than run 106 (2000#) as a result of increased bed inventory.
2. Clump disappearance time is about 10 to 15 seconds (5A and 6A). Rise times are relatively quick (channel 7A controls). These results compare favorably with run 79 (same conditions).
3. Bubbles seem well dispersed throughout the bed.
4. Vertical mixing is much better than horizontal mixing.

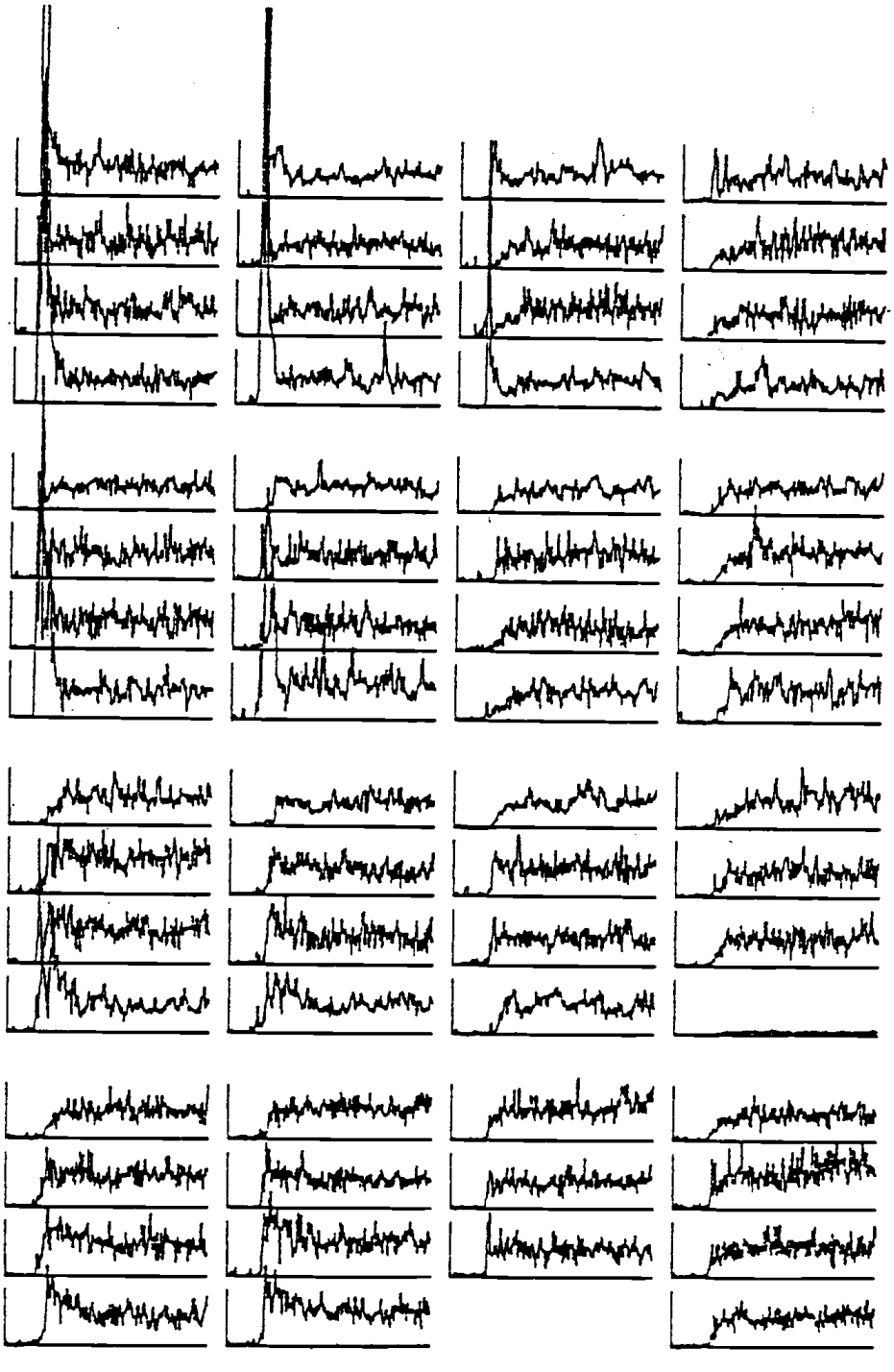

Figure 4.3. (Continued)

Run 111: .508 m (20"), 1134 kg (2500#), 3.35 m/s (11FPS), (see Run 82)

1. This run is quite similar to run 82. In both runs channel 8A is the location of the most persistent clump of tracer.
2. The rise times are approximately equal in both runs.
3. Therefore, the overall mixing times are the same in both runs.

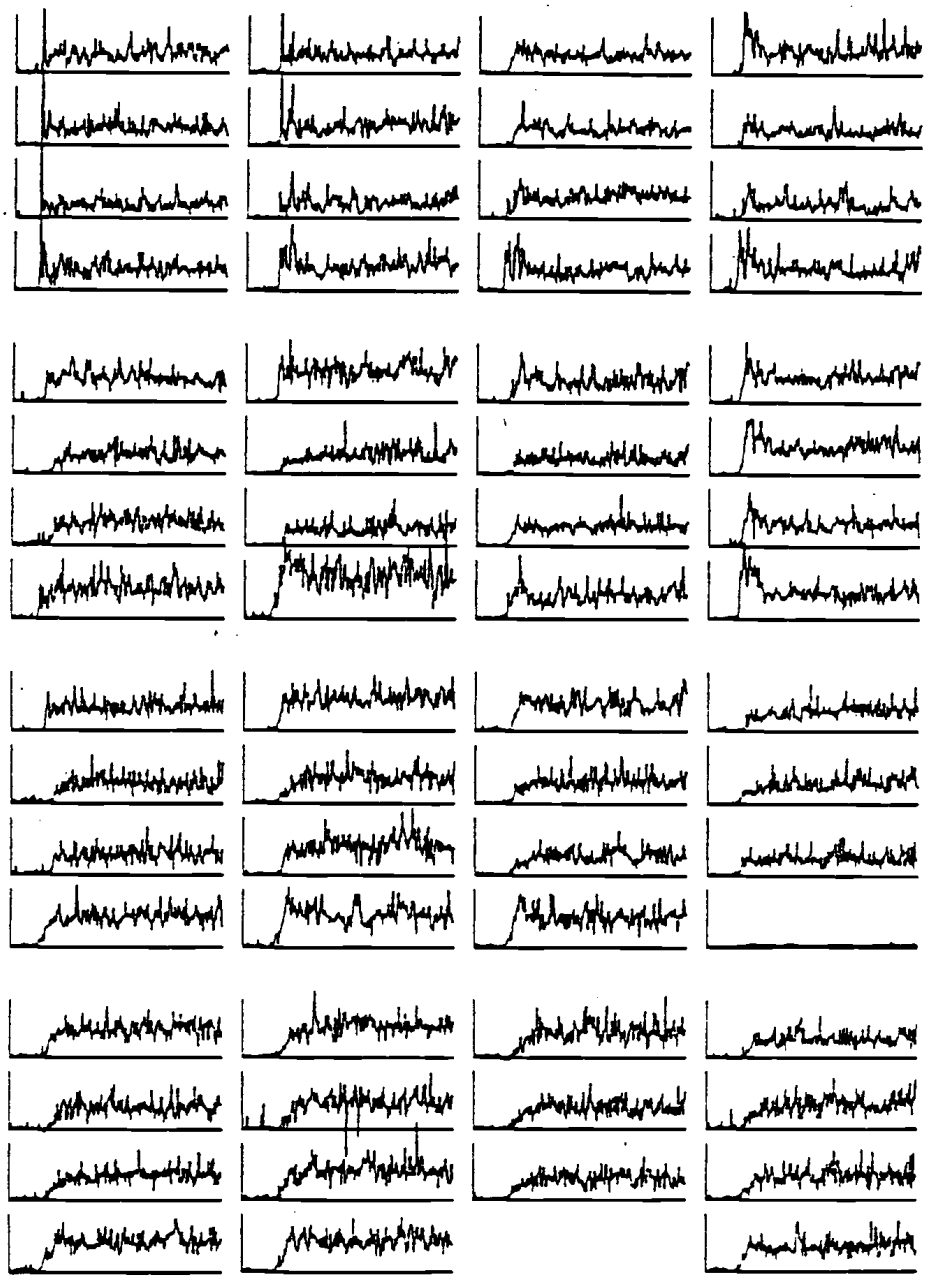

Figure 4.3. (Continued)

Run 112: .508 m (20"), 1361 kg (3000#), 1.52 m/s (5FPS),
(see Run 83)

1. There seems to be considerably more noise in this run than in run 83. Otherwise, the beds exhibit the same general characteristics.
2. The rise times are roughly equivalent in both runs. So, the overall mixing times are about the same.

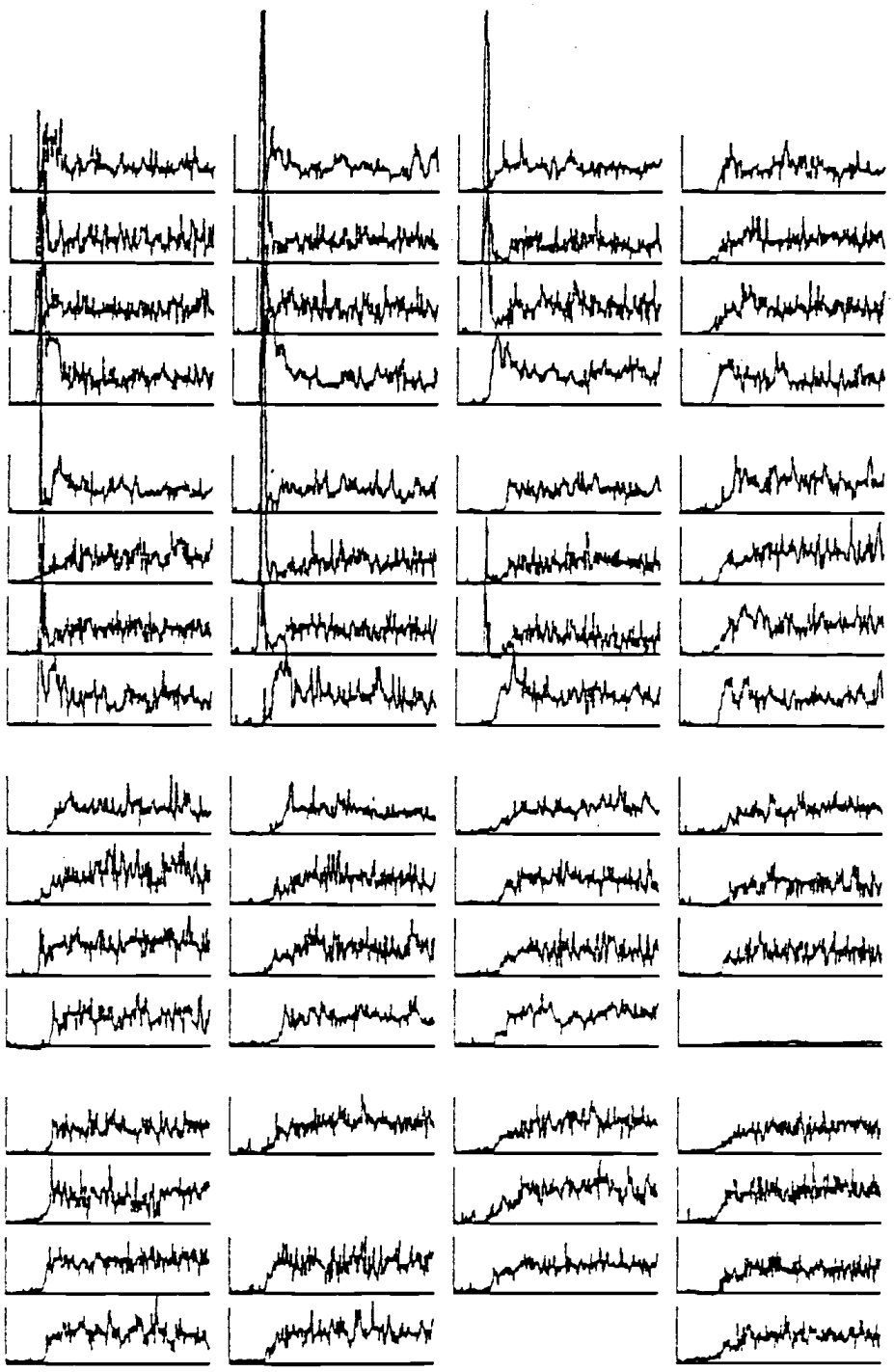

Figure 4.3. (Continued)

Run 113: .254 m (10"), 907 kg (2000#), .3 m/s (1FPS), EI-70 sand (d_p 0.17 mm (.0068 in))

1. This run differs from run 87 only by the height of the tube array above the distributor plate (10"). The array is now totally immersed in the bed media.
2. The concentration peaks are not nearly so sharp and high as those found in Run 87. Evidently, the tracer has some time to disperse before being detected by the probes.
3. As in Run 87, clumps of tracer seem to persist during their upswing through the center region (channels B and C on probes 2, 3, 6, 7, 10, 11, 14, 15) of the bed.
4. Again, it appears that the tracer prefers to move down the "1, 5, 9, 13" tube side of the bed after injection.
5. Bubbles appear to be small and few as seen by the relative infrequency of dropouts in the data.

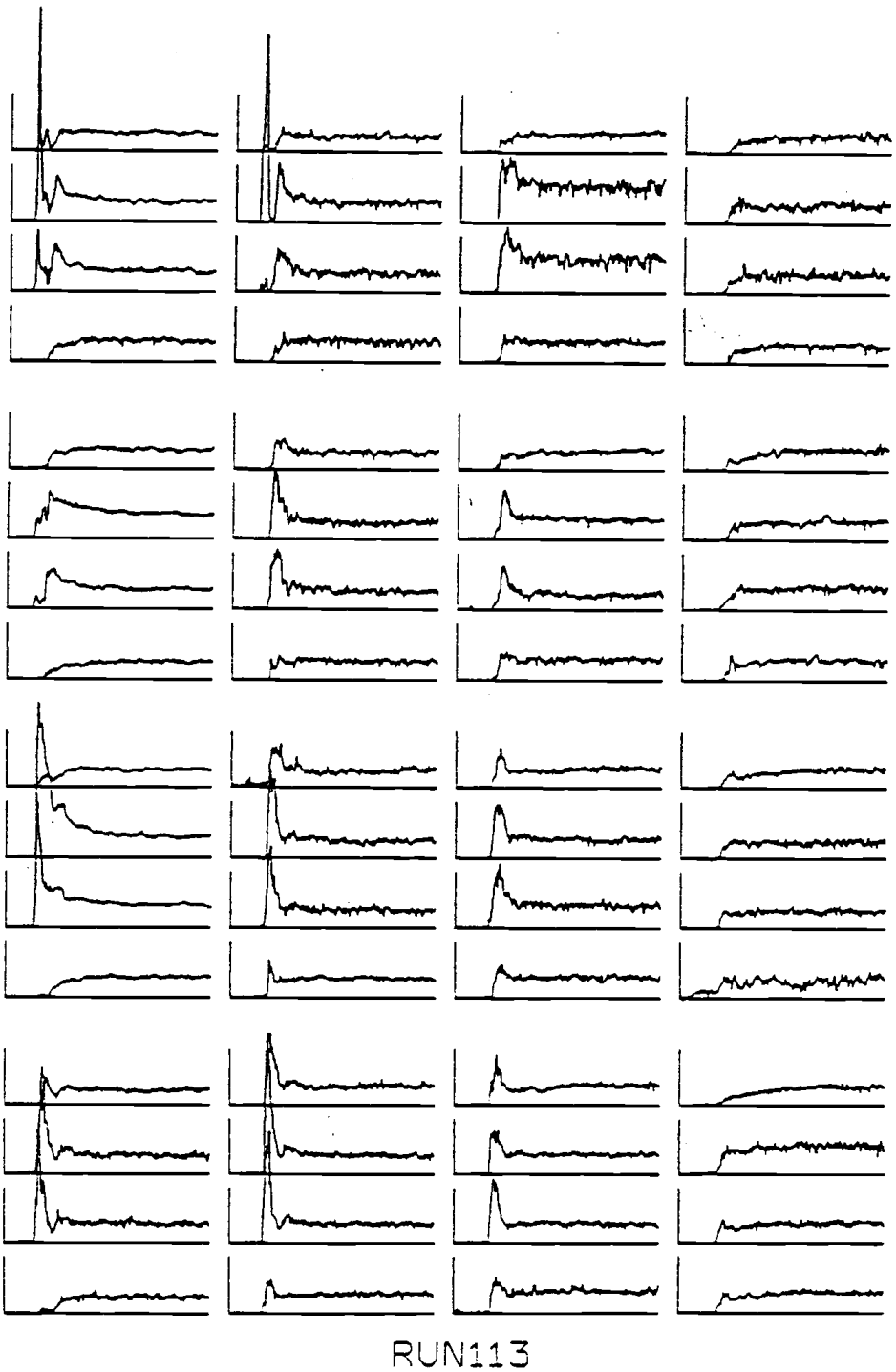

Figure 4.3. (Continued)

Run 114: .254 m (10"), 907 kg (2000#), 1.22 m/s (4FPS), EI-70 sand (d_p 0.17 mm (.0068 in))

1. A significant improvement in mixing has been realized in this run. The velocity of 4 FPS is fully responsible for this improvement as comparison with runs 87 and 113 will readily demonstrate.
2. Peaks of tracer are virtually absent.
3. Comments for runs 87 and 113 regarding bubbles are also applicable here.
4. Channel 12A was eliminated due to an electronic malfunction.

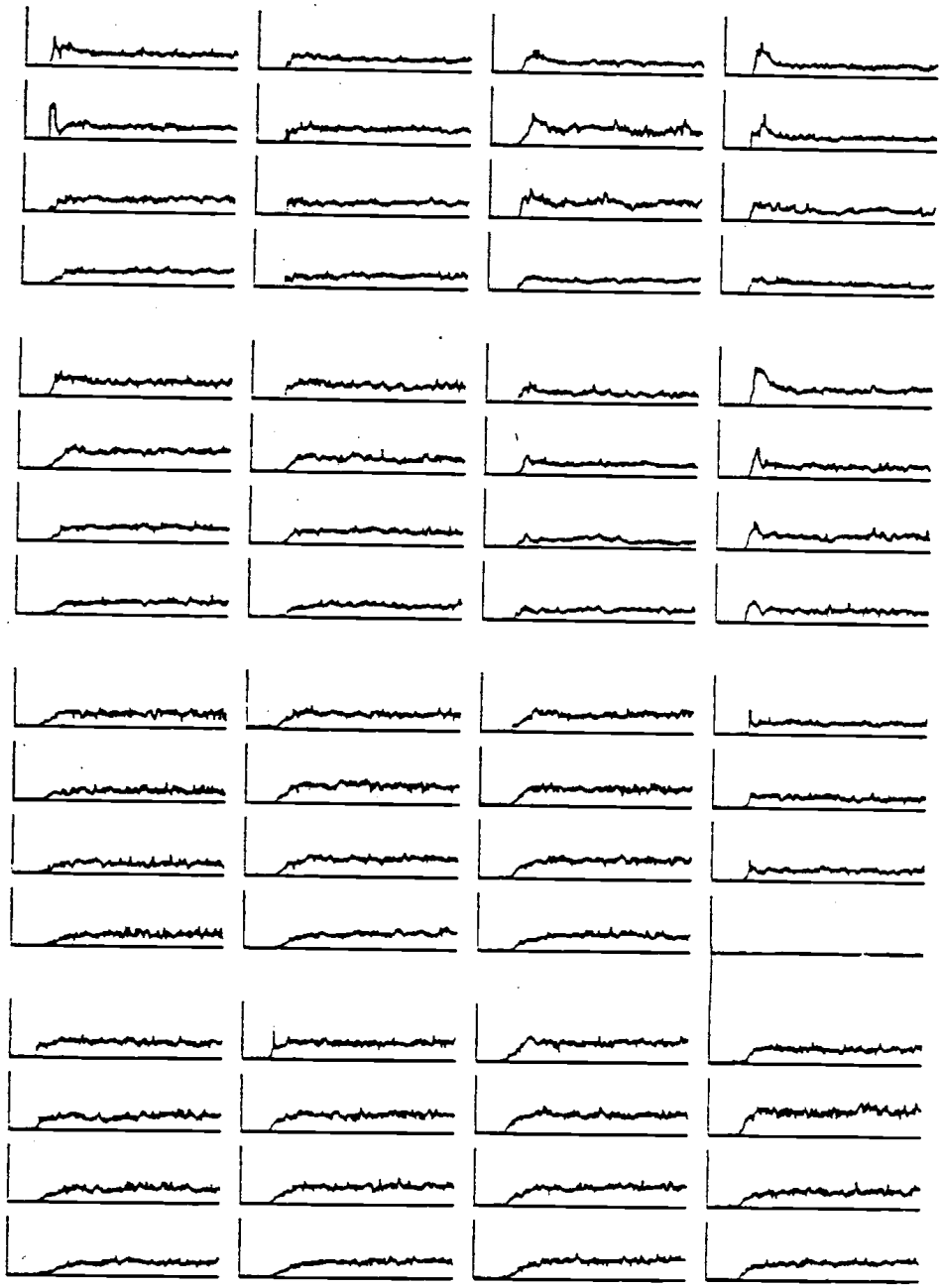

Figure 4.3. (Continued)

4.3 Closure: Conclusions Based on Observations

At high superficial gas velocities (2.74 m/s (9 FPS) and 3.35 m/s (11 FPS)) the tracer disperses rapidly throughout the bed, i.e. after eight to twelve seconds the tracer is fairly well distributed. Generally, the tracer appears to circulate down the sides and corners and up the middle or interior of the bed. The time of mixing seems to be somewhat better in the axial direction than in the lateral direction. Mixing is considerably slower at lower velocities.

The mass of bed media has a direct effect on mixing. As more media is added, faster mixing seems to occur. For example, when u_o = 2.13 m/s (7 FPS) and the height of the tube array above the distributor plate is .254 m (10 in), the tracer mixes much faster in 1361 Kg (3000 lbs) of sand than 907 Kg (2000 lbs) of sand. This conclusion is a bit misleading because there is more material above the tube array in the 1361 Kg (3000 lbs) bed and the ferrite tracer has more time to mix before reaching the probes.

Only three runs were done with finer bed media (EI-70 sand) due to problems with excessive elutriation. The successful runs indicate sluggish mixing at 0.3 m/s (1 FPS), but significantly better mixing at 1.22 m/s (4 FPS). It's possible that fine bed media promotes mixing to a greater extent than course bed media. Not enough data were taken to verify this hypothesis, though.

It seems evident that more numerous small tracer particles help eliminate the Poisson noise found in the earlier large tracer particle runs. In addition, small particles appear to move differently than large particles at low fluidizing velocities. This latter observation was brought up in the discussion of run 79 and run 65.

The inductance probes yield qualitative information about bed behavior. Bubble frequencies can be estimated from the raw data since the ferrite concentration and probe output briefly decrease as a bubble passes by. Thus, it is possible to qualitatively determine the degree of fluidization or mixing (which is a function of the number and size of bubbles) in different regions of the bed by the relative bubble frequencies, i.e. the signal dropouts, even from the "smoothed" data. Based on this criteria, one can readily distinguish three distinct regions of mixing. At the bottom of the tube array mixing is fairly uniform. Along the walls, bubble frequency and, hence, mixing is less; while in the center region the bubble frequency is generally the greatest. Thus, bubble-caused mixing is best at the center (or interior) of the bed. Schugerl's assertion [38] that the wall and center regions are distinct due to a low intensity of radial mixing is in accord with these findings.

V. UNSUCCESSFUL ANALYSIS AND MODELING EFFORTS

Various models were considered in an attempt to understand and characterize the dispersion of tracer in the .91 m x .91 m (3 ft x 3ft) fluidized bed. Initially, we contemplated writing a computer program which would follow the path of a simply connected volume (e.g., a box formed by a group of four probes) containing eighty percent of the tracer. This volume would expand with time because of tracer dispersion. In conjunction with this model, the tracer center of mass could be tabulated in terms of position and time. Eventually, we reverted to a more pertinent and concise version of this model referred to as the histogram approach, which is described in chapter six.

The Einstein random-walk model was considered next. The modelling equation is:

$$\overline{(\Delta Z)^2} = 3D(\Delta t)$$

where $\overline{(\Delta Z)^2}$ is the mean, square distance travelled by a tracer particle over a time interval (Δt) and D is the overall dispersion coefficient (with dimensions, L^2/t). This model is crude and, therefore, only yields an order of magnitude approximation of the dispersion coefficient. Since our bed has many tubes and relatively close walls compared to the distance between parallel walls in large-scale combustors, we decided that boundary effects (or reflecting barriers) would greatly

detract from even an order of magnitude estimation of D, the dispersion coefficient. Thus, we were compelled to discard the Einstein random-walk model.

A compartmental flow model developed by Chang and Fitzgerald [7] was our next approach. This model represents flow or nonflow (batch) systems in terms of well-mixed compartments with intercomparmental flows. Since measured tracer mass was not conserved within the tube array during a run (especially during the transient period - see mass balance plots in chapter six), this model was not viable. Bed media, i.e. sand and tracer, was always above and below the tube array as well as within it. Sometimes, due to noise and fluctuations, a material balance was not satisfied even when the bed was considered well-mixed. This lack of a material balance also ruled out any modelling efforts using the two-stirred tank model discussed in chapter two. In summary, if the probes had detected tracer in all regions of the bed, a material balance would have been satisfied and these two models could have been used.

Finally, in an attempt to quantify the mixing times observed for runs 74-112, the following measure was applied to the smoothed data.

Mean square measure of mixing (MSMM)

$$MSMM = \sum_{i=1}^{64} \frac{(C_{i,j} - C_i^*)^2}{C_i^*}$$

where: $C_{i,j}$ is the concentration measured by channel i at time j

C_i^* is the maximum concentration of channel i over the last 20 seconds of the run

j is time, which increments by .25 second intervals.

The mixing criterion, MSMM, measures the difference between a local instantaneous concentration and its final value. These differences are then normalized with respect to the final concentration and squared to accentuate unmixed states. The sum of these normalized and squared differences is taken over all 64 channels for each of 396 time intervals or approximately every .25 seconds.

Runs 74-112 have been analyzed using this measure (see Figure 5.1 - only four plots are included). Also, the MSMM curves for these runs were fit, in a least squares sense, with the following exponential:

$$MSMM = Ae^{Bt} + C$$

where A, B and C are constants determined by least squares analysis and t is time (seconds).

Table 5.1 summarizes the experimental conditions of each run. Note that all runs (74-112), except run 87 were conducted with EI-16 bed media ($\bar{d}_p \simeq 0.80$ mm (0.03 in)), ferrite tracer of similar size ($\bar{d}_p \simeq 1.6$ mm (0.06 in)) and a tube spacing of four inches. Tabulated alongside each run number is the weight of sand used, the height of the

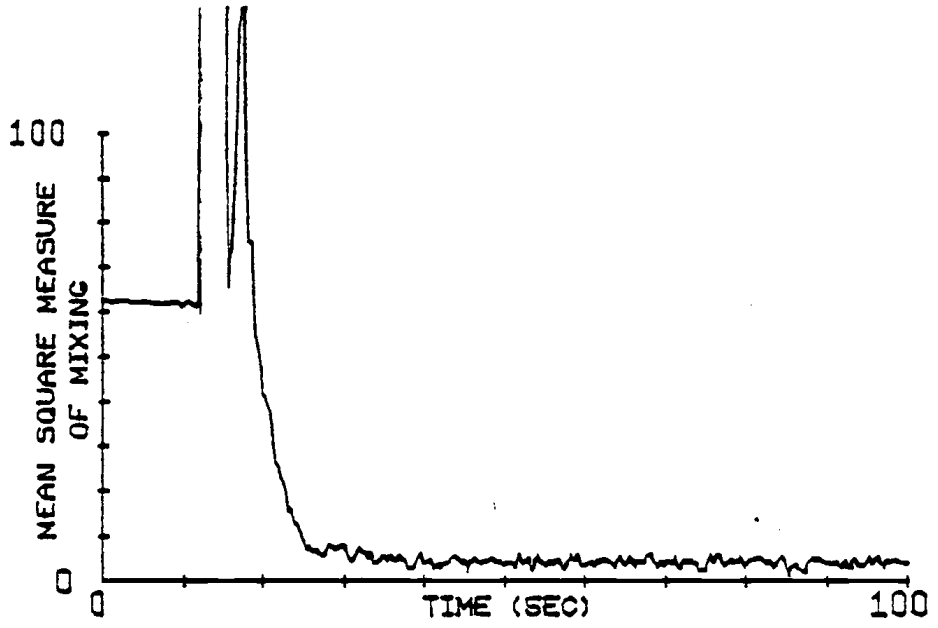

RUN79

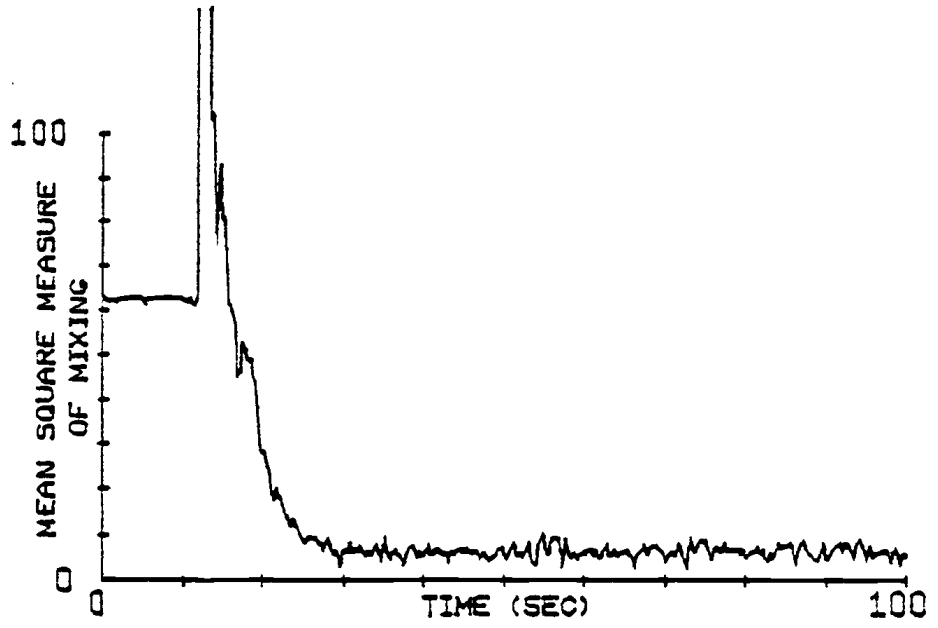

RUN80

Figure 5.1. Mean square measure of mixing curves.

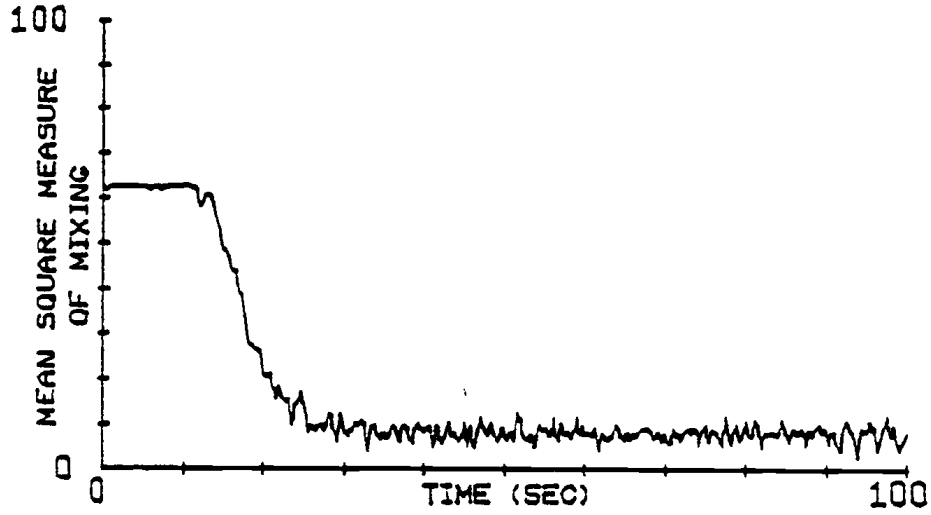

RUN81

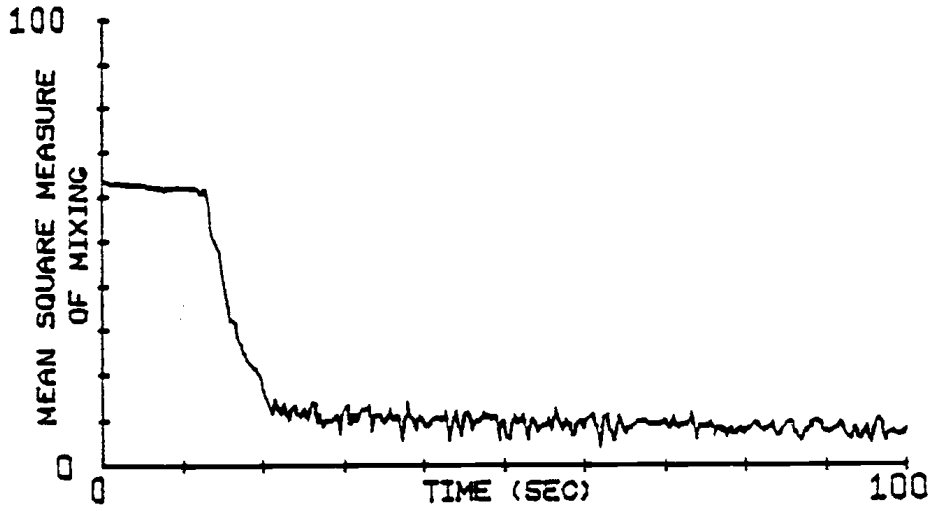

RUN82

Figure 5.1. (Continued)

Table 5.1

SUMMARY OF EXPERIMENTS, MSMM and OMT

Sand: EI-16 ($\bar{d}_p \simeq$ 0.8 mm (0103 in))

Tracer Size: $\bar{d}_p \simeq$ 1.6 mm (0.06 in)

Tube Spacing: 0.102m (4 in)

Run Number[3]	Weight of Sand kg (lbs)	Height of Array Above Oistributor m (in)	Superficial Gas Velocity m/s (FPS)	A	B	C	Overall Mixing Time (sec)
74	907 (2000)	.508 (20 in)	.91 (3)	102.1	- .1	11.7	28 sec.
75	907 (2000)	.508 (20 in)	2.13 (7)	59.0	- .4	6.5	12
76	907 (2000)	.508 (20 in)	1.52 (5)	59.3	- .3	7.2	12
77	907 (2000)	.508 (20 in)	3.35 (11)	40.5	- .3	8.7	9
78	907 (2000)	.508 (20 in)	2.74 (9)	109.7	- .4	8.0	9
79	1134(2000)	.508 (20 in)	1.52 (5)	166.7	- .2	11.9	15
80	1134(2000)	.508 (20 in)	2.13 (7)	85.6	- .2	5.7	14
81	1134(2000)	.508 (20 in)	2.74 (9)	47.5	- .2	7.8	12
82	1134(2000)	.508 (20 in)	3.35 (11)	44.6	- .3	9.1	11
83	1361(3000)	.508 (20 in)	1.52 (5)	100.7	- .2	4.6	19
84	1361(3000)	.508 (20 in)	2.13 (7)	67.0	- .2	6.8	15
85	1361(3000)	.508 (20 in)	2.74 (9)	45.4	- .2	8.0	14
86	1361(3000)	.508 (20 in)	3.35 (11)	37.3	- .2	9.6	12
87	907 (2000)	.508 (20 in)	0.30 (1.0)	65.0	- .3	10.3	21
88	1361(3000)	.254 (10 in)	1.52 (5)	52.0	- .3	4.3	19
89	1361(3000)	.254 (10 in)	2.13 (7)	40.8	- .3	6.2	20
90	1361(3000)	.254 (10 in)	2.74 (9)	39.0	- .2	8.0	18
91	1361(3000)	.254 (10 in)	3.05 (10)	39.5	- .2	7.8	21
92	1134(2500)	.254 (10 in)	1.52 (5)	76.4	- .2	3.4	14
93	1134(2500)	.254 (10 in)	2.13 (7)	44.3	- .3	5.7	16
95	1134(2500)	.254 (10 in)	3.35 (11)	40.4	- .2	7.6	21
96	907 (2000)	.254 (10 in)	1.52 (5)	--	--	--	19
97	907 (2000)	.254 (10 in)	2.13 (7)	--	--	--	11
98	907 (2000)	.254 (10 in)	2.74 (9)	40.7	- .3	6.9	18
99	907 (2000)	.254 (10 in)	3.35 (11)	39.1	- .2	7.6	14
102	1134(2500)	.254 (10 in)	1.52 (5)	--	--	--	12
103	1134(2500)	.254 (10 in)	2.13 (7)	48.3	- .2	5.4	15
104	1134(2500)	.254 (10 in)	2.74 (9)	39.9	- .2	7.9	18
105	1134(2500)	.254 (10 in)	3.20 (10.5)	37.0	- .2	7.6	19
106	907 (2000)	.254 (10 in)	1.52 (5)	--	--	--	19
107	907 (2000)	.254 (10 in)	2.13 (7)	59.1	- .3	5.2	12
108	907 (2000)	.254 (10 in)	2.74 (9)	--	--	--	11
109	907 (2000)	.254 (10 in)	3.35 (11)				19
110	1134(2500)	.508 (20 in)	1.52 (5)				13
111	1134(2500)	.508 (20 in)	3.35 (11)				10
112	1361(3000)	.508 (20 in)	1.52 (5)				15

[3] Run 87 was made with EI-70 sand ($\bar{d}_p \simeq$ 0.17 mm (0.0068 in))

tube array above the distributor plate, the superficial gas velocity, the constants A, B and C for the exponential fit of the MSMM curve and the overall mixing time. This overall mixing time is the time in seconds for the tracer concentration described by MSMM to enter the "noise band" about the equilibrium concentration, which, in turn, is defined as the maximum fluctuation of the MSMM curve about its mean value during the last twenty seconds of a run. The overall mixing time is redefined throughout the thesis for convenience.

Regression groups of B, the constant in the least squares fit of MSMM (i.e., $MSMM = Ae^{Bt} + C$), versus superficial gas velocity for two distances between the tube array and the distributor plate, and three bed inventories are provided on the pages that follow. Also, two groups of B versus weight of bed media are included. Brief descriptions and observations accompany these groups.

Since B has units of reciprocal seconds, the inverse of B, (1/B), behaves like a time constant. So, as B increases, mixing should also increase. This is the criterion used in the analysis of these groups.

Notation used in the text that follows is explained here:

B = Reciprocal time constant (sec^{-1}), (from $MSMM = Ae^{Bt} + C$)

U = Superficial gas velocity, m/s (FPS)

Weight = Bed Inventory, Kg (lbs)

Height = Distance between the distributor plate and the tube array, m (in)

DISCUSSION OF GROUPS

Group A1: B versus U
Weight = 1361 Kg (3000 lbs)
Height = .254 m (10 in)

Run	B (sec^{-1})	U m/s (FPS)
88	.3	1.52 (5)
89	.3	2.13 (7)
90	.2	2.74 (9)
91	.2	3.05 (10)

In this particular arrangement, B appears to increase as U decreases. This would lead us to believe that mixing is better at lower superficial gas velocities when 1361 Kg (3000 lbs) of sand are used and the height of the tube array above the distributor plate is .254 meters (10 inches).

Group A2: B versus U
Weight = 907 Kg (2000 lbs)
Height = .508 m (20 in)

Run	B (sec^{-1})	U m/s (FPS)
75	.4	2.13 (7)
76	.3	1.52 (5)
77	.3	3.35 (11)
78	.4	2.74 (9)

Mixing seems best at the intermediate gas velocities, namely 2.13 m/s and 2.74 m/s (7 FPS and 9 FPS).

Group A3: B versus U
Weight = 1134 Kg (2500 lbs)
Height = .254 m (10 in)

Run	B (sec^{-1})	U m/s (FPS)
92	.2	1.52 (5)
93	.3	2.13 (7)
95	.2	3.35 (11)
104	.2	2.74 (9)

Again, better mixing seems to occur at 2.13 m/s (7 FPS).

Group A4: B versus U
Weight = 1361 Kg (3000 lbs)
Height = .508 m (20 in)

Run	B (sec^{-1})	U m/s (FPS)
83	.2	1.52 (5)
84	.2	2.13 (7)
85	.2	2.74 (9)
86	.2	3.35 (11)

Mixing of solids seems about the same at all four gas velocities under these conditions.

Group A5: B versus Weight
U = 1.52 m/s (5 FPS)
Height = .254 m (10 in)

Run	B (sec^{-1})	Weight Kg (lbs)
88	.3	1361 (3000)
92	.2	1134 (2500)

At low gas velocities, 1.52 m/s (5 FPS), greater bed inventory seems to enhance solids mixing.

Group A6: B versus Weight
U = 2.13 m/s (7 FPS)
Height = .254 m (10 in)

Run	B (sec^{-1})	Weight Kg (lbs)
89	.3	1361 (3000)
93	.3	1134 (2500)
103	.2	1134 (2500)
107	.3	907 (2000)

Under these conditions, solids mixing may be best with 1134 Kg (2500 lbs) of bed media. Since runs 93 and 103 were done under the same experimental conditions, the scatter of data is quite evident. In other words, the data are not very reproducible.

On the following pages are regression groups of overall mixing time versus: (A) superficial gas velocity, (B) height of the tube array above the distributor plate and (C) weight of bed media (sand). Here, again, a brief description accompanies each group. Notation for these groups is shown below.

U = superficial gas velocity, m/s (FPS)

Height = Height of the tube array above the distributor plate, m (in)

Weight = Bed inventory, sand, Kg (lbs)

OMT = Overall mixing time (secs) - the time required for the MSMM curve to fall within the noise band about the equilibrium concentration.

DISCUSSION OF GROUPS

Group B1: OMT versus U
Height = .254 m (10 in)
Weight = 907 Kg (2000 lbs)

Run	OMT (secs)	U m/s (FPS)
96	19	1.52 (5)
106	19	1.52 (5)
97	11	2.13 (7)
107	12	2.13 (7)
98	18	2.74 (9)
108	11	2.74 (9)
99	12	3.35 (11)
109	17	3.35 (11)

Apparently the spread in overall mixing time (OMT) for runs performed under the same experimental conditions is greater as the superficial gas velocity increases. Therefore, mixing at higher velocities is quite erratic and not very reproducible.

Group B2: OMT versus U
Height = .254 m (10 in)
Weight = 1134 Kg (2500 lbs)

Run	OMT (secs)	U m/s (FPS)
92	14	1.52 (5)
102	12	1.52 (5)
93	16	2.13 (7)
103	15	2.13 (7)
104	18	2.74 (9)
95	21	3.35 (11)
105	19	3.35 (11)

This group indicates that OMT increases with superficial gas velocity, which seems contradictory.

Group B3: OMT versus Height
U = 1.52 m/s (5 FPS)
Weight = 907 Kg (2000 lbs)

Run	OMT (secs)	Height m (in)
76	12	.508 (20)
96	19	.254 (10)
106	19	.254 (10)

This group shows better mixing with increased height of the tube array above the distributor plate.

Group B4: OMT versus Height
U = 3.35 m/s (11 FPS)
Weight = 1134 Kg (2500 lbs)

Run	OMT (secs)	Height m (in)
82	11	.508 (20)
95	21	.254 (10)
105	19	.254 (10)

This group also shows better mixing of tracer with increased height of the tube array above the distributor plate.

Group B5: OMT versus Weight
U = 1.52 m/s (5 FPS)
Height = .254 m (10 in)

Run	OMT (secs)	Weight Kg (lbs)
88	19	1361 (3000)
92	14	1134 (2500)
102	12	1134 (2500)
96	19	907 (2000)
106	19	907 (2000)

Mixing with 1361 Kg (3000 lbs) and 907 Kg (2000 lbs) is about the same. The best mixing occurs with 1134 Kg (2500 lbs) of sand.

Group B6: OMT versus Weight
U = 3.35 m/s (11 FPS)
Height = .254 m (10 in)

Run	OMT (secs)	Weight Kg (lbs)
91	21	1361 (3000)
95	21	1134 (2500)
105	19	1134 (2500)
99	12	907 (2000)
109	17	907 (2000)

In this group one can see the variability caused by higher gas velocities. It appears that the fastest mixing occurs with 907 Kg (2000 lbs) of sand. Both 1361 Kg (3000 lbs) and 1134 Kg (2500 lbs) of bed inventory have almost the same effect on mixing.

In conclusion, the MSMM results were considered tentative and in some cases contradictory. In addition, MSMM only partially described local mixing. Values of B were misleading because they measured the rate of approach to equilibrium from the highest MSMM peak without regard to any horizontal shift. In other words, the B values measured "how" the MSMM curve fell to the equilibrium level and not "when" it fell to this level. Thus, a better measure of mixing was needed.

As far as overall mixing time (OMTs) were concerned, the data seemed fairly reproducible, except at higher superficial gas velocities where reproducibility was significantly impaired (see runs 98, 108 and 99, 109 in Table 5.2). In Table 5.2, replicate runs are in parentheses with their OMTs in the same respective order.

TABLE 5.2 Replicate Runs.

Replicate Runs	OMT (secs)
(92, 102)	(14, 12)
(93, 103)	(16, 15)
(95, 105)	(21, 19)
(96, 106)	(19, 19)
(97, 107)	(11, 12)
(98, 108)	(18, 11)
(99, 109)	(14, 19)

VI. SUCCESSFUL ANALYSIS

6.1 The Histogram Plots

In order to understand how fast clumps of ferrite tracer disperse within the tube array and, ergo, pollution control, histograms (see Figure 6.1) have been constructed over 1 second time intervals ascending in a Fibonacci sequence (i.e., 1,2,3,5,8,13,21,34,55...), where each number is the sum of the previous two. For example, the first six intervals are: 0-1 second, 1-2 seconds, 2-3 seconds, 4-5 seconds, 7-8 seconds and 12-13 seconds. This series was chosen because it describes exponential or natural decaying functions in a characteristic and, therefore, relevant manner. In our case, significant concentration changes occur relatively early in the mixing process, but as time progresses, the magnitudes of these changes diminish. Thus, it is vital to observe early changes, whereas those that occur later may be discounted and lumped together as the Fibonacci sequence does.

The abscissas of the histogram plots are divided into ten intervals of normalized concentration or $(\tilde{C}_i/C^*)$, where $\tilde{C}_i$ is the average concentration measured on channel i over a one second time interval and $\bar{C}^*$ is the average concentration sensed by all channels over the last ten seconds of a run (i.e., the well-mixed concentration). Values of the normalized concentration are plotted in the range from one to

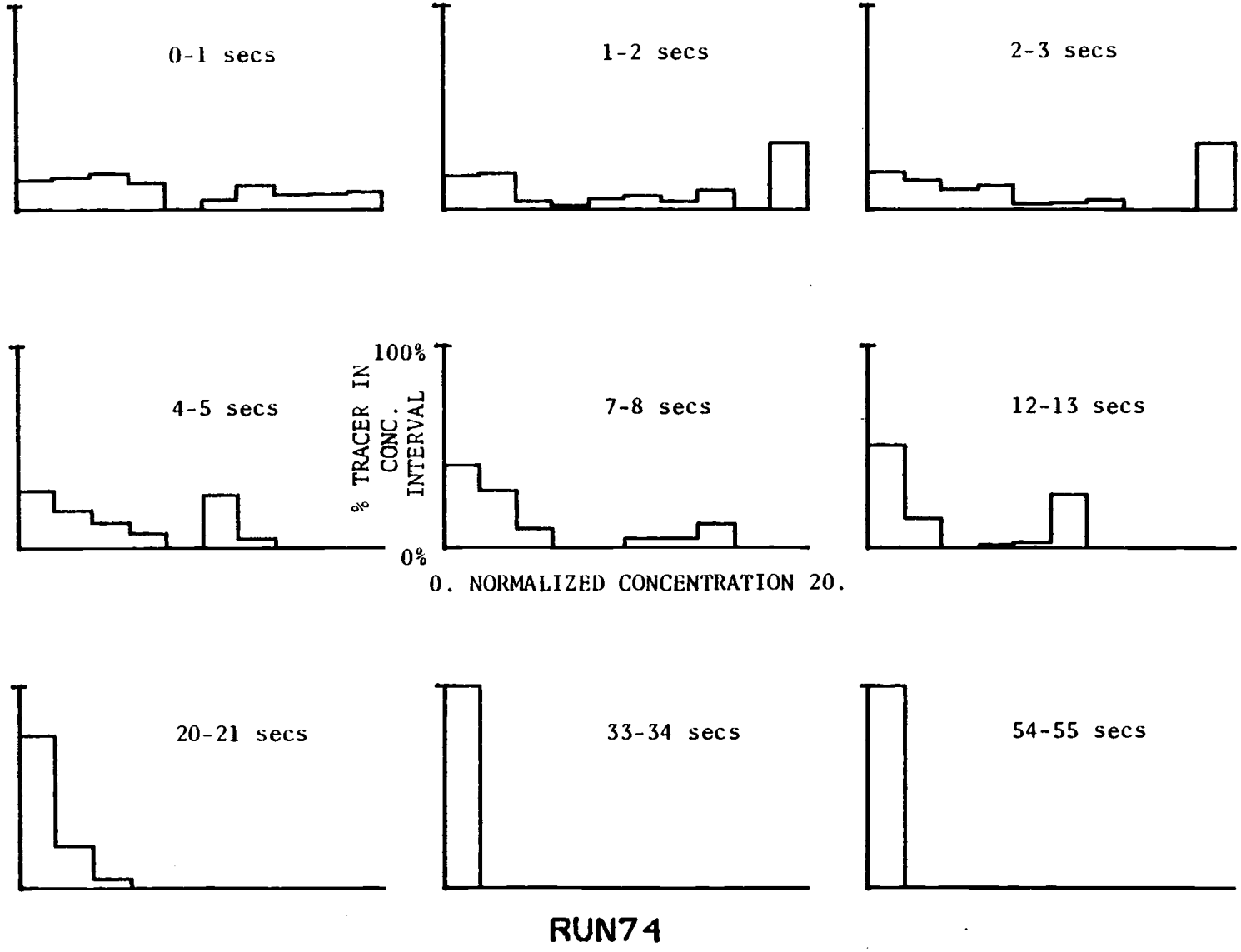

Figure 6.1. Histogram plots for runs 74 - 114.

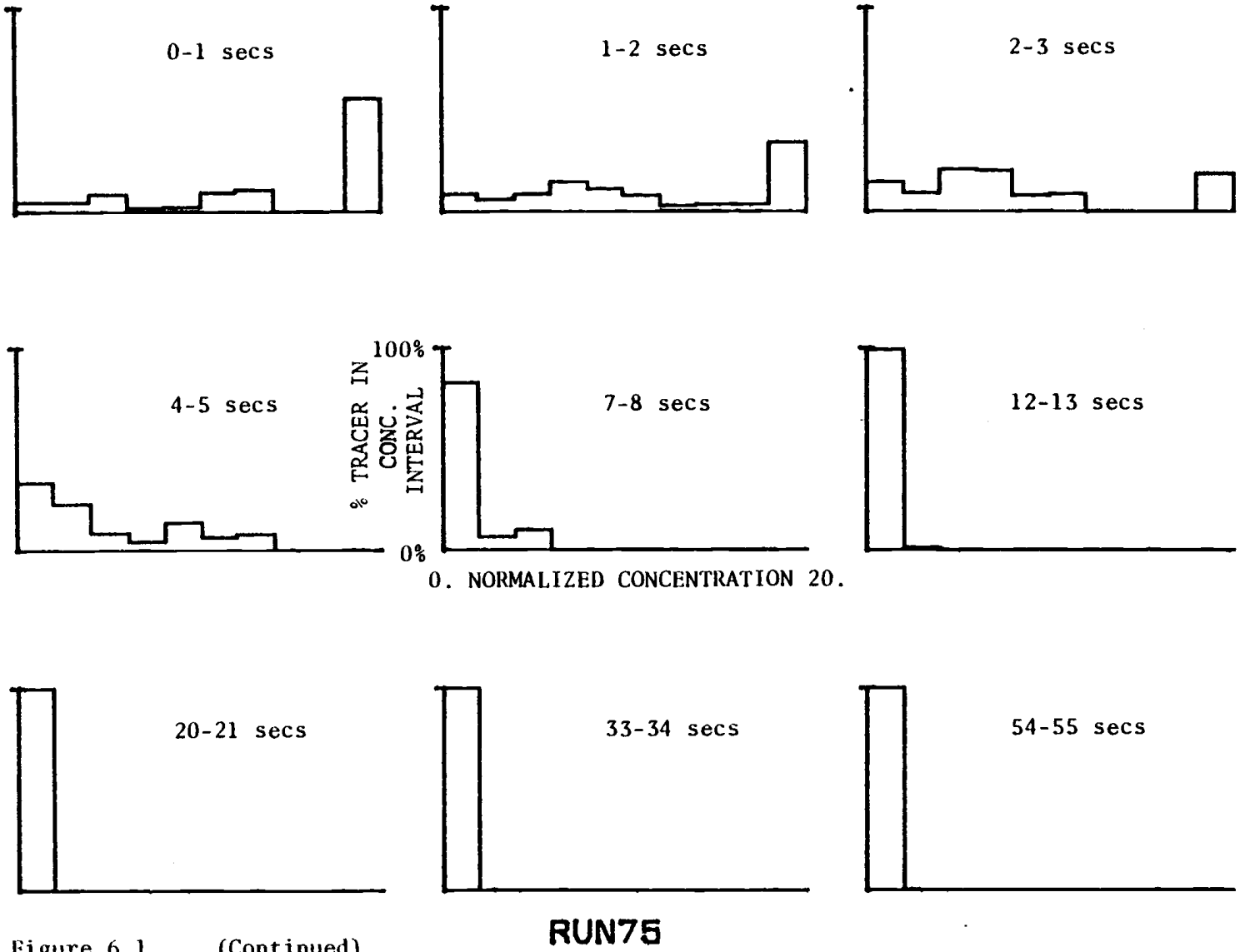

Figure 6.1. (Continued)

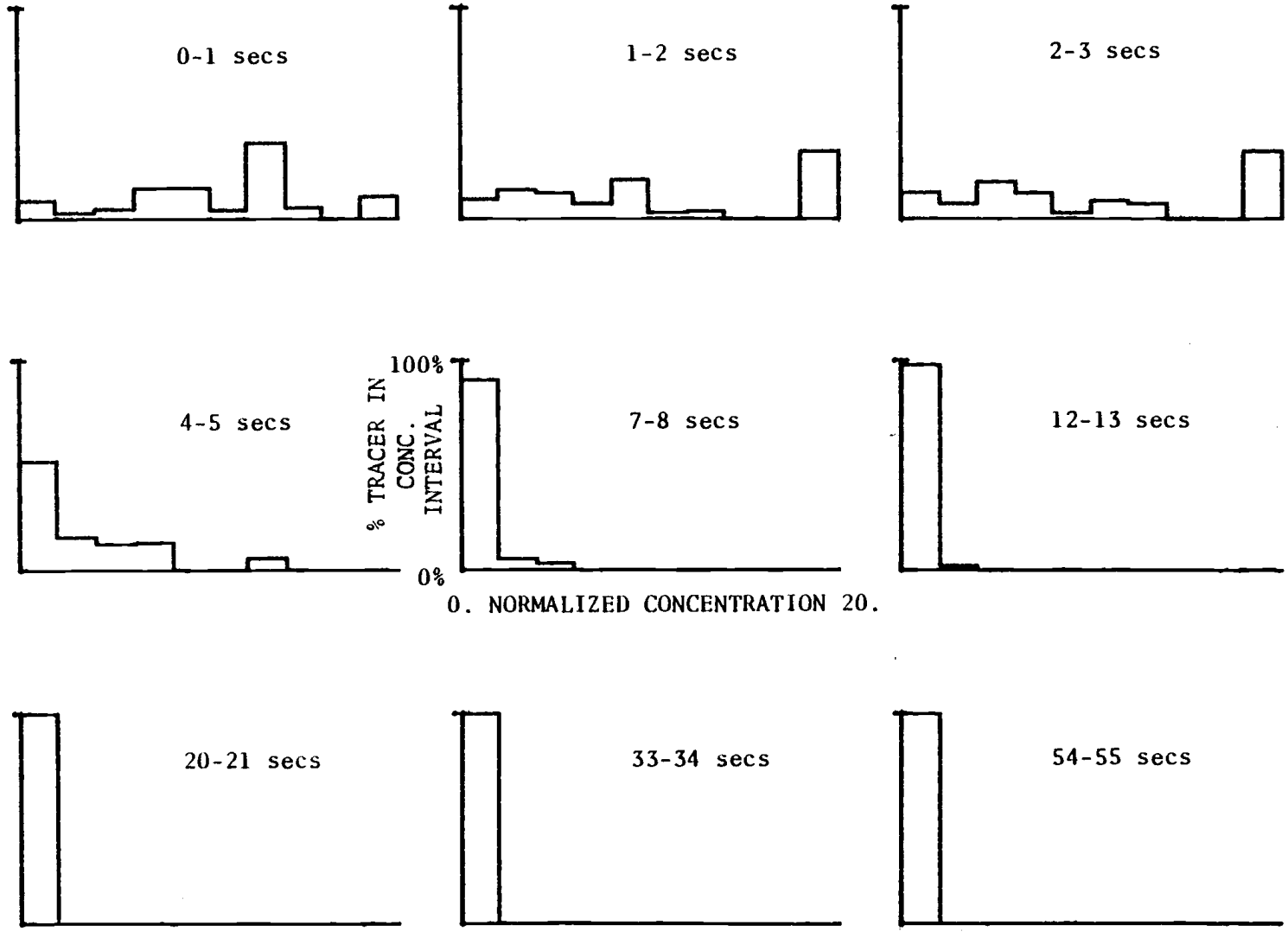

Figure 6.1. (Continued)

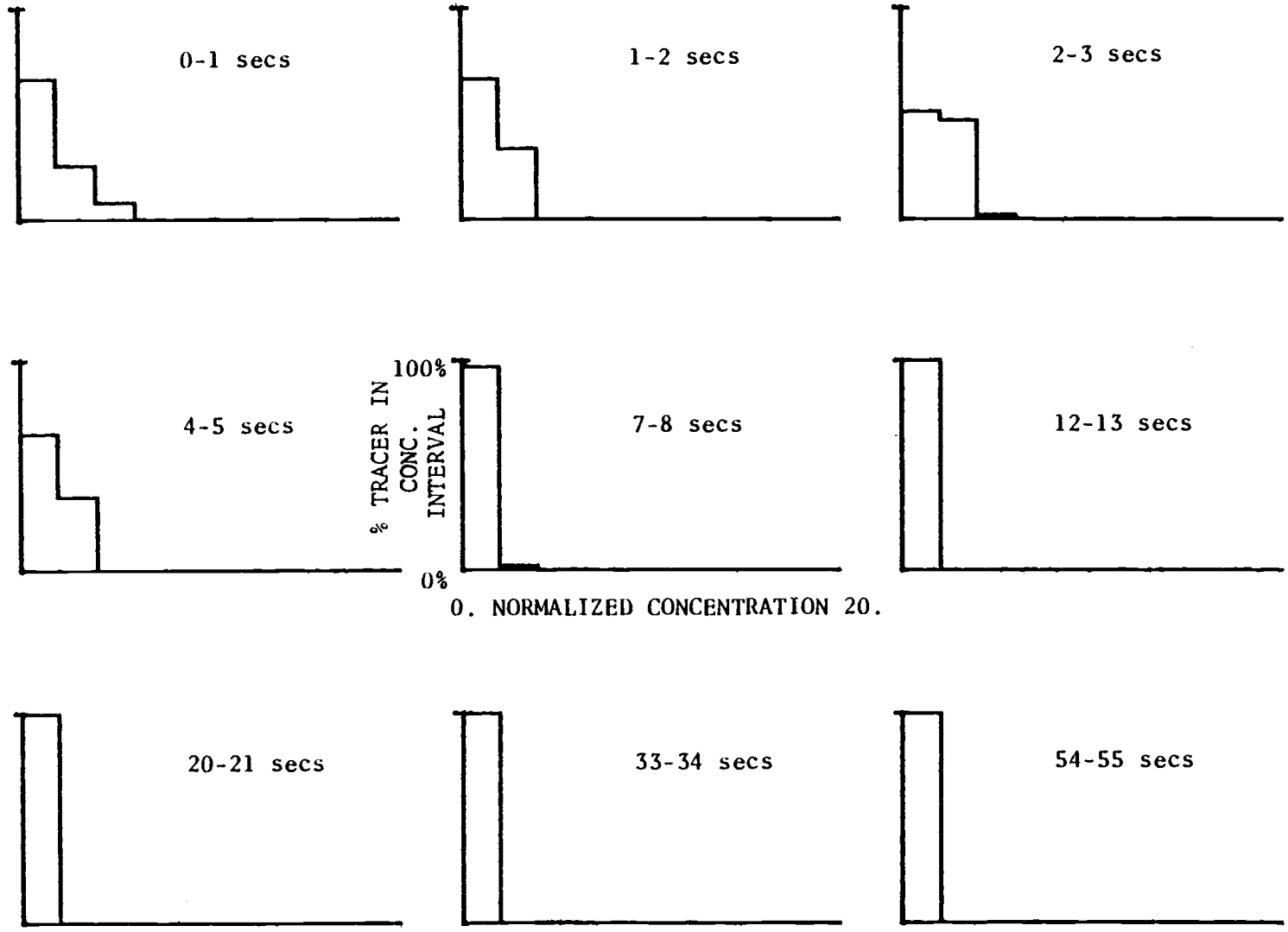

Figure 6.1. (Continued)

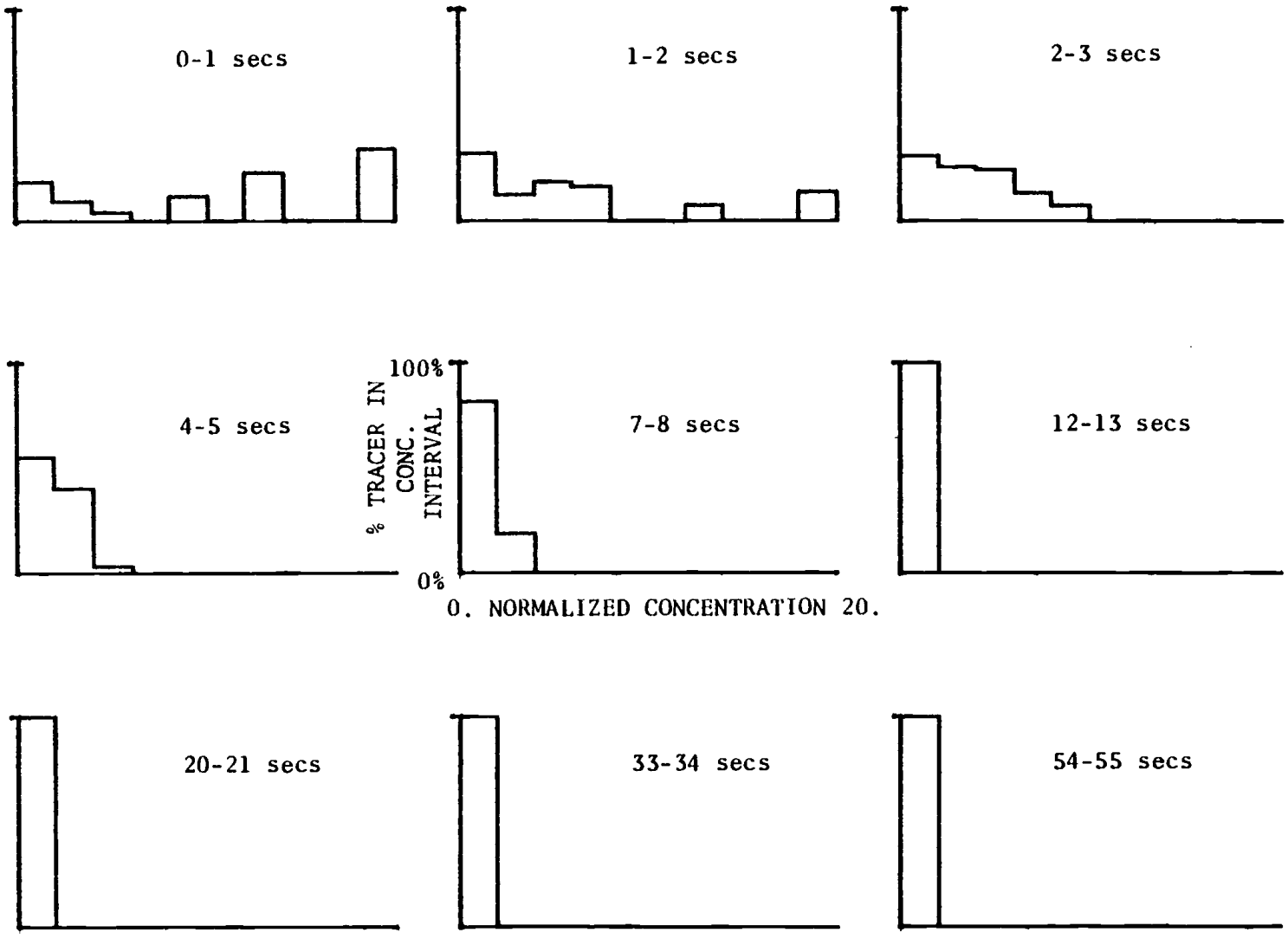

Figure 6.1. (Continued)

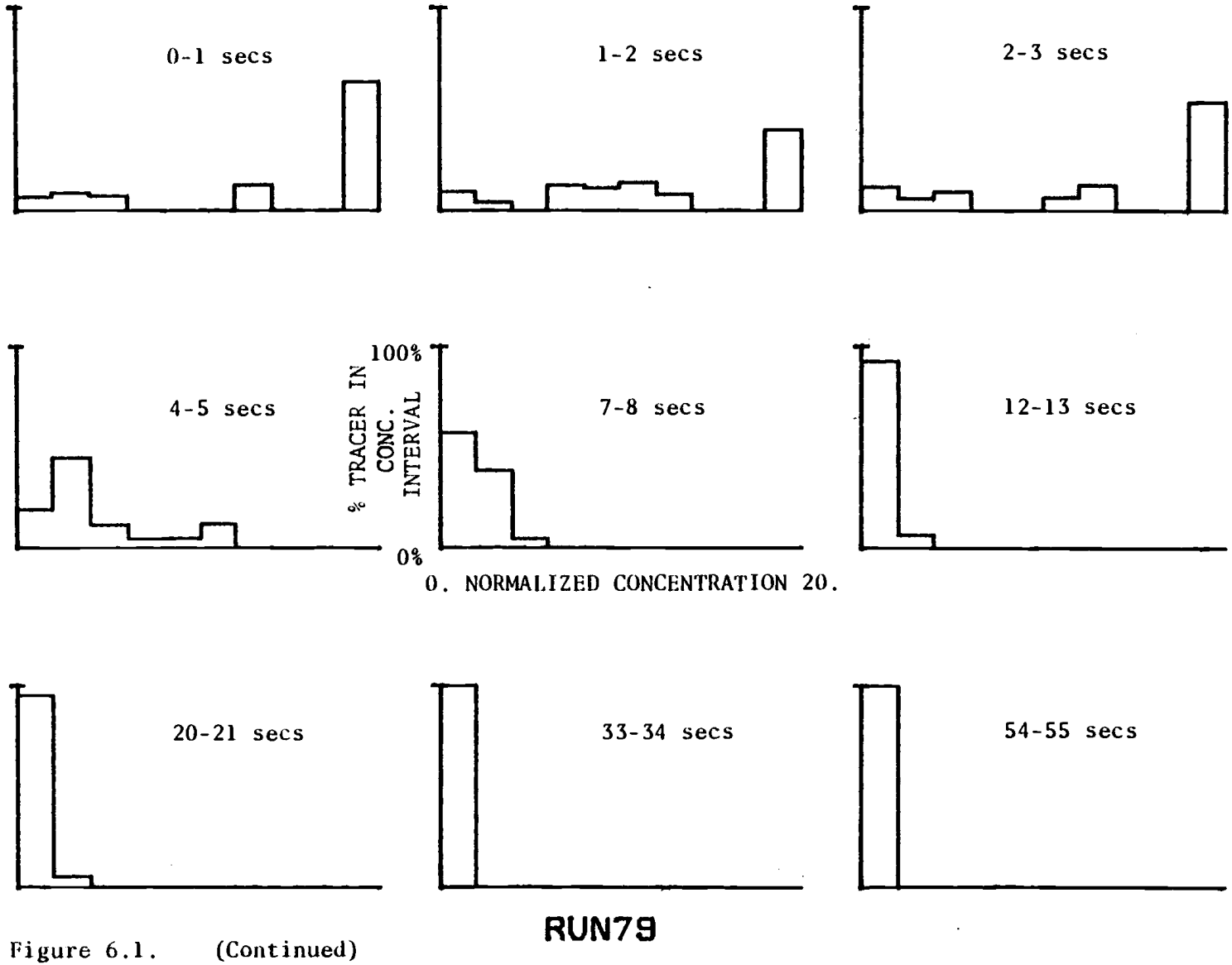

Figure 6.1. (Continued)

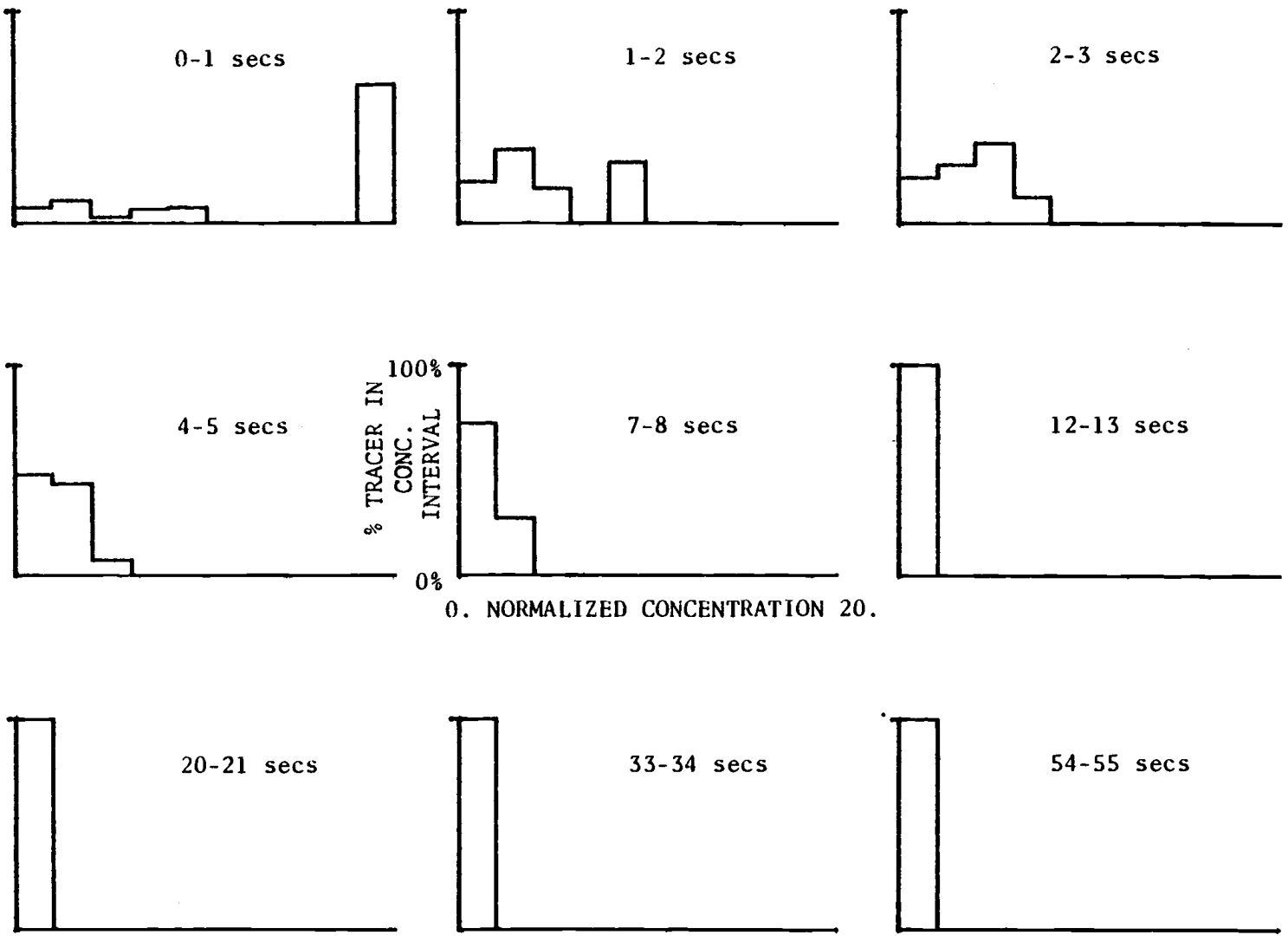

Figure 6.1. (Continued)

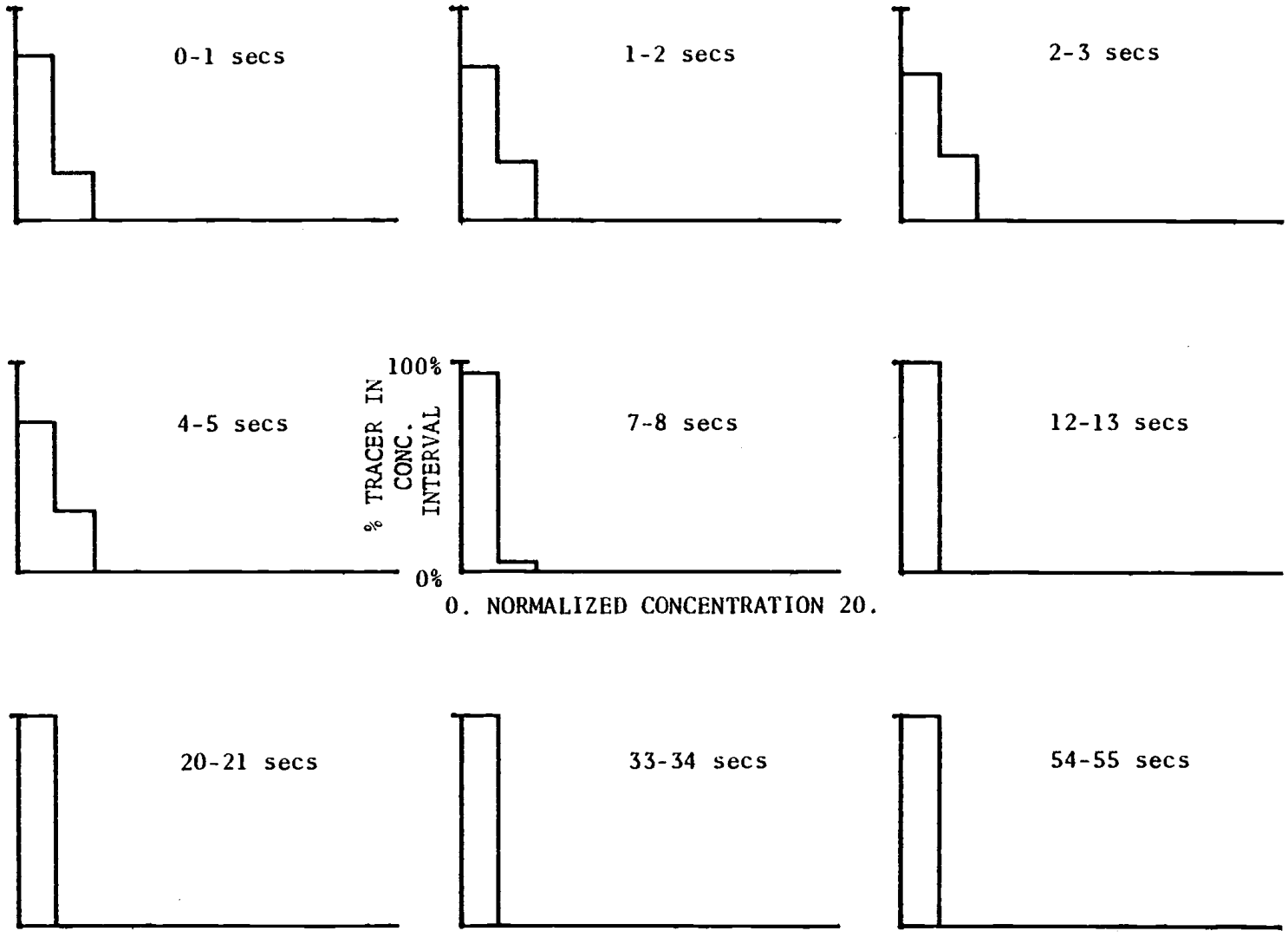

Figure 6.1. (Continued)

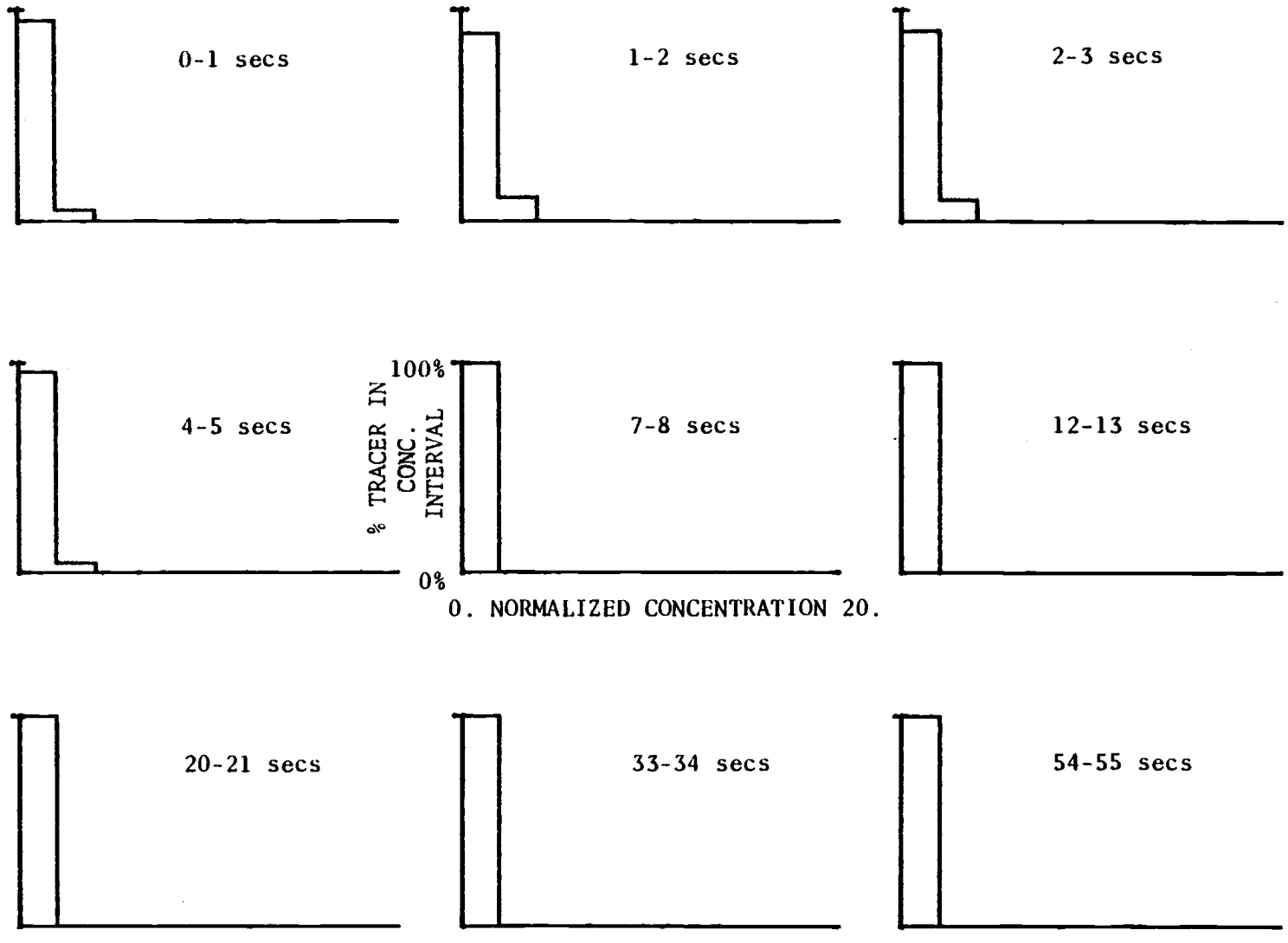

Figure 6.1. (Continued)

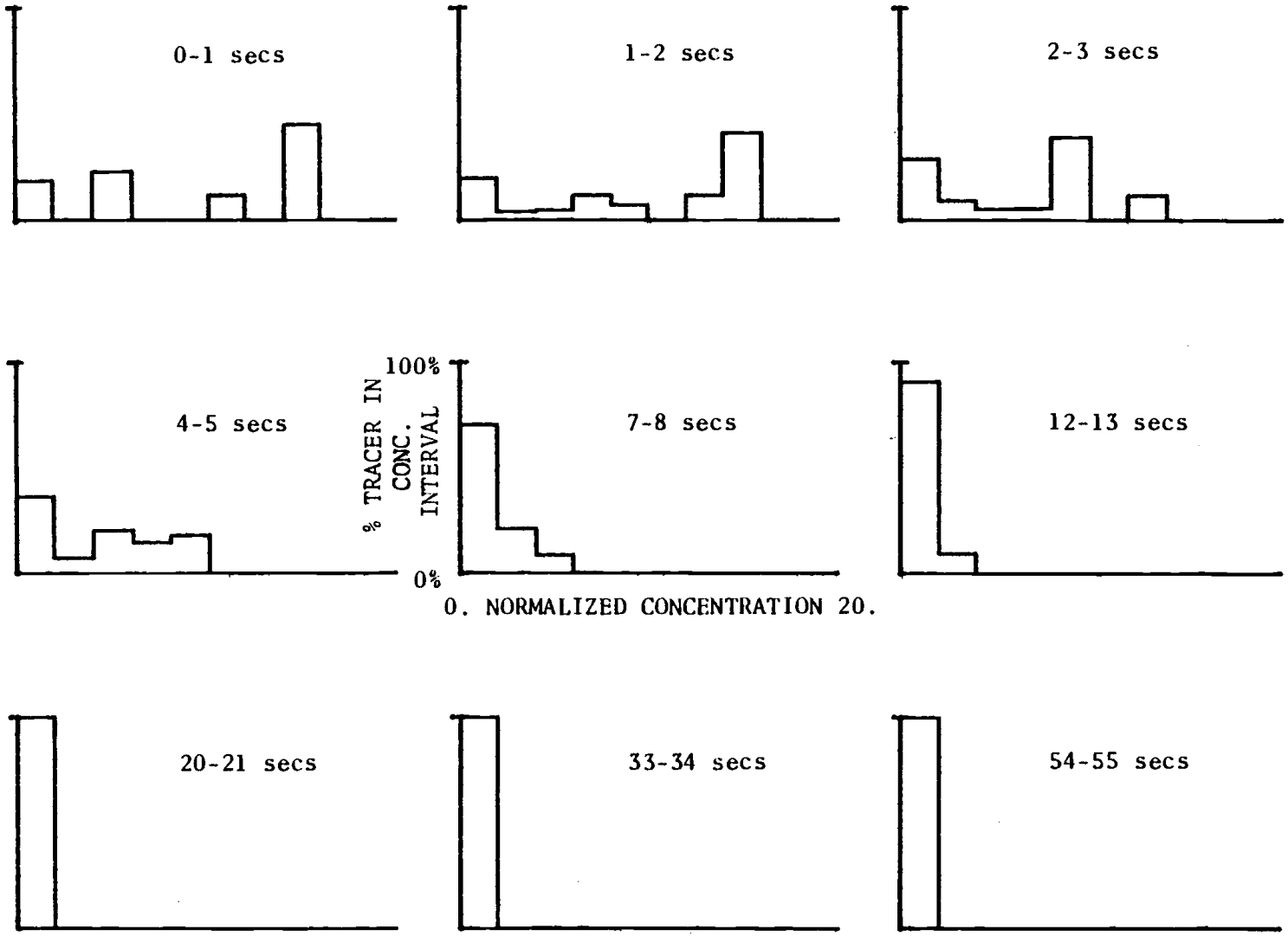

Figure 6.1. (Continued)

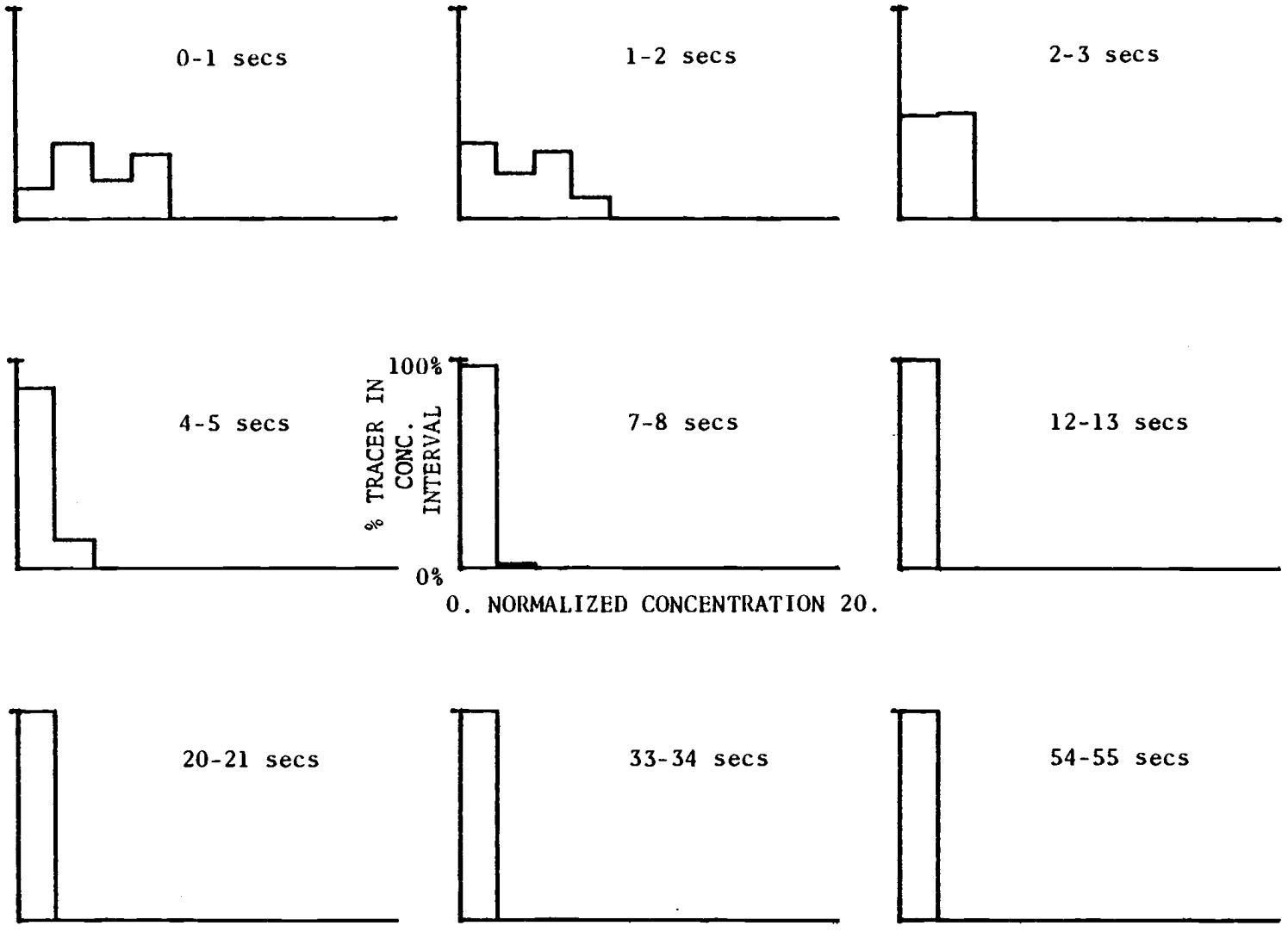

Figure 6.1. (Continued)

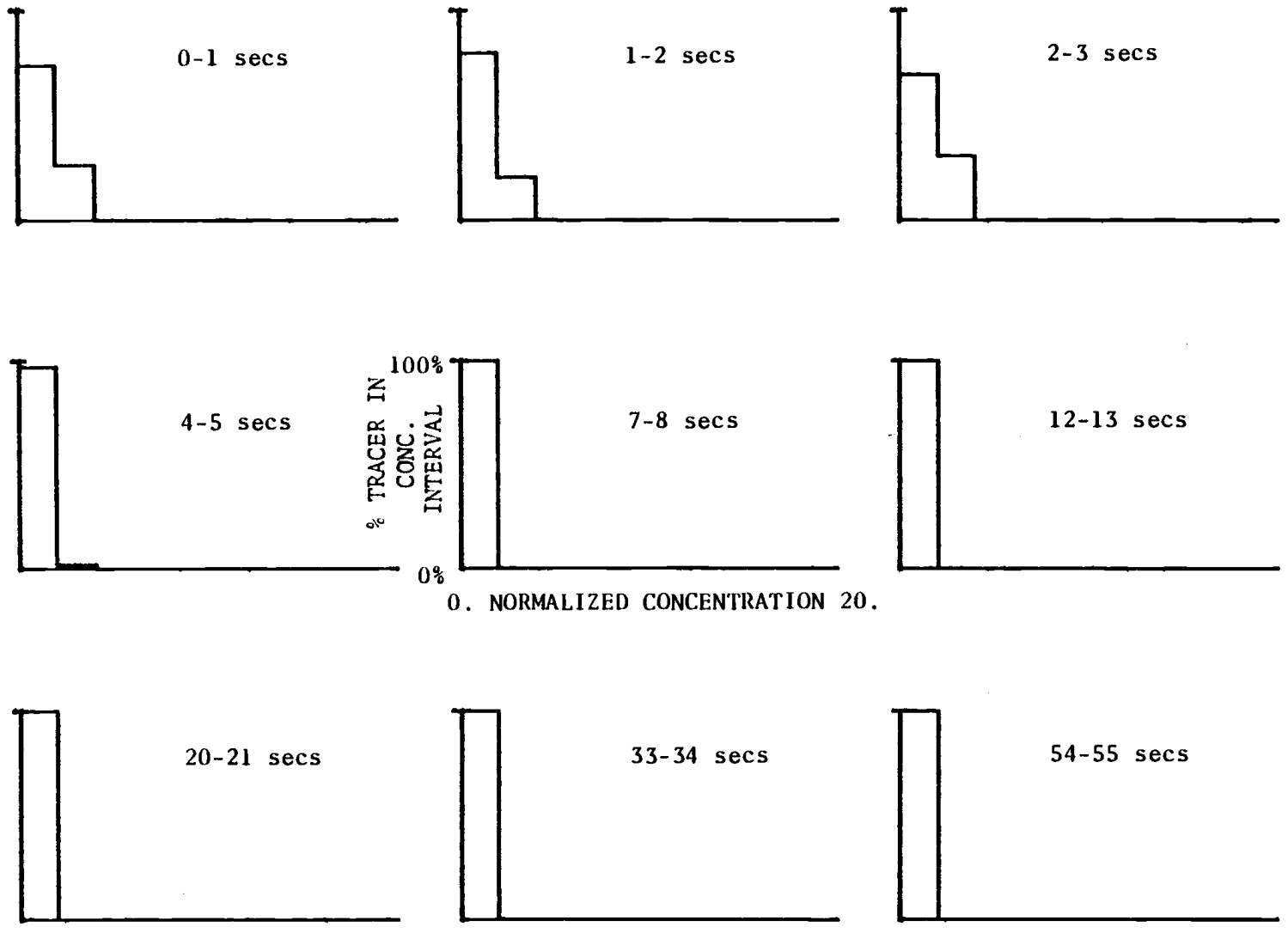

Figure 6.1. (Continued)

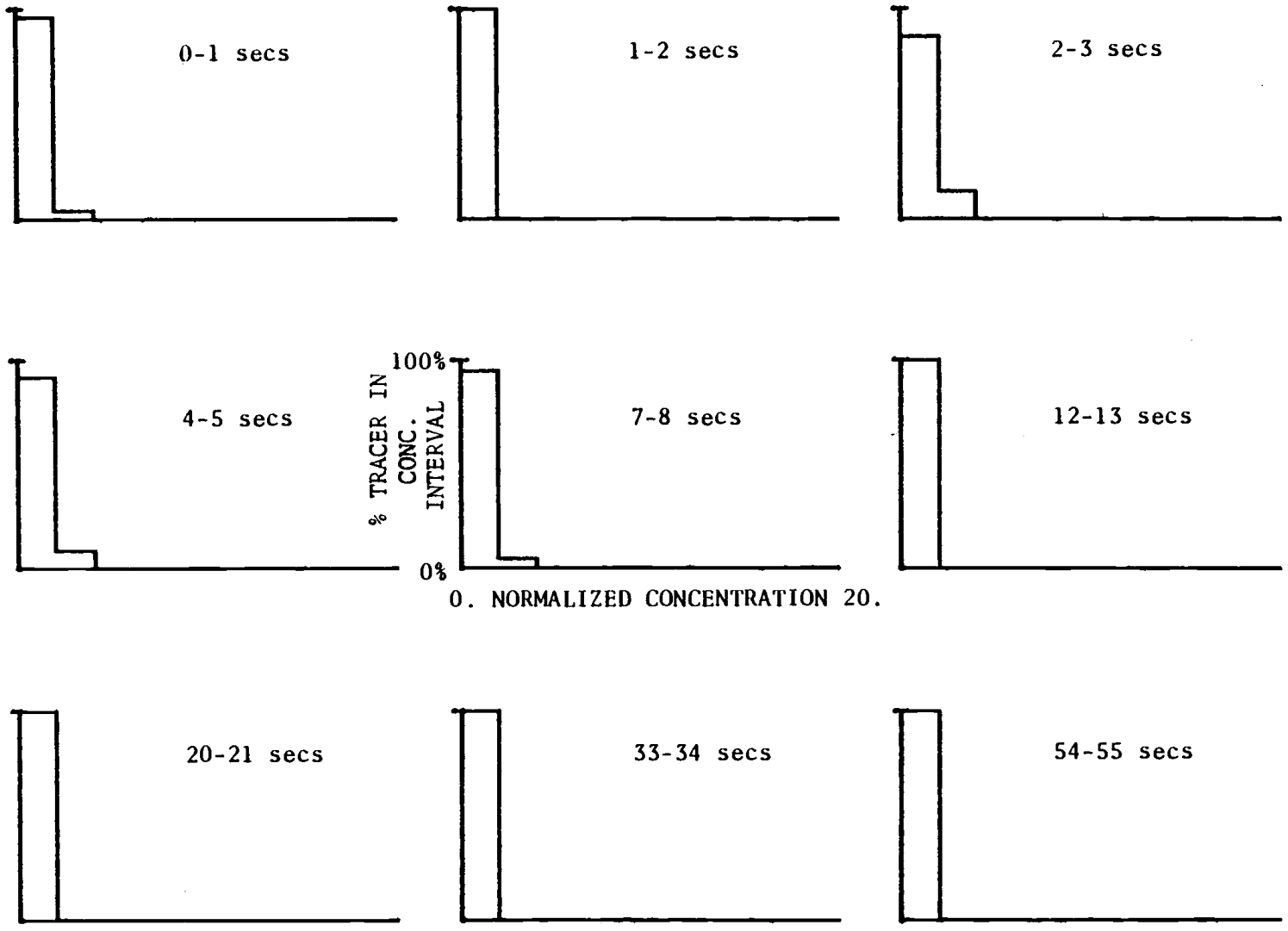

Figure 6.1. (Continued)

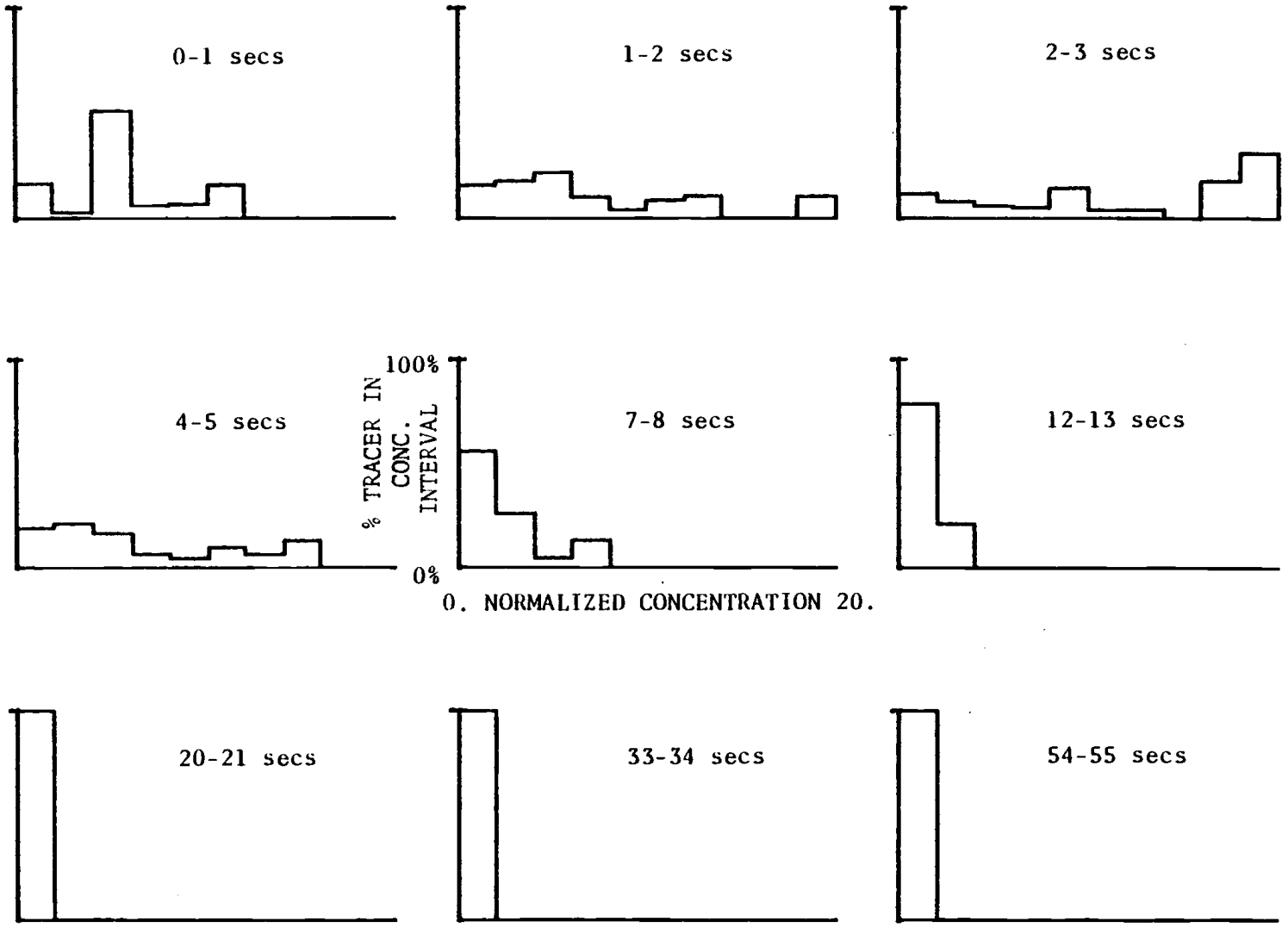

Figure 6.1. (Continued)

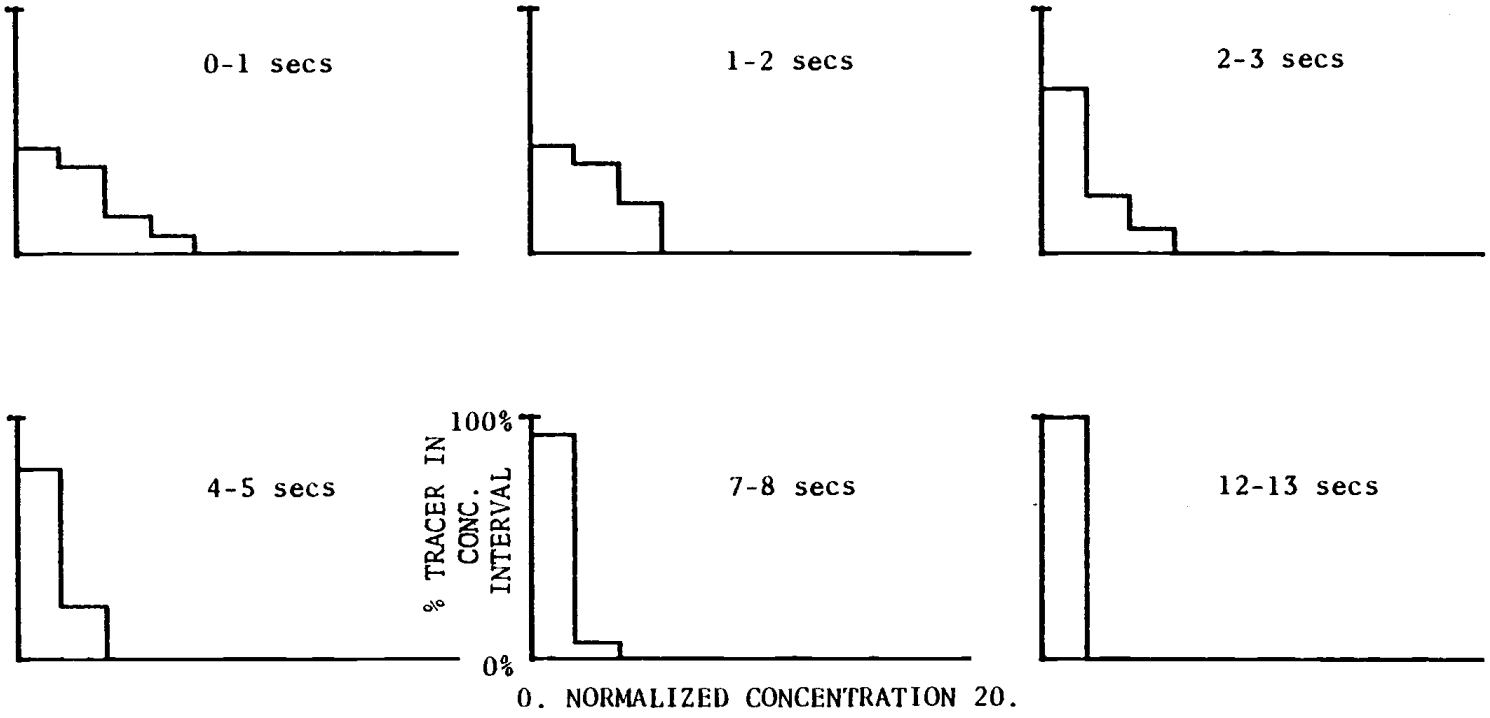

Figure 6.1. (Continued)

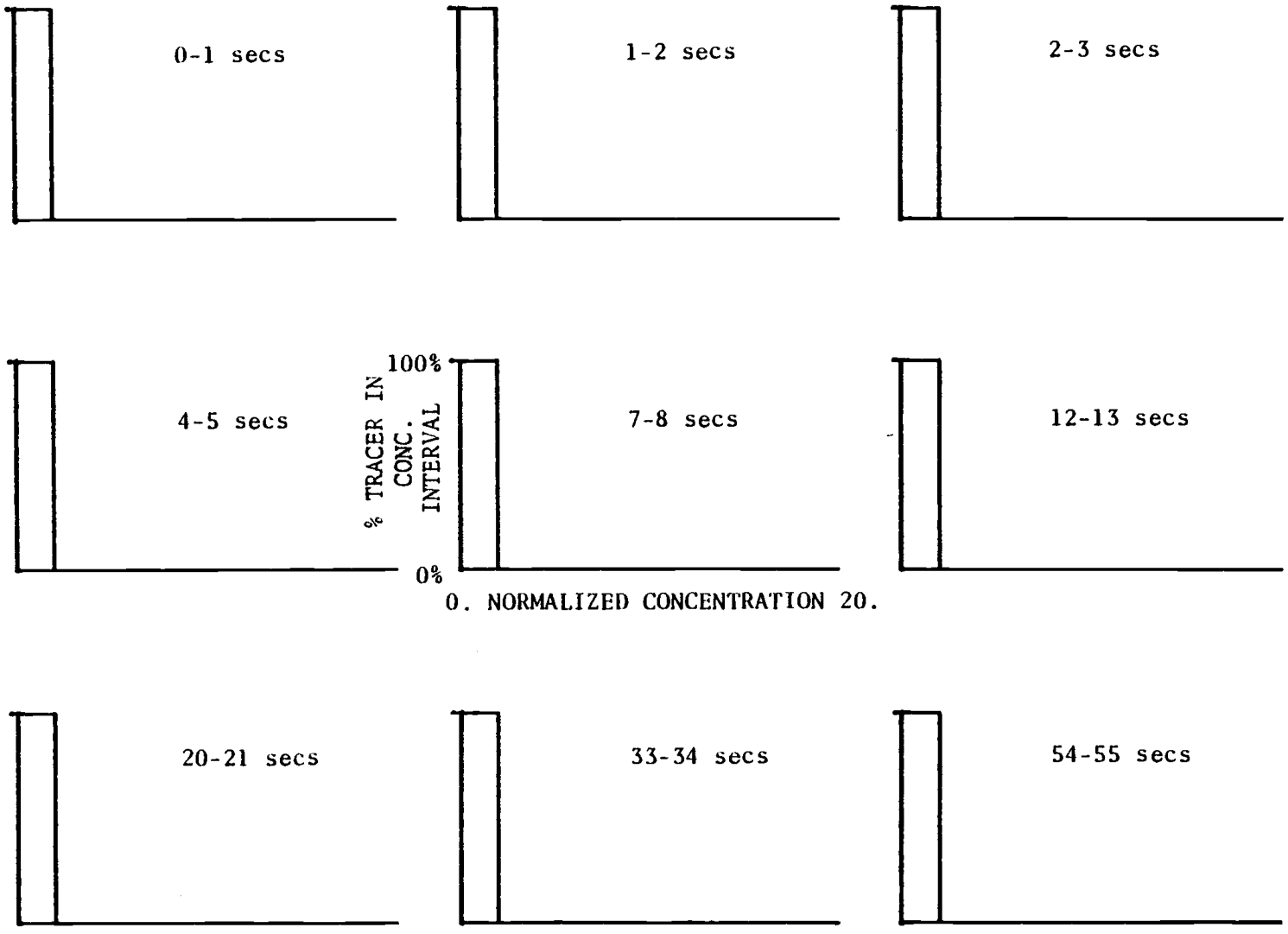

Figure 6.1. (Continued)

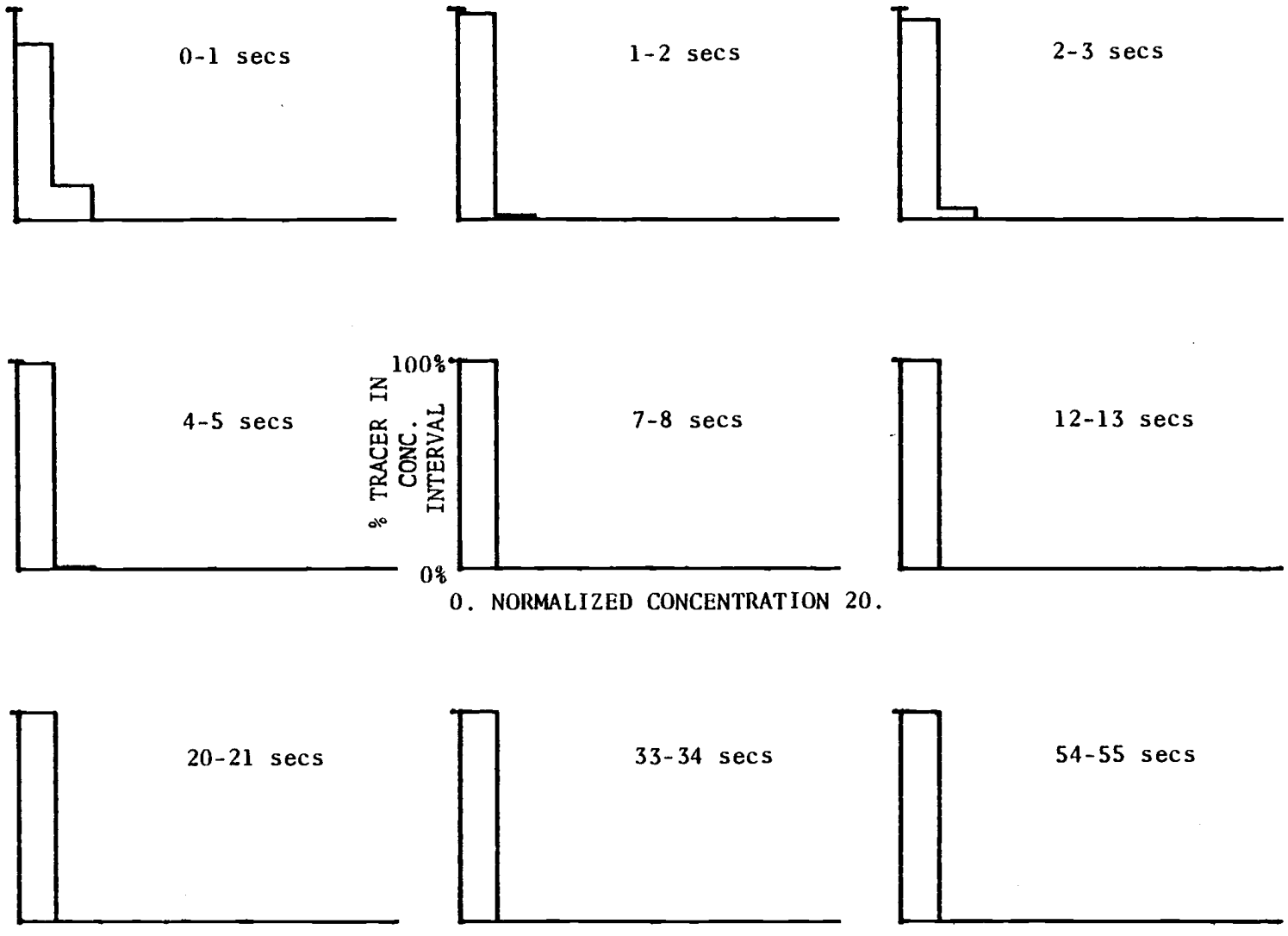

Figure 6.1. (Continued)

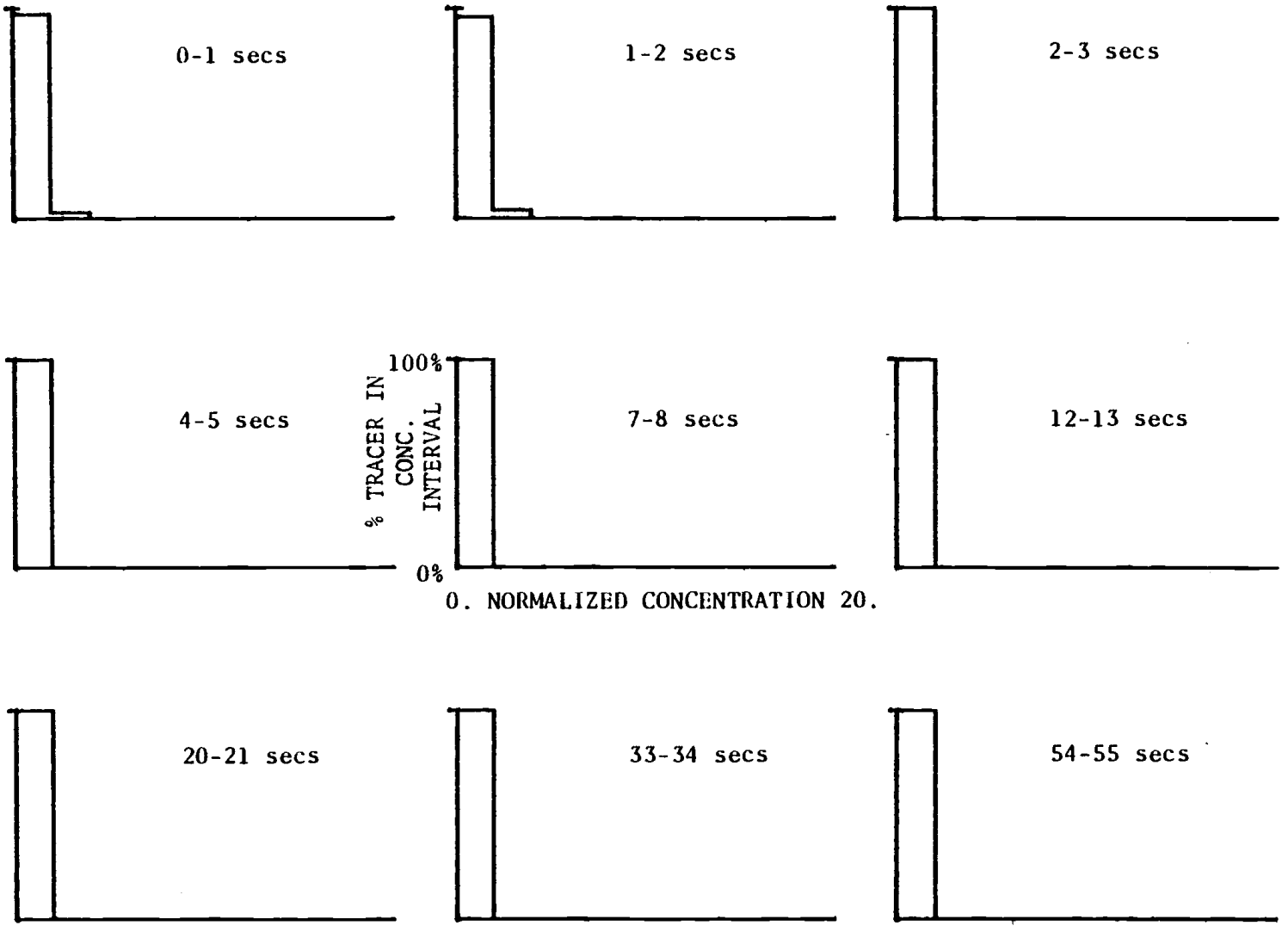

Figure 6.1. (Continued)

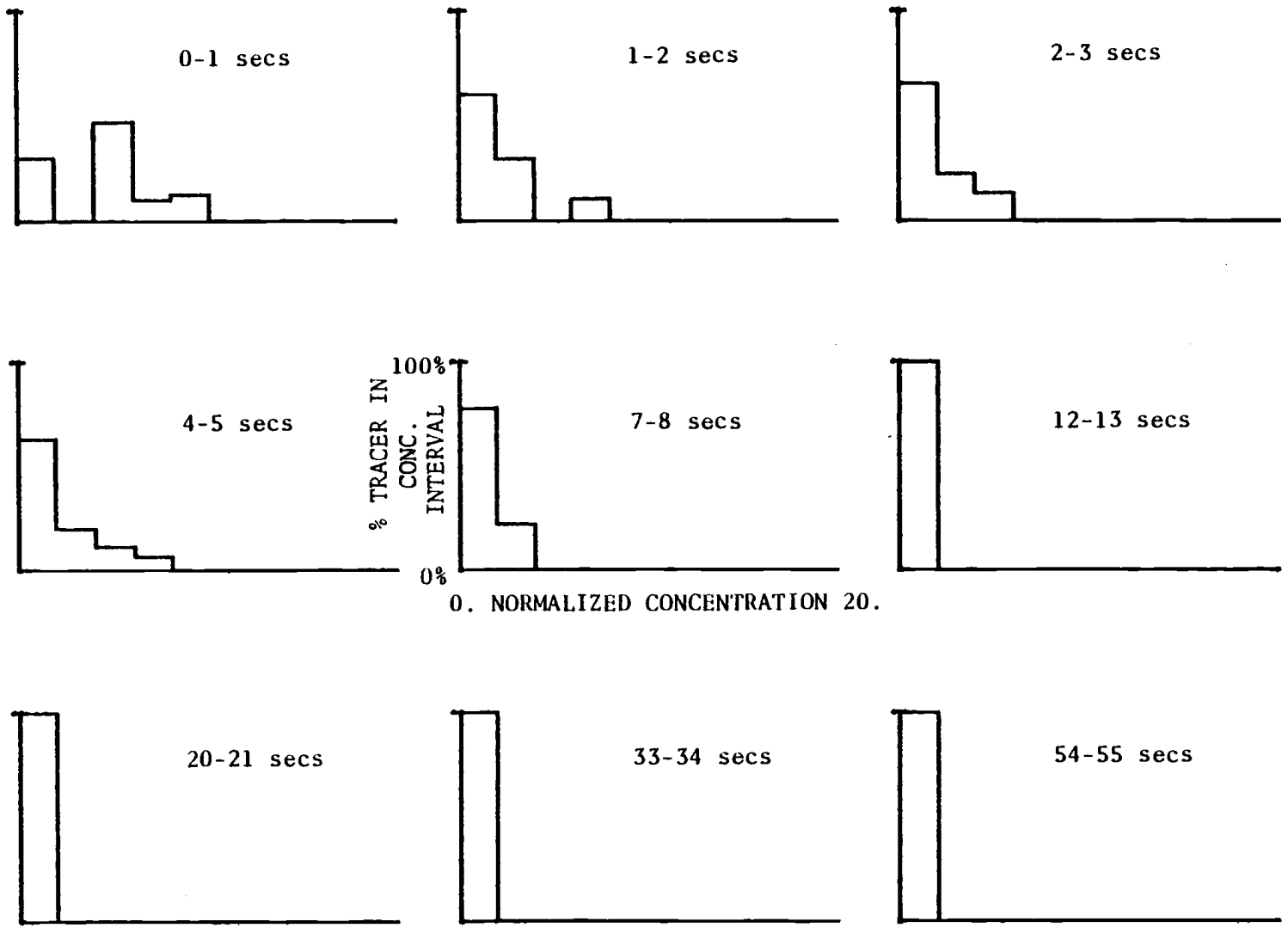

Figure 6.1. (Continued)

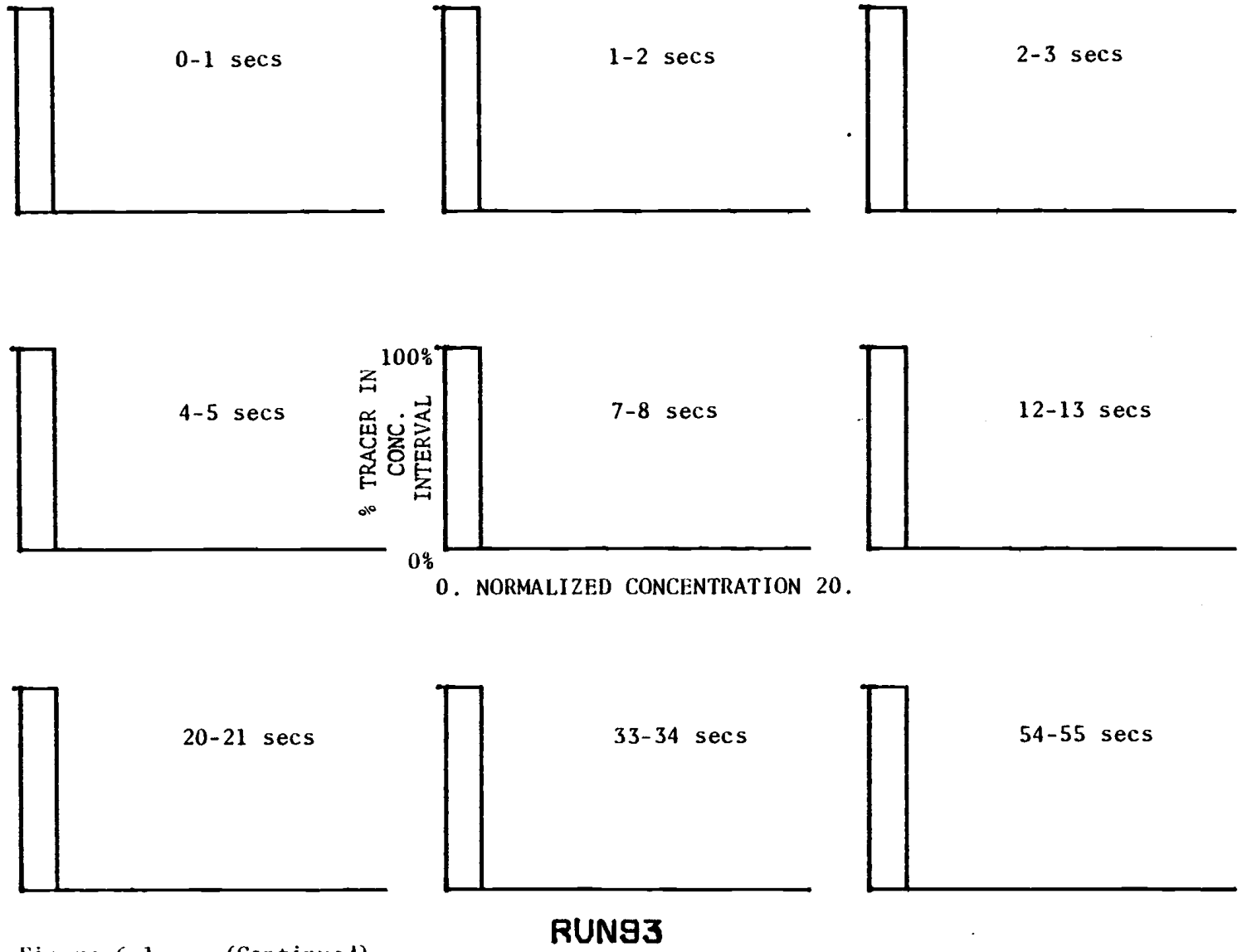

Figure 6.1. (Continued)

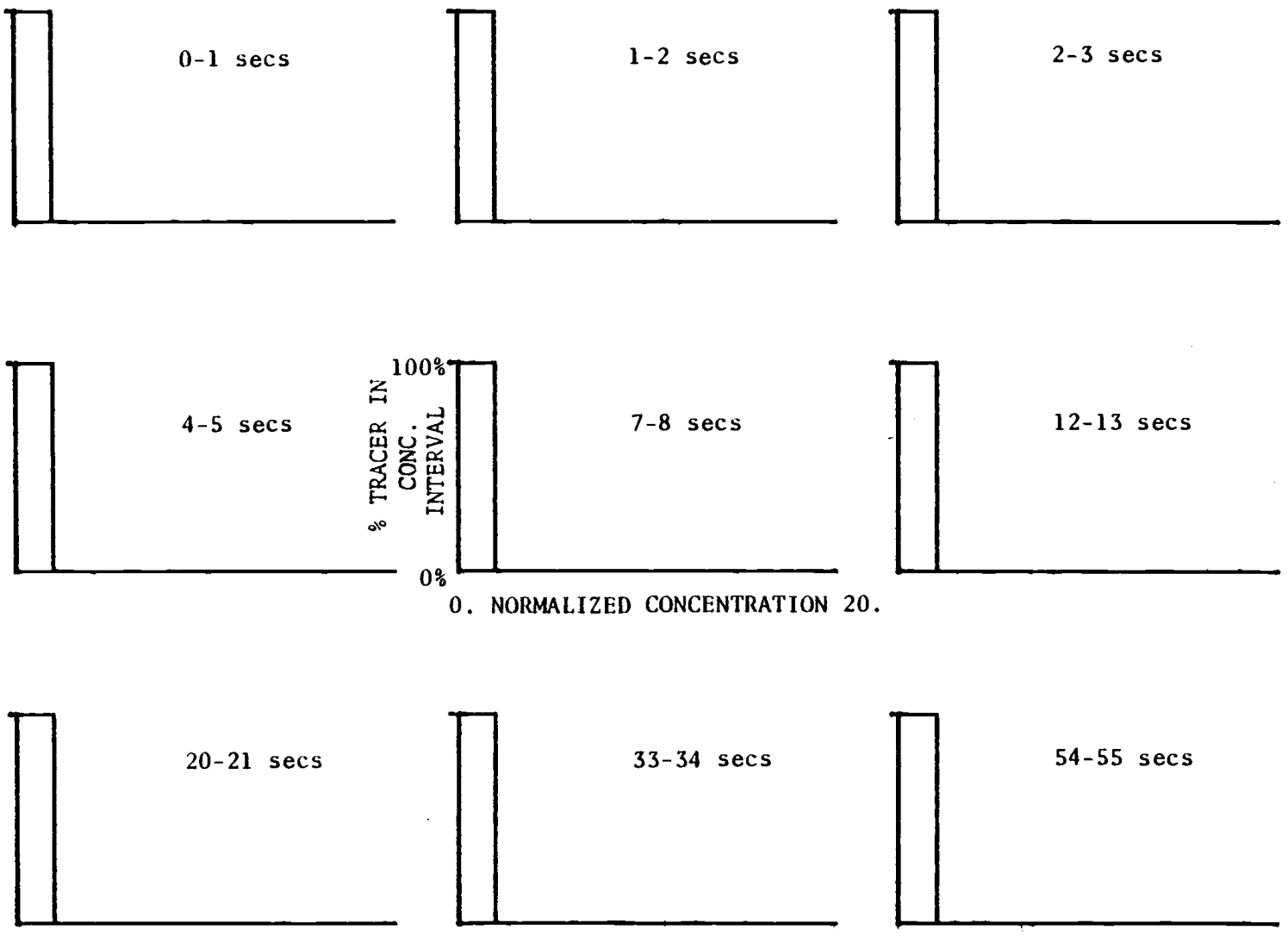

Figure 6.1. (Continued)

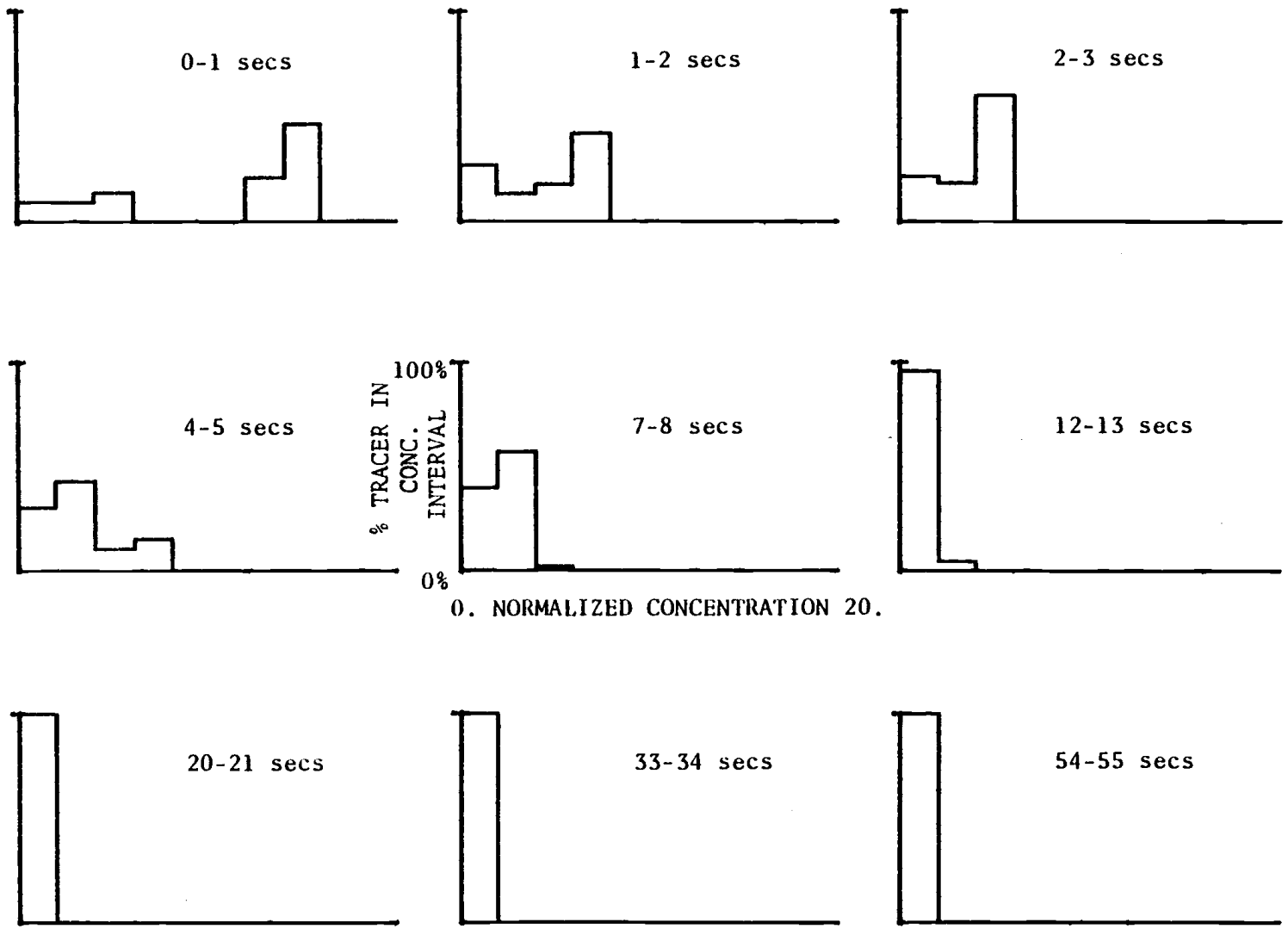

Figure 6.1. (Continued)

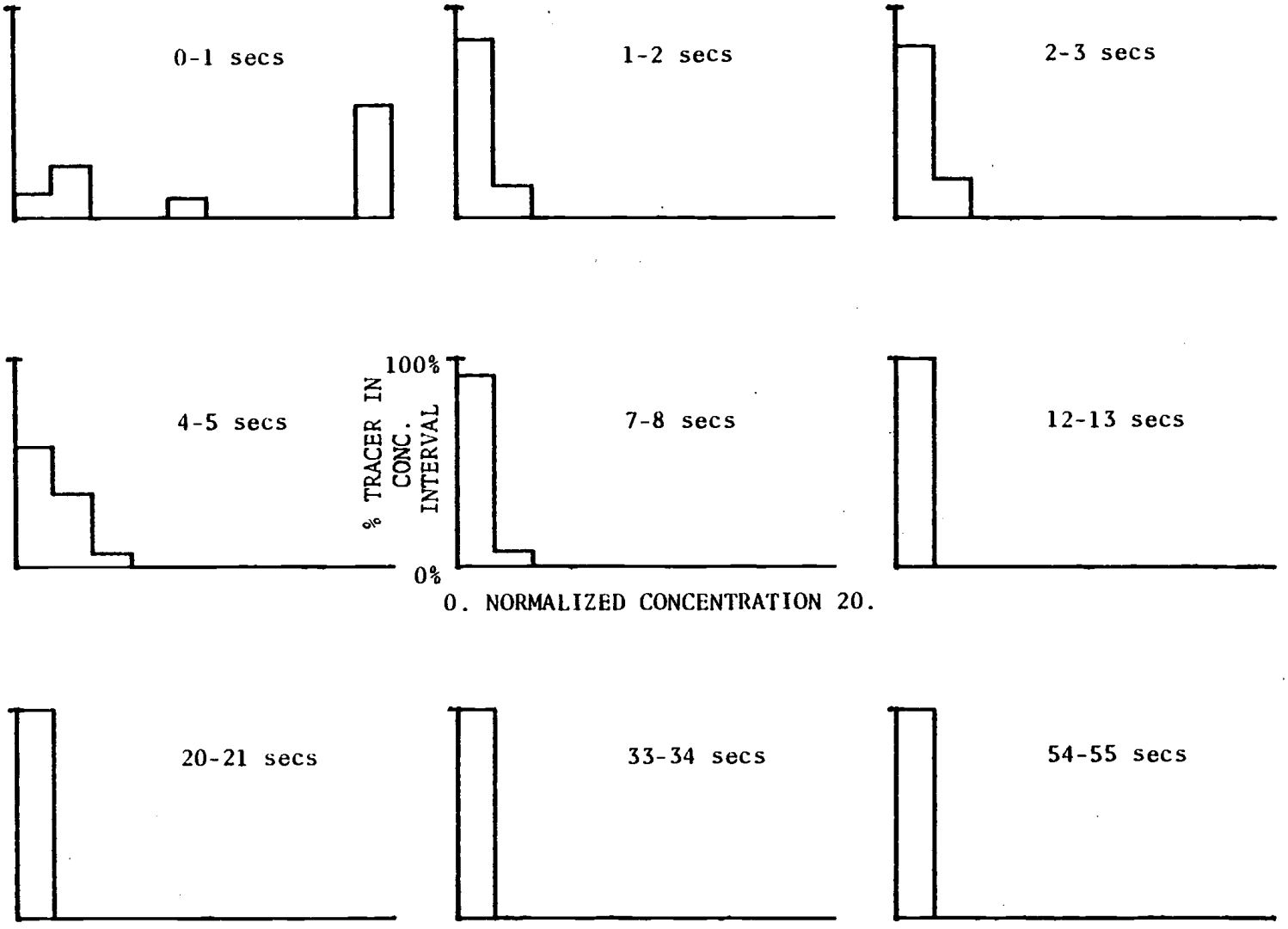

Figure 6.1. (Continued)

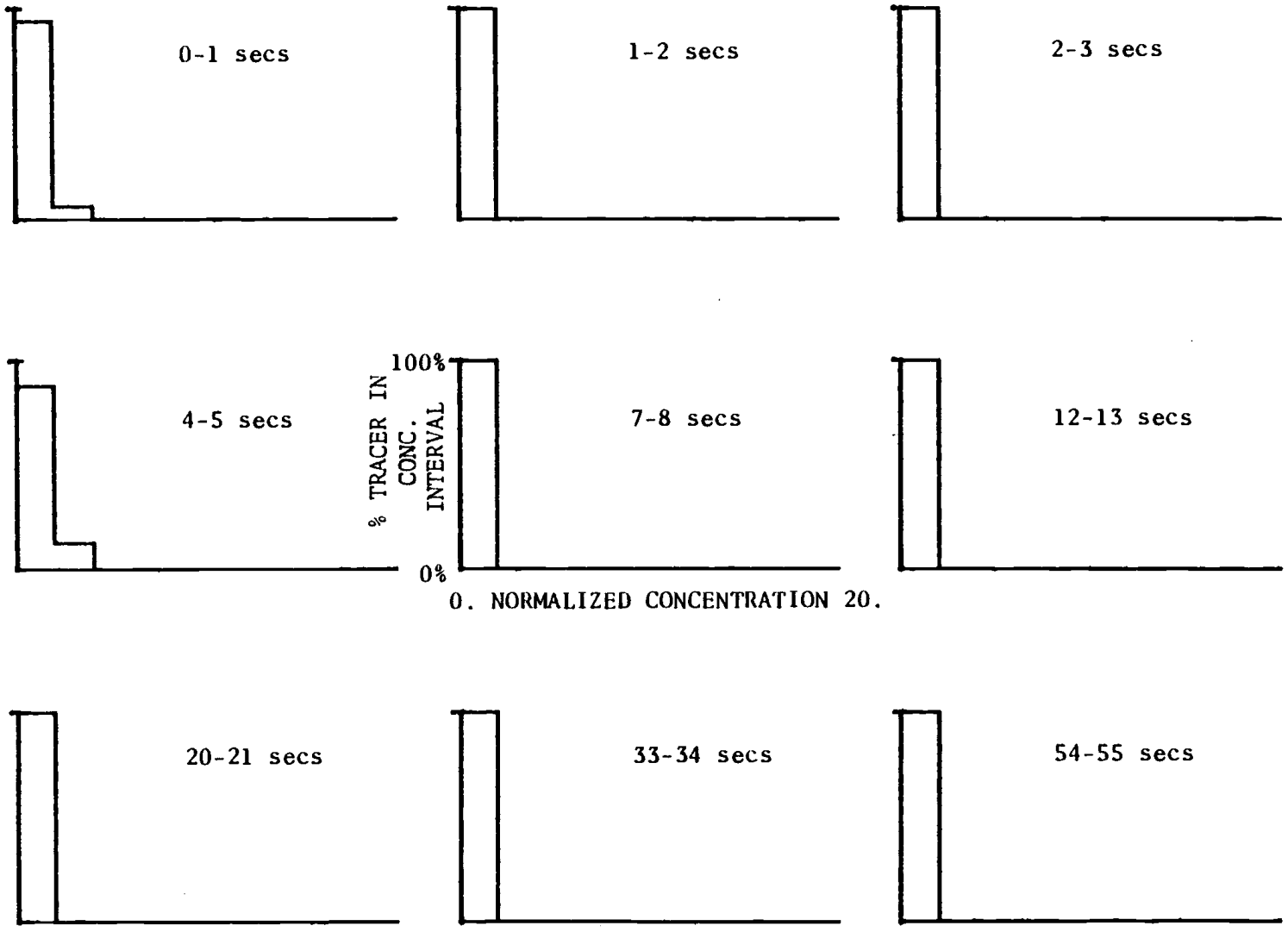

Figure 6.1. (Continued)

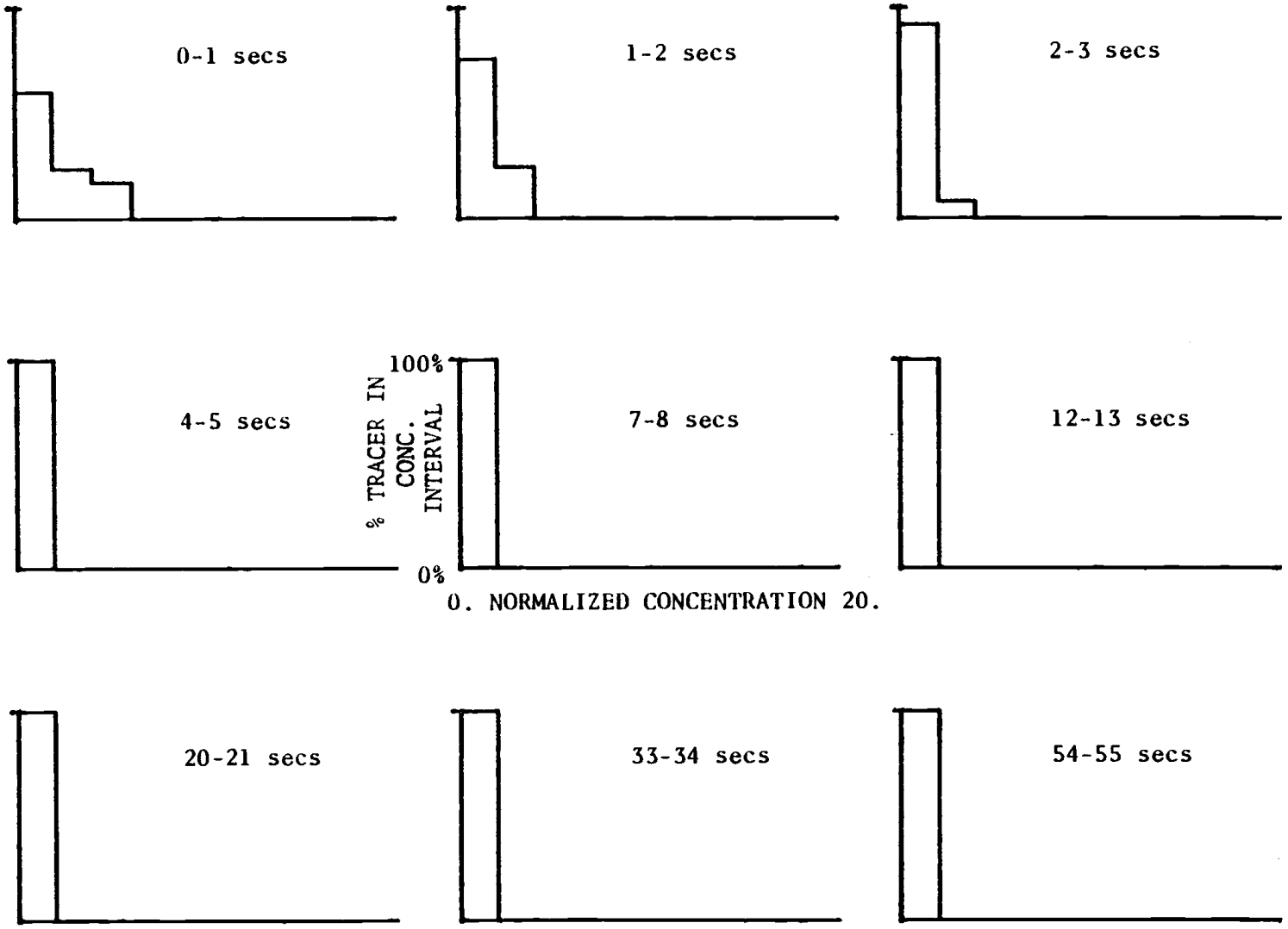

Figure 6.1. (Continued)

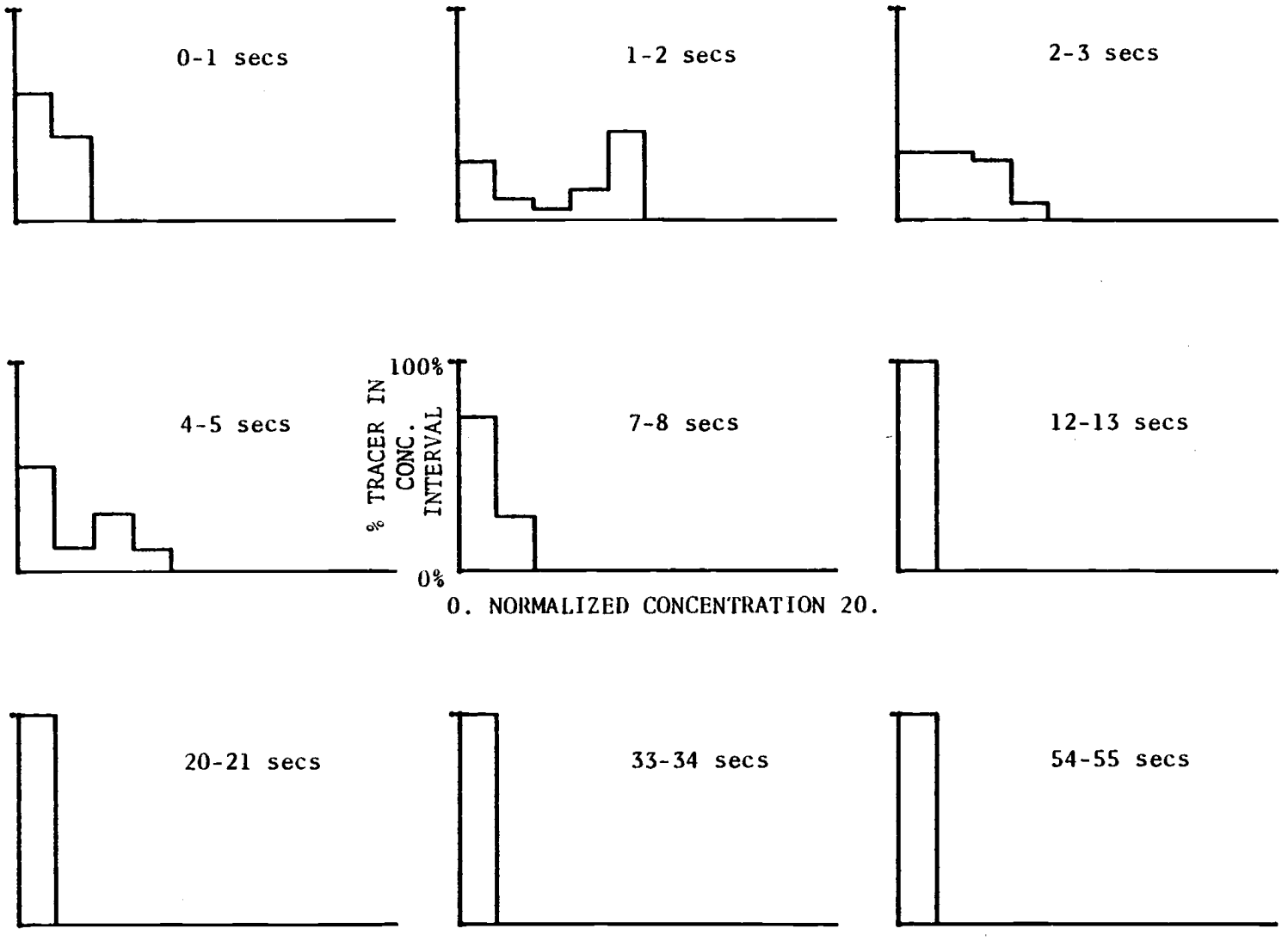

Figure 6.1. (Continued)

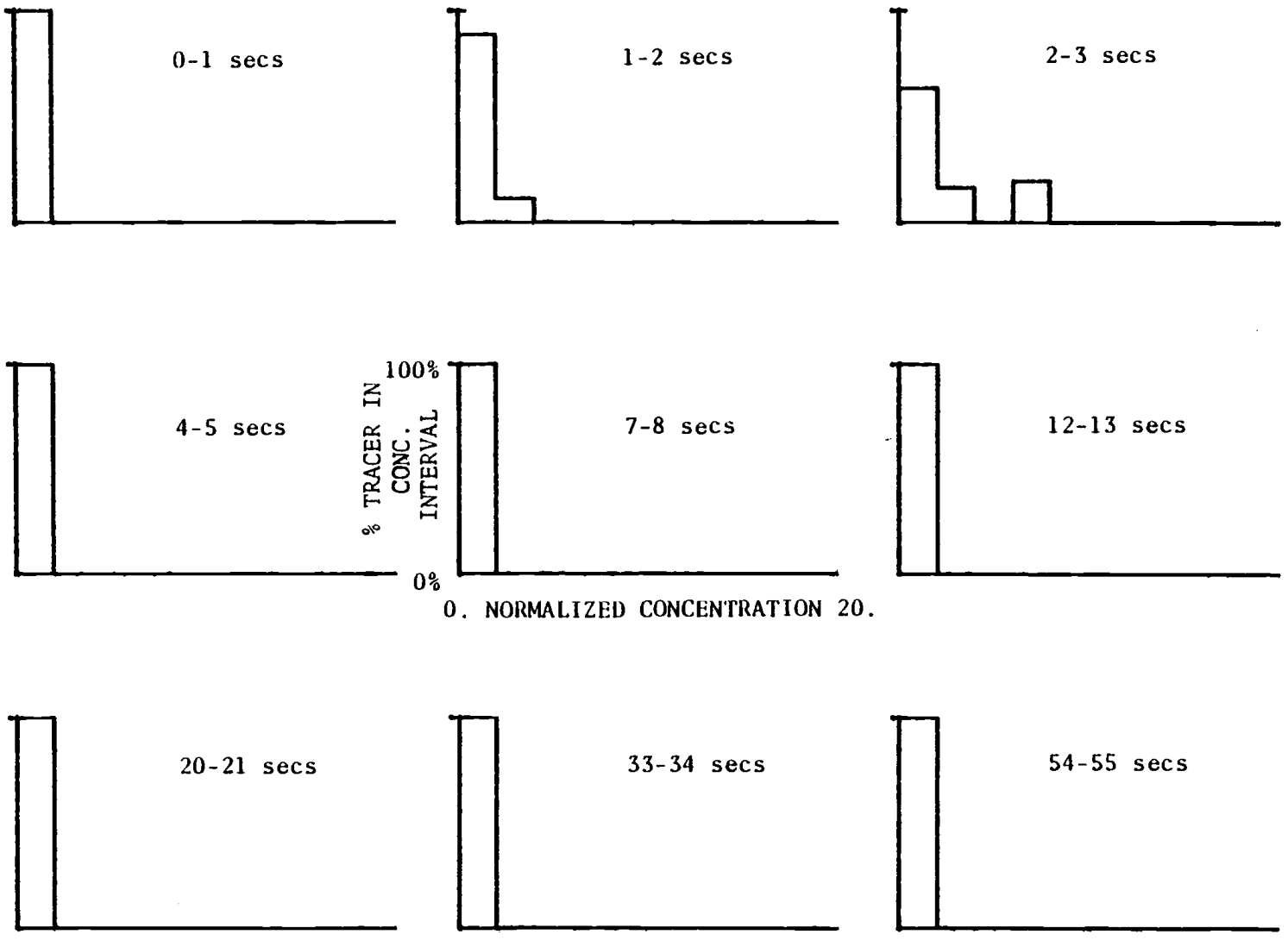

Figure 6.1. (Continued)

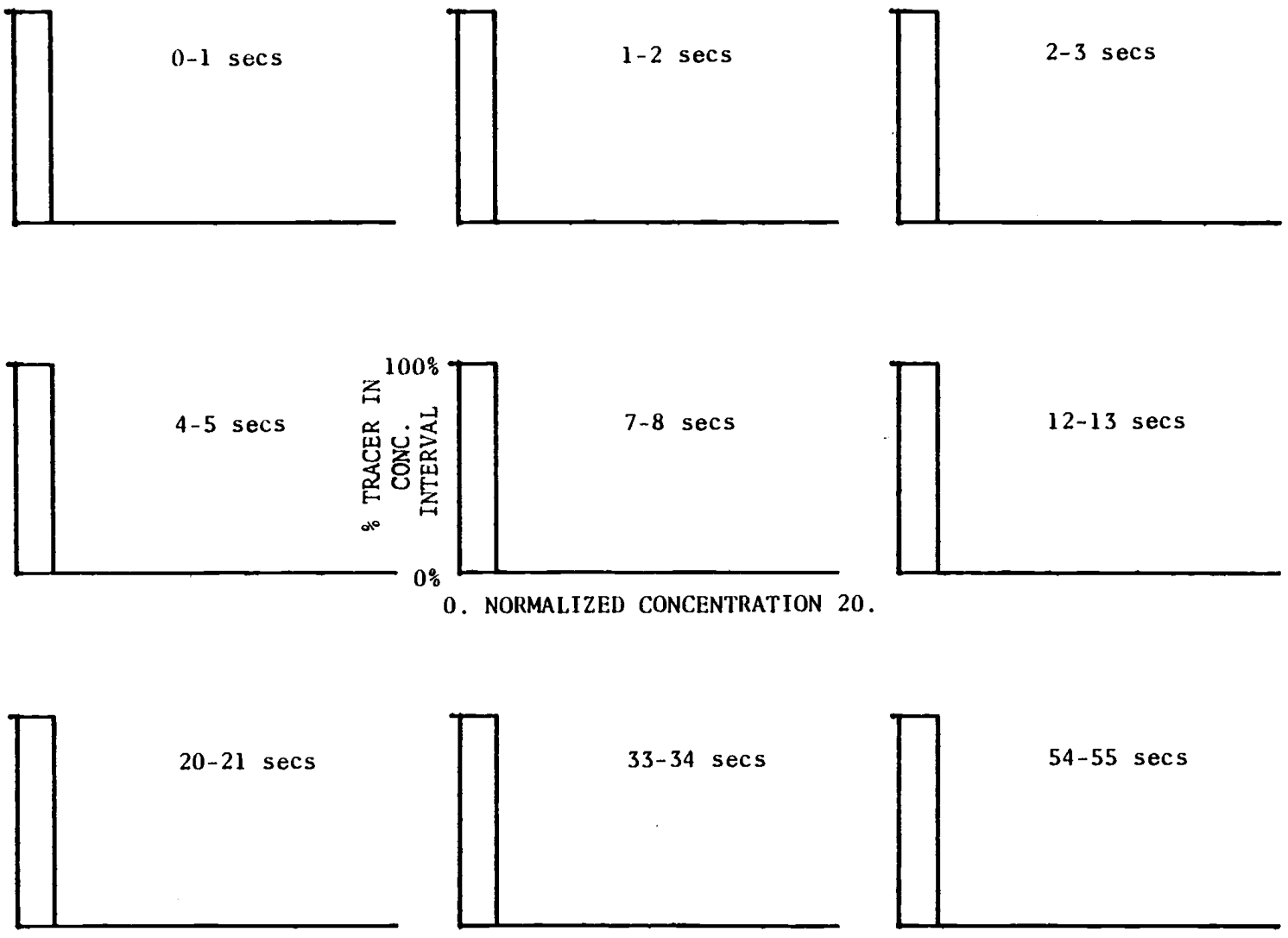

Figure 6.1. (Continued)

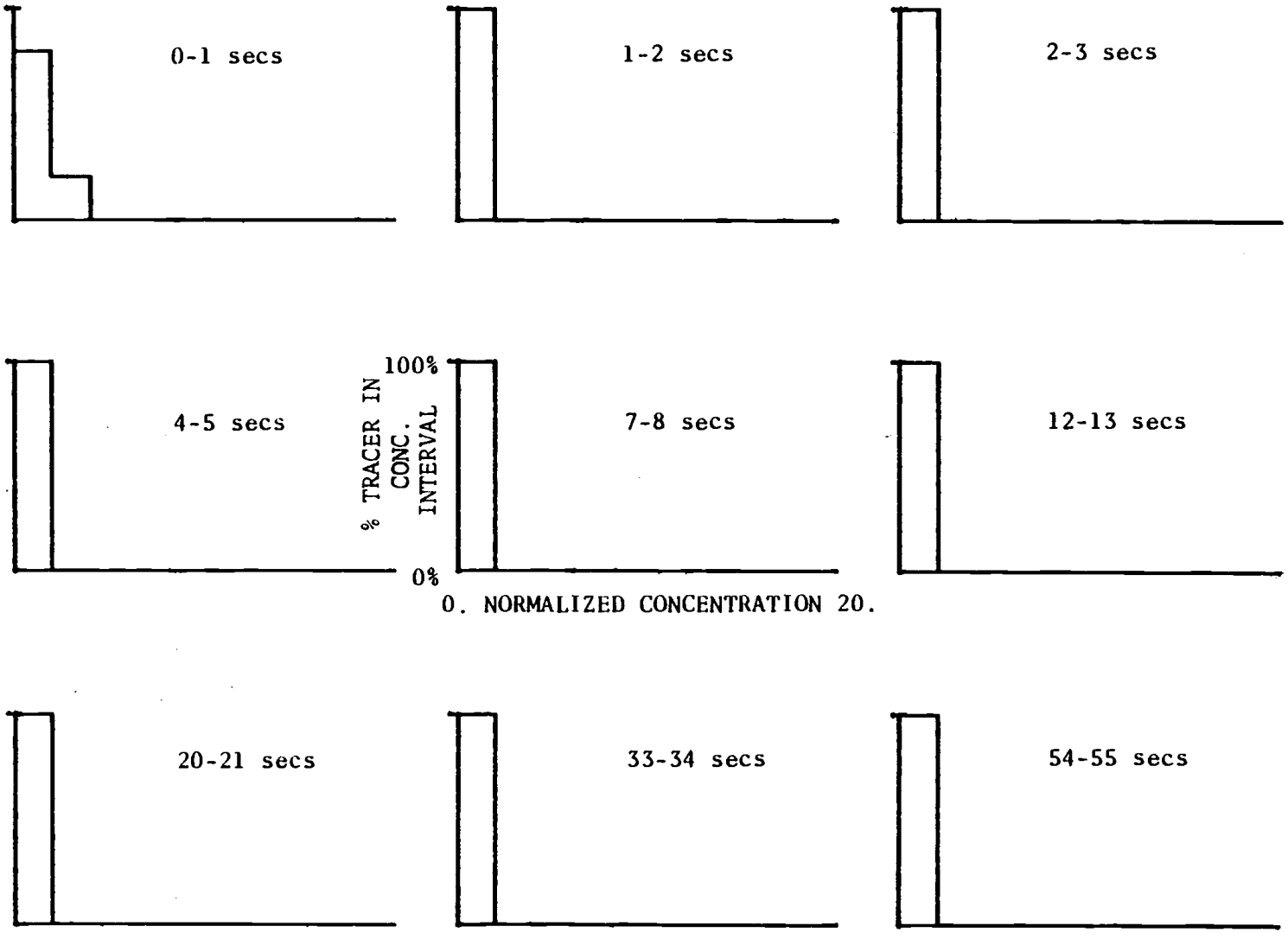

Figure 6.1. (Continued)

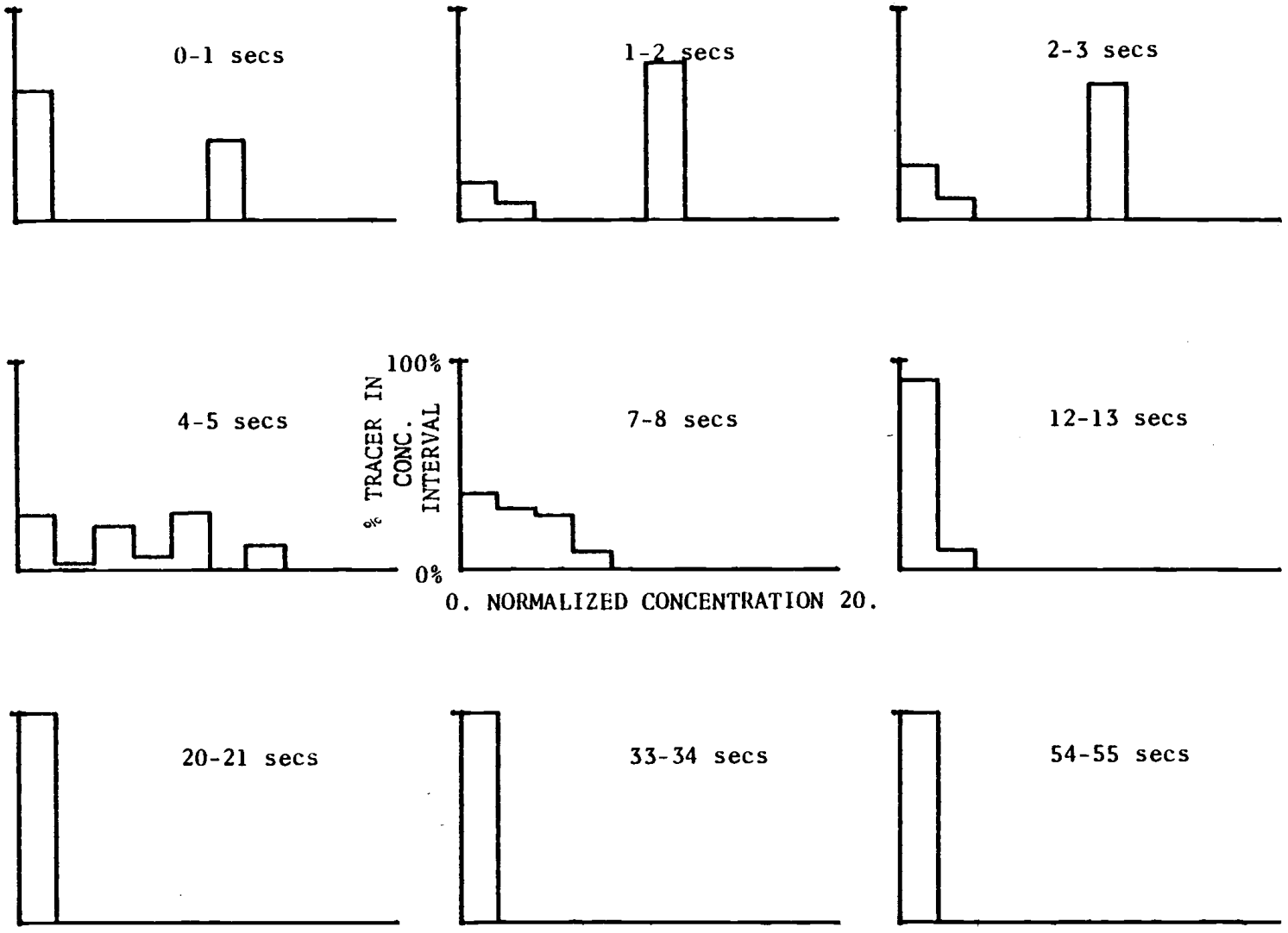

Figure 6.1. (Continued)

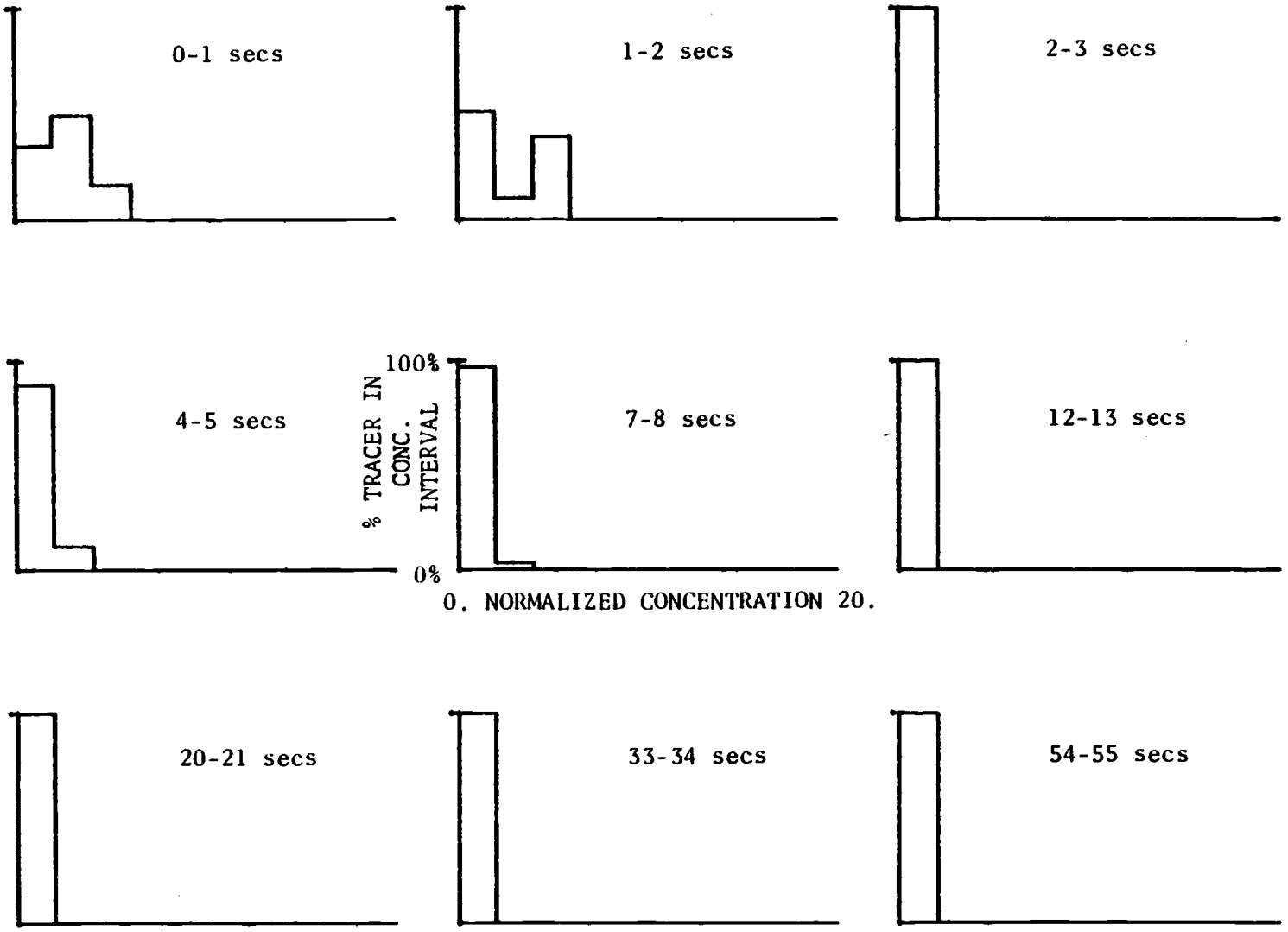

Figure 6.1. (Continued)

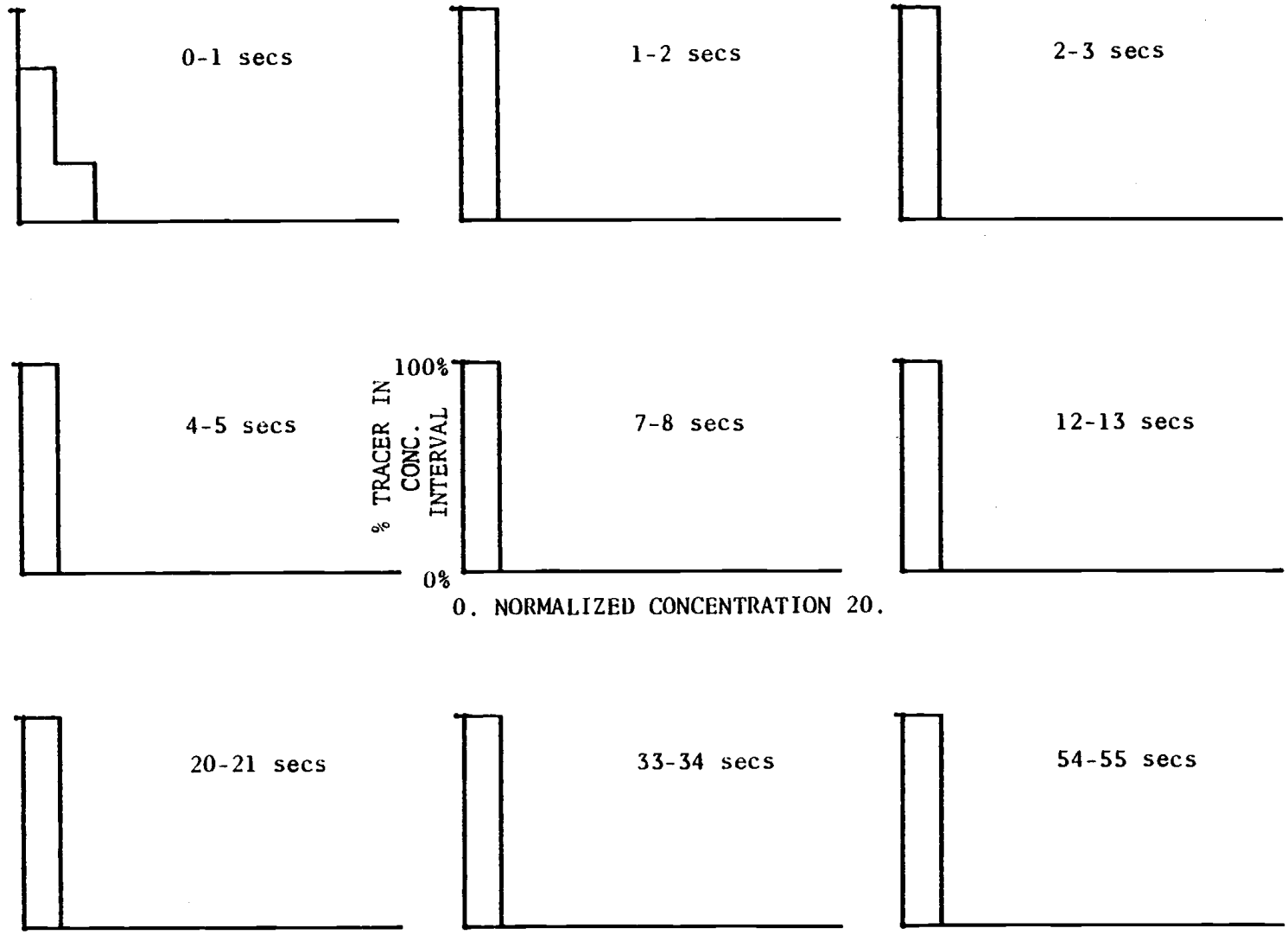

Figure 6.1. (Continued)

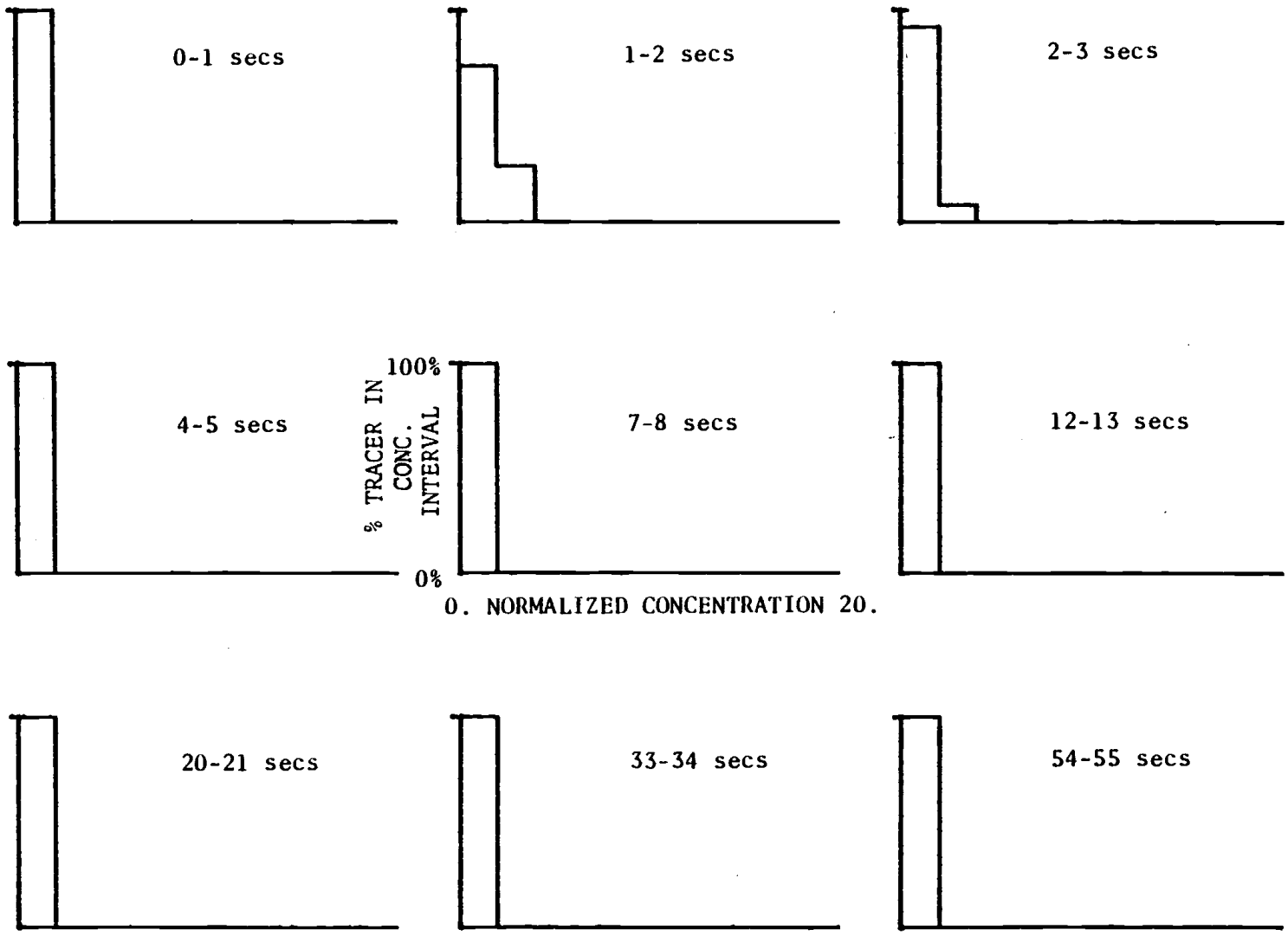

Figure 6.1. (Continued)

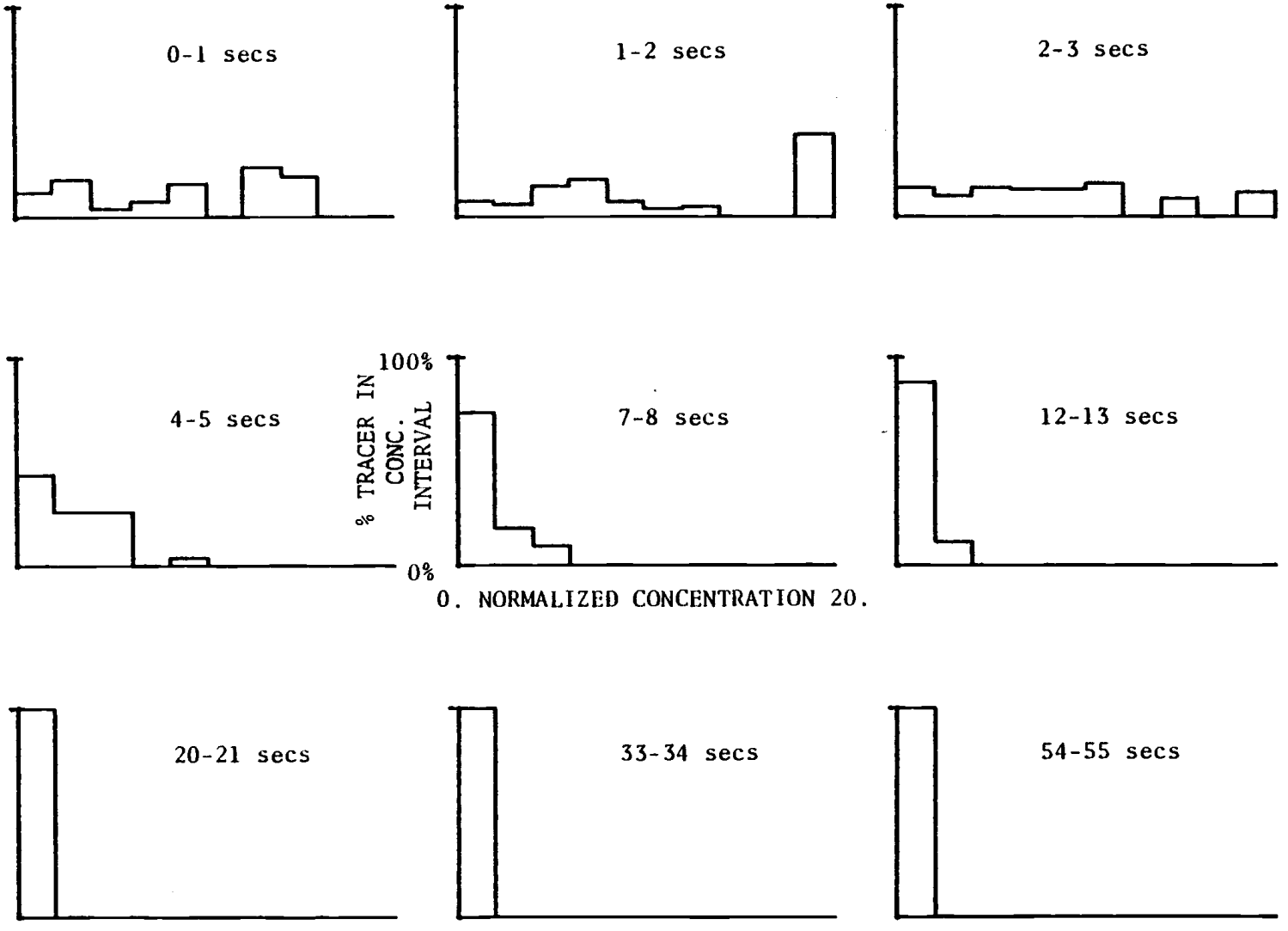

Figure 6.1. (Continued)

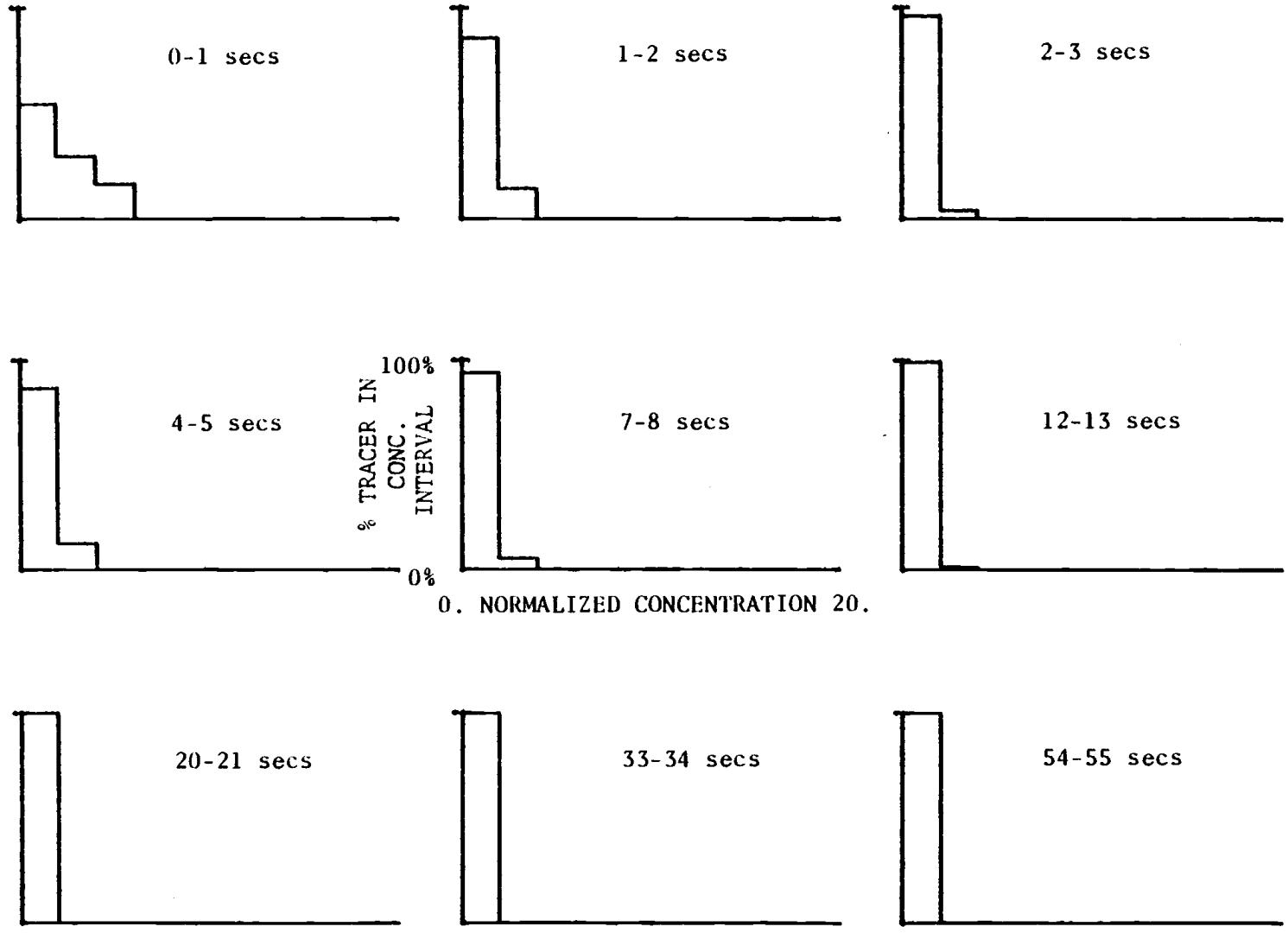

Figure 6.1. (Continued)

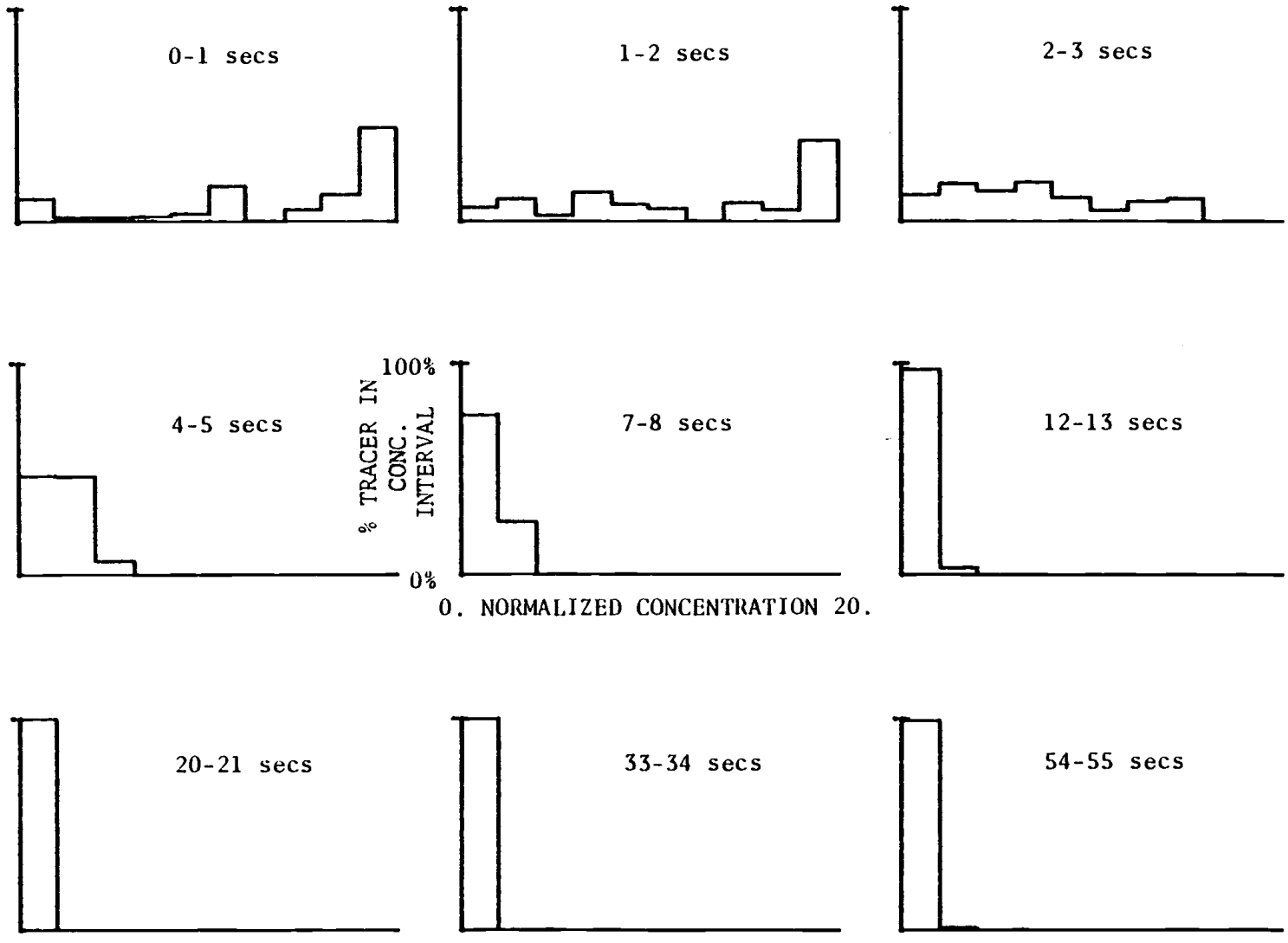

Figure 6.1. (Continued)

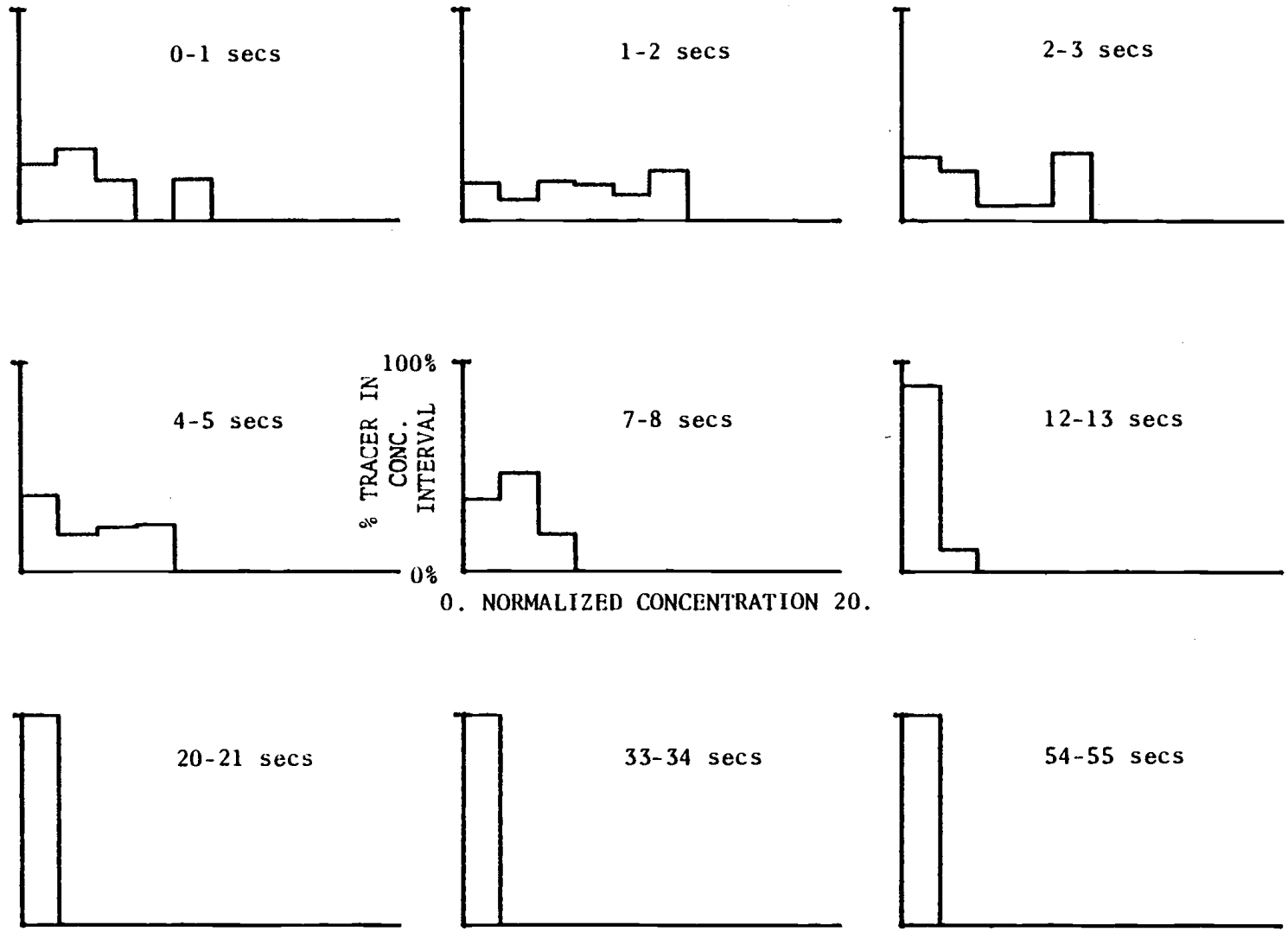

Figure 6.1. (Continued)

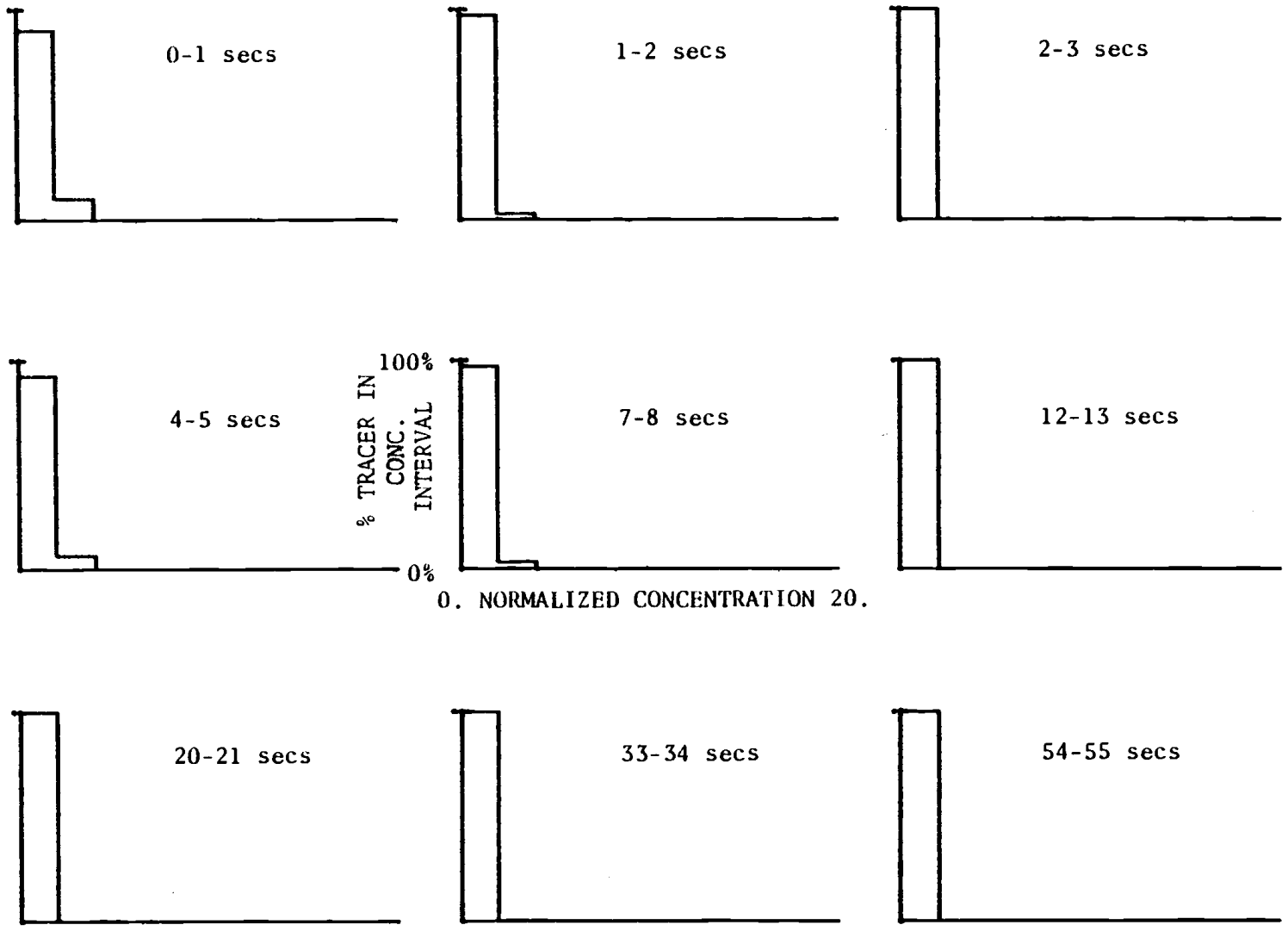

Figure 6.1. (Continued)

twenty. The ordinates on the other hand, are the percentages of total tracer (detected by the tube array) within each particular normalized concentration interval. Thus, be definition, the heights or percentages of tracer within each concentration interval (on one particular plot) always sum to 100%. However, the amount of tracer accounted for may vary among each of the nine plots describing a run. In fact, the mass balance plots (presented in section 6.3) show that the tracer does not satisfy a material balance during the early stages of a run.

Run 74 is representative of some of the more salient features of the histogram plots. A discussion of this run follows. During the first second of data collection (after tracer injection) there appear to be several different concentrations of tracer detected by the array ranging from $(\tilde{C}_i/\bar{C}^*) = 1$ to 20. In the next second (the 1-2 second interval), a clump (or clumps) of tracer $(\tilde{C}_i/\bar{C}^* \simeq 20)$ comes within the detection range of the probes. In the following two seconds (the 4-5 second interval), this clump has dispersed to a normalized concentration, $(C_i/\bar{C}^*)$, of about 12. Finally, sometime between the 20-21 and 33-34 second intervals, the tracer becomes uniformly distributed at its final concentration, i.e. $\tilde{C}_i/\bar{C}^* = 1$.

It is evident from Run 74 that clumps of tracer move in and out of the tube array. Thus, we have a puzzle which is missing some pieces, namely those portions of the bed outside the detection range of the probes. One can only guess what is happening in these external

regions. Tracer concentrations could be worse (or greater) than those observed in the early histogram plots (i.e., during the 0-1 second, 1-2 second and 2-3 second time intervals), especially when a good portion of the bed is above the tube array and near the injection port. This condition frequently occurs when 3000 lbs of sand are used; or the superficial gas velocity is 11 ft/sec; or the height of the array is only 10 in. above the distributor; or any combination of these factors is used.

6.2 The Normalized Tracer Average Concentration

Plots of normalized tracer average concentration versus time (see Figure 6.2) are used to determine an overall mixing time (OMT) for each run. Concentrations are averaged with respect to tracer rather than volume or space. This averaging is particularly relevant since it expresses how crowded the tracer is from the tracer's point of view. It is worthwhile to add that the normalized tracer average concentration is simply the mean concentration of the histograms. The ordinates of the normalized tracer average concentration plots are the same as the abscissas used for the histogram plots, i.e. values of $(\tilde{C}_i/\bar{C}^*)$ ranging from 1 to 20. Mean concentration values, $\bar{C}_j$, are calculated for each quarter second time interval, j, of data collection by squaring the concentration readings of each channel, summing these squared concentrations and, then, dividing by the sum of

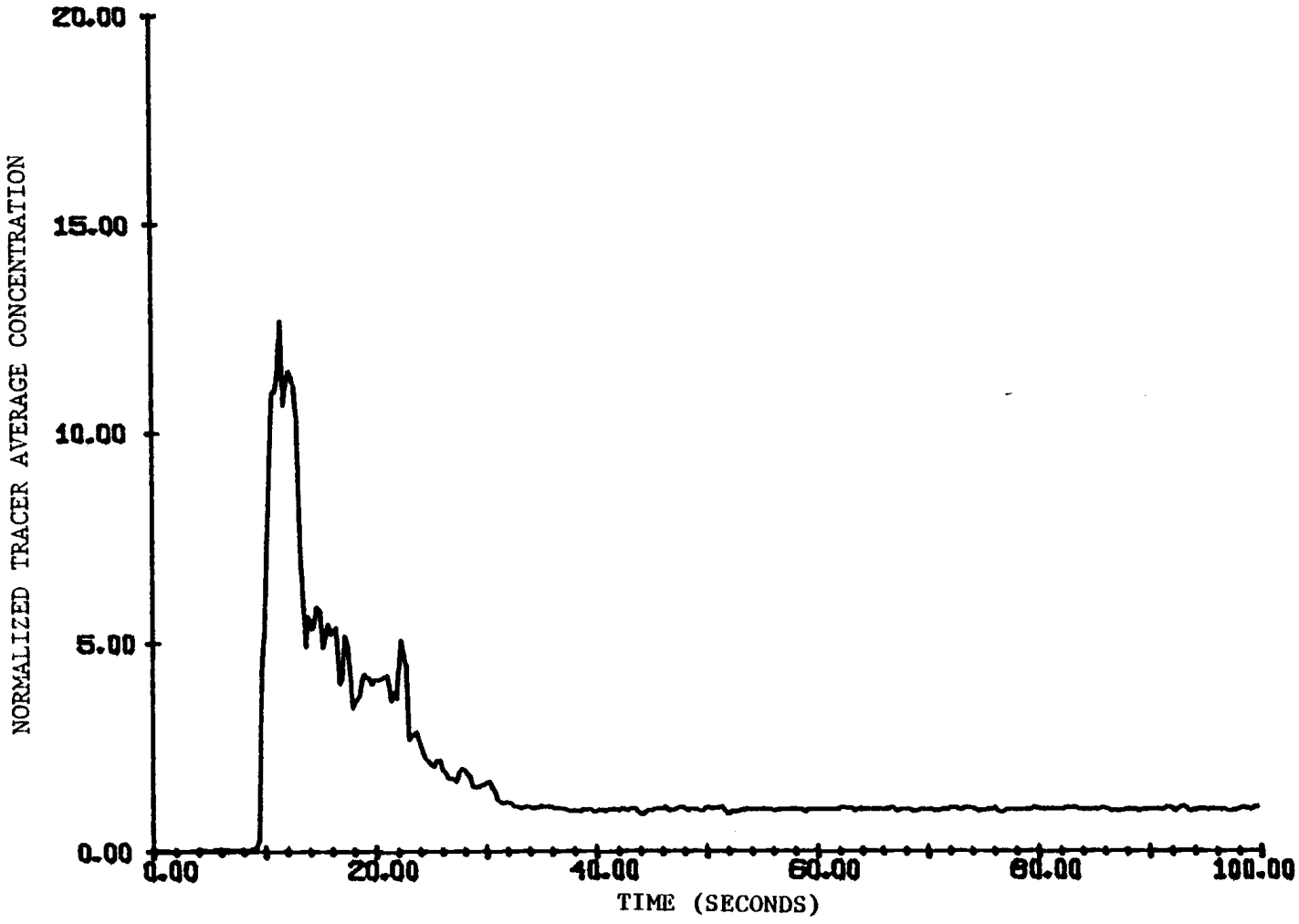

Figure 6.2 Normalized tracer plots.

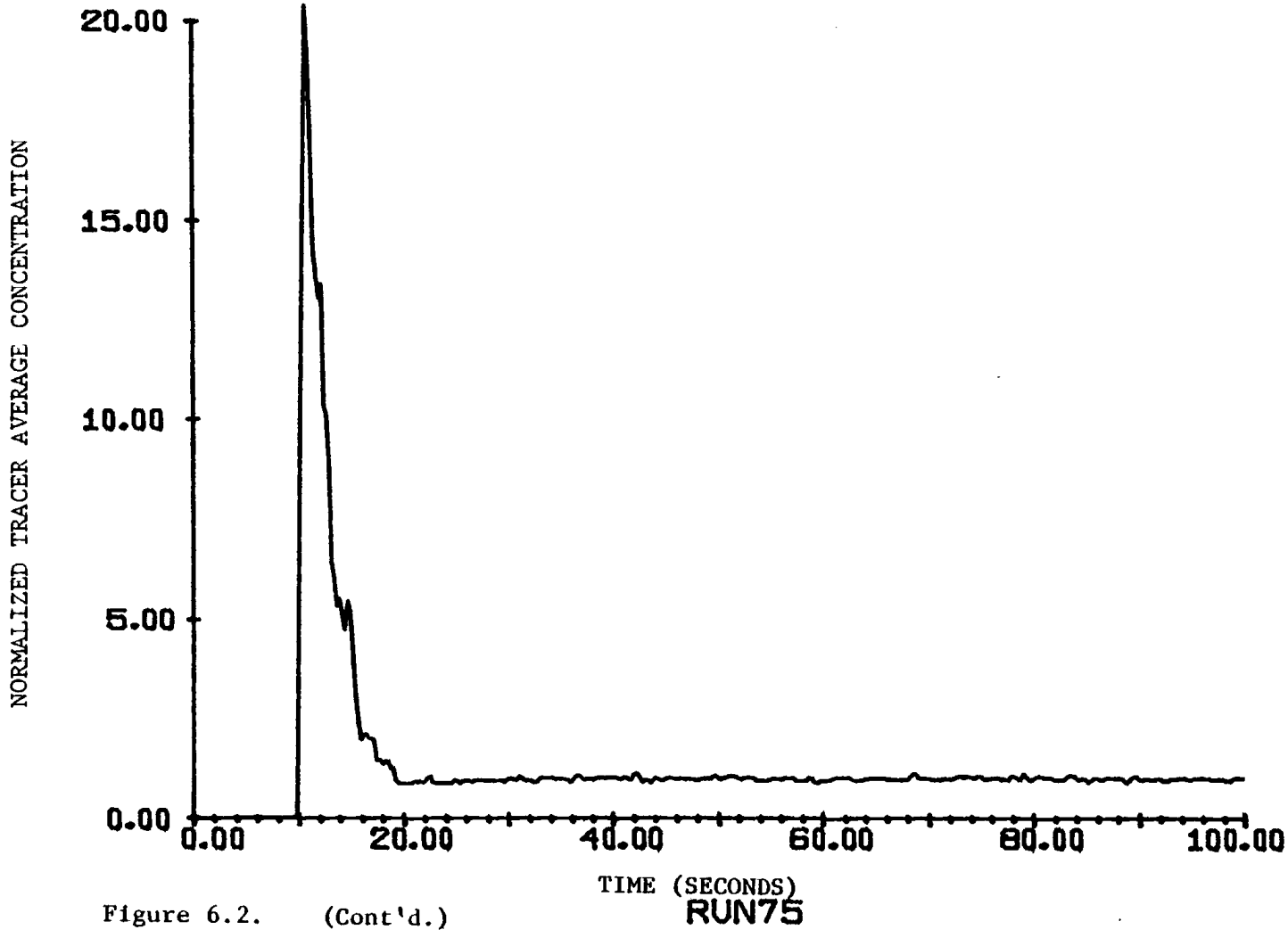

Figure 6.2. (Cont'd.)

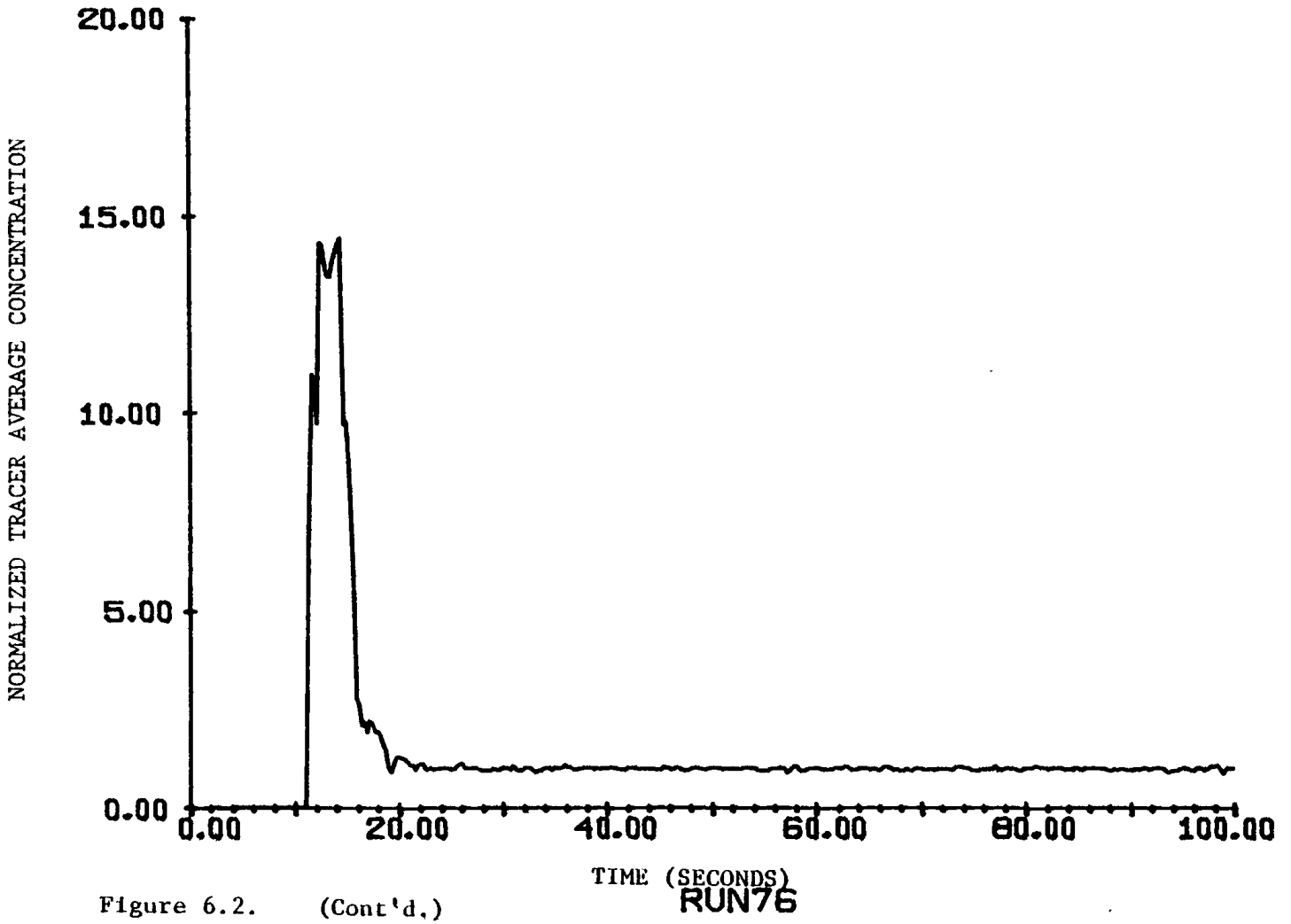

Figure 6.2. (Cont'd.)

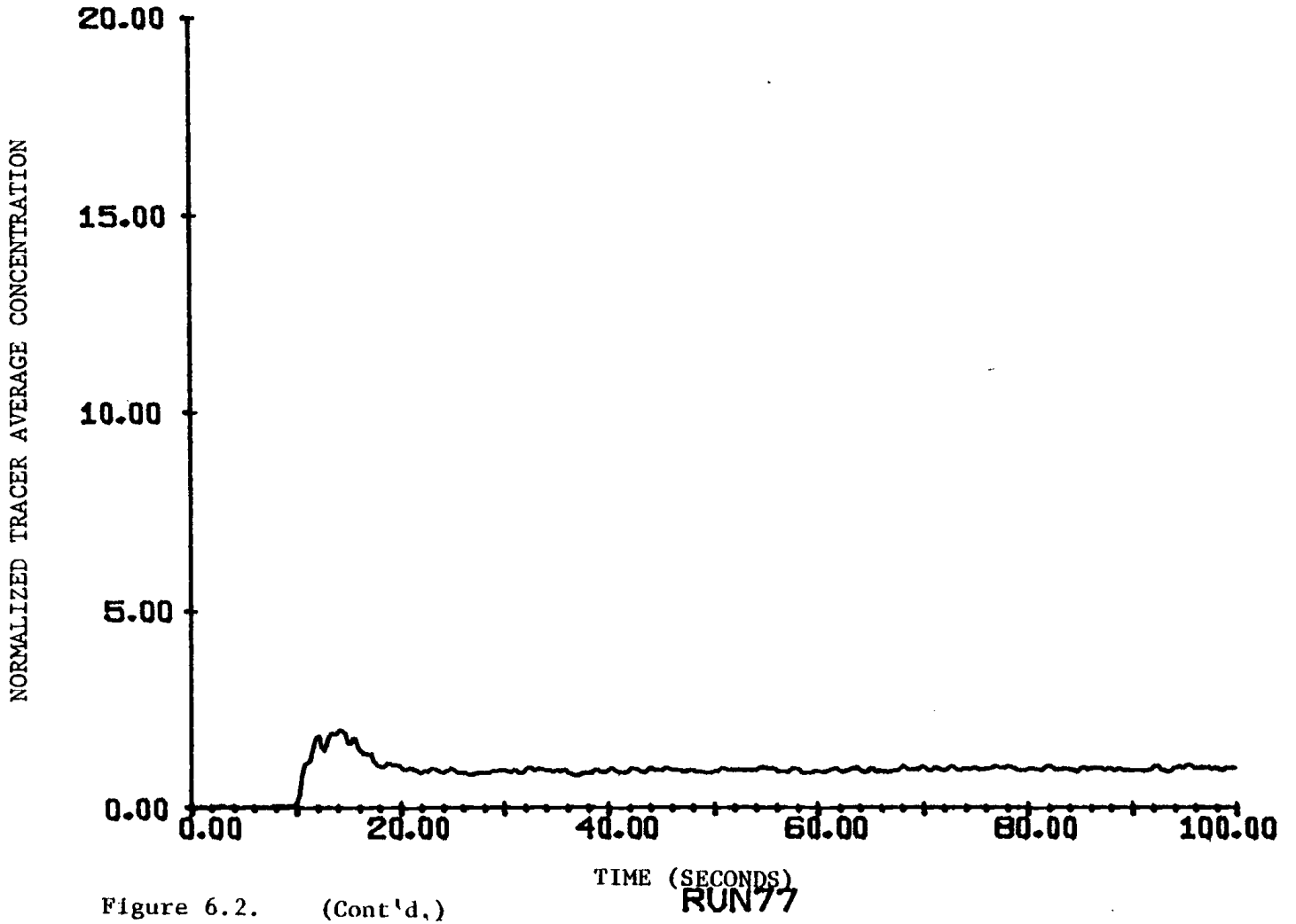

Figure 6.2. (Cont'd.)

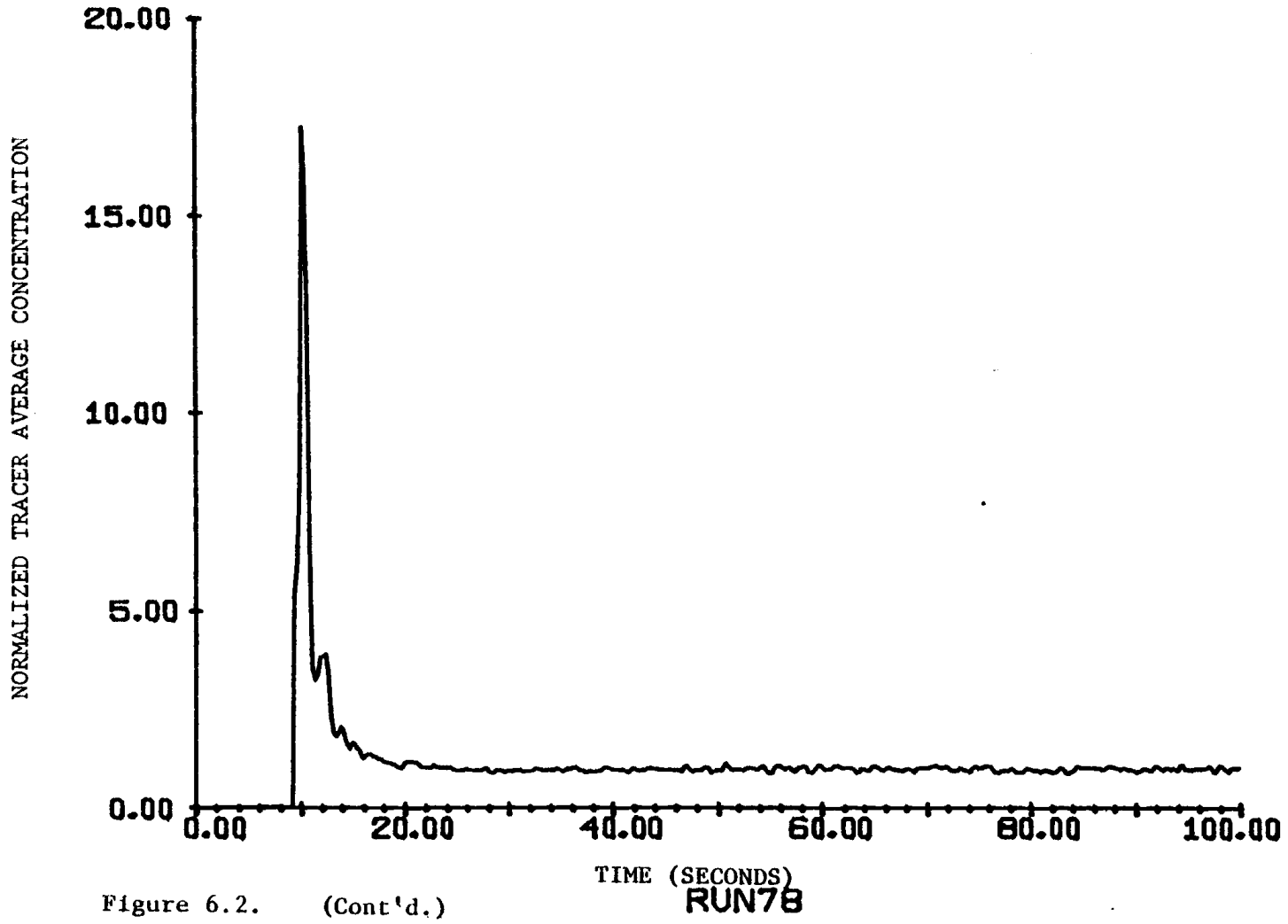

Figure 6.2. (Cont'd.)

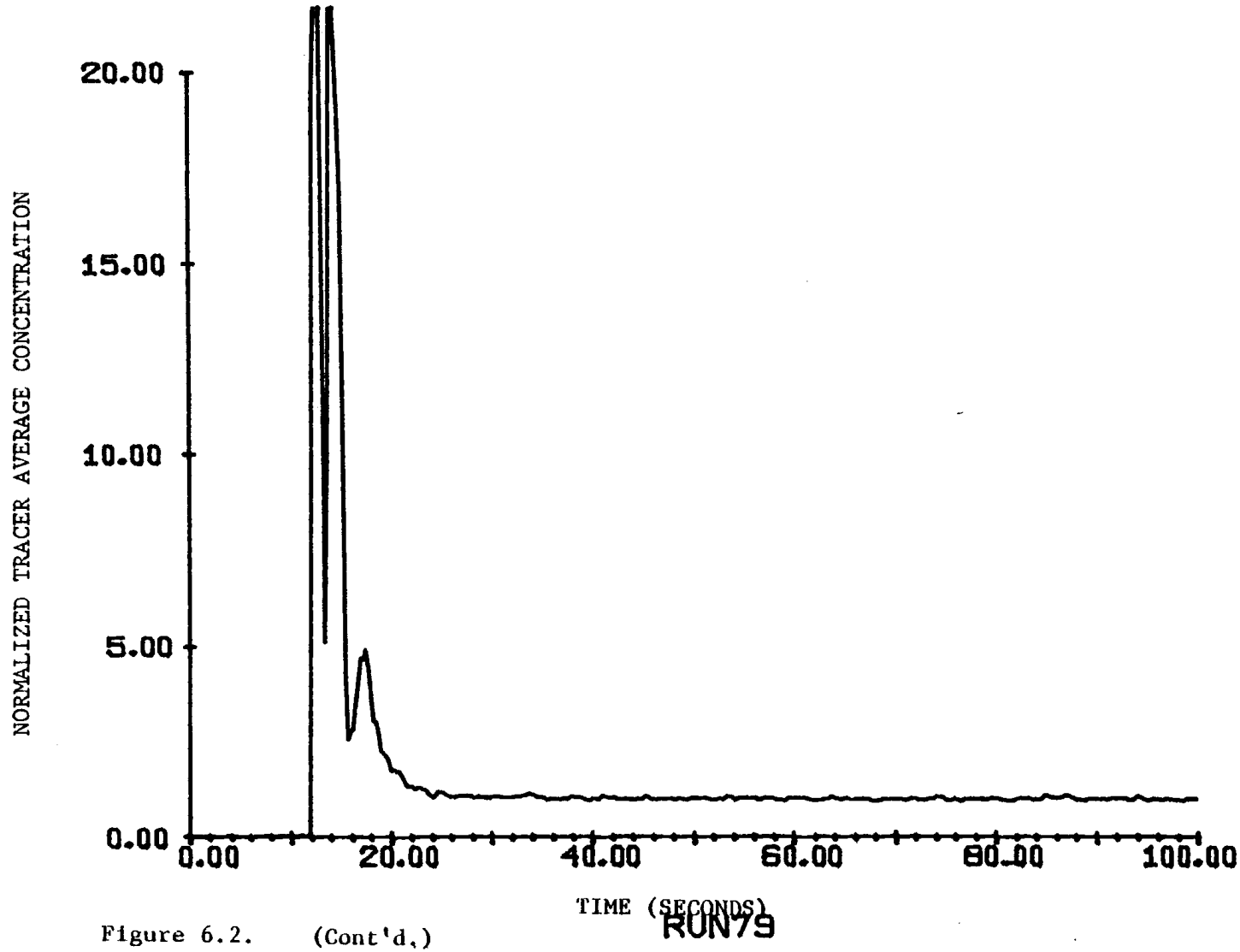

Figure 6.2. (Cont'd.)

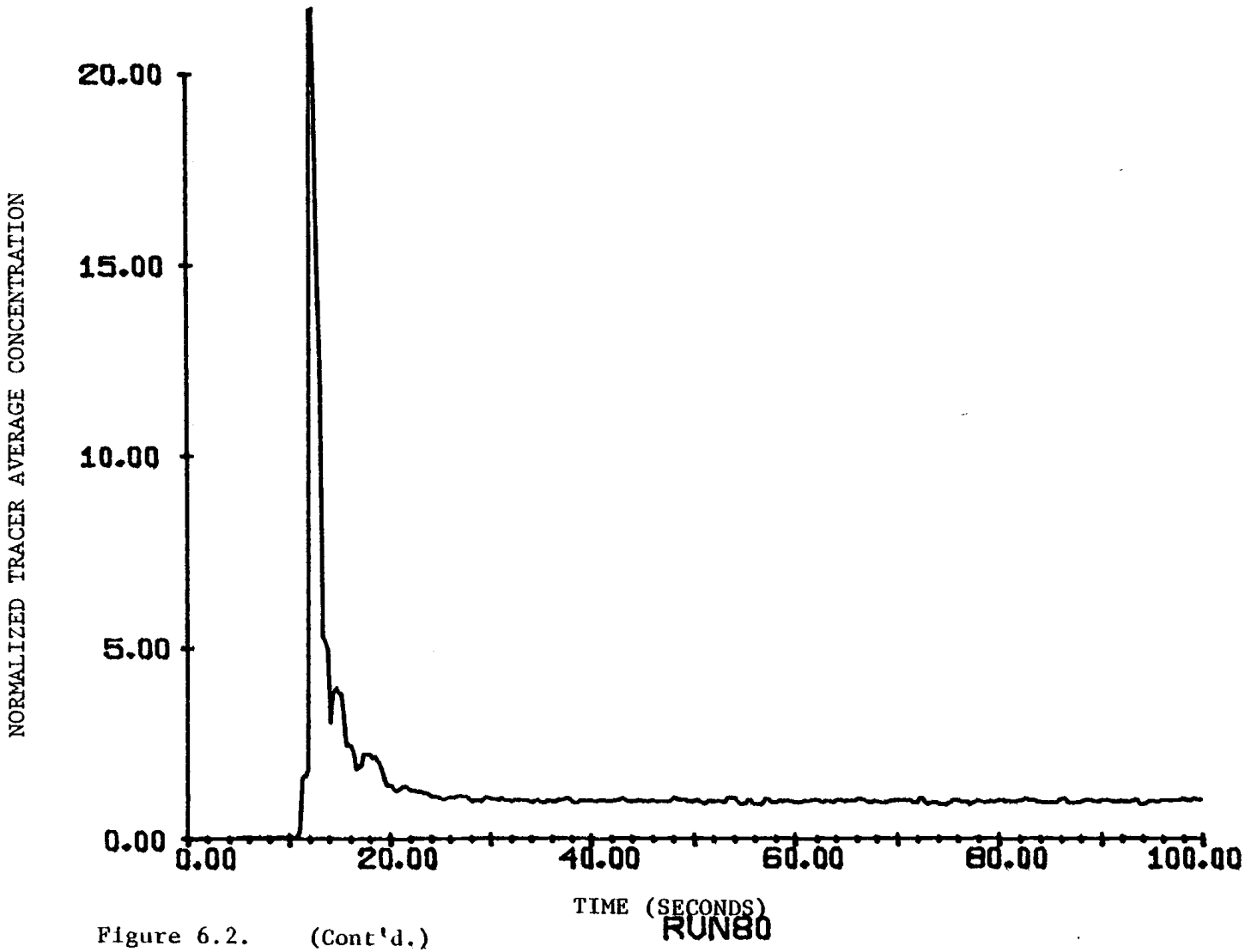

Figure 6.2. (Cont'd.)

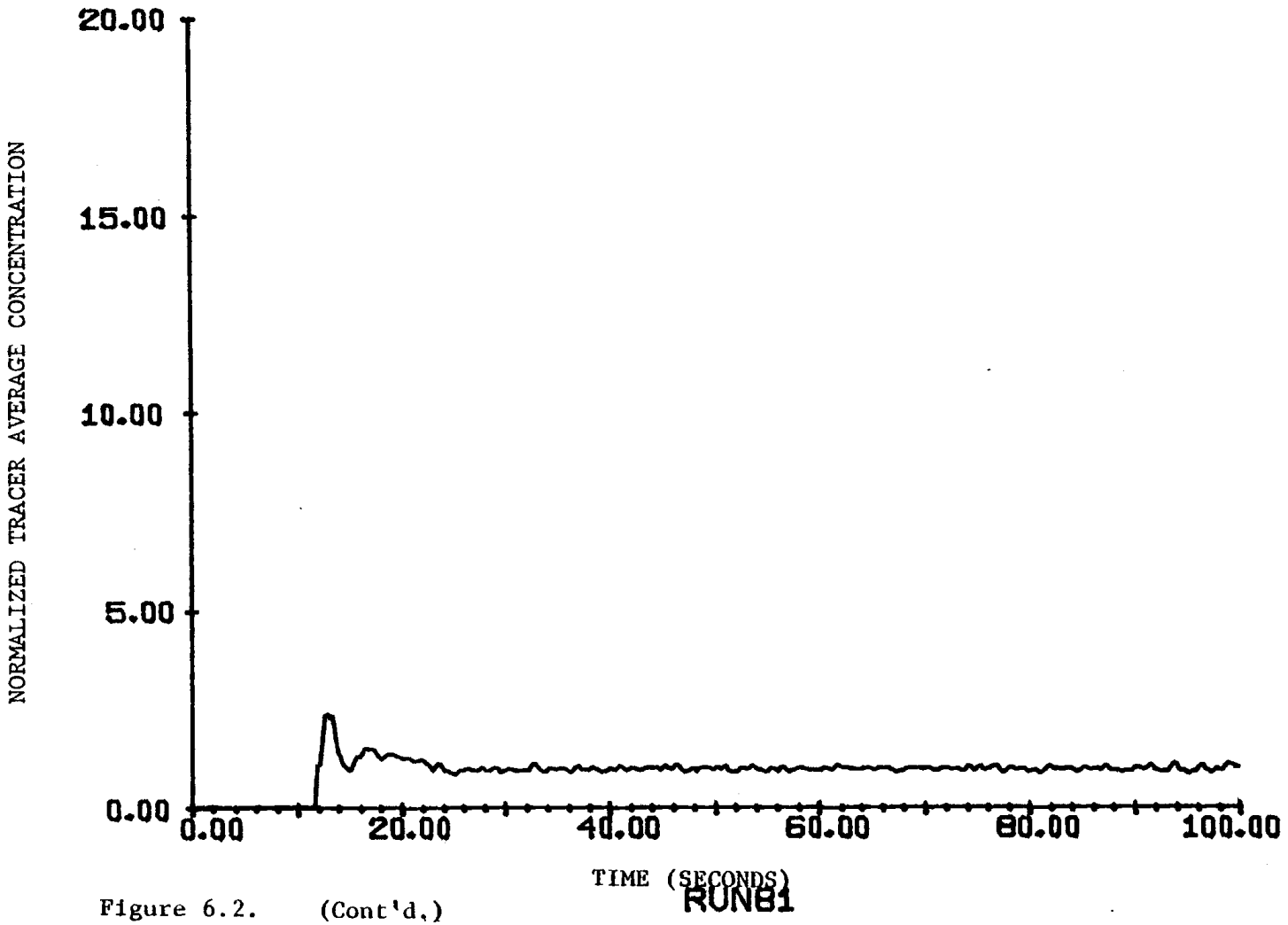

Figure 6.2. (Cont'd.)

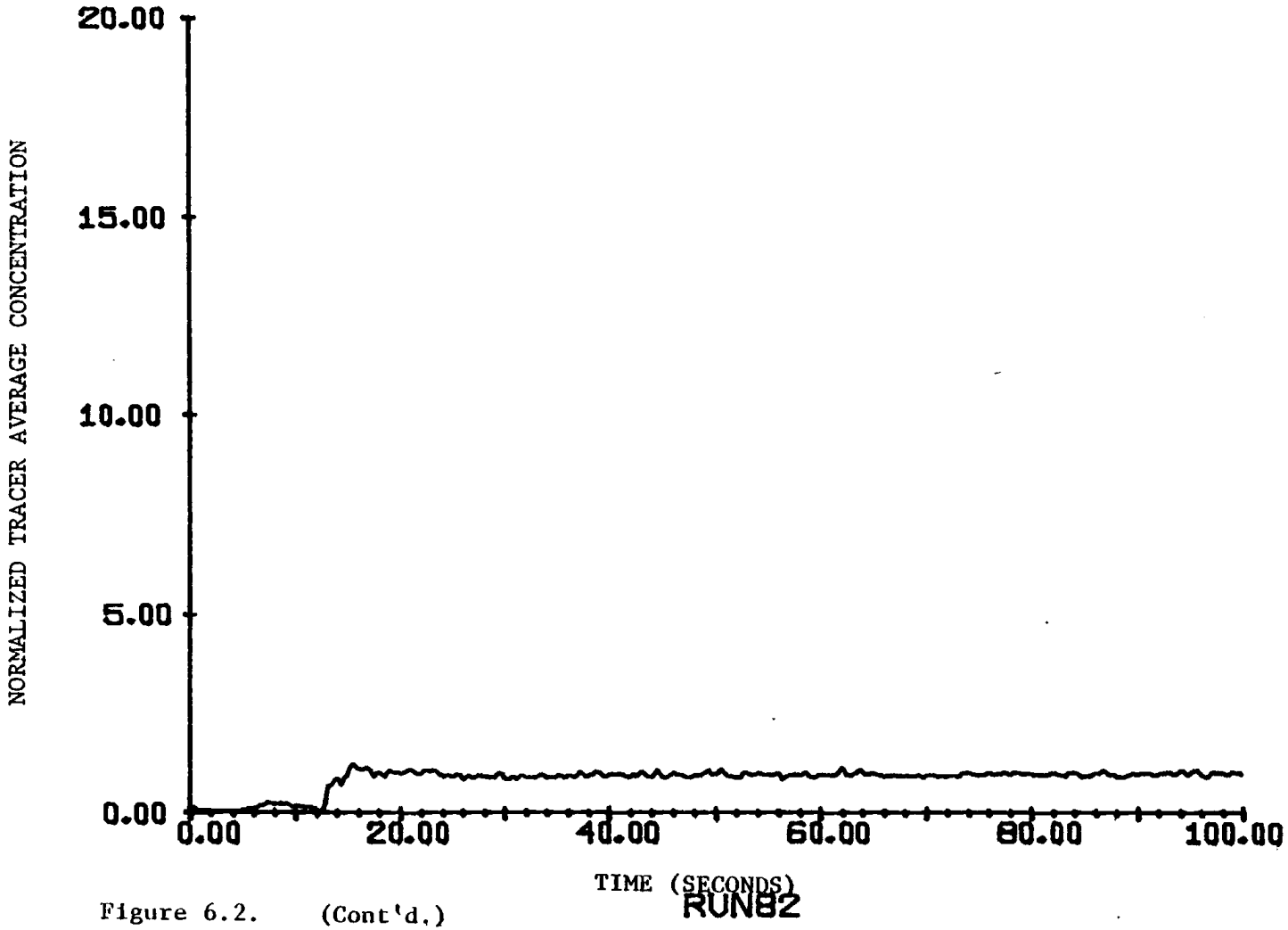

Figure 6.2. (Cont'd.)

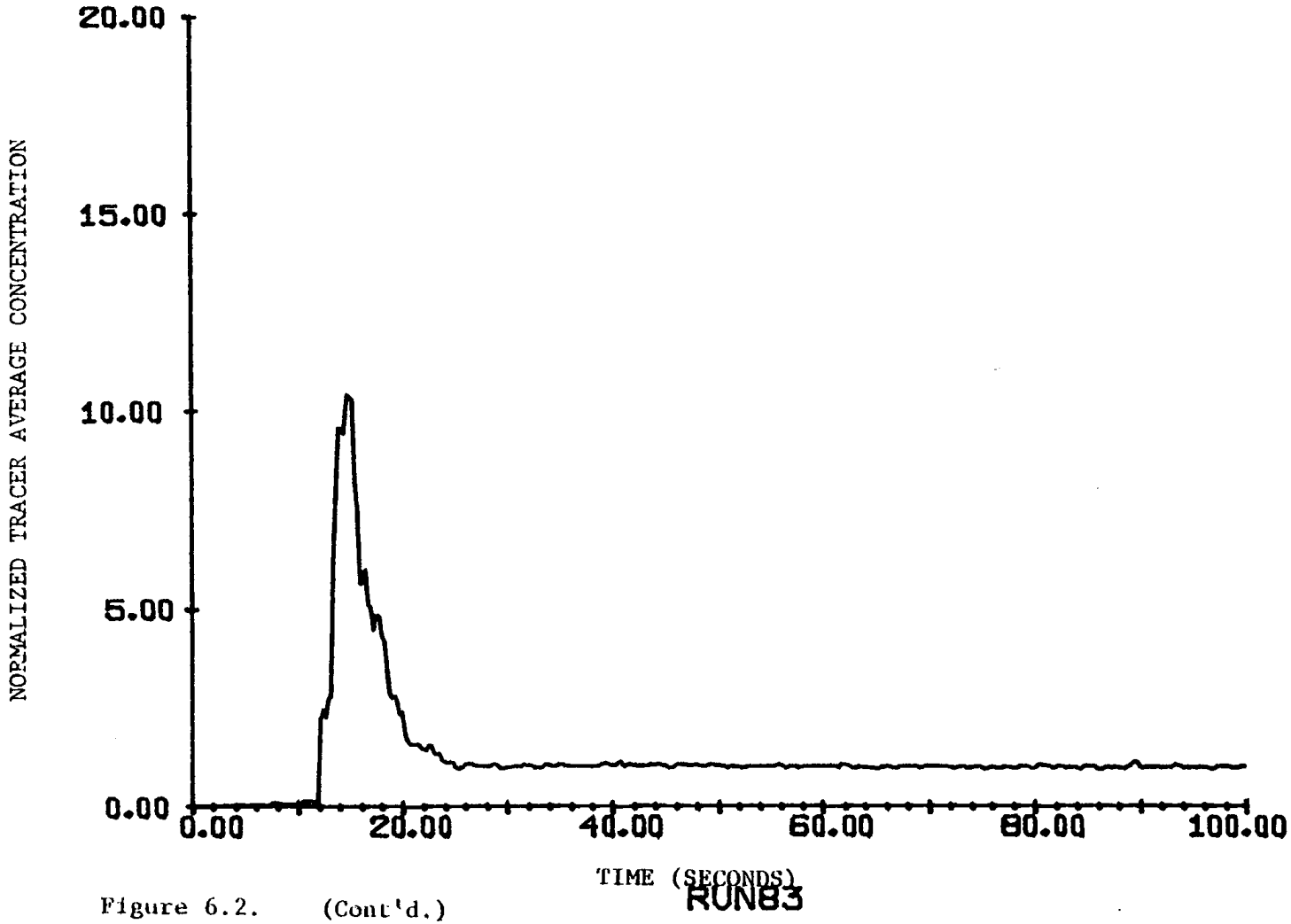

Figure 6.2. (Cont'd.)

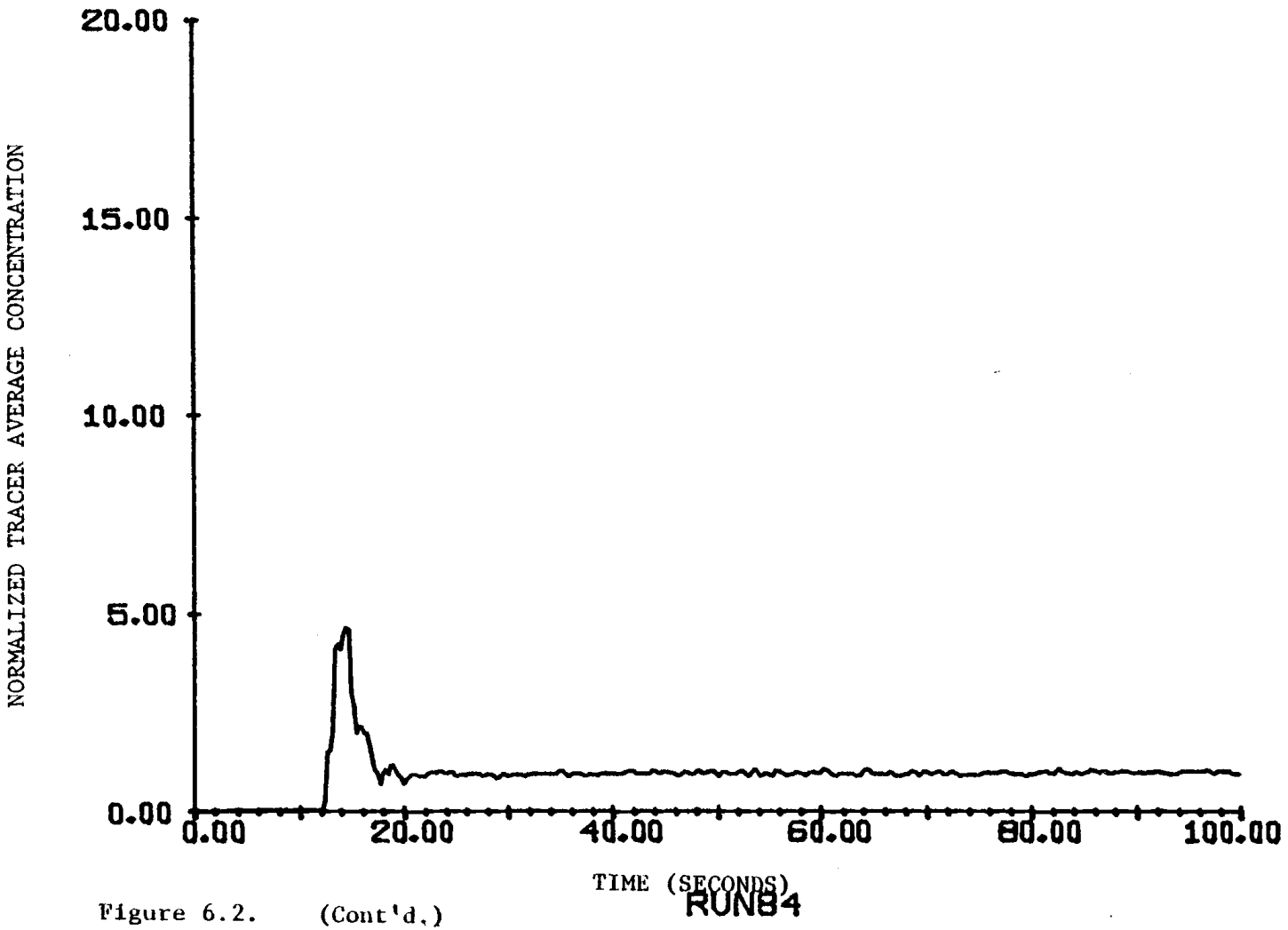

Figure 6.2. (Cont'd.)

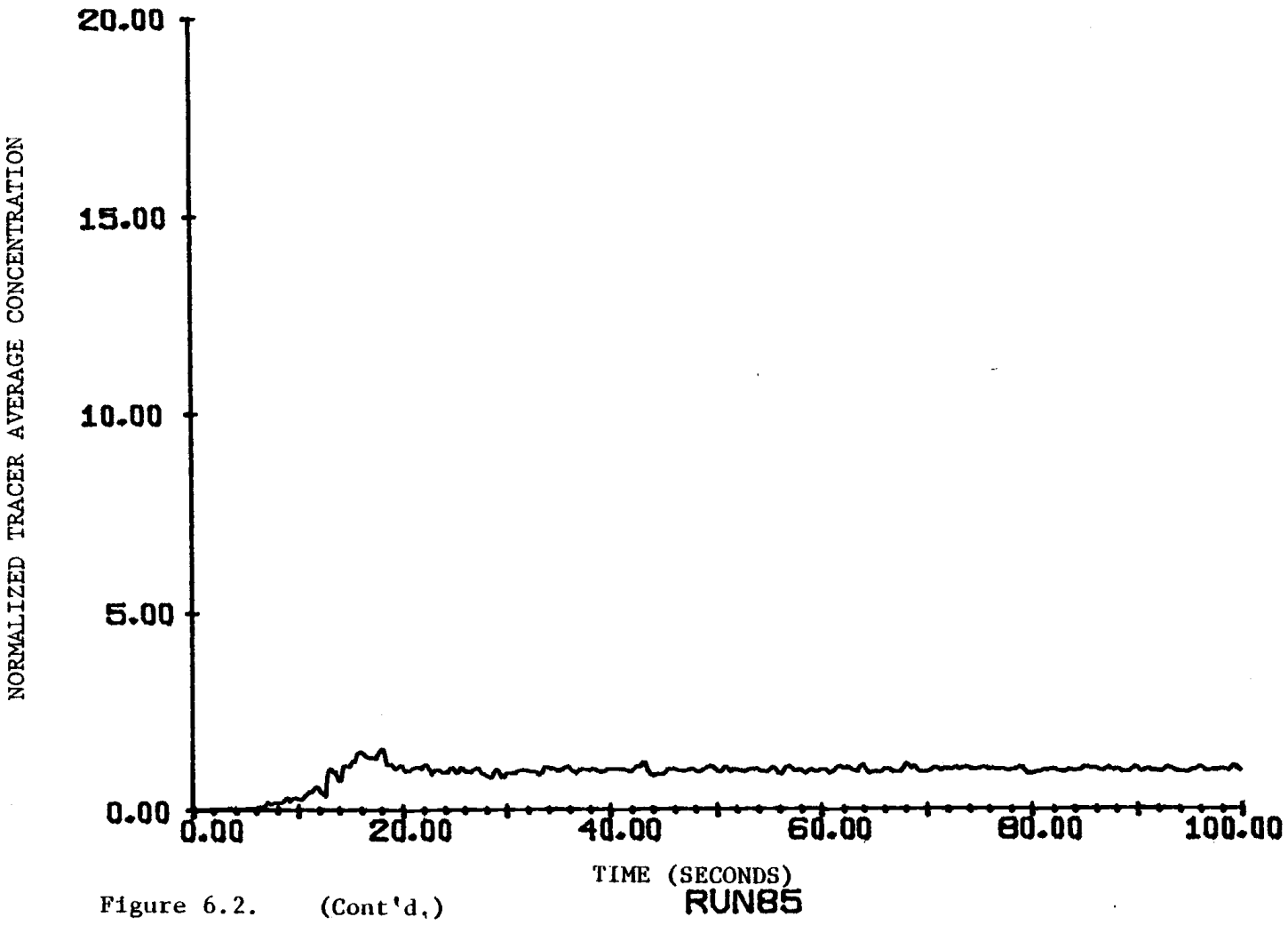

Figure 6.2. (Cont'd.)

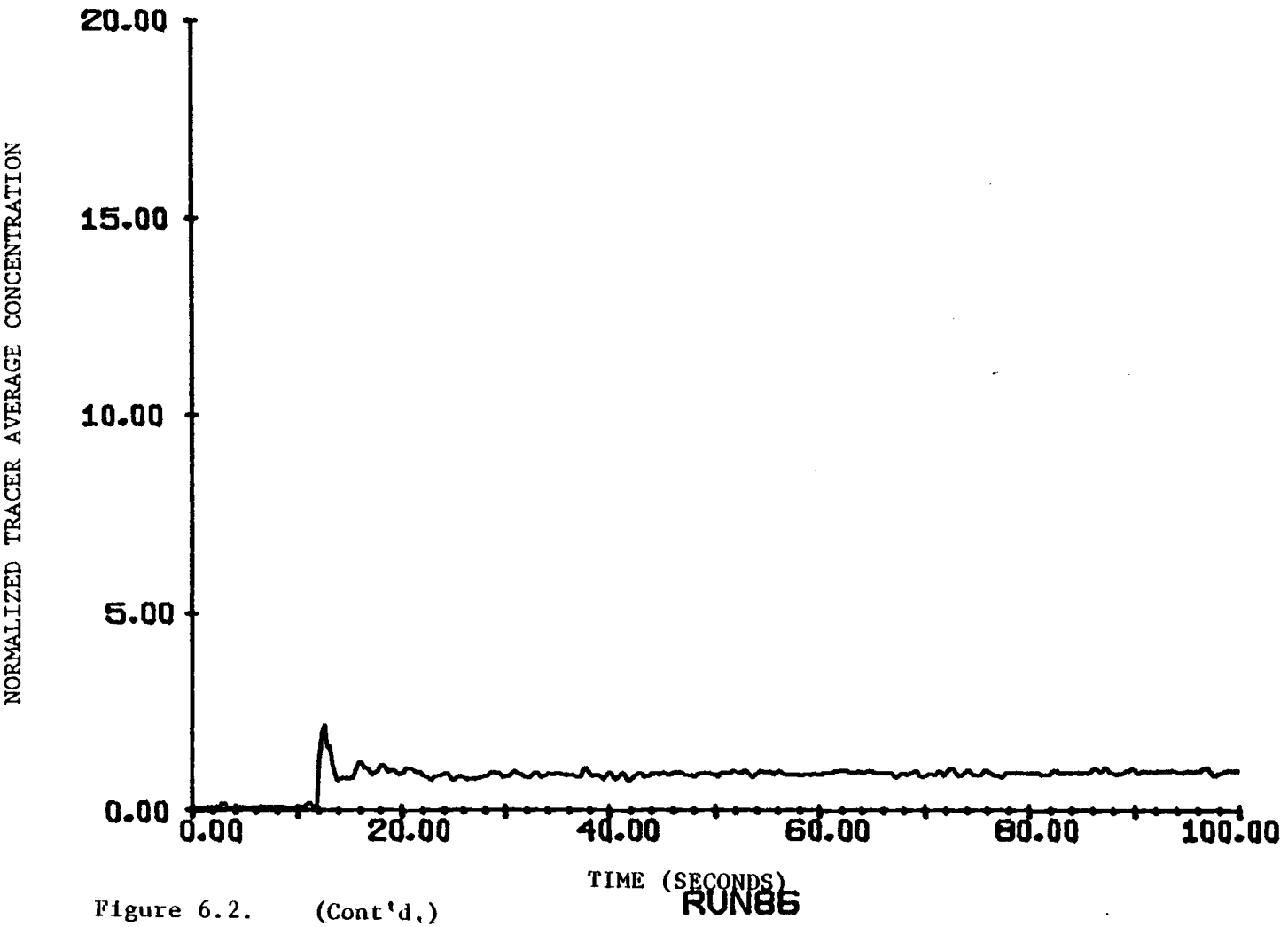

Figure 6.2. (Cont'd.)

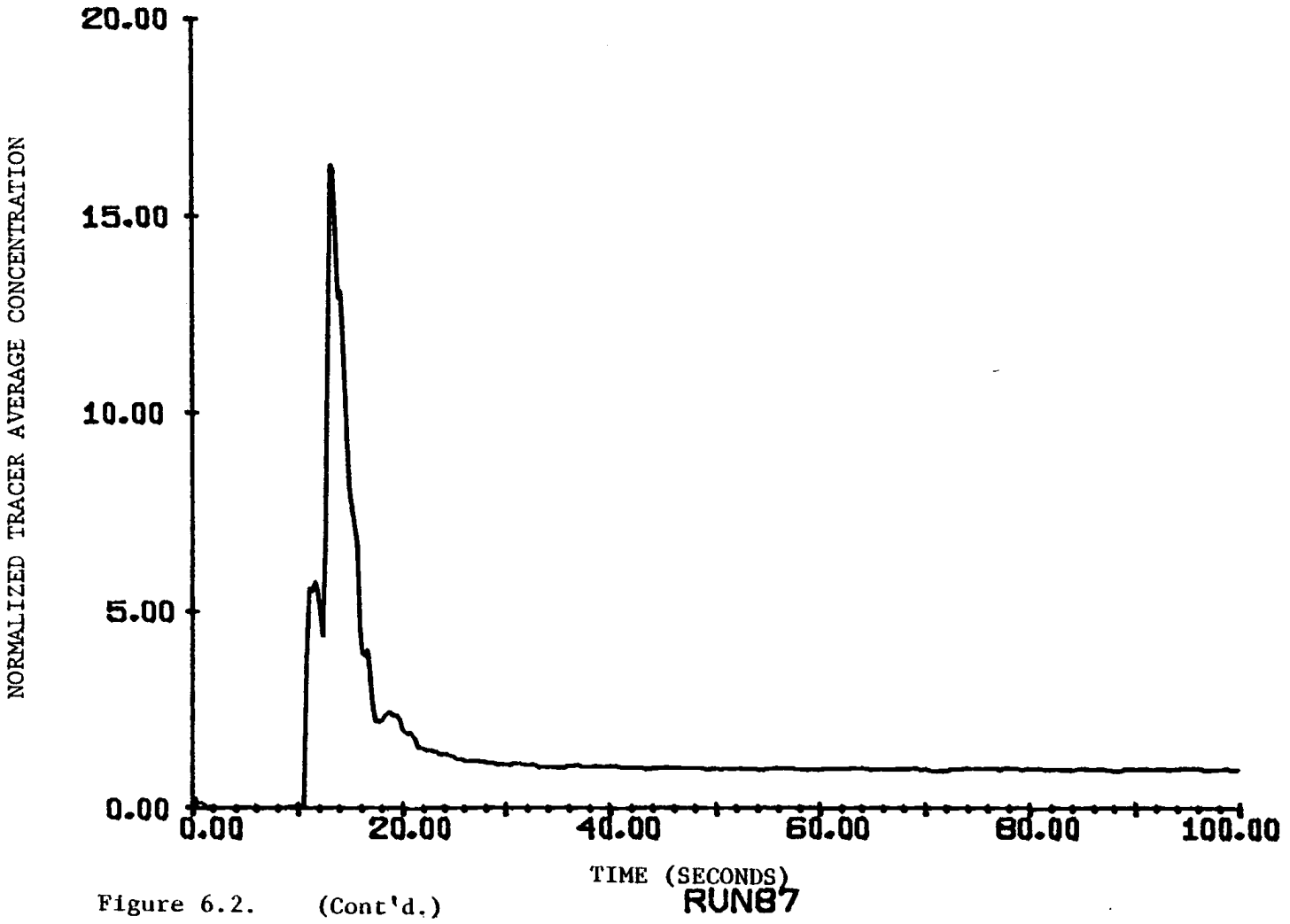

Figure 6.2. (Cont'd.)

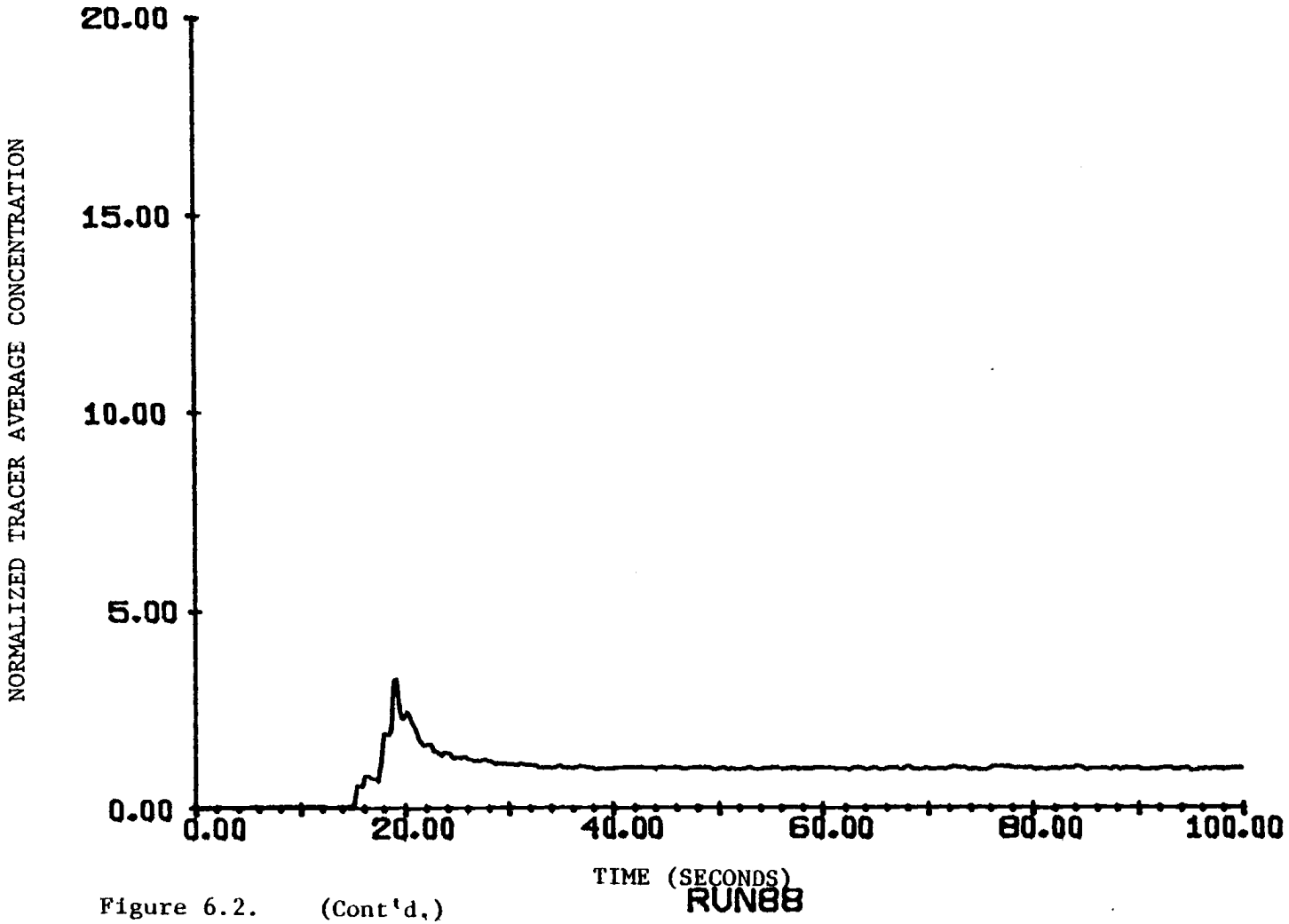

Figure 6.2. (Cont'd.)

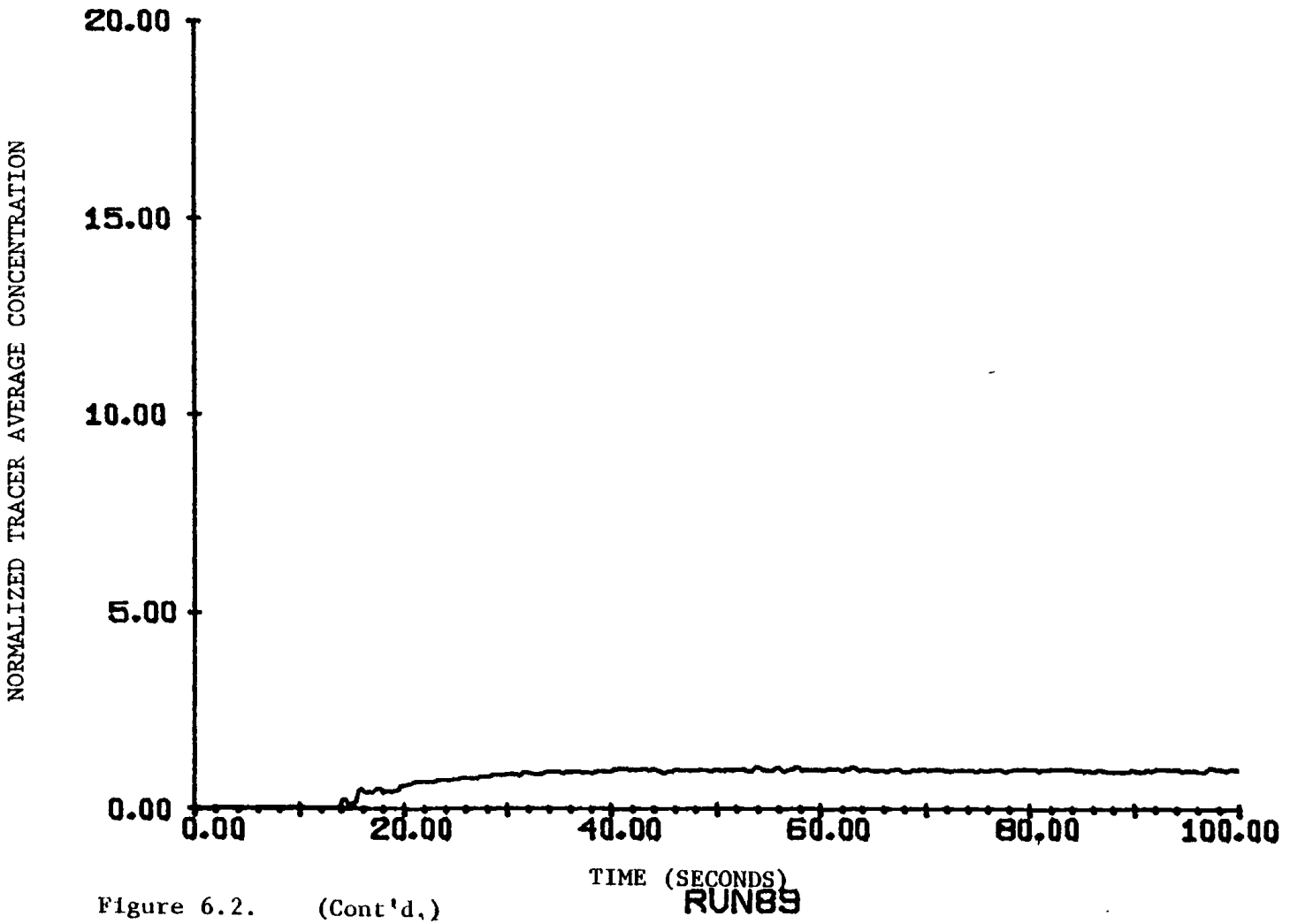

Figure 6.2. (Cont'd.)

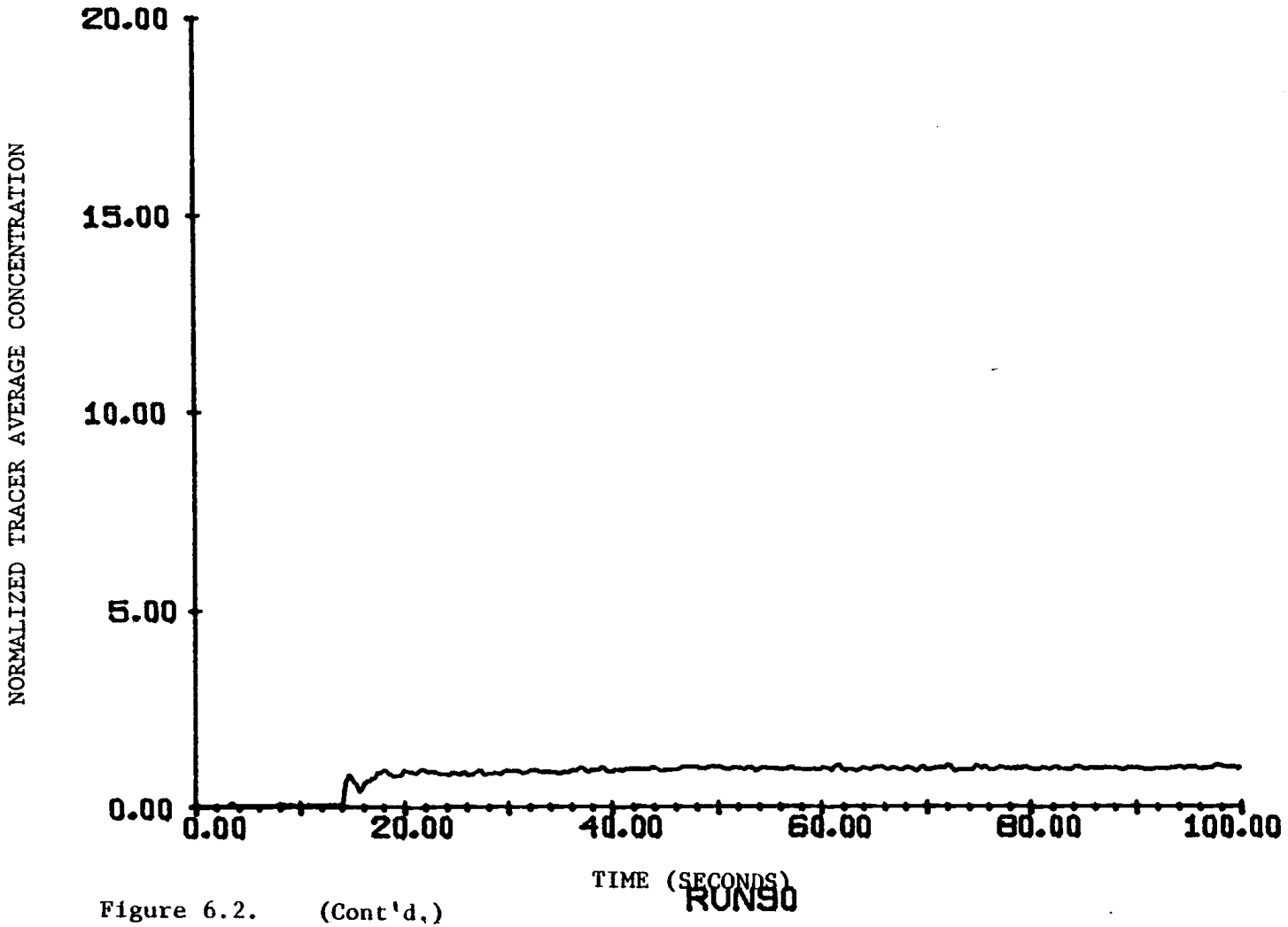

Figure 6.2. (Cont'd.)

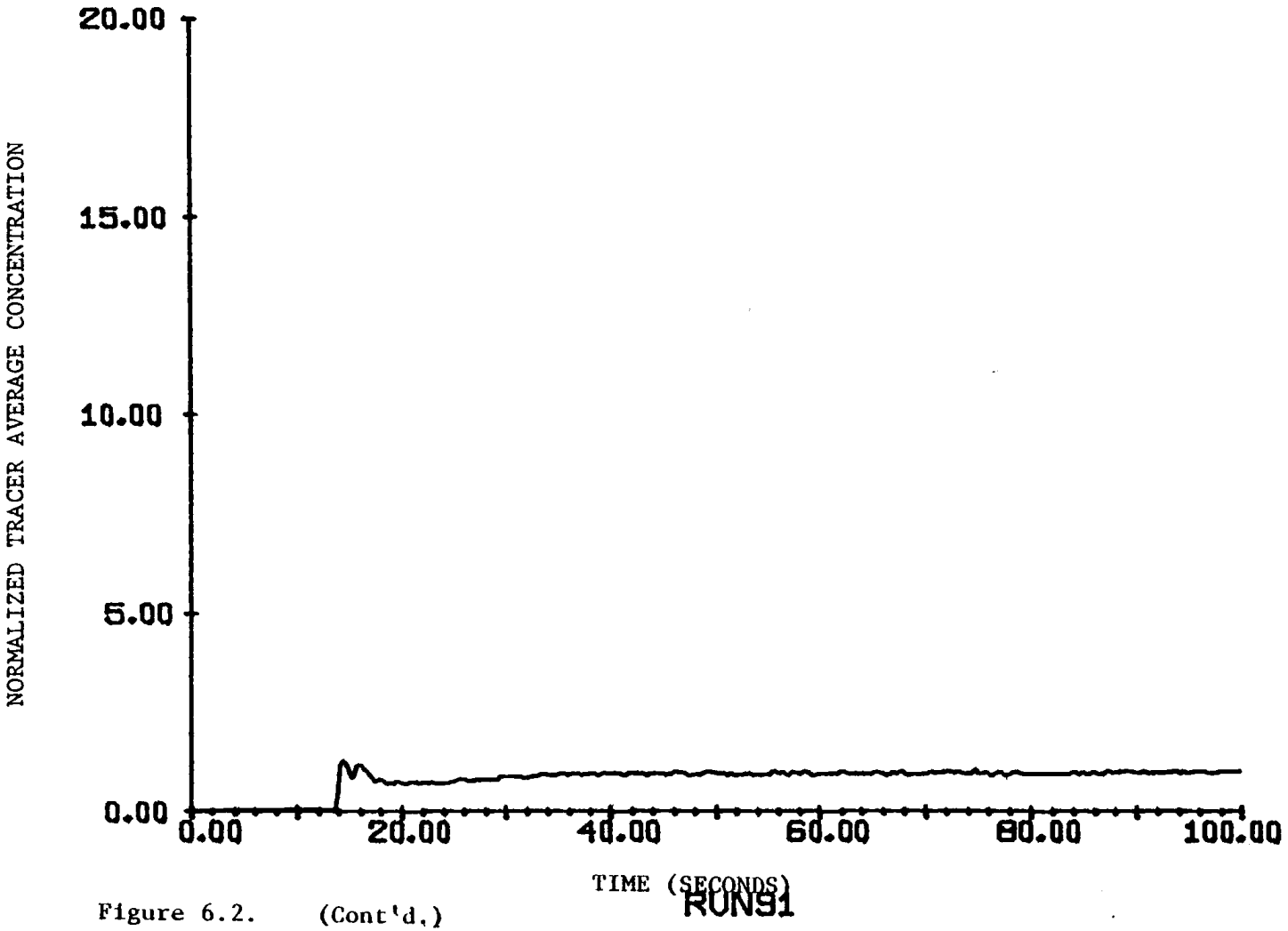

Figure 6.2. (Cont'd.)

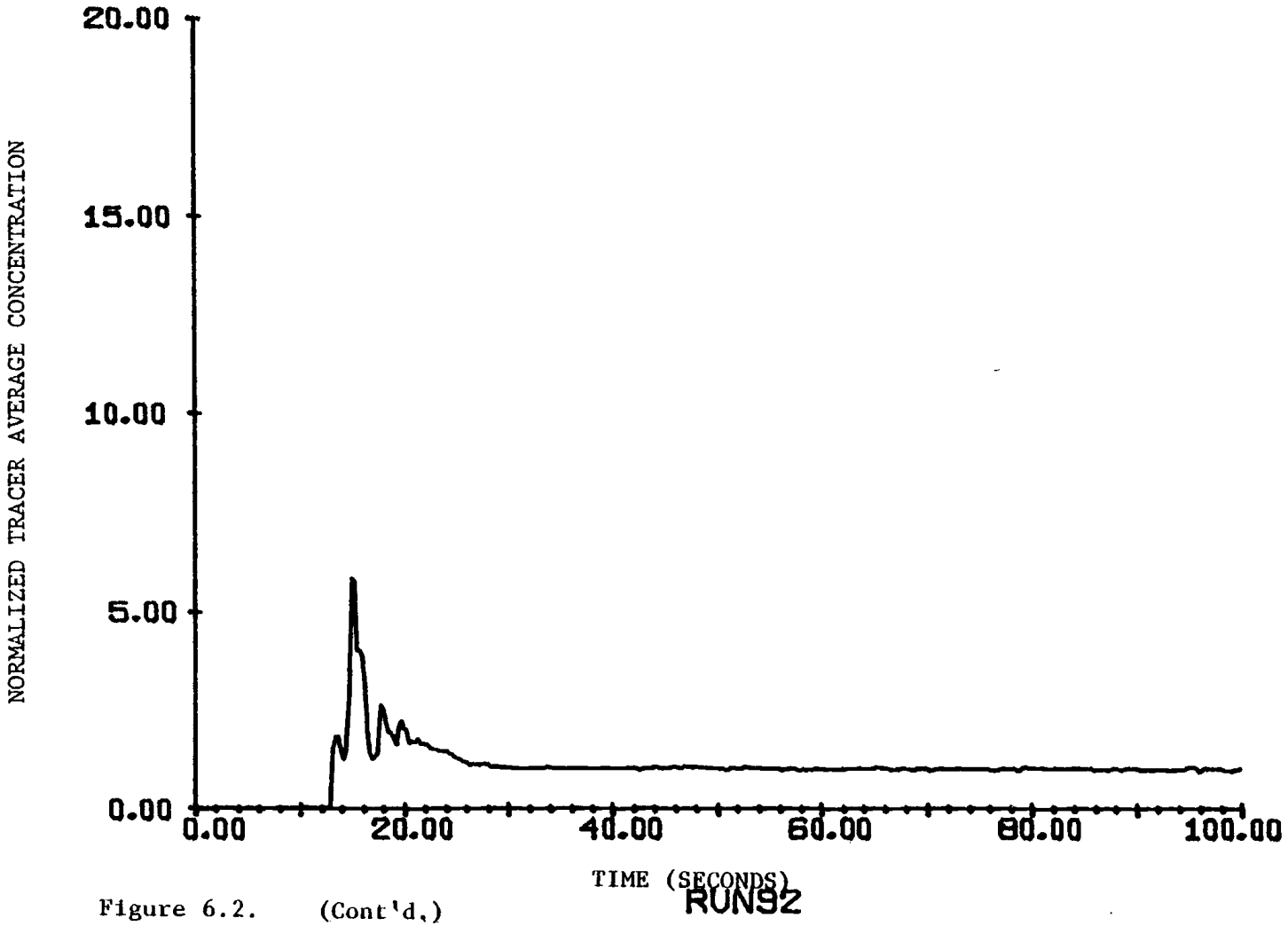

Figure 6.2. (Cont'd.)

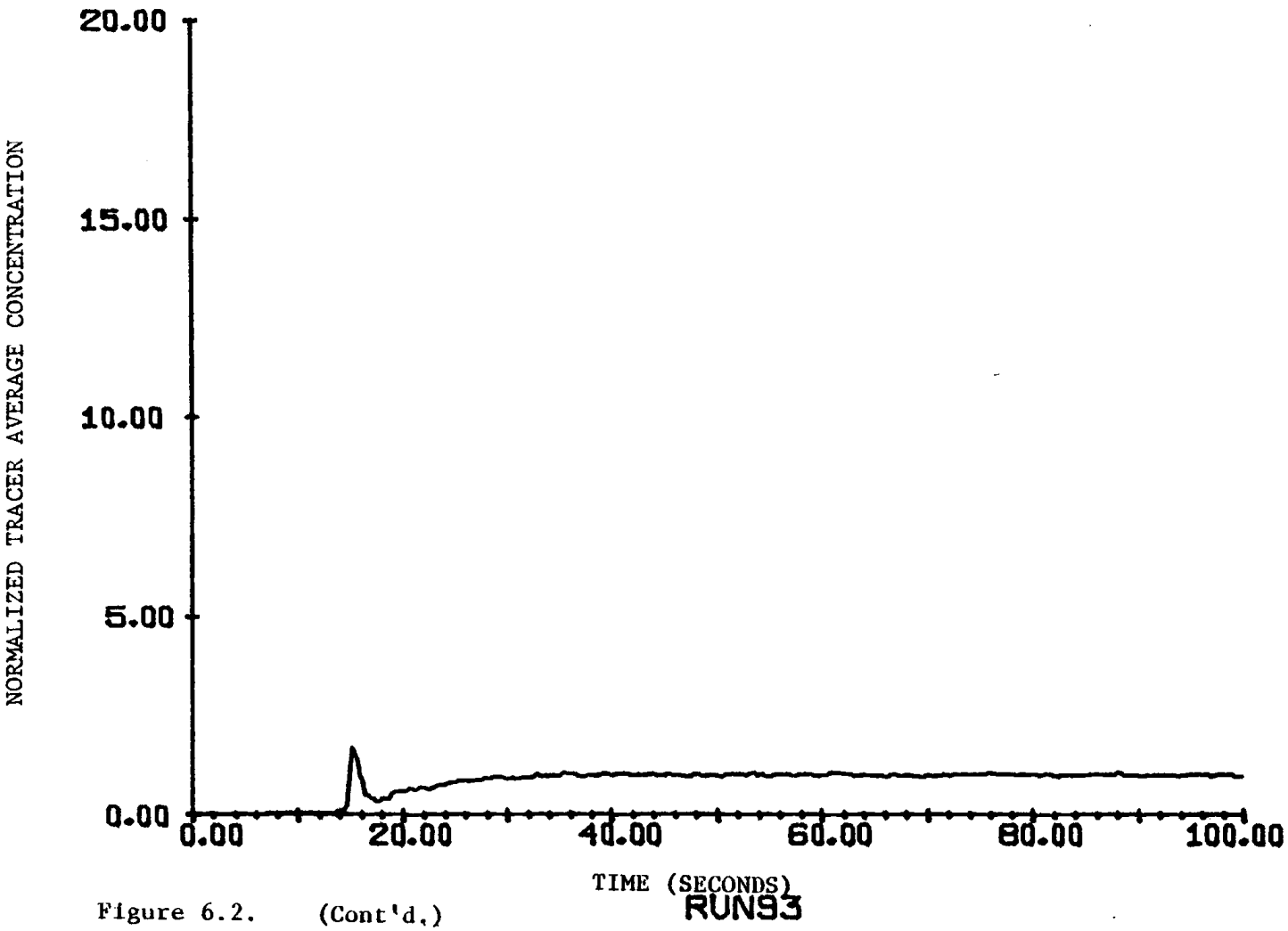

Figure 6.2. (Cont'd.)

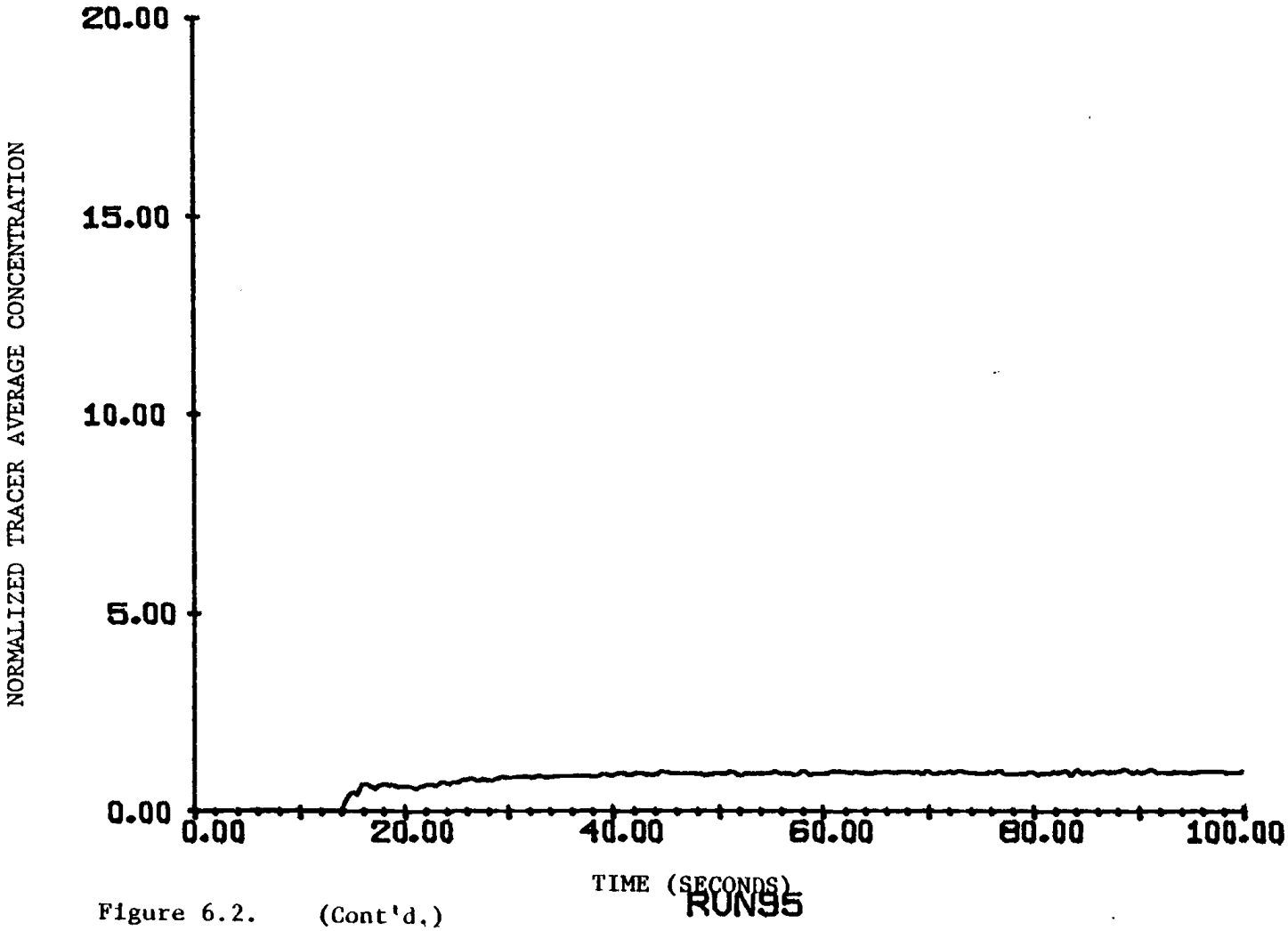

Figure 6.2. (Cont'd.)

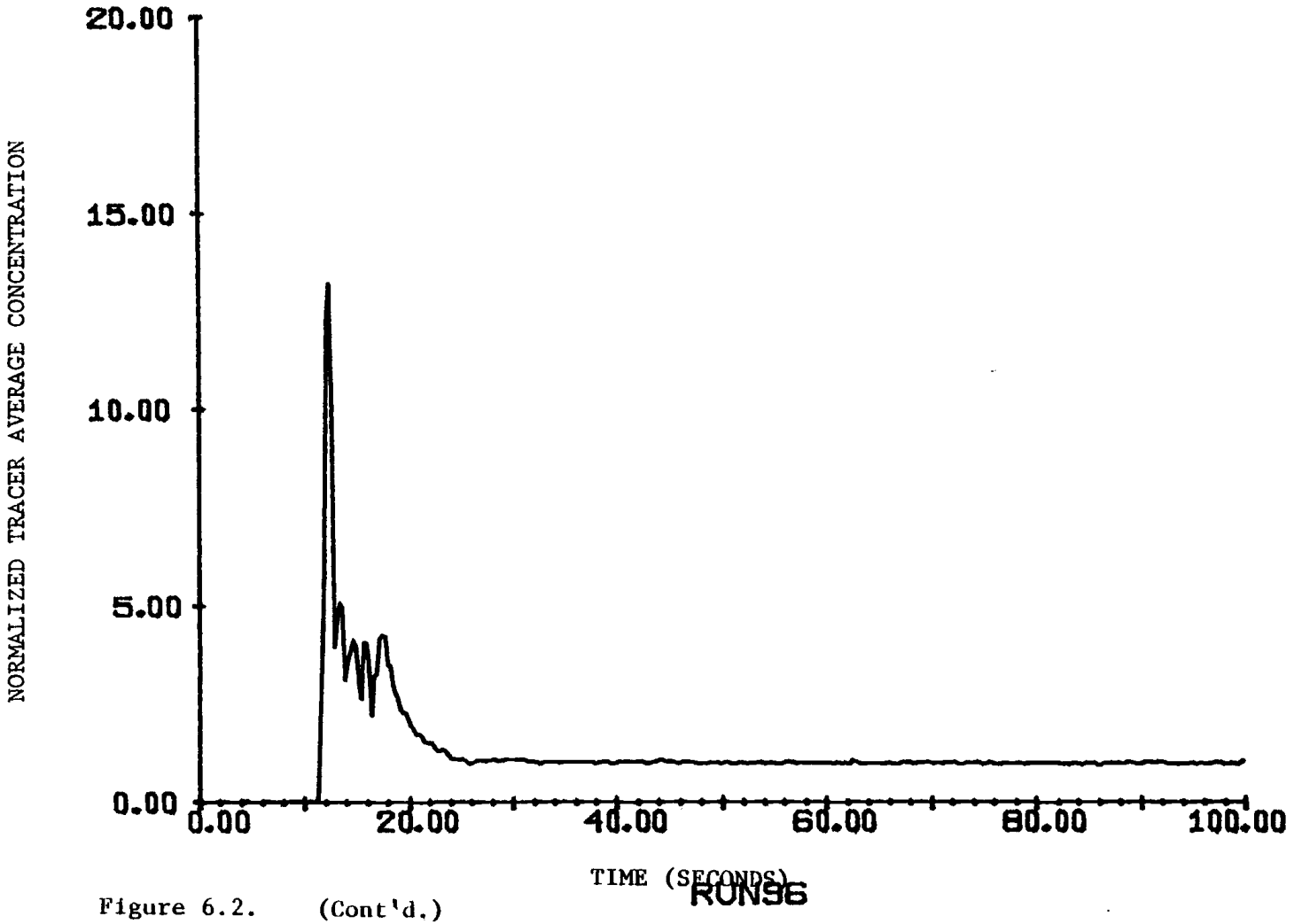

Figure 6.2. (Cont'd.)

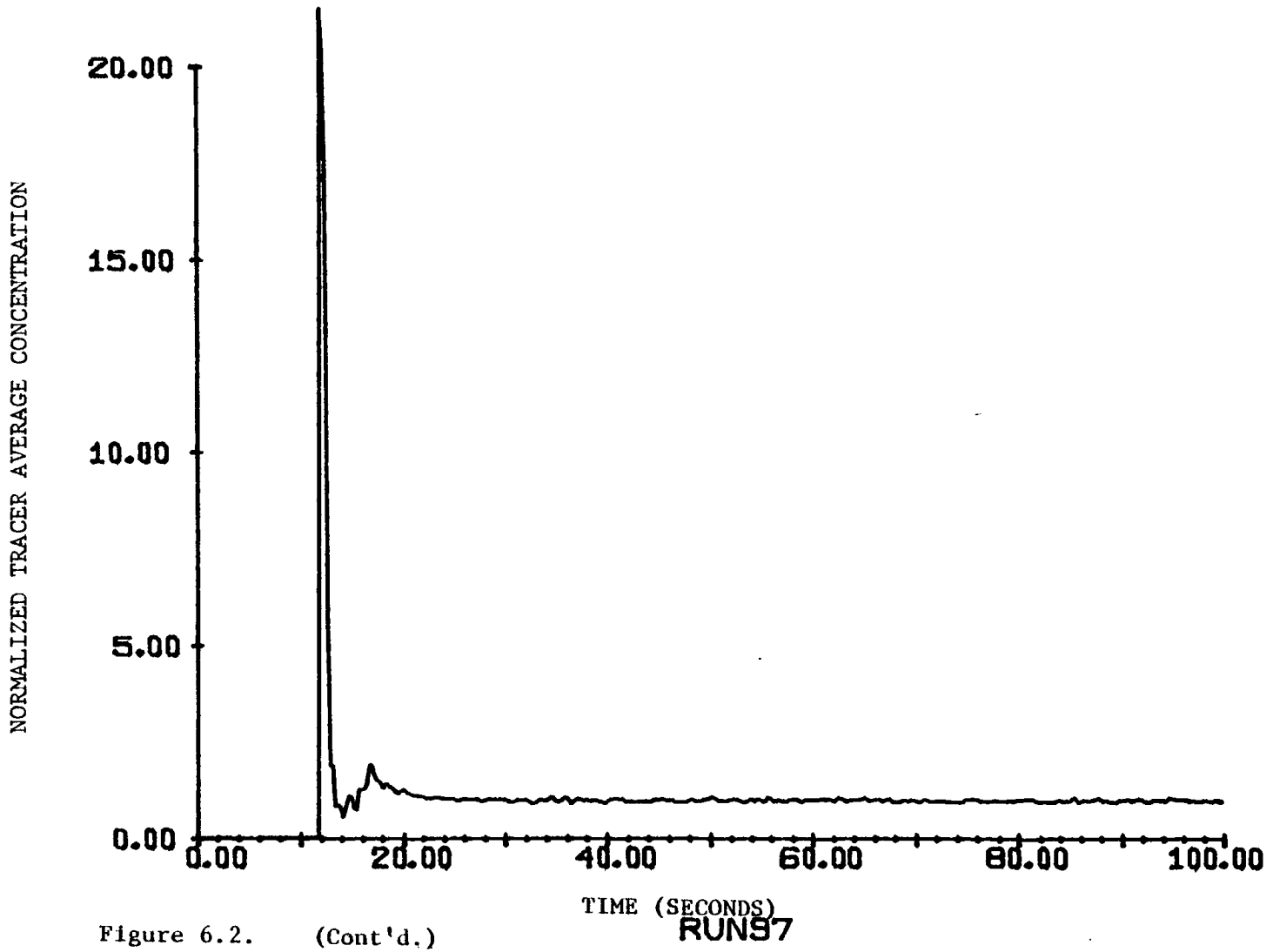

Figure 6.2. (Cont'd.)

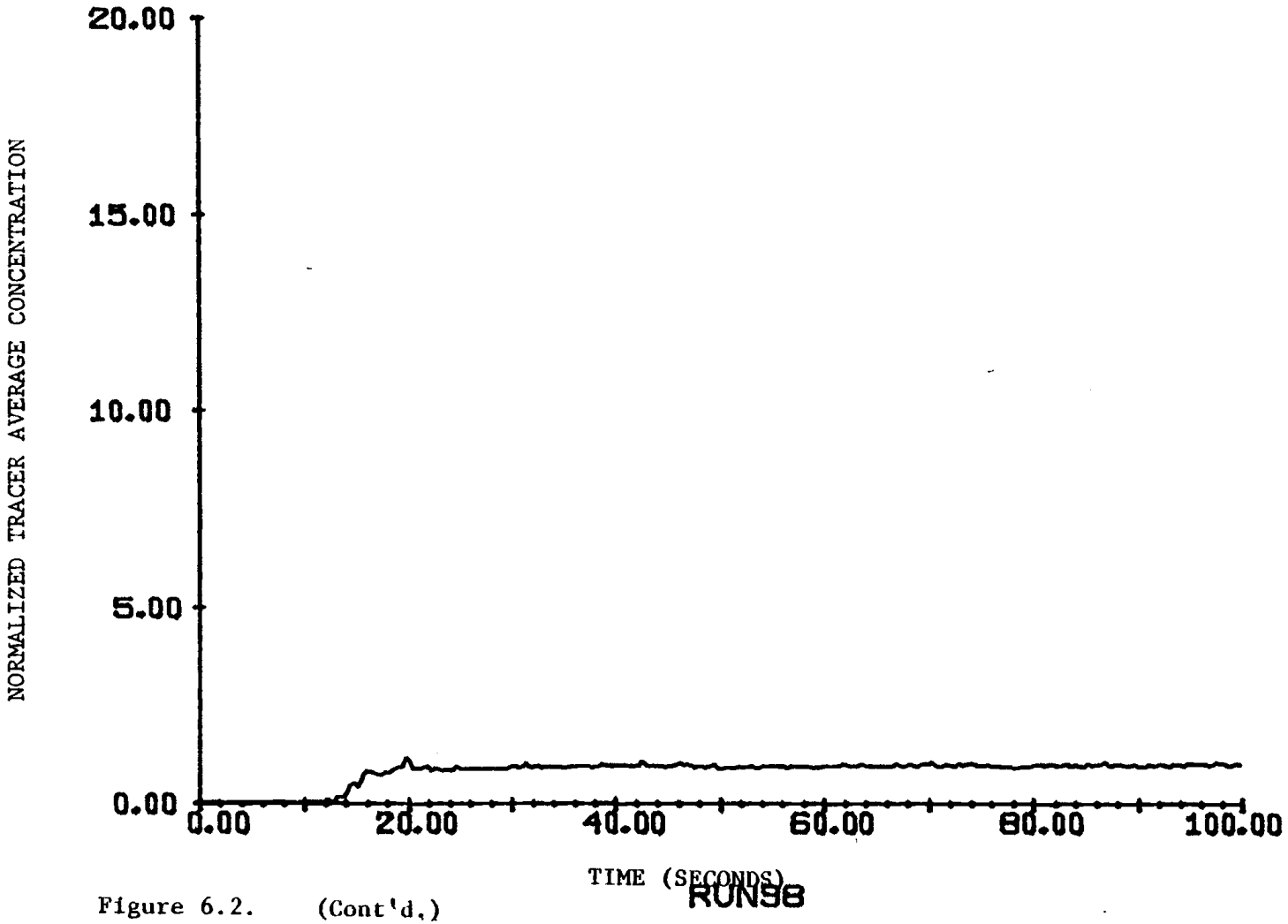

Figure 6.2. (Cont'd.)

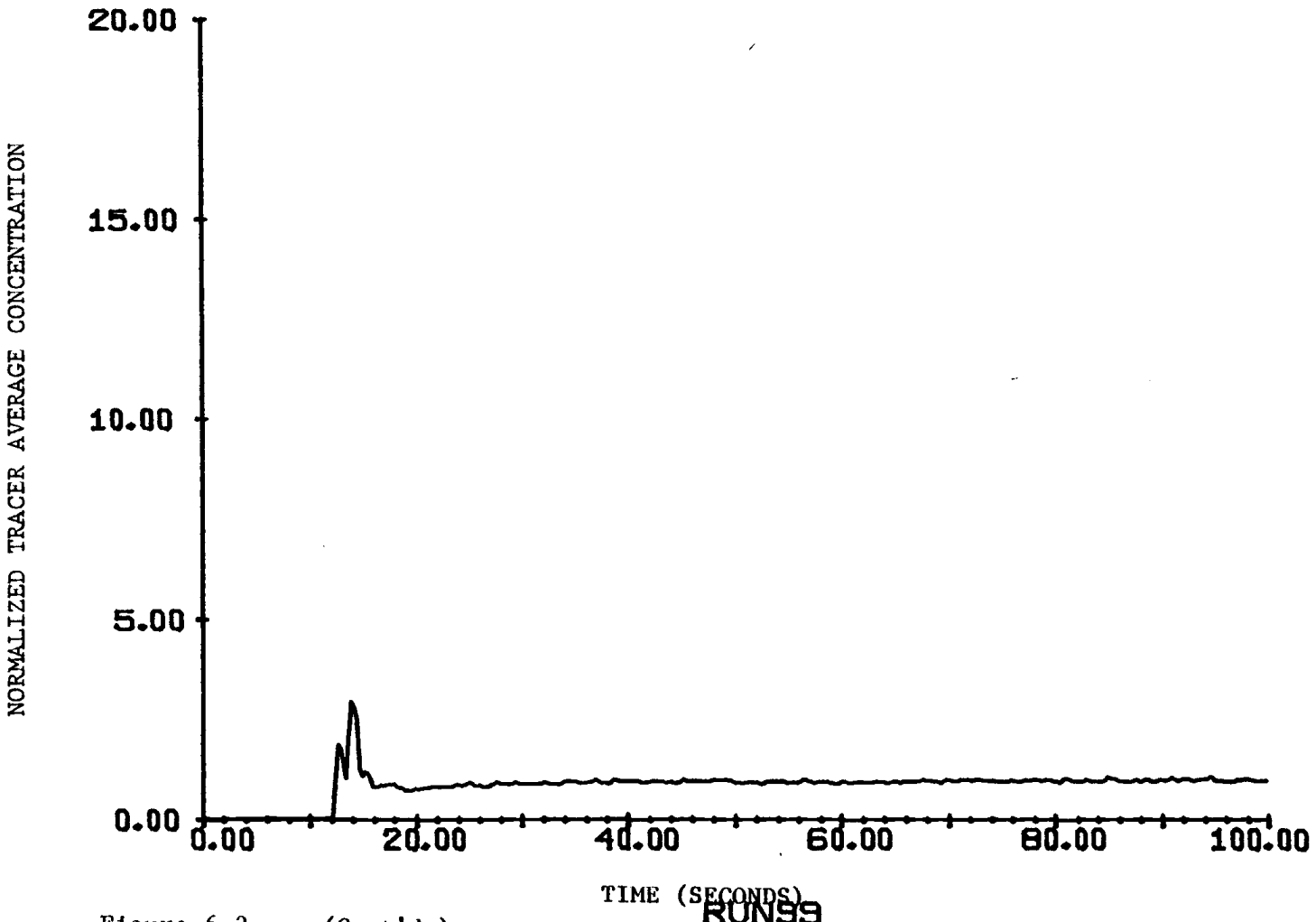

Figure 6.2. (Cont'd.)

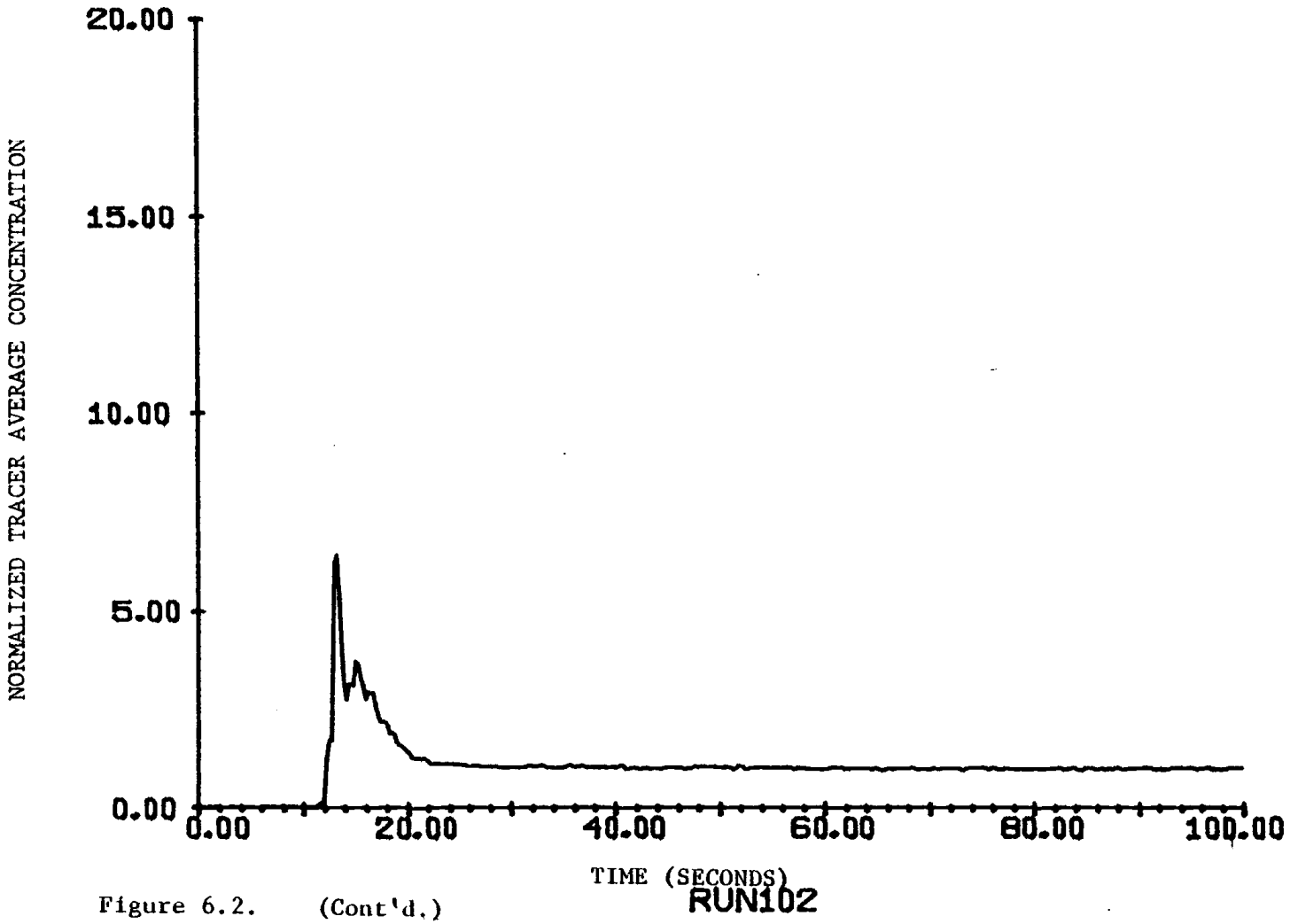

Figure 6.2. (Cont'd.)

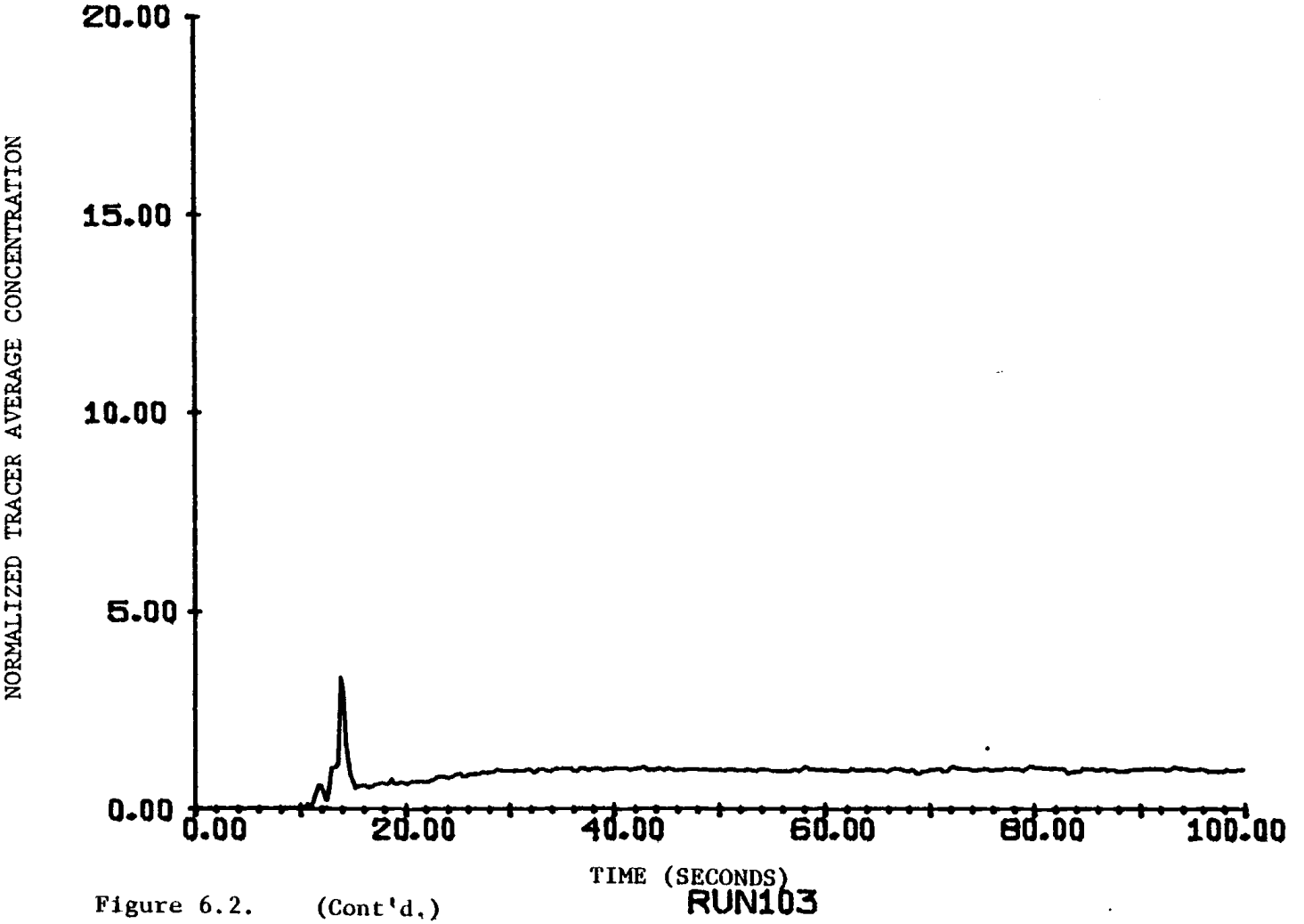

Figure 6.2. (Cont'd.)

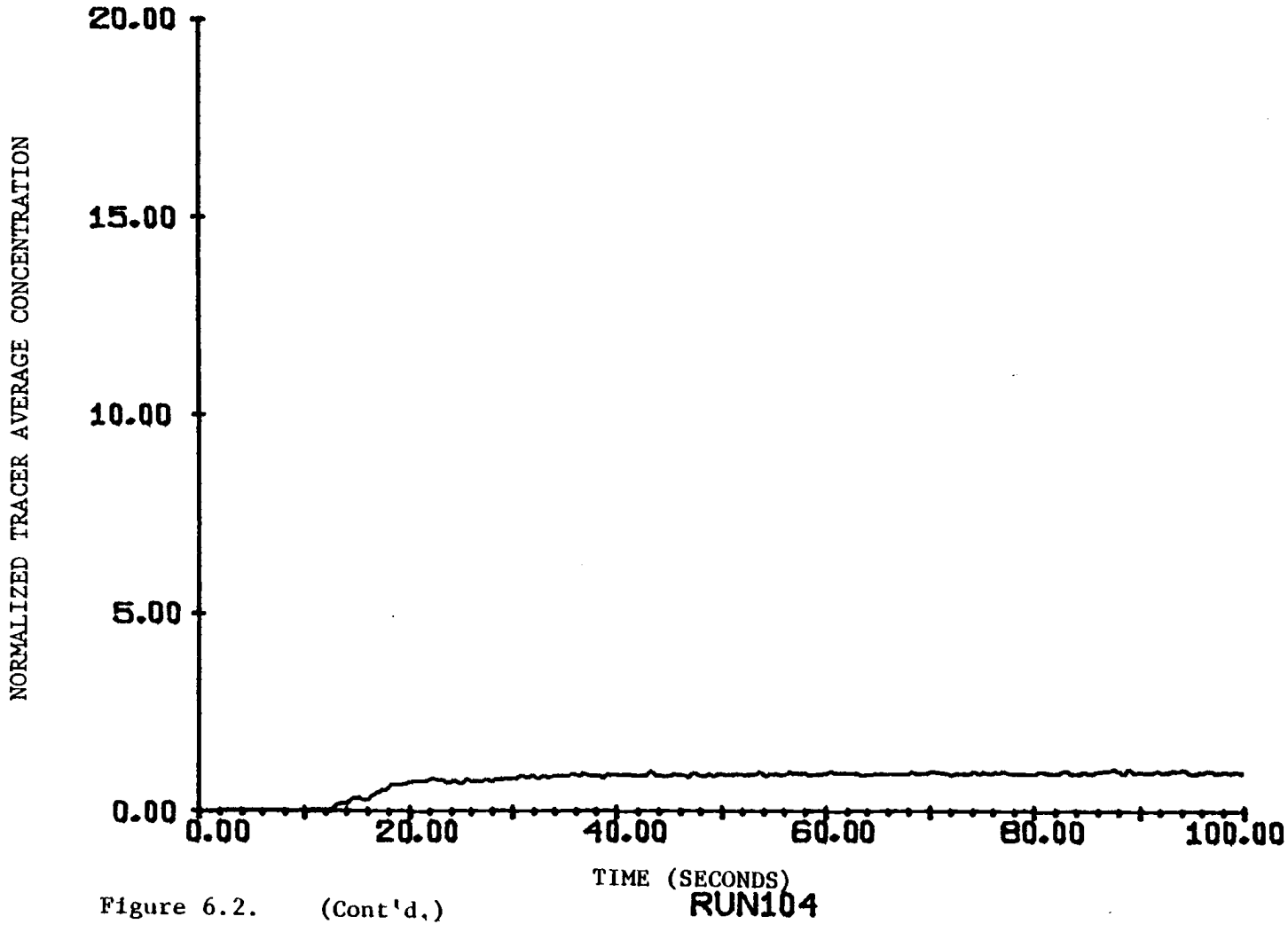

Figure 6.2. (Cont'd.)

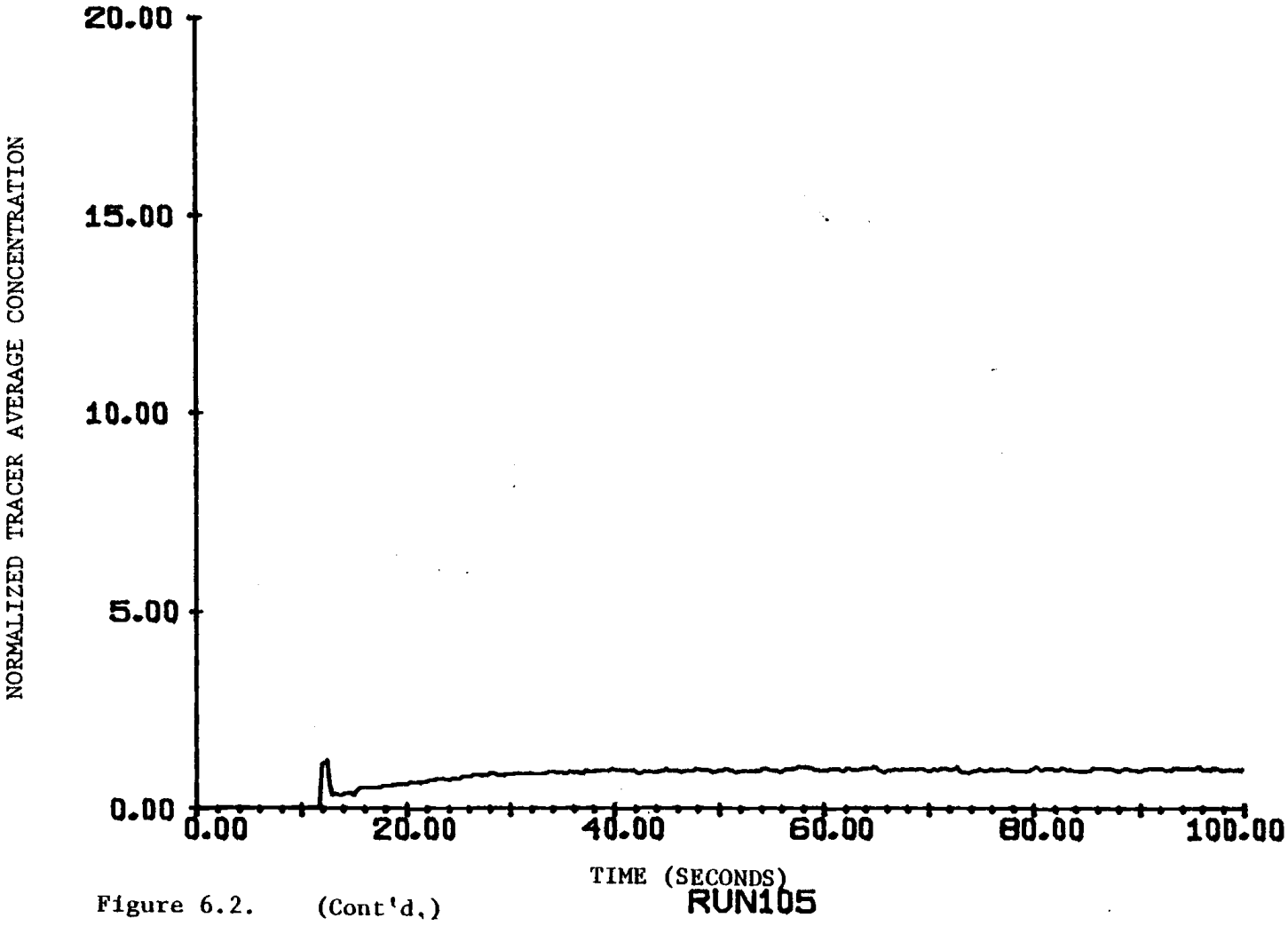

Figure 6.2. (Cont'd.)

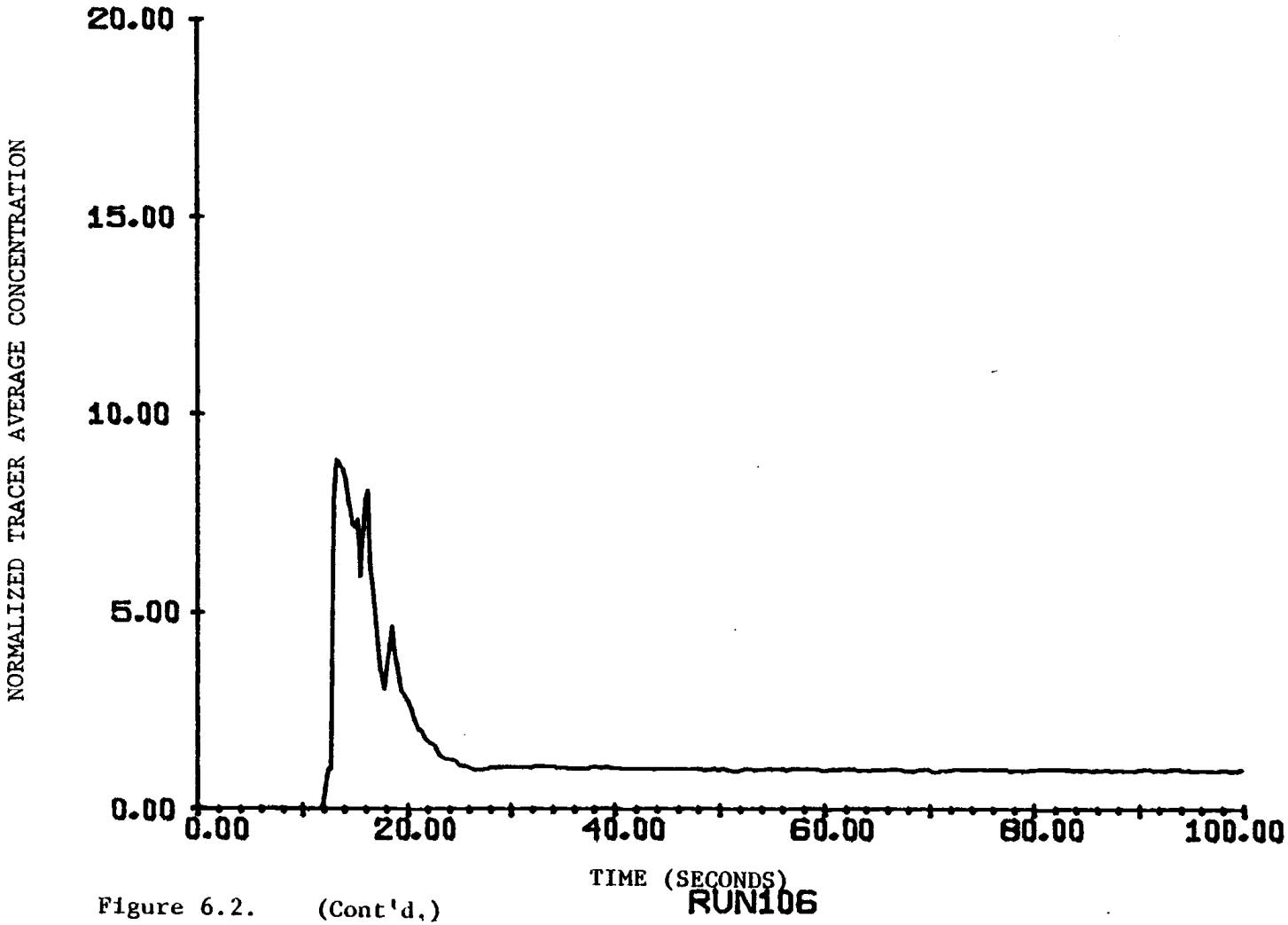

Figure 6.2. (Cont'd.)

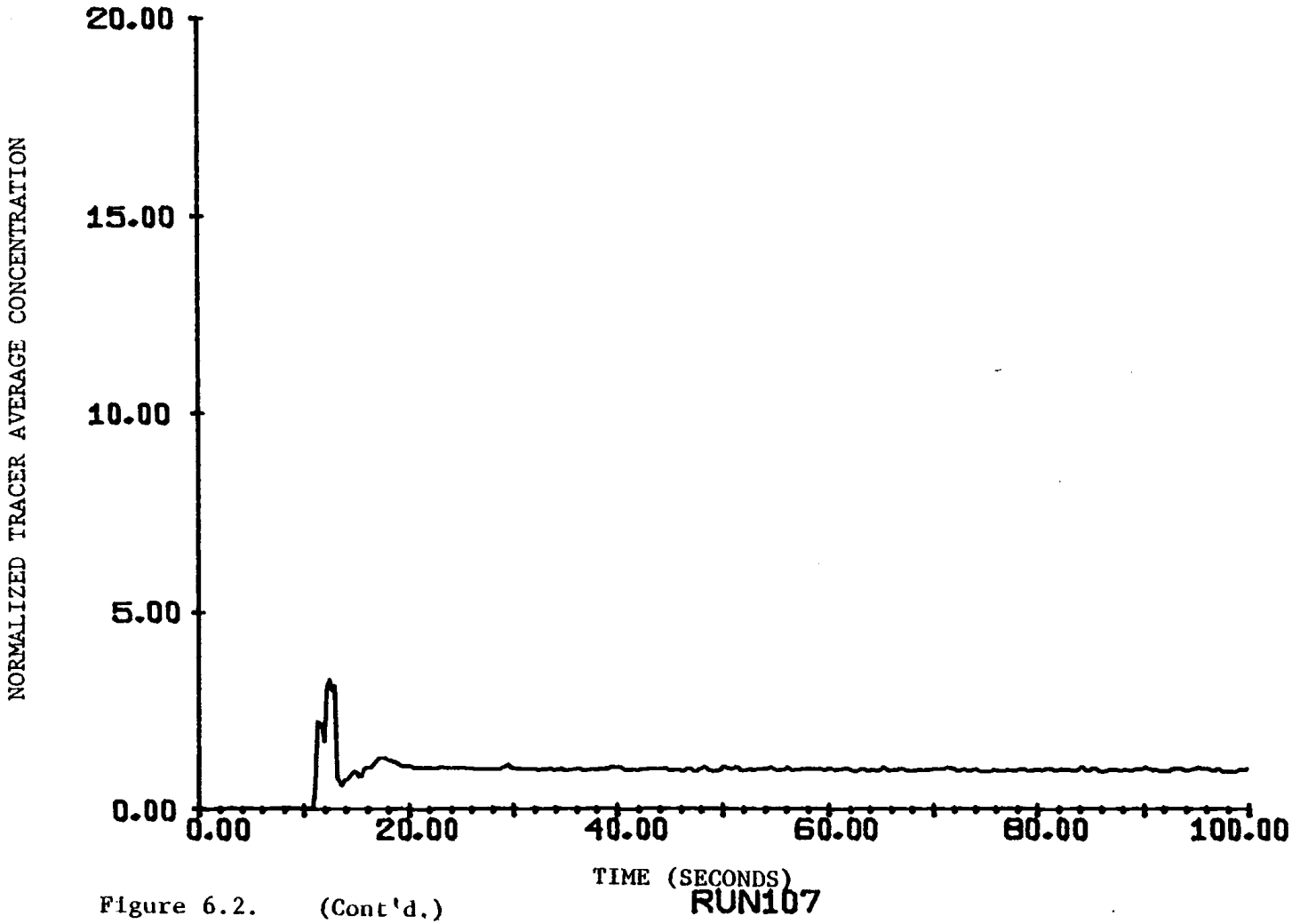

Figure 6.2. (Cont'd.)

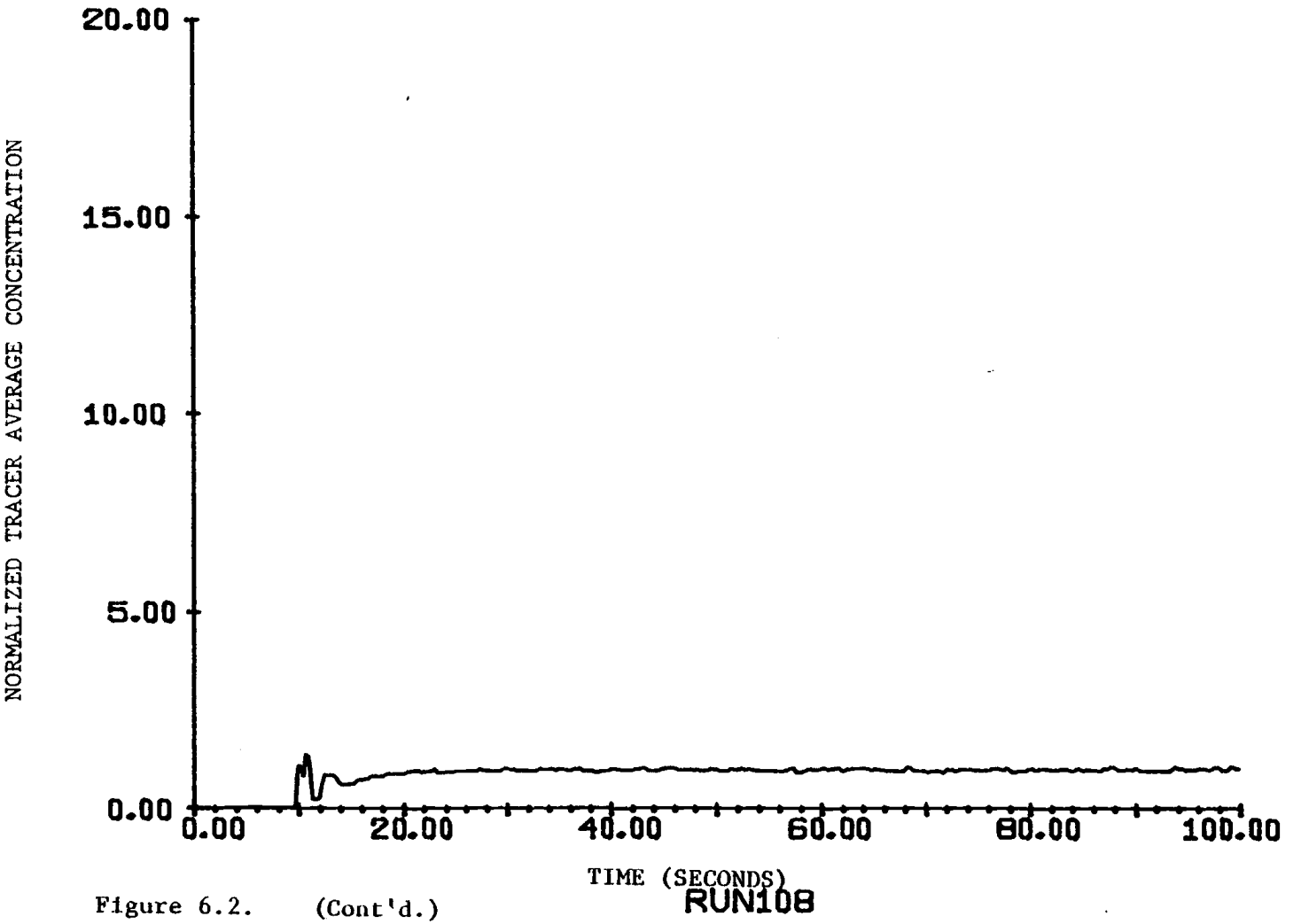

Figure 6.2. (Cont'd.)

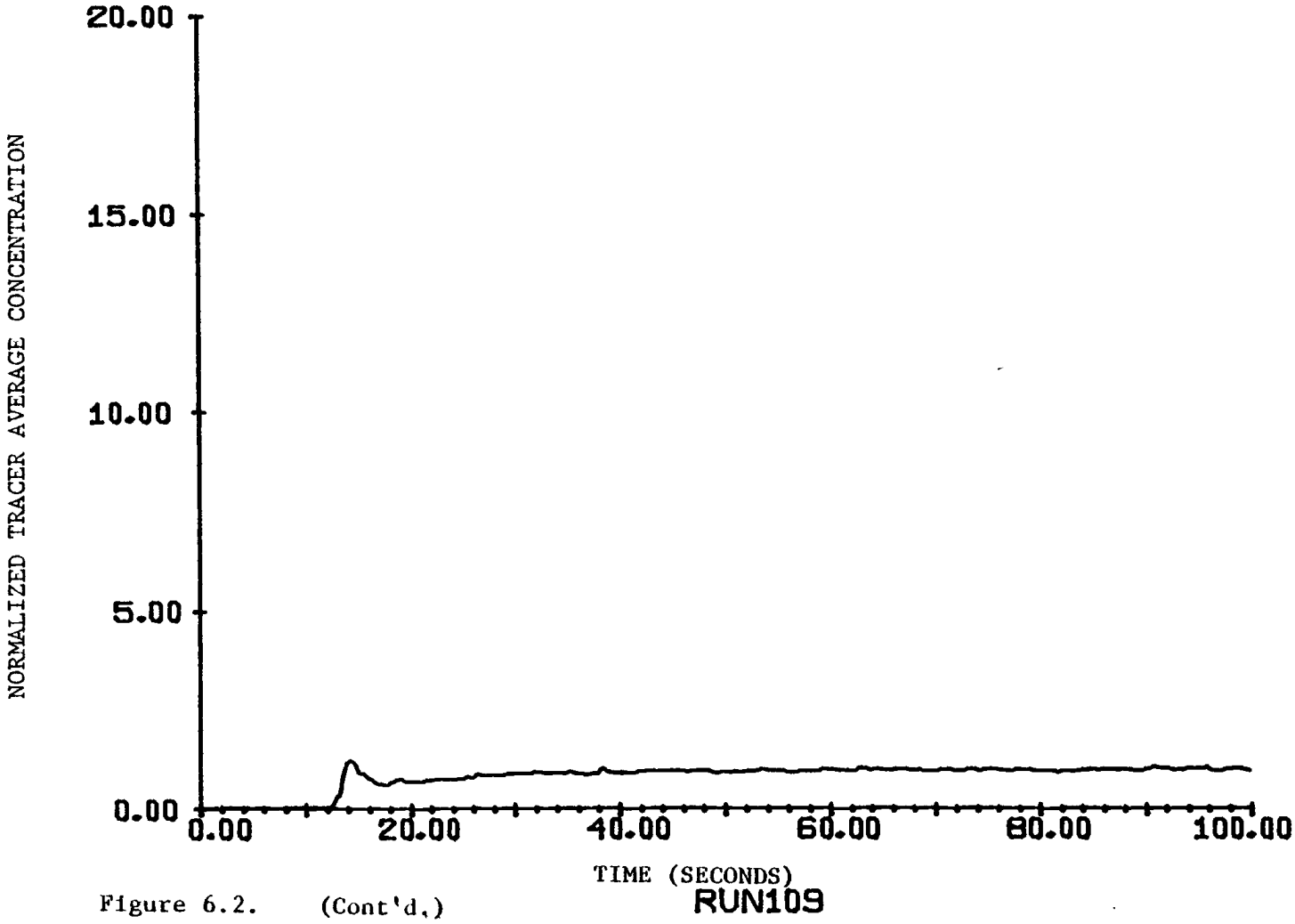

Figure 6.2. (Cont'd.)

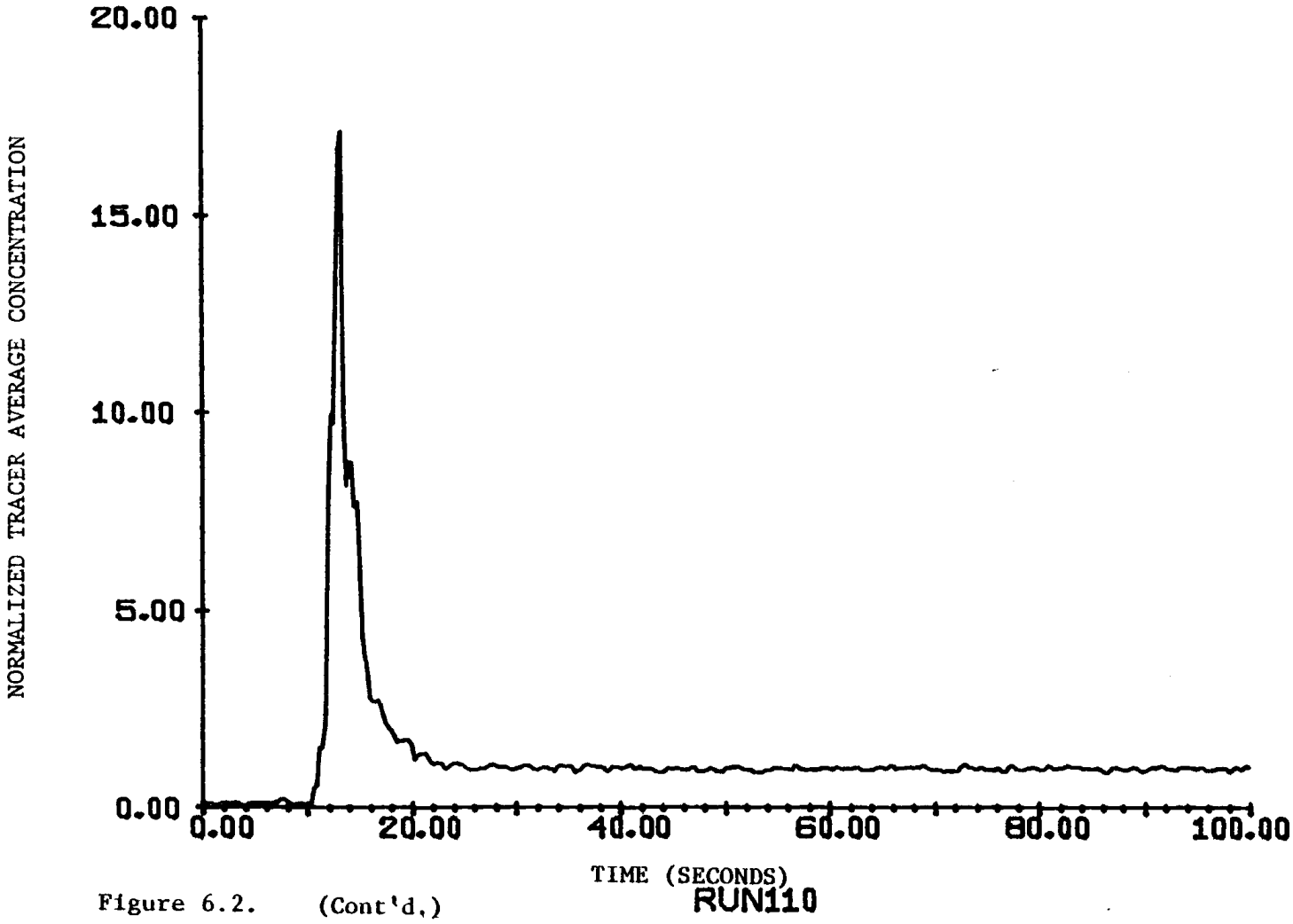

Figure 6.2. (Cont'd.)

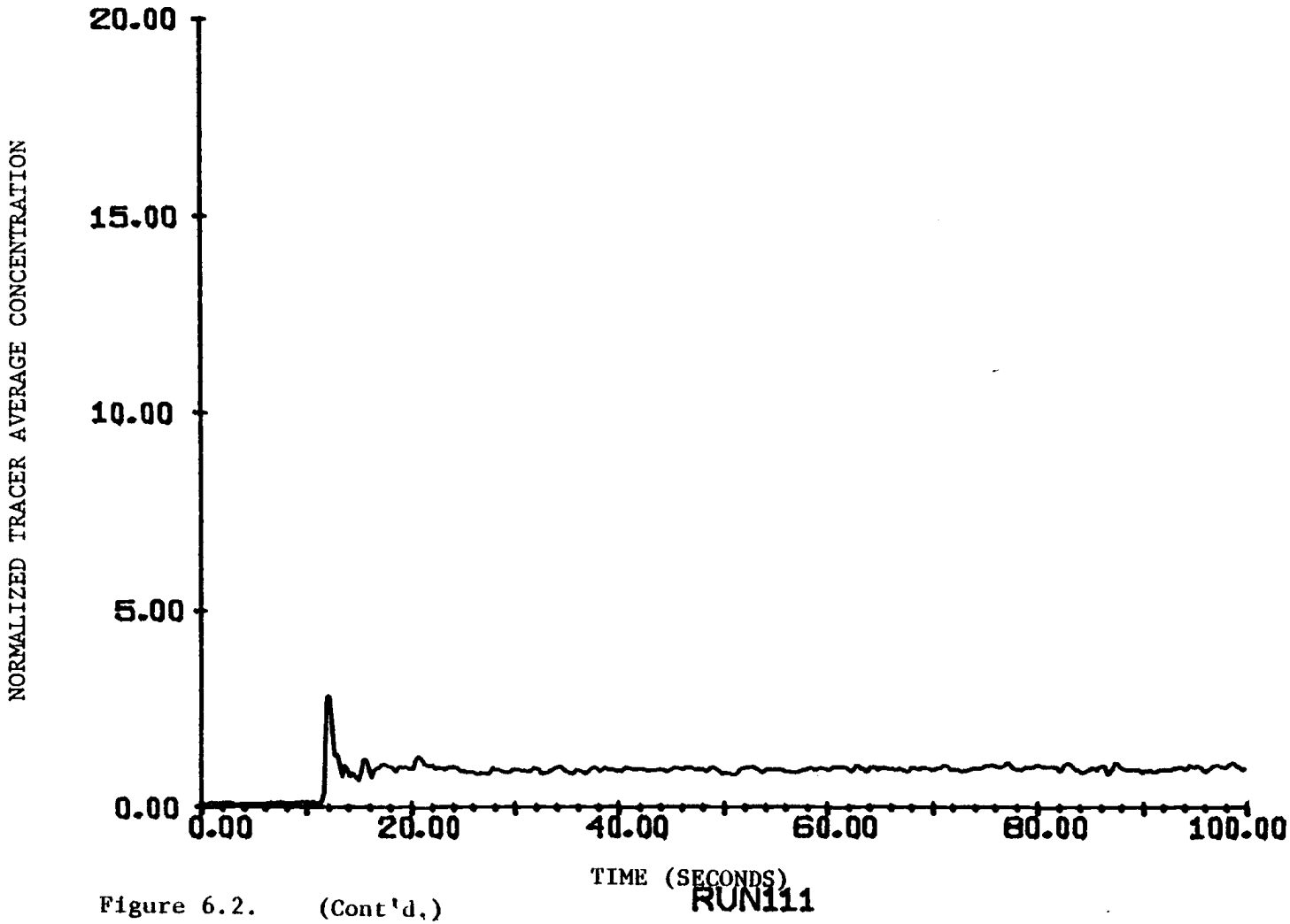

Figure 6.2. (Cont'd.)

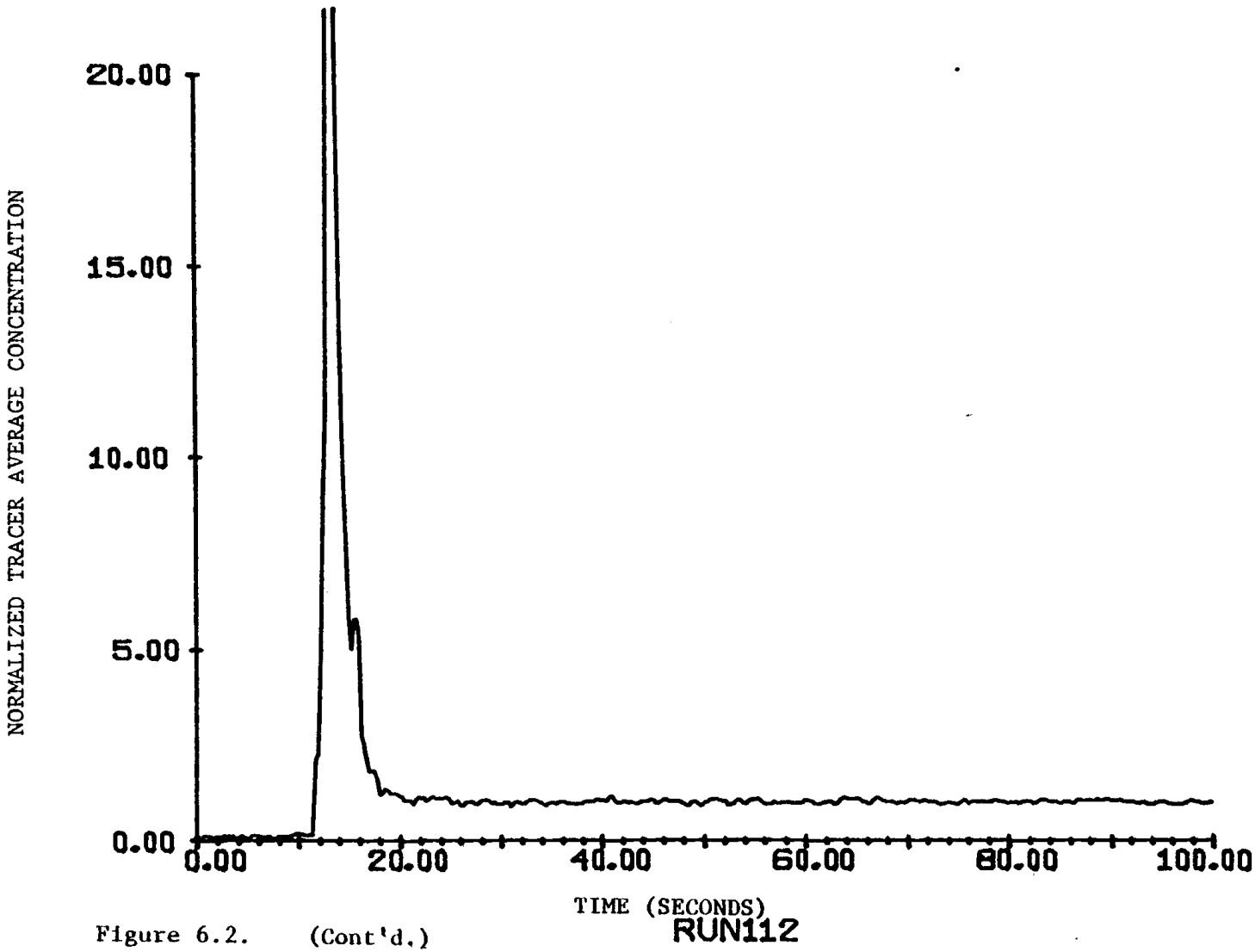

Figure 6.2. (Cont'd.)

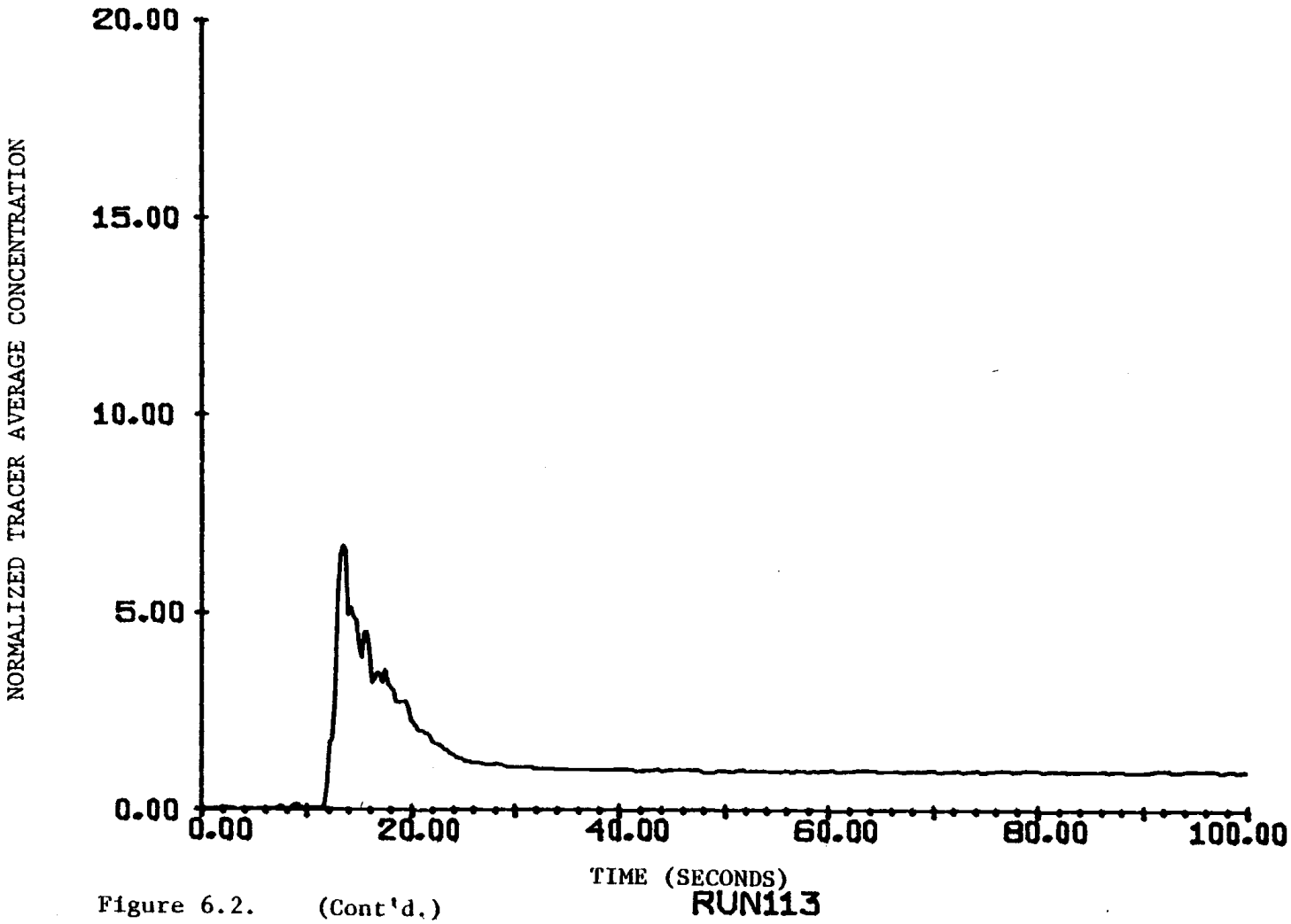

Figure 6.2. (Cont'd.)

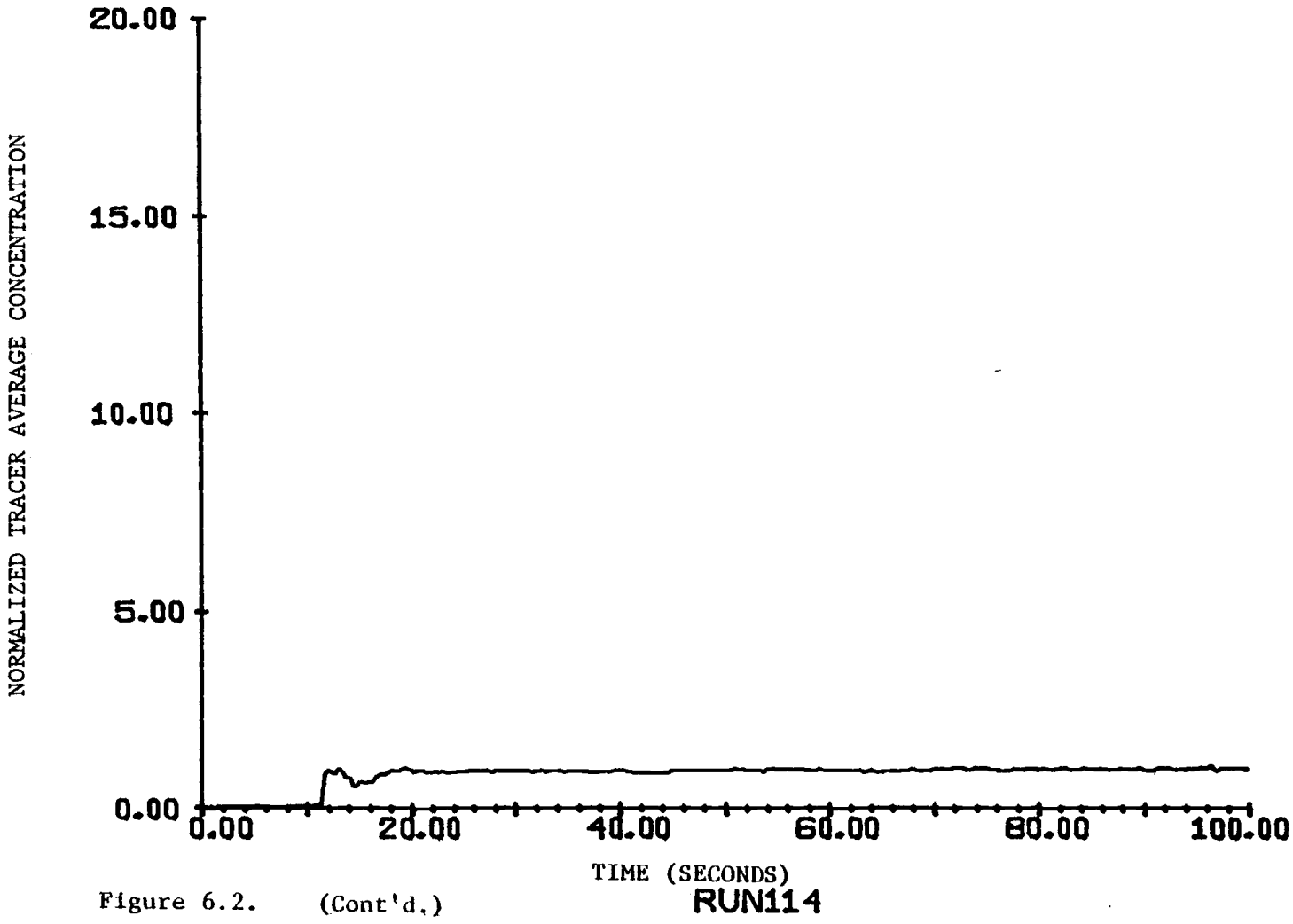

Figure 6.2. (Cont'd.)

concentrations. In terms of symbols, this becomes

$$\bar{C}_j = \left(\sum_{i=1}^{64} C_{i,j}^2\right) / \left(\sum_{i=1}^{64} C_{i,j}\right)$$

for one particular time interval, j, $C_{i,j}$ is the concentration reading on channel i, of which there are 64. This measure is consistent with the expectation of a particular concentration, which is defined to be the sum of concentrations times their respective probabilities or, discretely,

$$\bar{C}_j = \sum_{i=1}^{64} \left[C_{i,j} \; \frac{C_{i,j}}{\sum_{i=1}^{64} C_{i,j}} \right]$$

It is evident that this expectation becomes equal to the expression above for an almost instantaneous data sample (less than one-one hundredth of a second) since $\left(\sum_{i=1}^{64} C_{i,j}\right)$ is approximately constant. The normalized mean concentration, C_θ, is given by

$$C_\theta = (\bar{C}_j / \bar{C}^*) .$$

6.3 The Mass Balance Plots

The mass balances (see Figure 6.3) can also be used to determine approximate overall mixing times in a qualitative way. The ordinates are simply the sum of concentrations measured in data

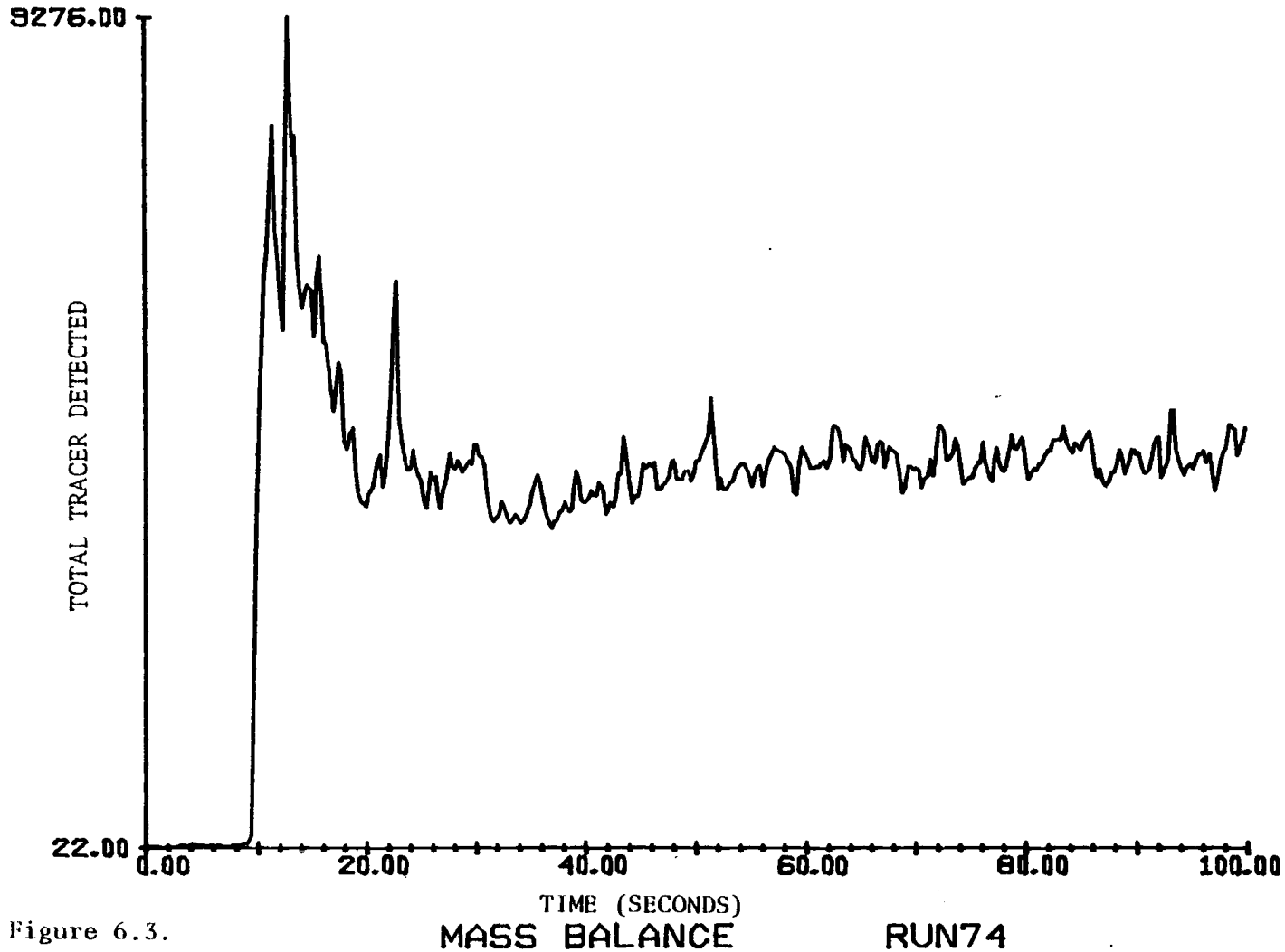
9276.00
22.00
TOTAL TRACER DETECTED
0.00
20.00
40.00
60.00
80.00
100.00
TIME (SECONDS)
MASS BALANCE
RUN74

Figure 6.3.

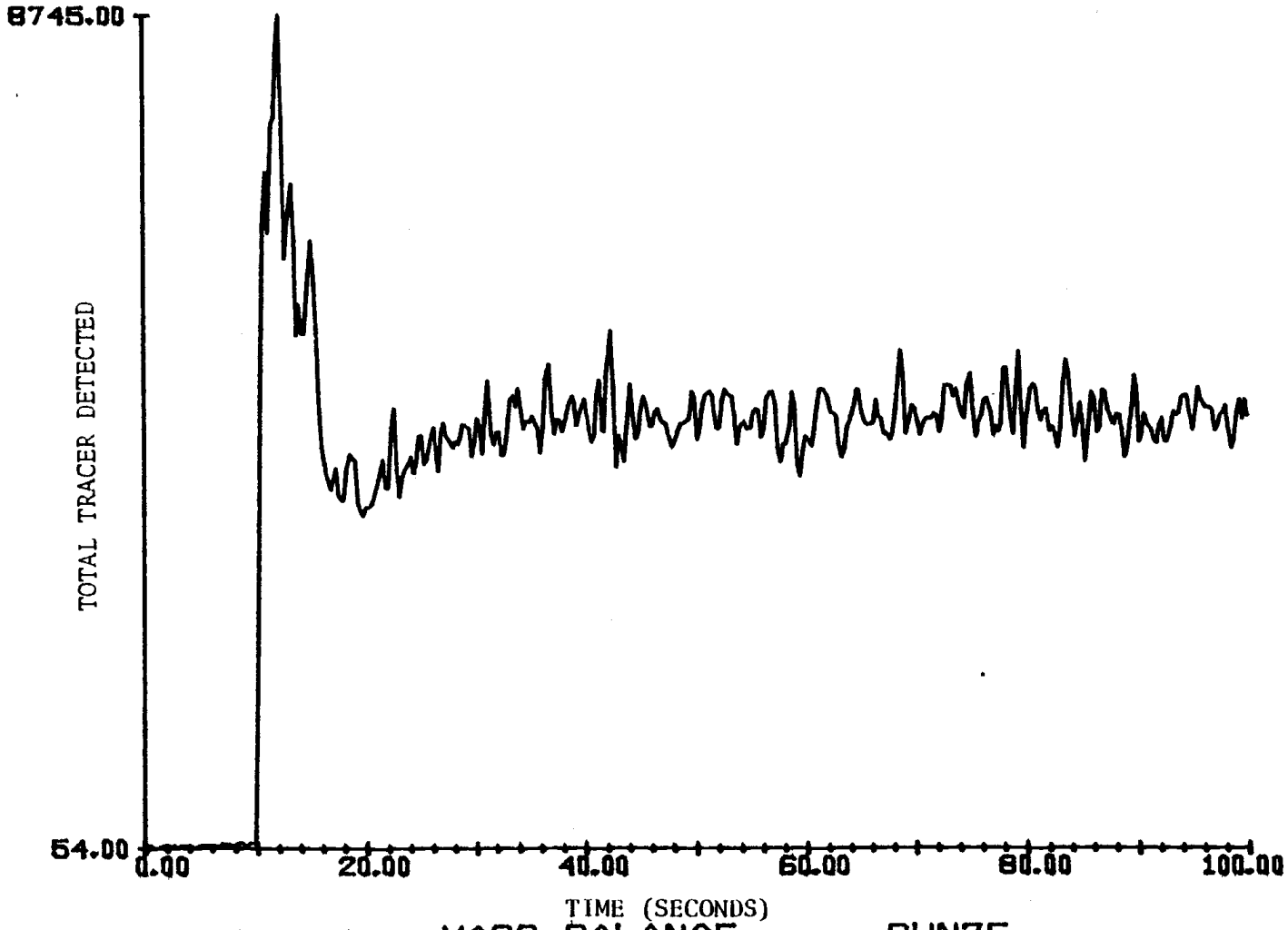

Figure 6.3. (Cont'd.)

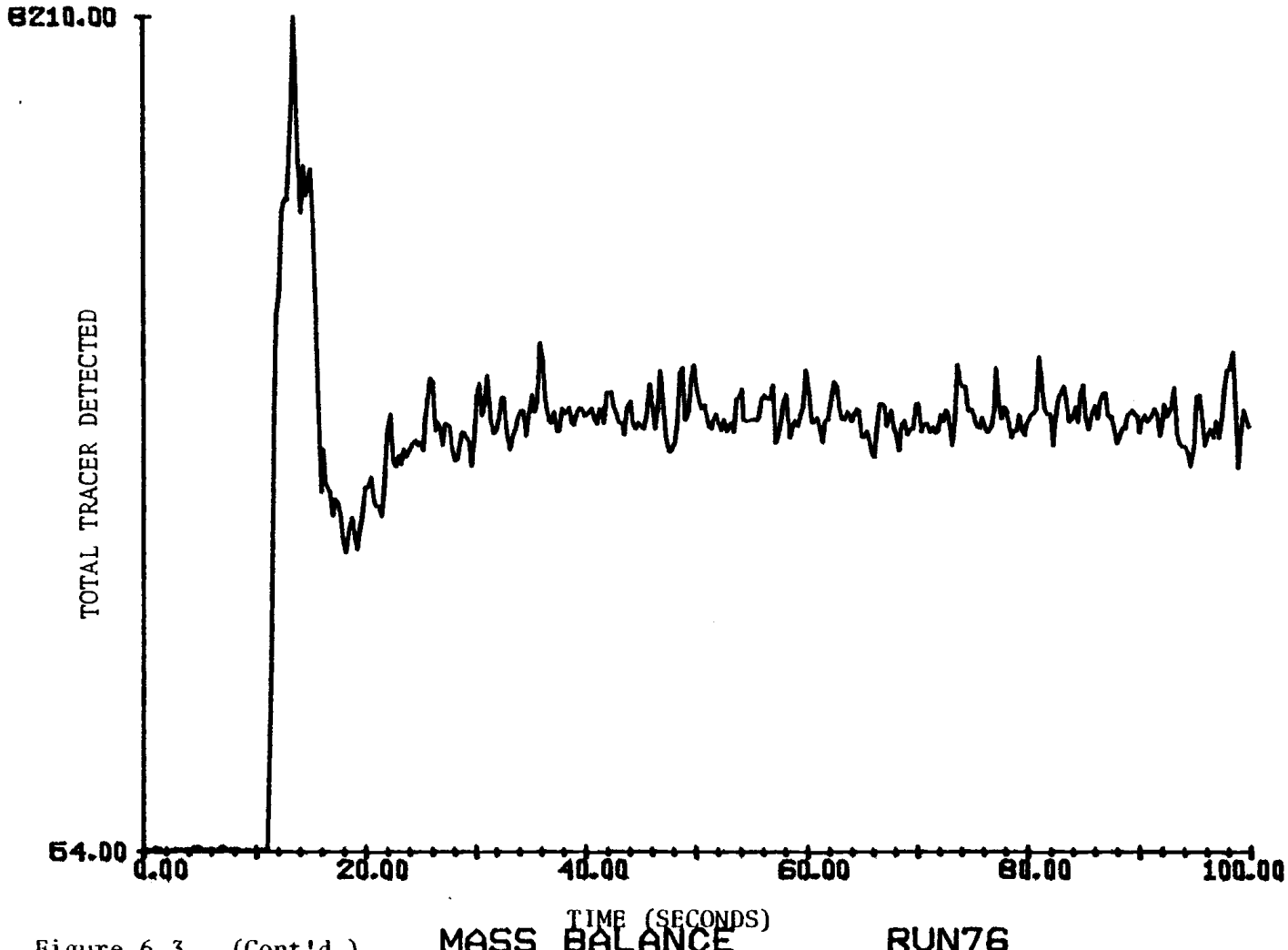

Figure 6.3. (Cont'd.)

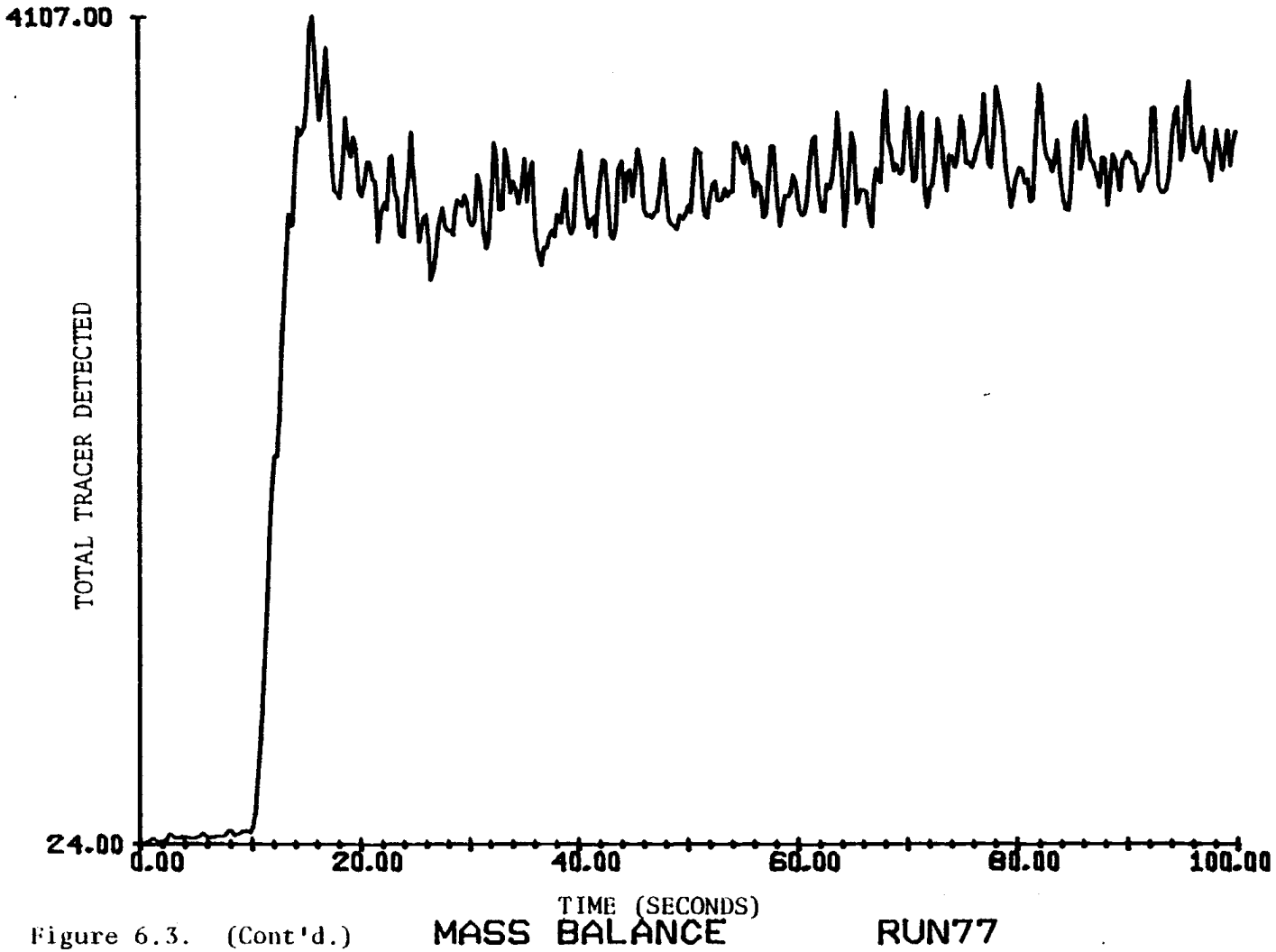

Figure 6.3. (Cont'd.)

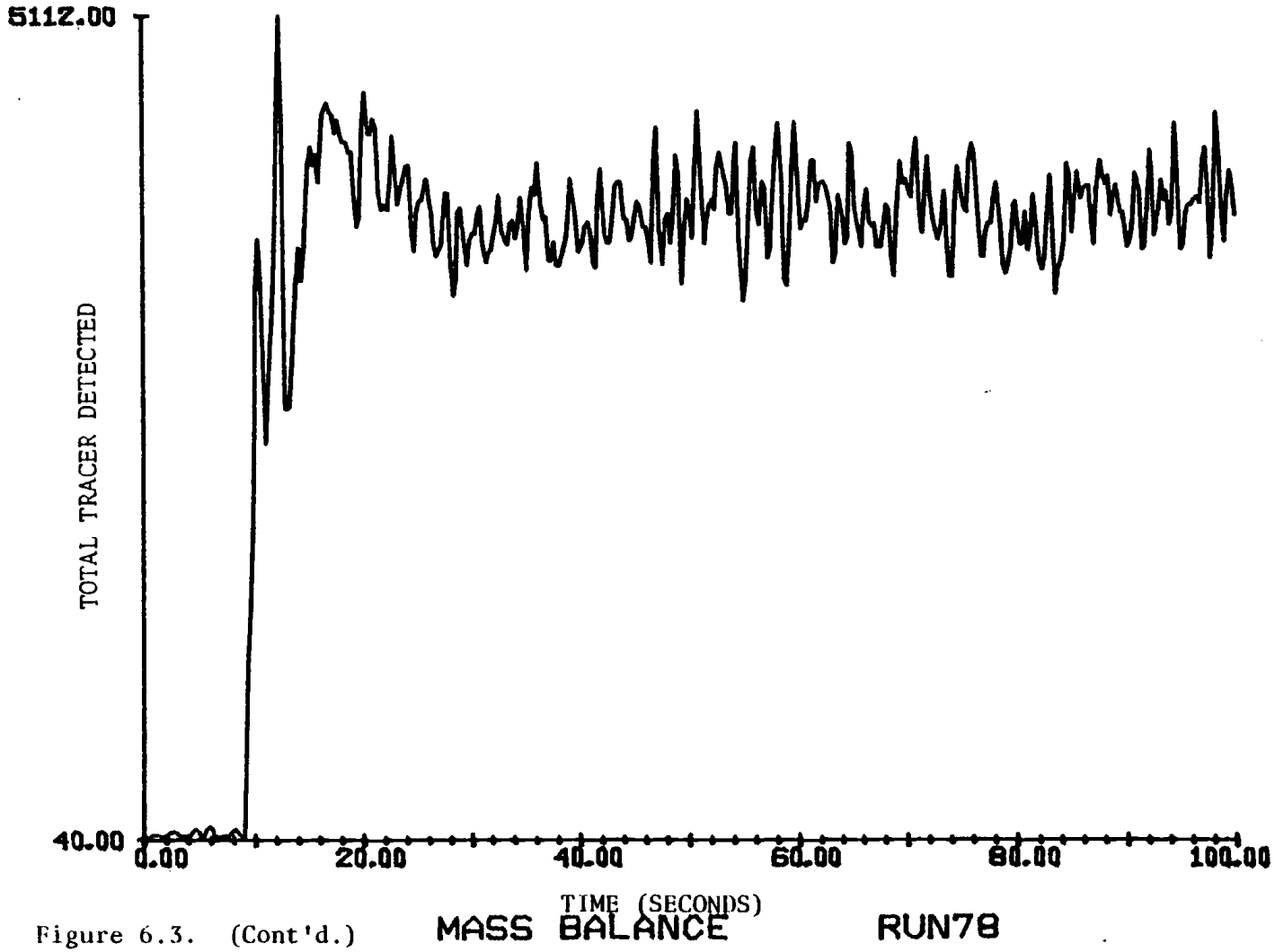

Figure 6.3. (Cont'd.)

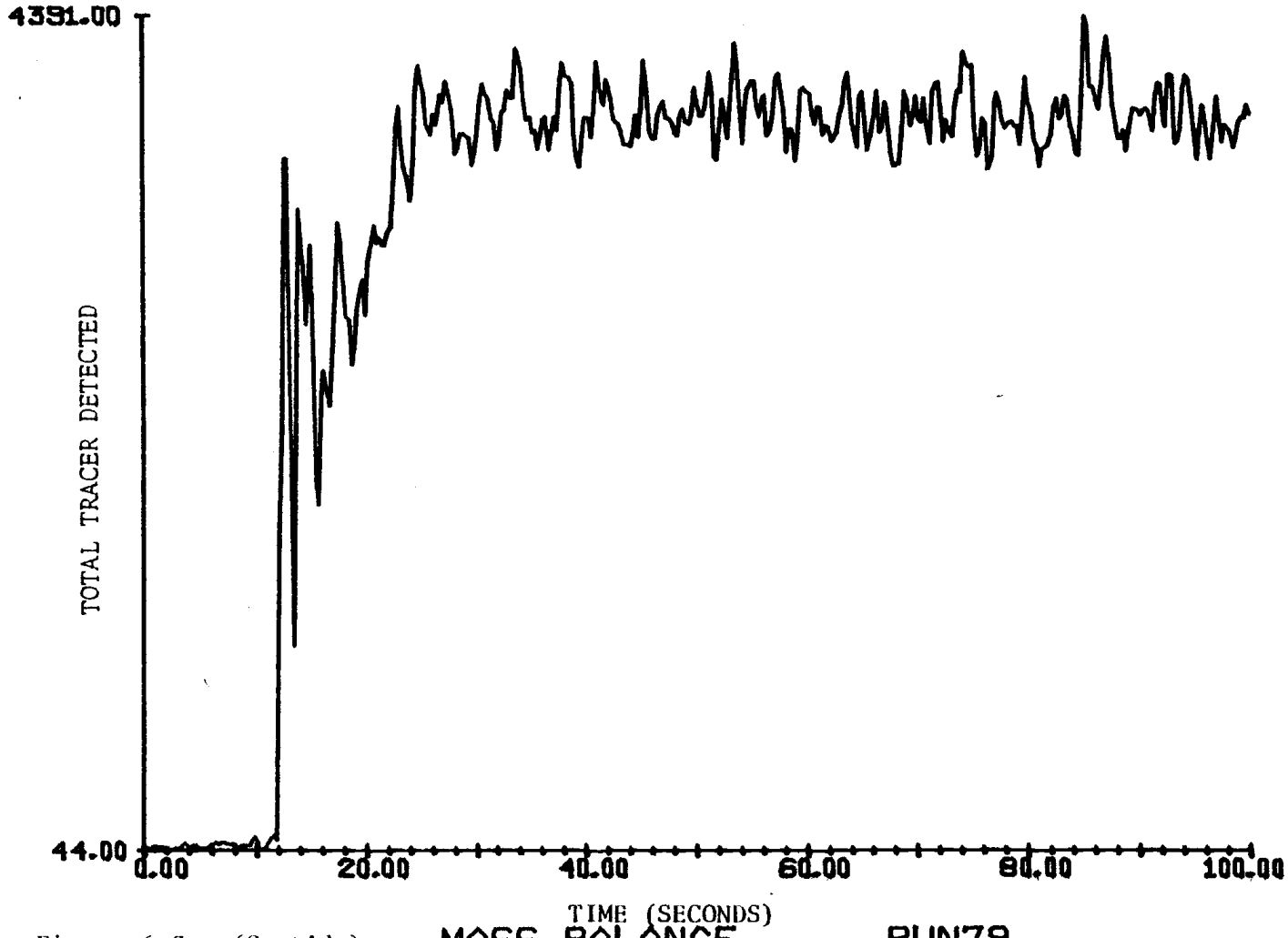

Figure 6.3. (Cont'd.)

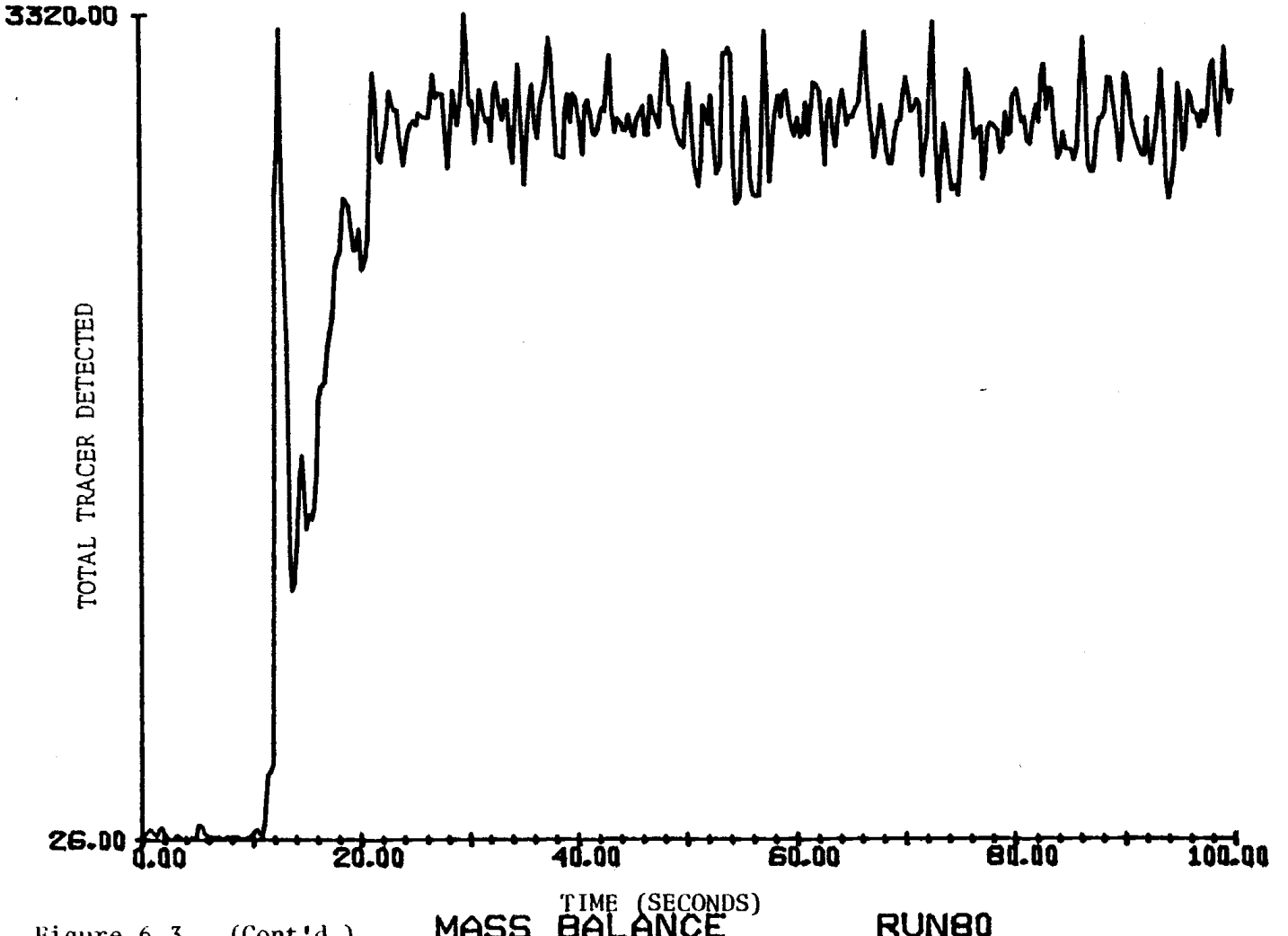

Figure 6.3. (Cont'd.)

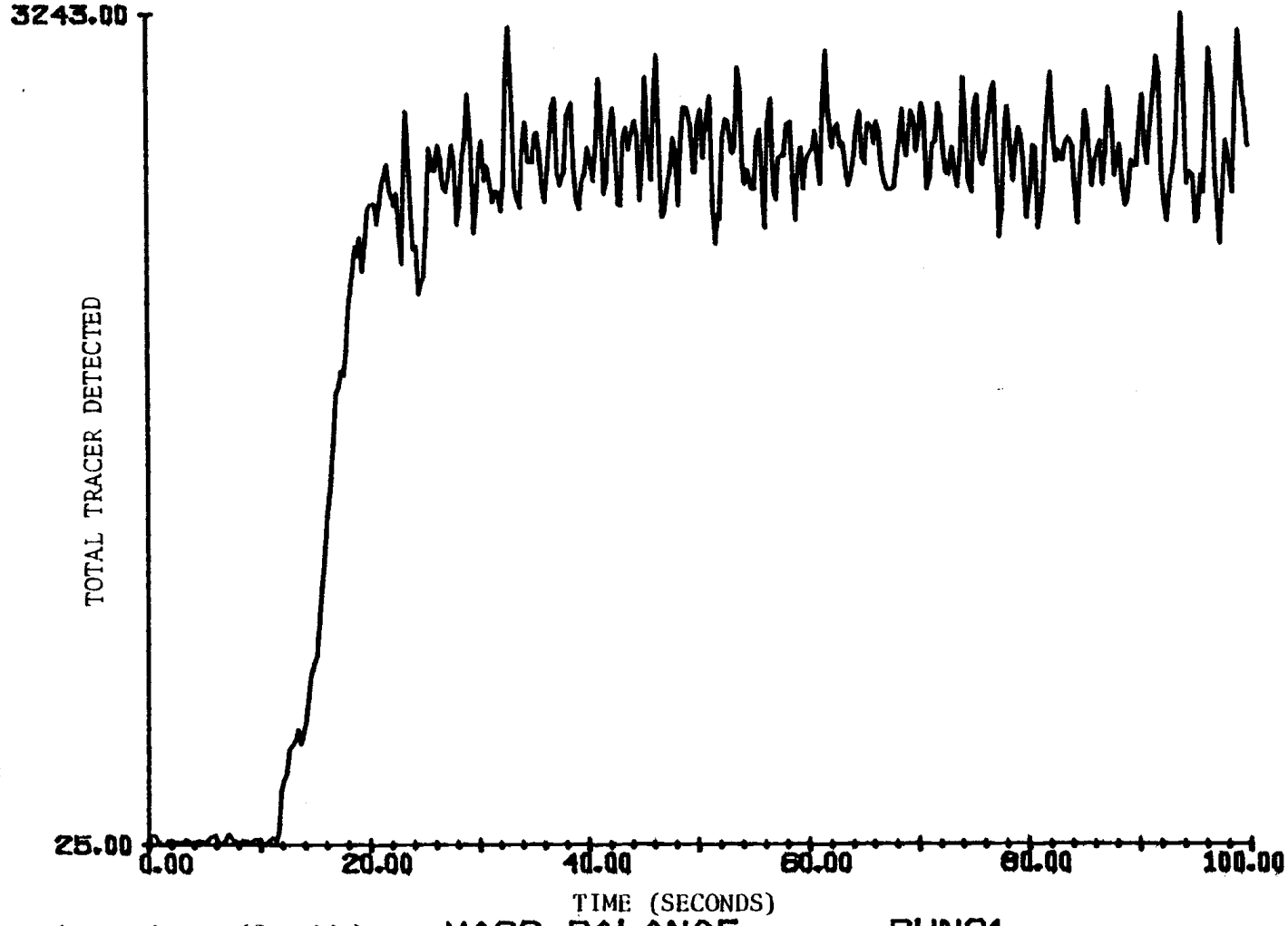

Figure 6.3. (Cont'd.)

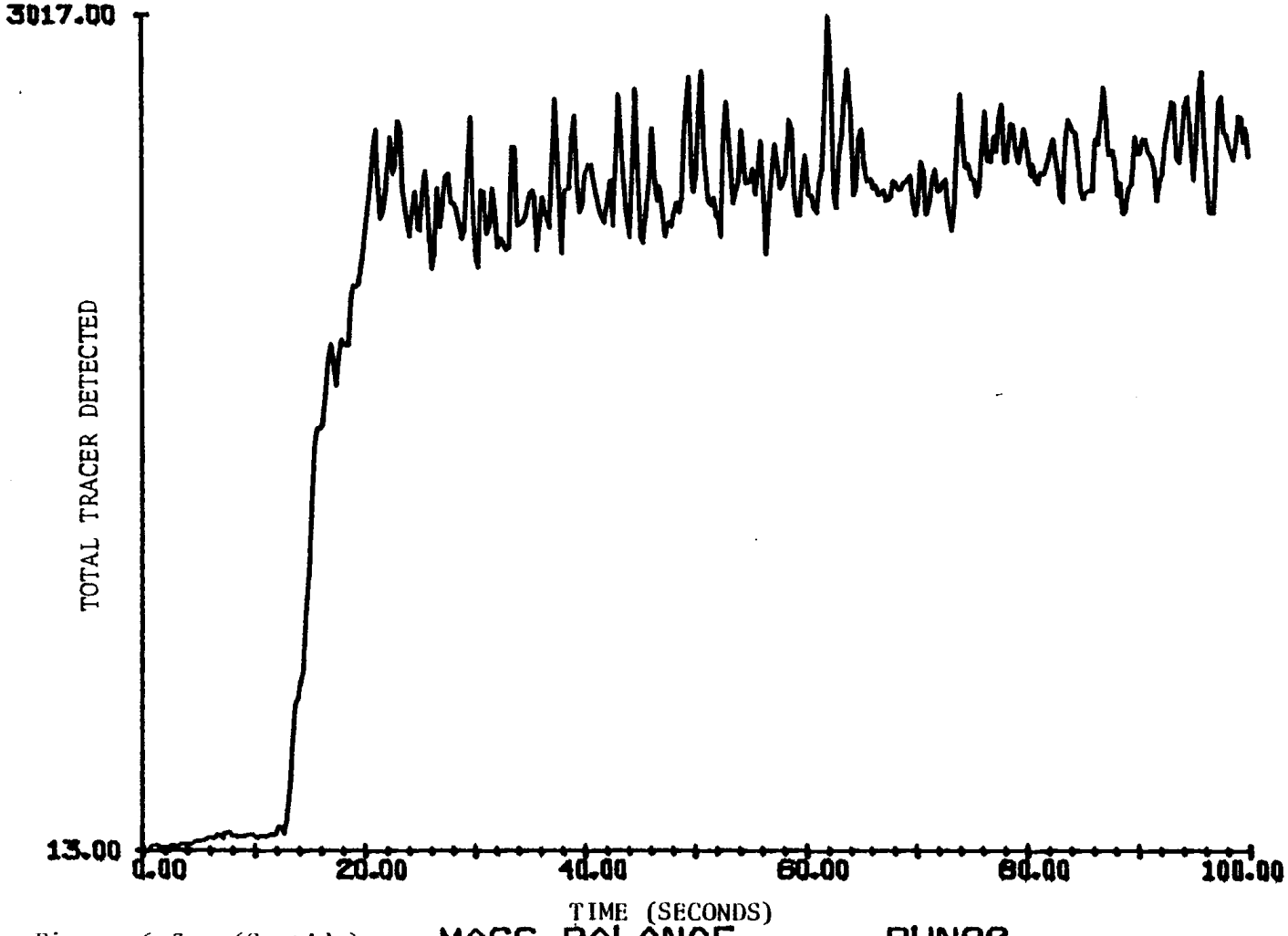

Figure 6.3. (Cont'd.)

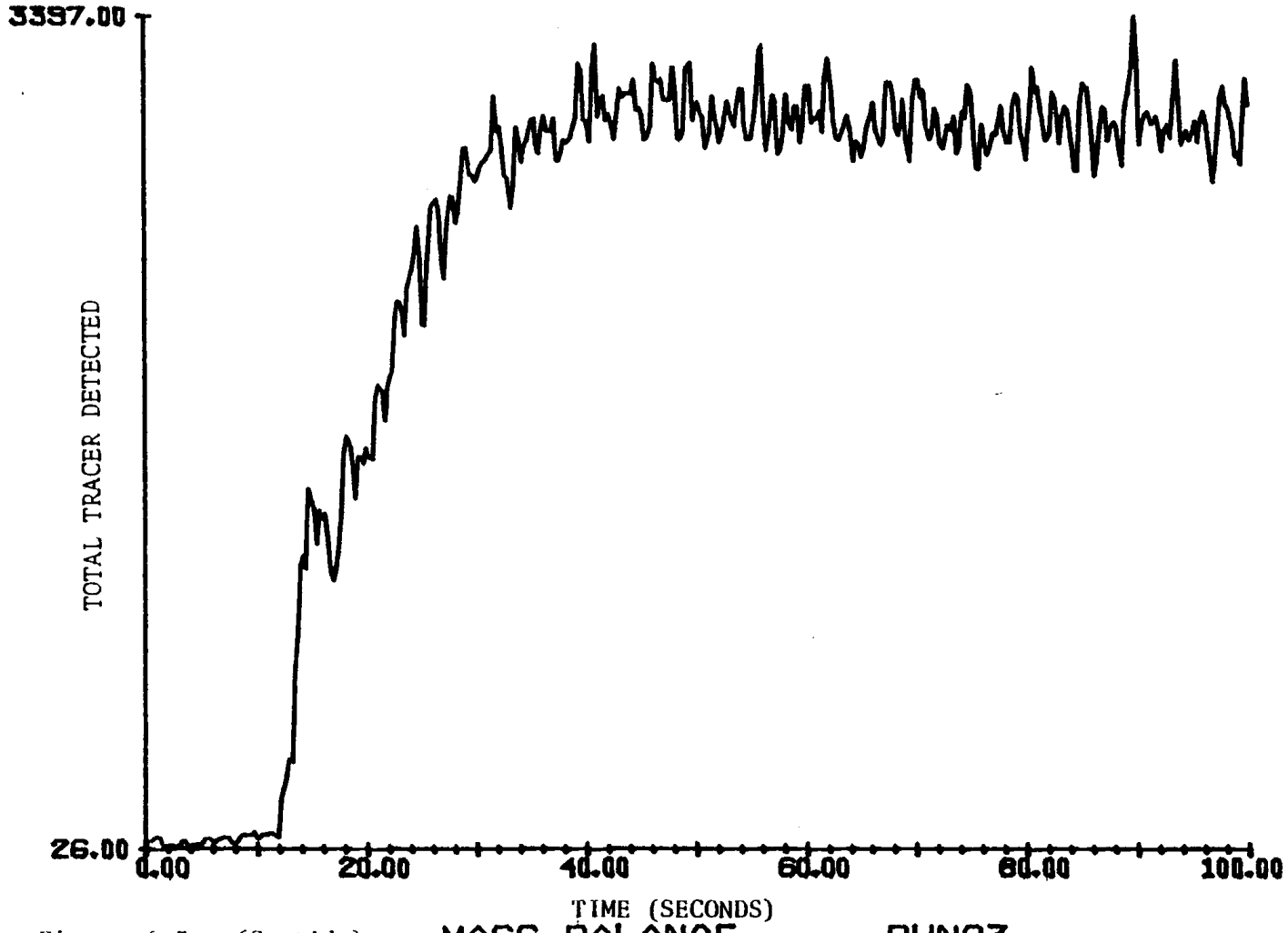

Figure 6.3. (Cont'd.)

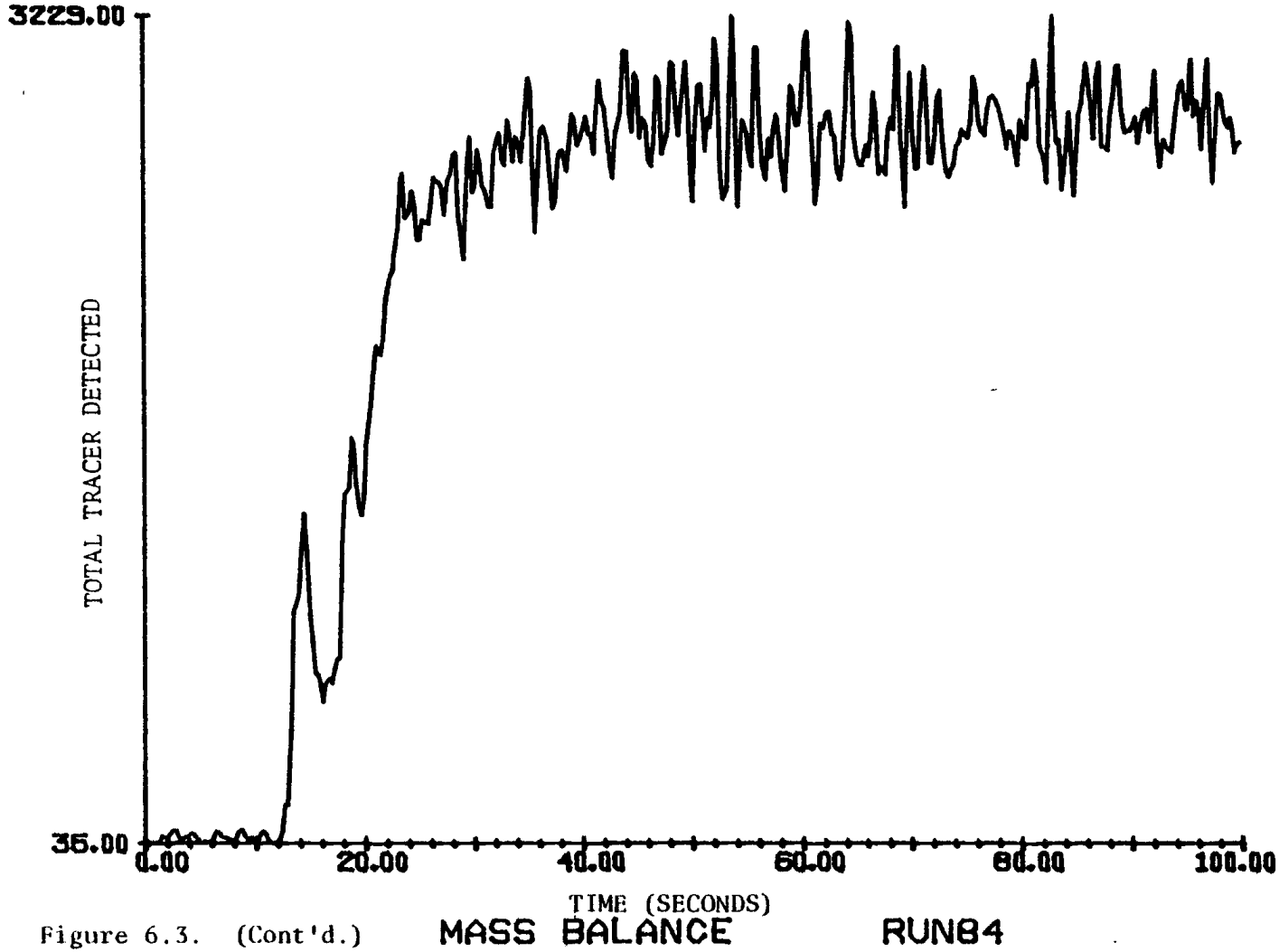

Figure 6.3. (Cont'd.)

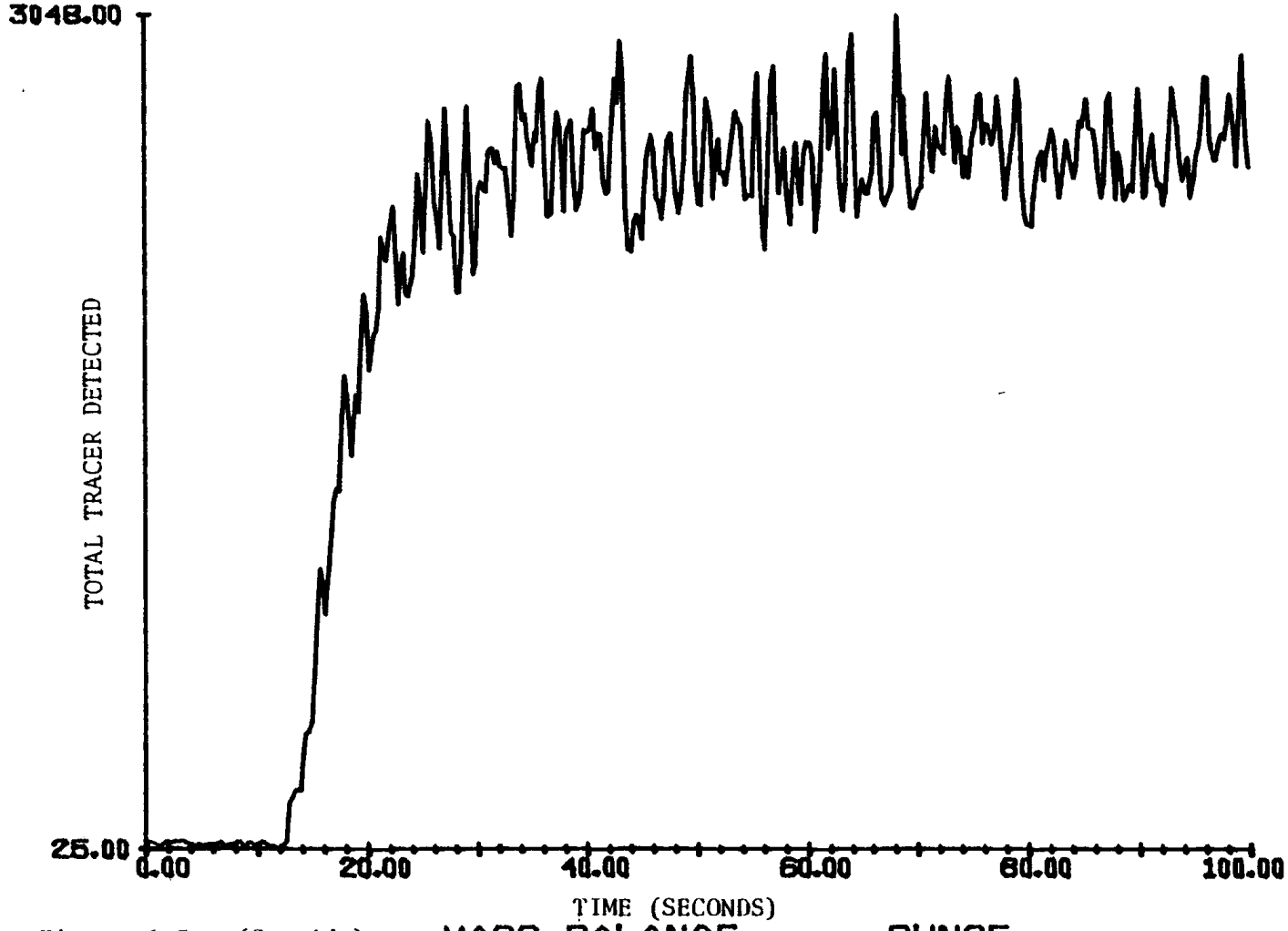

Figure 6.3. (Cont'd.)

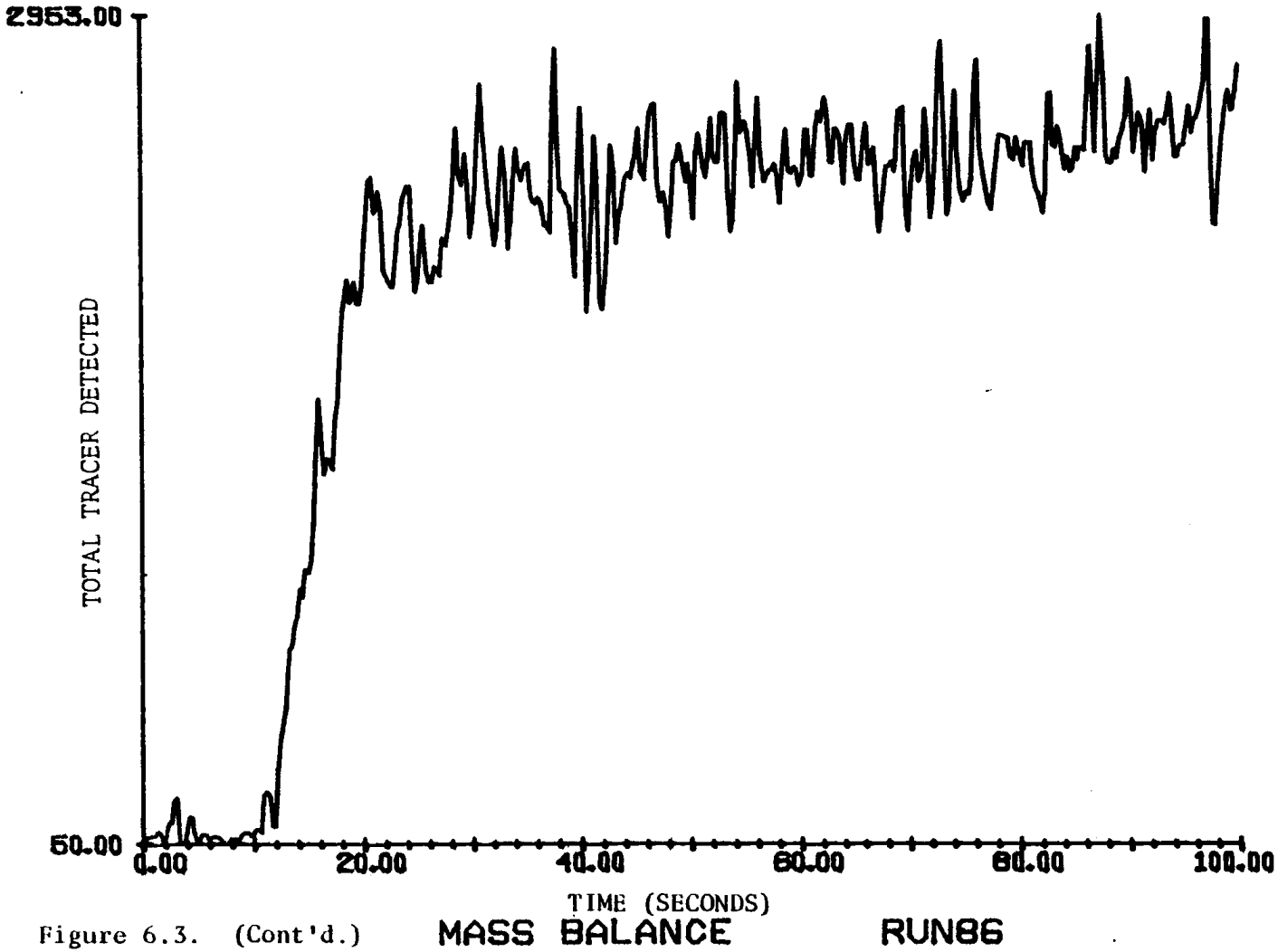

Figure 6.3. (Cont'd.)

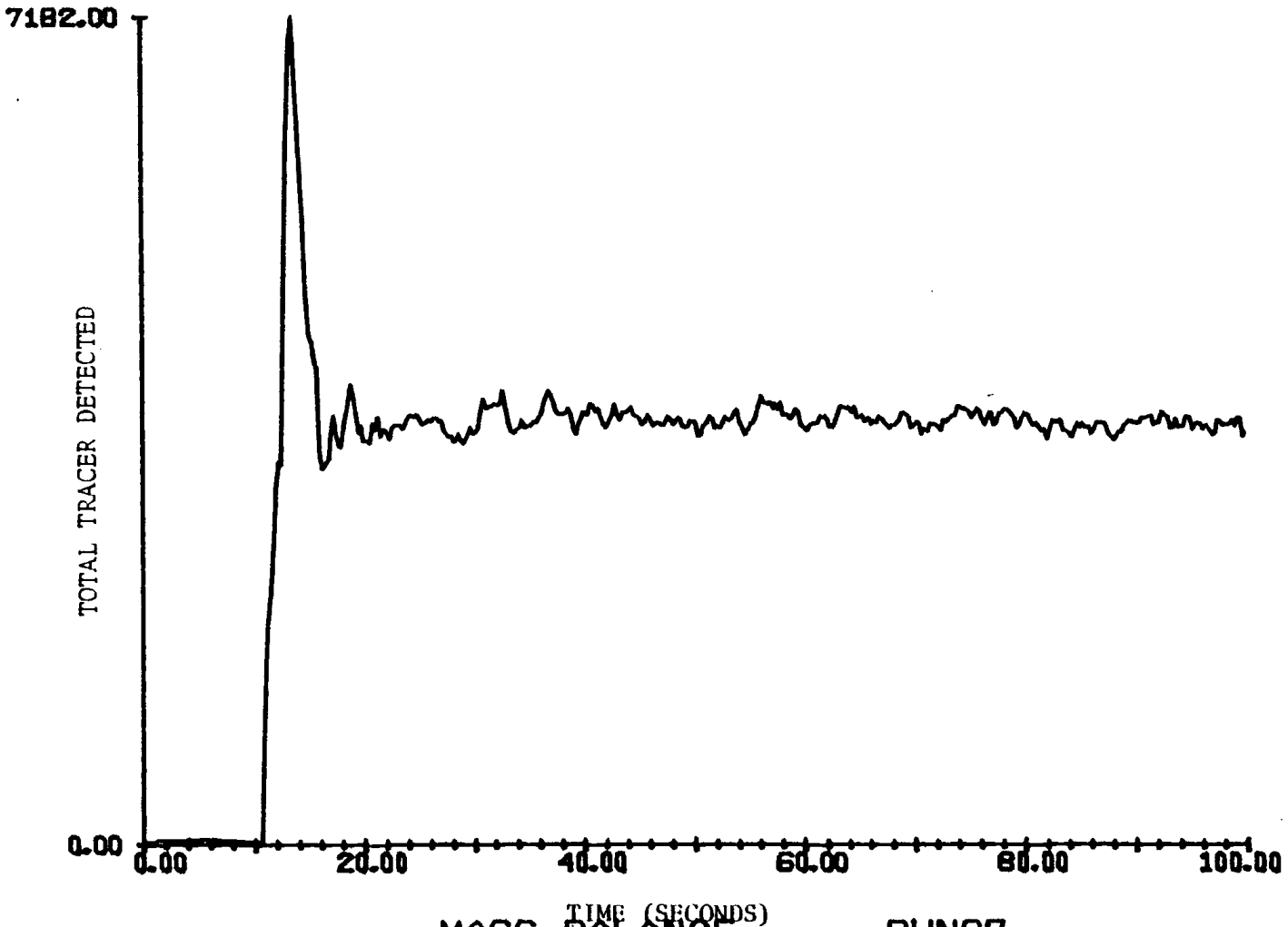

Figure 6.3. (Cont'd.)

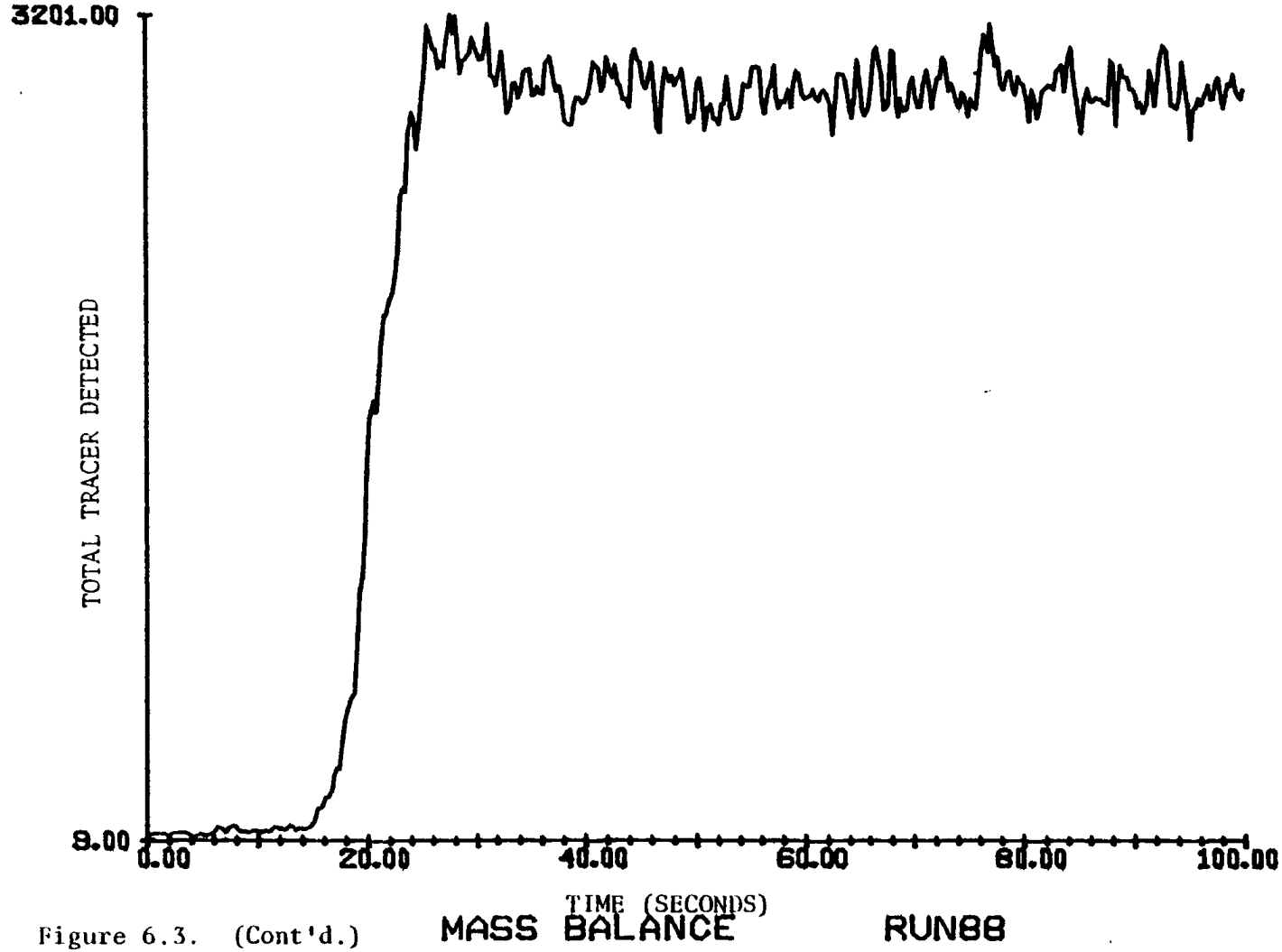

Figure 6.3. (Cont'd.)

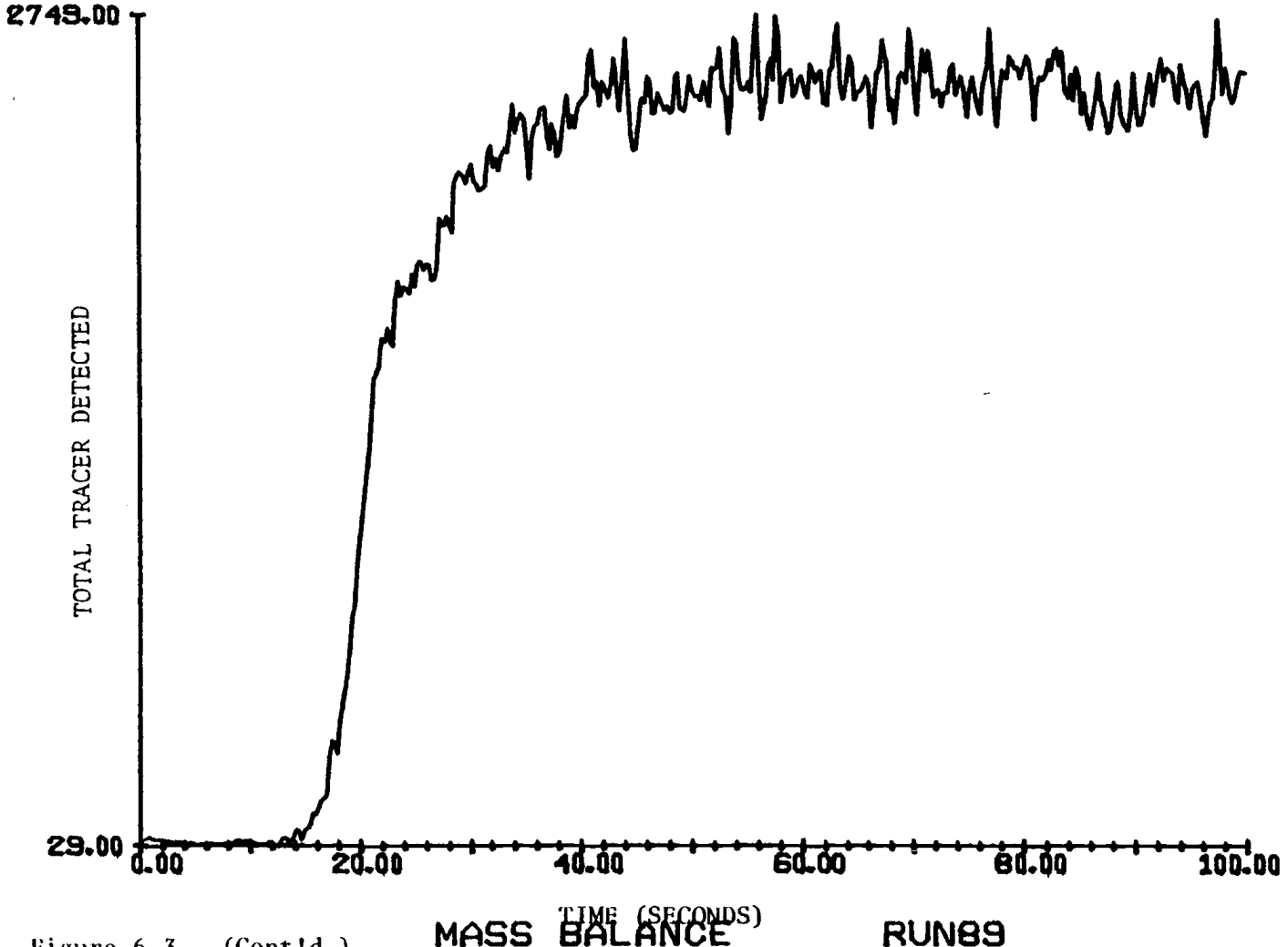

Figure 6.3. (Cont'd.)

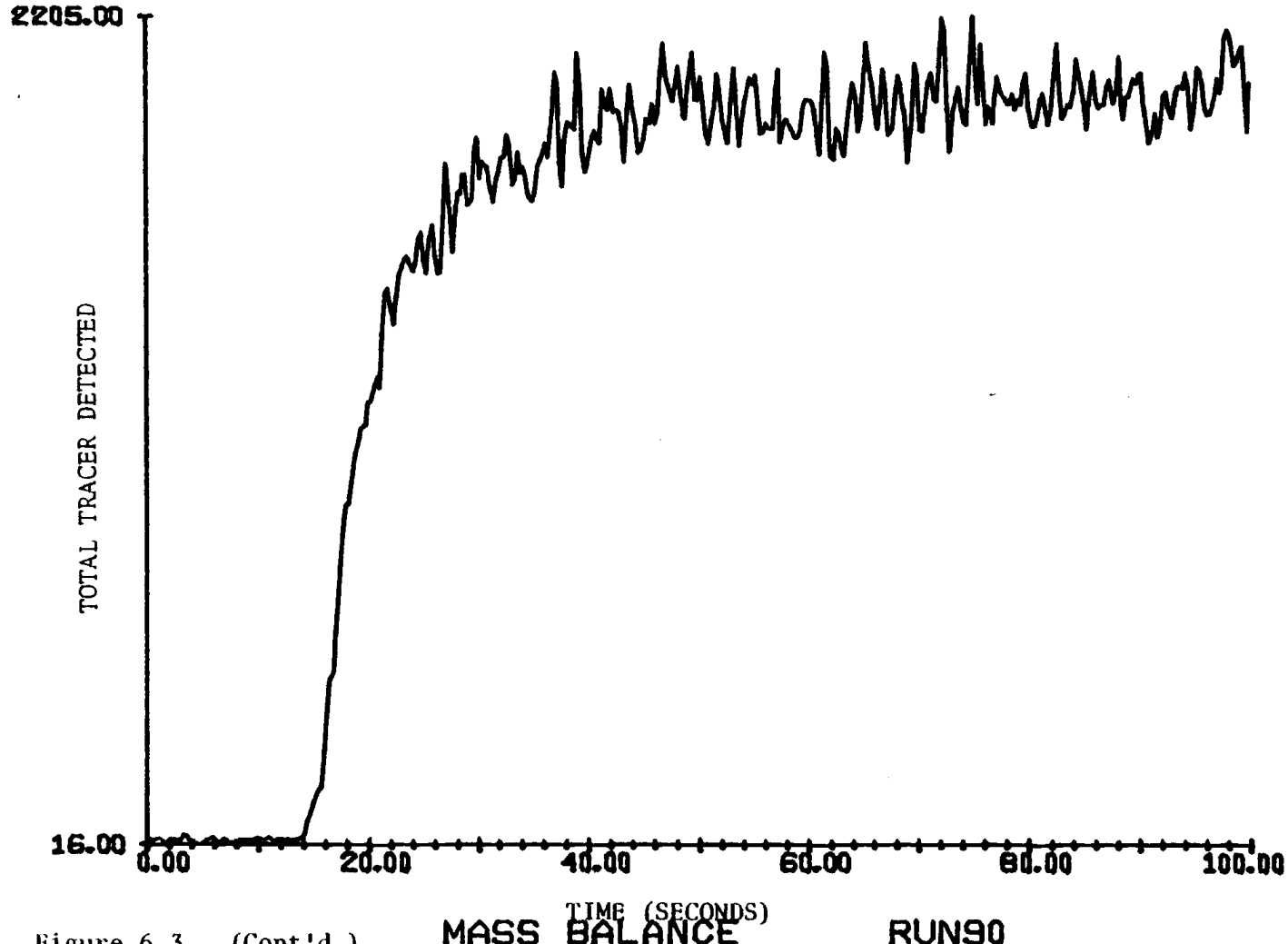

Figure 6.3. (Cont'd.)

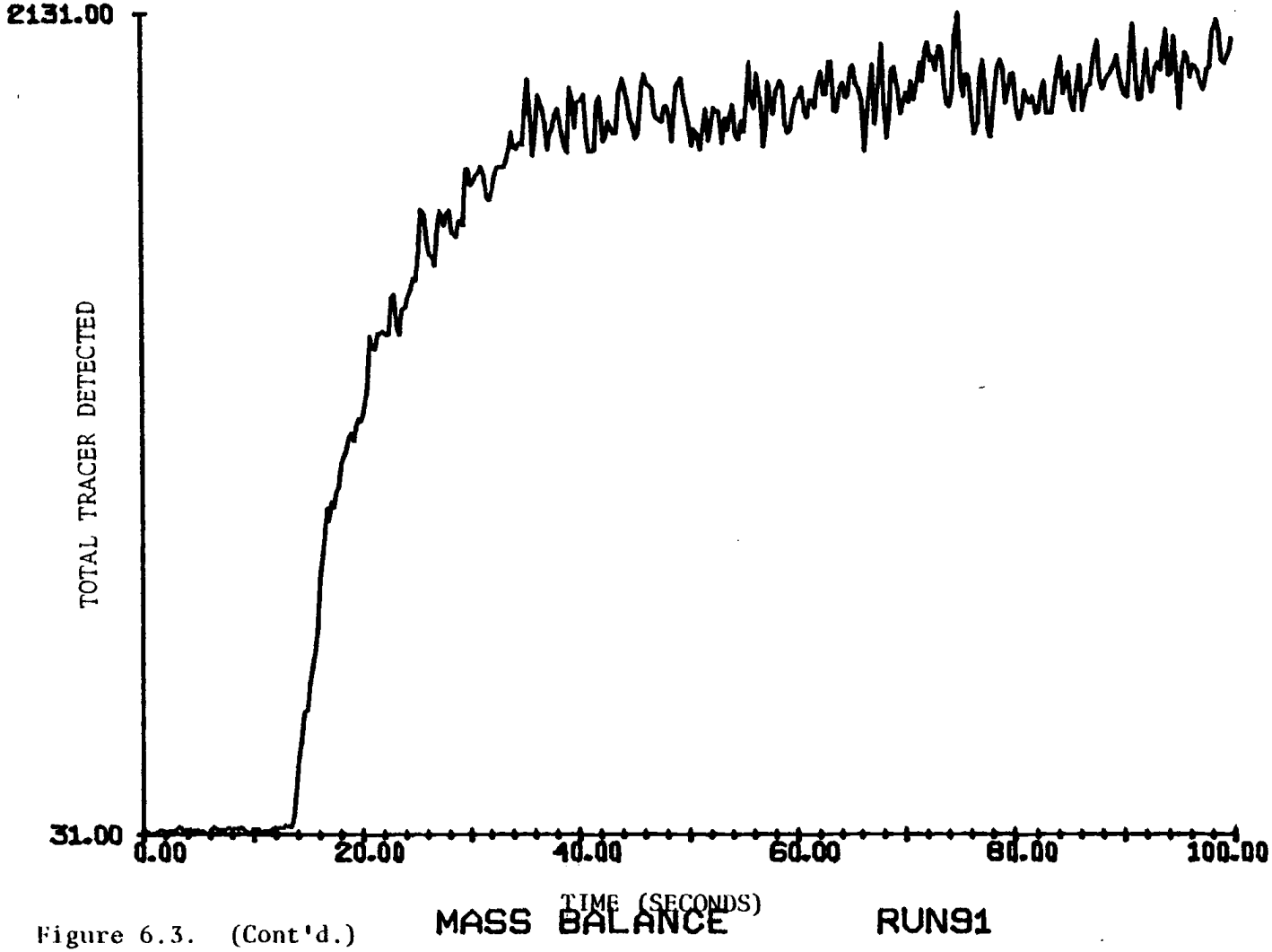

Figure 6.3. (Cont'd.)

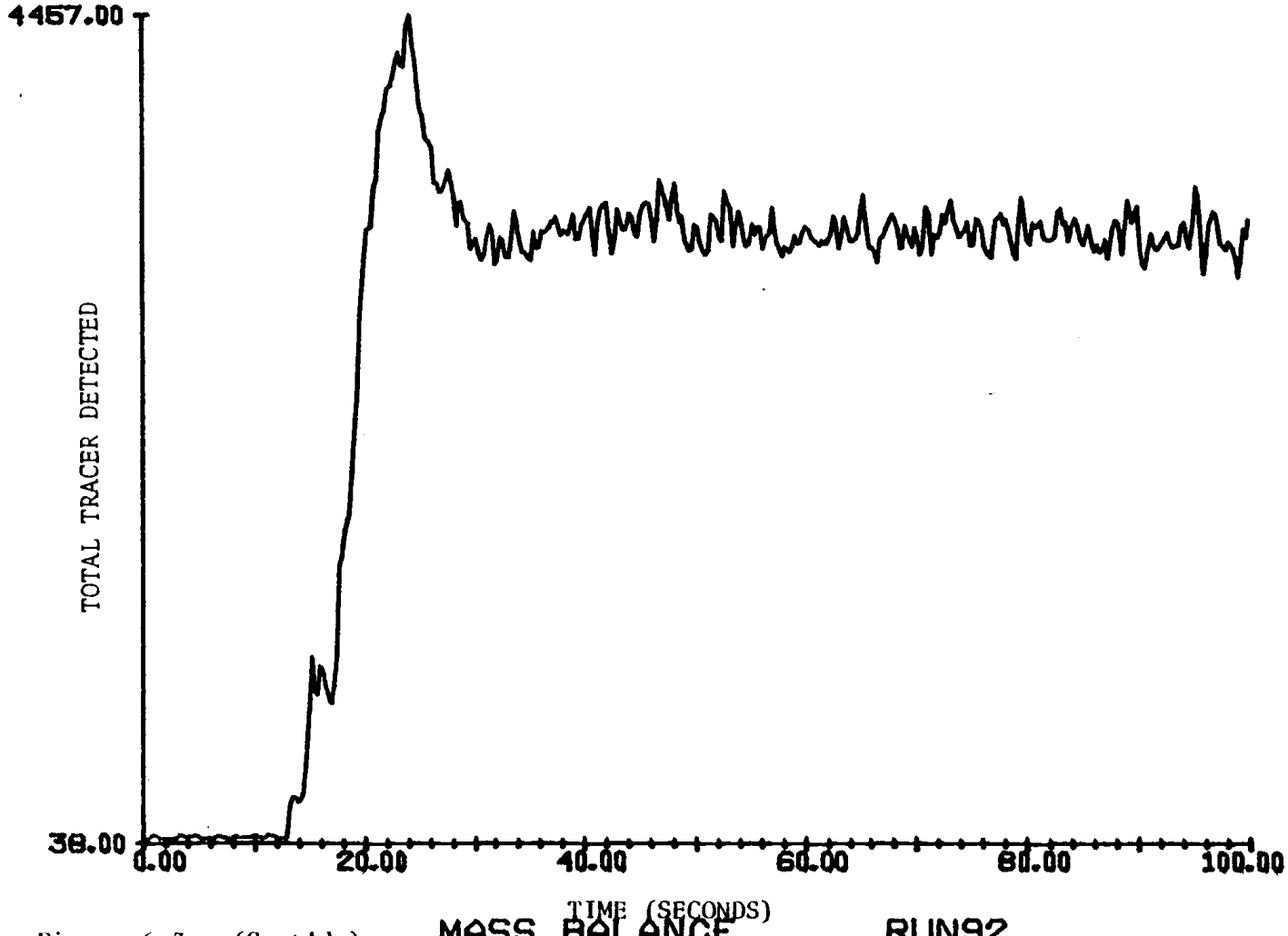

Figure 6.3. (Cont'd.)

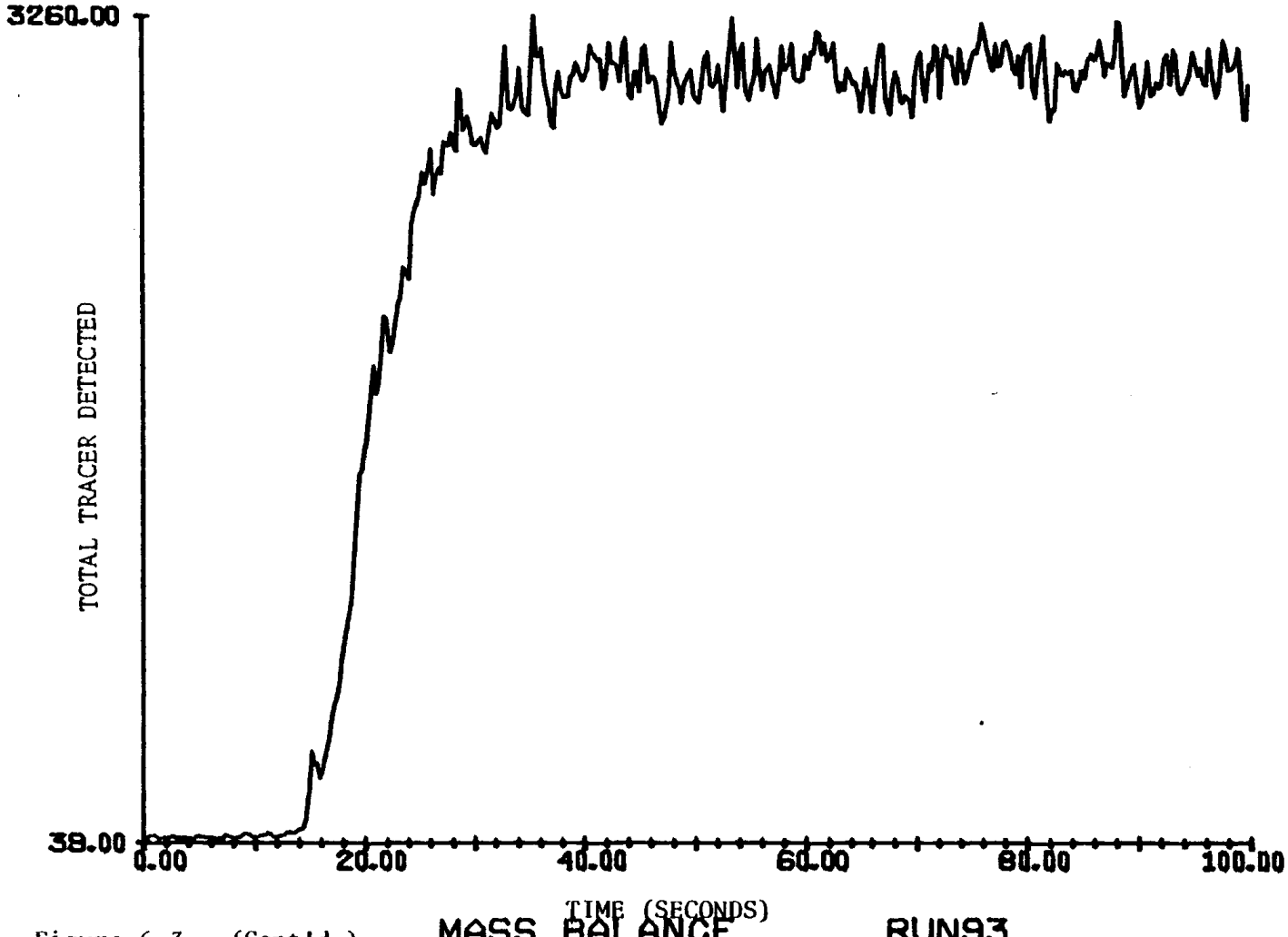

Figure 6.3. (Cont'd.)

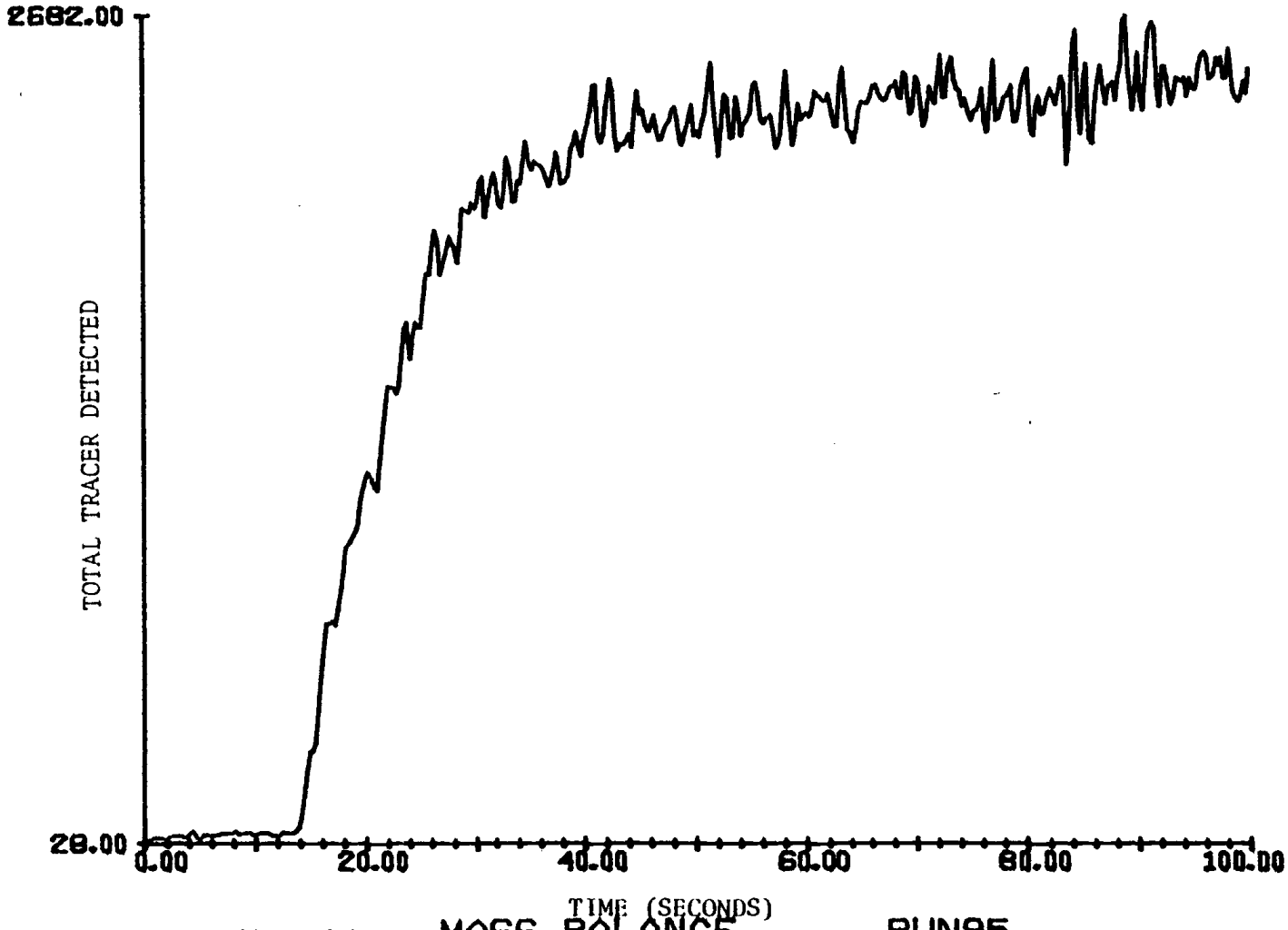

Figure 6.3. (Cont'd.)

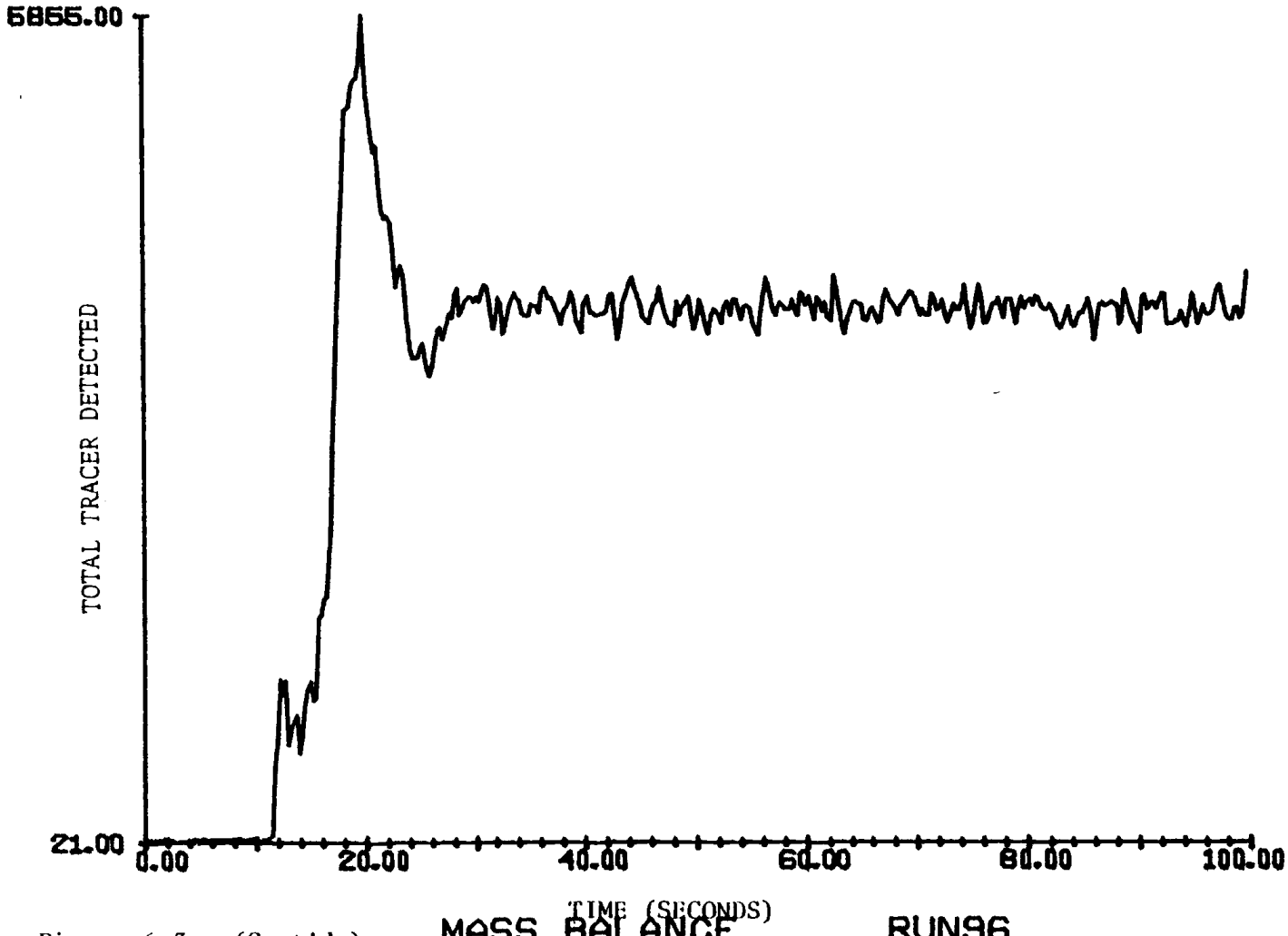

Figure 6.3. (Cont'd.)

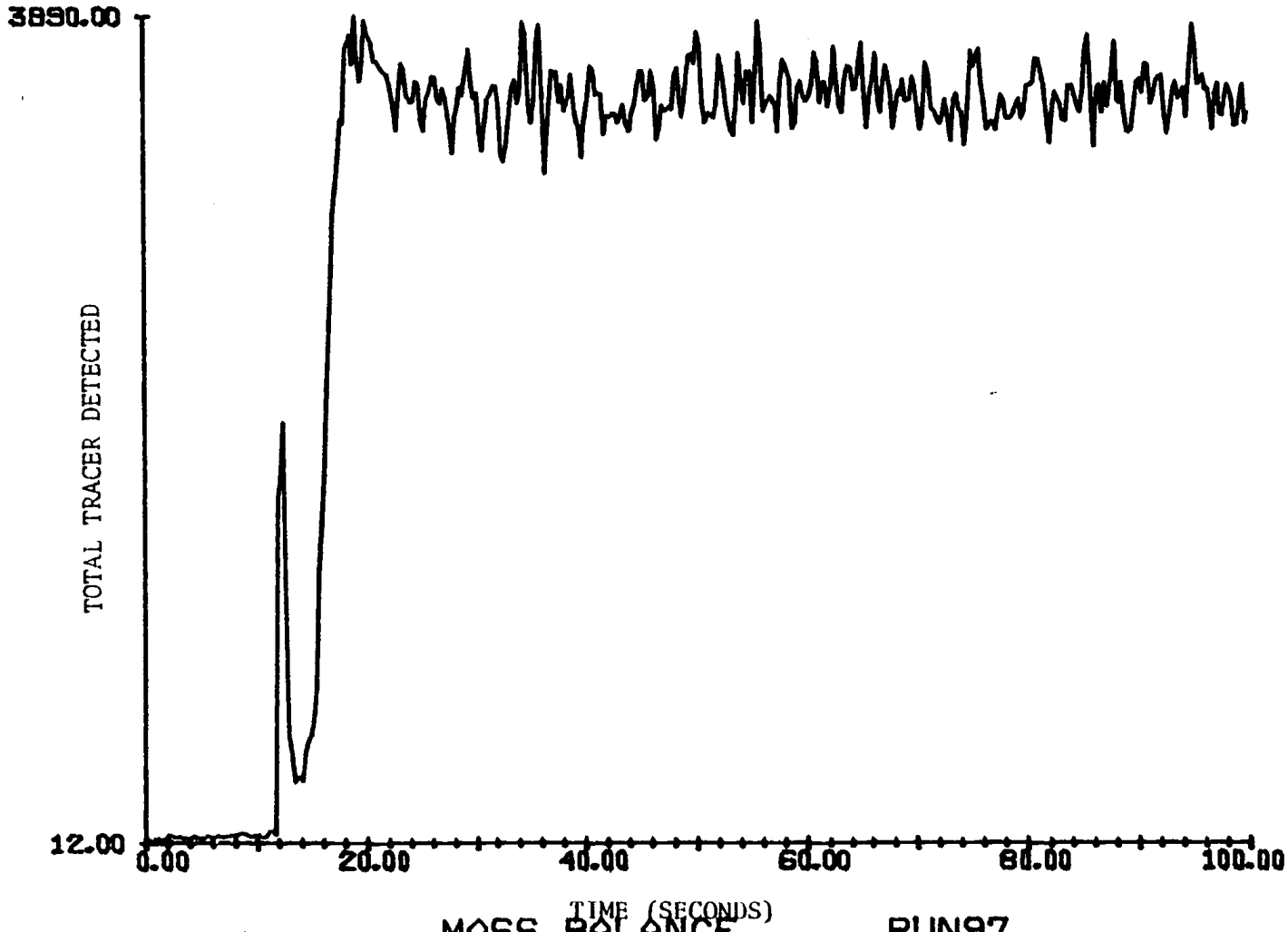

Figure 6.3. (Cont'd.)

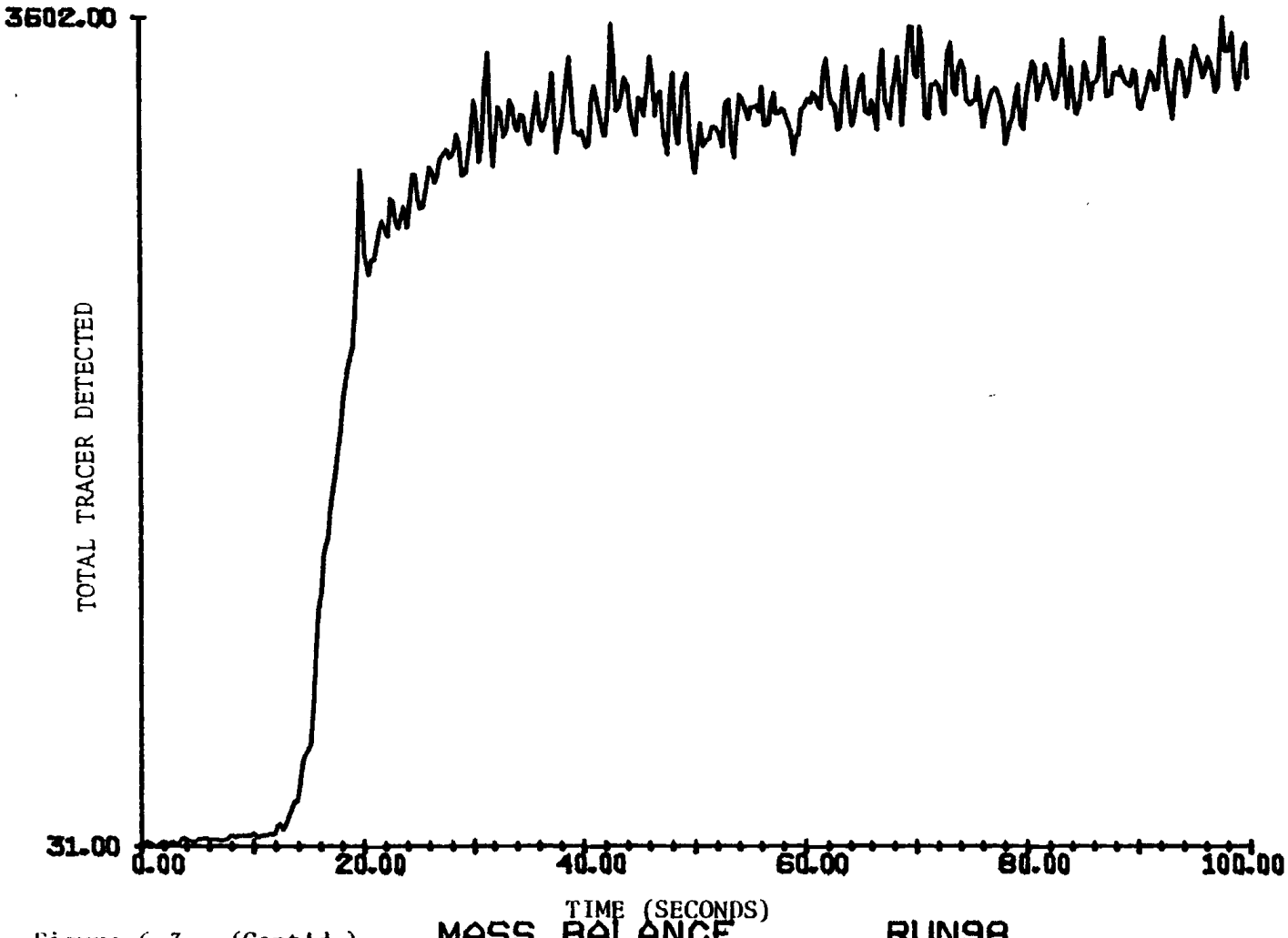

Figure 6.3. (Cont'd.)

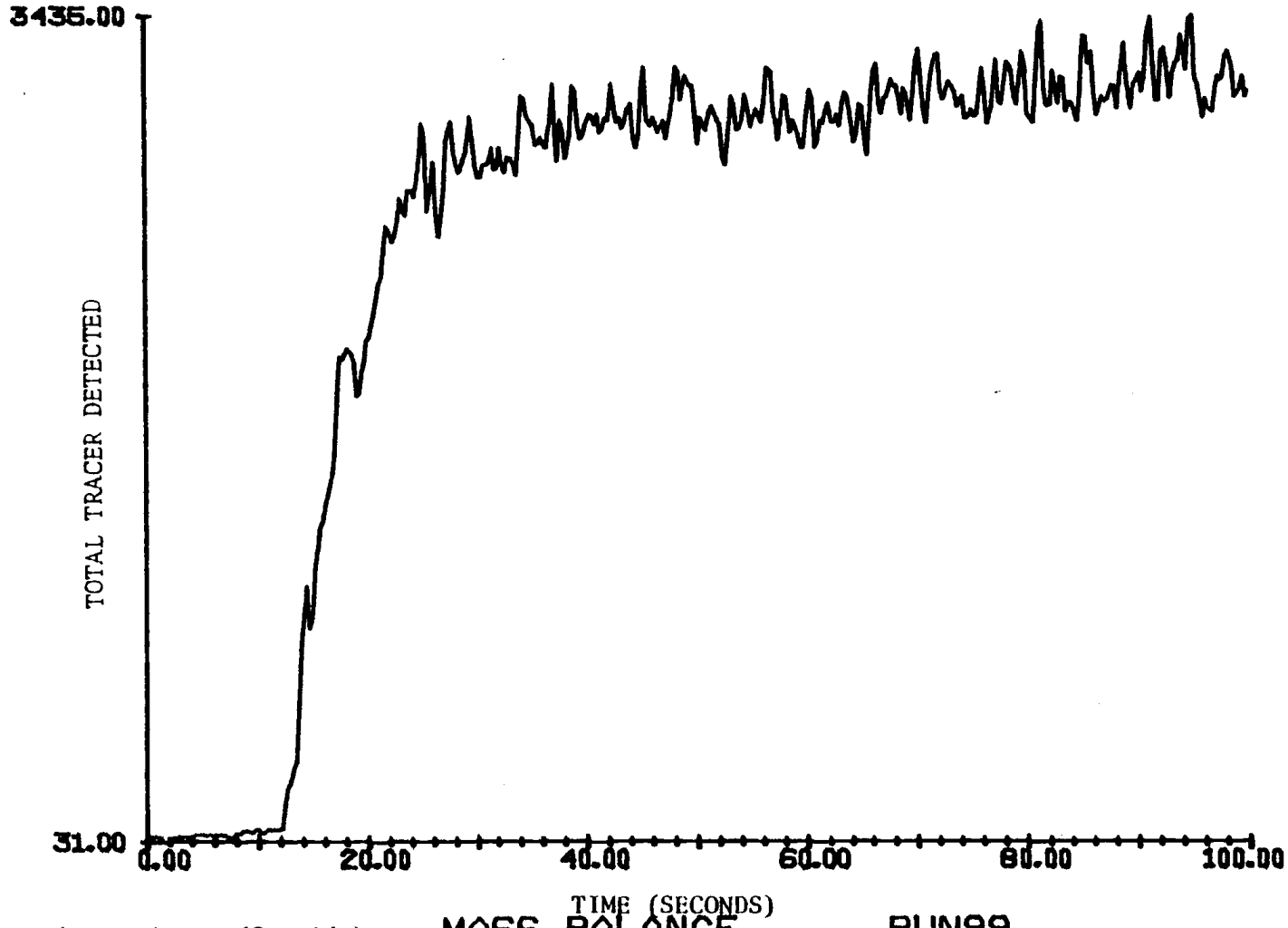

Figure 6.3. (Cont'd.)

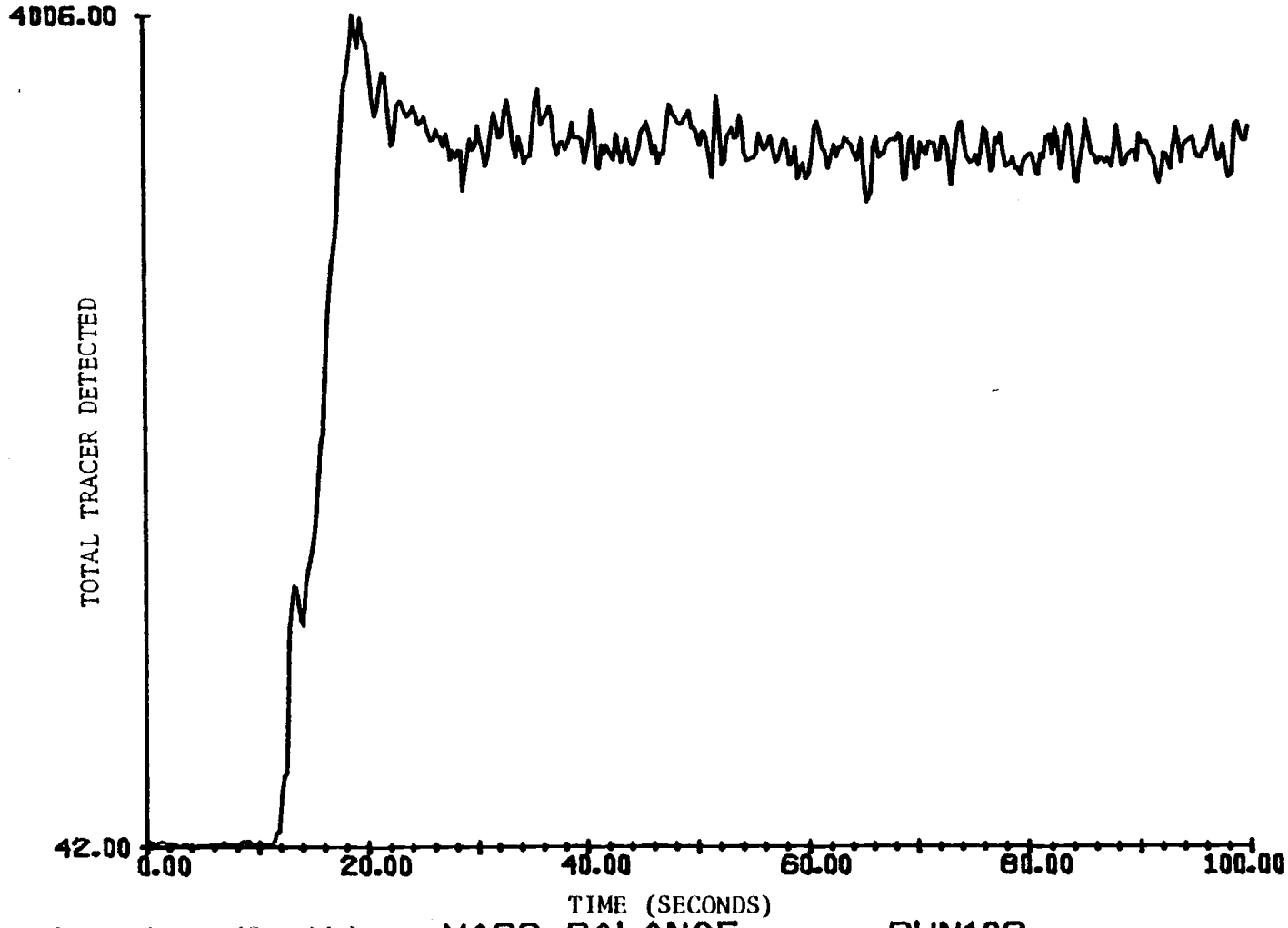

Figure 6.3. (Cont'd.)

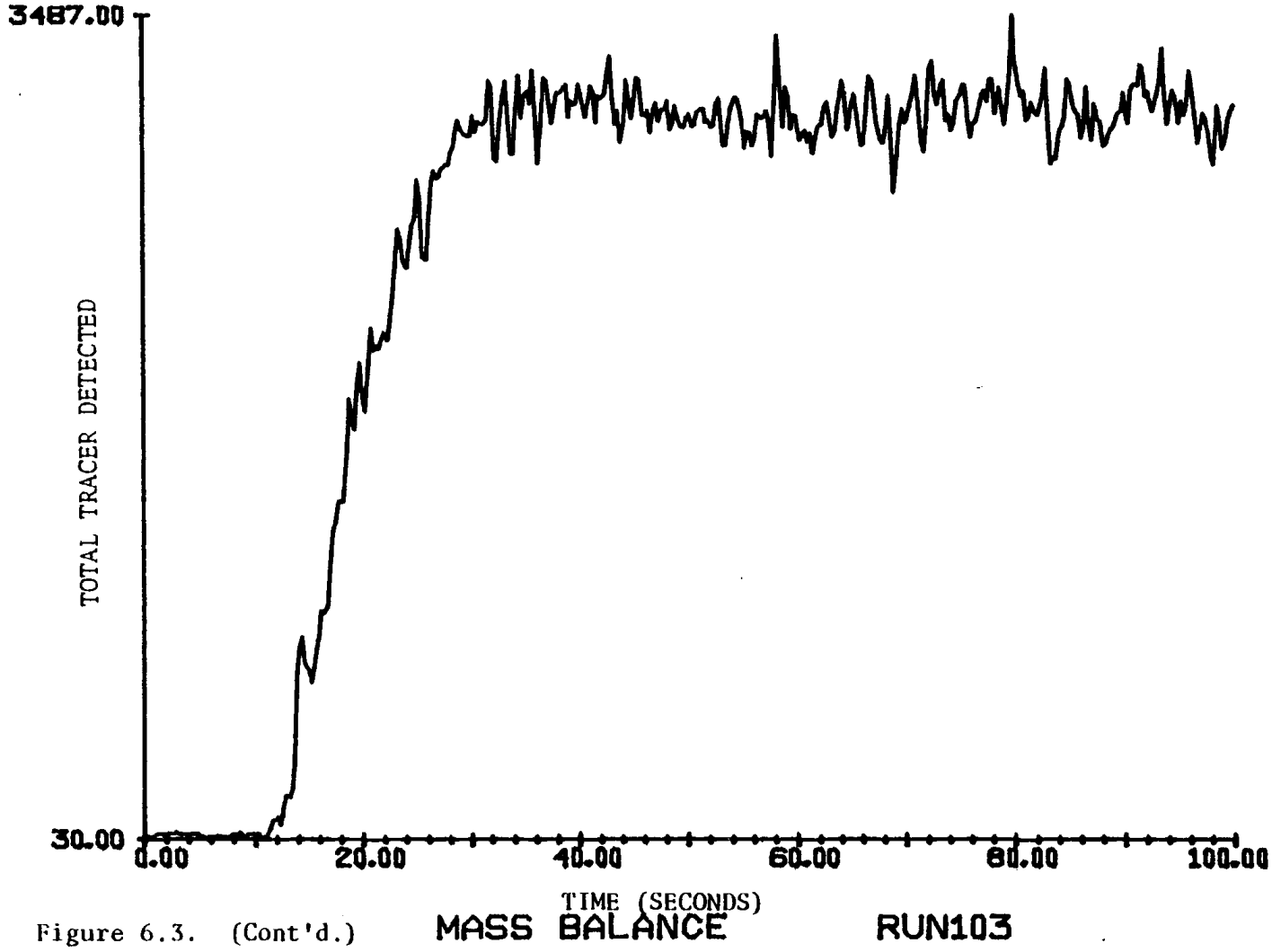

Figure 6.3. (Cont'd.)

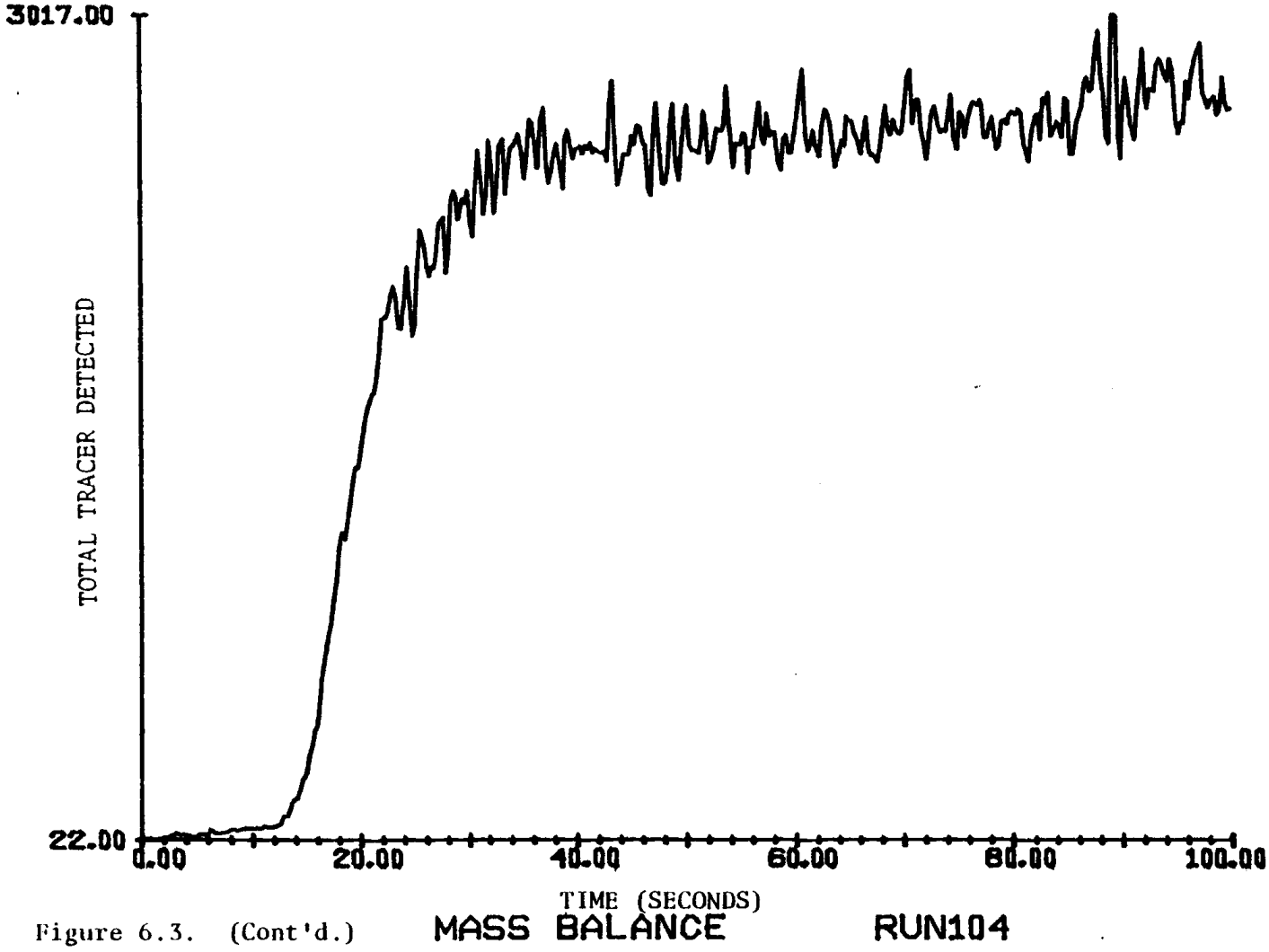

Figure 6.3. (Cont'd.)

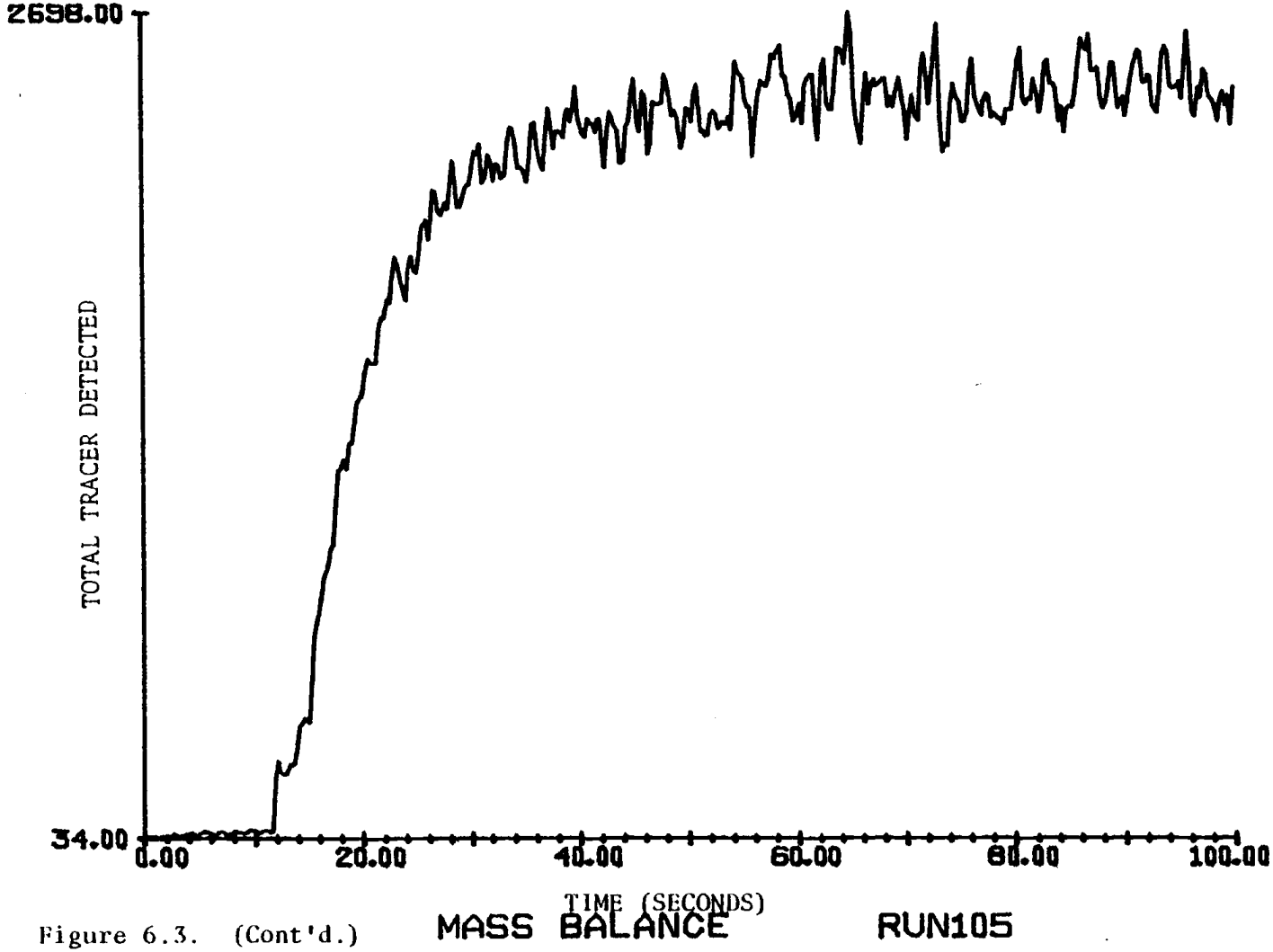

Figure 6.3. (Cont'd.)

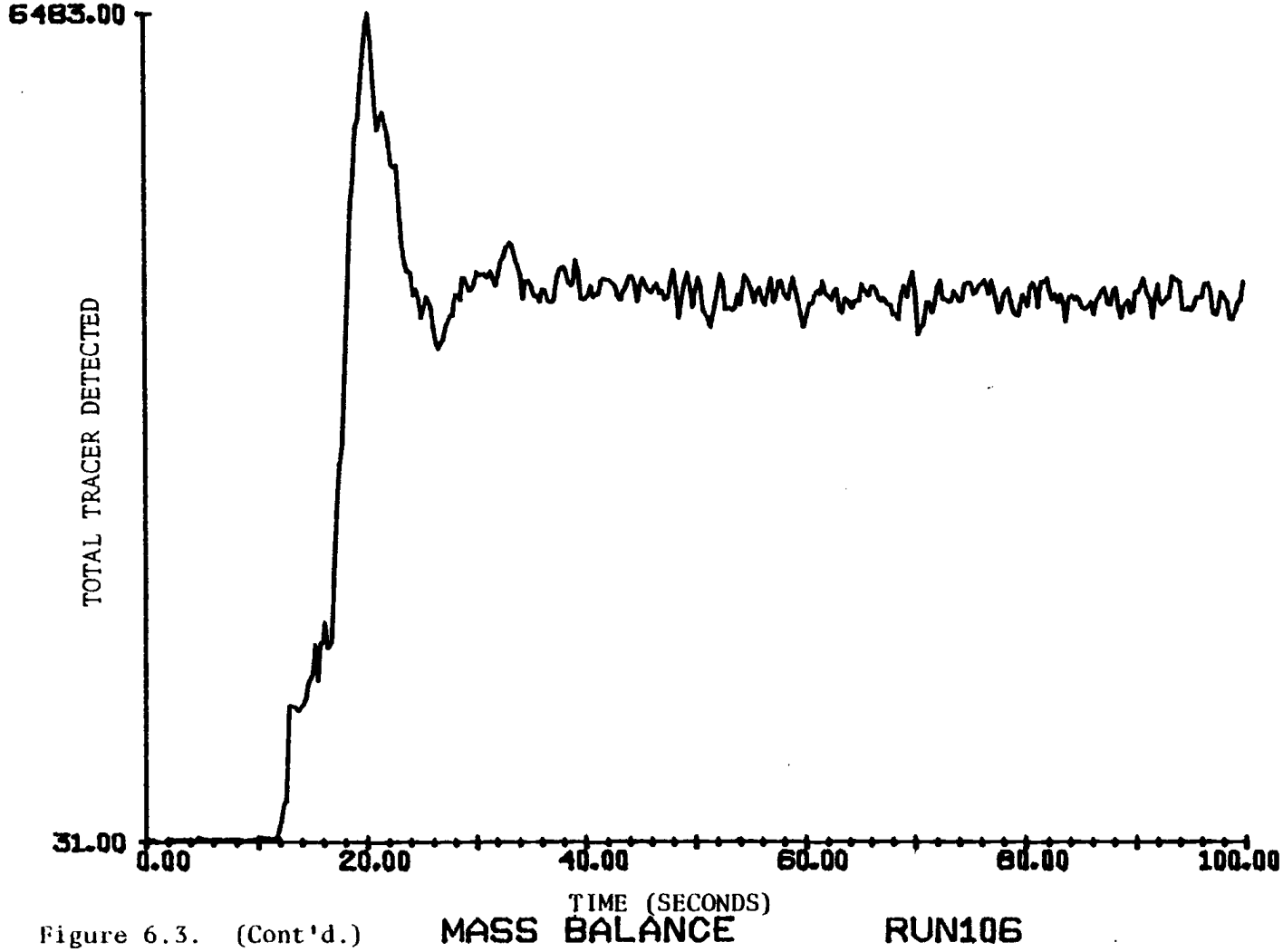

Figure 6.3. (Cont'd.)

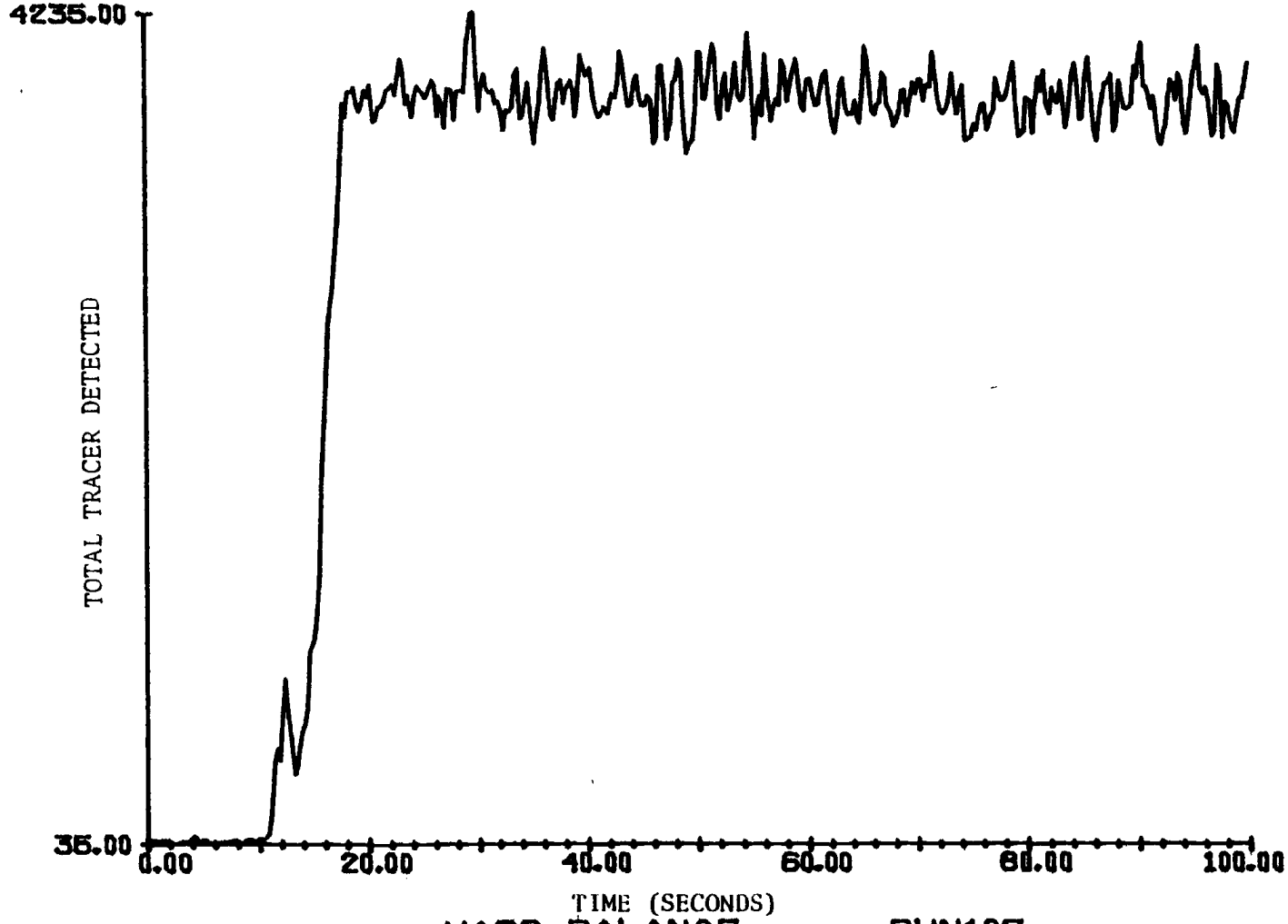

Figure 6.3. (Cont'd.)

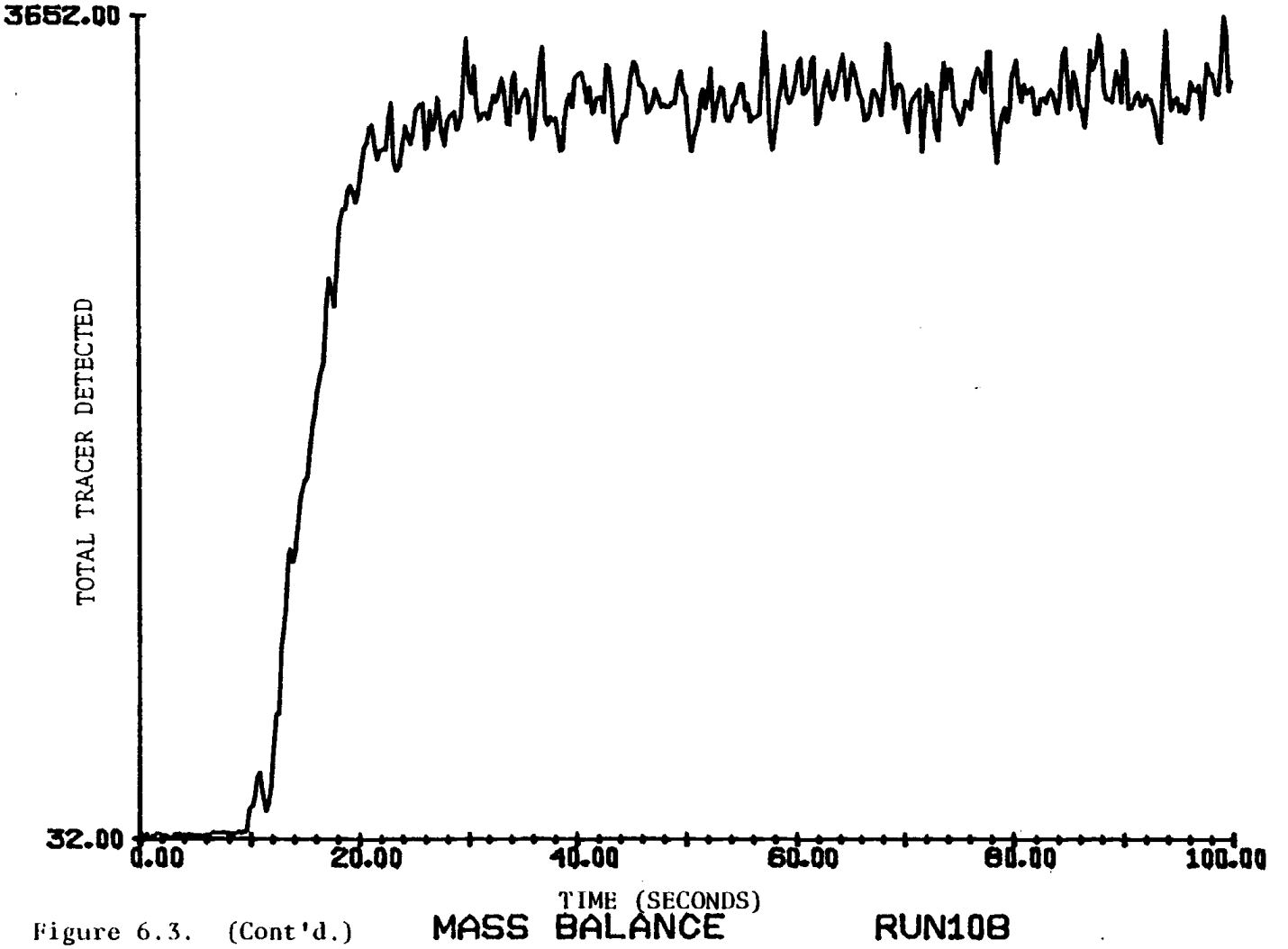

Figure 6.3. (Cont'd.)

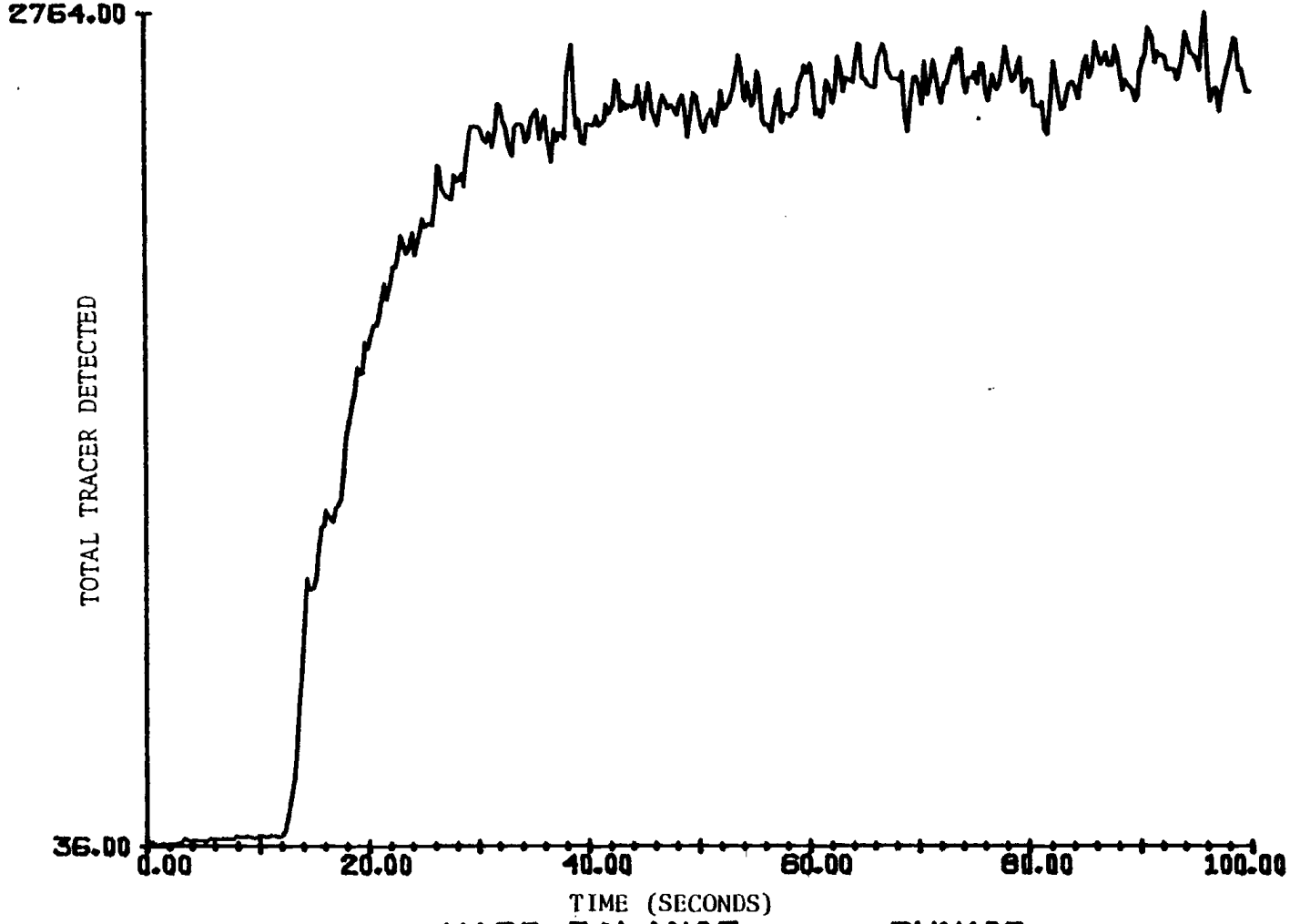

Figure 6.3. (Cont'd.)

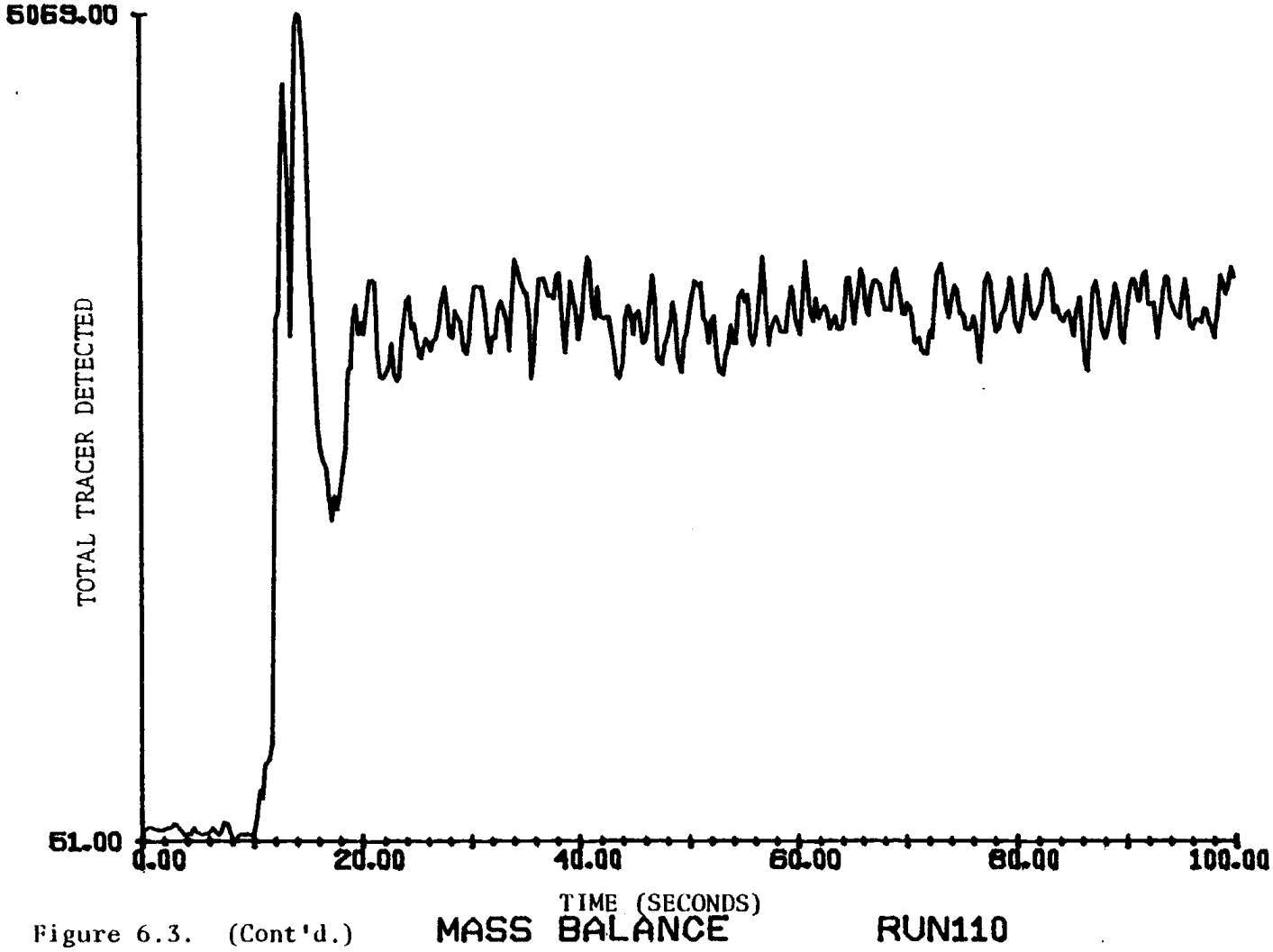

Figure 6.3. (Cont'd.)

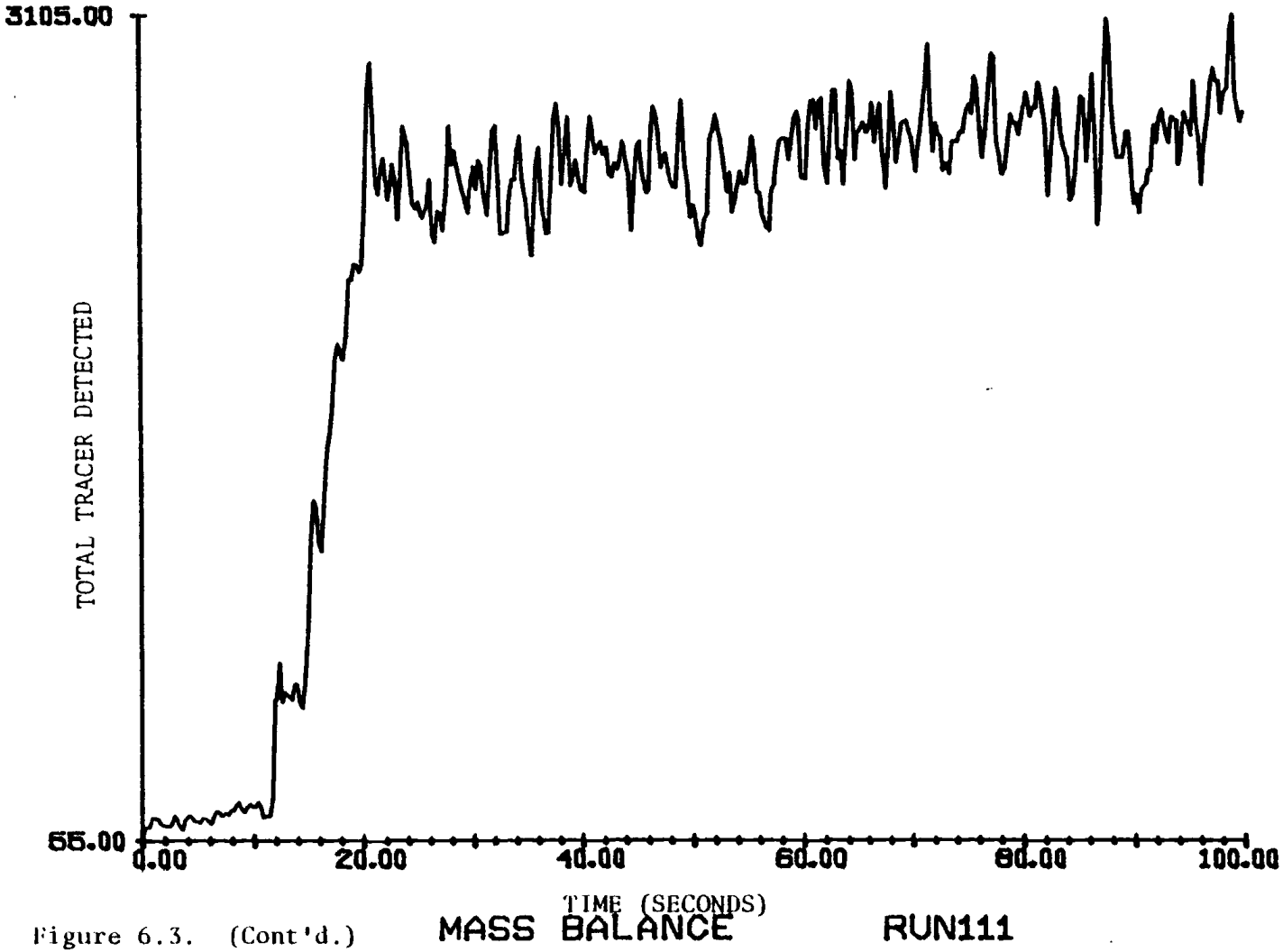

Figure 6.3. (Cont'd.)

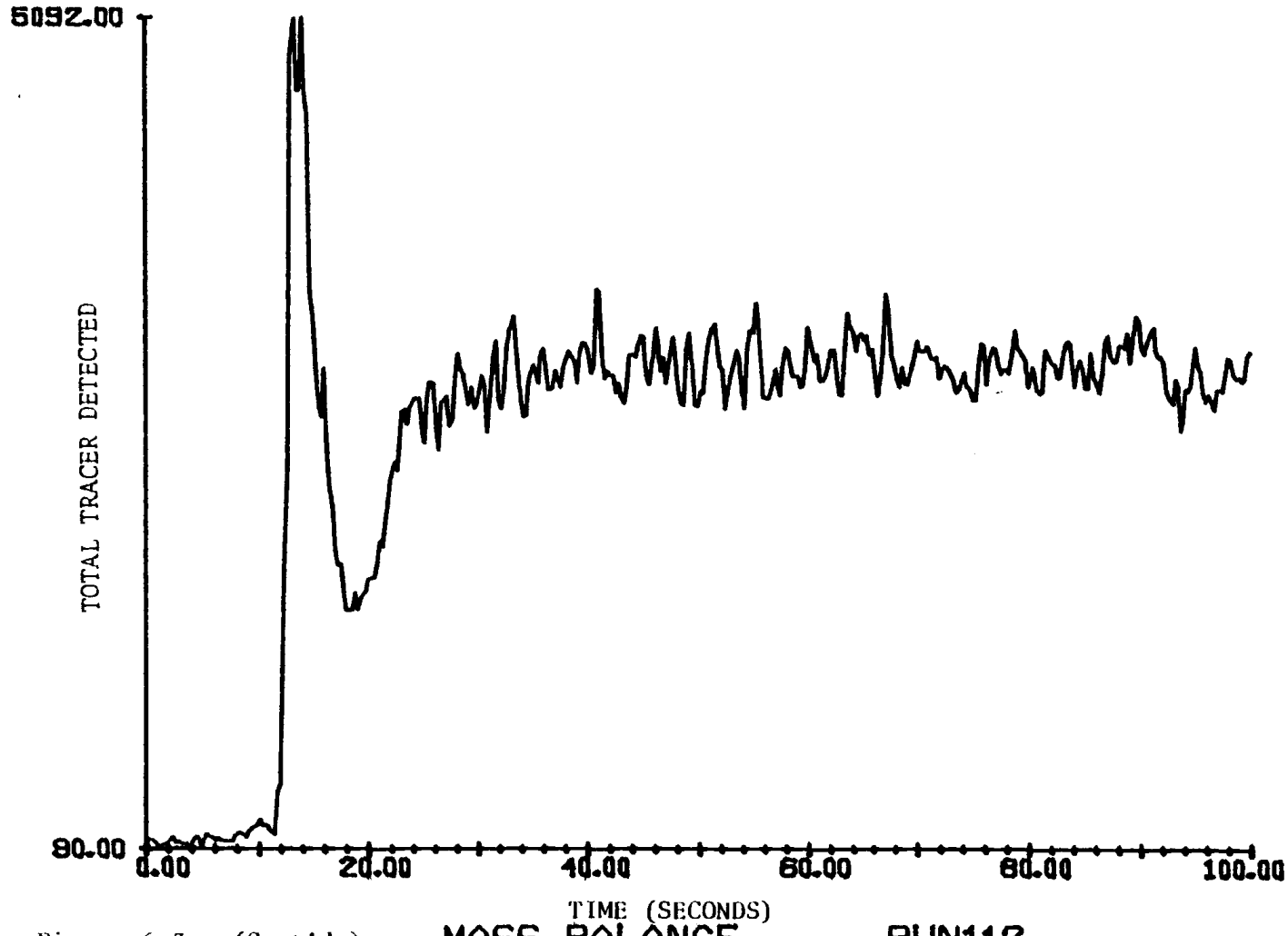

Figure 6.3. (Cont'd.)

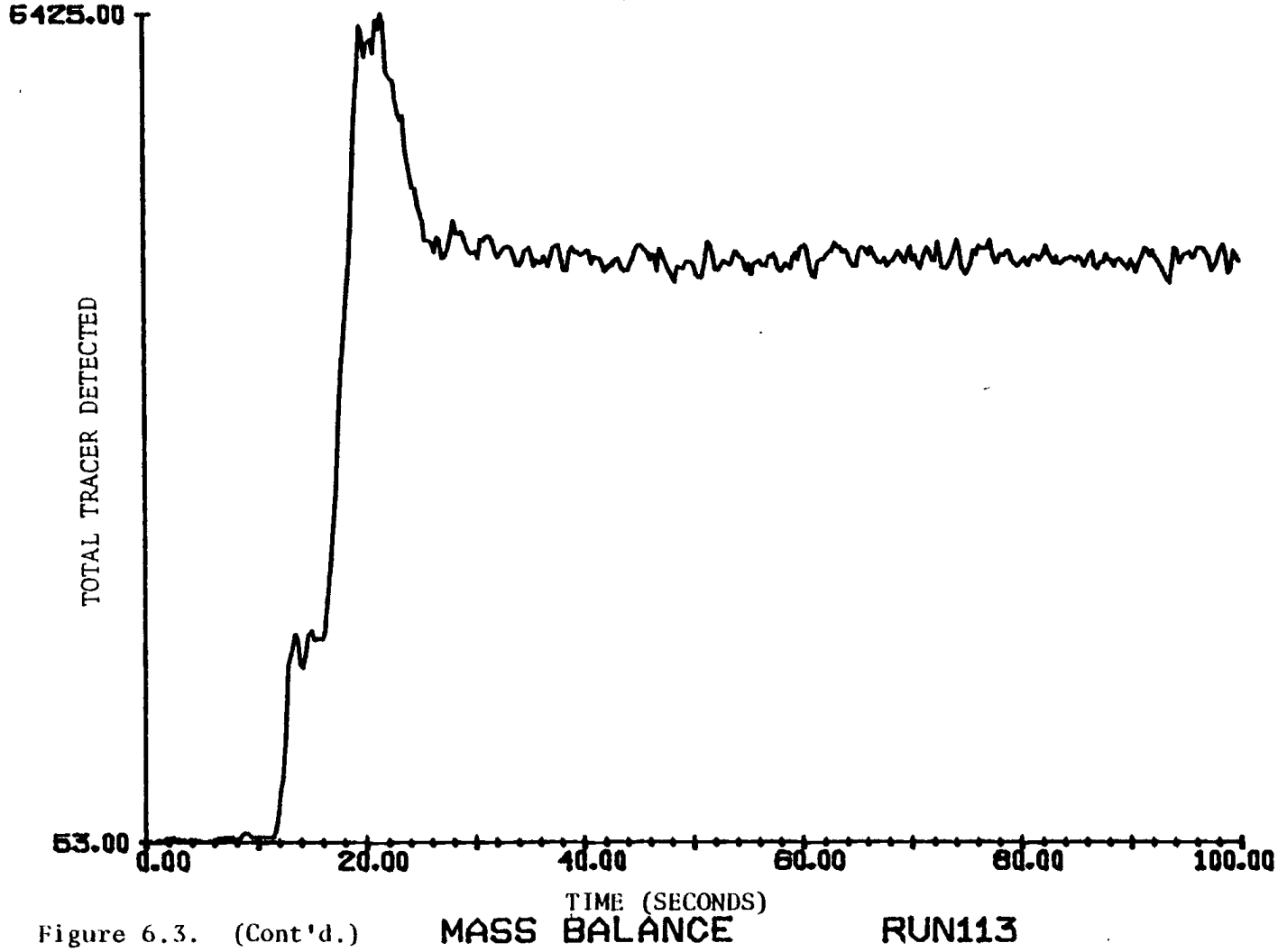

Figure 6.3. (Cont'd.)

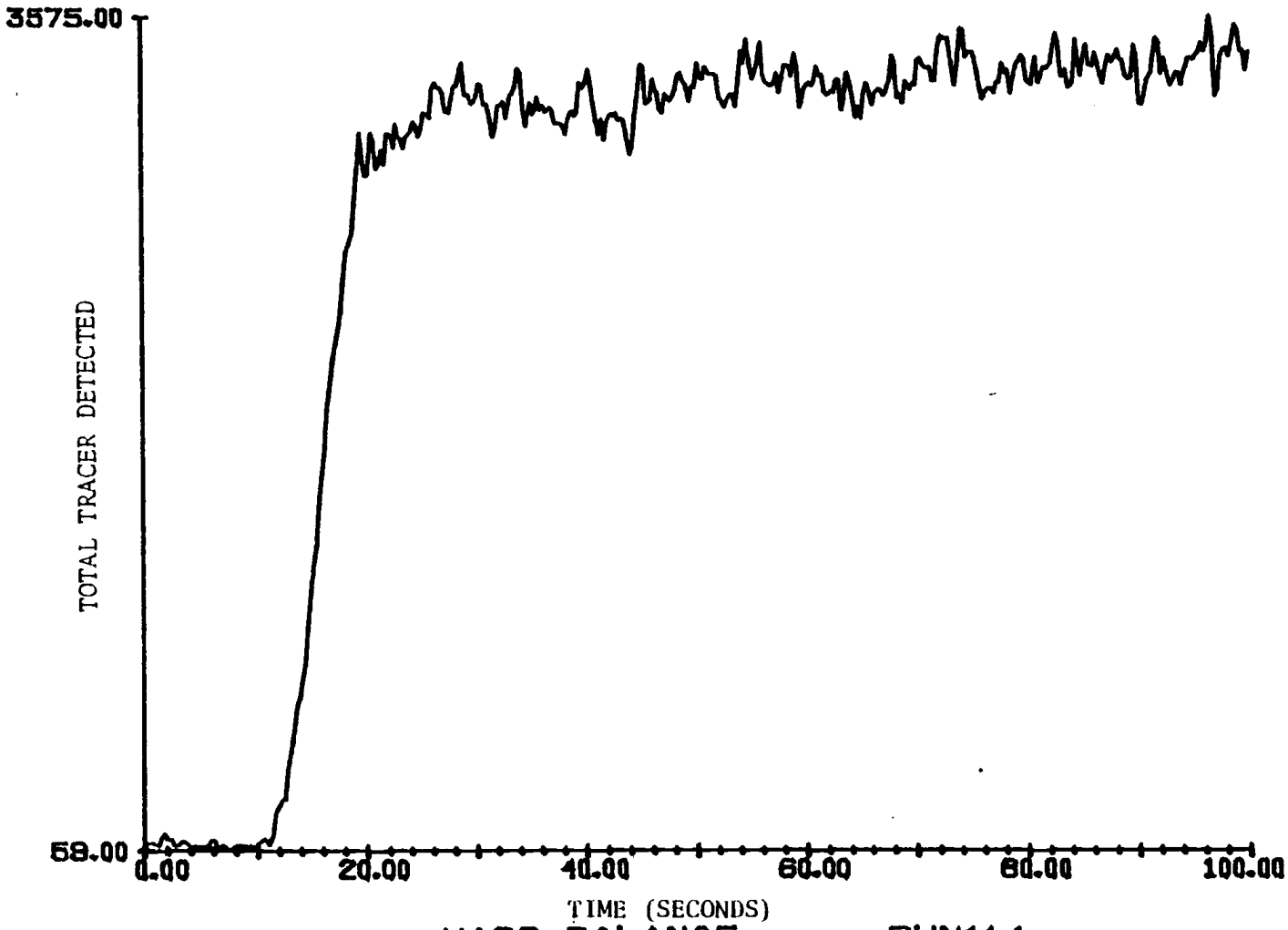

Figure 6.3. (Cont'd.)

units[4] for each quarter second time interval and the abscissas are time (in seconds). It is quite apparent that a material balance of tracer is not satisfied at the beginning of any run (i.e., the first 20 seconds or so).

6.4 Summary of Results

The overall mixing time (OMT) is the time required for the tracer concentration (the ordinates of the mass balance and normalized mean concentration) to enter the "noise band" about the equilibrium concentration. The equilibrium concentration is defined as the average concentration over the last 20 seconds of a run. These values appear in Table 6.1 along with other criteria of mixing. The first column is the run number, which is followed in parentheses by the weight of sand (lbs), height of the tube array above the distributor plate (in) and the superficial gas velocity (ft/sec). All runs were conducted in the .91 m x .91 m (3 ft x 3 ft) bed using ferrite tracer with an average surface diameter, $\bar{d}_p$, of .06 in (1.6 mm) and a density, $\bar{\rho}$, of 2400 Kg/m^3 (150 lb/ft^3) and sand with d_p = 0.8 mm (0.03 in) and $\bar{\rho}_{sand}$ = 2700 Kg/m^3 (169 lb/ft^3). The next column shows the first time interval in which all clumps of tracer have

---

[4] There are .005 volts signal/data unit and one volt is approximately equal to one volume percent tracer. Thus, there are 200 data units to one volume percent tracer.

TABLE 6.1 Criteria of Mixing (runs 74-86).

Run No.	First Time Interval With $\tilde{C}_i/\bar{C}^* < 10$	First Time Interval With $\tilde{C}_i/\bar{C}^* = 1$	OMTs (secs) Mass Balance	OMTs (secs) Normalized Tracer Average Concentration
74(2000#,20",3FPS)[5]	VII	VIII	32	28
75(2000#,20",7FPS)	V	~VI	22	14
76(2000#,20",5FPS)	V	~VI	16	15
77(2000#,20",11FPS)	I	~V	10	12
78(2000#,20",9FPS)	III	VI	14	15
79(2500#,20",5FPS)	V	VIII	15	17
80(2500#,20",7FPS)	II	VI	20	19
81(2500#,20',9FPS)	I	VI	16	15
82(2500#,20",11FPS)	I	~ IV	12	18
83(3000#,20",5FPS)	IV	VII	28	18
84(3000#,20",7FPS)	I	~V	25	16
85(3000#,20",9FPS)	I	~IV	16	14
86(3000#,20",11FPS)	I	~V	18	13

[5] Note that: 1 Kg = 2.2046 lbs, 1 in = .0254 m, 1 m/s = 3.29 FPS

reached a normalized concentration, $\tilde{C}_i/\bar{C}^*$, less than or equal to ten. In the third column, the first time interval of the well-mixed state ($\tilde{C}_i/\bar{C}^* = C_\theta = 1$) is tabulated. The last two columns are the overall mixing times (OMTs) as read from the mass balance and normalized mean concentration plots, respectively. The time intervals are as follows: I is the 0-1 second time interval, II is (1-2), III (2-3), IV (4-5), V (7-8), VI (12-13), VII (20-21), VIII (33-34), and IX (54-55).

6.5 Conclusions Based on Runs 74-86

It is quite evident that mixing is enhanced by increases in the superficial gas velocity. Run 74 (3 FPS) dramatically shows how poor mixing can be at low velocities. Overall mixing times (OMTs) are about the same when conditions are held constant at 20" and 5 FPS and different weights of sand are used (see runs 76, 79, 83). At 7 FPS and 20" the OMT rises and then falls as more sand is added (see runs 75, 80, and 84). The best run, in terms of all measures, is run 77 (2000#, 20", 11FPS). Many other runs (81, 82, 84, 85, 86) appear to mix as rapidly as run 77 when the criteria in the first column (i.e., $\tilde{C}_i/\bar{C}^* < 10$) is used. This criteria is probably the most important in terms of uneven combustion and sulfur retention in the bed. Thus, as one would expect, higher gas velocities and more sand (or limestone) will promote rapid dilution of injected particles (ferrite, coal or whatever).

OMTs based on the mass balance plots are questionable. It is possible for a mass balance to be satisfied while the bed, as a whole, remains unmixed. On the other hand, if the bed is well-mixed, a mass balance must be satisfied. Thus, OMTs based only on the normalized tracer average concentration will be used in the subsequent analysis of runs 87-114 (see Table 6.2).

6.6 Conclusions Based on Runs 74-114

In Table 6.3, the results of Tables 6.1 and 6.2 are grouped to show the effects of superficial gas velocity (the U groups), weight of the bed media (the W groups), and height of the tube array above the distributor plate (the H groups) on solids mixing. These groups are considered to be representative of general trends or tendencies in the data. Mixing criteria are shown in the same order as in Table 6.1 and 6.2. All OMTs are those read from the normalized tracer average concentration curves. Quantities in parentheses in Table 6.3 are replicate runs and their respective mixing criteria. The "studied" variable is the quantity which is varied in each group.

6.6.1 The U Groups

Groups U3 and U5 show a very definite increase in mixing efficiency as superficial gas velocity is increased. It appears that clumps of tracer have avoided detection by the probes in run 89,

TABLE 6.2 Criteria of Mixing (runs 87-114).

Run No.	First Time Interval With $\tilde{C}_i/\bar{C}^* < 10$	First Time Interval With $\tilde{C}_i/\bar{C}^* = 1$	OMT(secs) Normalized Tracer Average Concentration
87(2000#, 20"1FPS)	V	VII	22
88(3000#, 10", 5FPS)	I	VI	22
89(3000#, 10", 7FPS)	I	I	23
90(3000#, 10", 9FPS)	I	IV	12
91(3000#, 10", 10FPS)	I	III	10
92(2500#, 10", 5FPS)	I	VI	18
93(2500#, 10", 7FPS)	I	I	22
95(2500#, 10", 11FPS)	I	I	18
96(2000#, 10", 5FPS)	II	~ VI	14
97(2000#, 10", 7FPS)	II	VI	12
98(2000#, 10", 9FPS)	I	IV	10
99(2000#, 10", 11FPS)	I	IV	8
102(2500#, 10", 5FPS)	I	VI	12
103(2500#, 10", 7FPS)	I	IV	11
104(2500#, 10", 9FPS)	I	I	9
105(2500#, 10", 10.5FPS)	I	I	8
106(2000#, 10", 5FPS)	V	VII	16
107(2000#, 10", 7FPS)	I	~ VI	10
108(2000#, 10", 9FPS)	I	II	8
109(2000#, 10", 11FPS)	I	IV	8
110(2500#, 20", 5FPS)	IV	VII	12
111(2500#, 20", 11FPS)	I	VI	5
112(3000#, 20", 5FPS)	IV	~ VI	10
113(2000#, 10", 1FPS)[6]	I	VII	16
114(2000#, 10", 4FPS)	I	VI	7

[6] Runs 87, 113 and 114 were conducted with EI-70 sand ($\bar{d}_p \approx$ 0.17 mm (.0068 in)).

Also note: 1 Kg = 2.2046 lbs; 1 in = .0254 m; 1 m/s = 3.29 FPS.

TABLE 6.3 Grouping of Results.

Group	Run No.	Values of "Studied" Variable	Mixing Criteria
U1: 3000#, 10"	88	5FPS	I, VI, 22
	89	7FPS	I, I, 23
	90	9FPS	I, IV, 12
	91	10FPS	I, III, 10
U2: 2500#, 10"	92(102)	5FPS	I, VI, 18 (I, VI, 12)
	93(103)	7FPS	I, I, 22 (I, IV, 11)
	104	9FPS	I, I, 9
	95(105)	11FPS	I, I, 18 (I, I, 8)
U3: 2000#, 10"	96(106)	5FPS	II,~VI, 14 (V, VII, 16)
	97(107)	7FPS	II, VI, 12 (I,~VI, 10)
	98(108)	9FPS	I, IV, 10 (I, II, 8)
	99(109)	11FPS	I, IV, 8 (I, IV, 8)
U4: 3000#, 20"	83(112)	5FPS	IV, VII, 18 (IV,~VI, 10)
	84	7FPS	I,~V, 16
	85	9FPS	I,~IV, 14
	86	11FPS	I,~V, 13
U5: 2000#, 20"	76	5FPS	V,~VI, 15
	75	7FPS	V,~VI, 14
	78	9FPS	III, VI, 15
	77	11FPS	I,~V, 12
W1: 10", 5FPS	96(106)	2000#	II,~VI, 14 (V, VII, 16)
	92(102)	2500#	I, VI, 18 (I, VI, 12)
	88	3000#	I, VI, 22
W2: 10", 7FPS	97(107)	2000#	II, VI, 12 (I,~VI, 10)
	93(103)	2500#	I, I, 22 (I, IV, 11)
	89	3000#	I, I, 23
W3: 10", 11FPS	99(109)	2000#	I, IV, 8 (I, IV, 8)
	95(105)	2500#	I, I, 18 (I, I, 8)
	91	3000#	I, III, 10

TABLE 6.3 Continued

Group	Run No.	Values of "Studied" Variable	Mixing Criteria
W4: 20", 5FPS	76	2000#	V, ~VI, 15
	79(110)	2500#	V, VIII, 17 (IV, VII, 12)
	83(112)	3000#	IV, VII, 18 (IV, VI, 10)
W5: 20", 9FPS	78	2000#	III, VI, 15
	81	2500#	I, VI, 15
	85	3000#	I, IV, 14
W6: 20", 11FPS	77	2000#	I, ~V, 12
	82	2500#	I, ~IV, 18
	86	3000#	I, ~V, 13
H1: 3000#, 5FPS	88	10"	I, VI, 22
	83(112)	20"	IV, VII, 18 (IV, ~VI, 10)
H2: 3000#, 7FPS	89	10"	I, I, 23
	84	20"	I, ~V, 16
H3: 3000#, 11FPS	91	10"	I, III, 10
	86	20"	I, V, 18
H4: 2500#, 5FPS	92(102)	10"	I, VI, 18 (I, VI, 12)
	79(110)	20"	V, VIII, 17 (IV, VII, 12)
H5: 2500#, 11FPS	95(105)	10"	I, I, 18 (I, I, 8)
	82	20"	I, ~IV, 18
H6: 2000#, 5FPS	96(106)	10"	II, ~VI, 14 (V, VII, 16)
	76	20"	V, ~VI, 15
H7: 2000#, 11FPS	99(109)	10"	I, IV, 8 (I, IV, 8)
	77	20"	I, ~V, 12

thereby making group U1 appear slightly contradictory. The OMTs of replicate runs 95 and 105 are drastically different. Thus, OMT must not be a very good way to measure mixing. As far as the histogram criteria are concerned, group U2 is consistent with the hypothesis that increased gas velocity promotes mixing. According to the histogram criteria, mixing is worse when the height of the tube array above the distribution plate is decreased. A comparison of U1 with U4 and U3 with U5 will readily prove this assertion. Interestingly enough, the OMTs are not affected as greatly by changes in the height of the tube array.

6.6.2 The W Groups and H Groups

The W groups show that addition of bed media is accompanied by greater dilution and longer OMTs. Since enhancement of tracer dilution is the objective of this study, it is advisable to use 1361 Kg (3000 lbs) of bed media instead of 1134 Kg (2500 lbs) or 907 Kg (2000 lbs). Furthermore, the W groups reaffirm the conclusion that mixing is a direct function of superficial gas velocity. Groups W1, W3, W4, and W6 indicate that an increase in height is accompanied by sluggish mixing of tracer in the bed. This effect is attenuated at higher superficial gas velocities.

All H groups seem to indicate better mixing with the tube array in the .254 m (10 in) position rather than in the .508 m (20 in) position.

These groups also show greater dilution as the superficial gas velocity and or the weight of bed media is increased.

6.6.3 Replicate Runs

Replicate runs are tabulated in Table 6.4. Again, the quantities appearing in parentheses are the replicate runs are their respective mixing criteria. With regard to the histogram criteria, all runs seem fairly reproducible, except 93 and 103. OMTs are reproducible in the following pairs: 96(106), 97(107), 98(108), and 99(109). It seems that as the weight of bed media and the superficial gas velocity are increased, the variability in OMTs between replicate runs is also increased. This is shown in pairs 79(110), 83(112), 92(102), 93(103), and 95(105). Curiously, runs 99 and 109 at 3.35 m/s (11 FPS) mix at the same rate according to all criteria.

TABLE 6.4 Replicate Runs

Run Nos.	Conditions	Mixing Criteria
79(110)	2500#, 20", 5FPS	V, VIII, 17 (IV, VII, 12)
83(112)	3000#, 20", 5FPS	IV, VII, 18 (IV, ~VI, 10)
92(102)	2500#, 10", 5FPS	I, VI, 18 (I, VI, 12)
93(103)	2500#, 10", 7FPS	I, I, 22 (I, IV, 11)
95(105)	2500#, 10", 11FPS	I, I, 18 (I, I, 8)
96(106)	2000#, 10", 5FPS	II, ~VI, 14 (V, VII, 16)
97(107)	2000#, 10", 7FPS	II, VI, 12 (I, ~VI, 10)
98(108)	2000#, 10", 9FPS	I, IV, 10 (I, II, 8)
99(109)	2000#, 10", 11FPS	I, IV, 8 (I, IV, 8)

6.7 Movies of Tracer Concentration Profiles in the Fluidized Bed

Figure 6.4 shows a frame of a film describing the last ten seconds of Run 88 (3000#, 10", 5FPS). This figure is a concentration profile for each level of probes in the bed. Each vertex represents a probe. The heights of the vertices are proportional to the concentration of tracer in the vicinity of each probe. During the last 10 seconds of a run, tracer is fairly well-mixed. Thus, drops in concentration are the result of passing bubbles. The movie, therefore, describes bubble movement and frequency. Since bubbles are mostly responsible for solids mixing, it is possible to verify some of the conclusions made in chapter IV concerning distinct mixing regions in the bed. Careful observation of the movie reveals a preference of bubbles to rise in the interior regions of the bed as opposed to regions adjacent to the walls. Thus, mixing is best at the center of the bed. Along the bottom row of probes, bubbles seem evenly dispersed, but not as frequent as those found in the interior regions (channels B and C on tubes 2, 3, 6, 7, 10 and 11). Solids mixing in the region next to the distributor plate seems to be better than the wall regions, but worse than the interior regions. Again, these results are in accord with Schugerl's findings [38].

A movie of only the bottom row of probes was also made for the first ten seconds of run 88. It appears that tracer slides down along

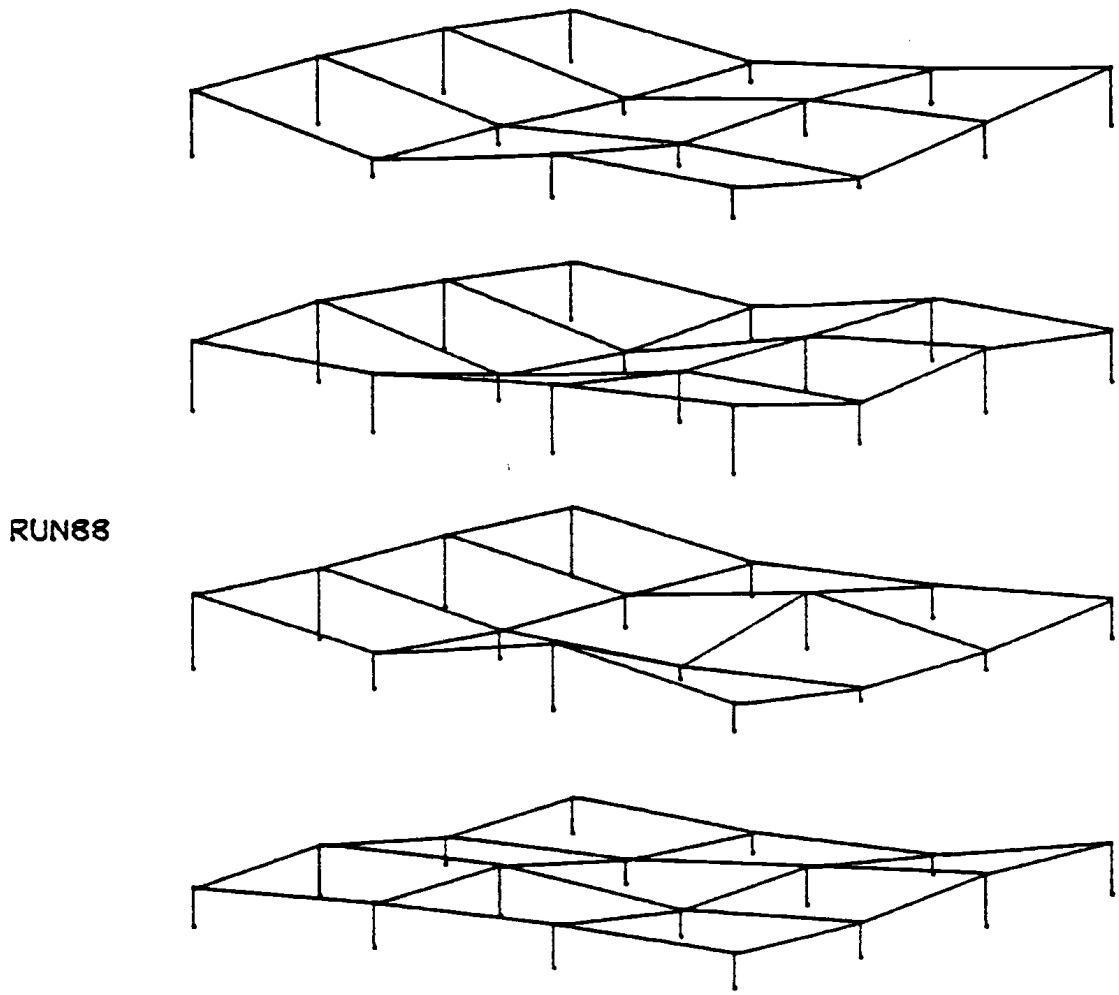

Figure 6.4. Concentration profile for each level of probes in the fluidized bed.

the walls and then moves up the center of the bed. This observation is in accord with the findings in chapter IV.

6.8 Closure

It appears that the histogram approach is consistent with itself and quite relevant to our study. OMTs, on the other hand, are misleading and sometimes contradictory. A significant deficiency in any approach is the lack of data from bed regions lying outside the detection range of the probes. Thus, it may appear that increases in the superficial gas velocity, increases in the amount of bed media and decreases in the height of the tube array all contribute to the enhancement of mixing; but, in reality, these changes may only shift the position of tracer injection away from the probes, thereby, allowing the tracer to disperse somewhat before being detected.

VII. OVERALL CONCLUSIONS

On the basis of the collected data and its analysis the following conclusions may be made:

1. At high gas velocities, 2.74 m/s (9 FPS) and 3.35 m/s (11 FPS), the ferrite tracer spreads rapidly (less than 10 seconds) throughout the bed. Low gas velocities are accompanied by sluggish mixing.
2. Though it may appear that increases in the superficial gas velocity, increases in the amount of bed media and decreases in the height of the tube array all contribute to the enhancement of mixing, in reality these changes may only place more bed media between the tracer injection port and the probes, thereby, allowing the tracer to disperse somewhat before being detected.
3. As shown by their lack of reproducibility, overall measures of solids spreading like OMT and MSMM fail to describe tracer dispersion in a consistent manner.
4. Although the data is slightly erratic it does show some distinct trends. The histogram criteria, gives a reasonable picture of how solids disperse. It measures tracer concentration with respect to itself. In effect, the histograms answer the question posed by a tracer particle -- "How

crowded am I?" Thus, this criteria measures "overshoot" of the normalized tracer average concentration very well. However, it fails to adequately describe slowly rising normalized tracer average concentration curves.

5. The concentration versus time plots and the concentration profile movie indicate that solids tend to circulate down the walls and up the center of the bed. The effects of the walls cause gulf-streaming and large scale eddies, even with an immersed tube bank. Therefore, it is not possible to divide the bed into well-mixed compartments with intercompartmental flows.
6. Bubble frequencies are greatest in the interior regions of the bed, whereas bubbles seem to avoid the wall regions. Thus, solids must flow down the walls and up the interior as stated in conclusion 5.
7. This work shows that tighter tube spacing enhances solids mixing. (Compare OMTs with study done by T. Fitzgerald et al. at Oregon State University - "Solid Tracer Studies in a Tube-Filled Fluidized Bed.")
8. More numerous small tracer particles helped eliminate the Poisson noise found in the earlier runs (50-73).
9. Industrial combustors always operate in the transient phase. Thus, burning coal particles are never well-mixed and

OMTs are not useful.

10. Char particles, on the other hand, are well-mixed because their residence time in the bed is greater than the observed OMTs.

VIII. DIRECTION OF FUTURE WORK

Future work dealing with solids movement will be directed toward bed scaling and dimensionless group modelling. The bed and tube array will be altered to test whether fluidization hydrodynamics can be correlated with the following four dimensionless groups:

$\left(\frac{\rho_s}{\rho_g}\right)$ — The ratio of solid density to gas density.

$\left(\frac{\bar{d}_p}{L}\right)$ — The ratio of particle size to a characteristic bed dimension.

$\left(\frac{U_o^2}{Lg}\right)$ — The ratio of superficial gas velocity squared to the product of the acceleration of gravity and a characteristic bed dimension - the Froude number.

$\left(\frac{\bar{d}_p U_o}{\nu}\right)$ — The ratio of the superficial gas velocity times particle size to the kinematic viscosity of the gas - the particle Reynold's number.

Jaycor Corporation has prepared a report [37] covering cold flow simulation theory, which is rigorously developed through dimensional analysis of the Navier-Stokes equations. An outline of the experimental approach, specifications and procedures necessary for verification of their theory is also presented.

I would also recommend a study of local solids velocity gradients at the bottom of the bed. Along with this investigation, one could

construct a map of tracer fluxes in the lower portion of the bed. This study is particularly significant in light of the Park et al. plume model [34] which describes coal particle devolitilization after its introduction to the bed. Essentially, coal must be injected at the bottom of the bed in order for its plume to be contained within the bed (i.e., not within the bed and the freeboard). Once instrumentation has been developed and refined, an investigation involving induced solids circulation patterns could commence. An investigator would be able to determine the variables (baffles, tube spacing, etc.) necessary to maximize the holding time of solids at the bottom of the bed and, thus, optimize conditions for coal combustion.

BIBLIOGRAPHY

1. Abrahami, S. N. and W. Resnick, Trans. Inst. Chem. Engrs., 52, 80 (1974).

2. Bart, R., Ph.D. Thesis, M.I.T., Cambridge, Mass. (1950).

3. Bondareva, A. K., "Particle Motion and Heat Transfer in Suspended Beds," Kand. Dissertat., Leningrad (1958).

4. Bondareva, A. K. and O. M. Todes, "Thermal Conduction in Fluid Bed Heat Transfer," Inzh.-Fiz. Zhurn., 3 (2), 105-110 (1960).

5. Brotz, W., Chem. Ing. Tech., 28, 165 (1956).

6. Burovoi, I. A. and G. I. Svetozarova, Int. Ch. E., 5 (4), (1965).

7. Chang, F. W., under the direction of Dr. Thomas J. Fitzgerald, Ph.D. Dissertation, Oregon State University (1976).

8. Colakyan, Manuk, Master's Thesis, Oregon State University (1978).

9. Cranfield, R. R., "Solids Mixing in Fluidized Beds of Large Particles," A. I. Ch. E. Symp. Series, 176 (74), 54-59 (1978).

10. Davidson, J. F. and D. Harrison, ed., Fluidization, Academic Press, London (1971).

11. Donlevy, B. T., Master's Thesis, Oregon State University (1977).

12. Furukawa, J. and T. Omae, "Liquid-like Properties of Fluidized Systems," Ind. Eng. Chem., 50 (5), 821-828 (1958).

13. Gabor, J. D., A. I. Che. E. Journal, 10, 345 (1964).

14. Geldart, D. and R. R. Cranfield, Chem. Engr. J., 3, 211 (1972).

15. Gilliland, E. R. and E. A. Mason, Ind. Eng. Chem., 41, 1191 (1949).

16. Hayakawa, T., W. Graham, and G. L. Osberg, Canadian J. Chem. Eng., 42, 99 (1964); Hayakawa, T. and S. Fujita, Ann. Rep. Asahi Glass Foundation, 12, 513 (1966).

17. Highley, J. and D. Merrick, "The Effect of Spacing Between Solid Feed Points on the Performance of a Large Fluidized-Bed Reactor," A. I. Ch. E. Symp. Series, 67 (116), (1971).

18. Katz, S. and F. A. Zenz, "Application of Radioactive Tracer," Petr. Ref., 33 (5), 203 (1954).

19. Kondukov, N. B. and Collaborators, Intern, Chem. Eng., 4, 43 (1964).

20. Kramers, H., "The Viscosity of a Bed of Fluidized Solids," Chem. Eng. Sci., 1, 35-37 (1951).

21. Kunii, D. and O. Levenspiel, Fluidization Engineering, John Wiley and Sons, Inc. (1969).

22. Kunii, D., K. Yoshida, and O. Levenspiel, Symp. on Fluidization, Tripartite Chem. Eng. Conf., Montreal (1968).

23. Leva, M., Fluidization, McGraw-Hill, N. Y. (1959).

24. Lewis, W. K., E. R. Gilliland, and H. Girouard, Chem. Eng. Progr. Symp. Series, 58 (38), 87 (1962).

25. Liu, F. F. and C. Orr, Jr., "Apparent Viscosity of Gas-Solid Fluidized Systems," J. Chem. Eng. Data, 5 (4), 430-432 (1960).

26. Massimilla, L. and I. W. Westwater, Photographic Study of Solid Gas Fluidization, A. I. Ch. E. J., 6 (1), 134-138 (1960).

27. Masson, H., "Solid Circulation Studies in a Gas Solid Fluid Bed," 33, 621-23 (1977).

28. Matheson, G., W. Herbst, and P. Holt, "Characteristics of Fluid Solid Systems," Ind. Eng. Chem., 41, 1099-1104 (1949).

29. May, W. G., Chem. Eng. Progr., 55, 49 (Dec. 1959).

30. McKenzie, E. C., "Burning Coal in Fluidized Beds," Chem. Eng., 85, 18 (1978).

31. Mireur, J. P. and K. B. Bischoff, "Mixing and Contacting Models for Fluidized Beds," A.I.Ch.E. J., 13 (5), 839-845 (1967).

32. Mori, Y. and K. Nakamura, Kagaku Kogaku (Chem. Eng. Japan), 29, 868 (1965).

33. Nguyen, H. V., A. B. Whitehead, and O. E. Potter, "Gas Backmixing, Solids Movement, and Bubble Activities in Large Scale Fluidized Beds," A.I.Ch.E. J., 23 (6), 913-917 (1977).

34. Park, D., O. Levenspiel, and T. J. Fitzgerald, "A Model for Large Scale Atmospheric Fluidized Bed Combustors," Paper Submitted for A.I.Ch.E. Meeting, San Francisco (1979).

35. Rowe, P. N. and B. A. Partridge, "Particle Movement Caused by Bubbles in a Fluidized Bed," Third Congress of European Federation of Chemical Engineering, London, June 2, 1962.

36. Rowe, P. N. and K. S. Sutherland, Trans. Inst. Chem. Engrs., 42, T55 (1964).

37. Scharff, M. F., S. R. Goldman, T. M. Flanigan, and T. K. Gregory, "Project to Provide an Experimental Plan for the Merc 6' x 6' Fluidized Bed Cold Test Model," U.S. Dept. of Energy, EY-77-C-21-8156 (1977).

38. Schugerl, K., "Mixed Regions in Fluidized Beds," Powder Tech., 3, 267-278 (1969).

39. Stemerding, S. (1955), Koninklijke Shell Lab, Amsterdam, Results reported by Reman (1955).

40. Sutherland, K. S., Trans. Inst. Chem. Engrs., 39, 188 (1961).

41. Todes, O. M. and A. K. Bondareva, Special Features of Technological Processes in Fluidized Beds, Khim. Nauka i Prom., 2 (2), 223-232 (1957).

42. Toomey, R. and H. Johnstone, Heat Transfer Between Beds of Fluidized Solids and the Walls of the Container, Chem. Eng. Progr. Symp. Ser., 49 (5), 51-63 (1953).

43. Trawinski, in "Hydrodynamics and Heat Transfer in Fluidized Beds," Zabrodsky, S. S., The M. I. T. Press, Cambridge, Mass. (1966).

44. Woolard, I. N. M. and O. E. Potter, A.I.Ch.E. J., 14, 388 (1968).

45. Zabrodsky, S. S., "Hydrodynamics and Heat Transfer in Fluidized Beds," Zenz, F. A., Trans., The M. I. T. Press, Cambridge, Mass. (1966).

APPENDIX A

Sand and Tracer Sieve Analysis

Colakyan [8] determined the mean surface diameter, d_p, and the minimum fluidization velocity, U_{mf}, of EI-16 sand to be 0.798 mm (0.0134 in) and 0.459 m/s (1.51 ft/s), respectively. The mean surface diameters of EI-16, EI-70 and the fine tracer were determined independently in the present study. Table A.1 shows the Tyler standard screens used in this analysis. Calculations are based on the method presented in Fluidization Engineering [21] using the formula:

$$\bar{d}_p = \frac{1}{\sum(x/d_p)_i}$$

where $\bar{d}_p$ is the mean surface particle size (mm), x_i is the fraction of material in size interval i and d_{p_i} is the average diameter of size interval i. Tables A.2, A.3 and A.4 show the results.

Table A.1. Tyler standard screens.

Standard Interval = $\sqrt{2}$, Aperture, in.	Interval = $\sqrt[4]{2}$, for Closer Sizing			
	Aperture, in.	Aperture, mm	Mesh Number	Wire Diameter, in.
1.050	1.050	26.67	.....	0.148
	0.883	22.43	.....	0.135
0.742	0.742	18.85	.....	0.135
	0.624	15.85	.....	0.120
0.525	0.525	13.33	.....	0.105
	0.441	11.20		0.105
0.371	0.371	9.423	.....	0.092
	0.312	7.925	2½	0.088
0.263	0.263	6.680	3	0.070
	0.221	5.613	3½	0.065
0.185	0.185	4.699	4	0.065
	0.156	3.962	5	0.044
0.131	0.131	3.327	6	0.036
	0.110	2.794	7	0.0326
0.093	0.093	2.362	8	0.032
	0.078	1.981	9	0.033
0.065	0.065	1.651	10	0.035
	0.055	1.397	12	0.028
0.046	0.046	1.168	14	0.025
	0.0390	0.991	16	0.0235
0.0328	0.0328	0.833	20	0.0172
	0.0276	0.701	24	0.0141
0.0232	0.0232	0.589	28	0.0125
	0.0195	0.495	32	0.0118
0.0164	0.0164	0.417	35	0.0122
	0.0138	0.351	42	0.0100
0.0116	0.0116	0.295	48	0.0092
	0.0097	0.248	60	0.0070
0.0082	0.0082	0.208	65	0.0072
	0.0069	0.175	80	0.0056
0.0058	0.0058	0.147	100	0.0042
	0.0049	0.124	115	0.0038
0.0041	0.0041	0.104	150	0.0026
	0.0035	0.088	170	0.0024
0.0029	0.0029	0.074	200	0.0021
	0.0024	0.061	230	0.0016
0.0021	0.0021	0.053	270	0.0016
	0.0017	0.043	325	0.0014
0.0015	0.0015	0.038	400	0.0010

TABLE A.2 EI-16 Sand Sieve Analysis

After run 60:

Cumulative Weight of a Representative 2.332 lb. Sample	With Diameter Smaller Than d_p (mm)	Tyler[7] Mesh
0	0.295	-48, +28
.220	0.589	-28, +20
.945	0.833	-20, +14
2.031	1.168	-14, +12
2.219	1.397	-12, +10
2.283	1.651	-10, +8
2.332	2.362	-8 , Pan

Diameter Range (mm)	d_{pi} (mm)	Weight Fraction in Interval (x_i)	$(x/d_p)_i$
.295 - .589	0.442	(.220-0)/2.332 = .0943	.213
.589 - .833	0.711	(.945-.22)/2.332 = .3109	.437
.833 - 1.168	1.001	(2.031-.945)/2.332 = .4657	.465
1.168 - 1.397	1.283	(2.219-2.031)/2.332 = .0806	.063
1.397 - 1.651	1.524	(2.283-2.219)/2.332 = .0274	.018
1.651 - 2.362	2.007	(2.332-2.283)/2.332 = .0210	.010
			$\sum$ = 1.207

$$d_p = \frac{1}{\sum_i \frac{1}{(x/d_p)_i}} = \frac{1}{1.207} = .828 \text{ mm } (.0326 \text{ in})$$

[7] Particles that pass through the 48-mesh screen but are retained on the 28-mesh screen are reported as -48, +28.

TABLE A.2 Continued.

After run 72:

Cumulative Weight of a Representative 1.119 lb. Sample	With Diameter Smaller Than d_p (mm)	Tyler Mesh
0	0.295	-48, +28
.192	0.589	-28, +20
.684	0.833	-20, +14
1.030	1.168	-14, +12
1.086	1.397	-12, +10
1.119	1.651	-10, +8
1.119	2.362	-8 , Pan

Diameter Range (mm)	d_{pi} (mm)	Weight Fraction in Interval (x_i)	$(x/d_p)_i$
.295 - .589	0.442	(.192-0)/1.119 = .1716	.388
.589 - .833	0.711	(.684-.192)/1.119 = .4397	.618
.833 - 1.168	1.001	(1.030-.684)/1.119 = .3092	.309
1.168 - 1.397	1.283	(1.086-1.030)/1.119 = .0500	.039
1.397 - 1.651	1.524	(1.119-1.086)/1.119 = .0295	.019
1.651 - 2.362	2.007	0.000	.000
		$\sum$ =	1.374

$$d_p = \frac{1}{1.374} = .728 \text{ mm } (.0287 \text{ in})$$

TABLE A.3 EI-70 Sand Sieve Analysis

After run 87:

Tyler Mesh Size	x_i	d_{p_i} (mm)	$(x/d_p)_i$
-35, +48	0.0064	.3560	0.0180
-48, +60	0.1089	.2715	.4011
-60, +65	0.3430	.2280	1.5044
-65, +80	0.1651	.1915	0.8621
-80, +100	0.1740	.1610	1.0807
-100, +150	0.1401	.1255	1.1163
-150, +170	0.0268	.0960	0.2792
-170, +200	0.0165	.0810	0.2037
Pan (+325)	0.0192	.0585	0.3282
	1.0000		$\sum$ = 5.7938

$$d_p = \frac{1}{5.7938} = 0.173 \text{ mm } (0.00680 \text{ in})$$

TABLE A.4 Fine Ferrite Tracer Sieve Analysis
(used in runs 74 - 114)

Cumulative Weight of a Representative 1.0 lb. Sample	With Diameter Smaller Than d_p (mm)	Tyler Mesh
0	.208	-65, +16
.085	.991	-16, +14
.157	1.168	-14, +12
.223	1.397	-12, +10
.348	1.651	-10, +8
.690	2.362	-8 , +6
.937	3.327	-6 , +3
1.000	6.680	-3 , Pan

Diameter Range (mm)	d_{pi} (mm)	Weight Fraction in Interval (x_i)	$(x/d_p)_i$
.208 - .991	0.600	(.085-0) = .085	.1417
.991 - 1.168	1.080	.157-.085 = .072	.0667
1.168 - 1.397	1.283	.066	.0514
1.397 - 1.651	1.524	.125	.0820
1.651 - 2.362	2.007	.342	.1704
2.362 - 3.327	2.845	.247	.0868
3.327 - 6.680	5.004	.063	.0126
			$\sum$ = .6116

$$d_p = \frac{1}{.6116} = 1.635 \text{ mm } (.0644 \text{ in})$$

APPENDIX B

Scaling Values for all 64 Channels:

Channel	ΔV (Voltage Difference)[8]	Scaling Value[9]
1A	1942	1.0029
B	2106	.9248
C	2761	.7054
D	1930	1.0091
2A	1658	1.1747
B	1896	1.0272
C	1609	1.2105
D	2112	.9222
3A	1986	.9807
B	1253	1.5544
C	1004	1.9400
D	1927	1.0107
4A	1957	.9952
B	1907	1.0213
C	1914	1.0176
D	1841	1.0579
5A	2155	.9038
B	2184	.8918
C	1693	1.1504
D	1844	1.0562
6A	2505	.7775
B	1775	1.0973
C	1821	1.0695
D	1705	1.1423
7A	1906	1.0218
B	2450	.7950
C	1972	.9876
D	1844	1.0562

---

[8] The voltage difference is given in terms of data units. There are .005 Volts per data unit.

[9] Scaled values are obtained by dividing the average voltage difference by the ΔV value of a particular probe.

APPENDIX B. Continued

Channel	ΔV (Voltage Difference)	Scaling Value
8A	1961	.9932
B	1755	1.1098
C	1963	.9922
D	1706	1.1416
9A	1976	.9856
B	2405	.8098
C	1801	1.0814
D	2401	.8112
10A	2171	.8971
B	2032	.9585
C	2045	.9524
D	2054	.9482
11A	1943	1.0024
B	1667	1.1684
C	1712	1.1376
D	1862	1.0460
12A	1680	1.1593
B	1879	1.0365
C	1939	1.0045
D	1988	.9797
13A	1857	1.0488
B	1677	1.1614
C	1707	1.1410
D	1768	1.1016
14A	2234	.8718
B	2299	.8472
C	2151	.9055
D	3169	.6146
15A	1678	1.1607
B	2311	.8428
C	2283	.8531
D	1960	.9937
16A	1850	1.0528
B	1964	.9917
C	1305	1.4924
D	1839	1.0591
	= 124,649	

$\overline{\Delta V}$ = Average ΔV = 1947.641

APPENDIX C

The Detection Circuit, Power Supply and Sine-Wave Generator

C.1 The Detection Circuit [10]

A simplified sketch of the inductance probe detection circuit and phasor representations of the driving, resistive and inductive voltage components appears in Figure C.1. Tracer concentrations in the bed rarely exceed two percent by volume. Therefore, the inductance of the coils could be expected to change by about two percent during an experimental run. However, as the bed warms up, its temperature can change by as much as 30°C (54°F). This temperature variation causes about a ten percent resistance change in the coils, which would easily drown out the two percent inductance change in the coils caused by the presence of tracer. This circuit is unique in that it circumvents the problem of heat-produced resistance changes in the detector coil. Since the resistive component of the active bridge output voltage is 90° out of phase with the driving voltage, their average product is zero. Hence, the bridge is only sensitive to inductance imbalance caused by the presence of ferrite tracer near the probe.

A brief mathematical description of the circuit and its temperature insensitivity follows. As shown in Figure C.1, the input to the

[10] Dr. Thomas J. Fitzgerald has applied for a patent on this circuit.

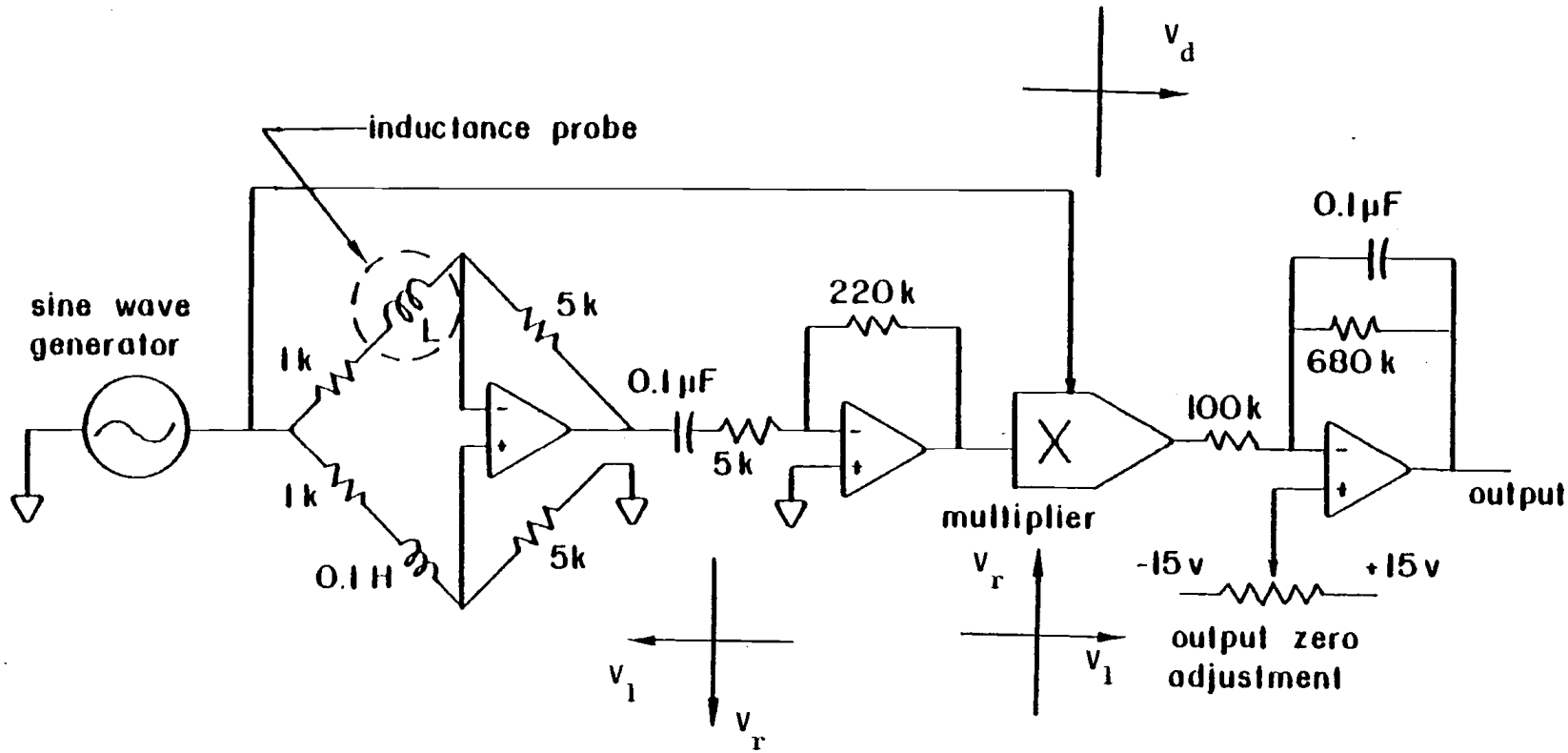

Figure C.1. Simplified inductance measuring circuit.

multiplier is:

$$v_d = V_d \sin(\omega t)$$

$$v_r + v_\ell = V_r \sin(\omega t + \pi/2) + V_\ell \sin(\omega t)$$

The output of the multiplier or averaging filter is:

$$v_{out} = \overline{V_d \sin(\omega t)\left[V_r \sin(\omega t + \pi/2) + V_\ell \sin(\omega t)\right]}$$

$$= \left[\overline{V_d V_r \sin(\omega t)\sin(\omega t + \pi/2)}\right] + \left[V_d V_\ell \sin^2(\omega t)\right]$$

$$= V_\ell\left[\overline{V_d \sin^2(\omega t)}\right]$$

$$= V_\ell[\text{CONSTANT}]$$

Thus, the output voltage is proportional to V_1 which is itself proportional to the ferrite tracer concentration near the inductor probe.

An inductance bridge card (containing four separate inductance bridge circuits) is shown in Figure C.2; and its schematic is shown in Figure C.3. The output from the multiplier is passed through a two time-constant filter to eliminate the carrier frequency and its harmonics from the output signal. Component values were chosen so that a one volume percent ferrite concentration in the vicinity of the

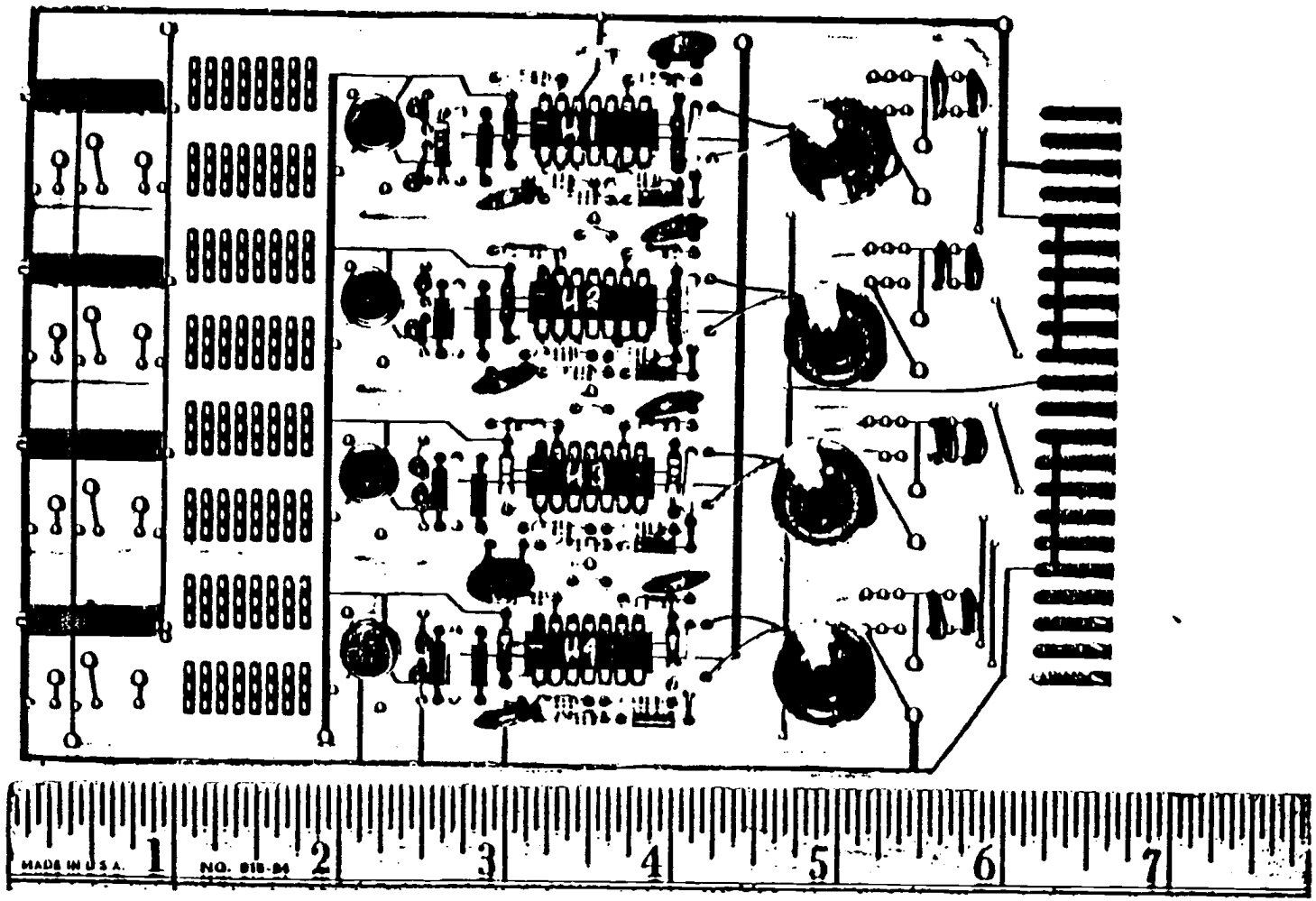

Figure C.2. Photograph of the component side of an inductance bridge card.

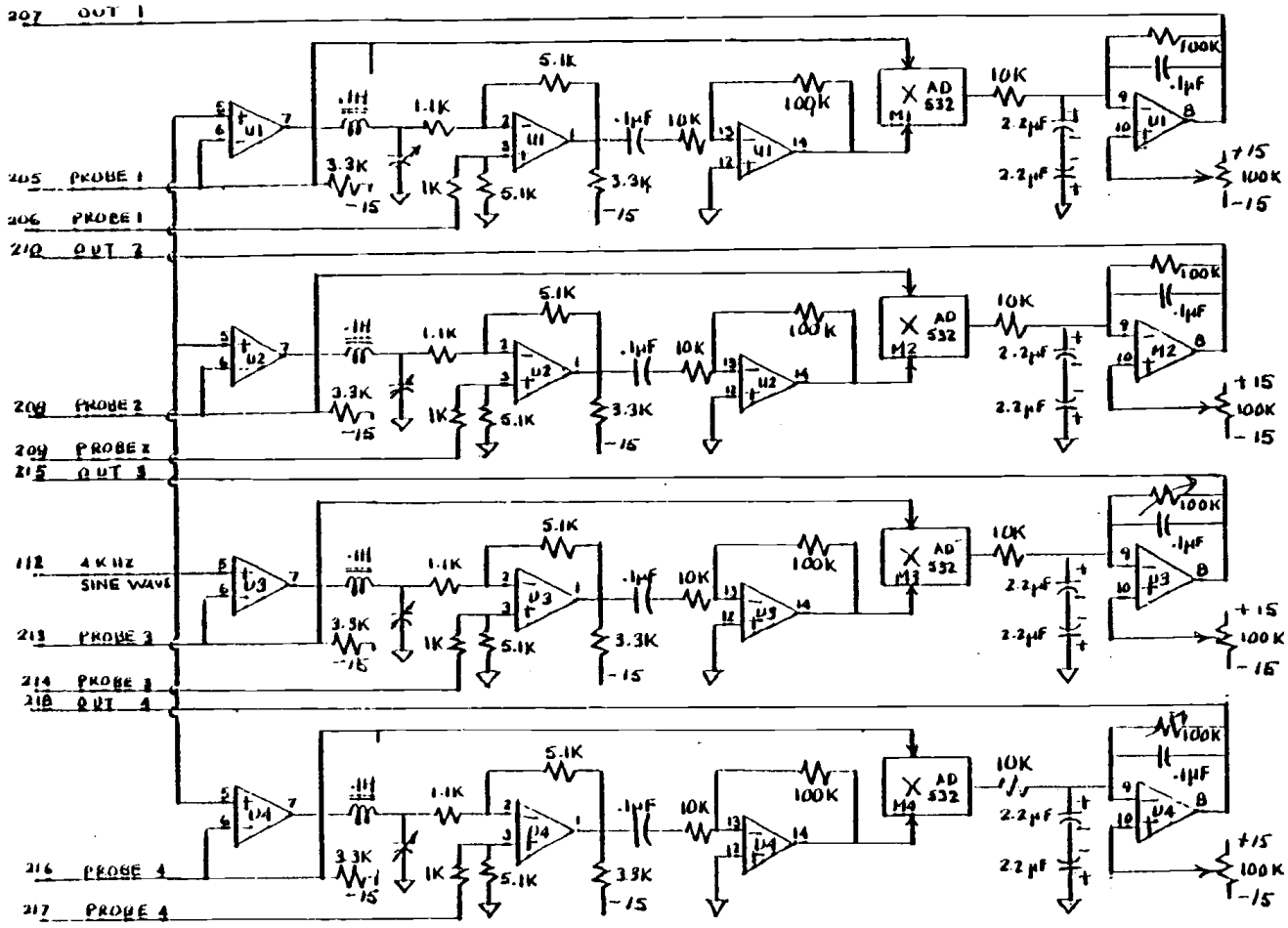

Figure C.3. Schematic drawing of an inductance bridge card. There are four inductance bridge amplifiers on a card.

probe produces approximately one volt at the output of the bridge circuit.

The only adjustable feature built into each circuit is the output D.C. level adjustment. This is necessary to compensate for drift in the electronics. The overall gain of each circuit ought to remain very nearly constant, and the gains of all the circuits should not vary by more than five percent from each other.

A $\pm$ 15 volt power supply (manufactured by Hewlett-Packard) is used to power all operational amplifiers. The common terminal of the supply is connected to earth ground; and the sense of the terminal is connected to the 15 volt bus of the inductor circuits.

The 4,000 Hz sine wave signal used to excite the inductance bridges is generated on the card which is schematically shown in Figure C.4. The oscillator is an Intersil 8038 voltage controlled oscillator which produces an approximately sinusoidal output. The frequency stability of the oscillator is good to better than 0.1 percent. The amplitude, which is determined by the power supply voltages, is stable to better than 0.1 percent, also. The output of the 8038 passes through a high pass filter to remove whatever DC component may be present, and then passes through an isolating follower amplifier. Since the sine wave is obtained by piecewise approximation, higher harmonics of the signal are still present. These harmonics are removed by Butterworth filters.

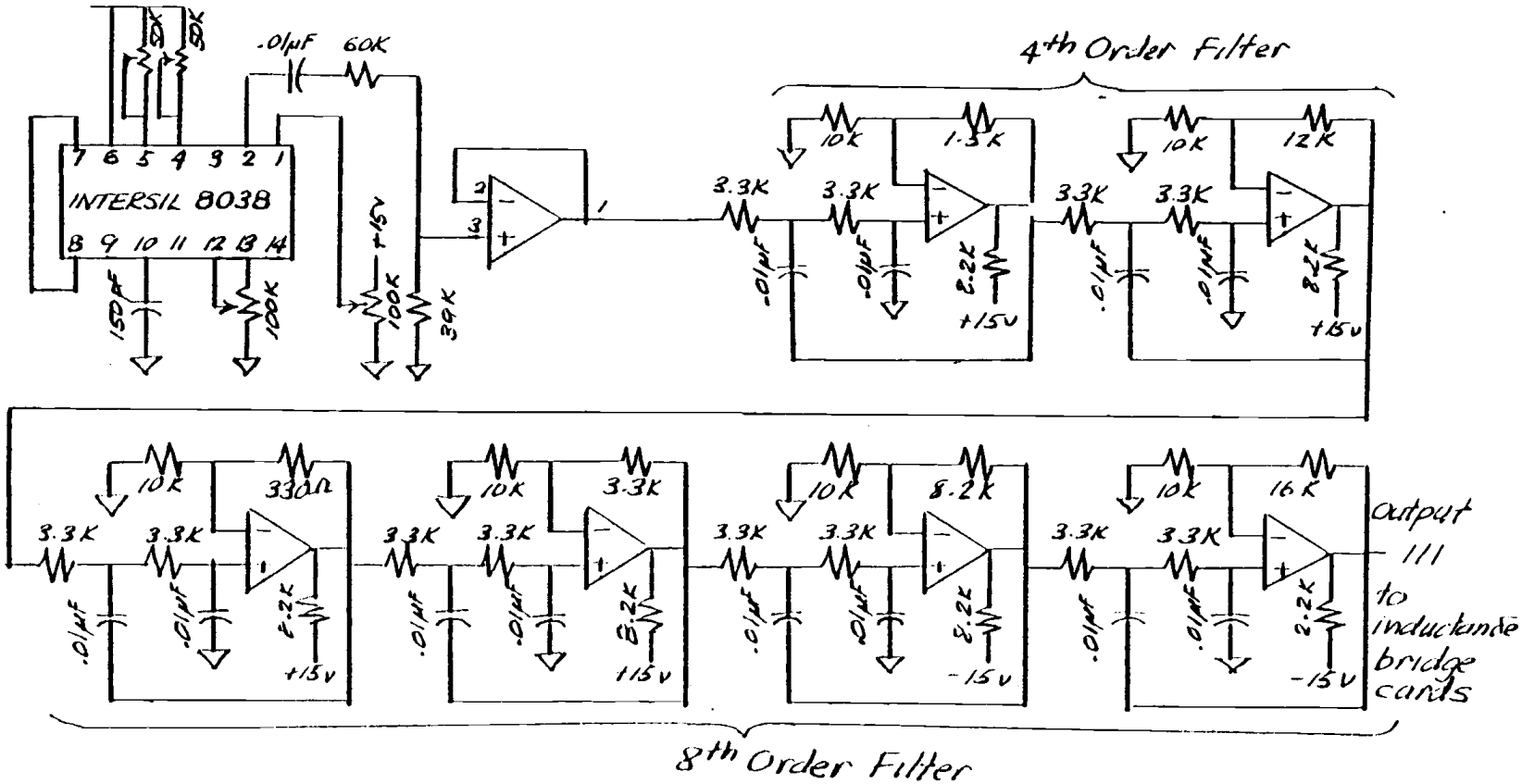

Figure C.4. The 4000 Hz. sine wave generator and Butterworth filters used for the inductance bridge circuits.